
Stability and Oscillations of Star Clusters in General Relativity

Von der Universität Bayreuth
zur Erlangung des Grades eines
Doktors der Naturwissenschaften (Dr. rer. nat.)
genehmigte Abhandlung

von
Sebastian Wolfschmidt
aus Kronach

1. Gutachter: Prof. Dr. Gerhard Rein
2. Gutachter: Prof. Dr. Mahir Hadžić
3. Gutachter: Prof. Dr. Håkan Andréasson

Tag der Einreichung: 17.07.2023

Tag des Kolloquiums: 21.11.2023

Preface

In this thesis, I have strived to compile a comprehensive collection of my research findings on the Einstein-Vlasov system gathered over the past several years. The work presented here builds in parts on the contributions of my colleagues and myself which have significantly influenced the direction and results of my research [45, 46, 47, 48]. I have made an effort to reference my prior work clearly throughout the dissertation.

In addition to the publications mentioned above, this thesis contains new results that go beyond the scope of my previous work. It represents an exploration of current open problems and is intended to advance knowledge in the field of collisionless equilibria in general relativity. Ultimately, I hope that this work contributes to the existing body of knowledge in the field and encourages further research and progress. I sincerely hope that the ideas and findings presented here will pave the way for future investigations.

Acknowledgments

I am deeply grateful to Prof. Gerhard Rein, whose lectures ignited my passion for mathematics from day one and who granted me the opportunity to pursue a doctorate under his guidance. He always maintained a friendly and open-minded but professional and rigorous research environment. This has greatly influenced my personal development over the many years. My gratitude also goes to Prof. Thomas Kriecherbauer, who always cultivated a pleasant working atmosphere and with whom I supervised numerous lectures, which were always perfectly organized by him.

I want to sincerely thank Christopher Straub, in whom I have found a close friend over the last few years. You provided invaluable insights to various research questions throughout my dissertation and many parts of the work would not have been developed without you. I wish you the best of luck for your future (academic) endeavors.

Nobody has been more important in this project than my newly wed wife Daniela. Your love and understanding have been the driving force behind my success. I am truly fortunate to have you as my partner in life, and I look forward to sharing many more achievements and adventures together.

I would also like to express my gratitude to the several other colleagues, friends, and family members who have accompanied and supported me along my academic journey. Each and every one of you has had a profound impact on my personal development and the individual I have become today.

With sincere appreciation and heartfelt thanks

Sebastian Wolfschmidt

Abstract

We study the dynamics of self-gravitating, collisionless matter in general relativity using the Einstein-Vlasov system, for which we consider the spherically symmetric, asymptotically flat case. We construct singularity-free stationary solutions and shells surrounding a black hole at the center. The properties of these steady states are thoroughly examined, including the single-well structure of the corresponding effective potential and the period function for particle motions. In the process, we introduce action-angle type variables. A numerical investigation provides further insights and evidence for the single-well structure for general isotropic steady states. We show that the metric coefficients, source terms, period function, and further macroscopic quantities are continuous along the redshift κ .

The linearized Einstein-Vlasov system around a fixed steady state is represented by a second-order evolution equation that is characterized by an Antonov-type operator \mathcal{L} . We prove that the essential spectrum of \mathcal{L} is strictly positive. By establishing a Birman-Schwinger principle, we characterize the issue of linear stability through a variational principle for the Mathur operator \mathcal{M} , which is a one-dimensional Hilbert-Schmidt operator. In addition, we obtain a quantitative bound on the number of unstable modes. As an application, we show that small shells surrounding a black hole are linearly stable.

By employing a continuity argument along the redshift, we prove that the Antonov operator has an isolated, positive eigenvalue under rather general assumptions. This leads directly to the existence of a linearly oscillating mode for the linearized system. In order to obtain this result, we show the continuity in κ of a projection operator that is not explicitly known and arises in the definition of the Mathur operator.

We numerically investigate non-linear stability with a particle-in-cell method. The study reveals different types of behavior for slightly perturbed equilibria: For stable steady states, we observe oscillating and damped solutions. Unstable configurations (fully or partially) collapse, disperse via a heteroclinic orbit, or perform a homoclinic orbit. The binding energy hypothesis is examined, and evidence for the existence of families of steady states with multiple stability changes is presented.

Linear stability is probed numerically by approximating the infimum of the spectrum of \mathcal{L} . The results show that linear and non-linear stability coincide. We confirm the existence of multiple stability changes on the linearized level. In addition, we investigate the existence of oscillating solutions and explore damping effects for isotropic polytropes.

Kurzfassung

Die Dynamik von selbstgravitierender, kollisionsfreier Materie in der allgemeinen Relativitätstheorie wird mit Hilfe des Einstein-Vlasov-Systems modelliert, wobei der sphärisch symmetrische, asymptotisch flache Fall betrachtet wird. Es werden singularitätsfreie stationäre Lösungen und Schalen mit schwarzem Loch im Zentrum konstruiert. Die Eigenschaften dieser stationären Zustände werden gründlich untersucht, einschließlich der “single-well”-Struktur des zugehörigen effektiven Potentials und der Periodenfunktion für Teilchenbewegungen. Dabei werden Variablen vom Typ der Wirkungs-Winkelkoordinaten eingeführt. Es wird gezeigt, dass die metrischen Koeffizienten, die Quellterme, die Periodenfunktion und weitere makroskopische Größen längs der Rotverschiebung κ stetig sind.

Das linearisierte Einstein-Vlasov-System um einen festen stationären Zustand wird durch eine Evolutionsgleichung zweiter Ordnung repräsentiert, der durch einen Antonov-Operator \mathcal{L} charakterisiert wird. Es wird bewiesen, dass das wesentliche Spektrum von \mathcal{L} strikt positiv ist. Über ein Birman-Schwinger-Prinzip wird das Problem der linearen Stabilität durch ein Variationsprinzip für den Mathur-Operator \mathcal{M} charakterisiert, welcher ein eindimensionaler Hilbert-Schmidt-Operator ist. Darüber hinaus erhält man eine quantitative Schranke für die Anzahl der instabilen Moden. Als Anwendung wird gezeigt, dass kleine Schalen, die ein Schwarzes Loch umgeben, linear stabil sind.

Durch Anwendung eines Stetigkeitsarguments entlang der Rotverschiebung wird unter recht allgemeinen Annahmen bewiesen, dass der Antonov-Operator einen isolierten, positiven Eigenwert besitzt. Dies führt direkt zur Existenz einer linear oszillierenden Mode für das linearisierte System. Um dieses Ergebnis zu erhalten, wird die Stetigkeit in κ eines nicht explizit bekannten Projektionsoperators gezeigt, welcher in der Definition des Mathur-Operators auftritt.

Eine numerische Untersuchung der nichtlinearen Stabilität wird mithilfe einer “particle-in-cell”-Methode durchgeführt. Die Studie zeigt verschiedene Arten von Verhalten für leicht gestörte Gleichgewichte: Oszillierende und gedämpfte Lösungen werden für stabile stationäre Zustände beobachtet. Instabile Konfigurationen kollabieren (komplett oder teilweise), zerfließen über einen heteroklinen Orbit oder führen einen homoklinen Orbit aus. Die Bindungsenergie-Hypothese wird geprüft, und es wird Evidenz für die Existenz von Familien stabiler Zustände mit mehreren Stabilitätswechseln präsentiert.

Lineare Stabilität wird numerisch untersucht, indem das Infimum des Spektrums von \mathcal{L} approximiert wird. Die Ergebnisse zeigen eine Übereinstimmung zwischen linearer und nicht-linearer Stabilität. Die Existenz von mehrfachen Stabilitätswechseln wird auf der linearisierten Ebene bestätigt. Darüber hinaus wird die Existenz von oszillierenden Lösungen untersucht und Dämpfungseffekte für isotrope polytrope Zustände erforscht.

Contents

1	Introduction	1
1.1	The Einstein-Vlasov system	1
1.1.1	The Schwarzschild coordinate system	4
1.1.2	The maximal areal coordinate system	7
1.2	Preliminaries and previous results	9
1.3	Methodology and outline of the thesis	11
2	Stationary solutions to the Einstein-Vlasov system	15
2.1	Definition and preliminaries	15
2.2	Construction	17
2.2.1	Singularity-free steady states	17
2.2.2	Matter shells with a Schwarzschild-singularity	23
2.3	Properties	32
2.3.1	The single-well structure	32
2.3.2	The periodic particle motions and the period function	39
2.3.3	A lower bound for the period function	41
2.3.4	An upper bound for the period function	43
2.3.5	Action-angle type variables	52
2.3.6	A preliminary bound on $\frac{2m}{r}$	55
2.4	Numerical investigation	56
2.4.1	General overview of macroscopic quantities	57
2.4.2	Single-well structure, bounds on $\frac{2m}{r}$, and the period function	62
3	Parameter dependence for steady state families	67
3.1	Metric coefficients and source terms along the redshift	68
3.2	Dependence in the case of the single-well structure	77
3.2.1	Continuity of the period function	80
3.2.2	Bounds on the period function	85
4	Linearization of the Einstein-Vlasov system	89
4.1	The class of steady states under consideration	89
4.2	The linearized Einstein-Vlasov system	91
4.2.1	Definition of the function spaces and operators	93
4.2.2	A second-order formulation	95
4.3	Properties of the operators	96
4.3.1	The transport operator \mathcal{T}	98
4.3.2	The essential operator \mathcal{B}	104

4.3.3	Two relative compactness results	119
4.3.4	Spectral properties of \mathcal{T} and \mathcal{B}	122
5	On linear stability of stationary solutions	129
5.1	Definition, previous results, and methodology	129
5.1.1	Definition of linear stability	129
5.1.2	Previous results on stability	132
5.1.3	Methodology of the Birman-Schwinger principle	135
5.2	A Birman-Schwinger principle	136
5.2.1	The operators \mathcal{L}_β	137
5.2.2	The Birman-Schwinger operator	142
5.3	The Mathur operator	145
5.3.1	Definition and functional analytic properties	145
5.3.2	Explicit representation	146
5.4	Results on linear stability	154
5.4.1	A reduced criterion for linear stability	154
5.4.2	Linear stability of matter shells with a Schwarzschild-singularity	156
6	On oscillating solutions	159
6.1	The class of steady states and methodology	160
6.2	Preliminary results	163
6.2.1	Approximating the quadratic form	165
6.2.2	A fixed-point method for the projection operator	169
6.2.3	Continuity of the projection operator	175
6.3	Existence of oscillating solutions	186
6.3.1	Continuity of the Mathur operator	186
6.3.2	On eigenvalues in the principal gap	189
7	Numerical investigation of non-linear stability	193
7.1	Setup and previous results	193
7.2	The numerical method	195
7.3	Singularity-free steady states	200
7.3.1	Stable steady states	200
7.3.2	Unstable steady states	204
7.3.3	Stability behavior along κ -families	212
7.4	Steady states surrounding a Schwarzschild black hole	215
7.4.1	Stable shells	216
7.4.2	Unstable shells	218
8	Numerical investigation of linear stability	225
8.1	Preliminaries and setup of the variational principle	225
8.2	The numerical method	230
8.3	Testing and verification	233
8.4	Results on linear stability	235

8.5	Results on oscillating modes and damping	238
9	Conclusion, open problems, and possible areas of further research	243
A	Derivation of the linearized system	245
B	Results from operator and spectral theory	249
C	Derivation of the equations for the reduced variational principle	253
D	Pseudo-codes	257
D.1	The steady state computation	257
D.2	The particle-in-cell method	257
D.3	The variational principle	259

List of Figures

2.1	The effective potential in the pure Schwarzschild case	26
2.2	Periodic orbits and action-angle type variables	55
2.3	Mass-radius spiral for various models	58
2.4	Binding-energy for various models	59
2.5	Metric coefficients and source terms of an isotropic steady state	59
2.6	Mass density and metric coefficient e^μ for a large redshift	60
2.7	Mass density and metric coefficient e^μ for a shell	60
2.8	A core-halo configuration	61
2.9	Metric coefficients for a shell with a singularity at the center	62
2.10	Convergence of static shells for $M_0 \rightarrow 0$	63
2.11	Maximal values of $\frac{2m}{r}$	64
2.12	The period function and Ω^{EL}	65
5.1	Qualitative configuration of the spectrum of the Antonov operator \mathcal{L}	133
5.2	Qualitative behavior of the functions γ_n	142
6.1	The idea behind obtaining an eigenvalue of \mathcal{L}	162
6.2	Discontinuous behavior of the bottom of the spectrum of \mathcal{L}	169
7.1	Oscillation of an isotropic steady state	201
7.2	Damping for the polytropic model	202
7.3	A stable core-halo configuration	203
7.4	A collapsing isotropic steady state	204
7.5	A collapsing isotropic steady state in (r, E) -space	205
7.6	A collapsing core-halo configuration	207
7.7	Evolution of the trapped mass and trapped radius	208
7.8	A heteroclinic orbit	209
7.9	A heteroclinic orbit in (r, E) -space	210
7.10	Heteroclinic orbits along the King model	211
7.11	Full dispersion for a polytrope	212
7.12	Stability behavior of the King model	213
7.13	Evidence against the binding energy hypothesis	214
7.14	A family of steady states with multiple stability changes	215
7.15	Oscillation for a shell	216
7.16	Damping for a shell	217
7.17	Indeterminable behavior of a stable shell	218
7.18	Unstable behavior of a shell	219

7.19	A homoclinic orbit in (r, E) -space	221
7.20	A fully dispersing shell	222
7.21	Homoclinic orbits along the redshift	223
8.1	Convergence test for the variational principle	234
8.2	Consistency test for linear and non-linear stability	235
8.3	Linear stability for the piecewise model with $n = 200$	236
8.4	Linear stability for the piecewise model with $n = 270$	237
8.5	Oscillation vs. damping along the polytropic index k	240
8.6	Oscillation vs. damping along the redshift κ	241

1 Introduction

Nothing has such power to broaden
the mind as the ability to investigate
systematically and truly all that
comes under thy observation in life.

Marcus Aurelius

Albert Einstein's theory of general relativity is widely considered as one of the foundational pillars of modern physics, having revolutionized our understanding of space, time, and gravity. Einstein's work on general relativity can be traced back to 1911, when he postulated the equivalence principle [36]. Prior to developing the notion of curved spacetime, Einstein used the combination of the equivalence principle with special relativity to predict that clocks operate at different rates in a gravitational field and that light rays bend under the influence of gravity. He spent several years refining his ideas and developing the mathematics necessary to express them. In 1915, his work culminated in the theory of general relativity [37, 38], which represented a radical departure from the previous understanding of gravity.

General relativity has stood the test of time and has been validated by numerous observations, including the explanation of the perihelion precession of Mercury [39], the deflection of light by the sun [34], and the detection of gravitational waves [1]. Einstein's theory predicts the existence of black holes [106]—some of the most extreme and mysterious objects in the universe—which are regions of spacetime where the gravitational pull is so strong that nothing can escape. This prediction has recently been confirmed through the first-ever image of a black hole, captured by the Event Horizon Telescope [41].

The behavior of matter in the presence of gravity is central to our understanding of the universe, from the motion of planets and stars to the structure and evolution of galaxies. One of the most fundamental questions that arises in the context of general relativity is therefore how matter generates and interacts with the gravitational field.

1.1 The Einstein-Vlasov system

The Einstein-Vlasov system stands as a mathematical model that describes the behavior of an ensemble of particles or gas moving under the influence of their mutual gravitational interactions, as described by the theory of general relativity. In this model, the particles are treated as a continuous distribution of mass, rather than discrete individual objects, and their dynamics are described by the Einstein field equations coupled to the Vlasov

equation, also known as the collisionless Boltzmann equation. We now present the Einstein-Vlasov system in its full generality before restricting it to spherical symmetry in the next section. We choose units where the gravitational constant and the speed of light are normalized to one. Concerning the notation for general relativity and the Einstein-Vlasov system, we follow [91, 112].

The object under investigation is a spacetime $(M, g_{\alpha\beta})$, where M is a time-orientable, four-dimensional manifold and $g_{\alpha\beta}$ is a Lorentzian metric with signature $(- + + +)$. Greek letters always run from 0 to 3. Indices can be lowered with the metric $g_{\alpha\beta}$ and raised with its inverse $g^{\alpha\beta}$. By writing x^α for local coordinates, the line element is given by

$$ds^2 = g_{\alpha\beta} dx^\alpha dx^\beta.$$

Henceforth, the Einstein summation convention is employed. The metric induces the Christoffel symbols

$$\Gamma_{\beta\gamma}^\alpha = \frac{1}{2} g^{\alpha\delta} (\partial_{x^\beta} g_{\gamma\delta} + \partial_{x^\gamma} g_{\beta\delta} - \partial_{x^\delta} g_{\beta\gamma})$$

and the geodesic equations

$$\frac{dx^\alpha}{d\tau} = p^\alpha, \quad \frac{dp^\alpha}{d\tau} = -\Gamma_{\beta\gamma}^\alpha p^\beta p^\gamma, \quad (1.1)$$

which can be viewed as equations of motion for particles or light rays in the gravitational field generated by the metric $g_{\alpha\beta}$. This is in analogy to Newton's equations of motion. The parameter τ corresponds to the proper time of an observer if the geodesic is timelike. The tangent bundle TM of the manifold M is equipped with the coordinates (x^α, p^β) , where p^β are the (canonical) coordinate basis components of the tangent vectors to the manifold M . The eight-dimensional tangent bundle TM —or rather an appropriate subset of TM —is the proper phase-space on which the particle density $f = f(x^\alpha, p^\beta)$ is defined. The Vlasov equation is consequently given by

$$p^\alpha \partial_{x^\alpha} f - \Gamma_{\beta\gamma}^\alpha p^\beta p^\gamma \partial_{p^\alpha} f = 0. \quad (1.2)$$

Since we aim to model (clusters of) galaxies, the particles are massive and travel along timelike geodesics, i.e., they move forward in time. The rest mass of a particle on a timelike geodesic is given by $-g_{\alpha\beta} p^\alpha p^\beta$ and is conserved along solutions to (1.1). Therefore, we restrict the particle density to the mass shell

$$PM := \{(x^\alpha, p^\beta) \in TM \mid g_{\alpha\beta} p^\alpha p^\beta = -1, p^\beta \text{ is future pointing}\},$$

which is a geodesically invariant, seven-dimensional submanifold of TM , where all particles have rest mass one. By employing Gaussian normal coordinates locally on M , the line element can be written as

$$ds^2 = g_{00} (dx^0)^2 + g_{ab} dx^a dx^b,$$

and solving for p^0 in $g_{\alpha\beta}p^\alpha p^\beta = -1$ yields

$$(p^0)^2 = -g^{00}(1 + g_{ab}p^a p^b).$$

Latin indices always run from 1 to 3. Due to the signature of the metric and p^β being future pointing on the mass shell PM , we obtain $p^0 > 0$ and

$$p^0 = \sqrt{-g^{00}}\sqrt{1 + g_{ab}p^a p^b}.$$

The coordinate $t := x^0$ can now be interpreted as a timelike coordinate because of

$$\frac{dx^0}{d\tau} = p^0 > 0$$

on PM . In particular, the geodesic equations (1.1) and the Vlasov equation (1.2) can be expressed in (t, x^a, p^b) on the mass shell via

$$\frac{dx^a}{dt} = \frac{p^a}{p^0}, \quad \frac{dp^a}{dt} = -\frac{1}{p^0}\Gamma_{\beta\gamma}^a p^\beta p^\gamma$$

and

$$\partial_t f + \frac{p^a}{p^0}\partial_{x^a} f - \frac{1}{p^0}\Gamma_{\beta\gamma}^a p^\beta p^\gamma \partial_{p^a} f = 0, \quad (1.3)$$

respectively.

In order to obtain a self-gravitating system of collisionless matter, the Vlasov equation (1.3) on the mass shell gets coupled to the Einstein field equations

$$G_{\alpha\beta} = 8\pi T_{\alpha\beta}, \quad (1.4)$$

where $G_{\alpha\beta}$ is the Einstein tensor determining the curvature of spacetime and $T_{\alpha\beta}$ is the energy-momentum tensor representing the matter and energy contained in M . We are only interested in the setting with a vanishing cosmological constant. The Einstein tensor is given by

$$G_{\alpha\beta} = R_{\alpha\beta} - \frac{1}{2}R g_{\alpha\beta},$$

where $R_{\alpha\beta}$ is the Ricci tensor and $R = R_\alpha^\alpha$ is the Ricci scalar. The Ricci tensor is in turn obtained from the Riemann curvature tensor

$$R_{\alpha\beta\gamma}{}^\delta = \partial_{x^\beta}\Gamma_{\alpha\gamma}^\delta - \partial_{x^\alpha}\Gamma_{\beta\gamma}^\delta + \Gamma_{\beta\varepsilon}^\delta\Gamma_{\alpha\gamma}^\varepsilon - \Gamma_{\alpha\varepsilon}^\delta\Gamma_{\beta\gamma}^\varepsilon$$

by setting $R_{\alpha\beta} = R_{\alpha\gamma\beta}{}^\gamma$. Therefore, the Einstein tensor is fully determined by the metric $g_{\alpha\beta}$ and contains second-order derivatives of this metric.

The particle distribution f induces the energy-momentum tensor via

$$T_{\alpha\beta} = \int p_\alpha p_\beta f |g|^{\frac{1}{2}} \frac{dp^1 dp^2 dp^3}{-p_0}, \quad (1.5)$$

where $|g|$ is the modulus of the determinant of the metric. The resulting equations (1.3), (1.4), and (1.5) constitute the *Einstein-Vlasov system in general coordinates*. We prescribe that the spacetime is asymptotically flat, which corresponds to the description of an isolated system. For a detailed derivation of the Einstein-Vlasov system from a kinetic-theory perspective, we refer the interested reader to [35] and the references there. In [29], the local well-posedness of the Cauchy problem for the Einstein-Vlasov system was first established by considering certain energy estimates in appropriate Sobolev spaces.

The goal of this work is to analyze stationary solutions to the asymptotically flat Einstein-Vlasov system. One trivial steady state is obtained by flat Minkowski space $g_{\alpha\beta} = \text{diag}(-1, 1, 1, 1)$ and $f = 0$. The non-linear stability of this setting was originally established in the spherical symmetry case in [91, 93] and proven recently in [43, 75] for general small perturbations. The second well-known steady state is given by the vacuum Schwarzschild metric

$$ds^2 = -\left(1 - \frac{2M}{r}\right)dt^2 + \left(1 - \frac{2M}{r}\right)^{-1}dr^2 + r^2(d\theta^2 + \sin^2(\theta)d\psi^2),$$

where a central black hole of $M > 0$ is surrounded by vacuum. The seminal work [30] shows that vacuum perturbations of Schwarzschild spacetime converge asymptotically to a member of the Schwarzschild family, modulo the Kerr solutions. The authors prove this on a non-linear level and without symmetry assumptions.

Currently, it is not possible to rigorously analyze questions regarding the stability or instability of non-trivial, time-independent solutions to the Einstein-Vlasov system without employing a symmetry assumption. From a mathematical point-of-view, the above-mentioned results for the Minkowski spacetime and the vacuum Schwarzschild spacetime rely on the matter being small, and the arguments are structurally different from the stability of non-trivial equilibria. We thus prescribe that the spacetime is spherically symmetric. We conduct our research in two coordinate systems which are presented in the following.

1.1.1 The Schwarzschild coordinate system

Einstein's field equations allow for coordinate freedom. For the *Schwarzschild coordinate system*, the line element is given by

$$ds^2 = -e^{2\mu(t,r)}dt^2 + e^{2\lambda(t,r)}dr^2 + r^2(d\theta^2 + \sin^2(\theta)d\psi^2), \quad (1.6)$$

where $(t, r, \theta, \psi) \in \mathbb{R} \times [0, \infty[\times [0, \pi] \times [0, 2\pi]$. The coordinates t and r can be interpreted as a time and radial variable, respectively. The polar angles θ and ψ parametrize the two-spheres of constant t and $r > 0$. The *metric coefficients* μ and λ are unknown functions in (t, r) that determine the metric of the spherically symmetric spacetime. We prescribe the boundary conditions $\mu(t, \infty) = 0 = \lambda(t, \infty)$ which ensure asymptotic flatness. In order to eliminate the artificial singularity that arises at $r = 0$, it is convenient to

introduce Cartesian coordinates

$$x = (x^1, x^2, x^3) = r(\sin(\theta) \cos(\psi), \sin(\theta) \sin(\psi), \cos(\theta)) \in \mathbb{R}^3 \quad (1.7)$$

and to express the metric, the Christoffel symbols, etc., in these coordinates. Furthermore, instead of the canonical momentum variables p^a , we use non-canonical momentum variables v^a given by

$$v^a = p^a + (e^\lambda - 1) \frac{x \cdot p}{r} \frac{x^a}{r}. \quad (1.8)$$

We have introduced the shorthand $x \cdot p = \delta_{ab} x^a p^b$, and in the following, we employ the notation $|\cdot|$ for the Euclidean norm on \mathbb{R}^3 . The change of momentum variables from p^a to v^a is advantageous, as it removes the dependency of the energy-momentum tensor on the metric coefficients. However, the characteristic flow of the Vlasov equation is no longer measure-preserving in (x, v) . By plugging (1.6), (1.7), and (1.8) into the Einstein-Vlasov system, a lengthy derivation yields the system which follows below. It is worth mentioning that the geometric aspects inherent in the Einstein equations are now fully eliminated, and only a coupled system of partial differential equations remains. We refer to [91] for a detailed discussion and derivation of the relevant geometric tensors and the energy-momentum tensor. The Vlasov equation for the particle distribution $f = f(t, x, v)$ is given by

$$\partial_t f + e^{\mu-\lambda} \frac{v}{\sqrt{1+|v|^2}} \cdot \partial_x f - \left(\dot{\lambda} \frac{x \cdot v}{r} + e^{\mu-\lambda} \mu' \sqrt{1+|v|^2} \right) \frac{x}{r} \cdot \partial_v f = 0. \quad (1.9)$$

Einstein's field equations are represented by

$$e^{-2\lambda}(2r\lambda' - 1) + 1 = 8\pi r^2 \rho_f, \quad (1.10)$$

$$e^{-2\lambda}(2r\mu' + 1) - 1 = 8\pi r^2 p_f, \quad (1.11)$$

$$\dot{\lambda} = -4\pi r e^{\lambda+\mu} j_f, \quad (1.12)$$

$$e^{-2\lambda} \left(\mu'' + (\mu' - \lambda') \left(\mu' + \frac{1}{r} \right) \right) - e^{-2\mu} \left(\ddot{\lambda} + \dot{\lambda}(\dot{\lambda} - \dot{\mu}) \right) = 8\pi q_f, \quad (1.13)$$

where the source terms arising from the energy-momentum tensor are

$$\rho_f(t, r) = \rho_f(t, x) = \int_{\mathbb{R}^3} \sqrt{1+|v|^2} f(t, x, v) dv, \quad (1.14)$$

$$p_f(t, r) = p_f(t, x) = \int_{\mathbb{R}^3} \left(\frac{x \cdot v}{r} \right)^2 f(t, x, v) \frac{dv}{\sqrt{1+|v|^2}}, \quad (1.15)$$

$$j_f(t, r) = j_f(t, x) = \int_{\mathbb{R}^3} \frac{x \cdot v}{r} f(t, x, v) dv, \quad (1.16)$$

$$q_f(t, r) = q_f(t, x) = \frac{1}{2} \int_{\mathbb{R}^3} \left| \frac{x \times v}{r} \right|^2 f(t, x, v) \frac{dv}{\sqrt{1+|v|^2}}. \quad (1.17)$$

Throughout the equations $x, v \in \mathbb{R}^3$. A prime or a dot always denotes a derivative with respect to $r = |x|$ or t , respectively, e.g., $\lambda' := \partial_r \lambda$ and $\dot{\lambda} := \partial_t \lambda$. As an aside, the terms ρ_f , p_f , j_f , and q_f can be interpreted as a mass, pressure, momentum, and tangential pressure density, respectively. The system is not complete without boundary conditions and initial data. We impose an asymptotically flat spacetime as mentioned above, i.e.,

$$\lim_{r \rightarrow \infty} \mu(t, r) = 0 = \lim_{r \rightarrow \infty} \lambda(t, r). \quad (1.18)$$

For the remaining boundary and initial conditions, we distinguish between two situations: On the one hand, we consider singularity-free spacetimes with a non-negative, spherically symmetric initial distribution

$$f(0) = \mathring{f} \in C_c^1(\mathbb{R}^3 \times \mathbb{R}^3).$$

A particle distribution $f = f(t, x, v)$ is called spherically symmetric if

$$f(t, x, v) = f(t, Ax, Av), \quad A \in \text{SO}(3),$$

i.e., if $f(t)$ is invariant under simultaneous rotation in x and v ; we comment further on spherical symmetry in Section 1.2. In addition, we prescribe that \mathring{f} satisfies

$$4\pi \int_0^r \rho_{\mathring{f}}(s) s^2 ds < \frac{r}{2}, \quad r > 0, \quad (1.19)$$

and impose that

$$\lambda(t, 0) = 0. \quad (1.20)$$

The latter condition is required to obtain a spacetime with a regular center. The estimate (1.19) is a necessary constraint on the initial data, as otherwise field equation (1.10) cannot be solved for $t = 0$ globally in r . We call (1.9)–(1.20) the *singularity-free Einstein-Vlasov system*.¹

On the other hand, we consider the setting where a Schwarzschild black hole of mass $M_0 > 0$ is situated at the center of the spacetime. In this case, Schwarzschild coordinates can only cover points of the spacetime where $r > 2M_0$. Therefore, we allow non-negative, spherically symmetric initial distributions $\mathring{f} \in C_c^1(\{x \in \mathbb{R}^3 \mid |x| > 2M_0\} \times \mathbb{R}^3)$ with

$$M_0 + 4\pi \int_{2M_0}^r \rho_{\mathring{f}}(s) s^2 ds < \frac{r}{2}, \quad r > 2M_0, \quad (1.21)$$

and we prescribe

$$\lim_{r \rightarrow \infty} e^{-2\lambda(t, r)} = 0. \quad (1.22)$$

The latter two conditions play the same role as (1.19) and (1.20) for the singularity-free

¹When using the expression *Einstein-Vlasov system*, we henceforth refer to the asymptotically flat, spherically symmetric setting in Schwarzschild coordinates. We implicitly refer to both the singularity-free case and the case with a singularity at the same time, unless stated otherwise.

system. Accordingly, we call (1.9)–(1.18), (1.21), and (1.22) the *Einstein-Vlasov system with a Schwarzschild-singularity of mass M_0* .

In both settings, the quantity

$$m(t, r) = 4\pi \int_0^r \rho_f(t, s) s^2 ds \quad (1.23)$$

is referred to as the quasi-local (Vlasov) mass, and necessarily $2m < r$ or $2(m + M_0) < r$ must hold.

At first sight, the Einstein-Vlasov system seems to be overdetermined due to the four field equations (1.10)–(1.13). As shown in [91], we can eliminate equations (1.12), (1.13) from the system and prove their validity a-posteriori if the Vlasov equation as well as (1.10), (1.11) are fulfilled. Furthermore, we substitute $\dot{\lambda}$ with field equation (1.12) in the Vlasov equation (1.9). This yields the modified Vlasov equation

$$\partial_t f + e^{\mu-\lambda} \frac{v}{\sqrt{1+|v|^2}} \cdot \partial_x f + \left(4\pi r e^{\mu+\lambda} j_f \frac{x \cdot v}{r} - e^{\mu-\lambda} \mu' \sqrt{1+|v|^2} \right) \frac{x}{r} \cdot \partial_v f = 0, \quad (1.24)$$

and one can prove that solving (1.10), (1.11), (1.14), (1.15), and (1.24) together with the corresponding boundary and initial conditions is equivalent to solving the Einstein-Vlasov system introduced above. In the following, we thus refer to (1.24) as the Vlasov equation for our purposes and dispense with (1.9).

1.1.2 The maximal areal coordinate system

Besides Schwarzschild coordinates, we introduce the maximal areal coordinate system, for which the line element is of the form

$$ds^2 = -(\alpha^2 + a^2 \beta^2) dt^2 + 2a^2 \beta dt dr + a^2 dr^2 + r^2 (d\theta^2 + \sin^2(\theta) d\psi^2).$$

The variables t , r , θ , and ψ are the same as in (1.6), and the metric coefficients α , a , and β are again functions of (t, r) ; we demand that α and a are strictly positive. Since we only use maximal areal coordinates for the numerical investigation in Chapter 7, we keep the discussion of the Einstein-Vlasov system in these coordinates fairly short. Overall, the structure is very similar to Schwarzschild coordinates but more involved due to the presence of a third metric coefficient β and the geometric “maximal slicing condition” which prescribes that hypersurfaces of constant t have vanishing mean curvature. For a thorough derivation and discussion, we refer to [44, 46].

The Einstein-Vlasov system in maximal areal coordinates is given by the following system of equations: The Vlasov equation

$$\begin{aligned} \partial_t f + \left[\frac{\alpha}{a} \frac{v}{\sqrt{1+|v|^2}} - \beta \frac{x}{r} \right] \cdot \partial_x f \\ + \left[\left(-\frac{\alpha'}{a} \sqrt{1+|v|^2} \frac{x}{r} + \frac{((a\beta)' - \dot{a}) x \cdot v}{a} \frac{x}{r} \right) \frac{x}{r} + \frac{\beta}{r} \left(v - \frac{x \cdot v}{r} \frac{x}{r} \right) \right] \cdot \partial_v f = 0 \end{aligned} \quad (1.25)$$

is coupled to the field equations²

$$K_\theta^\theta = \frac{\beta}{\alpha r}, \quad (1.26)$$

$$a' = 4\pi r \rho a^3 + \frac{3}{2} r (K_\theta^\theta)^2 a^3 + \frac{a}{2r} (1 - a^2), \quad (1.27)$$

$$(K_\theta^\theta)' = -3 \frac{K_\theta^\theta}{r} - 4\pi a j, \quad (1.28)$$

$$\alpha'' = \alpha' \left(\frac{a'}{a} - \frac{2}{r} \right) + 6\alpha a^2 (K_\theta^\theta)^2 + 4\pi \alpha a^2 (S + \rho), \quad (1.29)$$

$$\dot{a} = (a\beta)' + 2a\alpha K_\theta^\theta, \quad (1.30)$$

$$\dot{K}_\theta^\theta = -\frac{3}{2} (K_\theta^\theta)^2 \alpha - \frac{\alpha'}{ra^2} + \frac{\alpha}{2r^2} \left(1 - \frac{1}{a^2} \right) + 4\pi (\alpha p - a\beta j), \quad (1.31)$$

via the source terms as in (1.14)–(1.17), and

$$S_f(t, r) = p_f(t, r) + 2q_f(t, r) = \int_{\mathbb{R}^3} \frac{|v|^2}{\sqrt{1 + |v|^2}} f(t, x, v) dv. \quad (1.32)$$

The boundary conditions for the metric coefficients are

$$\lim_{r \rightarrow \infty} \alpha(t, r) = 1 = \lim_{r \rightarrow \infty} a(t, r), \quad \lim_{r \rightarrow \infty} \beta(t, r) = 0. \quad (1.33)$$

In the singularity-free setting, we prescribe $a(t, 0) = 1$, whereas we demand

$$\lim_{r \rightarrow 2M_0} \frac{1}{a^2(t, r)} = 0$$

in the case with a black hole of mass M_0 at the center.

We only consider compactly supported, non-negative initial data $f(0) = \mathring{f}$ such that (1.27) and (1.28) have solutions that exist for $r > 0$. Through the same mechanism as for Schwarzschild coordinates, we can eliminate \dot{a} in the Vlasov equation by field equation (1.30) and show that (1.30) as well as (1.31) are fulfilled a-posteriori for a reduced set of field equations; see [46, Sc. 2.3].

There are some key differences between the Einstein-Vlasov system in maximal areal coordinates compared to Schwarzschild coordinates. Maximal areal coordinates are able to cover parts of the spacetime that are trapped. A trapped surface is defined as a closed two-dimensional surface with the property that the expansion of any family of outgoing null geodesics (light rays) from the surface is negative everywhere on the surface. In other words, the surface has the property that the area of a small sphere centered on any point on the surface decreases as time progresses. In maximal areal coordinates, a

²We use the notation K_θ^θ , since $\frac{\beta}{\alpha r}$ is the $\theta\theta$ component of the extrinsic curvature tensor K_b^a .

trapped surface is present, if at some time t and radius $r > 0$ the inequality

$$\frac{1}{a(t, r)} < rK_{\theta}^{\theta}(t, r) \quad (1.34)$$

holds. The ability to describe trapped surfaces is a crucial advantage in the study of the formation of singularities.

In addition, the elliptic-type field equation (1.29) for α apparently yields more regularity compared to equation (1.11) for μ . Indeed, this simplifies some arguments in the proof of local existence [44, 46].

However, the trade-off for these beneficial properties is the more difficult structure of the Einstein-Vlasov system as a whole in maximal areal coordinates. In particular, the metric coefficients cannot be determined explicitly for given source terms. This makes the situation considerably worse for deriving analytical properties.

As mentioned above, we will come back to maximal areal coordinates when numerically studying the non-linear stability of steady states in Chapter 7, since the detection of trapped surfaces can be quite insightful in this case.

1.2 Preliminaries and previous results

Before we get to the main objectives of this work, we comment on some technical details, mention preliminary properties of the system, and review previous results. We limit the technicalities to the Schwarzschild coordinate case, but they can be transferred to maximal areal coordinates as well.

To begin, we note that spherical symmetry, as defined in the previous section, is conserved along regular solutions³ to the Einstein-Vlasov system. The spherical symmetry of the distribution function $f(t)$ allows us to eliminate three of the six variables (x, v) , since we can write f as a function of

$$r = |x|, \quad w = \frac{x \cdot v}{r}, \quad L = |x|^2|v|^2 - (x \cdot v)^2 = |x \times v|^2.$$

Under abuse of notation we write $f(t, x, v) = f(t, r, w, L)$. However, note that this introduces an artificial singularity at $r = 0$ which can make the analysis of the system more difficult. In (r, w, L) -variables, the (modified) Vlasov equation (1.24) becomes

$$\begin{aligned} & \partial_t f + e^{\mu-\lambda} \frac{w}{\sqrt{1+w^2 + \frac{L}{r^2}}} \partial_r f \\ & + \left(4\pi r e^{\lambda+\mu} j_f w - e^{\mu-\lambda} \mu' \sqrt{1+w^2 + \frac{L}{r^2}} + e^{\mu-\lambda} \frac{L}{r^3 \sqrt{1+w^2 + \frac{L}{r^2}}} \right) \partial_w f = 0. \end{aligned}$$

The field equations and the source terms remain unchanged, apart from transforming

³See [91, Def. 1.2.7] for a precise definition of a regular solution to the Einstein-Vlasov system.

the variables in the integrands of the source terms accordingly. The stability analysis central to this work relies mainly on (r, w, L) -coordinates since periodic particle orbits are better described in coordinates adapted to spherical symmetry. The spherical symmetry of f is also the reason why the source terms are radially symmetric functions, e.g., $\rho_f(t, r) = \rho_f(t, x)$ for $r = |x|$ and $x \in \mathbb{R}^3$.

Along regular, compactly supported solutions f to the Einstein-Vlasov system, it is easy to see that the ADM-mass

$$M := \iint_{\mathbb{R}^6} \sqrt{1 + |v|^2} f(t, x, v) d(x, v) = 4\pi \int_0^\infty \rho_f(t, s) s^2 ds$$

as well as the Casimir functionals

$$\iint_{\mathbb{R}^6} e^{\lambda(x)} \chi(f(t, x, v)) d(x, v) \tag{1.35}$$

are conserved quantities for every $\chi \in C^1([0, \infty[)$ with $\chi(0) = 0$. For the special case $\chi = \text{id}$, we obtain that the number of particles

$$N := \iint_{\mathbb{R}^6} e^{\lambda(t, x)} f(t, x, v) d(x, v) \tag{1.36}$$

is constant in time.

Let us comment on some known results for the Einstein-Vlasov system in spherical symmetry in the singularity-free case. For a general overview and introduction, we refer to [6, 91, 95].

The local existence of regular solutions together with a continuation criterion is established in [91, 93] for Schwarzschild coordinates and in [44, 46] for maximal areal coordinates. It is an open problem whether these solutions can always be continued globally in time. For matter bounded away from the spatial origin, the main result of [97] shows that solutions exist globally. A similar result is proven in [11] for outgoing initial data in maximal areal coordinates. The gravitational collapse of collisionless matter is studied in [7, 12, 13]. A first step towards proving the weak cosmic censorship hypothesis [28, 81] for collisionless matter is obtained in [32] by applying the results from [31]. The authors show that singularities for the Einstein-Vlasov system must emanate from the center and that the weak cosmic censorship hypothesis holds if a trapped surface forms.

For the setting with a central black hole, it is possible to show that global in-time solutions exist, by applying the continuation criterion from [91, 93]. However, the non-linear dynamics of the system with a singularity have not yet been studied in the literature.

There is a plethora of stationary solutions to the Einstein-Vlasov system [47, 83, 90, 96]. The existence of steady states to the axially symmetric Einstein-Vlasov system was shown in [14] and recently in [64] as a bifurcation from Kerr spacetime. Non-linear stability of steady states remains an open problem: An approach towards non-linear stability was tried in [113], but the work contains serious flaws, as pointed out in [9]. On

the contrary, the issue of linear stability is better understood: In [53, 54] it is proven that isotropic steady states are linearly stable if they are close to Newtonian, and the authors of [52] show that highly relativistic, isotropic equilibria are linearly unstable. Static shells surrounding a black hole are established by different means in [47, 63, 90], and linear stability of such shells is proven in [47]. Much work in the literature deals with the numerical investigation of stability; we refer to Chapter 7 for a detailed discussion. The existence of compactly supported stationary solutions to the massless Einstein-Vlasov system with a black hole at the center is shown in [8].

To conclude, we briefly discuss related results for the Vlasov-Poisson system—the Newtonian counterpart of the Einstein-Vlasov system: It is shown in [94] that solutions to the Einstein-Vlasov system converge to solutions to the Vlasov-Poisson system as the speed of light tends to infinity. The existence of regular global solutions to the Vlasov-Poisson system with general initial data is proven in [76, 82]. In sharp contrast to the Einstein-Vlasov system, all physically relevant isotropic steady states are known to be non-linearly stable, see [50, 72] and the references there. Recently, the quantitative behavior of perturbed stable steady states of the Vlasov-Poisson system has been studied in [55, 56, 69], which is closely related to the approach we will employ in Chapters 4 and 5.

1.3 Methodology and outline of the thesis

As the basis of the investigation, we construct classes of stationary solutions to the Einstein-Vlasov system in Chapter 2. After defining what we mean by a steady state in Section 2.1, we establish equilibria f_0 of the form

$$f_0(x, v) = \varphi(E(x, v), L(x, v))$$

with and without a singularity in Sections 2.2.1 and 2.2.2. The microscopic equation of state φ is a suitable function of the integrals of motion: the particle energy $E = e^\mu \sqrt{1 + |v|^2}$ and the angular momentum L . In a nutshell, the construction of steady states comes down to solving an integro-differential equation and making sure that the resulting solution has finite mass and radius. In Section 2.3, we thoroughly analyze important properties of these stationary solutions. At the core of this is the so-called *single-well structure* of the corresponding effective potential which allows us to uniquely characterize each particle trajectory by fixing the pair (E, L) . In Section 2.3.2, we prove the single-well structure for isotropic steady states that satisfy $6m < r$ and for small shells surrounding a black hole. Under the assumption of the single-well structure, we bound the period function $T = T(E, L)$ for the periods of the particle motions from above and away from zero in Sections 2.3.3 and 2.3.4. Moreover, we introduce action-angle type variables which are crucial for the analysis of linear stability later in the work. In Section 2.4, we conclude with a brief numerical investigation of stationary solutions which helps to justify the assumptions required for rigorous results in Chapters 5 and 6. In particular, we present evidence that all isotropic steady states have

single-well structure.

We determine the parameter dependence of families of isotropic steady states along the redshift κ in Chapter 3. This creates the groundwork for the continuity arguments used later in Chapter 6. In Section 3.1, we provide the continuous (differentiable) dependence of the metric coefficients and source terms along κ , whereas the quantities related to the single-well structure are studied in Section 3.2; the single-well structure in general and the period function in particular again require in-depth analysis. As one of the main results, we show in Proposition 3.2.7 that the period function is continuous along κ .

In Chapter 4, we derive and set up the linearized Einstein-Vlasov system around a fixed steady state that meets certain assumptions, e.g., φ has to be decreasing in the particle energy E . The linearized system is represented by a second-order evolution equation

$$\partial_t^2 f + \mathcal{L}f = 0$$

for the odd-in- w part of the perturbation f , where the *Antonov operator* \mathcal{L} is of the form

$$\mathcal{L} = -\mathcal{B}^2 - \mathcal{R} = -(\mathcal{T} + \mathcal{S})^2 - \mathcal{R}.$$

The transport operator \mathcal{T} corresponds to the characteristic flow of the steady state, and \mathcal{S} , \mathcal{R} are non-local, bounded operators. In Section 4.2.1, these operators are defined on an appropriately weighted L^2 -space H , and in Section 4.3, a comprehensive study of their properties is conducted. One of the crucial results is the proof that the inverse of $-\mathcal{B}^2$ exists on an appropriate subspace of H . As the main result, we determine the properties of the essential spectrum of the Antonov operator in Theorem 4.3.18 and show that it is non-negative and bounded away from zero.

Linear stability is defined through the positivity of the spectrum of the Antonov operator, i.e., $\inf(\sigma(\mathcal{L})) > 0$, which corresponds to the absence of non-positive eigenvalues. By deriving a Birman-Schwinger principle in Chapter 5, we show in Section 5.2 that eigenvalues ≤ 0 of \mathcal{L} are equivalent to eigenvalues ≥ 1 of the *Birman-Schwinger operator*

$$Q = -\sqrt{\mathcal{R}}\mathcal{B}^{-2}\sqrt{\mathcal{R}}.$$

The operator Q possesses favorable properties from a functional analysis point of view and can be reduced by observing that $\text{im}(Q) \subset \text{im}(\sqrt{\mathcal{R}})$, where the latter is isomorphic to a radial L^2 -space. In Section 5.3, we reduce the search for eigenvalues ≤ 0 of \mathcal{L} to the search for eigenvalues ≥ 1 of the so-called *Mathur operator* \mathcal{M} which is linear, bounded, symmetric, non-negative, compact, and of Hilbert-Schmidt type with a continuous integral kernel K that we determine semi-explicitly. As a result, linear stability is characterized through a one-dimensional variational principle in Theorem 5.4.1, and a Birman-Schwinger bound on the number of unstable modes follows in Theorem 5.4.3. As an application, we prove the linear stability of small shells surrounding a black hole in Theorem 5.4.4.

In Chapter 6, we initiate the search for (linearly) oscillating solutions to the Einstein-Vlasov system. The strategy is to obtain a positive eigenvalue of the Antonov operator as

it departs from the essential spectrum and becomes negative via a continuity argument along the redshift. A careful analysis of the operators along κ is necessary in Section 6.2. The main problem stems from the orthogonal projection operator Π_κ onto $\ker(\mathcal{B}_\kappa)$, which is not known explicitly but needs to be controlled since it appears in the Mathur operator \mathcal{M}_κ . In a lengthy endeavor, we prove the continuity of Π_κ along the redshift in Theorem 6.2.13 after deriving a fixed-point equation for the generator of Π_κ . This leads directly to the continuity of the Mathur operator \mathcal{M}_κ through its representation as a Hilbert-Schmidt operator. Due to the results from Chapter 5, we deduce the existence of an oscillating mode under suitable conditions in Theorem 6.3.4.

In Chapter 7, a numerical investigation is carried out in maximal areal coordinates with a focus on non-linear stability of steady states using a particle-in-cell method. After describing the algorithm in Section 7.2, we characterize the different types of behavior of the time evolution of slightly perturbed equilibria. In Section 7.3, we study singularity-free stationary solutions and obtain stable oscillations, but—for the first time for the Einstein-Vlasov system—we also observe damping effects when the microscopic equation φ is sufficiently regular. Unstable equilibria collapse to a black hole, lead to a *heteroclinic orbit*, or fully disperse. In Section 7.3.3, we provide evidence against the binding energy hypothesis and for the existence of families of steady states with multiple stability changes. In Section 7.4, we conduct a first investigation towards stability issues of (single) shells surrounding a black hole, for which we observe similar behavior as in the singularity-free case, apart from the existence of *homoclinic orbits*.

Finally, linear stability is numerically examined in Chapter 8 where we approximate the bottom of the spectrum of the Antonov operator. The numerical method introduced in Section 8.2 is mainly set up to provide a proof-of-concept for more refined algorithms. The results from Section 8.4 indicate that linear and non-linear stability coincide up to numerical accuracy. In particular, we confirm the results from the non-linear stability analysis regarding multiple stability changes for a family of steady states on a linear level. In Section 8.5, we explore whether oscillating solutions exist for isotropic polytropes or whether there is evidence for damping, by studying these behaviors along the redshift κ and the polytropic index k .

2 Stationary solutions to the Einstein-Vlasov system

Life is like riding a bicycle. To keep your balance, you must keep moving.

Albert Einstein

In this chapter, we study the construction and properties of time-independent solutions to the Einstein-Vlasov system in the singularity-free and the Schwarzschild-singularity case. In the first part, we define what we mean by a stationary solution in our context and deal with some preliminaries. In Section 2.2, self-consistent equilibria as well as static shells around a black hole are derived from scratch. We investigate important properties of these steady states in Section 2.3, where the focus lies on the notion of the (strict) single-well structure, which allows us to define the period function that we bound from above and away from zero under suitable conditions. This enables us to introduce so-called action-angle type variables. We conclude the chapter with a numerical investigation of the steady states in Section 2.4.

2.1 Definition and preliminaries

There exists an abundance of steady states to the spherically symmetric, asymptotically flat Einstein-Vlasov system which are physically reasonable, i.e., with finite mass and compact support. The main observation in order to construct static solutions is the following: Consider a sufficiently regular function of the form $f = \varphi(E, L)$, where

$$E = E(x, v) := e^{\mu(|x|)} \sqrt{1 + |v|^2} \quad (2.1)$$

is the *particle energy*, μ is the metric coefficient induced by f , and $L := |x \times v|^2$ is the (squared modulus of the) *angular momentum*. Then f formally solves the Vlasov equation (1.24) since E and L are preserved along the characteristic flow. The Einstein-Vlasov system is therefore reduced to solving the field equations. This motivates to use the following concept of a stationary solution to the Einstein-Vlasov system:

Definition 2.1.1. (a) Let $\mu \in C^1([0, \infty[)$ and define the particle energy $E = E(x, v)$ as in (2.1). A function $f: \mathbb{R}^3 \times \mathbb{R}^3 \rightarrow [0, \infty[$ with the property

$$f(x, v) = \varphi(E(x, v), L(x, v)), \quad (x, v) \in \{(\tilde{x}, \tilde{v}) \in \mathbb{R}^3 \times \mathbb{R}^3 \mid f(\tilde{x}, \tilde{v}) > 0\},$$

where $\varphi: \mathbb{R} \times \mathbb{R} \rightarrow [0, \infty[$, is called a stationary solution or steady state or equilibrium to the singularity-free Einstein-Vlasov system, if μ is the metric coefficient corresponding to f , i.e., if

$$\mu' = e^{2\lambda} \left(\frac{m}{r^2} + 4\pi r p_f \right), \quad \lim_{r \rightarrow \infty} \mu(r) = 0. \quad (2.2)$$

Here ρ_f and p_f are the densities induced by f via (1.14) and (1.15), m is the quasi-local mass (1.23) given by ρ_f , and $e^{-2\lambda} = 1 - \frac{2m}{r}$. If φ only depends on E , i.e., $f(x, v) = \varphi(E(x, v))$, the steady state is called isotropic.

- (b) We define a stationary solution or steady state or equilibrium to the Einstein-Vlasov system with a Schwarzschild-singularity of mass $M_0 > 0$ in the same manner but prescribe $\mu \in C^1(]2M_0, \infty[)$, replace m with $M_0 + m$, and only consider radii $r > 2M_0$.

In both cases, the ansatz φ is called the microscopic equation of state of the stationary solution f . When we mention a steady state of the Einstein-Vlasov system, we implicitly refer to both settings (a) and (b) simultaneously.

Even though the ansatz $f = \varphi(E, L)$ takes care of the (non-linear) Vlasov equation, finding stationary solutions is still a non-trivial problem since μ is determined by f , which itself depends on E and thus also on μ through (2.1). Our definition of steady states allows for density functions f which are not necessarily regular, because the Vlasov equation only has to be fulfilled in the sense that f can be written as a function of (E, L) . However, we obtain a classical solution of the time-independent Vlasov equation if φ is sufficiently regular.

Lemma 2.1.2. *Consider a stationary solution $f = \varphi(E, L)$ to the Einstein-Vlasov system. If $\varphi \in C_c^1(\mathbb{R} \times \mathbb{R})$ holds, $f \in C^1(\mathbb{R}^3 \times \mathbb{R}^3)$ and the time-independent Vlasov equation is solved in a classical sense, i.e.,*

$$\frac{v}{\sqrt{1+|v|^2}} \cdot \partial_x f - \sqrt{1+|v|^2} \mu' \frac{x}{r} \cdot \partial_v f = 0 \quad \text{on } \mathbb{R}^3 \times \mathbb{R}^3.$$

Proof. Since φ is compactly supported, the densities ρ_f and p_f are bounded, which implies that $\mu'(0) = 0$ by (2.2). Therefore, μ can be interpreted as a radially symmetric, continuously differentiable function on \mathbb{R}^3 , i.e., $\mu(r) = \mu(|x|) = \mu(x)$. Thus, $E = E(x, v)$ and $L = L(x, v) = |x \times v|^2$ are continuously differentiable, and we get that f is continuously differentiable by the chain rule. The time-independent Vlasov equation follows after noting $j_f = 0$ for $f = \varphi(E, L)$ by parity considerations. \square

The class of isotropic steady states is important in its own right since the dependency on L is not present in the microscopic equation of state. This leads to relations and estimates which generally hold for isotropic equilibria and which we will use repeatedly when dealing with such stationary solutions.

Lemma 2.1.3. *Consider an isotropic stationary solution $f = \varphi(E)$ to the Einstein-Vlasov system. Then $\rho_f(r)$ and $p_f(r)$ are monotonically decreasing in r , $p_f = q_f$, and $3p_f \leq \rho_f$.*

Proof. We plug the ansatz $f = \varphi(E)$ into the formulas for ρ_f, p_f, q_f from (1.14), (1.15), (1.17), respectively. A change of variables from v to (E, L) yields

$$\begin{aligned}\rho_f(r) &= 4\pi e^{-4\mu(r)} \int_{e^{\mu(r)}}^{\infty} E^2 \sqrt{E^2 - e^{2\mu(r)}} \varphi(E) dE, \\ p_f(r) &= \frac{4\pi}{3} e^{-4\mu(r)} \int_{e^{\mu(r)}}^{\infty} \left(E^2 - e^{2\mu(r)}\right)^{\frac{3}{2}} \varphi(E) dE = q_f(r),\end{aligned}$$

where we explicitly computed the integral over L . Let $0 \leq s \leq r$. Since μ is increasing, we get

$$\begin{aligned}\rho_f(s) &\geq 4\pi e^{-4\mu(r)} \int_{e^{\mu(r)}}^{\infty} E^2 \sqrt{E^2 - e^{2\mu(s)}} \varphi(E) dE \\ &\geq 4\pi e^{-4\mu(r)} \int_{e^{\mu(r)}}^{\infty} E^2 \sqrt{E^2 - e^{2\mu(r)}} \varphi(E) dE \geq \rho_f(r),\end{aligned}$$

and thus that $\rho_f(r)$ is decreasing in r . An analogous estimate holds for p_f . The observation

$$\left(\frac{x \cdot v}{r}\right)^2 + \frac{|x \times v|^2}{r^2} = |v|^2 \leq 1 + |v|^2$$

and $p_f = q_f$ imply $3p_f = p_f + 2q_f \leq \rho_f$. □

2.2 Construction

In this section, we derive stationary solutions for which we will analyze stability later on. We consider two situations which have to be treated slightly differently: steady states in a singularity-free setting and steady states which are situated around a black hole of mass M_0 at the center. We start off by constructing singularity-free steady states.

2.2.1 Singularity-free steady states

The construction of steady states for the Einstein-Vlasov system in the spherically symmetric and singularity-free case has been thoroughly covered in the literature. For our approach, we mainly refer to [83]. The primary difficulty arises from the fact that the support of the steady state should be compact with finite mass for physically reasonable configurations. In [83], this problem is solved for a large class of microscopic equations of state φ with help of what the authors call a ‘‘compact-support-Lemma’’. The techniques used in [83] are quite general and can also be applied, e.g., to the classical and relativistic Vlasov-Poisson system and related fluid models. For similar approaches, we refer to [90, 96].

Consider a microscopic equation of state of the form

$$f(x, v) = \varphi(E, L) = \Phi\left(1 - \frac{E}{E^0}\right)(L - L_0)_+, \quad (2.3)$$

where Φ is a suitable *ansatz function* specified below and $E^0 \in]0, 1[$ is a cut-off energy which bounds the possible energy values in the steady state support. Moreover, we prescribe $l > -\frac{1}{2}$ and $L_0 \geq 0$. The latter gives a lower bound for the angular momentum. In fact, $L_0 > 0$ leads to solutions with a vacuum region at the center of the steady state. The index $+$ denotes the positive part of a function, and we use the convention

$$x_+^l := \begin{cases} x^l, & x > 0, \\ 0, & x \leq 0. \end{cases}$$

Isotropic steady states are obtained in the special case where $l = 0 = L_0$. We point out that the explicit form of L -dependence in (2.3) is chosen only for simplicity, and our analysis can easily be extended to stationary states with more general L -dependencies. We demand that the ansatz function Φ satisfies the following conditions:

($\Phi 1$) $\Phi: \mathbb{R} \rightarrow [0, \infty[$, $\Phi \in L^\infty([0, 1])$, and $\Phi(\alpha) = 0$ for $\alpha \leq 0$.

($\Phi 2$) There exist constants $c_1, c_2 > 0$, $\alpha_0 > 0$, and $0 \leq k < l + \frac{3}{2}$ such that

$$c_1 \alpha^k \leq \Phi(\alpha) \leq c_2 \alpha^k, \quad \alpha \in]0, \alpha_0].$$

These properties together with the presence of the cut-off energy E^0 are sufficient to provide a compact support and finite mass, as we will see in Proposition 2.2.4. Obviously, ($\Phi 1$) and ($\Phi 2$) are quite loose conditions and allow for a variety of different ansatz functions. For example,

$$\Phi(\alpha) = (e^\alpha - 1)_+ \quad (2.4)$$

yields the so-called *King model* which is commonly used in the astrophysical literature to model globular clusters since it corresponds to an isothermal configuration [67]. The simple polytropic relation

$$\Phi(\alpha) = \alpha_+^k \quad (2.5)$$

with $0 \leq k < l + \frac{3}{2}$ yields static solutions referred to as *polytropes*.

By plugging the ansatz (2.3) with E given by (2.1) into the singularity-free Einstein-Vlasov system, we obtain a non-linear equation for the metric coefficient μ . However, the field equation for μ has a boundary condition at spatial infinity and contains the cut-off energy E^0 as another parameter, which makes the resulting equation difficult to handle. It is therefore advantageous to consider

$$y := \ln(E^0) - \mu$$

instead, in order to eliminate E^0 . After having solved for y , we will define the cut-off

energy E^0 accordingly. For y , we get the integro-differential equation

$$y'(r) = -\frac{1}{1 - \frac{8\pi}{r} \int_0^r s^2 G(s, y(s)) ds} \left(\frac{4\pi}{r^2} \int_0^r s^2 G(s, y(s)) ds + 4\pi r H(r, y(r)) \right), \quad y(0) = \kappa, \quad (2.6)$$

where $\kappa > 0$ is a given initial value. The functions G and H are defined for $(r, y) \in]0, \infty[\times \mathbb{R}$ by

$$G(r, y) := 2\pi c_l r^{2l} e^{(4+2l)y} g_l \left(1 - e^{-y} \sqrt{1 + \frac{L_0}{r^2}} \right), \quad (2.7)$$

$$H(r, y) := 2\pi d_l r^{2l} e^{(4+2l)y} h_l \left(1 - e^{-y} \sqrt{1 + \frac{L_0}{r^2}} \right), \quad (2.8)$$

where the functions $g_l, h_l:]-\infty, 1] \rightarrow \mathbb{R}$ are given by

$$g_l(z) := \begin{cases} \int_0^z \Phi(\alpha) (1-\alpha)^2 ((1-\alpha)^2 - (1-z)^2)^{l+\frac{1}{2}} d\alpha, & z \geq 0, \\ 0, & z < 0, \end{cases} \quad (2.9)$$

$$h_l(z) := \begin{cases} \int_0^z \Phi(\alpha) ((1-\alpha)^2 - (1-z)^2)^{l+\frac{3}{2}} d\alpha, & z \geq 0, \\ 0, & z < 0, \end{cases} \quad (2.10)$$

and

$$c_l := \int_0^1 \frac{s^l}{\sqrt{1-s}} ds, \quad d_l := \int_0^1 s^l \sqrt{1-s} ds.$$

In particular, G and H vanish for $e^{-y} \sqrt{1 + \frac{L_0}{r^2}} \geq 1$. These quantities arise from the coupling of the Vlasov equation (1.24) and the field equations (1.10), (1.11), since the mass density ρ_f and the pressure p_f are induced by the density f , which contains y through the energy dependency. More precisely,

$$\rho_f(r) = G(r, y(r)), \quad p_f(r) = H(r, y(r)), \quad r > 0.$$

First, we have to analyze the regularity of G and H , which was also done in similar contexts, e.g., in [83, Sc. 2.1.3], [90, Lem. 3.1], and [96, Lem. 2.2]. However, in these references, the more detailed arguments are often left out. For the sake of completeness, we provide the missing details here. Under the assumptions on Φ above, we obtain that g_l and h_l are sufficiently regular.

Lemma 2.2.1. *Let $l > -\frac{1}{2}$, $L_0 \geq 0$, and consider Φ that satisfies $(\Phi 1)$ and $(\Phi 2)$. Then $g_l \in C^1(]-\infty, 1[)$, $h_l \in C^2(]-\infty, 1[)$ and g_l, h_l are monotonically increasing.*

Proof. The proof comes down to applying Lebesgue's (dominated convergence) theorem.¹ We claim that

$$\tilde{g}_l(z) = (2l+1)(1-z) \int_0^z \Phi(\alpha)(1-\alpha)^2((1-\alpha)^2 - (1-z)^2)^{l-\frac{1}{2}} d\alpha$$

is the derivative of g_l on $]0, 1[$. For $z \in]0, 1[$ and $h > 0$ small, we estimate

$$\begin{aligned} & \left| \frac{g_l(z+h) - g_l(z)}{h} - \tilde{g}_l(z) \right| \\ & \leq \left| \frac{1}{h} \int_z^{z+h} \Phi(\alpha)(1-\alpha)^2((1-\alpha)^2 - (1-z-h)^2)^{l+\frac{1}{2}} d\alpha \right| \\ & \quad + \int_0^z \Phi(\alpha)(1-\alpha)^2 \left| \frac{((1-\alpha)^2 - (1-z-h)^2)^{l+\frac{1}{2}} - ((1-\alpha)^2 - (1-z)^2)^{l+\frac{1}{2}}}{h} \right. \\ & \quad \left. - (2l+1)(1-z)((1-\alpha)^2 - (1-z)^2)^{l-\frac{1}{2}} \right| d\alpha \\ & =: I_1 + I_2, \end{aligned}$$

and deal with the two terms separately. In both cases, we can bound $|\Phi(\alpha)| \leq \|\Phi\|_{L^\infty([0,1])}$ due to $(\Phi 1)$. We estimate the integrand in I_1 by

$$((1-\alpha)^2 - (1-z-h)^2)^{l+\frac{1}{2}} \leq ((1-z)^2 - (1-z-h)^2)^{l+\frac{1}{2}}, \quad \alpha \in]z, z+h[,$$

and thus

$$I_1 \leq C((1-z)^2 - (1-z-h)^2)^{l+\frac{1}{2}} \rightarrow 0, \quad h \rightarrow 0,$$

because of $l > -\frac{1}{2}$; note that $C > 0$ is independent of h .

The integrand in I_2 goes to zero pointwise almost everywhere for $h \rightarrow 0$ due to

$$\frac{d}{dz} \left(((1-\alpha)^2 - (1-z)^2)^{l+\frac{1}{2}} \right) = (2l+1)(1-z)((1-\alpha)^2 - (1-z)^2)^{l-\frac{1}{2}},$$

for every $\alpha \in]0, z[$. For the majorant, we apply the mean value theorem for $\alpha \in]0, z[$ and obtain

$$\begin{aligned} & \frac{((1-\alpha)^2 - (1-z-h)^2)^{l+\frac{1}{2}} - ((1-\alpha)^2 - (1-z)^2)^{l+\frac{1}{2}}}{h} \\ & = (2l+1)(1-z-\tilde{h}) \left((1-\alpha)^2 - (1-z-\tilde{h})^2 \right)^{l-\frac{1}{2}} \quad (2.11) \end{aligned}$$

for some $\tilde{h} \in]0, h[$, which depends on α . In the case $l \geq \frac{1}{2}$, we obtain $2l+1$ as an upper

¹Throughout the work, we only write *Lebesgue's theorem* as an abbreviation.

bound for (2.11). On the other hand, if $l < \frac{1}{2}$, we estimate

$$\left((1 - \alpha)^2 - (1 - z - \tilde{h})^2 \right)^{l - \frac{1}{2}} \leq \left((1 - \alpha)^2 - (1 - z)^2 \right)^{l - \frac{1}{2}}$$

and get an integrable majorant for (2.11), since $l > -\frac{1}{2}$. By Lebesgue's theorem, we have $I_1, I_2 \rightarrow 0$ as $h \xrightarrow{\geq} 0$. Therefore, g_l is right differentiable on $]0, 1[$ with right derivative \tilde{g}_l . Since g_l as well as \tilde{g}_l are continuous, we deduce that g_l is continuously differentiable with $\tilde{g}_l = g'_l$ on $]0, 1[$. In analogous fashion, we prove that h_l is differentiable with

$$h'_l(z) = (2l + 3)(1 - z) \int_0^z \Phi(\alpha) \left((1 - \alpha)^2 - (1 - z)^2 \right)^{l + \frac{1}{2}} d\alpha,$$

and—since h'_l is structurally similar to g_l —the same process yields that h'_l is differentiable again with

$$\begin{aligned} h''_l(z) &= -(2l + 3) \int_0^z \Phi(\alpha) \left((1 - \alpha)^2 - (1 - z)^2 \right)^{l + \frac{1}{2}} d\alpha \\ &\quad + (2l + 3)(2l + 1)(1 - z)^2 \int_0^z \Phi(\alpha) \left((1 - \alpha)^2 - (1 - z)^2 \right)^{l - \frac{1}{2}} d\alpha, \quad z \in]0, 1[. \end{aligned}$$

The continuity of g'_l and h''_l on $]0, 1[$ can be shown by another application of Lebesgue's theorem in a similar manner and comes down to using $l > -\frac{1}{2}$ for finding suitable integrable majorants. To summarize, we now have $g_l, h_l, h'_l \in C^1(]0, 1[\cup]-\infty, 0[)$, since g_l, h_l vanish on $] -\infty, 0[$. It thus remains to show that

$$\lim_{z \xrightarrow{\geq} 0} g_l(z), h_l(z), g'_l(z), h'_l(z), h''_l(z) = 0.$$

We limit the proof to the case g'_l and $l < \frac{1}{2}$. The remaining convergences follow via analogous or easier arguments. For $z > 0$, we have

$$|g'_l(z)| \leq C \int_0^z \left((1 - \alpha)^2 - (1 - z)^2 \right)^{l - \frac{1}{2}} d\alpha,$$

where $C > 0$ does not depend on z . We observe that

$$(1 - \alpha)^2 - (1 - z)^2 = (2 - \alpha - z)(z - \alpha) \geq z - \alpha, \quad z \in [0, \frac{1}{2}], \alpha \in [0, z],$$

and, because of $-\frac{1}{2} < l < \frac{1}{2}$,

$$|g'_l(z)| \leq C \int_0^z (z - \alpha)^{l - \frac{1}{2}} d\alpha = \frac{C}{l + \frac{1}{2}} z^{l + \frac{1}{2}} \rightarrow 0, \quad z \xrightarrow{\geq} 0.$$

To conclude, we note that the monotonicity claims follow from the explicit formulas for g'_l and h'_l above. \square

We translate the results for g_l, h_l to G, H in the following way:

Lemma 2.2.2. *Consider Φ that satisfies $(\Phi 1)$ and $(\Phi 2)$. Then,*

$$G \in C^1(]0, \infty[\times \mathbb{R}), \quad H \in C^2(]0, \infty[\times \mathbb{R}), \quad (2.12)$$

and G, H are increasing functions in the y -component. Moreover, the functions

$$]0, \infty[\times \mathbb{R} \ni (r, y) \mapsto r^{-2l}G(r, y), \quad r^{-2l}H(r, y), \quad r^{-2l}\partial_y G(r, y), \quad r^{-2l}\partial_y H(r, y),$$

can be extended continuously for $r \rightarrow 0$ onto $[0, \infty[\times \mathbb{R}$.

Proof. The regularity shown in Lemma 2.2.1 as well as the definitions (2.7), (2.8), imply (2.12) by the chain rule. The functions G and H are increasing in y , since g_l, h_l are increasing and due to $l > -\frac{1}{2}$. The continuous extension for $r = 0$ follows from the definition of G, H as well as the continuity and boundedness of g_l, h_l . \square

Since the Vlasov equation is only solved in the sense that f is constant along characteristics, as given in Definition 2.1.1, there is no guarantee that the fourth field equation (1.13) holds a-priori, which would be the case for classical solutions. This remaining second-order equation for μ is tightly connected to the so-called Tolman-Oppenheimer-Volkov equation which holds for spherically symmetric perfect fluids [112, Eqn. 6.2.19]

Lemma 2.2.3. *Let y be a solution of (2.6) on an interval $]0, R[$. Then $p_f = G(\cdot, y)$ is continuously differentiable and the Tolman-Oppenheimer-Volkov (TOV) equation*

$$p'_f(r) = y'(r)(p_f(r) + \rho_f(r)) - \frac{2}{r}(p_f(r) - q_f(r)) \quad (2.13)$$

holds on $]0, R[$, where q_f is the tangential pressure (1.17) induced by $f = \varphi(E, L)$.

Proof. A proof is found in [90, Lem. 3.3] and can be applied almost word by word. It involves using Lemma 2.2.2 and expressing q_f through p_f as well as an additional function similar to (2.7) and (2.8). \square

With these preliminary regularity considerations out of the way, we now obtain steady states as in [83, Thm. 4.1]:

Proposition 2.2.4. *Consider Φ that satisfies $(\Phi 1)$ and $(\Phi 2)$, and let $l > -\frac{1}{2}$ and $L_0 \geq 0$. For every $\kappa > 0$, there exists a unique solution $y \in C^1([0, \infty[)$ of (2.6) with*

$$y_\infty := \lim_{r \rightarrow \infty} y(r) < 0.$$

Defining $E^0 = \exp(y_\infty)$, $\mu = \ln(E^0) - y$, and

$$\lambda(r) := -\frac{1}{2} \ln \left(1 - \frac{8\pi}{r} \int_0^r s^2 G(s, y(s)) ds \right), \quad r > 0,$$

yields a (non-trivial) stationary solution to the singularity-free Einstein-Vlasov system, as defined in Definition 2.1.1(a), with $f = \varphi(E, L)$ as in (2.3). The solution is compactly supported and has finite mass. The Einstein field equation (1.13) is satisfied on $]0, \infty[$.

Proof. For the proof, we refer to [83]. We shortly recall the central idea: A contraction argument yields a unique, local solution y on a small interval which can be extended to a maximal solution by standard ODE theory and by controlling the denominator in (2.6) via the TOV equation (2.13) as in [90, Thm. 3.4]. The central difficulty is to obtain a compact support together with finite mass, which is shown by a “compact-support-Lemma”, cf. [83, Lem. 3.1]. The field equation (1.13) follows from the chain rule and the TOV equation. \square

For a fixed ansatz function Φ and values $l > -\frac{1}{2}$, $L_0 \geq 0$, we thus obtain a family of static solutions $(f_\kappa)_{\kappa>0}$, which are parameterized by $\kappa = y(0)$. For every $\kappa > 0$, this corresponds to a spherically symmetric star cluster in an equilibrium with finite expansion and mass.

Definition 2.2.5 (The κ -family). *Consider Φ , l , and L_0 as in Proposition 2.2.4. We call the induced family of steady states $(f_\kappa)_{\kappa>0}$ a κ -family. We denote the corresponding static quantities by a subscript κ , e.g., μ_κ , ρ_κ , etc., its cut-off energy by E^κ , and its Vlasov mass by M_κ .*

The value κ has an illustrative physical interpretation: It is closely related to the central redshift z_c of a photon which is emitted at the center of the steady state and received at spatial infinity. In fact, it holds that

$$z_c = \frac{e^\kappa}{E^0} - 1 = e^{-\mu(0)} - 1. \quad (2.14)$$

A more suitable quantity for our work is the *central-to-surface redshift*

$$z = e^\kappa - 1, \quad (2.15)$$

which is equivalent to considering κ . In particular, higher values of κ correspond to higher values of the central-to-surface redshift z . This can be interpreted as an indication that the configuration gets more relativistic as κ increases. Due to these relations, we will refer to κ as the *redshift* from now on.

2.2.2 Matter shells with a Schwarzschild-singularity

In addition to the singularity-free case, we explore steady states of the Einstein-Vlasov system with a Schwarzschild-singularity of given mass $M_0 > 0$. Even though the investigation is related to the singularity-free case in many aspects, some important structural differences arise so that it is convenient to consider this setting separately. The approach here is very similar to the one found in [47] but relies on a different parameter to obtain a slightly more diverse class of steady states. We discuss this in more detail and mention additional references in Remark 2.2.13.

The stationary solution shall be of the form

$$f(x, v) = \chi(r - r_0) \varphi(E(x, v), L(x, v)), \quad (2.16)$$

where χ is the Heaviside step function, i.e., $\chi(s) = 1$ for $s \geq 0$ and $\chi(s) = 0$ for $s < 0$, and $r_0 > 0$ is a parameter which we will determine later. For the microscopic equation of state φ , we use the ansatz of the form (2.3) with cut-off energy E^0 , $l > -\frac{1}{2}$, and $L_0 > 0$. As above, we impose that Φ satisfies $(\Phi 1)$ and $(\Phi 2)$.

Remark 2.2.6. (a) *The radial cut-off function χ ensures that only periodic orbits occur in the steady state. However, the resulting equilibrium will not depend on the particular choice of r_0 .*

(b) *In [47], condition $(\Phi 2)$ is replaced with the more general assumption that Φ is positive on some small interval $]0, \varepsilon[$. In our case, this is in general not sufficient to guarantee a compact support and finite mass, since our approach allows for a broader range of initial values for $y(3M_0)$ compared to [47].*

Due to the presence of the radial cut-off function, f will only be a solution of the Vlasov equation if the parameters $r_0, L_0 > 0$ and $y(3M_0)$ are chosen suitably. We derive such a choice of parameters by analyzing the metric quantity μ induced by f . According to (1.11), the equation for μ reads

$$\mu'(r) = \frac{1}{1 - \frac{2}{r}(M_0 + m(r))} \left(\frac{M_0 + m(r)}{r^2} + 4\pi r p_f(r) \right), \quad r > 2M_0, \quad (2.17)$$

together with the boundary condition $\lim_{r \rightarrow \infty} \mu(r) = 0$. Recall that m is induced by ρ_f via (1.23), where we set $\rho_f := 0$ on $[0, 2M_0]$.

It is instructive to consider the setting $f = 0$, i.e., where only the Schwarzschild black hole is situated at the center and no Vlasov matter is present. We denote all quantities in this case with an upper index zero. The pure Schwarzschild solution

$$\mu^0(r) = \frac{1}{2} \ln \left(1 - \frac{2M_0}{r} \right), \quad r > 2M_0, \quad (2.18)$$

solves (2.17) in the case $f = 0 = m$. The *effective potential* given by

$$\Psi_L^0(r) := e^{\mu^0(r)} \sqrt{1 + \frac{L}{r^2}} = \sqrt{1 - \frac{2M_0}{r}} \sqrt{1 + \frac{L}{r^2}}, \quad L \geq 0, \quad r > 2M_0, \quad (2.19)$$

encodes how particles move in the external potential of the black hole, which makes it an important quantity to study. We gather some of the main properties of Ψ_L^0 in the next lemma; see [27, § 19] or more recently [63, Apx. A].

Lemma 2.2.7. *The effective potential Ψ_L^0 in the pure Schwarzschild case has the following properties:*

(a) *For every $L \geq 0$, we have that $\lim_{r \rightarrow 2M} \Psi_L^0(r) = 0$ and $\lim_{r \rightarrow \infty} \Psi_L^0(r) = 1$.*

(b) For every $L > 12M_0^2$, there exist two unique zeros $r_L^0 > s_L^0 > 3M_0$ of $(\Psi_L^0)'$ given by

$$s_L^0 = \frac{L}{2M_0} \left(1 - \sqrt{1 - \frac{12M_0^2}{L}} \right), \quad r_L^0 = \frac{L}{2M_0} \left(1 + \sqrt{1 - \frac{12M_0^2}{L}} \right). \quad (2.20)$$

Furthermore, $(\Psi_L^0)''(s_L^0) < 0 < (\Psi_L^0)''(r_L^0)$, i.e., Ψ_L^0 attains a strict local maximum in s_L^0 and a strict local minimum in r_L^0 .

(c) The estimate $\Psi_L^0(r_L^0) < \min\{1, \Psi_L^0(s_L^0)\}$ holds, and $\Psi_L^0(s_L^0) > 1$ is equivalent to $L > 16M_0^2$.

(d) For every $L > 12M_0^2$ and $E \in]\Psi_L^0(r_L^0), \min\{1, \Psi_L^0(s_L^0)\}[$, there exist three unique radii

$$2M_0 < r_0^0(E, L) < s_L^0 < r_-^0(E, L) < r_L^0 < r_+^0(E, L)$$

such that

$$\Psi_L^0(r_0^0(E, L)) = E = \Psi_L^0(r_\pm^0(E, L)).$$

We illustrate these quantities in Figure 2.1. With this knowledge of the effective potential, we can specify the choice of the parameters remaining in the ansatz (2.16). We proceed similarly to the singularity-free setting and turn the cut-off energy E^0 into an unknown variable by considering $y := \ln(E^0) - \mu$. Due to Lemma 2.2.7, we set an initial value for y at $r = 3M_0$ and thus arrive at the equation²

$$y'(r) = -\frac{1}{1 - \frac{2}{r}(M_0 + m(r))} \left(\frac{M_0 + m(r)}{r^2} + 4\pi r p_f(r) \right), \quad y(3M_0) = \kappa + \ln(\sqrt{3}), \quad (2.21)$$

on $]2M_0, \infty[$ which should be compared with (2.6). We specify the admissible range for κ below. The initial value for $y(3M_0)$ is chosen such that it fits together well with the singularity-free case. Equation (2.21) is a closed system for y , since we can express ρ_f and p_f in terms of y by plugging (2.16) into (1.14) and (1.15):

$$\rho_f(r) = \chi(r - r_0) G(r, y(r)), \quad p_f(r) = \chi(r - r_0) H(r, y(r)), \quad r > 2M_0, \quad (2.22)$$

where G and H are defined in (2.7) and (2.8). In the pure Schwarzschild case $f = 0$, the solution of (2.21) is given by³

$$y^0(r) = \kappa - \frac{1}{2} \ln \left(1 - \frac{2M_0}{r} \right) = \kappa - \mu^0(r), \quad r > 2M_0.$$

²A general result for particle motions in the external potential of a Schwarzschild black hole states that stable orbits are only possible outside of the *photon sphere* which is situated at $r = 3M_0$. This is another reason why we choose the initial value of y at $r = 3M_0$.

³This is the “deeper” reason why we add $\ln(\sqrt{3})$ in the initial value for $y(3M_0)$: It gets rid of an additional term in the relation for μ^0 and y^0 .

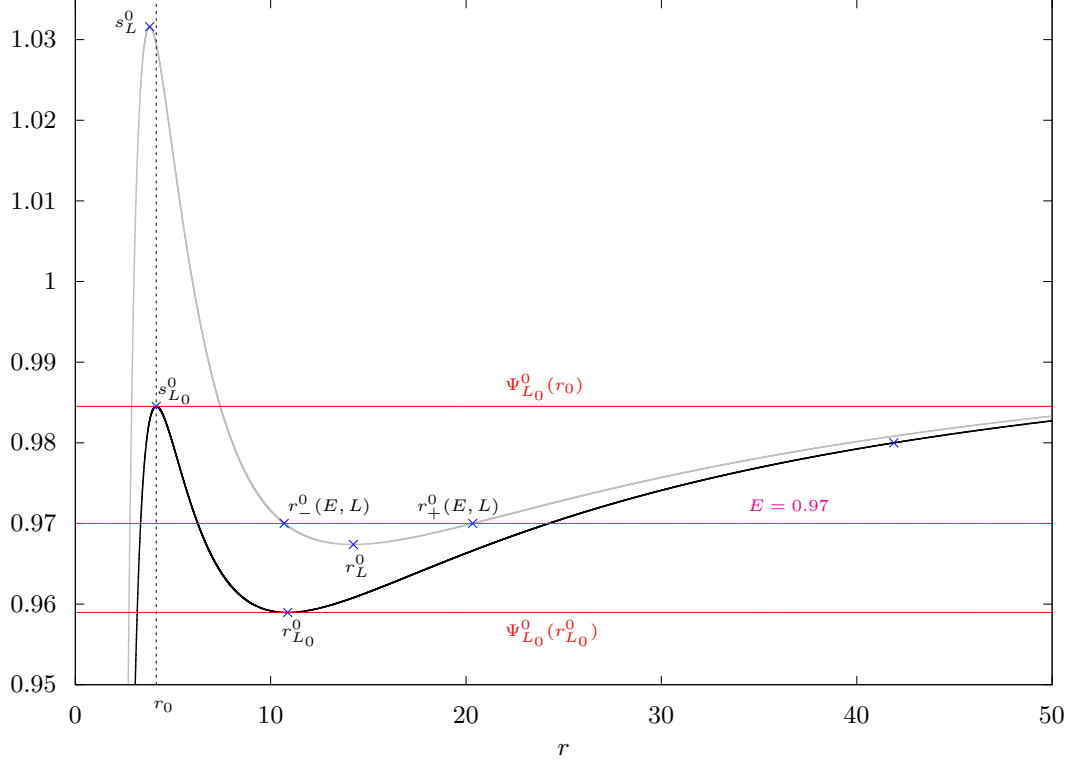


Figure 2.1: Illustration of the effective potential Ψ_L^0 in the pure Schwarzschild case for $M_0 = 1$, $L_0 = 15$. The black line corresponds to $\Psi_{L_0}^0$ and the grey line to Ψ_L^0 with $L = 18$. The value e^κ can be chosen between $\Psi_{L_0}^0(r_{L_0}^0)$ and $\Psi_{L_0}^0(r_0)$.

We can now specify how we choose κ and the parameters in the ansatz (2.16):

- (P1) Choose L_0 such that $L_0 > 12M_0^2$.
- (P2) Set $r_0 = s_{L_0}^0$, where $s_{L_0}^0 > 3M_0$ is defined in (2.20).
- (P3) Choose $\kappa \in \mathbb{R}$ such that

$$\Psi_{L_0}^0(r_{L_0}^0) < e^\kappa < \Psi_{L_0}^0(s_{L_0}^0).$$

To put it briefly, (P1) ensures that trapped orbits exist in the first place. The definition of r_0 in (P2) leads to $f(r, w, L) = 0$ for $r < r_0$. The lower bound in (P3) ensures that the solution is not trivial, i.e., $f \neq 0$, while the upper bound in (P3) yields that the matter is strictly bounded away from $r = r_0$ such that f does not have discontinuities arising from the Heaviside function χ in (2.16). This is the reason why κ is bounded from above unlike in the singularity-free case. As an aside, we note that the case $e^\kappa < \min\{1, \Psi_{L_0}^0(s_{L_0}^0)\}$

yields the same steady states, as derived in [47, Sc. 2.2]. The choice of these parameters together with the behavior of Ψ_L^0 is depicted in Figure 2.1. For the sake of completeness, we mention that the TOV equation (2.13) is also valid in the current setting with a Schwarzschild black hole at the center.

Lemma 2.2.8. *Let y be a solution of (2.21) on an interval $]2M_0, R[$. Then $p_f = G(\cdot, y)$ is continuously differentiable and the TOV equation*

$$p'_f(r) = y'(r)(p_f(r) + \rho_f(r)) - \frac{2}{r}(p_f(r) - q_f(r)), \quad (2.23)$$

holds on $]2M_0, R[$, where q_f is the tangential pressure (1.17) induced by

$$f = \chi(r - r_0)\varphi(E, L).$$

Proof. Except for technical details, the proof is the same as that of Lemma 2.2.3. \square

The next lemma deals with the existence and behavior of solutions of (2.21). In the proof, further details reveal why we have introduced conditions (P1)–(P3).

Lemma 2.2.9. *For every choice of parameters L_0, r_0, κ that satisfy (P1)–(P3), there exists a unique solution $y \in C^1(]2M_0, \infty[)$ of (2.21), where ρ_f, p_f , and the quasi-local mass m are given through the relations (2.22) and (1.23). It holds that*

$$2(M_0 + m(r)) < r, \quad y(r) \leq y^0(r), \quad r \in]2M_0, \infty[. \quad (2.24)$$

There exists $\varepsilon > 0$ such that

$$\rho_f(r) = 0 = p_f(r), \quad y(r) = y^0(r), \quad r \in]2M_0, r_0 + \varepsilon], \quad (2.25)$$

but ρ_f and p_f do not vanish on the whole domain $]2M_0, \infty[$. The limit

$$y_\infty := \lim_{r \rightarrow \infty} y(r)$$

exists with $y_\infty \in]-\infty, 0[$ and the relation

$$y_\infty = y(R_{\max}) + \frac{1}{2} \ln \left(1 - \frac{2}{R_{\max}}(M_0 + M) \right) \quad (2.26)$$

holds, where M is the total Vlasov mass given by

$$M := \lim_{r \rightarrow \infty} m(r) = 4\pi \int_{2M_0}^{R_{\max}} s^2 \rho(s) ds, \quad (2.27)$$

and $R_{\max} = \sup\{r > 2M_0 \mid \rho(r) > 0\} < \infty$.

Proof. Observe that $y = y^0$ defines the unique solution of (2.21) on $]2M_0, r_0[$. This is due to the presence of the radial cut-off function χ in (2.22) which implies $\rho_f(r) = 0 = p_f(r)$

for $2M < r \leq r_0$. We plug $r_0 = s_{L_0}^0$ into the explicit formula for y^0 and get that

$$e^{-y^0(r_0)} \sqrt{1 + \frac{L_0}{r_0^2}} = \Psi_{L_0}^0(r_0) e^{-\kappa} > 1,$$

which is equivalent to

$$\sqrt{1 - \frac{2M_0}{r_0}} \sqrt{1 + \frac{L_0}{r_0^2}} > e^\kappa$$

and by the choice $r_0 = s_{L_0}^0$, this holds if κ satisfies (P3). Therefore, since G and H vanish for $e^{-y} \sqrt{1 + \frac{L_0}{r^2}} > 1$, there exists $\varepsilon > 0$ such that $y = y^0$ solves (2.21) on $]2M_0, r_0 + \varepsilon[$. In particular,

$$G(r, y(r)) = 0 = H(r, y(r)), \quad r_0 < r \leq r_0 + \varepsilon,$$

which proves (2.25). By considering (2.21) with the new boundary condition $y(r_0 + \varepsilon) = y^0(r_0 + \varepsilon)$, the arguments from the singularity-free case can now be applied almost one-to-one. Uniqueness and local existence follow by basic ODE theory since $G, H \in C^1(]0, \infty[\times \mathbb{R})$, according to Lemma 2.2.2. For a proof that the solution can be extended to arbitrarily large radii, we refer to [90, Thm. 3.4]. The main difficulty is to show that the denominator on the right hand side of (2.21) does not vanish, which is achieved by using the TOV equation (2.23). The limiting behavior of y is deduced by applying the ‘‘compact-support-Lemma’’ from [83, Lem. 3.1] analogously to the singularity-free case; here condition ($\Phi 2$) is needed. Once we have determined $R_{\max} < \infty$, equation (2.26) follows explicitly from solving (2.21), because

$$y'(r) = \frac{1}{1 - \frac{2}{r}(M_0 + M)} \frac{M_0 + M}{r^2}, \quad r \geq R_{\max}.$$

It remains to show that the solution is not simply the vacuum solution, i.e., that there exists $r > r_0$ with $\rho_f(r) > 0$. We prove this by contradiction: Assume $\rho_f(r) = 0$ for every $r \in]2M_0, \infty[$. Then, as $0 \leq p_f(r) \leq \rho_f(r)$, we must have $y = y^0$ on $]2M_0, \infty[$ and we obtain

$$e^{-y(r)} \sqrt{1 + \frac{L_0}{r^2}} = e^{-y^0(r)} \sqrt{1 + \frac{L_0}{r^2}} = e^{-\kappa} \Psi_{L_0}^0(r).$$

Therefore, we need to show that $e^{-\kappa} \Psi_{L_0}^0(r) < 1$ for some radius $r > r_0$, because this implies $\rho_f(r) = G(r, y(r)) > 0$ which contradicts the assumption. If $\kappa > 0$, we are done by making r large enough. In the case where $\kappa \leq 0$, the lower bound for κ in condition (P3) comes into play: Since $e^\kappa < \min\{1, \Psi_{L_0}^0(r_0)\}$, Lemma 2.2.7(d) yields the existence of unique

$$r_0 = s_{L_0}^0 < r_-^0(e^\kappa, L_0) < r_{L_0}^0 < r_+^0(e^\kappa, L_0),$$

with the property $\Psi_{L_0}^0(r_\pm^0(e^\kappa, L_0)) = e^\kappa$. In particular, $\Psi_{L_0}^0(r_{L_0}^0) < e^\kappa$, which completes the contradiction for $\kappa \leq 0$. \square

From the solution y of (2.21), we can derive a stationary solution to the Einstein-Vlasov system—again similar to the singularity-free case.

Proposition 2.2.10. *Consider Φ that satisfies $(\Phi 1)$ and $(\Phi 2)$, and let $M_0 > 0$ and $l > -\frac{1}{2}$. For any choice of parameters L_0, r_0, κ that satisfy (P1)–(P3), let y be the solution of (2.21) provided by Lemma 2.2.9. Defining $E^0 = \exp(y_\infty)$, $\mu = \ln(E^0) - y$, and*

$$\lambda(r) := -\frac{1}{2} \ln \left(1 - \frac{2}{r} (M_0 + m(r)) \right), \quad r > 2M_0,$$

where

$$m(r) = 4\pi \int_{3M_0}^r s^2 G(s, y(s)) ds,$$

yields a (non-trivial) stationary solution to the Einstein-Vlasov system with Schwarzschild-singularity of mass M_0 , as defined in Definition 2.1.1(b) with $f = \chi(r - r_0)\varphi(E, L)$ as in (2.16). The solution is compactly supported and has finite mass. The Einstein field equation (1.13) is satisfied on $]2M_0, \infty[$.

Proof. Due to the properties of y shown in Lemma 2.2.9, it suffices to show

$$f(x, v) = \varphi(E(x, v), L(x, v)),$$

if $f(x, v) > 0$, which might only fail for $|x| = r_0$, because of the cut-off function χ . However, according to Lemma 2.2.9, we have $f(x, v) = 0$ for $|x| \in]2M_0, r_0 + \varepsilon]$. Moreover, the field equation (1.13) follows by the chain rule and the TOV equation (2.23). \square

To summarize, for a fixed ansatz function Φ and parameters M_0, L_0, l, κ chosen suitably, we obtain a steady state of the Einstein-Vlasov system with Schwarzschild-singularity of mass M_0 . The value κ has a similar interpretation as in the singularity-free case and will also be referred to as the redshift here; note that $\kappa < 0$ lacks a reasonable physical interpretation.

In contrast to Section 2.2.1, we do not only consider families of static solutions that are parameterized by κ , since using the mass of the central black hole M_0 or other parameters to describe families of steady states can be of interest. In particular, we can reproduce an analogue family of static solutions to the one introduced in [47], where a smallness parameter $\delta > 0$ is used to control the size of the Vlasov matter. We refer to it as a δ -family.

Definition 2.2.11 (The δ -family). *Consider Φ_0 that satisfies $(\Phi 1)$ and $(\Phi 2)$, and let $M_0 > 0$ and $l > -\frac{1}{2}$. Fix values for L_0, r_0, κ such that (P1)–(P3) and⁴*

$$E^{0, \text{vac}} := e^\kappa < 1$$

are satisfied. For $\delta > 0$, let f_δ be the steady state induced by the parameters above and $\Phi = \delta\Phi_0$ via Proposition 2.2.10. We call such a family of steady states $(f_\delta)_{\delta > 0}$ a

⁴We use the terminology $E^{0, \text{vac}}$, since this quantity corresponds to the limiting cut-off energy in the case where the mass of the Vlasov matter goes to zero, i.e., only the black hole at the center remains.

δ -family. We add the subscript δ to all relevant quantities, denote its cut-off energy by E^δ , and the Vlasov mass by M_δ .

We employ the following notation when using a δ -family: Let G_{Φ_0} and H_{Φ_0} be the induced functions by Φ_0 , according to (2.7) and (2.8). In particular, $G = \delta G_{\Phi_0}$ and $H = \delta H_{\Phi_0}$ correspond to

$$\rho_\delta(r) = G(r, y_\delta(r)) = \delta G_{\Phi_0}(r, y_\delta(r)), \quad p_\delta(r) = H(r, y_\delta(r)) = \delta H_{\Phi_0}(r, y_\delta(r)).$$

Note that such a choice of parameters, as made in the definition above, is possible because of Lemma 2.2.7(c). The prefactor $\delta > 0$ governs over the ‘‘size’’ of the Vlasov matter as δ becomes small. In fact, as in [47, Lem. 3.3], we can show that a δ -family converges uniformly to the pure Schwarzschild case in a suitable sense:

Lemma 2.2.12. *Consider a δ -family $(f_\delta)_{\delta>0}$. For every $\delta > 0$, the following properties hold:*

(a) *The radial support of f_δ is contained in $[R_{\min}^0, R_{\max}^0] \subset]3M_0, \infty[$, where*

$$R_{\min}^0 := r_-^0(E^{0,\text{vac}}, L_0), \quad R_{\max}^0 := r_+^0(E^{0,\text{vac}}, L_0); \quad (2.28)$$

see Lemma 2.2.7(d) for the definition of r_\pm^0 .

(b) *As $\delta \rightarrow 0$, the steady state quantities behave as follows: $\rho_\delta \rightarrow 0$, $p_\delta \rightarrow 0$, and $\lambda_\delta \rightarrow \lambda^0$ uniformly on $]2M_0, \infty[$, $M_\delta \rightarrow 0$, $E^\delta \rightarrow E^{0,\text{vac}}$, and*

$$(\mu_\delta)^{(k)} \rightarrow (\mu^0)^{(k)} \text{ uniformly on }]2M, \infty[, \quad k \in \{0, 1, 2\}, \quad (2.29)$$

where μ^0 is given by (2.18) and $\lambda^0 = \frac{1}{\mu^0}$.

Proof. For part (a), we first notice that $r_\pm^0(E^{0,\text{vac}}, L_0)$ are well defined because of (P3) and Lemma 2.2.7(d). For $r_0 = s_{L_0}^0$ as in (P2), Lemma 2.2.9 yields $y_\delta = y^0$ on $]2M_0, r_0]$. Consider $r \in [r_0, R_{\min}^0]$, then $y_\delta(r) \leq y^0(r)$ and $\Psi_{L_0}^0(r) \geq E^{0,\text{vac}}$ as per Lemma 2.2.7(d) imply

$$e^{-y_\delta(r)} \sqrt{1 + \frac{L_0}{r^2}} \geq e^{-y^0(r)} \sqrt{1 + \frac{L_0}{r^2}} = \frac{\Psi_{L_0}^0(r)}{E^{0,\text{vac}}} \geq 1,$$

and therefore $G(r, y_\delta(r)) = 0 = H(r, y_\delta(r))$. This proves $y_\delta(r) = y^0(r)$ and $f_\delta(x, v) = 0$ for $|x| \leq R_{\min}^0$. For the upper bound on the radial support, the same arguments are repeated for $r > R_{\max}^0$, which completes part (a).⁵

As to part (b), we start by showing the convergence of the density ρ_δ , which, due to (a), can be restricted to $[R_{\min}^0, R_{\max}^0]$. Since $R_{\min}^0 > 3M_0$, y_δ is decreasing, and $y_\delta \leq y^0$, we obtain that

$$G_{\Phi_0}(r, y_\delta(r)) \leq G_{\Phi_0}(r, y^0(3M_0)), \quad r \in [R_{\min}^0, R_{\max}^0],$$

⁵We emphasize that, for the proof, it is essential that $E^{0,\text{vac}} = e^\kappa < 1$. Otherwise, we would not be able to bound the radial support uniformly in δ . This is why we only get such a result for a δ -family and not for general families of steady states parameterized, e.g., in κ .

because G_{Φ_0} is an increasing function in the y -component, see Lemma 2.2.2. Hence, there exists $C > 0$ such that $G_{\Phi_0}(r, y_\delta(r)) \leq C$ for $r \in [R_{\min}^0, R_{\max}^0]$ and every $\delta > 0$, from which we deduce that $\rho_\delta \leq C\delta$. This immediately implies that $M_\delta \rightarrow 0$; recall (2.27). Analogous arguments are valid with ρ_δ replaced by p_δ . These convergences lead to $(y_\delta)' \rightarrow (y^0)'$ uniformly on $]2M_0, \infty[$.⁶ In particular, $\lambda_\delta \rightarrow \lambda^0$. After integration, we then deduce that $y_\delta \rightarrow y^0$ uniformly on $]2M_0, \infty[$ using similar arguments. Thus, $E^\delta \rightarrow E^{0,\text{vac}}$, and (2.29) for $k \in \{0, 1\}$ follows. Lastly, the uniform convergence of the second derivative of μ_δ follows from the field equation (1.13), which holds according to Proposition 2.2.10. \square

To conclude this section, we comment on some other and related approaches of constructing stationary solutions to the Einstein-Vlasov system around a black hole, which appear in the literature.

Remark 2.2.13. (a) *The existence of compactly supported stationary solutions with a Schwarzschild-singularity was originally proven in [90, Thm. 5.1] and the derivation is closely related to our work. In [90], the steady states are restricted to $L_0 > 16M_0^2$ and no families of equilibria were yet considered.*

(b) *The approach presented here is similar to the one found in [47, Sc. 2.2] but allows for equilibria that can reach arbitrarily close to $r = 3M_0$, whereas in [47] the solutions are bounded away from $r = 4M_0$. In addition, it is possible that the steady states in our work can be arbitrarily relativistic—as measured in the redshift k —which is not the case in [47].*

(c) *Stationary solutions surrounding a black hole are also derived in [63] via an entirely different strategy using a bifurcation argument. In short, steady states are implicitly obtained by perturbing the pure Schwarzschild case with a small amount of Vlasov matter. The main advantage of this method is that it can be generalized to obtain equilibria of the axisymmetric Einstein-Vlasov system with a Kerr black hole at the center [64]. This setting is out of reach in our approach.*

By nature of the implicit function theorem, the main result of [63] allows only for small shells that are not known explicitly. Moreover, the steady states are not suitable for our investigation from Chapter 4 onwards since we need to impose that $\partial_E \varphi < 0$ on the steady state support, which, by construction, is not possible in [63].

(d) *The spherically symmetric massless Einstein-Vlasov system is studied in [8]. The author proves the existence of static shells with finite mass and compact support surrounding a black hole. These stationary solutions are highly relativistic and the first known class of equilibria for the massless Einstein-Vlasov system.*

(e) *For the Vlasov-Poisson system, the existence of steady states with a fixed central point mass is shown in [105, Thm. 5.1] by minimizing a suitable energy-Casimir functional. The point mass can be interpreted as the non-relativistic counterpart*

⁶Recall (2.25) and note that $(y_\delta)'(r) \rightarrow 0$ as $r \rightarrow \infty$ uniformly in $\delta > 0$, since $2M_\delta < R_{\max}^0 - 2M_0$.

of the Schwarzschild black hole. In addition, the result in [105, Thm. 6.1] proves that these static solutions are non-linearly stable against spherically symmetric perturbations.

2.3 Properties

We now investigate important properties of the steady states derived in the previous section and aim to show these features under as few assumptions as possible. For various purposes throughout the investigation, we need to verify or assume a specific characteristic of the equilibrium: that the effective potential of the steady state has a so-called (*strict*) *single-well structure*. We can show this property for stationary solutions that are isotropic and satisfy $6m(r) < r$, and also for small matter shells surrounding a black hole. However, numerically the single-well structure holds for a much larger class of steady states, as we will argue in Section 2.4. The single-well structure is essential for the introduction of action-angle type variables in Section 2.3.5 and for the continuity of some quantities along a redshift-parameter, as we will see in Chapter 3. The *strict* single-well structure is needed to appropriately bound the period function from above and below in Section 2.3.3 and 2.3.4.

Unless stated otherwise, throughout the next subsections we consider a steady state f of the Einstein-Vlasov system with or without a Schwarzschild-singularity at the center, as derived in Section 2.2. Let μ , λ , E , and ρ , p be the static quantities corresponding to f and let

$$R_{\min} := \inf\{r > 0 \mid \rho(r) > 0\}, \quad R_{\max} := \sup\{r > 0 \mid \rho(r) > 0\}, \quad (2.30)$$

be the radial bounds of the steady state.

2.3.1 The single-well structure

We start by defining what we mean by a steady state having (strict) single-well structure. Our definition differs slightly from the one used in [47].

Definition 2.3.1. *Let f be a steady state of the Einstein-Vlasov system with or without a Schwarzschild-singularity of mass M_0 , as derived in Section 2.2. Let $E^0 \in]0, 1[$ be the corresponding cut-off energy, $L_0 \geq 0$ the lower bound on the angular momentum, and μ and ρ the induced metric coefficient and mass density, respectively. Furthermore, for $L \geq 0$, let the effective potential be given by*

$$\Psi_L(r) := e^{\mu(r)} \sqrt{1 + \frac{L}{r^2}}, \quad r > 2M_0, \quad (2.31)$$

where $M_0 = 0$ represents the singularity-free case. For $L > 0$, we define

$$I_L := \{r > 0 \mid \Psi_L(r) < E^0 \wedge \rho(r) > 0\},$$

and denote the set of all possible values of L in the steady state support as

$$\mathbb{L} := \{L > 0 \mid L \geq L_0, I_L \neq \emptyset\},$$

and the upper bound for the angular momentum as $L_{\max} := \sup(\mathbb{L})$.

- (a) The steady state is said to have single-well structure if for every $L \in \mathbb{L}$ there exists a unique radius $r_L \in I_L$ such that $\Psi'_L(r_L) = 0$.
- (b) The steady state is said to have strict single-well structure if in addition to (a) there exists a $a > 0$ such that $\Psi''_L(r_L) \geq a$ uniformly in $L \in \mathbb{L}$.

Even though the definition of the single-well structure for a steady state is easily understood, showing this property for relevant equilibria is quite difficult. In fact, it is known to be wrong for some static solutions.

Remark 2.3.2. (a) The main result in [104] proves that there exist steady states of the singularity-free Einstein-Vlasov system similar to the ones constructed in Section 2.2.1, which violate the single-well structure property in the anisotropic case, i.e., where an explicit L -dependency is present in the microscopic equation of state. Candidates for such steady states are numerically investigated in [16, Sc. 3.1], where the authors observe multiple nested static shells.

- (b) For the radial Vlasov-Poisson system—the non-relativistic counterpart to the Einstein-Vlasov system—, all relevant steady states have single-well structure [71, Lem. 2.1] and satisfy Jeans' theorem [19] which states that static solutions can only depend on the particle energy E and the angular momentum L .
- (c) It is an open question whether general isotropic steady states have (strict) single-well structure. We prove this statement for steady states satisfying the inequality $6m < r$ in Proposition 2.3.5. However, in Section 2.4 we will demonstrate numerically that this is the case for a large class of ansatz functions Φ , when the condition $6m < r$ is relaxed or even dropped.
- (d) Strictness of the single-well structure is tightly related to the period function being bounded from above, see Definition 2.3.7. In fact, it should be the case that a strict single-well structure is even necessary in order for the periods of the particle orbits to be bounded. We investigate this in more detail in Sections 2.3.2, 2.3.3, and 2.3.4.

The definition of the single-well structure immediately yields that for relevant values of L , the effective potential can only have one local minimum on the steady state support. This and further important properties are gathered in the upcoming lemma.

Lemma 2.3.3. Consider a steady state with single-well structure.

- (a) For $L \in \mathbb{L}$, it holds that $\Psi_L(r_L) = \min_{I_L} \Psi_L$.

(b) Let $L \in \mathbb{L}$. For every $E \in]\Psi_L(r_L), E^0[$, there exist two unique radii $r_{\pm}(E, L) \in I_L$ such that $r_-(E, L) < r_L < r_+(E, L)$ and $\Psi_L(r_{\pm}(E, L)) = E$.

(c) The functions r_{\pm} are differentiable on $\{(E, L) \mid L \in \mathbb{L}, E \in]\Psi_L(r_L), E^0[\}$ with

$$\frac{\partial r_{\pm}}{\partial E}(E, L) = \frac{1}{\Psi'_L(r_{\pm}(E, L))}.$$

In particular, r_{\pm} are continuous.

(d) $r_+(E, L)$ is strictly increasing in E and strictly decreasing in L . $r_-(E, L)$ is strictly decreasing in E and strictly increasing in L .

(e) The functions r_{\pm} can be extended continuously by

$$\lim_{E \xrightarrow{\Psi_L(r_L)} E^0} r_{\pm}(E, L) = r_L, \quad L \in \mathbb{L}, \quad (2.32)$$

$$\lim_{(E, L) \rightarrow (E^0, L_0)} r_+(E, L) = R_{\max}, \quad (2.33)$$

$$\lim_{(E, L) \rightarrow (E^0, L_0)} r_-(E, L) = R_{\min}. \quad (2.34)$$

The radial bound R_{\max} is the largest solution of $\Psi_{L_0}(r) = E^0$. Moreover, if $L_0 = 0$, the limit

$$r_+(E, 0) := \lim_{L \rightarrow 0} r_+(E, L)$$

exists for $E \in]e^{\mu(0)}, E^0[$.

(f) The set \mathbb{L} is an interval.

Proof. In the singularity-free situation, we have $\rho(r) = G(r, y(r)) > 0$, if and only if $e^{-y(r)} \sqrt{1 + \frac{L_0}{r^2}} < 1$, which is equivalent to $\Psi_{L_0}(r) < E^0$; see (2.7) and the definition of E^0 in Proposition 2.2.4. Hence, it holds that $I_L = \{r > 0 \mid \Psi_L(r) < E^0\}$. In the case of a central Schwarzschild-singularity, we have $\{\rho > 0\} = \{\Psi_{L_0} < E^0\} \cap]s_{L_0}^0, \infty[$ with $s_{L_0}^0$ given by Lemma 2.2.7(b).

In both settings, the minimum of Ψ_L is attained at r_L , since Ψ'_L has only one zero on I_L by definition of the single-well structure. From the characterization of I_L , we deduce that Ψ_L equals E^0 at the boundaries of I_L . This yields the claim in (b). In particular, I_L and the interior of the radial steady state support $\{\rho > 0\}$ are connected.

As to part (c), we fix $L \in \mathbb{L}$. The single-well structure implies $\Psi'_L(r_+(E, L)) \neq 0$ and by definition $\Psi_L(r_{\pm}(E, L)) = E$ for $E \in]\Psi_L(r_L), E^0[$. Therefore, $r_{\pm}(\cdot, L)$ is differentiable by the inverse function rule with

$$\frac{\partial r_{\pm}}{\partial E}(E, L) = \frac{1}{\Psi'_L(r_{\pm}(E, L))}, \quad E \in]\Psi_L(r_L), E^0[.$$

The differentiability with respect to L can be deduced from the implicit function theorem. Part (d) follows directly from (c) and from $\Psi_L(r)$ being increasing in L .

The claim in (2.32) can be derived from these monotonicity properties and from $R_{\min} < r_-(\cdot, L) < r_L < r_+(\cdot, L)$. The limit in (2.33) exists by the fact that $r_+(E, L)$ is increasing in E , decreasing in L , and bounded by R_{\max} . In addition, the limit must be equal to R_{\max} , because otherwise

$$\lim_{(E,L) \rightarrow (E^0, L_0)} r_+(E, L) < r_+(\tilde{E}, \tilde{L}) < R_{\max}$$

for some pair (\tilde{E}, \tilde{L}) with $\varphi(\tilde{E}, \tilde{L}) > 0$, which contradicts the monotonicity of r_+ . The same reasoning leads to (2.34). The final claim in (e) can be proven with similar arguments.

At last, we show that \mathbb{L} is an interval: By definition, we have $\mathbb{L} \subseteq [L_0, L_{\max}] \setminus \{0\}$. We now prove that $[L_0, L_{\max}] \setminus \{0\} \subseteq \mathbb{L}$, which implies the claim. For $L \in [L_0, L_{\max}] \setminus \{0\}$, choose $\bar{L} \in \mathbb{L}$ such that $L < \bar{L}$, which exists by the definition of L_{\max} . From $\Psi_L(r) \leq \Psi_{\bar{L}}(r)$ and the characterization of I_L above, we get $\emptyset \neq I_{\bar{L}} \subset I_L$, i.e., $L \in \mathbb{L}$. \square

We have to analyze the mapping $L \mapsto r_L$ further. For example, we need to prove that it is differentiable under suitable conditions which will be needed to show the strict single-well structure for isotropic steady states. Knowledge about r_L will also be important when dealing with the period function in the upcoming sections and is required for an upper bound on $\Psi_L''(r_L)$.

Lemma 2.3.4. *Consider a steady state with single-well structure and with $\Psi_L''(r_L) > 0$ for $L \in \mathbb{L}$.*

(a) *The mapping $\mathbb{L} \ni L \mapsto r_L$ is continuously differentiable and increasing with*

$$\frac{\partial r_L}{\partial L} = \frac{1}{\Psi_L''(r_L)} \frac{e^{\mu(r_L)}}{r_L^3} \left(1 + \frac{L}{r_L^2}\right)^{-\frac{3}{2}} > 0, \quad L \in \mathbb{L}.$$

(b) *The following estimate holds:*

$$\frac{4\pi}{3} \min_{[R_{\min}, r_L]} \rho \leq \frac{L}{r_L^4} \leq 8\pi \left(\max_{[R_{\min}, R_{\max}]} e^{2\lambda - 2\mu} \right) \sup_{[R_{\min}, R_{\max}]} \rho, \quad L \in \mathbb{L}. \quad (2.35)$$

(c) *The limit $r^* := \lim_{L \nearrow L_{\max}} r_L$ exists, and it holds that*

$$\Psi_{L_{\max}}(r^*) = E^0, \quad \Psi'_{L_{\max}}(r^*) = 0.$$

(d) *If the steady state is isotropic, $\lim_{L \rightarrow 0} r_L = 0$ is valid.*

Proof. Since $\Psi_L''(r_L) > 0$ for $L \in \mathbb{L}$, the implicit function theorem implies that $\mathbb{L} \ni L \mapsto r_L$ is continuously differentiable with

$$\frac{\partial r_L}{\partial L} = -\frac{(\partial_L \Psi_L')(r_L)}{\Psi_L''(r_L)}.$$

Making use of $\Psi_L'(r_L) = 0$ yields

$$(\partial_L \Psi_L')(r_L) = -\frac{e^{\mu(r_L)}}{r_L^3} \left(1 + \frac{L}{r_L^2}\right)^{-\frac{3}{2}},$$

and hence the claim in the lemma for the derivative of r_L . The estimates for $\frac{L}{r_L^4}$ in (b) can be derived from

$$\frac{L}{r_L^4} = \frac{\mu'(r_L)}{r_L} \left(1 + \frac{L}{r_L^2}\right) = e^{2\lambda(r_L) - 2\mu(r_L)} \Psi_L^2(r_L) \left(\frac{m(r_L)}{r_L^3} + 4\pi p(r_L)\right),$$

which follows from $\Psi_L'(r_L) = 0$ and (1.11). Inserting

$$m(r_L) \leq \frac{4\pi}{3} r_L^3 \sup_{[R_{\min}, R_{\max}]} \rho,$$

$\Psi_L(r_L) \leq 1$, and $0 \leq p \leq \rho$ gives the upper bound in (2.35). The lower bound follows from $\lambda \geq 0$, $\Psi_L \geq e^\mu$, $p \geq 0$, and from

$$m(r_L) \geq \frac{4\pi}{3} r_L^3 \min_{[R_{\min}, r_L]} \rho.$$

The limit in (c) exists due to $\partial_L r_L > 0$ from (a) and since $R_{\min} < r_L \leq R_{\max}$. From the continuity of $\Psi_L'(r)$ in (r, L) , we obtain

$$\Psi_{L_{\max}}'(r^*) = \lim_{L \nearrow L_{\max}} \Psi_L'(r_L) = 0.$$

Recalling the definition of \mathbb{L} in Definition 2.3.1 and considering $L_{\max} = \sup \mathbb{L}$, yields $\Psi_{L_{\max}}(r^*) = E^0$. As for (d), we apply (a) and (b). The fact that r_L is increasing in L implies that the limit of r_L for $L \rightarrow 0$ exists. According to the lower bound in (2.35) and the fact that ρ is decreasing in r because of Lemma 2.1.3, we have

$$\frac{4\pi}{3} \rho(r_L) = \frac{4\pi}{3} \min_{[0, r_L]} \rho \leq \frac{L}{r_L^4}, \quad L \in \mathbb{L}.$$

By choosing $R := r_{\bar{L}} < R_{\max}$ for some fixed $0 < \bar{L} < L_{\max}$, we obtain

$$r_{\bar{L}}^4 \leq \frac{3\bar{L}}{4\pi\rho(R)}, \quad 0 < \bar{L} < L_{\max},$$

i.e., $r_L \rightarrow 0$ as $L \rightarrow 0$. □

We now show that isotropic steady states have strict single-well structure, if $6m < r$ holds everywhere. Similar arguments have been used in [47, Lem. 3.2].

Proposition 2.3.5. *Consider a stationary solution to the singularity-free Einstein-Vlasov system, as constructed in Section 2.2.1. We require that the steady state is isotropic and satisfies*

$$\frac{2m(r)}{r} < \frac{1}{3}, \quad r > 0. \quad (2.36)$$

Then the steady state has strict single-well structure.

Proof. We start by showing that the steady state has single-well structure. The strictness will only follow a posteriori. Consider $L \in \mathbb{L}$. Since $\Psi_L(r) > E_0$ as $r \rightarrow 0$ and as $r \rightarrow \infty$, there exists at least one zero of Ψ'_L by the mean value theorem. In order to show that this is the only zero, we use that $\Psi'_L(r) = 0$ is equivalent to

$$\frac{1}{L} = \frac{1}{r^3 \mu'(r)} - \frac{1}{r^2}, \quad r > 0. \quad (2.37)$$

We prove that the right hand side of (2.37) is strictly monotonic on the steady state support. Since the underlying steady state is isotropic, we get $p = q$, according to Lemma 2.1.3. The field equations (1.10), (1.11), and (1.13) thus yield

$$\begin{aligned} \left(\frac{1}{r^3 \mu'} - \frac{1}{r^2} \right)' &= -\frac{e^{2\lambda}}{r^3 (\mu')^2} \left[16\pi p + 4\pi \rho + \frac{m}{r^3} \right. \\ &\quad \left. - e^{2\lambda} \left(48\pi^2 r^2 p^2 - 16\pi^2 r^2 \rho p + 28\pi p \frac{m}{r} - 4\pi \rho \frac{m}{r} + 4 \frac{m^2}{r^4} \right) \right]. \end{aligned}$$

Let $d(r)$ denote the term in the square brackets. By isotropy we obtain $3p \leq \rho$, and thus

$$\begin{aligned} d(r) &= 16\pi p + 4\pi \rho + \frac{m}{r^3} - e^{2\lambda} \left(16\pi^2 r^2 p(3p - \rho) + \frac{2m}{r} \left(14\pi p - 2\pi \rho + \frac{2m}{r^3} \right) \right) \\ &\geq 16\pi p + 4\pi \rho + \frac{m}{r^3} - 2 \left(e^{2\lambda} - 1 \right) \left(4\pi p + \frac{m}{r^3} \right), \end{aligned}$$

where we used that $\frac{2m}{r} = 1 - e^{-2\lambda}$. We observe that (2.36) is equivalent to $e^{2\lambda} - 1 \leq \frac{1}{2}$, from which we deduce that d is positive on $\{r > 0 \mid \rho(r) > 0\}$ and in particular on I_L . This proves that (2.37)—and thus $\Psi'_L = 0$ —has a unique solution on I_L and shows the single-well structure.

We now aim to apply Lemma 2.3.4 and thus have to provide that $\Psi''_L(r_L) > 0$. As above, fix $L \in \mathbb{L}$. From $\Psi'_L(r_L) = 0$, we get

$$\frac{L}{r_L^3} \frac{1}{1 + \frac{L}{r_L^2}} = \mu'(r_L), \quad (2.38)$$

which yields

$$\Psi_L''(r_L) = \Psi_L(r_L) \left(\mu''(r_L) + \frac{3\mu'(r_L)}{r_L} - 2(\mu'(r_L))^2 \right).$$

By inserting (1.13), $p = q$, and the identities

$$\begin{aligned} \mu' + \lambda' &= 4\pi r e^{2\lambda}(\rho + p), \\ \lambda' - 3\mu' + \frac{1}{r} &= 4\pi r e^{2\lambda}(\rho - 3p) + \frac{e^{2\lambda}}{r} \left(1 - \frac{6m}{r} \right), \end{aligned}$$

we arrive at

$$\Psi_L''(r_L) = \Psi_L(r_L) e^{2\lambda} \left[4\pi(\rho + 3p) + 4\pi\mu'(\rho - 3p) + \frac{\mu'}{r_L} \left(1 - \frac{6m}{r_L} \right) \right], \quad (2.39)$$

where all functions are evaluated at r_L . We make use of (2.38) in order to obtain

$$\Psi_L''(r_L) = \frac{e^{2\lambda+2\mu}}{\Psi_L(r_L)} \left[\left(1 + \frac{L}{r_L^2} \right) (4\pi(\rho + 3p) + 4\pi\mu'(\rho - 3p)) + \frac{L}{r_L^4} \left(1 - \frac{6m}{r_L} \right) \right].$$

Using $\Psi_L(r) \leq 1$, $\mu' \geq 0$, and $0 \leq 3p \leq \rho$ yields

$$\Psi_L''(r_L) \geq e^{2\mu(0)} \left[4\pi\rho(r_L) + \frac{L}{r_L^4} \left(1 - \frac{6m(r_L)}{r_L} \right) \right] > 0 \quad (2.40)$$

by (2.36). Hence, Lemma 2.3.4(a) implies that $L \mapsto r_L$ is continuously differentiable and increasing in L .

It remains to show that the single-well structure is strict, according to Definition 2.3.1(b). Fix $\bar{L} \in \mathbb{L}$. Then from the monotonicity of r_L , we obtain $r_L \leq r_{\bar{L}}$ for $0 < L \leq \bar{L}$.⁷ The estimate (2.40) yields

$$\Psi_L''(r_L) \geq 4\pi e^{2\mu(0)} \rho(r_L) \geq 4\pi e^{2\mu(0)} \rho(r_{\bar{L}}),$$

since isotropy implies that ρ is decreasing. For $L > \bar{L}$, we estimate

$$\Psi_L''(r_L) \geq e^{2\mu(0)} \frac{\bar{L}}{R_{\max}^4} \min_{r>0} \left(1 - \frac{6m(r)}{r} \right),$$

by again making use of (2.40). Therefore, for every $L \in \mathbb{L}$ we have

$$\Psi_L''(r_L) \geq e^{2\mu(0)} \min \left\{ 4\pi\rho(r_{\bar{L}}), \frac{\bar{L}}{R_{\max}^4} \min_{r>0} \left(1 - \frac{6m(r)}{r} \right) \right\} =: a,$$

which is independent of L and positive by the assumption that $6m(r) < r$ for $r > 0$.⁸

⁷Recall that \mathbb{L} is an interval, as shown in Lemma 2.3.3(f).

⁸We have $m(r) \approx r^2$ for small r and $m(r) = m(R_{\max})$ for $r \geq R_{\max}$, which implies that the minimum over $r > 0$ exists.

This implies the strict single-well structure and finishes the proof. \square

In the setting of a steady state with a central black hole, we have to find a different argument to assure the single-well structure. Since a δ -family is close to the pure Schwarzschild case for small values of δ , according to Lemma 2.2.12(b), we can salvage the strict single-well structure for $0 < \delta \ll 1$. This is also done in [47, Prop. 3.4]. We refer to [102, Apx. D] for a related analysis.

Proposition 2.3.6. *Consider a δ -family $(f_\delta)_{\delta>0}$ as in Definition 2.2.11. Then there exists $\delta_0 > 0$ such that f_δ has strict single-well structure for any $0 < \delta \leq \delta_0$.*

Proof. Recall the notation from Definition 2.2.11. Let $\Psi_{\delta,L}(r)$ be the corresponding effective potential given by (2.31) for $\delta > 0$, $L \geq L_0$, and $r > 2M_0$. Then, equation (2.24) and Lemma 2.2.12 imply that

$$\begin{aligned} I_{\delta,L} &:= \{r > 0 \mid \Psi_{\delta,L}(r) < E^\delta \wedge \rho_\delta(r) > 0\} \\ &\subset \{r \in [R_{\min}^0, R_{\max}^0] \mid \Psi_L^0(r) \leq E^{0,\text{vac}}\} =: J_L^0 \end{aligned}$$

for $\delta > 0$ and $L \geq L_0$.

If $J_L^0 \neq \emptyset$, then $r_L^0 \in J_L^0$ where r_L^0 is defined in Lemma 2.2.7. In this case, Ψ_L^0 behaves as follows on J_L^0 : There exists an open interval around r_L^0 , where $(\Psi_L^0)''$ is positive. To the left of that interval, $(\Psi_L^0)'$ is negative, and to the right of this interval, $(\Psi_L^0)'$ is positive; in both of the latter regions, $(\Psi_L^0)'$ is bounded away from zero. Using the uniform convergences (2.29) implies that $\Psi_{\delta,L}$ has the same properties on J_L^0 for $\delta \in]0, \delta_0]$ with some suitable $\delta_0 > 0$. The interval J_L^0 is empty for large L , which is why we only have to consider a compact L -interval and can thus choose δ_0 independent of L . \square

2.3.2 The periodic particle motions and the period function

In addition to the setup from the beginning of Section 2.3, we assume that the steady state has single-well structure, as stated in Definition 2.3.1, and also employ the notation from that definition.

In order to extract information about the particle motions, we analyze the characteristic flow of the steady state within (the interior of) its support

$$\Omega := \{(r, w, L) \in]0, \infty[\times \mathbb{R} \times]0, \infty[\mid f(r, w, L) > 0\}. \quad (2.41)$$

The characteristic system can be interpreted as the Hamiltonian-like ODE system

$$\dot{r} = e^{-\lambda(r)} \partial_w E(r, w, L) = e^{\mu(r)-\lambda(r)} \frac{w}{\sqrt{1 + w^2 + \frac{L}{r^2}}}, \quad (2.42a)$$

$$\dot{w} = -e^{-\lambda(r)} \partial_r E(r, w, L) = e^{\mu(r)-\lambda(r)} \left(\frac{L}{r^3 \sqrt{1 + w^2 + \frac{L}{r^2}}} - \mu'(r) \sqrt{1 + w^2 + \frac{L}{r^2}} \right). \quad (2.42b)$$

To be precise, the equation $\dot{L} = 0$ is also part of the characteristic system. However, this means that the angular momentum is constant along solutions and can be thought of as a parameter of the system. In addition, the particle energy E given by (2.1) is a conserved quantity. It is crucial to have good understanding of the particle motions in the steady state for the investigation in Chapters 5 and 6. In the upcoming lemma, we show that the particles move in periodic orbits, and we define the corresponding period function, which is an important quantity in the context of action-angle type variables. The period function can be derived formally by applying the inverse function theorem. We refer to Figure 2.2 on page 55 for an illustration of the periodic orbits. From the single-well structure, we are able to identify every particle orbit uniquely by fixing the energy E and the angular momentum L . We restrict the analysis to the case $L > 0$ as $\Omega \cap \{L = 0\}$ forms a set of measure zero which will not be of importance later on. In addition, we leave out circular orbits, i.e., where $E = \Psi_L(r_L)$, as the period of such an orbit is not easily defined.

Definition & Lemma 2.3.7. *Let f be a steady state with single-well structure and define*

$$\tilde{\Omega}^{EL} := \{(E(r, w, L), L) \mid (r, w, L) \in \Omega, L > 0, E(r, w, L) > \Psi_L(r_L)\}. \quad (2.43)$$

For $(E, L) \in \tilde{\Omega}^{EL}$, let $(R, W) = (R, W)(\cdot, E, L): \mathbb{R} \rightarrow \mathbb{R} \times \mathbb{R}$ be the maximal solution of (2.42), satisfying the initial condition $(R, W)(0, E, L) = (r_-(E, L), 0)$, where r_L and $r_{\pm}(E, L)$ are defined in Definition 2.3.1 and Lemma 2.3.3(b). The solution is time-periodic with period

$$T(E, L) := 2E \int_{r_-(E, L)}^{r_+(E, L)} \frac{e^{\lambda(r) - \mu(r)}}{\sqrt{E^2 - \Psi_L^2(r)}} dr. \quad (2.44)$$

The induced function $T: \tilde{\Omega}^{EL} \rightarrow]0, \infty[$ is called the period function. The orbit corresponding to the periodic motion is given by

$$\mathcal{O}_{EL} := \{(r, w) \mid E(r, w, L) = E, \rho(r) > 0\}.$$

Proof. From the single-well structure and the fact that the energy E is conserved, we obtain that

$$E = e^{\mu(R(\cdot, E, L))} \sqrt{1 + W(\cdot, E, L)^2 + \frac{L}{R(\cdot, E, L)^2}},$$

where the solution (R, W) exists. Observe that the radial component R of the solution stays in the interval I_L and the momentum component W is bounded since $\Psi_L(r) \leq E$; in particular, $I_L \neq \emptyset$, according to Definition 2.3.1. Due to $E > \Psi_L(r_L)$, the solution is non-constant, bounded, exists on \mathbb{R} , and is time-periodic with the orbit given by \mathcal{O}_{EL} ; the periodic behavior follows from standard arguments. Because of the single-well structure, \mathcal{O}_{EL} is bounded and connected. It does not contain any stationary solution of (2.42), since $E > \Psi_L(r_L)$ and $\Psi'_L(s) \neq 0$ for $s \in I_L \setminus \{r_L\}$ by Definition 2.3.1. \square

2.3.3 A lower bound for the period function

As in the non-relativistic setting [55, 69], the period function T and its properties are crucial in order to develop a Birman-Schwinger principle, see Chapter 5. In particular, we need to ensure that the period function is bounded away from zero and bounded from above uniformly in E and L . For the investigation in Section 3.2, it is essential to have explicit control over these bounds which makes deriving them quite painful.

We begin by showing that the period function is bounded away from zero if the steady state has strict single-well structure and if $L_0 > 0$ or $l \geq 0$ holds. We have to prescribe the latter condition to guarantee that ρ is bounded on $[0, \infty[$. Without the explicit bound and many missing details, a similar result is derived in [47] for some classes of steady states. As a first step, we show that Ψ''_L is bounded from above.

Lemma 2.3.8. *Let f be a steady state with strict single-well structure and $L_0 > 0$ or $l \geq 0$. The second-order derivative of the effective potential is uniformly bounded for every $L \in \mathbb{L}$ and $r \in [r_L, R_{\max}]$ by*

$$\Psi''_L(r) \leq N_{\Psi''} := 38\pi A(1 + 8\pi R_{\max}^2 A), \quad (2.45)$$

where

$$A := \left(\max_{[R_{\min}, R_{\max}] } e^{2\lambda - 2\mu} \right) \max_{[R_{\min}, R_{\max}] } \rho.$$

Proof. For $r \in [R_{\min}, R_{\max}]$, we compute

$$\Psi''_L(r) = \Psi_L(r) \left[\mu''(r) + \mu'(r)^2 - \frac{2\mu'(r)}{r^3} \frac{L}{1 + \frac{L}{r^2}} + \frac{L}{r^4} \frac{1}{\left(1 + \frac{L}{r^2}\right)^2} \left(3 + 2\frac{L}{r^2}\right) \right]. \quad (2.46)$$

Since $\mu'(r) \geq 0$, $0 < \Psi_L(r) \leq 1$, and $r_L > 0$, we obtain

$$\Psi''_L(r) \leq \mu''(r) + \mu'(r)^2 + 3\frac{L}{r^4}, \quad r \in [r_L, R_{\max}].$$

Lemma 2.3.4(b) thus yields

$$\Psi''_L(r) \leq \max_{[R_{\min}, R_{\max}]} (\mu'' + (\mu')^2) + 24\pi \left(\max_{[R_{\min}, R_{\max}]} e^{2\lambda - 2\mu} \right) \max_{[R_{\min}, R_{\max}]} \rho$$

for $r \in [r_L, R_{\max}]$. The maximum of ρ over $[R_{\min}, R_{\max}]$ is attained in the cases $L_0 > 0$ or $l \geq 0$, because if $L_0 > 0$ we have $R_{\min} > 0$, and if $l \geq 0$ and $L_0 = 0$, the boundedness of ρ over $[0, R_{\max}]$ follows from Lemma 2.2.2 and $\rho(r) = G(r, y(r))$. From the Einstein field equation (1.13), we have⁹

$$\mu'' + (\mu')^2 = \lambda' \mu' + \frac{\lambda' - \mu'}{r} + 8\pi e^{2\lambda} q. \quad (2.47)$$

⁹Recall that (1.13) holds in the singularity-free as well as in the singularity case, according to Propositions 2.2.4 and 2.2.10.

In addition, the field equations (1.10) and (1.11) imply

$$\frac{\lambda'}{r} = e^{2\lambda} \left(4\pi\rho - \frac{m}{r^3} \right), \quad \frac{\mu'}{r} = e^{2\lambda} \left(4\pi p + \frac{m}{r^3} \right),$$

and due to $m(r) \leq 2\pi r^3 \max_{[R_{\min}, R_{\max}]} \rho$, as well as $e^\mu \leq 1$, we obtain

$$\frac{\lambda'}{r}, \frac{\mu'}{r}, \frac{\lambda' - \mu'}{r} \leq 6\pi \left(\max_{[R_{\min}, R_{\max}]} e^{2\lambda - 2\mu} \right) \max_{[R_{\min}, R_{\max}]} \rho = 6\pi A.$$

Because of (2.47) and $0 \leq q \leq \rho$, we get

$$\mu'' + (\mu')^2 \leq (6\pi R_{\max} A)^2 + 6\pi A + 8\pi A \leq 14\pi A(1 + 8\pi R_{\max}^2 A),$$

and thus,

$$\Psi_L''(r) \leq 38\pi A(1 + 8\pi R_{\max}^2 A), \quad r \in [r_L, R_{\max}].$$

□

With this auxiliary lemma, we can now bound the period function from below.

Proposition 2.3.9. *Let f be a steady state with strict single-well structure and $L_0 > 0$ or $l \geq 0$. The period function corresponding to f is bounded from below by*

$$T(E, L) \geq 2e^{\mu(R_{\min})} \frac{1}{\sqrt{N_{\Psi''}}}, \quad (E, L) \in \tilde{\Omega}^{E, L}, \quad (2.48)$$

where $N_{\Psi''}$ is defined in (2.45).

Proof. We proceed in similar manner to [47, Lem. 3.6] and [55, Lem. B.4]. We fix $(E, L) \in \tilde{\Omega}^{E, L}$. Then $e^{\mu(R_{\min})} \leq E$ and

$$E^2 - \Psi_L^2(s) = (E - \Psi_L(s))(E + \Psi_L(s)) \leq 2(E - \Psi_L(s)), \quad s \in [r_-(E, L), r_+(E, L)],$$

imply the estimate

$$T(E, L) \geq \sqrt{2} e^{\mu(R_{\min})} S(E, L), \quad (2.49)$$

since $\lambda \geq 0$ and $\mu \leq 0$, where

$$S(E, L) := \int_{r_-(E, L)}^{r_+(E, L)} \frac{dr}{\sqrt{E - \Psi_L(r)}}.$$

Since Ψ_L attains its minimal value at $r_L > r_-(E, L)$, we get

$$S(E, L) \geq \frac{r_+(E, L) - r_-(E, L)}{\sqrt{E - \Psi_L(r_L)}} \geq \frac{r_+(E, L) - r_L}{\sqrt{E - \Psi_L(r_L)}}.$$

Using $\Psi'_L(r_L) = 0$ in the first-order Taylor expansion of Ψ_L yields

$$E = \Psi_L(r_+(E, L)) = \Psi_L(r_L) + \Psi''_L(s) \frac{(r_+(E, L) - r_L)^2}{2},$$

for some intermediate value $s \in]r_L, r_+(E, L)[$ and necessarily $\Psi''_L(s) > 0$ due to $E > \Psi_L(r_L)$. Rearranging this term and putting it into the estimate for S above gives

$$S(E, L) \geq \frac{\sqrt{2}}{\sqrt{\Psi''_L(s)}},$$

which together with (2.49) and Lemma 2.3.8 finishes the proof. \square

2.3.4 An upper bound for the period function

Bounding the period function from below is rather easy compared to deriving an explicit upper bound for T . We provide many of the involved details which are intentionally left out in [47]. The idea is similar to the non-relativistic setting [55, Apx. B] as the proof is divided into three steps: First, we bound T uniformly for values $L \geq L_1$, where $L_1 > 0$ is fixed, see Lemma 2.3.11. In Lemma 2.3.14, we bound T for values $E \leq E_1$, where $E_1 < E^0$ is fixed. The remaining gap is then closed in Lemma 2.3.15.

Alternatively, we could show the boundedness by extending T continuously onto the boundary of $\hat{\Omega}^{EL}$ using the techniques from [69, Thm. 3.13]. It is likely that this would be even more difficult than our approach.

In case the details are not of interest, the reader is invited to skip forward to Proposition 2.3.16, where we summarize the main result of this section. Before starting to bound T , we need to show an auxiliary result which guarantees that we can control Ψ'_L away from its zero r_L and Ψ''_L close to r_L independently from L .

Lemma 2.3.10. *Consider a steady state with strict single-well structure and fix $L_1 > 0$. Then there exist $a, q > 0$ such that, for every $L \in \mathbb{L}$ with $L \geq L_1$, it holds that*

- (i) $\Psi''_L \geq a$ on $[r_L - q, r_L + q] \cap \bar{I}_L$,
- (ii) $\Psi'_L \leq -a$ on $[R_{\min}, r_L - q] \cap \bar{I}_L$,
- (iii) $\Psi'_L \geq a$ on $[r_L + q, R_{\max}] \cap \bar{I}_L$.

In the cases (ii) and (iii), the sets may be empty. The interval I_L is given in Definition 2.3.1.

Proof. For fixed $L_1 > 0$, let

$$R_1 := \lim_{E \nearrow E^0} r_-(E, L_1) > 0,$$

which exists since $r_-(\cdot, L_1)$ is decreasing due to Lemma 2.3.3(d). The mapping

$$[R_1, R_{\max}] \times [L_1, L_{\max}] \ni (r, L) \mapsto \Psi''_L(r)$$

is uniformly continuous and, by the strict single-well structure, there exists $a_1 > 0$ with

$$\Psi_L''(r_L) \geq 2a_1, \quad L \in [L_1, L_{\max}].$$

This directly implies the existence of $q > 0$ with

$$\Psi_L''(r) \geq a_1, \quad r \in [r_L - q, r_L + q] \cap \bar{I}_L,$$

by the uniform continuity of Ψ_L'' .

For part (ii), we observe that the set

$$D_- := \{(r, L) \mid L \in [L_1, L_{\max}], r \in [R_{\min}, r_L - q] \cap \bar{I}_L\}$$

is compact (or empty) since r_L is continuous. If $D_- = \emptyset$, we are done and skip part (ii). In the case where $D_- \neq \emptyset$,

$$a_2 := - \max_{(r,L) \in D_-} \Psi_L'(r)$$

exists by continuity of $\Psi_L'(r)$ over D_- . Moreover, $a_2 > 0$, since $(r_L, L) \notin D_-$ and Ψ_L' has exactly one zero on I_L by the single-well structure. For (iii), an analogous argument holds. Overall, the claim in the lemma follows by choosing $a > 0$ small enough. \square

With the previous lemma at hand, the boundedness of T away from $L = 0$ is obtained in the next result. In order to simplify the investigation, we first consider

$$S(E, L) := \int_{r_-(E,L)}^{r_+(E,L)} \frac{dr}{\sqrt{E - \Psi_L(r)}}, \quad (E, L) \in \tilde{\Omega}^{EL} \quad (2.50)$$

and recover the estimates for T later in Proposition 2.3.16. A similar strategy in a more specific setting is used in [47, Proof of Lem. 3.6]. Related arguments can be found in [55, Prop. 2.8]

Lemma 2.3.11. *Consider a steady state with strict single-well structure and fix $L_1 > 0$. Then the estimate*

$$S(E, L) \leq \frac{4\sqrt{R_{\max}} + \sqrt{2}\pi}{\sqrt{a}} \quad (2.51)$$

holds for every $(E, L) \in \tilde{\Omega}^{EL}$ with $L \geq L_1$, where $a > 0$ depends on L_1 and is chosen according to Lemma 2.3.10.

Proof. For $L_1 > 0$, let $a, q > 0$ be the parameters given by Lemma 2.3.10. We split the integral $S(E, L)$ into three parts

$$\begin{aligned} S(E, L) &= \int_{r_-(E,L)}^{r_L - q} \frac{dr}{\sqrt{E - \Psi_L(r)}} + \int_{r_L - q}^{r_L + q} \frac{dr}{\sqrt{E - \Psi_L(r)}} + \int_{r_L + q}^{r_+(E,L)} \frac{dr}{\sqrt{E - \Psi_L(r)}} \\ &=: S_l(E, L) + S_m(E, L) + S_r(E, L) \end{aligned}$$

and estimate each term separately. In the case where $r_L - q < r_-(E, L)$ or $r_L + q > r_+(E, L)$, we replace $r_L \pm q$ by $r_{\pm}(E, L)$, respectively, i.e., the terms S_l or S_r vanish. If S_l is present, we obtain $\Psi'_L \leq -a$ on the domain of integration from Lemma 2.3.10(ii), i.e., the mean value theorem yields

$$E - \Psi_L(r) = \Psi_L(r_-(E, L)) - \Psi_L(r) \geq a(r - r_-(E, L)), \quad r \in [r_-(E, L), r_L - q].$$

Inserting this estimate into S_l gives

$$S_l(E, L) \leq \frac{1}{\sqrt{a}} \int_{r_-(E, L)}^{r_L - q} \frac{dr}{\sqrt{r - r_-(E, L)}} = \frac{2}{\sqrt{a}} \sqrt{r_L - q - r_-(E, L)} \leq \frac{2}{\sqrt{a}} \sqrt{R_{\max}}.$$

The term S_r can be treated analogously by using $\Psi'_L \geq a$ on $[r_L + q, r_+(E, L)]$ which yields

$$S_r(E, L) \leq \frac{2}{\sqrt{a}} \sqrt{R_{\max}}.$$

The middle term requires a more elaborate argument. We split S_m further into

$$S_m(E, L) = \int_{r_L - q}^{r_L} \frac{dr}{\sqrt{E - \Psi_L(r)}} + \int_{r_L}^{r_L + q} \frac{dr}{\sqrt{E - \Psi_L(r)}} =: S_m^-(E, L) + S_m^+(E, L).$$

By means of the single-well structure, $\Psi'_L > 0$ for $r > r_L$ and thus, changing variables via $\eta = \Psi_L(r)$, i.e., $r = r_+(\eta, L)$, yields

$$S_m^+(E, L) = \int_{\Psi_L(r_L)}^{\Psi_L(r_L + q)} \frac{d\eta}{\sqrt{(\Psi'_L(r_+(\eta, L)))^2 (E - \eta)}}. \quad (2.52)$$

We apply the mean value theorem for $\eta \in [\Psi_L(r_L), \Psi_L(r_L + q)]$ to obtain the existence of $\xi \in]\Psi_L(r_L), \Psi_L(r_L + q)[$ such that

$$\Psi'_L(r_+(\eta, L))^2 = \Psi'_L(r_+(\eta, L))^2 - \Psi'_L(r_L)^2 = \partial_{\eta}(\Psi'_L(r_+(\cdot, L))^2)(\xi)(\eta - \Psi_L(r_L)), \quad (2.53)$$

where we have extended $r_+(\eta, L)$ continuously by r_L for $\eta \xrightarrow{\geq} \Psi_L(r_L)$, according to Lemma 2.3.3(e). By explicitly computing the derivative in (2.53) and employing Lemma 2.3.3(c), we obtain

$$\frac{\Psi'_L(r_+(\eta, L))^2}{\eta - \Psi_L(r_L)} = 2\Psi'_L(r_+(\xi, L)) \frac{\Psi''_L(r_+(\xi, L))}{\Psi'_L(r_+(\xi, L))} = 2\Psi''_L(r_+(\xi, L)). \quad (2.54)$$

Since $r_+(\xi, L) \in [r_L, r_L + q]$, it follows that $\Psi''_L(r_+(\xi, L)) \geq a$ by the choice of a and q . Therefore, after inserting this result into (2.52), we explicitly calculate

$$S_m^+(E, L) \leq \frac{1}{\sqrt{2a}} \int_{\Psi_L(r_L)}^E \frac{d\eta}{\sqrt{(\eta - \Psi_L(r_L))(E - \eta)}} = \frac{\pi}{\sqrt{2a}}.$$

We proceed in the same way with S_m^- , recall the estimates for S_l and S_r above, and get

$$S(E, L) \leq \frac{4\sqrt{R_{\max}} + \sqrt{2}\pi}{\sqrt{a}}. \quad \square$$

We immediately obtain that S (and thus the period function T) is bounded from above in the case $L_0 > 0$, i.e., if the steady state is a shell with a vacuum region at the center.

Corollary 2.3.12. *Consider a steady state with strict single-well structure and $L_0 > 0$. Then the quantity $S(E, L)$ is bounded on $\tilde{\Omega}^{EL}$.*

Proof. The claim follows by setting $L_1 = L_0$ in Lemma 2.3.11. □

The situation gets a bit more delicate when $L_0 = 0$. In this case, we are only able to prove that $S(E, L)$ is bounded from above when $l = 0$ holds as well, i.e., if the underlying steady state is isotropic. However, we have reason to believe that this is no coincidence:

Remark 2.3.13. *Consider a steady state with single-well structure and $L_0 = 0$.*

- (a) *In the case where $l = 0$, we have $\varphi(E, L) = \varphi(E)$, i.e., an isotropic stationary solution. We bound the period function in the upcoming lemmata under suitable conditions.*
- (b) *In the case where $l > 0$, i.e.,*

$$\varphi(E, L) = \Phi\left(1 - \frac{E}{E^0}\right)L^l,$$

we claim that

$$\lim_{L \rightarrow 0} \Psi_L''(r_L) = 0.$$

In particular, the steady state cannot have strict single-well structure. Analogously to the proof of Proposition 2.3.9, we can show

$$S(E, L) \geq \frac{\sqrt{2}}{\sqrt{\Psi_L''(s)}}, \quad (E, L) \in \tilde{\Omega}^{EL},$$

for some intermediate value $s \in]r_L, r_+(E, L)[$. If we choose E close to $\Psi_L(r_L)$ and L close to 0, this lower bound implies that $S(E, L)$ gets large. In particular, the period function T is unbounded on $\tilde{\Omega}^{EL}$. We leave out the technical details.

In light of this remark, we intentionally dismiss the anisotropic case with $L_0 = 0$. It thus suffices to consider isotropes for which we demand that $6m(r) < r$ as in Proposition 2.3.5. As a counterpart to Lemma 2.3.11, we prove that T is bounded if we restrict it to values of E which are uniformly smaller than the cut-off energy E^0 . We refer to [55, Lem. B.2] for a related analysis in context of the Vlasov-Poisson system.

Lemma 2.3.14. *Consider an isotropic steady state that satisfies*

$$\frac{2m(r)}{r} < \frac{1}{3}, \quad r > 0, \quad (2.55)$$

fix $e^{\mu(0)} < E_1 < E^0$, and define $R_1 := r_+(E_1, 0)$. Then the estimate

$$T(E, L) \leq \sqrt{6\pi} \frac{\max_{[0, R_{\max}]} e^{\lambda - \mu}}{\sqrt{\min_{[0, R_1]} e^{2\mu + 2\lambda} \rho}}$$

holds for every $(E, L) \in \tilde{\Omega}^{EL}$ with $E \leq E_1$.

Proof. From Proposition 2.3.5, we know that the steady state has strict single-well structure. First, we observe that $R_1 < R_{\max}$ is well defined due to Lemma 2.3.3(d) and (e). Fix $(E, L) \in \tilde{\Omega}^{EL}$ with $E \leq E_1$ and abbreviate $r_{\pm} := r_{\pm}(E, L)$. The idea is to apply the maximum principle for the radial Laplacian $\Delta = \partial_r^2 + \frac{2}{r}\partial_r$ and show that Ψ_L^2 can be bounded on $[r_-, r_+]$ by an explicit function. For $c > 0$, we define an auxiliary function

$$U_c(r) := -\frac{2\pi c}{3} \frac{(r_+ - r)(r - r_-)(r + r_+ + r_-)}{r}, \quad r \in [r_-, r_+].$$

Applying the radial Laplacian shows that U_c solves the boundary value problem

$$\Delta U_c = 4\pi c \quad \text{on } [r_-, r_+], \quad (2.56)$$

$$U_c(r_{\pm}) = 0. \quad (2.57)$$

In addition, a lengthy calculation similar to (2.46) yields

$$\begin{aligned} \Delta_x(\Psi_L^2) &= \frac{1}{r^2} (r^2(\Psi_L^2)')' \\ &= 2e^{2\mu+2\lambda} \left[4\pi(\rho + 3p) + 4\pi r(p + \rho)\mu' + \frac{L}{r^4} \left(4\pi r^3(p + \rho)\mu' + 4\pi r^2(\rho - p) + 1 - \frac{6m}{r} \right) \right], \end{aligned} \quad (2.58)$$

which makes use of (1.10), (1.11), (1.13), and $p = q$. Putting (2.56) and (2.58) together implies

$$\Delta(U_c + E^2 - \Psi_L^2) < 4\pi c - 8\pi e^{2\mu+2\lambda} \rho,$$

since $6m < r$, $0 \leq p \leq \rho$, and $\mu' \geq 0$. We define

$$c := \min_{[0, R_1]} e^{2\mu+2\lambda} \rho > 0,$$

which is positive since ρ is decreasing and $\rho(r) > 0$ for $r \leq R_1 < R_{\max}$ in the isotropic

case. By using the boundary conditions (2.57), we obtain

$$\begin{aligned}\Delta(U_c + E^2 - \Psi_L^2) &< 0 \quad \text{on } [r_-, r_+], \\ \Psi_L^2(r_\pm) &= E^2,\end{aligned}$$

and thus the maximum principle for elliptic differential equations implies

$$U_c + E^2 - \Psi_L^2 > 0 \quad \text{on } [r_-, r_+].$$

We insert this estimate into the definition of the period function (2.44) and get

$$T(E, L) \leq 2 \left(\max_{[0, R_{\max}]} e^{\lambda - \mu} \right) \int_{r_-}^{r_+} \frac{dr}{\sqrt{-U_c(r)}}.$$

The integral can be bounded by

$$\begin{aligned}\int_{r_-}^{r_+} \frac{dr}{\sqrt{-U_c(r)}} &= \sqrt{\frac{3}{2\pi c}} \int_{r_-}^{r_+} \frac{1}{\sqrt{(r_+ - r)(r - r_-)}} \frac{\sqrt{r}}{\sqrt{r + r_+ + r_-}} dr \\ &\leq \sqrt{\frac{3}{2\pi c}} \int_{r_-}^{r_+} \frac{dr}{\sqrt{(r_+ - r)(r - r_-)}} = \sqrt{\frac{3\pi}{2c}}.\end{aligned}$$

Hence, we obtain the desired bound for $T(E, L)$. \square

By combining Lemma 2.3.11 and Lemma 2.3.14, it remains to control T for values of E close to E^0 and values of L close to $L_0 = 0$. Illustratively speaking, these are the orbits with the highest eccentricity. We close this gap in the next lemma. An analogous result in the non-relativistic case can be found in [55, Lem. B.3]

Lemma 2.3.15. *Consider an isotropic steady state that satisfies*

$$\frac{2m(r)}{r} < \frac{1}{3}, \quad r > 0. \quad (2.59)$$

There exists $e^{\mu(0)} < E_1 < E^0$ and $L_1 > 0$ such that for every $(E, L) \in \tilde{\Omega}^{EL}$ with $E_1 \leq E < E^0$ and $0 < L \leq L_1$ it holds that

$$T(E, L) \leq \left(\max_{[0, R_{\max}]} e^{\lambda - \mu} \right) \left(\frac{6R_{\max}}{\sqrt{\min\{e^{\mu(0)}, E^0 - E_1\}}} + \frac{4\sqrt{R_{\max}}}{\sqrt{\min_{[r_{2L_1}, R_{\max}]} (\Psi_{L_1}^2)'}} \right).$$

Proof. From Proposition 2.3.5, we know that the steady state has strict single-well structure. For $(E, L) \in \tilde{\Omega}^{EL}$, let $e^{\mu(0)} > \varepsilon > 0$ with $E - \varepsilon > \Psi_L(r_L)$. The main idea is to partition the orbit corresponding to (E, L) into the intervals

$$[r_-(E, L), r_-(E - \varepsilon, L)], \quad]r_-(E - \varepsilon, L), r_+(E - \varepsilon, L)[, \quad [r_+(E - \varepsilon, L), r_+(E, L)]; \quad (2.60)$$

recall the monotonicity properties of r_{\pm} from Lemma 2.3.3(d). Unsurprisingly, the most difficult part is controlling the period function on the first and last interval, i.e., near the turning points of the orbit. We start by analyzing T on the first interval:

Step 1: From $r_-(E, L)$ to $r_-(E - \varepsilon, L)$

Consider the formula for $\Delta(\Psi_L^2)$ in (2.58). From $6m < r$, $0 \leq p \leq \rho$, and $\mu' \geq 0$, we deduce

$$0 \leq \Delta(\Psi_L^2) = (\Psi_L^2)'' + \frac{4}{r}\Psi_L'\Psi_L,$$

and, as $\Psi_L' < 0$ on $[r_-(E, L), r_L[$, we obtain that Ψ_L^2 is convex on this interval. Hence, for every $\alpha \in [0, 1]$, we have

$$\begin{aligned} \Psi_L^2(\alpha r_-(E, L) + (1 - \alpha)r_-(E - \varepsilon, L)) &\leq (1 - \alpha)\Psi_L^2(r_-(E, L)) + \alpha\Psi_L^2(r_-(E - \varepsilon, L)) \\ &= (1 - \alpha)E^2 + \alpha(E - \varepsilon)^2 = E^2 + \alpha\varepsilon^2 - 2\alpha\varepsilon E. \end{aligned}$$

We choose

$$\alpha(r) = \frac{r - r_-(E, L)}{r_-(E - \varepsilon, L) - r_-(E, L)}, \quad r \in [r_-(E, L), r_-(E - \varepsilon, L)],$$

and obtain

$$E^2 - \Psi_L^2(r) \geq \alpha(r)(2\varepsilon E - \varepsilon^2) \geq \alpha(r)\varepsilon E,$$

since $E > e^{\mu(0)} > \varepsilon$ by choice of ε . With this result, we can estimate the first part of the period function via

$$\begin{aligned} \int_{r_-(E, L)}^{r_-(E - \varepsilon, L)} \frac{dr}{\sqrt{E^2 - \Psi_L^2(r)}} &\leq \int_{r_-(E, L)}^{r_-(E - \varepsilon, L)} \frac{dr}{\sqrt{\alpha(r)\varepsilon E}} \\ &= \frac{1}{\sqrt{\varepsilon E}} \int_{r_-(E, L)}^{r_-(E - \varepsilon, L)} \frac{\sqrt{r_-(E - \varepsilon, L) - r_-(E, L)}}{\sqrt{r - r_-(E, L)}} dr \\ &= 2 \frac{r_-(E, L) - r_-(E - \varepsilon, L)}{\sqrt{\varepsilon E}} \leq \frac{2R_{\max}}{\sqrt{\varepsilon E}}, \end{aligned} \quad (2.61)$$

where we have inserted the definition of $\alpha(r)$ and calculated the remaining integral.

Step 2: From $r_-(E - \varepsilon, L)$ to $r_+(E - \varepsilon, L)$

On $]r_-(E - \varepsilon, L), r_+(E - \varepsilon, L)[$, we have $\Psi_L(r) < E - \varepsilon$ by definition of r_{\pm} . Therefore,

$$\begin{aligned} \int_{r_-(E - \varepsilon, L)}^{r_+(E - \varepsilon, L)} \frac{dr}{\sqrt{E^2 - \Psi_L^2(r)}} &\leq \frac{r_+(E - \varepsilon, L) - r_-(E - \varepsilon, L)}{\sqrt{E^2 - (E - \varepsilon)^2}} \\ &\leq \frac{r_+(E - \varepsilon, L) - r_-(E - \varepsilon, L)}{\sqrt{\varepsilon E}} \leq \frac{R_{\max}}{\sqrt{\varepsilon E}}, \end{aligned} \quad (2.62)$$

because of $E > e^{\mu(0)} > \varepsilon$.

Step 3: From $r_+(E - \varepsilon, L)$ to $r_+(E, L)$

Unfortunately, we cannot deal with the last interval in (2.60) in the same way as the first one, since Ψ_L^2 is not necessarily convex there. We define

$$\gamma := \min_{[r_+(E-\varepsilon, L), r_+(E, L)]} (\Psi_L^2)' > 0,$$

which is positive because of the single-well structure and due to $r_L < r_+(E - \varepsilon, L)$. By the mean value theorem,

$$\Psi_L^2(r) \leq E^2 - \gamma(r_+(E, L) - r), \quad r \in [r_+(E - \varepsilon, L), r_+(E, L)],$$

gives rise to the estimate

$$\begin{aligned} \int_{r_+(E-\varepsilon, L)}^{r_+(E, L)} \frac{dr}{\sqrt{E^2 - \Psi_L^2(r)}} &\leq \frac{1}{\sqrt{\gamma}} \int_{r_+(E-\varepsilon, L)}^{r_+(E, L)} \frac{dr}{\sqrt{r_+(E, L) - r}} \\ &= 2 \frac{\sqrt{r_+(E, L) - r_+(E - \varepsilon, L)}}{\sqrt{\gamma}} \leq \frac{2\sqrt{R_{\max}}}{\sqrt{\gamma}}. \end{aligned} \quad (2.63)$$

We now aim at controlling γ independently from (E, L) . For this, we need the two limits

$$\begin{aligned} \lim_{(E, L) \rightarrow (E^0, 0)} r_+(E, L) &= R_{\max}, \\ \lim_{L \rightarrow 0} r_L &= 0, \end{aligned}$$

which were shown in Lemma 2.3.3(e) and Lemma 2.3.4(d). These limits imply that there exist $e^{\mu(0)} < \tilde{E}_1 < E^0$ and $0 < L_1 < L_{\max}$ such that¹⁰

$$r_+(E, L) \geq r_+(\tilde{E}_1, L_1) > r_{2L_1} > r_{L_1} \geq r_L, \quad \tilde{E}_1 > \Psi_L(r_L), \quad (2.64)$$

for every $(E, L) \in \tilde{\Omega}^{EL}$ with $\tilde{E}_1 \leq E < E^0$ and $0 < L \leq L_1$. The choice

$$E_1 := \frac{E^0 + \tilde{E}_1}{2}, \quad \varepsilon := \min\{e^{\mu(0)}, E^0 - E_1\}, \quad (2.65)$$

yields that for every $(E, L) \in \tilde{\Omega}^{EL}$ with $E_1 \leq E < E^0$ and $0 < L \leq L_1$, firstly, $E - \varepsilon \geq \tilde{E}_1$ and thus $r_+(E - \varepsilon, L) > r_{2L_1}$ from (2.64), and, secondly,

$$(\Psi_L^2)'(r) \geq (\Psi_{L_1}^2)'(r) \geq \min_{[r_{2L_1}, R_{\max}]} (\Psi_{L_1}^2)' > 0, \quad (2.66)$$

for every $r \in [r_+(E - \varepsilon, L), r_+(E, L)]$. The first estimate in (2.66) follows from the fact

¹⁰Here we also use that r_{\pm} and r_L are continuous from Lemma 2.3.3(c) and Lemma 2.3.4(a) as well as the corresponding monotonicity properties. In addition, we observe that $L \mapsto \Psi_L(r_L)$ is increasing and continuously differentiable, according to the chain rule.

that $(\Psi_L^2)'$ is decreasing in L since

$$\partial_L(\Psi_L^2)'(r) = 2e^{2\mu} \left(\frac{\mu'}{r^2} - \frac{1}{r} \right) \leq 0.$$

This derivative is non-positive because $\mu'(r)r \leq 1$ is equivalent to $4m \leq r$, which is valid due to assumption (2.59). Hence,

$$\gamma \geq \min_{[r_{2L_1}, R_{\max}]} (\Psi_{L_1}^2)'.$$

Note that ε —used also in the first and second steps—now only depends on E^0 , L_1 , and \tilde{E}_1 , and not on L anymore. In particular, $E - \varepsilon > \Psi_L(r_L)$ for all $E_1 \leq E < E^0$, $0 < L \leq L_1$ due to (2.64). To summarize, we merge (2.61), (2.62), and (2.63), the choice for ε , and the uniform estimate for γ in order to obtain

$$\begin{aligned} \int_{r_-(E,L)}^{r_+(E,L)} \frac{dr}{\sqrt{E^2 - \Psi_L^2(r)}} &\leq \frac{3R_{\max}}{\sqrt{\varepsilon E}} + \frac{2\sqrt{R_{\max}}}{\sqrt{\gamma}} \\ &\leq \frac{3R_{\max}}{\sqrt{E \min\{e^{\mu(0)}, E^0 - E_1\}}} + \frac{2\sqrt{R_{\max}}}{\sqrt{\min_{[r_{2L_1}, R_{\max}]} (\Psi_{L_1}^2)'}}. \end{aligned}$$

As per the definition of the period function in (2.44), we deduce the estimate claimed in the lemma. \square

We gather the previous results in one central proposition which establishes an upper bound on the possible periods of orbits appearing in the steady state. The fact that the bound is in some sense explicit will be used later when we analyze families of steady states in Chapter 3.

Proposition 2.3.16. *Consider a steady state of the Einstein-Vlasov system and define $Q := \max_{[R_{\min}, R_{\max}]} e^{\lambda - \mu}$. Then the following holds:*

- (a) *If $L_0 > 0$ and the steady state has strict single-well structure, the period function is bounded by*

$$T(E, L) \leq 2Q \left(\frac{4\sqrt{R_{\max}} + \sqrt{2}\pi}{\sqrt{a}} \right), \quad (E, L) \in \tilde{\Omega}^{EL},$$

where $a > 0$ is chosen according to $L_1 = L_0$ in Lemma 2.3.11.

- (b) *If the steady state is isotropic and satisfies*

$$\frac{2m(r)}{r} < \frac{1}{3}, \quad r > 0,$$

the period function is bounded by

$$T(E, L) \leq Q \max \left\{ 2 \left(\frac{4\sqrt{R_{\max}} + \sqrt{2}\pi}{\sqrt{a}} \right), \frac{\sqrt{6\pi}}{\min_{[0, R_1]} \sqrt{e^{2\mu+2\lambda}\rho}}, \right. \\ \left. \frac{6R_{\max}}{\sqrt{\min\{e^{\mu(0)}, E^0 - E_1\}}} + \frac{4\sqrt{R_{\max}}}{\sqrt{\min_{[r_{2L_1}, R_{\max}]} (\Psi_{L_1}^2)'}} \right\}$$

for $(E, L) \in \tilde{\Omega}^{EL}$, where the parameters L_1 and E_1 are given by Lemma 2.3.15, $R_1 = r_+(E_1, 0)$, and $a > 0$ is chosen according to L_1 in Lemma 2.3.11. We refer to Lemma 2.3.3(e) for the definition of $r_+(E_1, 0)$.

In both cases, the period function is bounded uniformly on $\tilde{\Omega}^{EL}$.

Proof. We observe that, in general,

$$T(E, L) \leq 2QE \int_{r_-(E, L)}^{r_+(E, L)} \frac{dr}{\sqrt{E - \Psi_L(r)} \sqrt{E + \Psi_L(r)}} \leq 2Q S(E, L).$$

Therefore, the claim in (a) follows from Lemma 2.3.11. For part (b), we use Lemma 2.3.15 in order to fix E_1 and L_1 and bound T on the set $\tilde{\Omega}^{EL} \cap \{E_1 \leq E < E^0\} \cap \{0 < L \leq L_1\}$. We can then apply Lemma 2.3.14 and Lemma 2.3.11 to obtain a bound for T on the sets $\tilde{\Omega}^{EL} \cap \{E \leq E_1\}$ and $\tilde{\Omega}^{EL} \cap \{L_1 \leq L\}$, respectively. We take the maximum over these bounds and arrive at the estimate for T . \square

2.3.5 Action-angle type variables

One of the main reasons why we deal with the concept of the single-well structure, is the goal of introducing so-called action-angle type variables similar to [47, Sc. 3.3] and [55, Sc. 5.1]. As described at the beginning of Section 2.3, we consider a steady state f of the Einstein-Vlasov system, and we prescribe that it has single-well structure, as stated in Definition 2.3.1.

For $(E, L) \in \tilde{\Omega}^{EL}$, let $(R, W) = (R, W)(\cdot, E, L)$ be the unique global solution to the characteristic system (2.42) with parameter L satisfying the initial condition $(R, W)(0, E, L) = (r_-(E, L), 0)$. As shown in Lemma 2.3.7, this solution is time-periodic with period $T(E, L) \in]0, \infty[$ and orbit $\mathcal{O}_{EL} = \{(r, w) \mid E(r, w, L) = E, \rho(r) > 0\}$. Now let

$$\tilde{\Omega} := \left\{ (r, w, L) \in \Omega \mid (E(r, w, L), L) \in \tilde{\Omega}^{EL} \right\}, \quad (2.67)$$

where Ω and $\tilde{\Omega}^{EL}$ are defined in (2.41) and (2.43), respectively. This point of view allows us to change variables from (r, w, L) to coordinates better adapted to the characteristic system.

Lemma 2.3.17. *Consider a steady state with single-well structure.*

(a) *For every $(r, w, L) \in \tilde{\Omega}$, there exists $\theta \in [0, 1[$ such that*

$$(r, w, L) = ((R, W)(\theta T(E, L), E, L), L),$$

where $E = E(r, w, L)$. *The change of variables*

$$\tilde{\Omega} \ni (r, w, L) \mapsto (\theta, E, L) \in [0, 1[\times \tilde{\Omega}^{EL} \quad (2.68)$$

is bijective.

(b) *For $(E, L) \in \tilde{\Omega}^{EL}$ and $r \in [r_-(E, L), r_+(E, L)]$, we call*

$$\theta(r, E, L) := \frac{E}{T(E, L)} \int_{r_-(E, L)}^r \frac{e^{\lambda(s) - \mu(s)}}{\sqrt{E^2 - \Psi_L^2(s)}} ds \in \left[0, \frac{1}{2}\right] \quad (2.69)$$

the angle function. For $(r, w, L) \in \tilde{\Omega}$, the variable θ from (a) is given by

$$\theta = \begin{cases} \theta(r, E(r, w, L), L), & \text{if } w \geq 0, \\ 1 - \theta(r, E(r, w, L), L), & \text{if } w < 0. \end{cases} \quad (2.70)$$

(c) *For $g \in L^1(\Omega)$, the identity*

$$\iiint_{\Omega} g(r, w, L) dr dw dL = \iint_{\tilde{\Omega}^{EL}} T(E, L) \int_0^1 e^{-\lambda(R(\theta T(E, L), E, L))} g(\theta, E, L) d\theta dE dL$$

holds, where $g(r, w, L) = g(\theta, E, L)$ under abuse of notation. Formally, integrals change via

$$dr dw dL = e^{-\lambda} T(E, L) d\theta dE dL. \quad (2.71)$$

Proof. For part (a), let $(r, w, L) \in \tilde{\Omega}$ and $E = E(r, w, L)$. We have $(r, w) \in \mathcal{O}_{EL}$, i.e., the pair lies in the orbit corresponding to the energy E and angular momentum L . The existence of $\theta \in [0, 1[$ thus follows from the characterization of \mathcal{O}_{EL} . Similarly, we deduce that the mapping in (2.68) is surjective. For its injectivity consider $(\theta, E, L), (\bar{\theta}, \bar{E}, \bar{L}) \in [0, 1[\times \tilde{\Omega}^{EL}$ such that

$$(r, w, L) := ((R, W)(\theta T(E, L), E, L), L) = ((R, W)(\bar{\theta} T(\bar{E}, \bar{L}), \bar{E}, \bar{L}), \bar{L}).$$

Then obviously $L = \bar{L}$ and $(r, w) \in \mathcal{O}_{EL} \cap \mathcal{O}_{\bar{E}L}$, which yields $E = E(r, w, L) = \bar{E}$ and thus $\theta = \bar{\theta}$, since $(R, W)(\cdot, E, L)$ is injective on $[0, T(E, L)[$. As to part (b), for fixed $(E, L) \in \tilde{\Omega}^{EL}$, the mapping

$$\left]0, \frac{1}{2}\right[\ni \theta \mapsto R(\theta T(E, L), E, L)$$

is continuously differentiable with derivative $T(E, L) \dot{R}(\theta T(E, L), E, L) > 0$, since

$\theta \in]0, \frac{1}{2}[$. By the inverse function theorem and the characteristic equation (2.42a), we get

$$\frac{\partial \theta}{\partial r}(r, E, L) = \frac{1}{T(E, L)} \frac{e^{\lambda(r) - \mu(r)} E}{\sqrt{E^2 - \Psi_L^2(r)}}, \quad r \in]r_-(E, L), r_+(E, L)[. \quad (2.72)$$

After integration in r and considering (E, L) as a function of (r, w, L) , we obtain (2.70) for $w \geq 0$. The case $w < 0$ follows analogously. The change of variables in (c) can be shown by first transforming from w to E via

$$\begin{aligned} \iiint_{\tilde{\Omega}} g(r, w, L) dr dw dL &= 2 \iiint_{\tilde{\Omega} \cap \{w \geq 0\}} g(r, w, L) dr dw dL \\ &= 2 \iint_{\tilde{\Omega}^{EL}} \int_{r_-(E, L)}^{r_+(E, L)} \frac{e^{-\mu(r)} E}{\sqrt{E^2 - \Psi_L^2(r)}} g\left(r, e^{-\mu(r)} \sqrt{E^2 - \Psi_L^2(r)}, L\right) dr dE dL \end{aligned}$$

and then changing from r to θ using (2.72). \square

To summarize, for a steady state f of the Einstein-Vlasov system with single-well structure, we call the variables (θ, E, L) introduced above the *action-angle type variables* corresponding to f . In particular, every function $g = g(r, w, L)$ can be written as

$$g(r, w, L) = g(\theta, E, L) \quad \text{for } (r, w, L) \in \tilde{\Omega},$$

under abuse of notation. The interpretation of these new variables is that the pair (E, L) —the “actions”—fixes an orbit of the characteristic flow of the steady state and θ —the “angle”—determines the position along this orbit. The underlying advantage from a mathematical point of view will become clear in Chapters 4, 5, and 6. The meaning of action-angle type variables is illustrated in Figure 2.2 for a fixed value of L .

Remark 2.3.18. (a) *As can be seen from (2.71), the change of variables*

$$\tilde{\Omega} \ni (r, w, L) \mapsto (\theta, E, L) \in [0, 1[\times \tilde{\Omega}^{EL}$$

is not volume preserving which would be the case for “true” action-angle variables [18, 70, 77]. This is why we call them action-angle “type” variables.

(b) *The sets Ω and $\tilde{\Omega}$, as well as*

$$\Omega^{EL} := \{(E(r, w, L), L) \mid (r, w, L) \in \Omega\} \quad (2.73)$$

and $\tilde{\Omega}^{EL}$ are equal up to sets of measure zero, respectively. This is the reason why it is sufficient to establish the change of variables on the (smaller) subsets. In fact, for circular orbits, i.e., where $E = \Psi_L(r_L)$, the notion of an angle variable breaks down since the corresponding orbit \mathcal{O}_{EL} is a singular point.

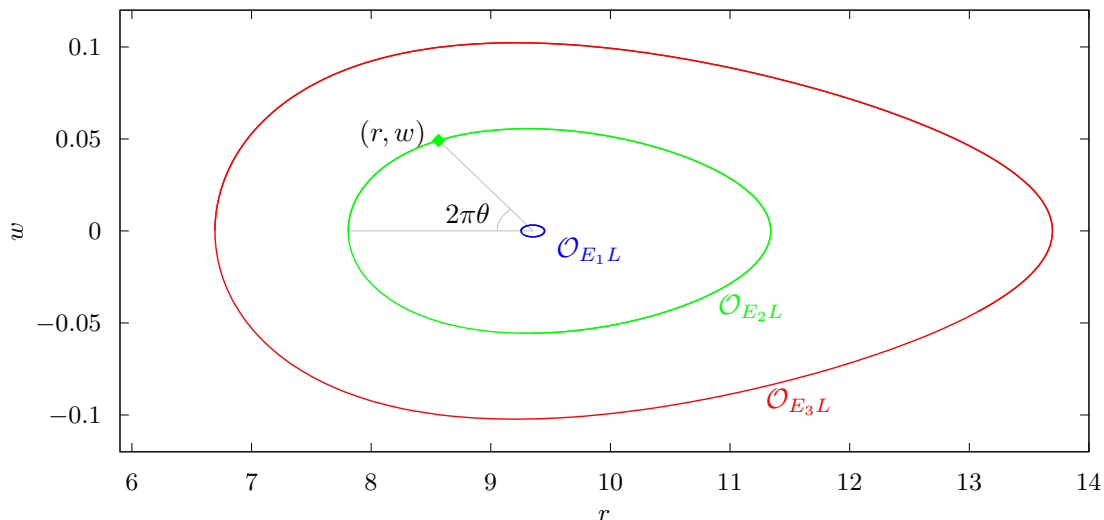


Figure 2.2: An illustration of the periodic orbits and the action-angle type variables for a stationary solution as in Section 2.2. The angular momentum $L > 0$ is fixed and the energies are chosen such that $\Psi_L(r_L) < E_1 < E_2 < E_3 < E^0$. For $E \rightarrow \Psi_L(r_L)$, the orbit becomes circular, while for $E \rightarrow E^0$ it has a more eccentric shape. Note that the illustrated angle $2\pi\theta$ is an approximation and not an analytical equality since θ is not linear.

2.3.6 A preliminary bound on $\frac{2m}{r}$

We close this section on a completely different issue compared to the previous results. At various points in our investigation we need to control the ratio $\frac{2m}{r}$, which yields an upper bound on the metric coefficient e^λ . It has long been conjectured that for stationary solutions to the Einstein-Vlasov system

$$\sup_{r>0} \frac{2m(r)}{r} < \frac{8}{9} \quad (2.74)$$

generally holds [5, 16], which can be interpreted as a type of Buchdahl inequality originally established for fluid spheres [26]. Indeed, in [16, Thm. 1] inequality (2.74) is shown to be valid under specific assumptions, e.g., for isotropic steady states. Numerical evidence in [16] also strongly indicated that it might hold true. In [4], it is shown that there exist steady states which come arbitrarily close to the ratio $\frac{8}{9}$, i.e., the bound should be sharp.

The main result from [5] establishes the bound (2.74), since there it is shown that

$$\sup_{r>0} \frac{2m(r)}{r} \leq \frac{(1 + 2\Theta)^2 - 1}{(1 + 2\Theta)^2}$$

holds for any static solution to the spherically symmetric Einstein equations, which

satisfies $p + 2q \leq \Theta\rho$, and $p, \rho, \geq 0$. Here, Θ is a non-negative constant. For the Einstein-Vlasov system, we have $0 \leq p + 2q \leq \rho$ and thus can choose $\Theta = 1$. This yields

$$\sup_{r>0} \frac{2m(r)}{r} \leq \frac{8}{9} \quad \text{and} \quad \sup_{r>0} e^{\lambda(r)} \leq 3 \quad (2.75)$$

for all stationary solutions considered in Section 2.2.

2.4 Numerical investigation

In order to gain a better understanding of the behavior of stationary solutions, as derived in Section 2.2, it is useful to investigate these equilibria numerically. Since most of the numerical work on the spherically symmetric Einstein-Vlasov system concerns the stability behavior of stationary solutions which we will deal with later in Chapter 7, we refer to that part of the work for a more detailed study of the numerical literature.

Let us quickly recall the results from Section 2.2. We prescribe an ansatz function Φ satisfying $(\Phi 1)$ and $(\Phi 2)$ such that the steady state is of the form

$$f(x, v) = \varphi(E, L) = \Phi \left(1 - \frac{E}{E_0} \right) (L - L_0)_+^l,$$

where $E^0 > 0$ is the cut-off energy, $L_0 \geq 0$ is a lower bound on the possible values of L in the steady state support, and $l > -\frac{1}{2}$. For these fixed parameters and every $\kappa > 0$, Proposition 2.2.4 proves the existence of a singularity-free, compactly supported stationary solution f_κ with finite mass, where $y = \ln(E^0) - \mu$ satisfies $y(0) = \kappa$. For equilibria surrounding a Schwarzschild black hole, we additionally prescribe a central mass $M_0 > 0$ and need to choose L_0 and $\kappa \in \mathbb{R}$ such that they satisfy (P1)–(P3). Proposition 2.2.10 then guarantees the existence of a compactly supported stationary solution f_κ with finite mass, where $y = \ln(E^0) - \mu$ satisfies $y(3M_0) = \kappa + \ln(\sqrt{3})$.

The conditions for Φ are not very restrictive, which allows for a large variety of possible ansatz functions. Common choices in the literature are the King model and the polytropes introduced in (2.4) and (2.5), respectively. A new family of ansatz functions is introduced in [48] by the author and colleagues. It is given as the piecewise linear function

$$\Phi_n(\eta) := \begin{cases} \frac{\eta}{10}, & \text{if } 0 < \eta \leq \frac{n}{1000}, \\ \frac{n-100000}{10n-10000} \eta + \frac{99n}{10n-10000}, & \text{if } \frac{n}{1000} < \eta, \\ 0, & \text{else,} \end{cases} \quad (2.76)$$

for $0 \leq n \leq 1000$ and we refer to these ansatz functions as the *piecewise model*. We only consider the isotropic case $L_0 = 0 = l$ when using the piecewise model. It is important to note that for $\eta < \frac{n}{1000}$ the ansatz $\Phi_n(\eta)$ is equal to the polytropic η_+^k with $k = 1$ up to a constant rescaling factor. The function is then continued by the unique straight line that connects the first part of the function continuously with the fixed value $\Phi_n(1) = 10$. We do not imply that these are physically relevant models arising in nature.

This family of models is selected primarily because of its novel characteristics and simple mathematical description. In particular, it exhibits unusual stability properties, as we will see in Chapter 7.

Once a model is prescribed, it is rather easy to numerically approximate stationary solutions. We simply solve the differential equation (2.6) by a radial midpoint method starting at the initial value $r = 0$ in the singularity-free case. In the setting with a singularity at the center, we solve (2.21) instead and start at $r = 3M_0$. In the process, we keep track of the quasi-local mass m . When we encounter a vacuum region, indicated by $e^{-y(r)}\sqrt{1 + \frac{L_0}{r^2}} > 1$, we can either cut-off the steady state there or search for another spatially separated shell. For our purposes, we always choose the former and thus do not study multi-shell solutions in this work.¹¹ Mathematically, this corresponds to multiplying the ansatz with an additional radial cut-off function at an appropriate radius. Note that this still yields a steady state of the Einstein-Vlasov system, as defined in Definition 2.1.1. Multi-shell solutions are extensively investigated numerically in [4, Sc. 3].

As a result of the calculation, we obtain an approximation on the metric coefficients λ , μ , as well as the (Vlasov-)mass M , cut-off energy E^0 , and number of particles N , see (1.36). We provide a pseudo-code of this algorithm in Appendix D.1.

2.4.1 General overview of macroscopic quantities

We begin by giving a general overview of the relevant macroscopic quantities of the singularity-free steady states under consideration. From [4, Thm. 2], it is known that for isotropic stationary solutions, the (R_{\max}, M) -relationship exhibits a spiraling behavior along the redshift κ , at least for large values of κ . This relation is plotted in Figure 2.3 for the isotropic King model, a polytropic shell model with $L_0 > 0$, as well as for the piecewise model introduced in (2.76) for $n = 90$. For the piecewise model, we notice that the behavior is radically different for small values of κ and a spiraling behavior only sets in after increasing κ sufficiently. The mass-radius relation is crucial for the related spherically symmetric Einstein-Euler system where matter is modeled as a perfect fluid. The work in [51] proves that linear stability of stationary solutions to the Einstein-Euler system may only change at “turning points” of the mass-radius spiral. Numerical evidence suggests that this is not the case for the Einstein-Vlasov system [45, 48].

Another important quantity is the so-called *binding energy* which was long thought of as an indicator for determining stability behavior, see Section 7.3.3 for a detailed discussion and the references there. The binding energy is defined as

$$E_b := \frac{N - M}{N} \tag{2.77}$$

and illustrated in Figure 2.4 for several models. Note that M includes only the Vlasov mass and not the mass of the central black hole M_0 , when considering shells with a

¹¹The research group with which the author is associated, is currently working on the study of solutions with multiple shells and it appears as if these arise quite naturally for shells surrounding a black hole.

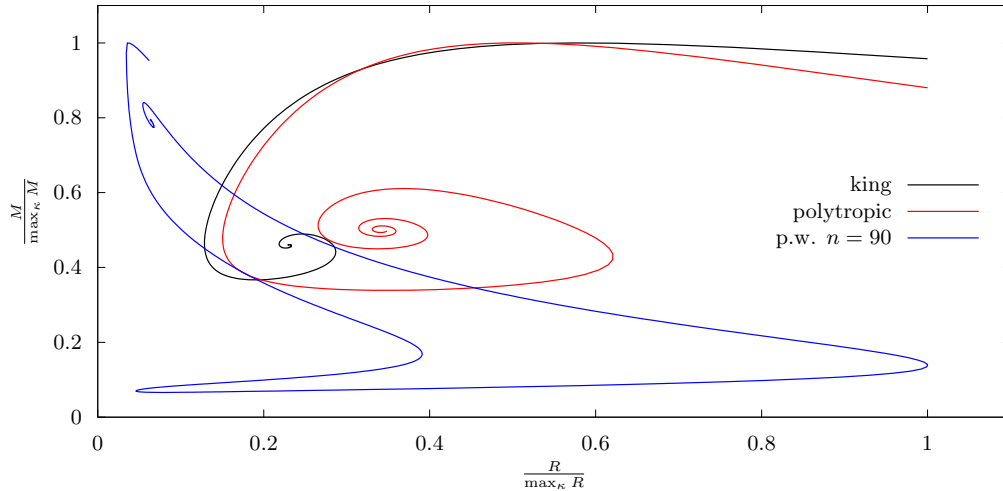


Figure 2.3: The relation of the ADM-mass M and the maximal radius R for the isotropic King model ($L_0 = 0 = l$), the polytropic model for $k = 1$, $l = 1$, and $L_0 = 0.05$, and the piecewise (p.w.) model for $n = 90$. The values of κ range from 0.05 to 4. For large values of κ , the relation of M and R approaches a limit in a spiraling form. We have normalized by dividing with the maximal mass and radius over all considered values of κ .

singularity at the center. For singularity-free equilibria, the binding energy always approaches zero for small values of κ , increases initially in κ , and eventually reaches a (local) maximum. After this, the behavior can be quite diverse. It can drop below zero and stay there (polytropic and king case), or resides close to the maximum and remain positive (p.w. $n = 270$ case), or decrease initially but develop a pronounced local maximum much later (p.w. $n = 90$ case).

As to the metric coefficients, Figure 2.5 shows e^μ , e^λ as well as the densities $4\pi r^2 \rho$, $4\pi r^2 p$ for the isotropic King model for a not too relativistic value of κ . We prefer this over plotting ρ and p , because it improves visibility. Moreover, we obtain insights over where the bulk of the mass of the steady state is located, as $4\pi r^2 \rho$ is the integrand of the quasi-local mass m . Since $4\pi r^2 p$ behaves similarly to $4\pi r^2 \rho$ and since e^λ can theoretically be obtained from $4\pi r^2 \rho$, we mainly choose to plot e^μ and $4\pi r^2 \rho$ in the following. By increasing the redshift value κ , the metric coefficients as well as the densities get more and more peaked, as illustrated in Figure 2.6. Adding an anisotropic part $L_0 > 0$ and $l \neq 0$ yields solutions that are bounded away from $r = 0$, as seen in Figure 2.7.

Stationary solutions obtained from the King model and polytropes behave quite similarly which is why we do not go into more detail for these ansatz functions. However, for the piecewise linear ansatz functions from (2.76), we obtain qualitatively different behavior, as already observed in [48]. The gradient difference for these piecewise linear ansatz functions implies that low energy particles, which are located near the center, can make the core extremely dense for larger values of κ . Around this dense center it is

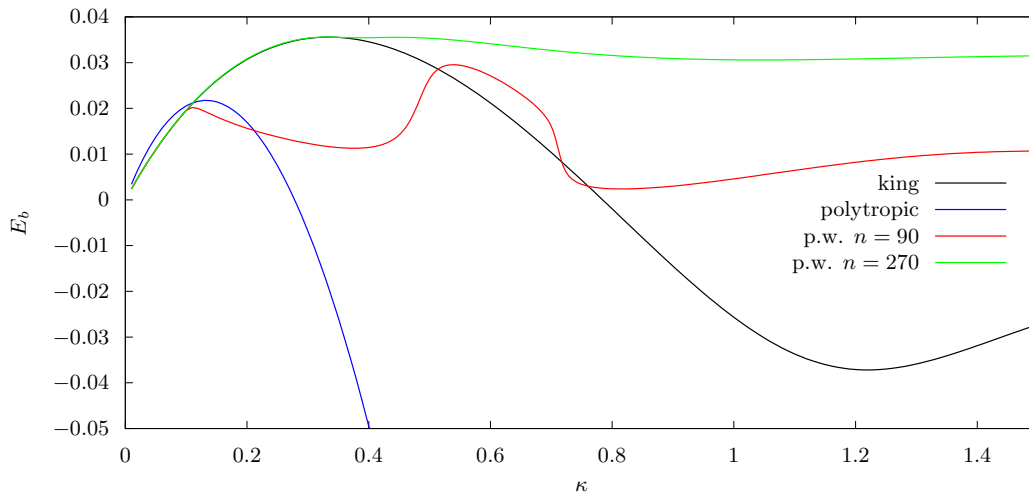


Figure 2.4: The binding energy E_b for the isotropic King model ($L_0 = 0 = l$), the polytropic model for $k = 1$, $l = 1$, and $L_0 = 0.05$, and the piecewise model for $n = 90$ and $n = 270$

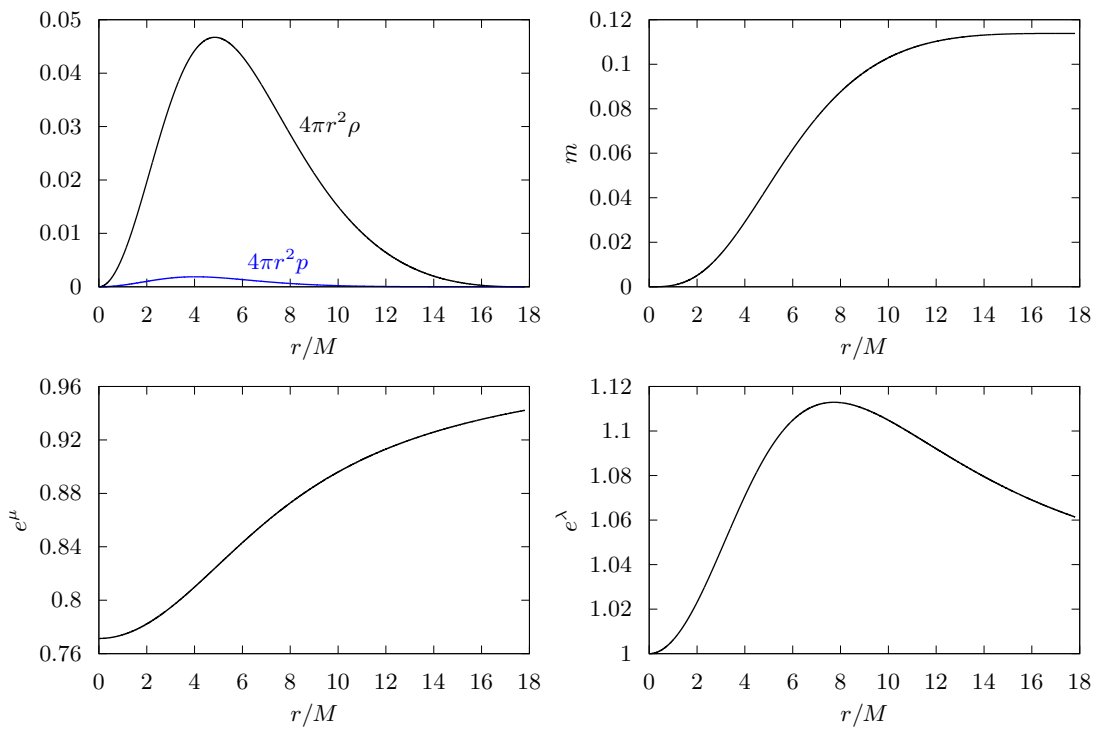


Figure 2.5: The densities $4\pi r^2\rho$, $4\pi r^2p$, the quasi-local mass m , and the metric coefficients e^μ , e^λ for the isotropic King model for $\kappa = 0.2$. The radius is given in multiples of the ADM-mass M to make it comparable to other models.

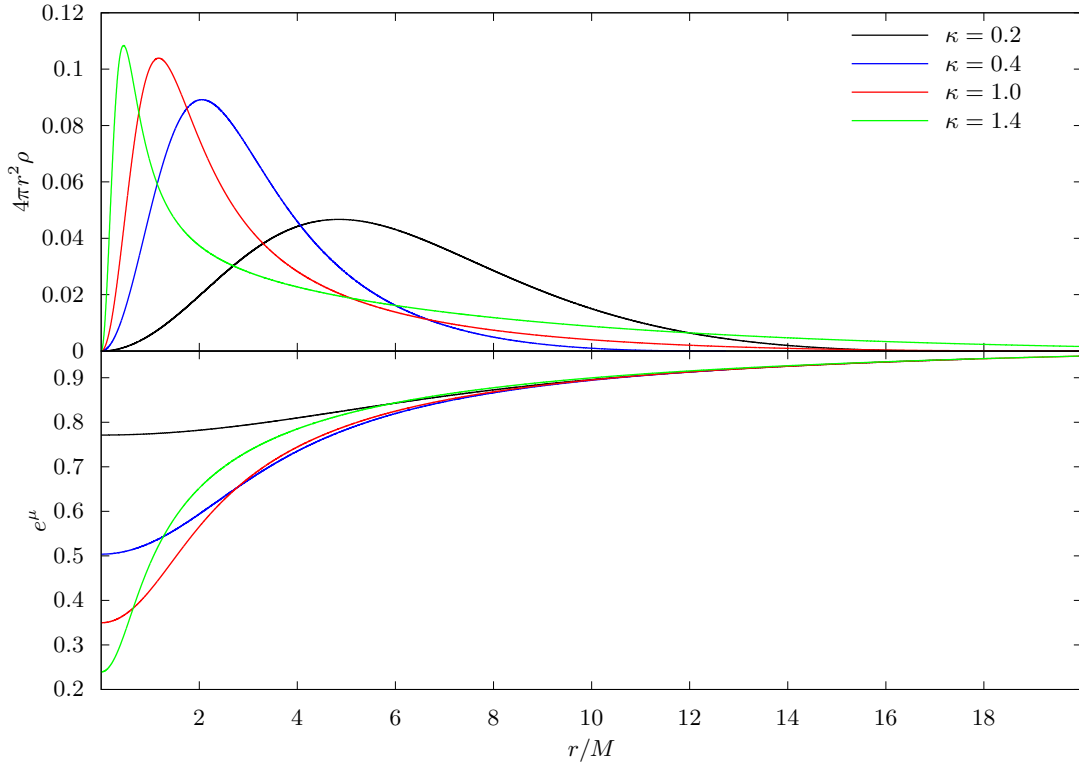


Figure 2.6: The weighted mass density $4\pi r^2 \rho$ and metric coefficient e^μ for the isotropic King model for different values of κ . The mass density peaks closer to $r = 0$ and $e^{\mu(0)}$ gets smaller rapidly. For better visibility, we have limited the plot to $r \leq 20M$.

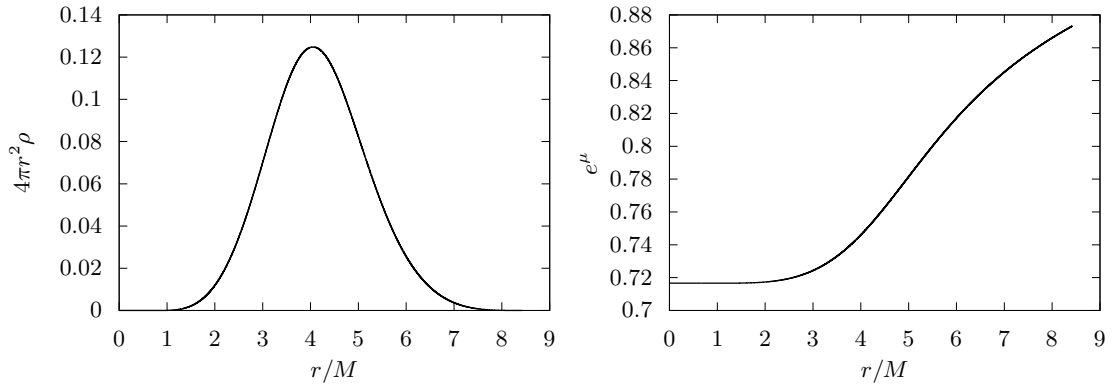


Figure 2.7: The weighted mass density $4\pi r^2 \rho$ and metric coefficient e^μ for an anisotropic polytrope with $k = 1$, $l = 1$, and $L_0 = 0.05$. For $0 < r < R_{\min}$, it holds that $\rho(r) = 0$ and $e^{\mu(r)} = e^{\mu(0)}$.

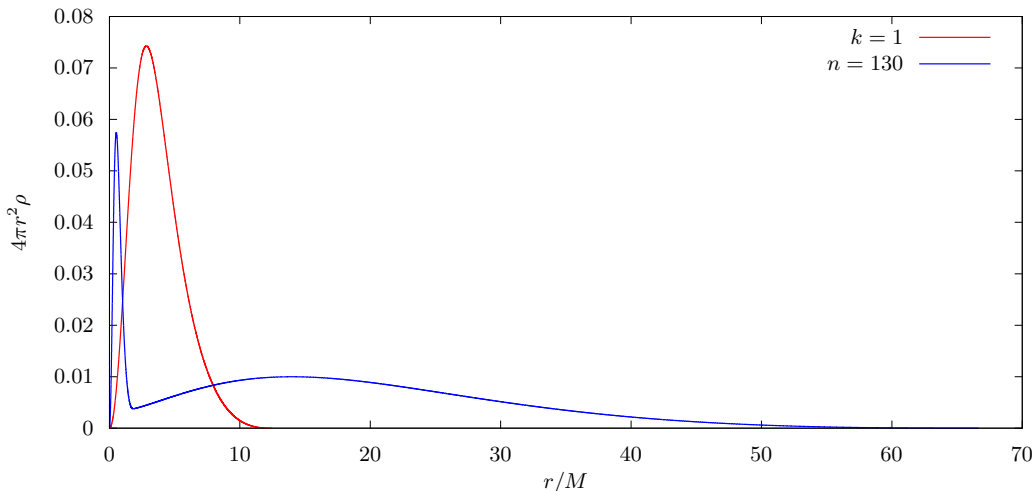


Figure 2.8: The weighted mass density $4\pi r^2 \rho$ of a *core-halo* configuration for $n = 130$ compared with the polytropic case $k = 1$ for the same value of $\kappa = 0.4$. We will see later that, numerically, the blue graph corresponds to a stable steady state and the red graph to an unstable one.

possible that a long tail of non-relativistic particles forms. This long tail is sometimes referred to as a *Newtonian halo* in the literature, cf. [21, 42]. An example of such a *core-halo* configuration is shown in Figure 2.8. These dense cores can have a stabilizing effect on the stationary solution, as discussed in [48].

For steady states surrounding a Schwarzschild black hole, the metric coefficients μ and λ go to $\mp\infty$, respectively, as $r \gtrsim 2M_0$. In fact, up to a constant, μ and λ equal the vacuum Schwarzschild metric for $2M_0 < r < R_{\min}$. The typical behavior of the metric coefficients compared to the vacuum Schwarzschild metric is depicted in Figure 2.9. The density ρ and the quasi-local mass m are qualitatively the same as in Figure 2.7. Note that we rescale the radial variable with the total mass

$$M_{\text{tot}} = M_0 + M,$$

where M is the Vlasov mass of the steady state.

If we reduce the central mass M_0 while keeping all other parameters fixed, the steady states eventually “converge” to the corresponding singularity-free shell with the same parameters. This is illustrated in Figure 2.10. However, note that this convergence might only be uniform on a compact subset of $]0, \infty[$, which contains the steady state supports, as μ and λ still diverge for $r \gtrsim 2M_0$ if $M_0 > 0$.

There are obviously many more limiting cases we could study. Recall that κ must fulfill $\Psi_{L_0}^0(r_{L_0}^0) < e^\kappa < \Psi_{L_0}^0(s_{L_0}^0)$, as demanded in (P3). In the case where $e^\kappa \gtrsim \Psi_{L_0}^0(r_{L_0}^0) < 1$, the radial support of the steady state radius is bounded as in (2.28) and the radial bound contracts to a point in this limit, i.e., the stationary solution is radially supported on

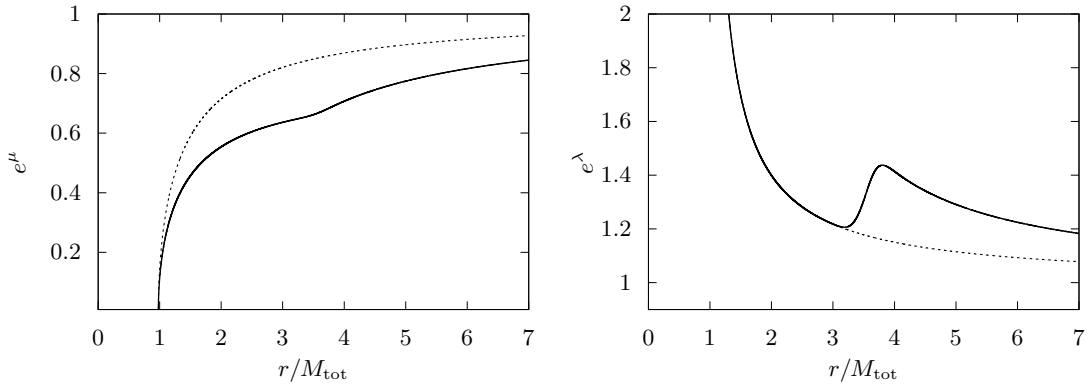


Figure 2.9: The metric coefficients e^μ and e^λ for a matter shell around a black hole with mass $M_0 = 1$ and parameters $k = 1$, $l = 1$, $L_0 = 30$, and $\kappa = 0.2$. The dashed lines correspond to the vacuum Schwarzschild case μ^0 and λ^0 . For $2M_0 < r < R_{\min}$, we have $\lambda = \lambda^0$.

smaller and smaller sets. The mass density also goes to zero in this case and we get the pure Schwarzschild metric in the limit. On the other hand, considering $e^\kappa \xrightarrow{\delta} \Psi_{L_0}^0(s_{L_0}^0)$ seems to yield a limiting non-trivial steady state. For a δ -family, as introduced in Definition 2.2.11, we have proven in Lemma 2.2.12 that the metric converges uniformly to the Schwarzschild metric as $\delta \rightarrow 0$. Therefore, letting $\delta \rightarrow 0$ or $\kappa \rightarrow \Psi_{L_0}^0(r_{L_0}^0)$ yields similar qualitative behavior.

2.4.2 Single-well structure, bounds on $\frac{2m}{r}$, and the period function

As we have seen in Section 2.3, the property of the steady state having strict single-well structure is of particular interest and difficult to obtain analytically. We were able to show the single-well structure in Propositions 2.3.5 and 2.3.6, for not too relativistic isotropic steady states and for small matter shells around a black hole, respectively. It would be desirable to verify the strict single-well structure for a larger class of stationary solutions. Luckily, we can quite easily test for this numerically.

As the strict single-well structure is known to be false for some static shells [104], we limit the analysis to isotropic steady states. Moreover, our goal is to numerically verify the assumptions needed for the investigation in Chapter 6, which is only carried out for isotropic steady states, as constructed in Section 2.2.1. We numerically test for the strict single-well structure in three steps:

1. We check for

$$\Gamma := \sup_{r \in]0, \infty[} \frac{2m}{r} < \frac{1}{3},$$

which is sufficient for the strict single-well structure as per Proposition 2.3.5. Note that we only need to check the supremum over the finite interval $]0, R_{\max}]$.

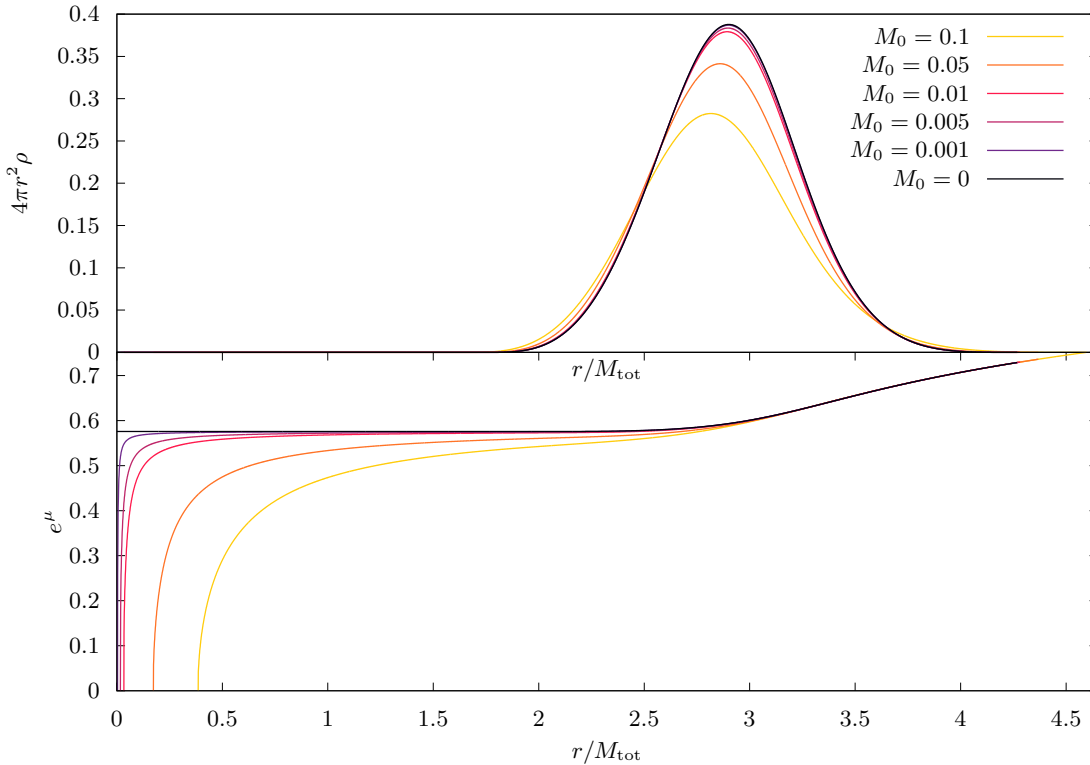


Figure 2.10: The mass density $4\pi r^2 \rho$ and metric coefficient e^μ for a static polytropic shell with $k = 1$, $l = 1$, $L_0 = 1$, $\kappa = 0.1$, surrounding a central black hole of different masses M_0 . The case $M_0 = 0$ corresponds to the singularity-free setting.

2. If the first step fails, we numerically check for a strict, unique minimum of the effective potential Ψ_L for $L \in [0, L_{\max}]$ on a discrete L -grid.
3. If the second step fails for some $L \in [0, L_{\max}]$, we output Ψ_L on the radial grid and check for the strict single-well structure by direct inspection. This happens only for large values of κ and is mainly due to numerical errors.

We summarize our findings in the following remark.

Remark 2.4.1. *Across all isotropic equilibria which we have studied through the three-step procedure described above, we find that the strict single-well structure is always valid, even for large values of κ . More precisely, we have checked the king model (2.4), isotropic polytropes (2.5) for various values of $0 \leq k \leq \frac{3}{2}$, and the piecewise model (2.76) for $n = 1, \dots, 1000$. The values of κ were chosen equidistantly in the interval $[0.05, 4]$. A reasonable conjecture is thus that the strict single-well structure holds for every isotropic steady state of the Einstein-Vlasov system, as derived in Section 2.2.1.¹² New*

¹²Note that all these models have in common that $\partial_E \varphi < 0$. However, we have also considered some

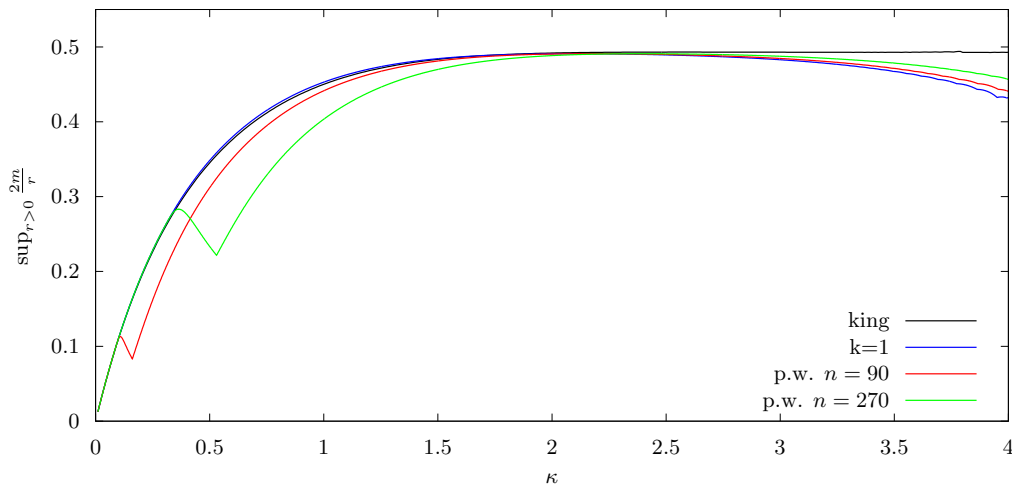


Figure 2.11: The value of $\sup_{r>0} \frac{2m}{r}$ for the isotropic King model, the isotropic polytropes for $k = 1$, and the piecewise model for $n = 90$ and $n = 270$.

techniques are required to analytically prove this hypothesis. The central problem consists of appropriately processing the pointwise terms arising from ρ and p together with the non-local terms μ and λ .

As we had to keep track of Γ in the preceding investigation, we illustrate another interesting property associated with isotropic steady states which we observe numerically.

Remark 2.4.2. *The models mentioned in Remark 2.4.1 all satisfy $\Gamma < \frac{1}{2}$. We conjecture that this holds for general isotropic steady states. As with the strict single-well structure, the analytical proof of this is an open problem. In [16, Thm. 1], it is shown that isotropic equilibria satisfy $\Gamma < \frac{8}{9}$, but our numerical evidence proposes that this bound is not sharp.*

We illustrate the values of Γ in Figure 2.11 for various models. The maximal values Γ_{\max} of Γ along families of steady states are listed in Table 2.1, where we also provide the minimal value of κ for which $\Gamma = \frac{1}{3}$ holds and denote this value as κ_{sws} . The value κ_{sws} is of interest in light of Proposition 2.3.5. The supremum Γ tends to get larger as κ increases. However, for the piecewise models in particular we observe that Γ decreases for relatively small κ . We speculate that this is tightly connected to the unusual stability behavior of these models which we study in Chapter 7. This also leads to κ_{sws} being larger compared to the polytropes or the king model, as shown in Table 2.1.

Closely related to the single-well structure is, of course, the period function T , which we examined in detail in Section 2.3. Especially the boundedness of the period function was of interest, and we could only show that it is bounded from above and below for isotropic steady states with $\Gamma < \frac{1}{3}$ as well as small shells surrounding a black hole, see

other piecewise models not introduced in this work, which have $\partial_E \varphi \geq 0$ on some interval(s). The strict single-well structure seems to hold there as well.

model	king	$k = \frac{1}{2}$	$k = 1$	$k = \frac{3}{2}$	$n = 90$	$n = 130$	$n = 270$
κ_{sWS}	0.467	0.406	0.459	0.509	0.552	0.596	0.762
Γ_{max}	0.494	0.494	0.491	0.493	0.491	0.491	0.491

Table 2.1: The approximate values κ_{sWS} and Γ_{max} along families of steady states. We consider the isotropic king model, polytropes for $k \in \{\frac{1}{2}, 1, \frac{3}{2}\}$, and the piecewise model for $n \in \{90, 130, 270\}$.

Sections 2.3.3 and 2.3.4. A numerical investigation of the boundedness of the period function is much more computationally expensive since we either have to calculate the integral (2.44) explicitly or approximate solutions to the characteristic system (2.42) on an appropriate grid in $(E, L) \in \Omega^{EL}$. We choose the latter approach and obtain $T(E, L)$ by keeping track of the time that elapses as characteristics travel from $r_-(E, L)$ to $r_+(E, L)$. This yields half of the period $T(E, L)$. The period function and the set Ω^{EL} is illustrated in Figure 2.12 for the king model and a static shell with a Schwarzschild singularity at the center.

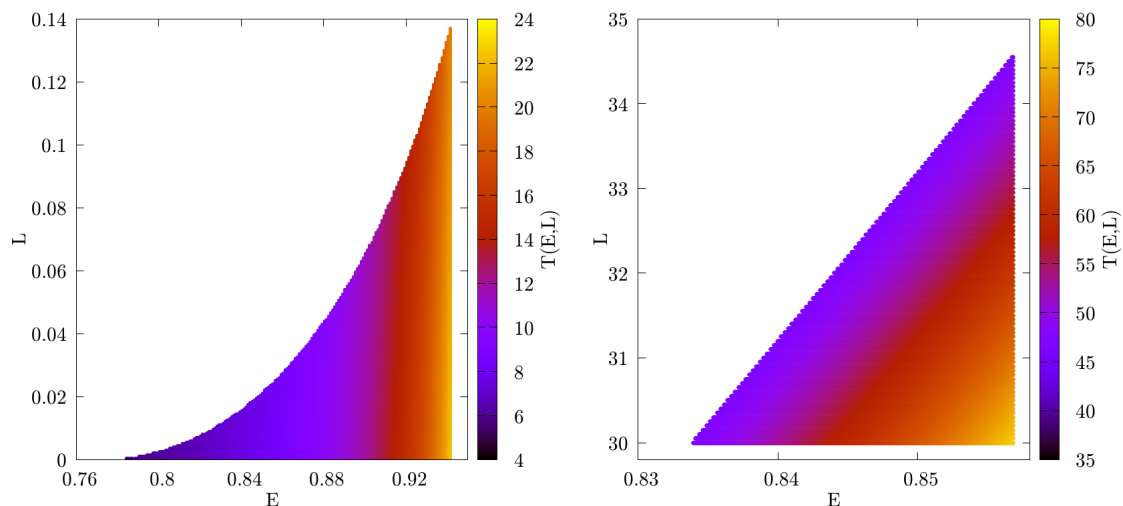


Figure 2.12: The set Ω^{EL} and the period function (color gradient) for the isotropic King model with $\kappa = 0.2$ on the left-hand side, and a polytropic steady state surrounding a Schwarzschild black hole of mass $M_0 = 1$ with parameters $k = 1$, $l = 1$, $L_0 = 30$, and $\kappa = 0.1$ on the right-hand side.

Remark 2.4.3. (i) For every isotropic stationary solution considered, numerical evidence suggests that the period function is bounded from above and away from zero. Due to limited computational resources, this study was only carried out for a subset of the models mentioned in Remark 2.4.1.

(ii) In Remark 2.3.13(b), we claimed that the case $L_0 = 0$ and $l > 0$ leads to an unbounded period function. We provide numerical evidence for this in Table 2.2, where we consider ever smaller values for L_0 for otherwise fixed parameters. This leads to an exploding period function as L_0 approaches zero. In fact, we observe that the supremum over T is reached as E and L both decrease, as claimed in Remark 2.3.13(b). Note, however, that this is quite delicate numerically.

L_0	10^{-2}	10^{-3}	10^{-4}	10^{-5}	10^{-6}	10^{-7}	10^{-8}
$\sup_{(E,L) \in \Omega^{EL}} T(E, L)$	22.0	31.0	43.3	62.3	89.4	124.2	188.1

Table 2.2: The approximate value of the supremum over the period function depending on the parameter L_0 for the polytropic model with $k = 1$, $l = 1$, and $\kappa = 0.2$.

We could, of course, put more effort into the numerical investigation and we are certain that there are still many interesting aspects to be discovered. For example, we could take a closer look at the period function for static shells with or without singularity, or investigate multiple, disjoint shells for some kind of “separated”-well structure. We leave this prospect open for future research.

3 Parameter dependence for steady state families

Some people want it to happen,
some wish it would happen,
others make it happen.

Michael Jordan

After dealing with individual steady states in the previous chapter, we now investigate families of stationary solutions. We consider a κ -family of steady states $(f_\kappa)_{\kappa>0}$ to the singularity-free Einstein-Vlasov system which is parametrized by the redshift κ , as defined in Definition 2.2.5.

We limit the analysis to this type of family but mention that analogous results can be shown for several types of families that might be constructed from the general existence theory in Proposition 2.2.4 and Proposition 2.2.10 as long as the parametrization of the family is in some sense regular. Therefore, the next subsections should rather serve as a blueprint and do not make heavy use of the explicit structure of the parametrization via κ . In particular, similar results hold for the δ -family introduced in Definition 2.2.11.

The main objective of this chapter is to show convergence and continuity results for relevant quantities, e.g., the metric components, the steady state support, the period function, etc., in the parameter κ .¹ In Section 3.1, we prove continuous differentiability of the metric coefficients and source terms. For further properties, we need to prescribe the strict single-well structure. This allows us to show in Section 3.2 that the period function is uniformly bounded and continuous. The results will be essential in Chapter 6, where we derive the existence of oscillating solutions from a continuity argument.

As in Definition 2.2.5, every quantity arises from a steady state f_κ with $\kappa > 0$ is from now on denoted by a subscript κ , e.g., μ_κ , m_κ , ρ_κ , and so forth. As an important notational artifact, we emphasize that E_κ corresponds to the energy

$$E_\kappa(r, w, L) = e^{\mu_\kappa(r)} \sqrt{1 + w^2 + \frac{L}{r^2}},$$

whereas E^κ is the cut-off energy corresponding to f_κ .

¹The reader should be warned that the following investigation will be very technical and can be omitted if the details are not of interest. Summarized in one sentence: Everything works out as expected in the sense that continuity and differentiability hold where desired.

3.1 Metric coefficients and source terms along the redshift

As a first step, we deduce that the quantities y_κ , ρ_κ , p_κ , and m_κ are uniformly continuous in κ for compact subsets in the radial variable r .²

Lemma 3.1.1. *Let $\eta > 0$ and $R > 0$. There exists $C > 0$ such that for every $\kappa > 0$ with $|\kappa - \eta| \leq 1$ and $r \in [0, R]$, it holds that*

$$\begin{aligned} |y_\kappa(r) - y_\eta(r)| &\leq C|\kappa - \eta|, \\ |y'_\kappa(r) - y'_\eta(r)| &\leq Cr^{2l}|\kappa - \eta|, \\ |m_\kappa(r) - m_\eta(r)| &\leq Cr^{2l+3}|\kappa - \eta|, \\ |\rho_\kappa(r) - \rho_\eta(r)|, |p_\kappa(r) - p_\eta(r)| &\leq Cr^{2l}|\kappa - \eta|. \end{aligned}$$

In particular, the functions

$$]0, \infty[^2 \ni (\kappa, r) \mapsto y_\kappa(r), y'_\kappa(r), m_\kappa(r), \rho_\kappa(r), p_\kappa(r),$$

are continuous.

Proof. The main idea of the proof is to employ Gronwall's inequality in order to control $|y_\kappa - y_\eta|$. Fix $\eta, R > 0$ and let $\kappa > 0$ with $|\kappa - \eta| \leq 1$ and $r \in [0, R]$ be arbitrary. Equation (2.6) and the triangle inequality yield

$$\begin{aligned} &|y'_\kappa(r) - y'_\eta(r)| \\ &\leq \left| \frac{1}{1 - \frac{2m_\kappa}{r}} \left| \frac{m_\kappa - m_\eta}{r^2} + 4\pi r(p_\kappa - p_\eta) \right| + \left| \frac{m_\kappa - m_\eta}{(1 - \frac{2m_\kappa}{r})(1 - \frac{2m_\eta}{r})} \right| \left| \frac{2m_\eta}{r^3} + 8\pi p_\eta \right| \right|. \end{aligned}$$

We apply the estimate (2.75) for $e^{2\lambda} = (1 - \frac{2m}{r})^{-1}$ and obtain

$$|y'_\kappa(r) - y'_\eta(r)| \leq C \left(\frac{1}{r^2} |m_\kappa(r) - m_\eta(r)| + r |p_\kappa(r) - p_\eta(r)| + \frac{1}{r} |m_\kappa(r) - m_\eta(r)| \right). \quad (3.1)$$

The constant $C > 0$ may change from line to line but remains independent of κ and r . We treat the terms on the right hand side of (3.1) separately. First, we note that the functions G and H from (2.7) and (2.8) are independent of κ . From $\rho_\kappa(r) = G(r, y_\kappa(r))$ and $y_\kappa(r) \leq \kappa \leq \eta + 1$, we get³

$$\begin{aligned} |m_\kappa(r) - m_\eta(r)| &\leq 4\pi \int_0^r s^{2+2l} \left\| s^{-2l} \partial_y G \right\|_{L^\infty([0, \eta+1] \times [0, R])} |y_\kappa(s) - y_\eta(s)| ds \\ &\leq Cr^{2l+2} \int_0^r |y_\kappa(s) - y_\eta(s)| ds \end{aligned} \quad (3.2)$$

²As a reminder, y_κ is the solution of (2.6) with $y(0) = \kappa$.

³Recall that y_κ is monotonically decreasing and $y_\kappa(0) = \kappa$.

by the mean value theorem and Lemma 2.2.2. A similar argument for $p_\kappa(r) = H(r, y_\kappa(r))$ yields

$$|p_\kappa(r) - p_\eta(r)| \leq Cr^{2l} |y_\kappa(r) - y_\eta(r)|. \quad (3.3)$$

Inserting this into (3.1) therefore implies

$$|y'_\kappa(r) - y'_\eta(r)| \leq Cr^{2l} \sup_{s \in [0, r]} |y_\kappa(s) - y_\eta(s)|, \quad (3.4)$$

and after integration

$$\sup_{[0, r]} |y_\kappa - y_\eta| \leq |\kappa - \eta| + C \int_0^r s^{2l} \sup_{[0, s]} |y_\kappa - y_\eta| ds.$$

We apply Gronwall's inequality to obtain

$$|y_\kappa(s) - y_\eta(s)| \leq C|\kappa - \eta|, \quad 0 \leq s \leq r,$$

since $l > -\frac{1}{2}$, which together with the previous estimates (3.2), (3.3), and (3.4) finishes the proof. \square

We need to show that $r_{\kappa, \pm}$, $R_{\kappa, \max}$, $R_{\kappa, \min}$, etc. are continuous in κ as well.⁴ Since these quantities are all given implicitly through the solution of an equation, i.e., as solutions of $\Psi_{\kappa, L} = E$ for suitable values E and L , we aim to employ the implicit function theorem. For this, however, we first need to show that the functions from the previous lemma are also continuously differentiable with respect to κ . It is convenient to first consider the differentiability of y_κ in κ , but we cannot simply argue with theorems from ordinary differential equations. We therefore formally derive and solve an equation that $\partial_\kappa y_\kappa$ has to fulfill if it exists. It then follows a-posteriori that the solution of said equation is indeed $\partial_\kappa y_\kappa$.

We write z_κ instead of $\partial_\kappa y_\kappa$, of which we do not yet know if it exists. By formally taking the derivative of (2.6) with respect to κ , we get

$$z'_\kappa = -\frac{2\tilde{m}_\kappa}{r\left(1 - \frac{2m_\kappa}{r}\right)^2} \left(\frac{m_\kappa}{r^2} + 4\pi r p_\kappa \right) - \frac{1}{1 - \frac{2m_\kappa}{r}} \left(\frac{\tilde{m}_\kappa}{r^2} + 4\pi r \tilde{p}_\kappa \right), \quad z_\kappa(0) = 1, \quad (3.5)$$

where

$$\tilde{m}_\kappa(r) = 4\pi \int_0^r s^2 \partial_y G(s, y_\kappa(s)) z_\kappa(s) ds, \quad (3.6)$$

$$\tilde{p}_\kappa(r) = \partial_y H(r, y_\kappa(r)) z_\kappa(r), \quad (3.7)$$

for $r > 0$. In the end, we will show that $\tilde{m}_\kappa = \partial_\kappa m_\kappa$ and $\tilde{p}_\kappa = \partial_\kappa p_\kappa$. Next, we solve this system of equations with techniques similar to the ones employed for solving (2.6).

⁴ $r_{\kappa, \pm}$ correspond to the radii which are defined in Lemma 2.3.3(b) and require the single-well structure. We deal with these issues later.

Lemma 3.1.2. *For every $\kappa > 0$, there exists a unique $z_\kappa \in C^1([0, \infty[)$, which solves (3.5)–(3.7). Moreover, the function*

$$]0, \infty[^2 \ni (\kappa, r) \mapsto z_\kappa(r)$$

is continuous.

Proof. Since the first part of the proof works for fixed $\kappa > 0$, we drop the index to lighten the notation. We rewrite (3.5) by inserting (3.6) and (3.7) via

$$z' = -\frac{a(r)}{r^2} \int_0^r s^2 \partial_y G(s, y(s)) z(s) ds - b(r) r \partial_y H(r, y(r)) z(r), \quad z(0) = 1, \quad (3.8)$$

where we have abbreviated

$$a(r) := \frac{4\pi}{1 - \frac{2m(r)}{r}} \left(\frac{\frac{2m(r)}{r} + 8\pi r^2 p(r)}{1 - \frac{2m(r)}{r}} + 1 \right), \quad b(r) := \frac{4\pi}{1 - \frac{2m(r)}{r}}, \quad (3.9)$$

which are positive and bounded by (2.75). We integrate (3.8) and obtain the integral equation

$$z(r) = 1 - \int_0^r \left(\frac{a(s)}{s^2} \int_0^s \sigma^2 \partial_y G(\sigma, y(\sigma)) z(\sigma) d\sigma + b(s) s \partial_y H(s, y(s)) z(s) \right) ds, \quad r \geq 0. \quad (3.10)$$

The existence of a local solution $z \in C^1([0, \delta])$ for $\delta > 0$ small enough now follows from a standard contraction argument which makes use of the fact that $s \partial_y G(s, y)$ and $s \partial_y H(s, y)$ are bounded⁵ on $[0, \delta] \times [0, \kappa]$. On $[\frac{\delta}{2}, \infty[$, equation (3.8) can be written as a two-dimensional ODE system with a linear right-hand side since H is twice continuously differentiable, according to Lemma 2.2.2. Therefore, the solution z can be extended uniquely to $[0, \infty[$.

It remains to show that z is continuous in κ . We reintroduce the index κ and fix $\eta, R > 0$. For every $\kappa > 0$ with $|\kappa - \eta| < \delta$, we have

$$\begin{aligned} |z_\kappa(r) - z_\eta(r)| &\leq \int_0^r |z'_\kappa(s) - z'_\eta(s)| ds \\ &\leq \int_0^r \left(|a_\kappa(s) - a_\eta(s)| \frac{|\tilde{m}_\eta(s)|}{4\pi s^2} + |a_\kappa(s)| \frac{|\tilde{m}_\kappa(s) - \tilde{m}_\eta(s)|}{4\pi s^2} \right. \\ &\quad \left. + |b_\kappa(s) - b_\eta(s)| |s \tilde{p}_\eta(s)| + |b_\kappa(s)| |s \tilde{p}_\kappa(s) - \tilde{p}_\eta(s)| \right) ds, \end{aligned} \quad (3.11)$$

where a_κ and b_κ are defined as in (3.9). The Buchdahl-type inequality (2.75) together

⁵Recall Lemma 2.2.2 for properties of G and H and use $s \partial_y G = s^{1+2l} s^{-2l} \partial_y G$ as well as $l > -\frac{1}{2}$. This lemma also yields that solving (3.8) is equivalent to solving (3.10).

with Lemma 3.1.1 yields that

$$|a_\kappa(s) - a_\eta(s)|, |b_\kappa(s) - b_\eta(s)| < \varepsilon, \quad s \in [0, R], \quad (3.12)$$

for $\delta > 0$ small enough. Furthermore, $\|s^{-2l}\partial_y G\|_{L^\infty([0,R]\times[0,\kappa])} \leq C$ follows from Lemma 2.2.2, where $C > 0$ is a constant that may depend on R, η and can change from line to line. This implies

$$|\tilde{m}_\eta(s)| \leq C \int_0^s \sigma^{2+2l}|z_\eta(\sigma)| d\sigma \leq Cs^{3+2l}, \quad s \in [0, R], \quad (3.13)$$

and, by the same argument for $\partial_y H$, we get $|s\tilde{p}_\eta(s)| \leq Cs^{1+2l}$. In addition, $|a_\kappa(s)| + |b_\kappa(s)| \leq C$ for $s \in [0, R]$, if $\delta > 0$ is small. Since $\sigma^{-2l}\partial_y G$ is uniformly continuous on $[0, R] \times [0, \eta + 1]$ and $l > -\frac{1}{2}$, we get

$$\begin{aligned} \frac{|\tilde{m}_\kappa(s) - \tilde{m}_\eta(s)|}{s^2} &\leq C \int_0^s |\partial_y G(\sigma, y_\kappa(\sigma))z_\kappa(\sigma) - \partial_y G(\sigma, y_\eta(\sigma))z_\eta(\sigma)| d\sigma \\ &\leq C \int_0^s \left| \sigma^{-2l}\partial_y G(\sigma, y_\kappa(\sigma)) - \sigma^{-2l}\partial_y G(\sigma, y_\eta(\sigma)) \right| \sigma^{2l}|z_\eta(\sigma)| d\sigma \\ &\quad + C \int_0^s \left| \sigma^{-2l}\partial_y G(\sigma, y_\kappa(\sigma)) \right| \sigma^{2l}|z_\kappa(\sigma) - z_\eta(\sigma)| d\sigma \\ &\leq C\varepsilon + C \int_0^s \sigma^{2l}|z_\kappa(\sigma) - z_\eta(\sigma)| d\sigma \end{aligned} \quad (3.14)$$

for $s \in [0, R]$. Similarly, we obtain

$$s|\tilde{p}_\kappa(s) - \tilde{p}_\eta(s)| \leq C\varepsilon + Cs^{1+2l}|z_\kappa(s) - z_\eta(s)|, \quad s \in [0, R]. \quad (3.15)$$

By putting the bounds above as well as (3.12)–(3.15) into (3.11) and again using $l > -\frac{1}{2}$, we deduce

$$\sup_{[0,r]} |z_\kappa - z_\eta| \leq C\varepsilon + C \int_0^r \sup_{[0,s]} |z_\kappa - z_\eta| ds, \quad r \in [0, R],$$

which—via Gronwall’s inequality—implies

$$|z_\kappa(r) - z_\eta(r)| \leq C\varepsilon, \quad r \in [0, R],$$

for every $\kappa > 0$ with $|\kappa - \eta| < \delta$, i.e., we have continuity in κ . □

With the solution z_κ of (3.5) at hand, we can prove that $\kappa \mapsto y_\kappa$ is differentiable with continuous derivative z_κ .

Lemma 3.1.3. For $r \in [0, \infty[$, the function

$$]0, \infty[\ni \kappa \mapsto y_\kappa(r)$$

is continuously differentiable with $\partial_\kappa y_\kappa(r) = z_\kappa(r)$.

Proof. The proof is structurally similar to the proof of the continuity of z_κ in Lemma 3.1.2. Fix $R > 0$ and $r \in [0, R]$. Let $\kappa > 0$ and $h \in [-1, 1] \setminus \{0\}$ with $\kappa + h > 0$. First, we estimate

$$\begin{aligned} \left| \frac{y_{\kappa+h}(r) - y_\kappa(r)}{h} - z_\kappa(r) \right| &= \left| \frac{\kappa + h - \kappa}{h} + \int_0^r \frac{y'_{\kappa+h}(s) - y'_\kappa(s)}{h} ds - 1 - \int_0^r z'_\kappa(s) ds \right| \\ &\leq \int_0^r \left| \frac{y'_{\kappa+h}(s) - y'_\kappa(s)}{h} - z'_\kappa(s) \right| ds. \end{aligned} \quad (3.16)$$

According to (2.6) and (3.5)–(3.7), we obtain

$$\begin{aligned} &\left| \frac{y'_{\kappa+h}(s) - y'_\kappa(s)}{h} - z'_\kappa(s) \right| \\ &= \left| \frac{1}{h} \left[\frac{1}{1 - \frac{2m_{\kappa+h}(s)}{s}} \left(\frac{m_{\kappa+h}(s)}{s^2} + 4\pi s p_{\kappa+h}(s) \right) - \frac{1}{1 - \frac{2m_\kappa(s)}{s}} \left(\frac{m_\kappa(s)}{s^2} + 4\pi s p_\kappa(s) \right) \right] \right. \\ &\quad \left. - \frac{2\tilde{m}_\kappa(s)}{s \left(1 - \frac{2m_\kappa(s)}{s} \right)^2} \left(\frac{m_\kappa(s)}{s^2} + 4\pi s p_\kappa(s) \right) - \frac{1}{1 - \frac{2m_\kappa(s)}{s}} \left(\frac{\tilde{m}_\kappa(s)}{s^2} + 4\pi s \tilde{p}_\kappa(s) \right) \right| \\ &\leq \left| \frac{1}{h} \left(\frac{1}{1 - \frac{2m_{\kappa+h}(s)}{s}} - \frac{1}{1 - \frac{2m_\kappa(s)}{s}} \right) - \frac{2\tilde{m}_\kappa(s)}{s \left(1 - \frac{2m_\kappa(s)}{s} \right)^2} \right| \left| \frac{m_{\kappa+h}(s)}{s^2} + 4\pi s p_{\kappa+h}(s) \right| \\ &\quad + \left| \frac{2\tilde{m}_\kappa(s)}{s \left(1 - \frac{2m_\kappa(s)}{s} \right)^2} \right| \left| \frac{m_{\kappa+h}(s) - m_\kappa(s)}{s^2} + 4\pi s (p_{\kappa+h}(s) - p_\kappa(s)) \right| \\ &\quad + \frac{1}{s^2 \left(1 - \frac{2m_\kappa(s)}{s} \right)} \left| \frac{m_{\kappa+h}(s) - m_\kappa(s)}{h} - \tilde{m}_\kappa(s) \right| + \frac{4\pi s}{1 - \frac{2m_\kappa(s)}{s}} \left| \frac{p_{\kappa+h}(s) - p_\kappa(s)}{h} - \tilde{p}_\kappa(s) \right| \\ &=: T_1(s) + T_2(s) + T_3(s) + T_4(s) \end{aligned} \quad (3.17)$$

for $s \in [0, R]$, after repeatedly applying the triangle inequality. The goal now is to construct a ‘‘Gronwall-loop’’ by estimating these terms appropriately for small values of h . For this, let $\varepsilon > 0$. From the explicit estimates in Lemma 3.1.1, we know that

$$\left| \frac{m_{\kappa+h}(s)}{s^2} + 4\pi s p_{\kappa+h}(s) \right| \leq C, \quad s \in [0, R],$$

due to $|h| \leq 1$, where $C > 0$ is a constant that may depend on κ and R but never on h or r . This bound and the mean value theorem applied to $]0, \frac{s}{2}[\ni x \mapsto \frac{1}{1-\frac{2x}{s}}$ yield the existence of $\eta_s > 0$ between $m_{\kappa+h}(s)$ and $m_\kappa(s)$ such that

$$\begin{aligned} T_1(s) &\leq C \left| \frac{1}{s(1-\frac{2\eta_s}{s})^2} \left(\frac{m_{\kappa+h}(s) - m_\kappa(s)}{h} \right) - \frac{\tilde{m}_\kappa(s)}{s \left(1 - \frac{2m_\kappa(s)}{s}\right)^2} \right| \\ &\leq C \left| \frac{1}{(1-\frac{2\eta_s}{s})^2} - \frac{1}{\left(1 - \frac{2m_\kappa(s)}{s}\right)^2} \right| \left| \frac{\tilde{m}_\kappa(s)}{s} \right| + \frac{C}{s(1-\frac{2\eta_s}{s})^2} \left| \frac{m_{\kappa+h}(s) - m_\kappa(s)}{h} - \tilde{m}_\kappa(s) \right| \\ &=: T_{11}(s) + T_{12}(s). \end{aligned}$$

For T_{11} , we can establish the bound

$$\left| \frac{\tilde{m}_\kappa(s)}{s} \right| \leq Cs^{2+2l}, \quad (3.18)$$

as in (3.13), and choose h small such that

$$\left| \frac{1}{(1-\frac{2\eta_s}{s})^2} - \frac{1}{\left(1 - \frac{2m_\kappa(s)}{s}\right)^2} \right| < \varepsilon$$

uniformly in $s \in [0, R]$, which is possible because of Lemma 3.1.1 and the choice of η_s ; recall the Buchdahl-type inequality (2.75). Hence, with (3.18) we get the estimate

$$T_{11}(s) \leq C\varepsilon. \quad (3.19)$$

We deal with T_{12} by again using the mean value theorem in order to obtain

$$\begin{aligned} T_{12}(s) &= \frac{C}{s} \left| \int_0^s \sigma^2 \left(\frac{G(\sigma, y_{\kappa+h}(\sigma)) - G(\sigma, y_\kappa(\sigma))}{h} - \partial_y G(\sigma, y_\kappa(\sigma)) z_\kappa(\sigma) \right) d\sigma \right| \\ &\leq C \int_0^s \sigma^{1+2l} \left| \sigma^{-2l} \partial_y G(\sigma, \xi_\sigma) \frac{y_{\kappa+h}(\sigma) - y_\kappa(\sigma)}{h} - \sigma^{-2l} \partial_y G(\sigma, y_\kappa(\sigma)) z_\kappa(\sigma) \right| d\sigma \end{aligned}$$

for intermediate values ξ_σ between $y_{\kappa+h}(\sigma)$ and $y_\kappa(\sigma)$. Since $\sigma^{-2l} \partial_y G$ is uniformly continuous on $[0, R] \times [0, \kappa + |h|]$ from Lemma (2.2.2) and $l > -\frac{1}{2}$, we get

$$T_{12}(s) \leq C\varepsilon + C \int_0^s \sigma^{1+2l} \left| \frac{y_{\kappa+h}(\sigma) - y_\kappa(\sigma)}{h} - z_\kappa(\sigma) \right| d\sigma, \quad s \in [0, R], \quad (3.20)$$

if $|h|$ is chosen small enough. The term T_2 is considerably easier. The prior results (2.75)

and (3.18) yield

$$T_2(s) \leq C \left| \frac{m_{\kappa+h}(s) - m_{\kappa}(s)}{s^2} \right| + C |p_{\kappa+h}(s) - p_{\kappa}(s)|, \quad (3.21)$$

and therefore, by making $|h|$ small, $T_2(s) \leq C\varepsilon$ for $s \in [0, R]$ from the estimates in Lemma 3.1.1. Furthermore, the Buchdahl-type inequality (2.75) implies

$$T_3(s) \leq \frac{1}{s^2} \left| \frac{m_{\kappa+h}(s) - m_{\kappa}(s)}{h} - \tilde{m}_{\kappa}(s) \right|.$$

In similar fashion to T_{12} , we obtain

$$T_3(s) \leq C\varepsilon + C \int_0^s \sigma^{2l} \left| \frac{y_{\kappa+h}(\sigma) - y_{\kappa}(\sigma)}{h} - z_{\kappa}(\sigma) \right| d\sigma, \quad s \in [0, R], \quad (3.22)$$

where we used $l > -\frac{1}{2}$ and made $|h|$ small enough. With the remaining term T_4 we proceed in the same way since all arguments for G above also work for H . More precisely,

$$\begin{aligned} T_4(s) &\leq Cs \left| \frac{H(s, y_{\kappa+h}(s)) - H(s, y_{\kappa}(s))}{h} - \partial_y H(s, y_{\kappa}(s)) z_{\kappa}(s) \right| \\ &\leq C\varepsilon + Cs^{1+2l} \left| \frac{y_{\kappa+h}(s) - y_{\kappa}(s)}{h} - z_{\kappa}(s) \right|, \quad s \in [0, R]. \end{aligned} \quad (3.23)$$

We insert the estimates (3.19)–(3.23) into (3.17) and, because of $l > -\frac{1}{2}$, get

$$\left| \frac{y'_{\kappa+h}(s) - y'_{\kappa}(s)}{h} - z'_{\kappa}(s) \right| \leq C\varepsilon + C \sup_{\sigma \in [0, s]} \left| \frac{y_{\kappa+h}(\sigma) - y_{\kappa}(\sigma)}{h} - z_{\kappa}(\sigma) \right|, \quad s \in [0, R],$$

which together with (3.16) implies

$$\sup_{[0, r]} \left| \frac{y_{\kappa+h} - y_{\kappa}}{h} - z_{\kappa} \right| \leq C\varepsilon + C \int_0^r \sup_{[0, s]} \left| \frac{y_{\kappa+h} - y_{\kappa}}{h} - z_{\kappa} \right| ds, \quad r \in [0, R].$$

Overall, Gronwall's inequality yields

$$\left| \frac{y_{\kappa+h}(r) - y_{\kappa}(r)}{h} - z_{\kappa}(r) \right| \leq C\varepsilon,$$

if $|h|$ is chosen small enough, which finishes the proof since $\varepsilon > 0$ was arbitrary. \square

Fortunately, this was one of the more difficult steps in the analysis on parameter-dependence in κ . The regularity of metric coefficients and source term can be shown rather easily from the previous lemma.

Proposition 3.1.4. *The functions*

$$]0, \infty[^2 \ni (\kappa, r) \mapsto \rho_\kappa(r), p_\kappa(r), m_\kappa(r), \lambda_\kappa(r), \mu_\kappa(r), \mu'_\kappa(r)$$

are continuously differentiable, and for $r > 0$ it holds that

$$\begin{aligned} \partial_\kappa \rho_\kappa(r) &= \partial_y G(r, y_\kappa(r)) \partial_\kappa y_\kappa(r), \\ \partial_\kappa p_\kappa(r) &= \partial_y H(r, y_\kappa(r)) \partial_\kappa y_\kappa(r), \\ \partial_\kappa m_\kappa(r) &= 4\pi \int_0^r s^2 \partial_\kappa \rho_\kappa(s) ds, \\ \partial_\kappa \lambda_\kappa(r) &= -\frac{2 \partial_\kappa m_\kappa(r)}{r} e^{2\lambda_\kappa(r)}, \\ \partial_\kappa \mu'_\kappa(r) &= 2 \partial_\kappa \lambda_\kappa(r) e^{2\lambda_\kappa(r)} \left(\frac{m_\kappa(r)}{r^2} + 4\pi r p_\kappa(r) \right) + e^{2\lambda_\kappa(r)} \left(\frac{\partial_\kappa m_\kappa(r)}{r^2} + 4\pi r \partial_\kappa p_\kappa(r) \right), \\ \partial_\kappa \mu_\kappa(r) &= -\int_r^\infty \partial_\kappa \mu'_\kappa(s) ds. \end{aligned}$$

Moreover, the cut-off energy $]0, \infty[\ni \kappa \mapsto E^\kappa \in]0, 1[$ is continuously differentiable.

Proof. As $\rho_\kappa(r) = G(r, y_\kappa(r))$ and $p_\kappa(r) = H(r, y_\kappa(r))$, the continuous differentiability follows from Lemma 2.2.2, Lemma 3.1.3, and the chain rule. We can differentiate m_κ as a parameter-dependent integral, since

$$|\partial_\kappa \rho_\kappa(s)| \leq C s^{2l} |z_\kappa(s)| \leq C s^{2l}, \quad s \in [0, R],$$

is an integrable majorant over $[0, R]$, where $R > 0$ is fixed. The remaining claims can be deduced analogously from the field equations (1.10) and (1.11). To complete the proof, we note that Proposition 2.2.4 implies that the cut-off energy is given by

$$E^\kappa = e^{\mu_\kappa(r) + y_\kappa(r)}, \quad r \in]0, \infty[,$$

which yields its continuous differentiability. \square

As an application of the continuous differentiability of the quantities shown above, we prove that the support of the steady state Ω_κ given by (2.41) is well behaved for values of κ , which are close to each other. More precisely, we can locally uniformly approximate the sets Ω_κ by compact subsets. This will be enormously important later since we can then restrict the analysis to a set which is independent of κ .

Lemma 3.1.5. *Let $\eta > 0$.*

- (a) *For every $\varepsilon > 0$, there exists a compact set K and $\delta > 0$ such that for every $\kappa > 0$ with $|\kappa - \eta| < \delta$ it holds that $K \subset \Omega_\kappa$,*

$$\iiint_{\Omega_\kappa \setminus K} dr dw dL < \varepsilon, \quad (3.24)$$

and, for every $r \in [R_{\min}, R_{\max}]$,

$$\iint_{\{(w,L) \mid (r,w,L) \in \Omega_\kappa \setminus K\}} dw dL < \varepsilon. \quad (3.25)$$

(b) For $\delta > 0$ small enough, there exists a compact set U such that for every $\kappa > 0$ with $|\kappa - \eta| < \delta$ it holds that $\Omega_\kappa \subset U$.

Proof. For $\kappa > 0$, the interior of the steady state support is given by

$$\Omega_\kappa = \{(r, w, L) \in]0, \infty[\times \mathbb{R} \times]0, \infty[\mid E_\kappa(r, w, L) < E^\kappa, L > L_0\}.$$

For $\varepsilon > 0$, we define

$$K := \{(r, w, L) \in \Omega_\eta \mid E_\eta(r, w, L) \leq E^\eta - 2\varepsilon, L \geq L_0 + \varepsilon\}$$

and make ε small enough such that $K \neq \emptyset$. The set K is bounded since Ω_η is bounded. In particular, due to $\mu_\eta(r) \geq \mu_\eta(0)$ we get

$$\frac{L_0 + \varepsilon}{r^2} \leq \frac{e^{2\mu_\eta(r)}}{e^{2\mu_\eta(0)}} \left(1 + w^2 + \frac{L}{r^2}\right) \leq \frac{(E^\eta - \varepsilon)^2}{e^{2\mu_\eta(0)}}$$

for $(r, w, L) \in K$. Therefore, if $(r_n, w_n, L_n)_{n \in \mathbb{N}} \subset K$ is convergent, this implies that $(r_n)_{n \in \mathbb{N}}$ is bounded away from zero and the sequence must converge in K , i.e., K is compact. For $\delta > 0$ small enough, the compactness of K and the continuity of the energy in (κ, r, w, L) from Proposition 3.1.4 yield

$$E_\kappa(r, w, L) \leq E^\eta - \varepsilon \leq E^\kappa - \frac{\varepsilon}{2}$$

for $(r, w, L) \in K$ and $|\kappa - \eta| < \delta$, where the latter estimate follows from the continuity of the cut-off energy shown in Lemma 3.2.1. This proves $K \subset \Omega_\kappa$ for $|\kappa - \eta| < \delta$. In addition, we have

$$\Omega_\kappa \setminus K = \left\{ (r, w, L) \in \Omega_\kappa \mid E_\eta(r, w, L) > E^\eta - \varepsilon \vee L < L_0 + \varepsilon \right\}$$

and thus define

$$\begin{aligned} M_1 &:= \left\{ (r, w, L) \in \Omega_\kappa \mid E_\eta(r, w, L) > E^\eta - \varepsilon \right\}, \\ M_2 &:= \left\{ (r, w, L) \in \Omega_\kappa \mid L < L_0 + \varepsilon \right\}, \end{aligned}$$

with $\Omega_\kappa \setminus K \subset M_1 \cup M_2$. We first note that for $\delta > 0$ small enough

$$w^2 + \frac{L}{r^2} = e^{-2\mu_\kappa(r)} (E_\kappa)^2 - 1 \leq C$$

and

$$E_\kappa(r, w, L) \geq E_\kappa(r, 0, L_0) = \Psi_{\kappa, L_0} > E^\kappa$$

holds for every $r \geq R_\eta + 1$, because E^κ is continuous and $\lim_{r \rightarrow \infty} e^{\mu_\kappa(r)} = 1$. We conclude that Ω_κ is uniformly bounded in κ with

$$r, w^2, L, \frac{L}{r^2} \leq C, \quad (r, w, L) \in \Omega_\kappa, \quad (3.26)$$

for some $C > 0$ independent of κ .

Let us estimate the integrals over M_1 and M_2 . Since the cut-off energy E^κ is continuous in κ , we can choose $\delta > 0$ such that

$$|E_\eta(r, w, L) - E^\eta| < \varepsilon, \quad (r, w, L) \in M_1,$$

In particular, we get

$$M_1 \subset \{(r, w, L) \in [0, R_\eta] \times \mathbb{R} \times]L_0, \infty[\mid |E_\eta(r, w, L) - E^\eta| < \varepsilon\},$$

where $R_\eta > 0$ is a bound on the radial variable obtained from $E_\eta(r, w, L) < E^\eta + \varepsilon < 1$ after making $\varepsilon > 0$ sufficiently small. A change of variables via $w \mapsto E_\eta(r, w, L)$ yields

$$\begin{aligned} \iiint_{M_1} dr dw dL &\leq \int_0^{R_\eta} \int_{E^\eta - \varepsilon}^{E^\eta + \varepsilon} \int_{L_0}^{r^2(E^2 e^{-2\mu_\eta(r)} - 1)} \frac{2e^{-2\mu_\eta(r)} E}{\sqrt{E^2 e^{-2\mu_\eta(r)} - 1 - \frac{L}{r^2}}} dL dE dr \\ &\leq \int_0^{R_\eta} \int_{E^\eta - \varepsilon}^{E^\eta + \varepsilon} 4r^2 E e^{-2\mu_\eta(r)} \sqrt{E^2 e^{-2\mu_\eta(r)} - \frac{L_0}{r^2}} dE dr \leq C\varepsilon \end{aligned}$$

with $C > 0$ independent of κ . As to M_2 , we use (3.26) in order to obtain

$$\iiint_{M_2} dr dw dL \leq C \int_{L_0}^{L_0 + \varepsilon} dL = C\varepsilon.$$

These estimates together with $\Omega_\kappa \setminus K \subset M_1 \cup M_2$ imply (3.24). In order to obtain (3.25), we perform the same estimates as above without the radial integral. This still yields the factor ε due to the integral over (E, L) . Part (b) was already established in (3.26). \square

3.2 Dependence in the case of the single-well structure

The next step consists of showing that the maximal radius $R_{\kappa, \max}$ and the total mass M_κ is continuous in κ . If we naively try to prove that $R_{\kappa, \max}$ is continuous, we encounter the obstacle that multi-shell solutions [16] could lead to discontinuities in the maximal radius. In order to avoid such a situation, we have to prescribe that the singularity-free steady state f_κ has (strict) single-well structure, as introduced in Definition 2.3.1. Throughout this section, we consider an open interval $I_{\text{sws}} \subset]0, \infty[$ such that f_κ has strict single-well structure for $\kappa \in I_{\text{sws}}$.

Lemma 3.2.1. *Consider the minimal and maximal radius $R_{\kappa,\min}$, $R_{\kappa,\max}$, the maximal angular momentum $L_{\kappa,\max}$, and the ADM-mass M_κ corresponding to f_κ . The mappings*

$$I_{\text{sws}} \ni \kappa \mapsto R_{\kappa,\min}, R_{\kappa,\max}, L_{\kappa,\max}, M_\kappa$$

are continuously differentiable.

Proof. From Proposition 3.1.4, we know that the function⁶

$$F(\kappa, r) := \Psi_{\kappa, L_0}(r) - E^\kappa, \quad (\kappa, r) \in I_{\text{sws}} \times]0, \infty[,$$

is continuously differentiable and $R_{\kappa,\max}$ solves $F(\kappa, R_{\kappa,\max}) = 0$, as we have proven in Lemma 2.3.3(e). From the single-well structure, we deduce that⁷

$$\partial_r F(\kappa, R_{\kappa,\max}) = \partial_r \Psi_{\kappa, L_0}(R_{\kappa,\max}) > 0,$$

and thus the implicit function theorem yields the claim for $R_{\kappa,\max}$. For $R_{\kappa,\min}$, we proceed analogously and note $R_{\kappa,\min} = 0$ for $L_0 = 0$. As to $L_{\kappa,\max}$, we define

$$G(\kappa, r, L) := \begin{pmatrix} \Psi_{\kappa, L}(r) - E^\kappa \\ \Psi'_{\kappa, L}(r) \end{pmatrix}, \quad (\kappa, r, L) \in I_{\text{sws}} \times]0, \infty[\times]0, \infty[,$$

which is continuously differentiable due to the previous results. From Lemma 2.3.4(c), we observe that

$$G(\kappa, r_\kappa^*, L_{\kappa,\max}) = 0$$

for every $\kappa \in I_{\text{sws}}$, where

$$r_\kappa^* = \lim_{L \nearrow L_{\kappa,\max}} r_{\kappa, L}.$$

Moreover, we calculate

$$\det(D_{(r, L)} G)(\kappa, r_\kappa^*, L_{\kappa,\max}) = -\Psi''_{\kappa, L_{\kappa,\max}}(r_\kappa^*) \partial_L \Psi_{\kappa, L}(r_\kappa^*) > 0,$$

which is positive according to the strict single-well structure. The implicit function theorem implies that $I_{\text{sws}} \ni \kappa \mapsto (r_\kappa^*, L_{\kappa,\max})$ is continuously differentiable. At last, the ADM-mass is given by

$$M_\kappa = m_\kappa(R_{\kappa,\max}),$$

which is continuously differentiable due to Proposition 3.1.4 and the chain rule. \square

We obtain more information about the regularity of quantities specific to the single-well structure through the implicit function theorem. In particular, we analyze $r_{\kappa, L}$ and $r_{\kappa, \pm}(E, L)$, defined in Definition 2.3.1 and Lemma 2.3.3(b), respectively.

⁶Recall the definition of the effective potential $\Psi_{\kappa, L}$ in (2.31).

⁷To be precise, we have to treat $L_0 = 0$ separately. However, in this case $\Psi_{\kappa, L_0} = e^{\mu_\kappa}$ and the claim follows from the strict monotonicity of μ_κ .

Corollary 3.2.2. *The mapping*

$$\{(\kappa, L) \mid \kappa \in I_{\text{sws}}, L \in]L_0, L_{\kappa, \max}[\} \ni (\kappa, L) \mapsto r_{\kappa, L}$$

is continuously differentiable.

Proof. For every pair (κ, L) in the set above, $\Psi'_{\kappa, L}(r_{\kappa, L}) = 0$ holds by Definition 2.3.1, and, since we assume strict single-well structure, $\Psi''_{\kappa, L}(r_{\kappa, L}) > 0$. The implicit function theorem implies the claim. \square

In order to derive a regularity result for $r_{\kappa, \pm}$, we first need to introduce sets that describe the steady state support along κ . We recall the definition of $\tilde{\Omega}_\kappa$ from (2.67) as well as $\tilde{\Omega}_\kappa^{EL}$ from (2.43), and we define

$$\Gamma := \left\{ (\kappa, r, w, L) \mid \kappa \in I_{\text{sws}}, (r, w, L) \in \tilde{\Omega}_\kappa \right\}, \quad (3.27)$$

$$\Gamma^{EL} := \left\{ (\kappa, E, L) \mid \kappa \in I_{\text{sws}}, (E, L) \in \tilde{\Omega}_\kappa^{EL} \right\}, \quad (3.28)$$

which contain all “relevant” values of (r, w, L) and (E, L) appearing in the steady state supports along the parameter $\kappa \in I_{\text{sws}}$.

Lemma 3.2.3. *The sets Γ and Γ^{EL} are open.*

Proof. From the definition of Γ , we have

$$(\kappa, r, w, L) \in \Gamma \iff \kappa \in I_{\text{sws}}, \quad \Psi_{\kappa, L}(r_{\kappa, L}) < E_\kappa(r, w, L) < E^\kappa, \quad L > L_0,$$

where $E_\kappa(r, w, L) = e^{\mu_\kappa(r)} \sqrt{1 + w^2 + \frac{L}{r^2}}$. Likewise, we can characterize

$$(\kappa, E, L) \in \Gamma^{EL} \iff \kappa \in I_{\text{sws}}, \quad \Psi_{\kappa, L}(r_{\kappa, L}) < E < E^\kappa, \quad L > L_0.$$

The proof that these sets are open now comes down to the fact that all quantities are continuous in their parameters; see Proposition 3.1.4, Lemma 3.2.1, and Corollary 3.2.2. \square

Corollary 3.2.4. *The mappings*

$$\Gamma^{EL} \ni (\kappa, E, L) \mapsto r_{\kappa, \pm}(E, L)$$

are continuously differentiable.

Proof. According to Lemma 2.3.3, we have $\Psi_{\kappa, L}(r_{\kappa, \pm}(E, L)) = E$, and

$$r_{\kappa, -}(E, L) < r_{\kappa, L} < r_{\kappa, +}(E, L), \quad (\kappa, E, L) \in \Gamma^{EL}.$$

The single-well structure yields $\Psi'_{\kappa, L}(r_{\kappa, \pm}(E, L)) \neq 0$, and thus the implicit function theorem is applicable. \square

3.2.1 Continuity of the period function

The derivation of regularity for the period function T defined in (2.44) is one of the main objectives in the analysis of parameter dependence along κ . First, we need to ensure that solutions to the characteristic system are regular in a suitable sense. Recall that we consider a family of singularity-free steady states $(f_\kappa)_{\kappa>0}$ restricted to $\kappa \in I_{\text{sWS}}$, where I_{sWS} is introduced at the beginning of Section 3.2.

It is convenient to slightly reformulate the analysis of the characteristic system compared to Section 2.3.2 and switch from a description in (E, L) to (r, w, L) coordinates. Similar to Definition 2.3.7, for $(r, w, L) \in \tilde{\Omega}_\kappa$, let

$$(R_\kappa, W_\kappa) = (R_\kappa, W_\kappa)(\cdot, r, w, L): \mathbb{R} \rightarrow \mathbb{R} \times \mathbb{R}$$

be the maximal solution to the characteristic system (2.42) with parameter L satisfying the initial condition $(R_\kappa, W_\kappa)(0, r, w, L) = (r_{\kappa,-}(E_\kappa(r, w, L), L), 0)$. Obviously, this solution now also depends on κ .

Lemma 3.2.5. *The solution to the characteristic system*

$$\mathbb{R} \times \Gamma \ni (t, \kappa, r, w, L) \mapsto (R_\kappa, W_\kappa)(t, r, w, L)$$

is continuously differentiable.

Proof. We can interpret L and κ as parameters of the system. The right-hand side of the characteristic system (2.42) is continuously differentiable on Γ due to Proposition 3.1.4. Note that $r > 0$ on Γ . Furthermore, the initial condition

$$(R_\kappa, W_\kappa)(0, r, w, L) = (r_{\kappa,-}(E_\kappa(r, w, L), L), 0)$$

is continuously differentiable as a function on Γ by Corollary 3.2.4 and the chain rule. The claim therefore follows from the standard theory of continuous differentiable dependence on initial values and parameters for ordinary differential equations. \square

The next goal is to show that the period function is continuous on Γ^{EL} by making use of the previous results. For this, we need a result similar to Lemma 2.3.10, which is in some sense uniform in κ . This will also be useful later when we bound the period function uniformly in κ .

Lemma 3.2.6. *Let $\eta \in I_{\text{sWS}}$ and fix $L_1 > 0$. There exist $\delta, a, q > 0$ such that for every $\kappa \in I_{\text{sWS}}$ with $|\kappa - \eta| < \delta$ and $L_1 \leq L < L_{\kappa, \text{max}}$ it holds that*

- (i) $\Psi''_{\kappa, L} \geq a$ on $[r_{\kappa, L} - q, r_{\kappa, L} + q] \cap \bar{I}_{\kappa, L}$,
- (ii) $\Psi'_{\kappa, L} \leq -a$ on $[R_{\kappa, \text{min}}, r_{\kappa, L} - q] \cap \bar{I}_{\kappa, L}$,
- (iii) $\Psi'_{\kappa, L} \geq a$ on $[r_{\kappa, L} + q, R_{\kappa, \text{max}}] \cap \bar{I}_{\kappa, L}$.

In the cases (ii) and (iii), the sets may be empty. The interval $I_{\kappa, L}$ is given in Definition 2.3.1.

Proof. The proof is similar to the one in Lemma 2.3.10, but we have to take care of the dependence in κ . For $\delta > 0$ and $q > 0$ small enough⁸, consider the sets

$$\begin{aligned} J_{\delta,q} &:= \{(\kappa, L) \mid \kappa \in [\eta - \delta, \eta + \delta], L \in [L_1, L_{\kappa,\max}]\}, \\ K_{\delta,q} &:= \{(\kappa, r, L) \mid (\kappa, L) \in J_{\delta,q}, r \in [r_{\kappa,L} - q, r_{\kappa,L} + q]\}, \end{aligned}$$

which are compact since $L_{\kappa,\max}$ and $r_{\kappa,L}$ are continuous as per Lemma 3.2.1 and Corollary 3.2.2. Therefore,

$$\begin{aligned} J_{\delta,q} \ni (\kappa, L) &\mapsto r_{\kappa,L}, \\ K_{\delta,q} \ni (\kappa, r, L) &\mapsto \Psi''_{\kappa,L}(r), \end{aligned}$$

are uniformly continuous. By the strict single-well structure, there exists $a > 0$ such that

$$\Psi''_{\eta,L}(r_{\eta,L}) \geq a,$$

for $L_1 \leq L \leq L_{\kappa,\max}$. These two observations imply the claim in (i) after possibly making δ and a smaller.

By using the values for δ and q from part (i) and making them smaller if necessary, we use similar arguments and deduce that

$$\{(\kappa, r, L) \mid (\kappa, L) \in J_{\delta,q}, r \in [R_{\kappa,\min}, r_{\kappa,L} - q]\}$$

is compact, and thus $\Psi'_{\kappa,L}(r)$ attains its minimum on this set. Moreover, the minimum is bounded away from zero. This yields (ii). Part (iii) follows analogously. \square

The continuity of the period function (2.44) can now be deduced from the continuity results in Proposition 3.1.4 and Lemma 3.2.6.

Proposition 3.2.7. *The period function*

$$\Gamma^{EL} \ni (\kappa, E, L) \mapsto T_{\kappa}(E, L) = 2E \int_{r_{\kappa,-}(E,L)}^{r_{\kappa,+}(E,L)} \frac{e^{\lambda_{\kappa}(r) - \mu_{\kappa}(r)}}{\sqrt{E^2 - \Psi_{\kappa,L}^2(r)}} dr$$

is continuous.

Proof. The goal is to apply Lebesgue's dominated convergence theorem as well as the continuity of $r_{\kappa,\pm}$ and $\Psi_{\kappa,L}$ derived above. Finding suitable integrable majorants is the main difficulty here and they are obtained in a manner similar to the proof of Lemma 2.3.11.

Fix $(\bar{\kappa}, \bar{E}, \bar{L}) \in \Gamma^{EL}$ and choose $\delta_0, a, q > 0$ according to Lemma 3.2.6. We split the

⁸In particular, we choose these parameters small such that $\eta > \delta$ and $r_{\kappa,L} > q$ for $\kappa \in [\eta - \delta, \eta + \delta]$ and $L \in [L_1, L_{\kappa,\max}]$, which is possible because of continuity and $L_1 > 0$.

period function into the three parts

$$\begin{aligned}
 T_l(\kappa, E, L) &:= 2E \int_{r_{\kappa,-}(E,L)}^{\max\{r_{\kappa,L}-q, r_{\kappa,-}(E,L)\}} \frac{e^{\lambda_\kappa(r)-\mu_\kappa(r)}}{\sqrt{E^2 - \Psi_{\kappa,L}^2(r)}} dr, \\
 T_m(\kappa, E, L) &:= 2E \int_{\max\{r_{\kappa,L}-q, r_{\kappa,-}(E,L)\}}^{\min\{r_{\kappa,L}+q, r_{\kappa,+}(E,L)\}} \frac{e^{\lambda_\kappa(r)-\mu_\kappa(r)}}{\sqrt{E^2 - \Psi_{\kappa,L}^2(r)}} dr, \\
 T_r(\kappa, E, L) &:= 2E \int_{\min\{r_{\kappa,L}+q, r_{\kappa,+}(E,L)\}}^{r_{\kappa,+}(E,L)} \frac{e^{\lambda_\kappa(r)-\mu_\kappa(r)}}{\sqrt{E^2 - \Psi_{\kappa,L}^2(r)}} dr,
 \end{aligned}$$

for which obviously $T = T_l + T_m + T_r$. We separately show that T_l , T_m , and T_r are continuous in $(\bar{\kappa}, \bar{E}, \bar{L})$. Choose $0 < \delta \leq \delta_0$ such that for every

$$(\kappa, E, L) \in D_\delta := \left\{ (\tilde{\kappa}, \tilde{E}, \tilde{L}) \in]0, \infty[^3 \mid |\tilde{\kappa} - \bar{\kappa}|, |\tilde{E} - \bar{E}|, |\tilde{L} - \bar{L}| \leq \delta \right\}$$

it holds that

$$(\kappa, E, L) \in \Gamma^{EL}, \quad R_{\kappa,\max} \leq R_{\bar{\kappa},\max} + 1, \quad \frac{1}{2}r_{\bar{\kappa},-}(\bar{E}, \bar{L}) \leq r_{\kappa,-}(E, L).$$

This is possible due to Lemma 3.2.3 and the continuity properties shown previously. We first deal with T_l and consider the case where $r_{\bar{\kappa},-}(\bar{E}, \bar{L}) < r_{\bar{\kappa},\bar{L}} - q$. We choose $\delta > 0$ small such that $r_{\kappa,-}(E, L) < r_{\kappa,L} - q$ for every $(\kappa, E, L) \in D_\delta$, which is possible because of the continuity derived in Corollaries 3.2.2 and 3.2.4. After changing variables

$$T_l(\kappa, E, L) = 2E \int_0^1 \frac{(r_{\kappa,L} - q - r_{\kappa,-}(E, L)) e^{(\lambda_\kappa - \mu_\kappa)(s(r_{\kappa,L} - q - r_{\kappa,-}(E, L)) + r_{\kappa,-}(E, L))}}{\sqrt{E^2 - \Psi_{\kappa,L}^2(s(r_{\kappa,L} - q - r_{\kappa,-}(E, L)) + r_{\kappa,-}(E, L))}} ds,$$

where the integrand converges for $\delta \rightarrow 0$ because of the continuity of all relevant quantities. More precisely, we use that $\Psi_{\kappa,L}(r)$ and the metric coefficients are uniformly continuous for $|\kappa - \bar{\kappa}| \leq \delta$, $|L - \bar{L}| \leq \delta$, and $r \in [\frac{1}{2}r_{\bar{\kappa},-}(\bar{E}, \bar{L}), R_{\bar{\kappa},\max} + 1]$ by the choice of δ above. In order to obtain an integrable majorant, we use that $e^{\lambda_\kappa - \mu_\kappa}$ is uniformly bounded, $E + \Psi_{\kappa,L} \geq E$, and observe

$$E - \Psi_{\kappa,L}(r) \geq a(r - r_{\kappa,-}(E, L)), \quad r \in [r_{\kappa,-}(E, L), r_{\kappa,L} - q],$$

from the choice of a and the mean value theorem. Hence,

$$\begin{aligned}
 &\frac{r_{\kappa,L} - q - r_{\kappa,-}(E, L)}{\sqrt{E - \Psi_{\kappa,L}(s(r_{\kappa,L} - q - r_{\kappa,-}(E, L)) + r_{\kappa,-}(E, L))}} \\
 &\leq \frac{\sqrt{r_{\kappa,L} - q - r_{\kappa,-}(E, L)}}{\sqrt{a}} \frac{1}{\sqrt{s}} \leq \frac{\sqrt{R_{\bar{\kappa},\max} + 1}}{\sqrt{a} \sqrt{s}}.
 \end{aligned}$$

Applying Lebesgue's dominated convergence theorem yields the continuity of T_l in $(\bar{\kappa}, \bar{E}, \bar{L})$ in this case. It remains to show the continuity if $r_{\bar{\kappa},-}(\bar{E}, \bar{L}) \geq r_{\bar{\kappa},\bar{L}} - q$, for which $T_l(\bar{\kappa}, \bar{E}, \bar{L}) = 0$ holds. Due to the continuity of $r_{\kappa,-}$ and $r_{\kappa,L}$, the scenario " $>$ " is trivial. In the case where $r_{\bar{\kappa},-}(\bar{E}, \bar{L}) = r_{\bar{\kappa},\bar{L}} - q$, we estimate

$$|T_l(\kappa, E, L)| \leq C \frac{\sqrt{r_{\kappa,L} - q - r_{\kappa,-}(E, L)}}{\sqrt{a}},$$

as above with $C > 0$ independent of $(\kappa, E, L) \in D_\delta$ and $r_{\kappa,-}(E, L) < r_{\kappa,L} - q$. The right-hand side goes to zero as $\delta \rightarrow 0$, since $r_{\bar{\kappa},-}(\bar{E}, \bar{L}) = r_{\bar{\kappa},\bar{L}} - q$. For $r_{\kappa,-}(E, L) \geq r_{\kappa,L} - q$, we again have $T_l(\kappa, E, L) = 0$. This proves the continuity of T_l . For the term T_r , we argue in similar manner and leave out the details.

We split the term T_m further into

$$\begin{aligned} T_m(\kappa, E, L) &= 2E \int_{\max\{r_{\kappa,L}-q, r_{\kappa,-}(E,L)\}}^{r_{\kappa,L}} \frac{e^{\lambda_\kappa(r)-\mu_\kappa(r)}}{\sqrt{E^2 - \Psi_{\kappa,L}^2(r)}} dr \\ &\quad + 2E \int_{r_{\kappa,L}}^{\min\{r_{\kappa,L}+q, r_{\kappa,+}(E,L)\}} \frac{e^{\lambda_\kappa(r)-\mu_\kappa(r)}}{\sqrt{E^2 - \Psi_{\kappa,L}^2(r)}} dr \\ &=: T_m^-(\kappa, E, L) + T_m^+(\kappa, E, L) \end{aligned}$$

and show the continuity for both terms separately. Let us first consider T_m^+ and the case $r_{\bar{\kappa},\bar{L}} + q < r_{\bar{\kappa},+}(\bar{E}, \bar{L})$. Due to the single-well structure, we have $\Psi'_{\kappa,L} > 0$ for $r > r_{\kappa,L}$ and can switch variables (twice) via $\eta = \Psi_{\kappa,L}(r)$, i.e., $r = r_{\kappa,+}(\eta, L)$, which implies

$$\begin{aligned} T_m^+(\kappa, E, L) &= 2E \int_{\Psi_{\kappa,L}(r_{\kappa,L})}^{\Psi_{\kappa,L}(r_{\kappa,L}+q)} \frac{e^{\lambda_\kappa(r_{\kappa,+}(\eta,L))-\mu_\kappa(r_{\kappa,+}(\eta,L))}}{\sqrt{\left(\Psi'_{\kappa,L}(r_{\kappa,+}(\eta,L))\right)^2 (E^2 - \eta^2)}} d\eta \\ &= (\Psi_{\kappa,L}(r_{\kappa,L} + q) - \Psi_{\kappa,L}(r_{\kappa,L})) \int_0^1 \frac{e^{\lambda_\kappa(r_{\kappa,+}(\eta(s),L))-\mu_\kappa(r_{\kappa,+}(\eta(s),L))}}{\sqrt{\left(\Psi'_{\kappa,L}(r_{\kappa,+}(\eta(s),L))\right)^2 (E^2 - \eta^2(s))}} ds, \end{aligned} \tag{3.29}$$

where $\eta(s) = (\Psi_{\kappa,L}(r_{\kappa,L} + q) - \Psi_{\kappa,L}(r_{\kappa,L}))s + \Psi_{\kappa,L}(r_{\kappa,L})$ for $s \in [0, 1]$. Since

$$D_\delta \ni (\kappa, \eta, L) \mapsto \Psi'_{\kappa,L}(r_{\kappa,+}(\eta, L)), \quad e^{\lambda_\kappa(r_{\kappa,+}(\eta,L))-\mu_\kappa(r_{\kappa,+}(\eta,L))}$$

are uniformly continuous, we get pointwise convergence in the integrand of (3.29) for $\delta \rightarrow 0$. Moreover, the methods used in (2.53) and (2.54) in the proof of Lemma 2.3.11

can be applied word-by-word to yield⁹

$$\frac{\Psi'_{\kappa,L}(r_{\kappa,+}(\eta, L))^2}{\eta - \Psi_{\kappa,L}(r_{\kappa,L})} \geq 2a, \quad \eta \in]\Psi_{\kappa,L}(r_{\kappa,L}), \Psi_{\kappa,L}(r_{\kappa,L} + q)[.$$

Therefore,

$$\begin{aligned} & \frac{\Psi_{\kappa,L}(r_{\kappa,L} + q) - \Psi_{\kappa,L}(r_{\kappa,L})}{\sqrt{(\Psi'_{\kappa,L}(r_{\kappa,+}(\eta(s), L)))^2 (E - \eta(s))}} \\ & \leq \frac{1}{\sqrt{2a} \sqrt{s} \sqrt{\frac{E - \Psi_{\kappa,L}(r_{\kappa,L})}{\Psi_{\kappa,L}(r_{\kappa,L} + q) - \Psi_{\kappa,L}(r_{\kappa,L})} - s}} \leq \frac{1}{\sqrt{2a} \sqrt{s(1-s)}} \end{aligned}$$

for every $s \in [0, 1]$, which yields an integrable majorant. Lebesgue's theorem proves the continuity of T_m^+ . The case $r_{\bar{\kappa},\bar{L}} + q \geq r_{\bar{\kappa},+}(\bar{E}, \bar{L})$ as well as the term T_m^- can be treated with the same techniques. \square

A similar result can be deduced for the angle function defined in (2.69), which is another quantity that has to be controlled for the analysis in Chapter 6.

Proposition 3.2.8. *The angle function*

$$\theta_{\kappa}(r, E, L) = \frac{E}{T_{\kappa}(E, L)} \int_{r_{\kappa,-}(E, L)}^r \frac{e^{\lambda_{\kappa}(s) - \mu_{\kappa}(s)}}{\sqrt{E^2 - \Psi_{\kappa,L}^2(s)}} ds$$

is continuous on the set where $(\kappa, E, L) \in \Gamma^{EL}$ and $r \in]r_{\kappa,-}(E, L), r_{\kappa,+}(E, L)[$. For fixed $(\kappa, E, L) \in \Gamma^{EL}$, the function $\theta_{\kappa}(\cdot, E, L)$ can be continuously extended onto $[0, \infty[$ by

$$\theta_{\kappa}(r, E, L) = \begin{cases} 0, & \text{if } r \leq r_{\kappa,-}(E, L), \\ \frac{1}{2}, & \text{if } r \geq r_{\kappa,+}(E, L). \end{cases} \quad (3.30)$$

Proof. Note that the set on which the angle function is defined is open because Γ^{EL} is open and r_{\pm} are continuous, see Lemma 3.2.3 and Corollary 3.2.4. Since the proof is very alike to the proof of Proposition 3.2.7, we only refer to the general procedure and leave out the details. We fix a point $(\bar{\kappa}, \bar{r}, \bar{E}, \bar{L})$ in the domain of definition, choose $\delta_0, a, q > 0$ according to Lemma 3.2.6, and split the angle function into

$$\theta_{\kappa}(r, E, L) = \frac{E}{T_{\kappa}(E, L)} \begin{cases} \int_{r_{\kappa,-}(E, L)}^r \cdots, & \text{if } r \leq r_{\kappa,L} - q, \\ \int_{r_{\kappa,-}(E, L)}^{r_{\kappa,L} - q} \cdots + \int_{r_{\kappa,L} - q}^r \cdots, & \text{if } r_{\kappa,L} - q < r \leq r_{\kappa,L} + q, \\ \int_{r_{\kappa,-}(E, L)}^{r_{\kappa,L} - q} \cdots + \int_{r_{\kappa,L} - q}^{r_{\kappa,L} + q} \cdots + \int_{r_{\kappa,L} + q}^r \cdots, & \text{if } r > r_{\kappa,L} + q, \end{cases}$$

⁹This estimate is possible uniformly since a does not depend on κ because of Lemma 3.2.6.

for (κ, r, E, L) close to $(\bar{\kappa}, \bar{r}, \bar{E}, \bar{L})$. If $r_{\kappa, L} + q > r_{\kappa, +}(E, L)$ or $r_{\kappa, L} - q < r_{\kappa, -}(E, L)$, we replace $r_{\kappa, L} \pm q$ with $r_{\kappa, \pm}(E, L)$, respectively. We observe that $T_{\kappa}(E, L)$ is continuous because of Proposition 3.2.7. Moreover, the terms which do not depend on r were already treated explicitly in the proof of Proposition 3.2.7, while the terms depending on r can be dealt with the same techniques as in said proof, i.e., we use Lebesgue's theorem and apply the different cases in Lemma 3.2.6 to control the integrand. The cases $\bar{r} = r_{\bar{L}, \bar{\kappa}} \pm q$ have to be considered separately in similar fashion to the border cases in the proof of Proposition 3.2.7.

The continuous extension of $\theta_{\kappa}(\cdot, E, L)$ onto $[0, \infty[$ is obtained by the limiting behavior

$$\lim_{r \xrightarrow{>} r_{\kappa, -}(E, L)} \theta_{\kappa}(r, E, L) = 0$$

as well as

$$\lim_{r \xrightarrow{<} r_{\kappa, +}(E, L)} \theta_{\kappa}(r, E, L) = \frac{T_{\kappa}(E, L)}{2T_{\kappa}(E, L)} = \frac{1}{2}.$$

□

3.2.2 Bounds on the period function

As a final project, we prove that the period function can be bounded away from zero and from above locally uniformly in the redshift parameter. For this, we pursue the same strategy as in Sections 2.3.3 and 2.3.4. More precisely, we show that the bounds obtained in Propositions 2.3.9 and 2.3.16 can be generalized to include a dependence in κ . As in Proposition 2.3.9, we prescribe that $L_0 > 0$ or $l \geq 0$ to get a lower bound.

Proposition 3.2.9. *Let $L_0 > 0$ or $l \geq 0$. For every $\eta \in I_{\text{sWS}}$, there exists $\delta > 0$ and $c > 0$ such that*

$$T_{\kappa}(E, L) \geq c, \quad \kappa \in [\eta - \delta, \eta + \delta], \quad (E, L) \in \tilde{\Omega}_{\kappa}^{EL}.$$

Proof. Fix $\eta > 0$ and let $\delta > 0$ be such that $[\eta - \delta, \eta + \delta] \subset I_{\text{sWS}}$. Proposition 2.3.9 implies

$$T_{\kappa}(E, L) \geq 2e^{\mu_{\kappa}(R_{\kappa, \min})} \frac{1}{\sqrt{N_{\kappa}}}$$

with

$$N_{\kappa} = 38\pi \left(\max_{[R_{\kappa, \min}, R_{\kappa, \max}]} e^{2\lambda_{\kappa} - 2\mu_{\kappa}} \right) \max_{[R_{\kappa, \min}, R_{\kappa, \max}]} \rho_{\kappa} \cdot \left(1 + 8\pi R_{\kappa, \max}^2 \left(\max_{[R_{\kappa, \min}, R_{\kappa, \max}]} e^{2\lambda_{\kappa} - 2\mu_{\kappa}} \right) \max_{[R_{\kappa, \min}, R_{\kappa, \max}]} \rho_{\kappa} \right).$$

We now choose $0 < \delta < 1$ such that $R_{\kappa, \max} \leq R_{\eta, \max} + 1 =: R$ and $E^{\kappa} \geq \frac{1}{2}E^{\eta}$. First, consider the case $L_0 = 0$, i.e., $l \geq 0$. Together with the Buchdahl-type inequality (2.75),

we get

$$N_\kappa \leq C \left(\max_{[0,R]} e^{2y_\kappa} \right) \max_{[0,R]} \rho_\kappa \left(1 + \left(\max_{[0,R]} e^{2y_\kappa} \right) \max_{[0,R]} \rho_\kappa \right).$$

Moreover, y_κ and ρ_κ are uniformly bounded for $\kappa \in [\eta - \delta, \eta + \delta]$ and $r \in [0, R]$ due to Lemma 3.1.1 and $l \geq 0$. On the other hand, if $L_0 > 0$, we can bound $R_{\kappa, \min} \geq \frac{1}{2} R_{\eta, \min} > 0$ by making δ small, and proceed similarly to above with the radial steady state support uniformly bounded away from zero. \square

For the upper bound, we have to restrict the accessible steady states further, as it is the case in Proposition 2.3.16.

Proposition 3.2.10. *Let $L_0 > 0$ or let f_κ be isotropic with*

$$\frac{2m_\kappa(r)}{r} < \frac{1}{3}, \quad r > 0,$$

for $\kappa \in I_{\text{sws}}$. For every $\eta \in I_{\text{sws}}$, there exists $\delta > 0$ and $C > 0$ such that

$$T_\kappa(E, L) \leq C, \quad \kappa \in [\eta - \delta, \eta + \delta], \quad (E, L) \in \tilde{\Omega}_\kappa^{EL}.$$

Proof. Fix $\eta \in I_{\text{sws}}$. In the case $L_0 > 0$, we choose $\delta_0, a, q > 0$ according to Lemma 3.2.6 and $0 < \delta \leq \delta_0$. We can apply Proposition 2.3.16(a) to obtain

$$T_\kappa(E, L) \leq 2Q_\kappa \left(\frac{4\sqrt{R_{\kappa, \max}} + \sqrt{2}\pi}{\sqrt{a}} \right), \quad (E, L) \in \tilde{\Omega}_\kappa^{EL},$$

where $Q_\kappa = \max_{[R_{\kappa, \min}, R_{\kappa, \max}]} e^{\lambda_\kappa - \mu_\kappa}$. Now T can be bounded uniformly in κ , since $Q_\kappa \leq C$ and because $R_{\kappa, \max}$ is continuous by Lemma 3.2.1.

In the isotropic case, we apply Proposition 2.3.16(b), but we have to make sure that E_1 and L_1 —which are chosen in step 3 of the proof of Lemma 2.3.15—can be chosen independently of $\kappa \in [\eta - \delta, \eta + \delta]$. Recall that $r_{\kappa, +}(E, L)$ and $r_{\kappa, L}$ are continuous in (κ, E, L) and (κ, L) , respectively, due to Corrolaries 3.2.2 and 3.2.4. In addition, we have shown monotonicity properties for these quantities in Lemmas 2.3.3(d) and 2.3.4(a). Because of this, we can choose $\tilde{E}_1, \tilde{E}_2, L_1 > 0$ with the following properties for every $\kappa \in [\eta - \delta, \eta + \delta]$, $\tilde{E}_2 < E < E^\kappa$, and $0 < L < L_1$:

$$(i) \quad \Psi_{\kappa, L}(r_{\kappa, L}) < \tilde{E}_1 < \tilde{E}_2 < E^\kappa \text{ and } 0 < L_1 < L_{\kappa, \max},$$

$$(ii) \quad r_{\kappa, +}(E, L) > r_{\eta, +}(\tilde{E}_1, L) > r_{\eta, 2L_1} > r_{\kappa, L},$$

after possibly shrinking δ ; this is the counterpart to (2.64). We now choose $E_1 > 0$ with $\tilde{E}_2 < E_1 < E^\kappa$ for every $\kappa \in [\eta - \delta, \eta + \delta]$, and we define

$$\varepsilon := \min_{\kappa \in [\eta - \delta, \eta + \delta]} \left(\min \left\{ e^{\mu_\kappa(0)}, E^\kappa - E_1 \right\} \right).$$

From this, we deduce that for every $\kappa \in [\eta - \delta, \eta + \delta]$ and $(E, L) \in \Omega_\kappa^{EL}$ with $E_1 < E < E^\kappa$ and $0 < L < L_1$ it holds that firstly, $E - \varepsilon > \tilde{E}_2$, and thus $r_{\kappa,+}(E - \varepsilon, L) > r_{\eta,2L_1}$ due to (ii), and secondly,

$$(\Psi_{\kappa,L}^2)'(r) \geq \min_{(\kappa,s) \in [\eta-\delta, \eta+\delta] \times [r_{\eta,2L_1}, R_{\eta,\max}+1]} (\Psi_{\kappa,L_1}^2)'(s) > 0$$

for $r_{\kappa,+}(E - \varepsilon, L) < r < r_{\kappa,+}(E, L)$. Therefore, we can bound

$$\int_{r_{\kappa,+}(E-\varepsilon,L)}^{r_{\kappa,+}(E,L)} \frac{dr}{\sqrt{E^2 - \Psi_{\kappa,L}^2(r)}}$$

uniformly for the relevant values of κ and (E, L) , as in the proof of Lemma 2.3.15.¹⁰

Moreover, in the estimate from Proposition 2.3.16(b), we can choose R_1 independent of κ , e.g., by setting $R_1 = \frac{1}{2}r_{\eta,+}(E_1, 0)$ and making $\delta > 0$ smaller if necessary. By Lemma 3.2.6, the parameter $a > 0$ is independent of κ as well which finally yields via Proposition 2.3.16(b) that

$$T(E, L) \leq Q_\kappa \max \left\{ 2 \left(\frac{4\sqrt{R_{\kappa,\max}} + \sqrt{2}\pi}{\sqrt{a}} \right), \frac{\sqrt{6\pi}}{\sqrt{\min_{[0,R_1]} e^{2\mu_\kappa + 2\lambda_\kappa} \rho_\kappa}}, \right. \\ \left. \frac{6R_{\kappa,\max}}{\sqrt{\min\{e^{\mu_\kappa(0)}, E^\kappa - E_1\}}} + \frac{4\sqrt{R_{\kappa,\max}}}{\sqrt{\min_{[\eta-\delta, \eta+\delta] \times [r_{\eta,2L_1}, R_{\eta,\max}+1]} (\Psi_{\kappa,L_1}^2)'}} \right\}$$

for every $\kappa \in [\eta - \delta, \eta + \delta]$ and $(E, L) \in \tilde{\Omega}_\kappa^{EL}$ for suitable parameters a , E_1 , L_1 , and R_1 , as described above. By continuity considerations, this estimate can be bounded further by a constant independent of κ . □

This concludes our investigation of the steady state families. We could have put even more work into the details when dealing with the dependence on κ . However, the arguments that we shortened were already part of Section 2.3, and we refer the reader to this section for more details. Most of the work done in this chapter is necessary much later in Chapter 6. We now continue our work by analyzing the linearized Einstein-Vlasov system to access the question of linear stability.

¹⁰For the complete proof, we would have to consider the proof of Lemma 2.3.15 in detail and repeat most of the steps word-by-word, which we omit here.

4 Linearization of the Einstein-Vlasov system

I can calculate the motion of
heavenly bodies but not
the madness of people.

Isaac Newton

The main focus of this work is to analyze whether stationary solutions to the spherically symmetric, asymptotically flat Einstein-Vlasov system are stable or unstable under small perturbations. The comprehensive introduction on equilibria and families of steady states in the previous two chapters can be seen as a necessary preliminary for what follows next. A first step towards stability analysis consists of linearizing the system close to a steady state and studying its dynamic behavior. The linearized Einstein-Vlasov system and analysis of linear stability is, e.g., considered in [47, 52, 53, 54, 59, 60, 61, 62]. For a detailed recap of what is known about linear stability, we refer to Section 5.1.

In this chapter, we start by providing the class of steady states for which our analysis is possible in Section 4.1. The main condition that we need to prescribe is the (strict) single-well structure of the effective potential, as introduced in Definition 2.3.1. We then formulate the linearized Einstein-Vlasov system and introduce the corresponding operators in Section 4.2. The linearized system is represented by a second-order in time evolution equation governed by a self-adjoint, unbounded operator. The relevant operators are thoroughly analyzed in Section 4.3. In particular, we provide valuable information about the spectral properties of these operators. This lays the groundwork for the spectral analysis in Chapter 5.

4.1 The class of steady states under consideration

Throughout the investigation in this chapter and in Chapter 5, we consider a steady state f_0 with or without a Schwarzschild-singularity at the center, as derived in Proposition 2.2.4 and Proposition 2.2.10, respectively. We denote its metric coefficients, source terms, etc., with a subscript zero, e.g., $\mu_0, \lambda_0, \rho_0, p_0$. In the case of a spacetime with a singularity, M_0 stands for the mass of the central black hole. Similar to [47, Sc. 4.1], we have to prescribe more specific properties that need to be fulfilled by the steady state.

The distribution function f_0 is of the form

$$f_0(r, w, L) = \varphi(E(r, w, L), L), \quad (r, w, L) \in \Omega_0,$$

for some appropriate microscopic equation of state $\varphi: \mathbb{R}^2 \rightarrow [0, \infty[$. Here E is the particle energy induced by μ_0 via (2.1) and Ω_0 is the interior of the steady state support defined in (2.41). In addition, let R_{\min} and R_{\max} be the radial bounds of the steady state, as defined in (2.30). We further impose the following conditions on f_0 :

- (S1) The steady state has single-well structure, as introduced in Definition 2.3.1(a).
- (S2) The period function T , defined in (2.44), is bounded and bounded away from zero on the set $\tilde{\Omega}_0^{EL}$, which is given by (2.43).
- (S3) The microscopic equation of state φ is continuously differentiable with respect to E on $\tilde{\Omega}_0^{EL}$ with $\varphi' := \partial_E \varphi < 0$ on $\tilde{\Omega}_0^{EL}$. On $\mathbb{R}^2 \setminus \tilde{\Omega}_0^{EL}$, we set $\varphi' := 0$.
- (S4) There exists $C > 0$ such that

$$\int_{\mathbb{R}^3} |\varphi'(E, L)| dv = \frac{\pi}{r^2} \int_0^\infty \int_{\mathbb{R}} |\varphi'(E, L)| dw dL \leq C, \quad r \in]R_{\min}, \infty[. \quad (4.1)$$

At first glance, these conditions may seem confusing and rather restrictive. In both the singularity-free and the Schwarzschild-singularity case, condition (S1) is mandatory in order to introduce action-angle type variables as in Section 2.3.5, which will be used heavily in the following analysis. In particular, condition (S1) is required for (S2), which enables us to control the periodic particle motions. Condition (S3) is necessary to obtain a Hilbert space as the domain of definition for the linearized operators. Lastly, we prescribe (S4) for mere technical reasons.

The detailed analysis of the properties of steady states in Section 2.3 allows us to verify (S1)–(S4) for a broad family of stationary solutions:

Remark 4.1.1. (a) *We have seen in Proposition 2.3.5 that isotropic steady states fulfill (S1) if they are not too relativistic, i.e., if $6m < r$ holds. Moreover, in this case the period function satisfies (S2) because of Propositions 2.3.9 and 2.3.16(b). As mentioned in Remarks 2.4.1 and 2.4.3, numerical simulations demonstrate that the (strict) single-well structure and the bounds on the period functions are valid for a much larger class of equilibria. In particular, we conjecture that (S1) and (S2) hold true for general isotropic static solutions.*

(b) *In the case of stationary solutions surrounding a Schwarzschild black hole, as constructed in Proposition 2.2.10, the results in Propositions 2.3.6, 2.3.9, and 2.3.16(a) prove (S1) as well as (S2) if the mass of the Vlasov matter is sufficiently small compared to the mass of the black hole. As in part (a), numerical evidence indicates that this holds in much more generality.*

(c) *In the setting of an anisotropic steady state without a singularity, we are not able to show that the strict single-well structure is present—not even in special cases. This is to be expected for some cases since multi-shells are known to exist, as already*

commented on in Remark 2.3.2(a). However, if one can confirm the strict single-well structure numerically or with help of new techniques, we obtain that (S2) holds by Propositions 2.3.9 and 2.3.16(a) in the case where $L_0 > 0$ or $l \geq 0$.

- (d) We prescribe (S3) such that the relevant function space H , which we introduce in Section 4.2.1, becomes a Hilbert space. From a physics point of view, $\varphi' < 0$ means that more energetic stars are less common compared to less energetic stars. This is a reasonable assumption, as also argued in [59]. For example, $\varphi' < 0$ is fulfilled by the King model (2.4), the polytropes (2.5), and by most ansatz functions used in the literature.
- (e) The technical assumption (S4) is, for example, satisfied if the energy-dependency Φ for the steady states from Section 2.2 is chosen suitably. It is, e.g., true if Φ' is bounded. In addition, (S4) can be verified in the case where $L_0 > 0$, since the integral over L can be calculated explicitly, and due to $\Phi \in L^\infty([0, 1])$, as well as $R_{\min} > 0$.

4.2 The linearized Einstein-Vlasov system

We use the same linearization of the spherically symmetric, asymptotically flat Einstein-Vlasov system in Schwarzschild coordinates, as introduced by Ipser & Throne in [62], and subsequently also used in [47, 52, 53, 54]. For $0 < \varepsilon \ll 1$ and a suitably smooth function $f = f(t, r, w, L): \mathbb{R} \times [0, \infty[\times \mathbb{R} \times [0, \infty[\rightarrow \mathbb{R}$ with $f(t)$ supported on Ω_0 for $t \in \mathbb{R}$, we plug

$$f_0 + \varepsilon f + \mathcal{O}(\varepsilon^2)$$

into the Einstein-Vlasov system with or without a Schwarzschild black hole at the center and dispense with terms of order $\mathcal{O}(\varepsilon^2)$. For a detailed derivation of the following equations, we refer to Appendix A. The linearized Vlasov equation reads

$$\partial_t f = -e^{-\lambda_0} \{f, E\} + 4\pi r |\varphi'| e^{3\mu_0 + \lambda_0} \frac{w^2}{E} j_f - e^{2\mu_0 - \lambda_0} |\varphi'| w \mu'_f, \quad (4.2)$$

where

$$\{g, h\} := \partial_x g \cdot \partial_v h - \partial_v g \cdot \partial_x h = \partial_r g \partial_w h - \partial_w g \partial_r h$$

is the Poisson bracket of two spherically symmetric, differentiable functions $g(x, v) = g(r, w, L)$ and $h(x, v) = h(r, w, L)$. The linearized metric coefficients λ_f and μ_f are determined by

$$(r e^{-2\lambda_0} \lambda_f)' = 4\pi r^2 \rho_f, \quad (4.3)$$

$$\mu'_f = 4\pi r e^{2\lambda_0} p_f + \left(2\mu'_0 + \frac{1}{r}\right) \lambda_f, \quad (4.4)$$

where the source terms ρ_f , p_f , and j_f are the same as in (1.14)–(1.16). The boundary conditions are given by

$$\lim_{r \rightarrow \infty} \mu_f(t, r) = 0 = \lim_{r \rightarrow \infty} \lambda_f(t, r). \quad (4.5)$$

In the singularity-free case, we prescribe

$$\lambda_f(0) = 0, \quad (4.6)$$

while

$$\lambda_f(3M_0) = 0, \quad (4.7)$$

if there is a Schwarzschild black hole of mass M_0 at the center¹. Integrating (4.3) yields that

$$\lambda_f(r) = \frac{4\pi e^{2\lambda_0(r)}}{r} \int_{R_{\min}}^r \rho_f(s) s^2 ds, \quad r \in]2M_0, \infty[, \quad (4.8)$$

for $M_0 \geq 0$, where $M_0 = 0$ represents the singularity-free case. In summary, equations (4.2)–(4.6) are referred to as the linearized, singularity-free Einstein-Vlasov system on $[0, \infty[\times \mathbb{R} \times [0, \infty[$, whereas (4.2)–(4.5) together with (4.7) constitute the linearized Einstein-Vlasov system with a Schwarzschild-singularity of mass M_0 on $]2M_0, \infty[\times \mathbb{R} \times [0, \infty[$.

It is now possible to analyze the linearized Einstein-Vlasov system as a new dynamical system. A natural question is that of the existence of global-in-time solutions for given initial data at $t = 0$. For the singularity-free case, this is covered in [53, Thm. 5.1]. The proof can be adapted to obtain an analogous result in the setting with a singularity at the center. For our purposes, however, this is not needed since we analyze stability from a spectral analysis point of view.

As an aside, we derived the linearized system in canonical momentum variables to see if it behaves structurally differently. Unsurprisingly, it turns out that the two linearized systems are equivalent by applying a simple transformation of variables. Furthermore, we tried to transfer the setup of the linearized system from Schwarzschild to maximal areal coordinates. Firstly, it is much longer and more involved. Secondly, we did not find a way to bring the linearized system into a nice form, let alone show that the resulting linearized operators are self-adjoint which is the case in Schwarzschild coordinates, as we will see later.

In order to define and analyze linear stability properly, it turns out very useful to reformulate the linearized Einstein-Vlasov system as a second-order evolution equation for f . As preparation, we define several operators in the next subsection to keep notation short.

¹By construction of f_0 in Section 2.2.2, we have $3M_0 < R_{\min}$, i.e., it suffices to set a boundary condition at $r = 3M_0$.

4.2.1 Definition of the function spaces and operators

We now introduce suitable function spaces and the operators for which we conduct spectral analysis in Chapter 5. The approach is similar to the ones used in [47, 52, 55]. Most of our analysis takes place on the weighted L^2 -space

$$H := \left\{ f : \Omega_0 \rightarrow \mathbb{R} \text{ measurable} \mid \|f\|_H < \infty \right\}, \quad (4.9)$$

which we equip with the norm²

$$\|f\|_H^2 := 4\pi^2 \iiint_{\Omega_0} \frac{e^{\lambda_0(r)}}{|\varphi'(E, L)|} |f(r, w, L)|^2 dr dw dL.$$

Recall that $\varphi' < 0$ almost everywhere (a.e.) on Ω_0^{EL} by (S3). We thus obtain a real Hilbert space $(H, \langle \cdot, \cdot \rangle_H)$, where the scalar product is given by

$$\langle f, g \rangle_H := 4\pi^2 \iiint_{\Omega_0} \frac{e^{\lambda_0(r)}}{|\varphi'(E, L)|} f(r, w, L) g(r, w, L) dr dw dL, \quad g, h \in H.$$

While carrying out the spectral analysis, we sometimes have to allow for complex-valued functions as well. In this case, the scalar product is given by taking the complex conjugate of g in the integral above. As usual, we identify functions in H which are equal up to sets of measure zero, i.e., if they are equal a.e. We extend functions $f \in H$ by 0 to all of \mathbb{R}^3 . In Section 4.2.2, we will see that functions which are odd in w play a prominent role in our investigation. Therefore, we split $f \in H$ into its odd-in- w part f_- and even-in- w part f_+ defined by

$$f_{\pm}(r, w, L) = \frac{1}{2}(f(r, w, L) \pm f(r, -w, L)), \quad (r, w, L) \in \Omega_0,$$

i.e., $f = f_+ + f_-$ with $f_{\pm}(r, w, L) = \pm f_{\pm}(r, -w, L)$ for almost every (a.e.) value of $(r, w, L) \in \Omega_0$.³ The subspace of odd-in- w functions is denoted by

$$\mathcal{H} := \{f \in H \mid f \text{ is odd in } w \text{ a.e. on } \Omega_0\} \subset H. \quad (4.10)$$

As in [55, Rem. 5.3], we note that parity with respect to w can be translated to parity with respect to the angle variable defined in Section 2.3.5:

Remark 4.2.1. *Consider the function spaces*

$$\begin{aligned} L^{2,\text{odd}}(]0, 1[) &:= \{y \in L^2(]0, 1[) \mid y(\theta) = -y(1 - \theta) \text{ for a.e. } \theta \in]0, 1[\}, \\ L^{2,\text{even}}(]0, 1[) &:= \{y \in L^2(]0, 1[) \mid y(\theta) = y(1 - \theta) \text{ for a.e. } \theta \in]0, 1[\}. \end{aligned}$$

²To keep notation short, we do not always write out the dependence of $E = E(r, w, L)$ in full. We hope that this leads to no ambiguities.

³Note that Ω_0 is symmetric with respect to w , since f_0 is even in w by virtue of the ansatz $f_0 = \varphi(E, L)$.

For every $f \in H$, we can characterize

$$f \text{ is odd in } w \text{ a.e.} \Leftrightarrow f(\cdot, E, L) \in L^{2,\text{odd}}(]0, 1[) \text{ for a.e. } (E, L) \in \Omega_0^{EL}, \quad (4.11)$$

$$f \text{ is even in } w \text{ a.e.} \Leftrightarrow f(\cdot, E, L) \in L^{2,\text{even}}(]0, 1[) \text{ for a.e. } (E, L) \in \Omega_0^{EL}, \quad (4.12)$$

where $f = f(\theta, E, L)$ is expressed in action-angle type variables associated with f_0 .

The *transport operator* corresponding to the steady state's characteristic flow is a crucial quantity in the context of linear stability. For a suitably regular function f , it is given by

$$\begin{aligned} \mathcal{T}f &:= -e^{-\lambda_0} \{f, E\} \\ &= -e^{\mu_0 - \lambda_0} \left(\partial_r f \frac{w}{\sqrt{1 + w^2 + \frac{L}{r^2}}} - \partial_w f \left(\mu'_0 \sqrt{1 + w^2 + \frac{L}{r^2}} - \frac{L}{r^3 \sqrt{1 + w^2 + \frac{L}{r^2}}} \right) \right), \end{aligned} \quad (4.13)$$

and arises naturally from the first-order linearized Vlasov equation (4.2). Let $(R, W)(\cdot, r, w, L): \mathbb{R} \rightarrow]0, \infty[\times \mathbb{R}$ be a solution to the characteristic system (2.42) with initial data

$$(R(0, r, w, L), W(0, r, w, L), L) = (r, w, L) \in \Omega_0.$$

Then the transport operator can be written as

$$\mathcal{T}f(r, w, L) = \frac{d}{dt} [f(R(t, r, w, L), W(t, r, w, L), L)], \quad f \in C^1(\Omega_0),$$

i.e., \mathcal{T} computes the derivative of f along characteristics of the underlying steady state. The transport operator is comprehensively studied in [100]. As in this reference, we have to extend this definition to a weak sense such that we can define \mathcal{T} on a dense subset of H . In addition, we introduce a related operator \mathcal{B} , which we call the *essential operator*.⁴ Both of these operators were also defined in [47, Def. 4.2] and [52, Def. 4.11].

Definition 4.2.2. (a) For a function $f \in H$, the transport term $\mathcal{T}f$ exists weakly if there exists some $h \in H$ such that for every test function $\xi \in C_c^1(\Omega_0)$,

$$\langle f, \mathcal{T}\xi \rangle_H = -\langle h, \xi \rangle_H.$$

In this case, we set $\mathcal{T}f = h$ in a weak sense. The domain of \mathcal{T} is defined as

$$D(\mathcal{T}) := \{f \in H \mid \mathcal{T}f \text{ exists weakly}\},$$

and the resulting operator $\mathcal{T}: D(\mathcal{T}) \rightarrow H$ is called the transport operator.

⁴This terminology is due to the fact that \mathcal{B} determines the essential spectrum of the Antonov operator \mathcal{L} , which we introduce below as well. Moreover, \mathcal{B} is the main—or *essential*—operator that we have to handle throughout the investigation of linear stability.

(b) The essential operator $\mathcal{B}: D(\mathcal{T}) \rightarrow H$ is defined by

$$\mathcal{B}f := \mathcal{T}f + \mathcal{S}f,$$

where $\mathcal{S}: H \rightarrow H$ is given by

$$\mathcal{S}f := -4\pi r |\varphi'| e^{2\mu_0 + \lambda_0} \left(wp_f - \frac{w^2}{\sqrt{1 + w^2 + \frac{L}{r^2}}} jf \right).$$

(c) The response operator $\mathcal{R}: H \rightarrow H$ is defined by

$$\mathcal{R}f := 4\pi |\varphi'| e^{3\mu_0} (2r\mu'_0 + 1) w jf.$$

(d) The Antonov operator $\mathcal{L}: D(\mathcal{L}) \cap \mathcal{H} \rightarrow \mathcal{H}$ is defined on

$$D(\mathcal{L}) := D(\mathcal{T}^2) := \{f \in H \mid f \in D(\mathcal{T}), \mathcal{T}f \in D(\mathcal{T})\}$$

and given by

$$\mathcal{L} := -\mathcal{B}^2 - \mathcal{R}.$$

Remark 4.2.3. The test function space $C_c^1(\Omega_0)$ is dense in H . Therefore, the transport operator is well defined, because for $f \in D(\mathcal{T})$ the transport term $\mathcal{T}f$ is uniquely determined a.e. if it exists.

As shown in [100, Prop. 1], we have $\langle f, \mathcal{T}g \rangle_H = -\langle \mathcal{T}f, g \rangle_H$ for $f, g \in C_c^1(\Omega_0)$. In particular, the weak and the classical definition (4.13) agree for $f \in C_c^1(\Omega_0)$, and we deduce

$$C_c^1(\Omega_0) \subset D(\mathcal{T}),$$

which implies that \mathcal{T} is densely defined on H .

Before coming to the properties of the operators introduced above, we transform the linearized Einstein-Vlasov system to a system which is second-order in time.

4.2.2 A second-order formulation

The procedure of formulating the linearized Einstein-Vlasov system as a second-order evolution equation goes back to Antonov, who used it in the context of non-relativistic galactic dynamics [17]. The same method was used for the Einstein-Vlasov system in [62] and subsequently in [47, 52].

Let us formally derive the second-order formulation. We write $f = f_+ + f_-$, where f_\pm are the even-in- w and odd-in- w parts of f introduced in the previous section. The linearized Vlasov equation (4.2) can be written as

$$\partial_t f = \mathcal{B}f - |\varphi'| e^{2\mu_0 - \lambda_0} \left(2\mu'_0 + \frac{1}{r} \right) w \lambda_f,$$

after using the definition of the essential operator \mathcal{B} and (4.4). Since \mathcal{B} reverses parity with respect to w and $\lambda_f = \lambda_{f_+}$, which we will show later in detail, we get

$$\partial_t f_- = \mathcal{B}f_+ - |\varphi'|e^{2\mu_0 - \lambda_0} \left(2\mu'_0 + \frac{1}{r}\right) w \lambda_{f_+}, \quad (4.14)$$

$$\partial_t f_+ = \mathcal{B}f_-. \quad (4.15)$$

By inserting the latter equation into the former, we obtain

$$\begin{aligned} \partial_t^2 f_- &= \mathcal{B}\mathcal{B}f_- - |\varphi'|e^{2\mu_0 - \lambda_0} \left(2\mu'_0 + \frac{1}{r}\right) w \lambda_{\mathcal{B}f_-} \\ &= \mathcal{B}^2 f_- + 4\pi|\varphi'|e^{3\mu_0} (2r\mu'_0 + 1) w j_{f_-} = \mathcal{B}^2 f_- + \mathcal{R}f_- = -\mathcal{L}f_-, \end{aligned}$$

where we applied the identity⁵ $\lambda_{\mathcal{B}f_-} = -4\pi r e^{\mu_0 + \lambda_0} j_{f_-}$, which follows by an integration by parts. This yields the following lemma, partly also given in [52, Lem. 4.21].

Lemma 4.2.4. *A formal linearization of the spherically symmetric Einstein-Vlasov system takes the form*

$$\partial_t^2 f_- + \mathcal{L}f_- = 0, \quad (4.16)$$

where \mathcal{L} is the Antonov operator. More precisely, $f \in C^2(\mathbb{R} \times \Omega_0)$ solves the linearized Einstein-Vlasov system if, and only if, f_- solves (4.16), $\partial_t f_+ = \mathcal{B}f_-$ holds, and (4.3), (4.4) as well as the boundary conditions (4.5) and (4.6) or (4.7) are valid for the singularity-free or singularity case, respectively.

Proof. For the proof, we only note that the derivation above is possible rigorously for $f \in C^2(\mathbb{R} \times \Omega_0)$. Equations (4.14) and (4.15) are fulfilled in the case where f solves the linearized Einstein-Vlasov system, as well as if (4.16) and $\partial_t f_+ = \mathcal{B}f_-$ holds. \square

The Antonov operator \mathcal{L} therefore governs the behavior of solutions to the linearized system, and we will see later that \mathcal{L} has some beneficial properties, e.g., it is self-adjoint. This is why we define linear stability of a steady state through \mathcal{L} in Definition 5.1.2. We emphasize that \mathcal{L} only determines the evolution of the odd-in- w part of the linear perturbation f , and we have thus defined \mathcal{L} only on the subspace \mathcal{H} consisting of odd-in- w functions.

4.3 Properties of the operators

Deriving various properties of the operators from Definition 4.2.2 is a technical but vital endeavor. We still consider a stationary solution to the Einstein-Vlasov system, as described in Section 4.1. The current section has much overlap with [47, Sc. 5], even though we do provide more details throughout the lengthy proofs and computations. The main result of this section is a thorough understanding of the transport operator \mathcal{T}

⁵This identity will be proven rigorously later in (4.41) and can also be interpreted as the linearization of the field equation (1.12).

and the essential operator \mathcal{B} summarized in Propositions 4.3.2 and 4.3.5, respectively. Furthermore, we control the essential spectrum of these operators and the Antonov operator in Theorem 4.3.18. The reader is invited to skip forward to these references in case the details are not of interest.

From this point forwards, for a given triple of action-angle type variables (θ, E, L) , as introduced in Section 2.3.5, we denote the radial coordinate and the radial momentum by $R = R(\theta, E, L)$ and $W = W(\theta, E, L)$, respectively. More precisely,⁶

$$\partial_\theta R = T(E, L)e^{\mu_0(R)-\lambda_0(R)} \frac{W}{\sqrt{1+W^2+\frac{L}{R^2}}}, \quad (4.17a)$$

$$\partial_\theta W = T(E, L)e^{\mu_0(R)-\lambda_0(R)} \left(\frac{L}{R^3 \sqrt{1+W^2+\frac{L}{R^2}}} - \mu'_0(R) \sqrt{1+W^2+\frac{L}{R^2}} \right), \quad (4.17b)$$

where we prescribe $(R, W)(0, E, L) = (r_-(E, L), 0)$ and $(R, W)(\frac{1}{2}, E, L) = (r_+(E, L), 0)$ with $0 < r_-(E, L) < r_+(E, L)$ defined for a.e. $(E, L) \in \Omega_0^{EL}$ by Lemma 2.3.3(b). We often leave out the explicit dependency on (θ, E, L) to shorten notation. We start with an important identity that is also used in [47, 52, 59].

Lemma 4.3.1. *The following identity holds:*

$$\frac{\pi}{r^2} \int_0^\infty \int_{\mathbb{R}} w^2 |\varphi'(E(r, w, L), L)| dw dL = \frac{e^{-2\lambda_0(r)-\mu_0(r)}}{4\pi r} (\lambda'_0 + \mu'_0)(r), \quad r \in]2M_0, \infty[, \quad (4.18)$$

where $M_0 = 0$ represents the singularity-free case.

Proof. By the chain rule, we have $w \partial_E \varphi(E, L) = e^{-2\mu_0(r)} E \partial_w \varphi(E, L)$. Therefore, $|\varphi'| = -\partial_E \varphi$ implies

$$\begin{aligned} \int_0^\infty \int_{\mathbb{R}} w^2 |\varphi'(E, L)| dw dL &= -e^{-2\mu_0(r)} \int_0^\infty \int_{\mathbb{R}} w E \partial_w (\varphi(E(r, w, L), L)) dw dL \\ &= e^{-2\mu_0(r)} \int_0^\infty \int_{\mathbb{R}} \left(E + e^{2\mu_0(r)} \frac{w^2}{E} \right) \varphi(E, L) dw dL, \end{aligned}$$

where we integrated by parts in the second step. The boundary terms vanish for fixed (r, L) , because for large w we have $E(r, w, L) > E^0$, i.e., $\varphi = 0$ there. We thus obtain

$$\frac{\pi}{r^2} \int_0^\infty \int_{\mathbb{R}} w^2 |\varphi'(E(r, w, L), L)| dw dL = e^{-\mu_0(r)} (\rho_0 + p_0)(r),$$

which together with the field equations (1.10), (1.11) yields the claim in the lemma. \square

⁶This is a slightly different notation than the relation of (r, w, L) and (θ, E, L) in Lemma 2.3.17(a), where the period function $T(E, L)$ is also plugged into the first argument of R and W . We have thus rescaled the time variable in $(R, W)(\cdot, E, L)$ such that it takes values in $[0, 1]$ instead of $[0, T(E, L)]$.

4.3.1 The transport operator \mathcal{T}

As mentioned above, the transport operator has been comprehensively covered in the literature. We recall many important properties from these references and prove most of them here; see Remark 4.3.3 for a more detailed discussion. We employ action-angle type variables (θ, E, L) introduced in Section 2.3.5 in order to transform \mathcal{T} into a one-dimensional differential operator along the angle variable θ , which simplifies a lot of the proofs compared to (r, w, L) -coordinates. In order to show this property of \mathcal{T} , the function spaces

$$H_\theta^1 := \{y \in H^1(]0, 1[) \mid y(0) = y(1)\}, \quad (4.19)$$

$$H_\theta^2 := \{y \in H^2(]0, 1[) \mid y(0) = y(1) \text{ and } \dot{y}(0) = \dot{y}(1)\} = \{y \in H_\theta^1 \mid \dot{y} \in H_\theta^1\} \quad (4.20)$$

are useful to characterize the necessary regularity with respect to the angle variable. Note that the Sobolev embeddings $H^1(]0, 1[) \hookrightarrow C([0, 1])$ and $H^2(]0, 1[) \hookrightarrow C^1([0, 1])$ hold, i.e., the boundary conditions in H_θ^1 and H_θ^2 are prescribed for the continuous representatives.

We now show that \mathcal{T} and \mathcal{T}^2 act as differential operators with respect to θ . First, we formulate the following central proposition and then prove its claims step by step throughout this section.

Proposition 4.3.2. (a) *The transport operator $\mathcal{T}: \mathcal{D}(\mathcal{T}) \rightarrow H$ is well defined and skew-adjoint as a densely defined operator on H , i.e., $\mathcal{T}^* = -\mathcal{T}$. Moreover, $\mathcal{T}^2: \mathcal{D}(\mathcal{T}^2) \rightarrow H$ is self-adjoint.*

(b) *\mathcal{T} reverses w -parity, i.e., $(\mathcal{T}f)_\pm = \mathcal{T}(f_\mp)$ for $f \in \mathcal{D}(\mathcal{T})$, in particular, $f \in \mathcal{D}(\mathcal{T})$ is equivalent to $f_\pm \in \mathcal{D}(\mathcal{T})$ and the restricted operator $\mathcal{T}^2: \mathcal{D}(\mathcal{T}^2) \cap \mathcal{H} \rightarrow \mathcal{H}$ is self-adjoint as a densely defined operator on \mathcal{H} .*

(c) *For every $f \in \mathcal{D}(\mathcal{T})$, there exists a sequence $(f_n)_{n \in \mathbb{N}} \subset C_c^\infty(\Omega_0)$ such that*

$$f_n \rightarrow f, \quad \mathcal{T}f_n \rightarrow \mathcal{T}f \quad \text{in } H \text{ as } n \rightarrow \infty,$$

and $(\partial_r f_n), (\partial_w f_n)$ are bounded in H .

(d) *The domains of \mathcal{T} and \mathcal{T}^2 can be characterized by*

$$\begin{aligned} \mathcal{D}(\mathcal{T}) &= \left\{ f \in H \mid f(\cdot, E, L) \in H_\theta^1 \text{ for a.e. } (E, L) \in \Omega_0^{EL} \right. \\ &\quad \left. \text{and } \iint_{\Omega_0^{EL}} \frac{T(E, L)^{-1}}{|\varphi'(E, L)|} \int_0^1 |\partial_\theta f(\theta, E, L)|^2 d\theta dE dL < \infty \right\}, \\ \mathcal{D}(\mathcal{T}^2) &= \left\{ f \in H \mid f(\cdot, E, L) \in H_\theta^2 \text{ for a.e. } (E, L) \in \Omega_0^{EL} \right. \\ &\quad \left. \text{and } \sum_{j=1}^2 \iint_{\Omega_0^{EL}} \frac{T(E, L)^{1-2j}}{|\varphi'(E, L)|} \int_0^1 |\partial_\theta^j f(\theta, E, L)|^2 d\theta dE dL < \infty \right\}. \end{aligned}$$

In addition,

$$\begin{aligned} (\mathcal{T}f)(\theta, E, L) &= -\frac{1}{T(E, L)} (\partial_\theta f)(\theta, E, L), \quad f \in \mathcal{D}(\mathcal{T}), \\ (\mathcal{T}^2 f)(\theta, E, L) &= \frac{1}{T(E, L)^2} (\partial_\theta^2 f)(\theta, E, L), \quad f \in \mathcal{D}(\mathcal{T}^2), \end{aligned}$$

for a.e. $(\theta, E, L) \in [0, 1] \times \Omega_0^{EL}$.

(e) The kernel of \mathcal{T} consists of functions only depending on (E, L) , i.e.,

$$\ker(\mathcal{T}) = \left\{ f \in H \mid \exists g: \mathbb{R}^2 \rightarrow \mathbb{R} \text{ s.t. } f(r, w, L) = g(E(r, w, L), L) \text{ a.e. on } \Omega_0 \right\}. \quad (4.21)$$

The range and the orthogonal complement of the kernel of \mathcal{T} are equal and given by

$$\text{im}(\mathcal{T}) = \ker(\mathcal{T})^\perp = \left\{ f \in H \mid \int_0^1 f(\theta, E, L) d\theta = 0 \text{ for a.e. } (E, L) \in \Omega_0^{EL} \right\}. \quad (4.22)$$

(f) The mapping $\mathcal{T}: \mathcal{D}(\mathcal{T}) \cap \ker(\mathcal{T})^\perp \rightarrow \text{im}(\mathcal{T})$ is bijective. Its inverse $\mathcal{T}^{-1}: \text{im}(\mathcal{T}) \rightarrow \mathcal{D}(\mathcal{T}) \cap \ker(\mathcal{T})^\perp$ is given by

$$(\mathcal{T}^{-1}f)(\theta, E, L) = -T(E, L) \left(\int_0^\theta f(\tau, E, L) d\tau - \int_0^1 \int_0^\tau f(\sigma, E, L) d\sigma d\tau \right), \quad (4.23)$$

for a.e. $(\theta, E, L) \in [0, 1] \times \Omega_0^{EL}$, is bounded, and reverses w -parity.

Before we come to the proof, a comment is in order since most of these properties were already shown in similar contexts in the existing literature.

Remark 4.3.3. (a) The transport operator is thoroughly examined in [100] and an overview as in Proposition 4.3.2 can be found in [47, Prop. 5.1]. It should be mentioned that in [100], many of the features of the transport operator are derived without relying on action-angle type variables. The approach in [100] is therefore more difficult but also more general since action-angle type variables are only known to exist for limited classes of steady states, as discussed in detail in Section 2.3. In particular, not all of the properties given above require the existence of the single-well structure, as stated in Definition 2.3.1.

(b) For relevant results from operator theory, we refer to Appendix B. In particular, a short recollection of the terms skew-adjoint and self-adjoint operator can be found in Definition B.1.

(c) Most of the properties introduced above were originally derived for the transport operator corresponding to the Vlasov-Poisson system. For example, a result similar

to Proposition 4.3.2(d) is derived in [55, Lem. 5.2, Cor. 5.4]. Proposition 4.3.2(e) should be compared with [55, Lem. 5.5] and [100, Thm. 2.3].

- (d) In the non-relativistic setting, the transport operator is inverted in [50, Sc. 3.2] without using action-angle type variables, and in [55, Proof of Prop. 8.6.] via a Fourier series approach. We choose to invert \mathcal{T} by integrating in the angle variable and have to subtract the correct element in $\ker(\mathcal{T})$ in order to obtain an element in $\ker(\mathcal{T})^\perp = \text{im}(\mathcal{T})$. This approach is more useful for the upcoming investigation.

As a first part of the proof, we recall that the transport operator is skew-adjoint and that it can be approximated by smooth functions. Since most of these properties were already shown in the literature, we skim over the details.

Proof of Proposition 4.3.2(a)–(c). The operator \mathcal{T} is well defined, as explained in Remark 4.2.3. The fact that \mathcal{T} is skew-adjoint is proven in [100, Thm. 2.2]. We note that in [100], only isotropic steady states are considered. However, the methods employed there work with our different class of stationary solutions as well—also in the setting with a Schwarzschild black hole at the center. The parity properties in (b) can be deduced immediately from the weak definition of \mathcal{T} . The self-adjointness of \mathcal{T}^2 in (a) follows from von Neumann’s theorem, cf. [87, Thm. X.25]; the restricted operator is self-adjoint due to parity considerations. For the approximation by smooth functions, we refer to [100, Prop. 2] and add that the same methods, which are used in this reference in order to bound $(\mathcal{T}f_n)$, can be employed to obtain bounds on $(\partial_r f_n)$ and $(\partial_w f_n)$ as well. \square

We now provide the proof of Proposition 4.3.2(d), which was left out in [47] as it is quite similar to the non-relativistic case.

Proof of Proposition 4.3.2(d). The proof relies on methods similar to [55, Lem. 5.2], which we recall here. We start by examining the assertions for $\text{D}(\mathcal{T})$ and \mathcal{T} . Lemma 2.3.17 and the chain rule imply

$$(\mathcal{T}h)(\theta, E, L) = -\frac{1}{T(E, L)}(\partial_\theta h)(\theta, E, L), \quad h \in C_c^1(\Omega_0). \quad (4.24)$$

Consider $f \in \text{D}(\mathcal{T})$. By using the weak definition of \mathcal{T} and changing variables from (r, w, L) to (θ, E, L) via (2.71), we obtain

$$\begin{aligned} -4\pi^2 \iint_{\Omega_0^{EL}} \frac{1}{|\varphi'(E, L)|} \int_0^1 \partial_\theta h(\theta, E, L) f(\theta, E, L) d\theta dE dL &= \langle f, \mathcal{T}h \rangle_H = -\langle \mathcal{T}f, h \rangle_H \\ &= -4\pi^2 \iint_{\Omega_0^{EL}} \frac{T(E, L)}{|\varphi'(E, L)|} \int_0^1 h(\theta, E, L) (\mathcal{T}f)(\theta, E, L) d\theta dE dL \end{aligned} \quad (4.25)$$

for every $h \in C_c^1(\Omega_0)$. In particular, this holds for $h(\theta, E, L) = \chi(\theta)\xi(E, L)$ with $\chi \in C_c^\infty([0, 1])$ and $\xi \in C_c^\infty(\Omega_0^{EL})$. Inserting this into the equation above and using

that ξ can be chosen arbitrarily, implies⁷

$$\int_0^1 \frac{d\chi}{d\theta}(\theta) f(\theta, E, L) d\theta = T(E, L) \int_0^1 \chi(\theta) (\mathcal{T}f)(\theta, E, L) d\theta \quad (4.26)$$

for a.e. $(E, L) \in \Omega_0^{EL}$. This holds for every $\chi \in C_c^\infty(]0, 1[)$ and thus $f(\cdot, E, L)$ is weakly differentiable with

$$\partial_\theta f(\cdot, E, L) = -T(E, L)(\mathcal{T}f)(\cdot, E, L) \in L^2(]0, 1[)$$

for a.e. $(E, L) \in \Omega_0^{EL}$. In particular,

$$4\pi^2 \iint_{\Omega_0^{EL}} \frac{T(E, L)^{-1}}{|\varphi'(E, L)|} \int_0^1 |\partial_\theta f(\theta, E, L)|^2 d\theta dEdL = \|\mathcal{T}f\|_H^2 < \infty.$$

For the boundary condition $f(0, E, L) = f(1, E, L)$, we observe that (4.26) is valid for $\chi = 1$ as well because this still induces $h \in C_c^1(\Omega_0)$. Therefore,

$$0 = -T(E, L) \int_0^1 (\mathcal{T}f)(\theta, E, L) d\theta = \int_0^1 \partial_\theta f(\theta, E, L) d\theta = f(1, E, L) - f(0, E, L)$$

for a.e. $(E, L) \in \Omega_0^{EL}$ from an integration by parts for functions in $H^1(]0, 1[)$, which holds for the continuous representative of f .

For the reverse implication, we consider $f \in H$ with $f(\cdot, E, L) \in H_\theta^1$ for a.e. $(E, L) \in \Omega_0^{EL}$ and

$$\iint_{\Omega_0^{EL}} \frac{T(E, L)^{-1}}{|\varphi'(E, L)|} \int_0^1 |\partial_\theta f(\theta, E, L)|^2 d\theta dEdL < \infty. \quad (4.27)$$

Every test function $h \in C_c^1(\Omega_0)$ satisfies

$$h(\cdot, E, L) \in C^1(]0, 1[), \quad h(0, E, L) = h(1, E, L),$$

directly from the definition of action-angle type variables, see Lemma 2.3.17. Therefore, (4.24) and an integration by parts similar to (4.25) above yield

$$\langle f, \mathcal{T}h \rangle_H = 4\pi^2 \iiint_{\Omega_0} \frac{e^{\lambda_0}}{|\varphi'(E, L)|} \frac{(\partial_\theta f)(r, w, L)}{T(E, L)} h(r, w, L) dr dw dL, \quad h \in C_c^1(\Omega_0),$$

which, together with the weak definition of the transport operator, implies that

$$\mathcal{T}f = -\frac{1}{T(E, L)} \partial_\theta f$$

⁷Note that we can choose the set of measure zero independently of χ by considering a countable subset of $C_c^\infty(]0, 1[)$, which is dense in $H^1(]0, 1[)$.

holds weakly. In addition, we have $f \in D(\mathcal{T})$, because $\mathcal{T}f \in H$ from (4.27). This finishes the proof for the characterization of $D(\mathcal{T})$ and the properties of \mathcal{T} . By applying this result to $\mathcal{T}f$ instead of f , we obtain the claims for both $D(\mathcal{T}^2)$ and \mathcal{T}^2 . \square

From the representation of the transport operator in part (d), it is an easy task to determine the kernel of \mathcal{T} and consequently show that the range (or image) of \mathcal{T} is closed.

Proof of Proposition 4.3.2(e). The fact that every function $g = g(E, L) \in H$ is an element in $\ker(\mathcal{T})$ follows from Proposition 4.3.2(d) because obviously $g(E, L) \in H_\theta^1$ for a.e. $(E, L) \in \Omega_0^{EL}$ and $\partial_\theta g = 0$. Conversely, let $f \in \ker(\mathcal{T})$, i.e., according to Proposition 4.3.2(d), we have $f(\cdot, E, L) \in H_\theta^1$ with $\partial_\theta f(\cdot, E, L) = 0$ for a.e. $(E, L) \in \Omega_0^{EL}$. This implies

$$f(\theta, E, L) = f(0, E, L) + \int_0^\theta \partial_\theta f(\theta, E, L) d\theta = f(0, E, L)$$

for a.e. $(E, L) \in \Omega_0^{EL}$ and thus shows (4.21).

From [25, Cor. 2.18(iv)], we deduce $\ker(\mathcal{T})^\perp = \overline{\text{im}(\mathcal{T})}$ and therefore only have to prove $\ker(\mathcal{T})^\perp \subseteq \text{im}(\mathcal{T})$. For $g \in \ker(\mathcal{T})^\perp$, we show that there exists $f \in D(\mathcal{T})$ such that $\mathcal{T}f = g$, which implies $g \in \text{im}(\mathcal{T})$. We define the function $f: \Omega_0 \rightarrow \mathbb{R}$ through

$$f(\theta, E, L) := -T(E, L) \int_0^\theta g(\tau, E, L) d\tau,$$

which is weakly differentiable in θ with $\partial_\theta f(\cdot, E, L) = -T(E, L)g(\cdot, E, L)$ for a.e. $(E, L) \in \Omega_0^{EL}$. Moreover,

$$|f(\theta, E, L)|^2 \leq T(E, L)^2 \int_0^1 |g(\tau, E, L)|^2 d\tau$$

and therefore $f \in H$ due to

$$\|f\|_H^2 \leq 4\pi^2 \iint_{\Omega_0^{EL}} \frac{T(E, L)^3}{|\varphi'(E, L)|} \int_0^1 |g(\tau, E, L)|^2 d\tau dE dL \leq \sup_{\tilde{\Omega}_0^{EL}} (T^2) \|g\|_H^2,$$

where we recall from (S2) that T is bounded on $\tilde{\Omega}_0^{EL}$. Since $g \in \ker(\mathcal{T})^\perp$, we get

$$0 = \langle g, h \rangle_H = 4\pi^2 \iint_{\Omega_0^{EL}} \frac{T(E, L)}{|\varphi'(E, L)|} \left(\int_0^1 g(\theta, E, L) d\theta \right) h(E, L) dE dL$$

for every $h = h(E, L) \in \ker(\mathcal{T})$, and thus

$$\int_0^1 g(\theta, E, L) d\theta = 0$$

for a.e. $(E, L) \in \Omega_0^{EL}$. Combining these results yields $f \in H^1(]0, 1[)$ as well as

$f(0, E, L) = f(1, E, L)$, and hence $f \in \mathcal{D}(\mathcal{T})$ by Proposition 4.3.2(d) because of

$$\iint_{\Omega_0^{EL}} \frac{T(E, L)^{-1}}{|\varphi'(E, L)|} \int_0^1 |\partial_\theta f(\theta, E, L)|^2 d\theta dE dL = \|g\|_H^2 < \infty.$$

We have $\mathcal{T}f = g$ by Proposition 4.3.2(d), i.e., $g \in \text{im}(\mathcal{T})$. \square

Proof of Proposition 4.3.2(f). For $g \in \text{im}(\mathcal{T})$, we define

$$(\mathcal{G}g)(\theta, E, L) = -T(E, L) \left(\int_0^\theta g(\tau, E, L) d\tau - \int_0^1 \int_0^\tau g(\sigma, E, L) d\sigma d\tau \right)$$

and aim to prove $\mathcal{G} = \mathcal{T}^{-1}$. We first show that $\mathcal{G}g \in \mathcal{D}(\mathcal{T})$ with help of Proposition 4.3.2(d). For a.e. $(E, L) \in \Omega_0^{EL}$, we observe $\mathcal{G}g(\cdot, E, L) \in H_\theta^1$, because⁸

$$|(\mathcal{G}g)(\cdot, E, L)|^2 \leq C \int_0^1 |g(\tau, E, L)|^2 d\tau \quad (4.28)$$

and since $\mathcal{G}g$ is weakly differentiable in θ with $\partial_\theta(\mathcal{G}g)(\cdot, E, L) = -T(E, L)g(\cdot, E, L)$. Moreover $(\mathcal{G}g)(0, E, L) = (\mathcal{G}g)(1, E, L)$ due to $\int_0^1 g(\tau, E, L) d\tau = 0$ for a.e. $(E, L) \in \Omega_0^{EL}$ by (4.22). We again apply the characterization (4.22) and obtain

$$\int_0^1 (\mathcal{G}g)(\theta, E, L) d\theta = -T(E, L) \left(\int_0^1 \int_0^\theta g(\tau, E, L) d\tau d\theta - \int_0^1 \int_0^\sigma g(\tau, E, L) d\tau d\sigma \right) = 0$$

for a.e. $(E, L) \in \Omega_0^{EL}$, which implies $\mathcal{G}g \in \ker(\mathcal{T})^\perp$. Therefore, the mapping $\mathcal{G}: \text{im}(\mathcal{T}) \rightarrow \mathcal{D}(\mathcal{T}) \cap \ker(\mathcal{T})^\perp$ is well defined. For $g \in \text{im}(\mathcal{T})$, we compute

$$\begin{aligned} & (\mathcal{T}\mathcal{G}g)(\theta, E, L) \\ &= \frac{1}{T(E, L)} \partial_\theta \left(T(E, L) \left(\int_0^\theta g(\tau, E, L) d\tau - \int_0^1 \int_0^\sigma g(\tau, E, L) d\tau d\sigma \right) \right) = g(\theta, E, L) \end{aligned}$$

for a.e. $(E, L) \in \Omega_0^{EL}$, where we employed the representation of \mathcal{T} from Proposition 4.3.2(d). Lastly, this part of the proposition together with (4.22) also yields

$$\begin{aligned} (\mathcal{G}\mathcal{T}f)(\theta, E, L) &= \int_0^\theta \partial_\theta f(\tau, E, L) d\tau - \int_0^1 \int_0^\sigma \partial_\theta f(\tau, E, L) d\tau d\sigma \\ &= f(\theta, E, L) - \int_0^1 f(\sigma, E, L) d\sigma = f(\theta, E, L) \end{aligned}$$

for $f \in \mathcal{D}(\mathcal{T}) \cap \ker(\mathcal{T})^\perp$ and a.e. $(E, L) \in \Omega_0^{EL}$. We thus deduce that $\mathcal{G} = \mathcal{T}^{-1}$ and that \mathcal{T}^{-1} is bounded because of (4.28). The fact that \mathcal{T} reverses w -parity immediately implies the same property for \mathcal{T}^{-1} ; see also Remark 4.2.1. \square

⁸The constant $C > 0$ does not depend on g . Note again that T is bounded on $\tilde{\Omega}_0^{EL}$ from (S2).

With this in-depth knowledge of the transport operator \mathcal{T} at hand, we can now turn to the essential operator \mathcal{B} . Its analysis is more involved.

4.3.2 The essential operator \mathcal{B}

In order to derive a Birman-Schwinger principle for the operator $\mathcal{L} = -\mathcal{B}^2 - \mathcal{R}$, we need a comprehensive understanding of the essential operator \mathcal{B} defined in Definition 4.2.2(b). We want to derive more or less analogous results for \mathcal{B} , as for \mathcal{T} gathered in Proposition 4.3.2. This turns out more difficult than the analysis for \mathcal{T} since \mathcal{B} introduces non-local terms via p_f and j_f , and because we do not have access to action-angle type variables that are in some sense adapted to \mathcal{B} .

The main difficulties arise from the inversion of \mathcal{B} and \mathcal{B}^2 . We need to determine $(\mathcal{B}^2)^{-1}$ as explicitly as possible for two key reasons: Firstly, we have to ascertain that the spectrum of \mathcal{B}^2 restricted to odd-in- w functions stays away from zero, which we do in Section 4.3.4. Secondly, by construction we need $(\mathcal{B}^2)^{-1}$ in order to derive a Birman-Schwinger principle in Chapter 5.

As in [47, Def. 5.7], the following operator $\tilde{\mathcal{B}}^{-1}$ turns out quite useful and is actually a right-inverse of \mathcal{B} . We will see later in Lemma 4.3.10 that $\tilde{\mathcal{B}}^{-1}$ is well defined.

Definition 4.3.4. *The operator $\tilde{\mathcal{B}}^{-1}: \ker(\mathcal{B})^\perp \rightarrow \mathcal{D}(\mathcal{T})$ is defined by*

$$\begin{aligned} \tilde{\mathcal{B}}^{-1}f := & \mathcal{T}^{-1} \left(f + |\varphi'| e^{2\mu_0} \lambda_f \frac{w^2}{E} \right) \\ & + 4\pi |\varphi'| E e^{-\lambda_0 - \mu_0} \int_r^{R_{\max}} e^{(3\lambda_0 + \mu_0)(s)} p_{\mathcal{T}^{-1}(f + |\varphi'| e^{2\mu_0} \lambda_f \frac{w^2}{E})(s)} s \, ds. \end{aligned} \quad (4.29)$$

We proceed in a similar manner as in the previous section and first state all the properties of \mathcal{B} in the upcoming proposition. The reader should be warned that some steps of the subsequent proofs are quite technical and peppered with many non-trivial calculations.

Proposition 4.3.5. *(a) The essential operator $\mathcal{B}: \mathcal{D}(\mathcal{T}) \rightarrow H$ is well defined and skew-adjoint as a densely defined operator on H , i.e., $\mathcal{B}^* = -\mathcal{B}$. Moreover, $\mathcal{B}^2: \mathcal{D}(\mathcal{T}^2) \rightarrow H$ is self-adjoint.*

(b) \mathcal{B} reverses w -parity, i.e., $(\mathcal{B}f)_\pm = \mathcal{B}(f_\mp)$ for $f \in \mathcal{D}(\mathcal{T})$. Moreover, \mathcal{B}^2 conserves w -parity, and the restricted operator $\mathcal{B}^2 = \mathcal{B}^2|_{\mathcal{H}}: \mathcal{D}(\mathcal{T}^2) \cap \mathcal{H} \rightarrow \mathcal{H}$ is self-adjoint as a densely defined operator on \mathcal{H} .

(c) For every $f \in \mathcal{D}(\mathcal{T})$, there exists a sequence $(f_n)_{n \in \mathbb{N}} \subset C_c^\infty(\Omega_0)$ such that

$$f_n \rightarrow f, \quad \mathcal{B}f_n \rightarrow \mathcal{B}f \quad \text{in } H \text{ as } n \rightarrow \infty,$$

and $(\partial_r f_n), (\partial_w f_n)$ are bounded in H .

(d) There exists a bijective mapping between $\ker(\mathcal{T})$ and $\ker(\mathcal{B})$, where

$$\ker(\mathcal{B}) = \left\{ g + 4\pi|\varphi'|Ee^{-\lambda_0-\mu_0} \int_r^{R_{\max}} e^{(3\lambda_0+\mu_0)(s)} p_g(s) s ds \mid g \in \ker \mathcal{T} \right\}. \quad (4.30)$$

(e) It holds that $\text{im}(\mathcal{B}) = \text{im}(\mathcal{B}^2)$, $\ker(\mathcal{B}) = \ker(\mathcal{B}^2)$, $\mathcal{H} \subset \ker(\mathcal{B})^\perp = \text{im}(\mathcal{B})$, and

$$\ker(\mathcal{B})^\perp = \left\{ f \in H \mid \int_0^1 \left(f^+ |\varphi'| e^{2\mu_0(R)} \lambda_f(R) \frac{W^2}{E} \right) d\theta = 0 \text{ for a.e. } (E, L) \in \Omega_0^{EL} \right\}, \quad (4.31)$$

where the notation introduced at the beginning of Section 4.3 is used, i.e., $R = R(\theta, E, L)$ and $W = W(\theta, E, L)$.

(f) The operator $\mathcal{B}: \text{D}(\mathcal{T}) \cap \ker(\mathcal{B})^\perp \rightarrow \text{im}(\mathcal{B})$ is bijective. The bounded and skew-symmetric inverse is given by

$$\mathcal{B}^{-1} = (\text{id} - \Pi) \tilde{\mathcal{B}}^{-1}, \quad (4.32)$$

with $\tilde{\mathcal{B}}^{-1}$ defined in Definition 4.3.4 and $\Pi: H \rightarrow \ker(\mathcal{B})$ being the orthogonal projection⁹ onto $\ker(\mathcal{B})$. Moreover, \mathcal{B}^{-1} reverses w -parity.

(g) The operator $\mathcal{B}^2: \text{D}(\mathcal{T}^2) \cap \ker(\mathcal{B}^2)^\perp \rightarrow \text{im}(\mathcal{B}^2)$ is bijective. The bounded and symmetric inverse is given by

$$(\mathcal{B}^2)^{-1} = \mathcal{B}^{-1} \mathcal{B}^{-1} =: \mathcal{B}^{-2}. \quad (4.33)$$

Moreover, \mathcal{B}^{-2} conserves w -parity.

(h) There exists $C > 0$ such that

$$\|\mathcal{B}f\|_H \geq C\|f\|_H, \quad f \in \text{D}(\mathcal{T}) \cap \ker(\mathcal{B})^\perp. \quad (4.34)$$

Before attending to the proof—we do this step by step in this section—some preliminary results are necessary in order to show the claims in Proposition 4.3.5. For example, we have to analyze the source terms and ensure that they are in some sense bounded operators. The next lemma draws on and extends [47, Lem. 5.2]. Throughout the upcoming proofs, $C > 0$ denotes a constant that may depend on steady state quantities but never on elements in H or $r \in]2M_0, \infty[$.

Lemma 4.3.6. (a) *The mappings*

$$\begin{aligned} H \ni f &\mapsto |\varphi'| \rho_f, |\varphi'| p_f, |\varphi'| j_f \in H, \\ H \ni f &\mapsto r^2 \rho_f, r^2 p_f, r^2 j_f \in L^2([R_{\min}, R_{\max}]) \end{aligned}$$

⁹We refer to Definition B.2 and Lemma B.3 for details and further references on orthogonal projections.

are bounded, where ρ_f, p_f, j_f are defined in (1.14)–(1.16). The mapping

$$H \ni f \mapsto \lambda_f \in L^2([R_{\min}, R_{\max}])$$

is compact with λ_f given by (4.8).

(b) For $f \in C_c^1(\Omega_0)$,

$$p'_f = -\mu'_0(\rho_f + p_f) - \frac{2}{r}(p_f - q_f) - e^{\lambda_0 - \mu_0} j_{\mathcal{T}f}, \quad (4.35)$$

$$j'_f = -2\left(\mu'_0 + \frac{1}{r}\right)j_f - e^{\lambda_0 - \mu_0} \rho_{\mathcal{T}f}. \quad (4.36)$$

The mappings

$$D(\mathcal{T}) \ni f \mapsto |\varphi'| (rp_f)' \in H, \quad D(\mathcal{T}) \ni f \mapsto |\varphi'| (rj_f)' \in H$$

are well defined and bounded, if $D(\mathcal{T})$ is equipped with the norm $\|\cdot\|_H + \|\mathcal{T}\cdot\|_H$ and the derivatives are taken in the weak sense.

Proof. In the following, we repeatedly use that the steady state support is compact. We apply the Cauchy-Schwarz inequality and obtain

$$|\rho_f(r)| \leq \rho_{|f|}(r) \leq C \left(\int_{\mathbb{R}^3} |\varphi'(E, L)| dv \right)^{\frac{1}{2}} \left(\int_{\mathbb{R}^3} \frac{|f|^2}{|\varphi'(E, L)|} dv \right)^{\frac{1}{2}}, \quad r > 2M_0, \quad (4.37)$$

with $C > 0$ independent from r by using (S4), which readily proves that

$$H \ni f \mapsto r^2 \rho_f \in L^2([R_{\min}, R_{\max}])$$

is bounded. Furthermore, (4.37) and (S4) also imply

$$\| |\varphi'| \rho_f \|_H^2 \leq \int_{\mathbb{R}^3} \int_{\mathbb{R}^3} e^{\lambda_0} |\varphi'(E, L)| |\rho_f|^2 dx dv \leq C \|f\|_H^2.$$

The boundedness for the mappings involving p_f and j_f follows from $|j_f|, |p_f| \leq \rho_{|f|}$. For the compactness of $f \mapsto \lambda_f$, let $(f_n)_{n \in \mathbb{N}} \subset H$, which converges weakly to 0 in H . The explicit formula (4.8) yields

$$\|\lambda_{f_n}\|_{L^2([R_{\min}, R_{\max}])}^2 = \int_{R_{\min}}^{R_{\max}} \frac{e^{4\lambda_0(r)}}{r^2} \left\langle e^{-\lambda_0} |\varphi'| \sqrt{1 + w^2 + \frac{L}{s^2}} \mathbb{1}_{[R_{\min}, r]}, f_n \right\rangle_H^2 dr. \quad (4.38)$$

It is easy to see that for every $r \in [R_{\min}, R_{\max}]$ the function

$$\Omega_0 \ni (s, w, L) \mapsto e^{-\lambda_0(s)} |\varphi'(E(s, w, L), L)| \sqrt{1 + w^2 + \frac{L}{s^2}} \mathbb{1}_{[R_{\min}, r]}(s)$$

is an element of H , and by the weak convergence of (f_n) in H , we deduce that the scalar product in (4.38) converges to zero pointwise in $r \in [R_{\min}, R_{\max}]$. In addition, the Cauchy-Schwarz inequality and (S4) yield

$$\left\langle e^{-\lambda_0} |\varphi'| \sqrt{1 + w^2 + \frac{L}{s^2}} \mathbb{1}_{[R_{\min}, r]}, f_n \right\rangle_H^2 \leq C \|f_n\|_H^2,$$

which is uniformly bounded in n due to the weak convergence of (f_n) ; recall also that φ' vanishes outside of Ω_0 . Hence, Lebesgue's theorem implies that the term in (4.38) goes to zero as $n \rightarrow \infty$, which proves the compactness.

As to part (b), for $r > 2M_0$ and $f \in C_c^1(\Omega_0)$, we compute

$$\begin{aligned} p'_f(r) &= -\frac{2}{r} p_f(r) + \frac{\pi}{r^2} \int_0^\infty \int_{\mathbb{R}} \frac{w^2 L}{r^3 \left(1 + w^2 + \frac{L}{r^2}\right)^{\frac{3}{2}}} f(r, w, L) \, dw dL \\ &\quad + \frac{\pi}{r^2} \int_0^\infty \int_{\mathbb{R}} \frac{w^2}{\sqrt{1 + w^2 + \frac{L}{r^2}}} \partial_r f(r, w, L) \, dw dL. \end{aligned} \quad (4.39)$$

By solving for $\partial_r f$ in the transport term (4.13), we obtain

$$\begin{aligned} &\frac{\pi}{r^2} \int_0^\infty \int_{\mathbb{R}} \frac{w^2}{\sqrt{1 + w^2 + \frac{L}{r^2}}} \partial_r f(r, w, L) \, dw dL \\ &= \frac{\pi}{r^2} \int_0^\infty \int_{\mathbb{R}} w \left(-e^{\lambda_0(r) - \mu_0(r)} \mathcal{T}f + \partial_w f \left(\mu'_0 \sqrt{1 + w^2 + \frac{L}{r^2}} - \frac{L}{r^3 \sqrt{1 + w^2 + \frac{L}{r^2}}} \right) \right) \, dw dL \\ &= -e^{\lambda_0(r) - \mu_0(r)} j_{\mathcal{T}f} - \mu'_0(\rho_f + p_f) + \frac{2}{r} q_f - \frac{\pi}{r^2} \int_0^\infty \int_{\mathbb{R}} \frac{w^2 L}{r^3 \left(1 + w^2 + \frac{L}{r^2}\right)^{\frac{3}{2}}} f(r, w, L) \, dw dL \end{aligned}$$

after an integration by parts. Boundary terms vanish due to the compact support of f . Putting this into (4.39) gives the claim in (4.35). A similar calculation shows

$$\begin{aligned} j'_f(r) &= -\frac{2}{r} j_f \\ &\quad + \frac{\pi}{r^2} \int_0^\infty \int_{\mathbb{R}} \left(-e^{\lambda_0(r) - \mu_0(r)} \mathcal{T}f \sqrt{1 + w^2 + \frac{L}{r^2}} + \partial_w f \left(\mu'_0 \left(1 + w^2 + \frac{L}{r^2}\right) - \frac{L}{r^3} \right) \right) \, dw dL \end{aligned}$$

and integrating by parts in w yields (4.36). In order to prove the last claim in (b), we first show that the weak derivative exists. More precisely, that there exists $h \in L^1_{\text{loc}}(\Omega_0)$ with

$$\langle r p_f, \partial_r \xi \rangle_{L^2(\Omega_0)} = -\langle h, \xi \rangle_{L^2(\Omega_0)}, \quad \xi \in C_c^\infty(\Omega_0), \quad (4.40)$$

i.e., $(r p_f)' = h$ in a weak sense. According to Proposition 4.3.2(c), there exists a sequence

$(f_n)_{n \in \mathbb{N}} \subset C_c^\infty(\Omega_0)$ such that

$$f_n \rightarrow f, \quad \mathcal{T}f_n \rightarrow \mathcal{T}f \quad \text{in } H \text{ as } n \rightarrow \infty.$$

Together with part (a), we can thus write

$$\begin{aligned} \langle rp_f, \partial_r \xi \rangle_{L^2(\Omega_0)} &= \left\langle |\varphi'| rp_f, e^{-\lambda_0} \partial_r \xi \right\rangle_H \\ &= \lim_{n \rightarrow \infty} \left\langle |\varphi'| rp_{f_n}, e^{-\lambda_0} \partial_r \xi \right\rangle_H = - \lim_{n \rightarrow \infty} \left\langle |\varphi'| (rp_{f_n})', e^{-\lambda_0} \xi \right\rangle_H \end{aligned}$$

after an integration by parts. From (4.35) we get

$$(rp_{f_n})' = -r\mu_0'(\rho_{f_n} + p_{f_n}) - p_{f_n} + 2q_{f_n} - re^{\lambda_0 - \mu_0} j_{\mathcal{T}f_n} =: h_n.$$

The choice of (f_n) and part (a) imply that $|\varphi'|h_n$ converges to $|\varphi'|h$ in H for $n \rightarrow \infty$ with

$$h := -r\mu_0'(\rho_f + p_f) - p_f + 2q_f - re^{\lambda_0 - \mu_0} j_{\mathcal{T}f}.$$

Therefore, we get

$$\langle rp_f, \partial_r \xi \rangle_{L^2(\Omega_0)} = - \left\langle |\varphi'|h, e^{-\lambda_0} \xi \right\rangle_H = - \langle h, \xi \rangle_{L^2(\Omega_0)},$$

which proves (4.40). The boundedness now follows from the result in (a) via

$$\| |\varphi'| (rp_f)' \|_H = \| |\varphi'| h \|_H \leq C (\| |\varphi'| \rho_f \|_H + \| |\varphi'| j_{\mathcal{T}f} \|_H) \leq C (\| f \|_H + \| \mathcal{T}f \|_H).$$

The assertions for $(rj_f)'$ follow in a similar manner. \square

We now show the first few properties of the essential operator \mathcal{B} stated in the main proposition of this section.

Proof of Proposition 4.3.5(a)–(c). Due to Definition 4.2.2(b), we have $\mathcal{B} = \mathcal{T} + \mathcal{S}$ and, according to Lemma 4.3.6(a), the operator \mathcal{S} is well defined and bounded on H . Moreover, \mathcal{S} is skew-symmetric since for $f, g \in H$, it holds that

$$\begin{aligned} \langle \mathcal{S}f, g \rangle_H &= \left\langle -4\pi r |\varphi'| e^{2\mu_0 + \lambda_0} \left(wp_f - \frac{w^2}{\sqrt{1 + w^2 + \frac{L}{r^2}}} j_f \right), g \right\rangle_H \\ &= (4\pi)^2 \int_{R_{\min}}^{R_{\max}} e^{2\mu_0 + 2\lambda_0} r^3 (p_g j_f - p_f j_g) dr. \end{aligned}$$

Hence, $\mathcal{B} = \mathcal{T} + \mathcal{S}$ is skew-adjoint as per the Kato-Rellich theorem [87, Thm. X.12] with domain $D(\mathcal{B}) := D(\mathcal{T})$. Thus, von Neumann's theorem [87, Thm. X.25] implies that \mathcal{B}^2 is self-adjoint on the domain $D(\mathcal{B}^2) := \{f \in D(\mathcal{B}) \mid \mathcal{B}f \in D(\mathcal{B})\}$. We claim that $D(\mathcal{B}^2) = D(\mathcal{T}^2)$. To see this equality, it remains to show that $\mathcal{S}f \in D(\mathcal{T})$ for $f \in D(\mathcal{T})$,

which we accomplish via the weak definition of \mathcal{T} . For $\xi \in C_c^1(\Omega_0)$, we have

$$\begin{aligned} \langle \mathcal{S}f, \mathcal{T}\xi \rangle_H &= 4\pi \left\langle |\varphi'| e^{3\mu_0} \left(\frac{w^2}{\sqrt{1+w^2+\frac{L}{r^2}}} r p_f - \frac{w^3}{1+w^2+\frac{L}{r^2}} r j_f \right), \partial_r \xi \right\rangle_H \\ &- 4\pi \left\langle |\varphi'| e^{3\mu_0} \left(w r p_f - \frac{w^2}{\sqrt{1+w^2+\frac{L}{r^2}}} r j_f \right) \left(\mu'_0 e^{-\mu_0} E - \frac{L}{r^3 \sqrt{1+w^2+\frac{L}{r^2}}} \right), \partial_w \xi \right\rangle_H, \end{aligned}$$

where we can integrate by parts in both terms since $\partial_r(r p_f)$ as well as $\partial_r(r j_f)$ exist weakly, according to Lemma 4.3.6(b), and the remaining terms are continuously differentiable in r and w , respectively. Boundary terms vanish because ξ has compact support. Therefore, we get

$$\langle \mathcal{S}f, \mathcal{T}\xi \rangle_H = -\langle h, \xi \rangle_H$$

for a suitable function h . By computing h explicitly (via the product rule for weak derivatives), it is easy to see that $h \in H$ due to $f \in D(\mathcal{T})$ and Lemma 4.3.6(b).

Since \mathcal{T} and \mathcal{S} reverse w -parity, so does \mathcal{B} . In addition, \mathcal{B}^2 preserves w -parity which proves Proposition 4.3.5(b). Lastly, the approximation property follows directly from Proposition 4.3.2(c) and the fact that \mathcal{S} is bounded. \square

As in [47, Lem. 5.4], an additional auxiliary result is needed which will be crucial across the investigation. The first of these identities can be interpreted as the linearized version of the field equation (1.12).

Lemma 4.3.7. *Let $f \in D(\mathcal{T})$. Then the following identities hold for a.e. $r \in [R_{\min}, \infty[$:*

$$\lambda_{\mathcal{B}f}(r) = -4\pi r e^{(\mu_0+\lambda_0)(r)} j_f(r), \quad (4.41)$$

$$\lambda_{e^{\mu_0+\lambda_0} \mathcal{T}f}(r) = -4\pi r e^{(2\mu_0+2\lambda_0)(r)} j_f(r). \quad (4.42)$$

Proof. By Propositions 4.3.2(c) and 4.3.5(c), we can approximate $f \in D(\mathcal{T})$ and simultaneously $\mathcal{T}f$ or $\mathcal{B}f$, respectively, with smooth functions. Because of Lemma 4.3.6(a), it is therefore sufficient to show (4.41) and (4.42) for $f \in C_c^\infty(\Omega_0)$.

We insert (4.13) into (4.8) and integrate by parts to obtain

$$\begin{aligned} &\lambda_{\mathcal{T}f}(r) \\ &= -\frac{4\pi^2 e^{2\lambda_0(r)}}{r} \int_{R_{\min}}^r \int_0^\infty \int_{\mathbb{R}} e^{(\mu_0-\lambda_0)(s)} \left(w \partial_r f - \partial_w f \left(\mu'_0(s) \left(1 + w^2 + \frac{L}{s^2} \right) - \frac{L}{s^3} \right) \right) dw dL ds \\ &= -4\pi r e^{(\mu_0+\lambda_0)(r)} j_f(r) - \frac{4\pi e^{2\lambda_0(r)}}{r} \int_{R_{\min}}^r (\mu'_0 + \lambda'_0)(s) e^{(\mu_0-\lambda_0)(s)} j_f(s) s^2 ds \end{aligned} \quad (4.43)$$

for $r \geq R_{\min}$. Moreover, plugging $\mathcal{S}f$ into (4.8) yields

$$\begin{aligned} \lambda_{\mathcal{S}f}(r) &= \frac{16\pi^3 e^{2\lambda_0(r)}}{r} \int_{R_{\min}}^r \int_0^\infty \int_{\mathbb{R}} s |\varphi'| e^{(2\mu_0 + \lambda_0)(s)} \left(w \sqrt{1 + w^2 + \frac{L}{s^2}} p_f(s) - w^2 j_f(s) \right) dw dL ds \\ &= -\frac{16\pi^2 e^{2\lambda_0(r)}}{r} \int_{R_{\min}}^r s^3 e^{(2\mu_0 + \lambda_0)(s)} j_f(s) \left(\frac{\pi}{s^2} \int_0^\infty \int_{\mathbb{R}} |\varphi'| w^2 dw dL \right) ds, \end{aligned}$$

where we have used that the first term vanishes since it is odd in w . By (4.18), we get

$$\lambda_{\mathcal{S}f}(r) = \frac{4\pi e^{2\lambda_0(r)}}{r} \int_{R_{\min}}^r (\mu'_0 + \lambda'_0)(s) e^{(\mu_0 - \lambda_0)(s)} j_f(s) s^2 ds,$$

which together with (4.43) implies (4.41). Similar to (4.43), we obtain¹⁰

$$\begin{aligned} \lambda_{e^{\mu_0 + \lambda_0} \mathcal{T}f}(r) &= -\frac{4\pi^2 e^{2\lambda_0(r)}}{r} \int_{R_{\min}}^r \int_0^\infty \int_{\mathbb{R}} e^{2\mu_0(s)} \left(w \partial_r f - \partial_w f \left(\mu'_0(s) \left(1 + w^2 + \frac{L}{s^2} \right) - \frac{L}{s^3} \right) \right) dw dL ds \\ &= -4\pi r e^{(2\mu_0 + 2\lambda_0)(r)} j_f(r) \end{aligned}$$

and thus (4.42). \square

With the knowledge about $\ker(\mathcal{T})$ from Proposition 4.3.2(e), we can now characterize elements in the kernel of \mathcal{B} explicitly and find a bijective mapping from $\ker(\mathcal{T})$ to $\ker(\mathcal{B})$, see [47, Lem. 5.5]. With the next lemma we prove the claim in Proposition 4.3.5(d).

Lemma 4.3.8. (a) *The kernel of \mathcal{B} is given by*

$$\ker(\mathcal{B}) = \left\{ g + 4\pi |\varphi'| E e^{-\lambda_0 - \mu_0} \int_r^{R_{\max}} e^{(3\lambda_0 + \mu_0)(s)} p_g(s) s ds \mid g = g(E, L) \in \ker \mathcal{T} \right\}.$$

When $f \in \ker(\mathcal{B})$ is of the form above, we refer to g as the generator of f . This generator is given by

$$g(E, L) = f\left(\frac{1}{2}, E, L\right) - 4\pi |\varphi'(E, L)| E \int_{r_+(E, L)}^{R_{\max}} e^{2\lambda_0(s)} p_f(s) s ds$$

for a.e. $(E, L) \in \Omega_0^{EL}$. Moreover,

$$f(\theta, E, L) = g(E, L) + 4\pi |\varphi'(E, L)| E \int_{R(\theta, E, L)}^{R_{\max}} e^{2\lambda_0(s)} p_f(s) s ds \quad (4.44)$$

holds for $\theta \in [0, 1]$ and a.e. $(E, L) \in \Omega_0^{EL}$.

¹⁰The weight $e^{\mu_0 + \lambda_0}$ is chosen such that only the boundary term remains after integrating by parts.

(b) *The mappings*

$$\ker(\mathcal{T}) \ni g \mapsto g + 4\pi|\varphi'|Ee^{-\lambda_0-\mu_0} \int_r^{R_{\max}} e^{(3\lambda_0+\mu_0)(s)} p_g(s) s ds \in \ker(\mathcal{B}), \quad (4.45)$$

$$\ker(\mathcal{B}) \ni f \mapsto f\left(\frac{1}{2}, E, L\right) - 4\pi|\varphi'|E \int_{r_+(E,L)}^{R_{\max}} e^{2\lambda_0(s)} p_f(s) s ds \in \ker(\mathcal{T}) \quad (4.46)$$

are well defined, bijective, and inverse to each other. In particular, the generator of $f \in \ker(\mathcal{B})$ is uniquely determined.

Proof. We prove that every $f \in \ker(\mathcal{B})$ is of the form claimed in (a). From (4.41) we obtain $0 = \lambda_{\mathcal{B}f} = -4\pi r e^{\mu_0+\lambda_0} j_f$, which implies $j_{f_-} = j_f = 0$. We split $\mathcal{B}f$ into its odd-in- w and even-in- w part¹¹

$$\mathcal{B}f_+ = \mathcal{T}f_+ - 4\pi r |\varphi'| e^{2\mu_0+\lambda_0} w p_{f_+} = 0, \quad (4.47)$$

$$\mathcal{B}f_- = \mathcal{T}f_- + 4\pi r |\varphi'| e^{2\mu_0+\lambda_0} \frac{w^2}{\sqrt{1+w^2+\frac{L}{r^2}}} j_{f_-} = 0, \quad (4.48)$$

and therefore $\mathcal{T}f_- = 0$ from $j_f = 0$. However, $\ker(\mathcal{T})$ only contains functions which are even in w because of Proposition 4.3.2(e), which yields that $f = f_+$. We express (4.47) in action-angle type variables and apply Proposition 4.3.2(d) in order to obtain¹²

$$\frac{1}{T(E, L)} \partial_\theta f(\theta, E, L) = -4\pi R |\varphi'(E, L)| e^{(2\mu_0+\lambda_0)(R)} W p_f(R) \quad (4.49)$$

for $\theta \in [0, 1]$ and a.e. $(E, L) \in \Omega_0^{EL}$. Integrating this equation in $\theta \in [0, \frac{1}{2}]$ implies¹³

$$f(\theta, E, L) = f\left(\frac{1}{2}, E, L\right) + 4\pi |\varphi'(E, L)| T(E, L) \int_\theta^{\frac{1}{2}} \left(R e^{(2\mu_0+\lambda_0)(R)} W p_f(R) \right) (\tau, E, L) d\tau.$$

We change variables in the integral through $s = R(\tau, E, L)$ and recall (2.72), which yields

$$\begin{aligned} f(\theta, E, L) &= f\left(\frac{1}{2}, E, L\right) + 4\pi |\varphi'(E, L)| E \int_{R(\theta, E, L)}^{r_+(E, L)} e^{2\lambda_0(s)} p_f(s) s ds \\ &= g(E, L) + 4\pi |\varphi'(E, L)| E \int_{R(\theta, E, L)}^{R_{\max}} e^{2\lambda_0(s)} p_f(s) s ds, \end{aligned}$$

where g is the generator of f , as defined above. This proves (4.44). We deduce that f

¹¹Recall that \mathcal{B} and \mathcal{T} reverse parity in w and that $f_\pm \in \mathcal{D}(\mathcal{T})$, according to Proposition 4.3.2(b).

¹²As mentioned at the beginning of Section 4.3, R and W have to be considered as functions of (θ, E, L) .

¹³Recall that $f(\cdot, E, L) \in H_\theta^1$ for a.e. $(E, L) \in \Omega_0^{EL}$, i.e., the evaluation $f(\cdot, E, L)$ at $\theta = \frac{1}{2}$ is well defined for the representative that is continuous in θ .

has to be of the form

$$f(\theta, E, L) = g(E, L) + |\varphi'(E, L)|E H(R(\theta, E, L)),$$

for some function $H \in C^1([R_{\min}, R_{\max}])$ depending on f with $H(R_{\max}) = 0$. Using (4.49) yields the differential equation

$$\partial_r H = -4\pi r e^{2\lambda_0} (p_g + p_{|\varphi'|_{EH}}), \quad H(R_{\max}) = 0. \quad (4.50)$$

We can simplify this via (4.18), which implies

$$p_{|\varphi'|_{EH}}(r) = H(r) e^{\mu_0(r)} \frac{\pi}{r^2} \int_0^\infty \int_{\mathbb{R}} w^2 |\varphi'| dw dL = H(r) \frac{e^{-2\lambda_0(r)}}{4\pi r} (\lambda'_0 + \mu'_0)(r),$$

and therefore (4.50) is equivalent to

$$\partial_r \left(e^{\mu_0 + \lambda_0} H \right) = -4\pi r e^{3\lambda_0 + \mu_0} p_g, \quad H(R_{\max}) = 0.$$

We integrate this equation and get

$$H(r) = 4\pi e^{-\mu_0 - \lambda_0} \int_r^{R_{\max}} e^{(3\lambda_0 + \mu_0)(s)} p_g(s) s ds, \quad r \in [R_{\min}, R_{\max}],$$

which proves the first inclusion in (a). For the reverse inclusion, we show that the function

$$f(\theta, E, L) = g(E, L) + 4\pi |\varphi'(E, L)| E e^{(-\lambda_0 - \mu_0)(R)} \int_R^{R_{\max}} e^{(3\lambda_0 + \mu_0)(s)} p_g(s) s ds,$$

defined for $(\theta, E, L) \in [0, 1] \times \Omega_0^{EL}$, is in $\ker(\mathcal{B})$ for every $g = g(E, L) \in \ker(\mathcal{T})$. We first must ascertain that $f \in D(\mathcal{T})$, which we accomplish through the characterization in Proposition 4.3.2(d). In detail, we observe $f(\cdot, E, L) \in L^2(]0, 1[)$, because it is bounded in θ . Moreover, $f(\cdot, E, L)$ is weakly differentiable in θ with

$$\begin{aligned} & \partial_\theta f(\theta, E, L) \\ &= -4\pi R |\varphi'| T e^{(2\mu_0 + \lambda_0)(R)} W \left(p_g(R) + \frac{e^{(-\mu_0 - 3\lambda_0)(R)}}{R} (\mu'_0 + \lambda'_0)(R) \int_R^{R_{\max}} e^{3\lambda_0 + \mu_0} p_g s ds \right), \end{aligned}$$

which is again a function in $L^2(]0, 1[)$ due to Lemma 4.3.6(a). The remaining condition $f(0, E, L) = f(1, E, L)$ for a.e. $(E, L) \in \Omega_0^{EL}$ is fulfilled because of $R(0, E, L) = r_-(E, L) = R(1, E, L)$. Proposition 4.3.2(d) furthermore implies

$$\mathcal{T}f = 4\pi r |\varphi'| e^{2\mu_0 + \lambda_0} w \left(p_g + \frac{e^{-\mu_0 - 3\lambda_0}}{r} (\mu'_0 + \lambda'_0) \int_r^{R_{\max}} e^{3\lambda_0 + \mu_0} p_g s ds \right). \quad (4.51)$$

For $\mathcal{B}f$, we compute

$$p_f = p_g + \frac{e^{-3\lambda_0 - \mu_0}}{r} (\lambda'_0 + \mu'_0) \int_r^{R_{\max}} e^{3\lambda_0 + \mu_0} p_g s \, ds \quad (4.52)$$

by again using (4.18). This equation together with (4.51) and the definition of $\mathcal{B}f$ yields

$$\mathcal{B}f = \mathcal{T}f - 4\pi r |\varphi'| e^{2\mu_0 + \lambda_0} w p_f = 0,$$

because f is even in w , which finishes the proof of (a).

The mappings in part (b) are well defined because of the considerations made above. The inverse property follows from a lengthy calculation for which we briefly provide the details: Firstly, we plug (4.45) into (4.46), i.e., we take $g \in \ker(\mathcal{T})$ and define

$$f := g + 4\pi |\varphi'| E e^{-\lambda_0 - \mu_0} \int_r^{R_{\max}} e^{(3\lambda_0 + \mu_0)(s)} p_g(s) s \, ds.$$

As in (4.52), we get

$$p_f(r) = p_g(r) + e^{-3\lambda_0(r) - \mu_0(r)} \frac{\mu'_0(r) + \lambda'_0(r)}{r} \int_r^{R_{\max}} e^{(3\lambda_0 + \mu_0)(s)} p_g(s) s \, ds, \quad r > R_{\min},$$

and, therefore, $R(\frac{1}{2}, E, L) = r_+(E, L) =: r_+$ yields

$$\begin{aligned} f\left(\frac{1}{2}, E, L\right) &= 4\pi |\varphi'| E \int_{r_+}^{R_{\max}} e^{2\lambda_0(s)} p_f(s) s \, ds \\ &= g(E, L) + 4\pi |\varphi'| E e^{-\lambda_0(r_+) - \mu_0(r_+)} \int_{r_+}^{R_{\max}} e^{(3\lambda_0 + \mu_0)(s)} p_g(s) s \, ds \\ &\quad - 4\pi |\varphi'| E \int_{r_+}^{R_{\max}} \left(e^{2\lambda_0(s)} p_g(s) s - \partial_r \left(e^{-\lambda_0 - \mu_0} \right) (s) \int_s^{R_{\max}} e^{(3\lambda_0 + \mu_0)(\sigma)} p_g(\sigma) \sigma \, d\sigma \right) ds. \end{aligned}$$

An integration by parts in the last term cancels the second and third term such that only $g = g(E, L)$ remains, as desired; note that all these assertions hold for a.e. $(E, L) \in \Omega_0^{EL}$. Secondly, for a function $f \in \ker(\mathcal{B})$, we know from part (a) that

$$g := f\left(\frac{1}{2}, \cdot, \cdot\right) - 4\pi |\varphi'| E \int_{r_+}^{R_{\max}} e^{2\lambda_0(s)} p_f(s) s \, ds$$

is the generator of f , i.e.,

$$f = g + 4\pi |\varphi'| E e^{-\lambda_0 - \mu_0} \int_r^{R_{\max}} e^{(3\lambda_0 + \mu_0)(s)} p_g(s) s \, ds,$$

which is simply (4.46) inserted into (4.45). This finishes the proof. \square

To conclude, we can describe $\ker(\mathcal{B})$ in similar fashion to $\ker(\mathcal{T})$, but we must add an extra term to the “generating” function $g = g(E, L)$. We emphasize that we could have used an integration from R_{\min} to r in this characterization. However, this choice would only complicate the description of $\ker(\mathcal{B})^\perp$, which is why we integrate from r to R_{\max} instead. As in [47, Lem. 5.6], we identify the orthogonal complement of the kernel of \mathcal{B} via an integral over the angle variable θ .

Lemma 4.3.9. *Let $f \in H$. Then, $f \in \ker(\mathcal{B})^\perp$ is equivalent to*

$$\int_0^1 \left(f(\theta, E, L) + |\varphi'(E, L)| e^{2\mu_0(R)} \lambda_f(R) \frac{W^2}{E} \right) d\theta = 0 \text{ for a.e. } (E, L) \in \Omega_0^{EL}, \quad (4.53)$$

i.e., $f + |\varphi'| e^{2\mu_0} \lambda_f \frac{w^2}{E} \in \ker(\mathcal{T})^\perp$. In particular, $\mathcal{H} \subset \ker(\mathcal{B})^\perp$.

Proof. By definition, we have $f \in \ker(\mathcal{B})^\perp$ if, and only if,

$$\langle f, h \rangle_H = 0, \quad h \in \ker(\mathcal{B}).$$

From the characterization of elements in $\ker(\mathcal{B})$ in Lemma 4.3.8, this is equivalent to

$$\begin{aligned} 0 &= \iiint_{\Omega_0} \frac{e^{\lambda_0}}{|\varphi'|} f \left(g + 4\pi |\varphi'| E e^{-\lambda_0 - \mu_0} \int_r^{R_{\max}} e^{(3\lambda_0 + \mu_0)(s)} p_g(s) s ds \right) dr dw dL \\ &= \iiint_{\Omega_0} \frac{e^{\lambda_0}}{|\varphi'|} f g dr dw dL + 4 \int_{R_{\min}}^{R_{\max}} r^2 \rho_f \int_r^{R_{\max}} e^{(3\lambda_0 + \mu_0)(s)} p_g(s) s ds dr \end{aligned} \quad (4.54)$$

for every $g = g(E, L) \in \ker \mathcal{T}$. We rewrite the source term ρ_f using the linearized field equation (4.3) and integrate by parts for the second term in order to obtain¹⁴

$$\begin{aligned} 4 \int_{R_{\min}}^{R_{\max}} r^2 \rho_f \int_r^{R_{\max}} e^{3\lambda_0 + \mu_0} p_g s ds dr &= \frac{1}{\pi} \int_{R_{\min}}^{R_{\max}} \left(r e^{-2\lambda_0} \lambda_f \right)' \int_r^{R_{\max}} e^{3\lambda_0 + \mu_0} p_g s ds dr \\ &= \frac{1}{\pi} \int_{R_{\min}}^{R_{\max}} e^{\lambda_0 + \mu_0} \lambda_f p_g r^2 dr = \iiint_{\Omega_0} e^{\lambda_0 + 2\mu_0} \lambda_f \frac{w^2}{E} g(E, L) dr dw dL. \end{aligned}$$

This enables us to express condition (4.54) equivalently as

$$\begin{aligned} 0 &= \iiint_{\Omega_0} g(E, L) e^{\lambda_0(r)} \left(\frac{f(r, w, L)}{|\varphi'(E, L)|} + e^{2\mu_0(r)} \lambda_f(r) \frac{w^2}{E} \right) dr dw dL \\ &= \iiint_{\Omega_0^{EL}} g(E, L) T(E, L) \int_0^1 \left(\frac{f(\theta, E, L)}{|\varphi'(E, L)|} + e^{2\mu_0(R)} \lambda_f(R) \frac{W^2}{E} \right) d\theta dE dL \end{aligned}$$

after transforming the integral from (r, w, L) to action-angle type variables, according to (2.71). Since $g \in \ker(\mathcal{T})$ is arbitrary and the period function is positive, the integral

¹⁴The boundary terms vanish when integrating by parts since $\lambda_f(R_{\min}) = 0$ by (4.8). Note that this is the reason why we chose to integrate from r to R_{\max} in the characterization of $\ker(\mathcal{B})$, as commented on above.

over (E, L) must vanish a.e. and (4.53) is proven.

The fact that odd-in- w functions f are elements in $\ker(\mathcal{B})^\perp$ follows from the observation that $\lambda_f = 0$ and that $\int_0^1 f(\theta, \cdot, \cdot) d\theta = 0$ holds a.e. by the characterization of w -parity in Remark 4.2.1. \square

It is now possible to analyze the range of \mathcal{B} . The result is structurally the same as for the transport operator in (4.22), i.e., we identify the range and the orthogonal complement of the kernel of \mathcal{B} . We first show that the operator $\tilde{\mathcal{B}}^{-1}$ introduced in Definition 4.3.4 is a right-inverse of \mathcal{B} . We emphasize that, as far as the author knows, this right-inverse is not deducible from any general procedure. Its derivation involved a lot of trial and error.

We would certainly prefer to provide the true inverse of \mathcal{B} , but we are unable to explicitly construct \mathcal{B}^{-1} . The difficulty of this endeavor arises from the fact that the orthogonal projection onto $\ker(\mathcal{B})$ is not known explicitly, as we will see later. The next lemma is also part of [47, Lem. 5.8, Prop. 5.9]

Lemma 4.3.10. *The operator $\tilde{\mathcal{B}}^{-1}$ given in (4.29) is well defined, bounded, reverses w -parity, and for every $f \in \ker(\mathcal{B})^\perp$ it holds that $\mathcal{B}\tilde{\mathcal{B}}^{-1}f = f$. Moreover,*

$$\text{im}(\mathcal{B}) = \ker(\mathcal{B})^\perp,$$

and the range of \mathcal{B} is closed.

Proof. Lemma 4.3.9 implies that $f + |\varphi'|e^{2\mu_0}\lambda_f\frac{w^2}{E} \in \ker(\mathcal{T})^\perp$ for every $f \in \ker(\mathcal{B})^\perp$, i.e., we can apply the inverse \mathcal{T}^{-1} to this function and obtain an element in $D(\mathcal{T})$, according to Proposition 4.3.2(f). In addition, Lemma 4.3.6(a) and Proposition 4.3.2(d) yield that the second term in the definition of $\tilde{\mathcal{B}}^{-1}$ is in $D(\mathcal{T})$, since $R(\cdot, E, L)$ is differentiable and $R(0, E, L) = r_-(E, L) = R(1, E, L)$ for a.e. $(E, L) \in \Omega_0^{EL}$. Hence, $\tilde{\mathcal{B}}^{-1}$ is well defined. The boundedness follows from Proposition 4.3.2(f) and Lemma 4.3.6(a).

Consider an odd-in- w function $f \in \ker(\mathcal{B})^\perp$. Then $\lambda_f = 0$ and, since \mathcal{T}^{-1} reverses w -parity, $\mathcal{T}^{-1}f$ is even in w . The second term in $\tilde{\mathcal{B}}^{-1}f$ is always even in w . Conversely, if f is even in w , the second part vanishes because $\mathcal{T}^{-1}(f + |\varphi'|e^{2\mu_0}\lambda_f\frac{w^2}{E})$ is odd in w . This proves the parity-reversing property of $\tilde{\mathcal{B}}^{-1}$.

We need to show the right-inverse property of $\tilde{\mathcal{B}}^{-1}$. For $f \in \ker(\mathcal{B})^\perp$, we calculate

$$\begin{aligned} \mathcal{B}\tilde{\mathcal{B}}^{-1}f &= \mathcal{T}\tilde{\mathcal{B}}^{-1}f + \mathcal{S}\tilde{\mathcal{B}}^{-1}f \\ &= f + |\varphi'|\frac{e^{2\mu_0}w^2}{E}\lambda_f - 4\pi|\varphi'|we^{2\mu_0-\lambda_0}\partial_r\left(e^{-\lambda_0-\mu_0}\int_r^{R_{\max}}e^{3\lambda_0+\mu_0}p_{\mathcal{T}^{-1}(f+|\varphi'|e^{2\mu_0}\lambda_f\frac{w^2}{E})}(s)s\,ds\right) \\ &\quad + 4\pi r|\varphi'|e^{2\mu_0+\lambda_0}\left(e^{\mu_0}\frac{w^2}{E}j_{\tilde{\mathcal{B}}^{-1}f} - wp_{\tilde{\mathcal{B}}^{-1}f}\right) \\ &= f + |\varphi'|\frac{e^{2\mu_0}w^2}{E}\left(\lambda_f + 4\pi re^{\mu_0+\lambda_0}j_{\tilde{\mathcal{B}}^{-1}f}\right) \\ &\quad - 4\pi|\varphi'|e^{2\mu_0-\lambda_0}w\left(\partial_r\left(e^{-\lambda_0-\mu_0}\int_r^{R_{\max}}e^{3\lambda_0+\mu_0}p_{\mathcal{T}^{-1}(f+|\varphi'|e^{2\mu_0}\lambda_f\frac{w^2}{E})}(s)s\,ds\right) + re^{2\lambda_0}p_{\tilde{\mathcal{B}}^{-1}f}\right), \end{aligned}$$

by applying Proposition 4.3.2(d) and the chain rule. A comparison of coefficients yields that the following two equations have to be fulfilled in order for $\mathcal{B}\tilde{\mathcal{B}}^{-1}f = f$ to hold:

$$\lambda_f = -4\pi r e^{\mu_0 + \lambda_0} j_{\tilde{\mathcal{B}}^{-1}f}, \quad (4.55)$$

$$\begin{aligned} p_{\tilde{\mathcal{B}}^{-1}f} &= p_{\mathcal{T}^{-1}(f + |\varphi'| e^{2\mu_0} \lambda_f \frac{w^2}{E})} \\ &+ \frac{1}{r} (\lambda'_0 + \mu'_0) e^{-3\lambda_0 - \mu_0} \int_r^{R_{\max}} e^{(3\lambda_0 + \mu_0)(s)} p_{\mathcal{T}^{-1}(f + |\varphi'| e^{2\mu_0} \lambda_f \frac{w^2}{E})}(s) s \, ds. \end{aligned} \quad (4.56)$$

Since $g := f + |\varphi'| e^{2\mu_0} \lambda_f \frac{w^2}{E} \in \text{im}(\mathcal{T}) = \ker(\mathcal{T})^\perp$ due to Proposition 4.3.2(f), we get

$$\lambda_{e^{\mu_0 + \lambda_0} g} = -4\pi r e^{2\mu_0 + 2\lambda_0} j_{\mathcal{T}^{-1}g}$$

from (4.42), which together with $j_{\tilde{\mathcal{B}}^{-1}f} = j_{(\tilde{\mathcal{B}}^{-1}f)_-} = j_{\mathcal{T}^{-1}g}$ and (4.8) yields

$$\begin{aligned} -4\pi r e^{2\mu_0 + 2\lambda_0} j_{\tilde{\mathcal{B}}^{-1}f} &= \lambda_{e^{\mu_0 + \lambda_0} g} = \frac{4\pi e^{2\lambda_0}}{r} \int_{R_{\min}}^r e^{\mu_0 + \lambda_0} \rho_g s^2 \, ds \\ &= \frac{4\pi e^{2\lambda_0}}{r} \int_{R_{\min}}^r e^{\mu_0 + \lambda_0} \left(\rho_f + e^{\mu_0} \lambda_f \left(\frac{\pi}{s^2} \int_0^\infty \int_{\mathbb{R}} w^2 |\varphi'| \, dw dL \right) \right) s^2 \, ds \\ &= \frac{4\pi e^{2\lambda_0}}{r} \left(\int_{R_{\min}}^r e^{\mu_0 + \lambda_0} \rho_f s^2 \, ds + \frac{1}{4\pi} \int_{R_{\min}}^r s e^{-2\lambda_0} \lambda_f \partial_s (e^{\mu_0 + \lambda_0}) \, ds \right) \\ &= \frac{4\pi e^{2\lambda_0}}{r} \left(\int_{R_{\min}}^r e^{\mu_0 + \lambda_0} \rho_f s^2 \, ds + \frac{1}{4\pi} r e^{\mu_0 - \lambda_0} \lambda_f - \frac{1}{4\pi} \int_{R_{\min}}^r \partial_s (s e^{-2\lambda_0} \lambda_f) e^{\mu_0 + \lambda_0} \, ds \right) \\ &= e^{\mu_0 + \lambda_0} \lambda_f. \end{aligned} \quad (4.57)$$

Here we made use of (4.3) and (4.18) as well as of an integration by parts. This shows the validity of (4.55). Equation (4.56) follows from plugging the definition of $\tilde{\mathcal{B}}^{-1}f$ into p and calculating

$$\begin{aligned} p_{\tilde{\mathcal{B}}^{-1}f} &= p_{\mathcal{T}^{-1}(f + |\varphi'| e^{2\mu_0} \lambda_f \frac{w^2}{E})} \\ &+ 4\pi e^{-\lambda_0} \left(\int_r^{R_{\max}} e^{(3\lambda_0 + \mu_0)(s)} p_{\mathcal{T}^{-1}(f + |\varphi'| e^{2\mu_0} \lambda_f \frac{w^2}{E})}(s) s \, ds \right) \frac{\pi}{r^2} \int_0^\infty \int_{\mathbb{R}} w^2 |\varphi'| \, dw dL \\ &= p_{\mathcal{T}^{-1}(f + |\varphi'| e^{2\mu_0} \lambda_f \frac{w^2}{E})} + \frac{\lambda'_0 + \mu'_0}{r} e^{-\mu_0 - 3\lambda_0} \int_r^{R_{\max}} e^{3\lambda_0 + \mu_0} p_{\mathcal{T}^{-1}(f + |\varphi'| e^{2\mu_0} \lambda_f \frac{w^2}{E})}(s) s \, ds, \end{aligned}$$

from (4.18). Therefore, we have $\mathcal{B}\tilde{\mathcal{B}}^{-1}f = f$ and conclude $\ker(\mathcal{B})^\perp \subset \text{im}(\mathcal{B})$. Since \mathcal{B} is skew-adjoint, we obtain $\ker(\mathcal{B})^\perp = \overline{\text{im}(\mathcal{T})}$ from [25, Cor. 2.18(iv)] and thus deduce $\ker(\mathcal{B})^\perp = \text{im}(\mathcal{B})$. \square

The goal is to invert \mathcal{B} and \mathcal{B}^2 appropriately. The actual inverse of \mathcal{B} must satisfy

$$\mathcal{B}^{-1}f \in \text{im}(\mathcal{B}) = \ker(\mathcal{B})^\perp,$$

which is why we need to project elements of H onto the kernel of \mathcal{B} in order to obtain \mathcal{B}^{-1} from $\tilde{\mathcal{B}}^{-1}$. We denote the orthogonal projection of elements in H onto $\ker(\mathcal{B})$ by $\Pi: H \rightarrow \ker(\mathcal{B})$. For more details on orthogonal projections, we refer the reader to Definition B.2, Lemma B.3, and the references there. As a first step, we identify the kernel and range of \mathcal{B}^2 , see [47, Lem. 5.10].

Lemma 4.3.11. *The kernel and image of \mathcal{B}^2 are given by*

$$\ker(\mathcal{B}^2) = \ker(\mathcal{B}), \quad \text{im}(\mathcal{B}^2) = \text{im}(\mathcal{B}).$$

Proof. The inclusion $\ker(\mathcal{B}^2) \supset \ker(\mathcal{B})$ is obvious. By the skew-adjointness of \mathcal{B} , we get

$$0 = \langle \mathcal{B}^2 f, f \rangle_H = -\langle \mathcal{B} f, \mathcal{B} f \rangle_H = -\|\mathcal{B} f\|_H^2$$

for $f \in \ker(\mathcal{B}^2)$, and therefore $\mathcal{B} f = 0$, which gives $\ker(\mathcal{B}^2) \subset \ker(\mathcal{B})$. The fact that $\text{im}(\mathcal{B}^2) \subset \text{im}(\mathcal{B})$ is trivial. For the reverse inclusion, we consider $f \in \text{im}(\mathcal{B})$, i.e., there exists $\tilde{h} \in D(\mathcal{T})$ with $\mathcal{B}\tilde{h} = f$. We set

$$h := (\text{id} - \Pi)\tilde{h} \in \ker(\mathcal{B})^\perp$$

such that $\mathcal{B}h = \mathcal{B}\tilde{h} = f$. Lemma 4.3.10 yields $h \in \text{im}(\mathcal{B})$, which implies that $\mathcal{B}g = h$ for some $g \in D(\mathcal{T})$. We now have $\mathcal{B}^2 g = \mathcal{B}h = f$ and thus $f \in \text{im}(\mathcal{B}^2)$. \square

After deriving these properties for \mathcal{B} and $\tilde{\mathcal{B}}^{-1}$, we are now able to complete the proof of Proposition 4.3.5. In summary, only the invertibility of \mathcal{B} and \mathcal{B}^2 remains to be proven. For the parts (f) and (g), similar arguments were carried out in [47, Lems. 5.11 & 5.12]

Proof of Proposition 4.3.5(d)–(h). For the sake of completeness, we mention that (d) follows from the explicit characterization of $\ker(\mathcal{B})$ made in Lemma 4.3.8. The assertions in (e) were shown in Lemmas 4.3.9, 4.3.10 and 4.3.11.

As to part (f), we have to prove that \mathcal{B} is invertible and that the formula (4.32) holds. The operator

$$(\text{id} - \Pi)\tilde{\mathcal{B}}^{-1}: \text{im}(\mathcal{B}) \rightarrow H$$

is well defined and bounded because of Lemma 4.3.10. In addition, as per definition of the orthogonal projection onto $\ker(\mathcal{B})$ we have

$$\text{im}((\text{id} - \Pi)\tilde{\mathcal{B}}^{-1}) \subset \text{im}(\text{id} - \Pi) = \ker(\mathcal{B})^\perp \cap D(\mathcal{T}), \quad (4.58)$$

since for $f \in D(\mathcal{T})$ it holds that $(\text{id} - \Pi)f \in D(\mathcal{T})$ due to $\text{im}(\Pi) = \ker(\mathcal{B}) \subset D(\mathcal{T})$. We now show that $\mathcal{B}: D(\mathcal{T}) \cap \ker(\mathcal{B})^\perp \rightarrow \text{im}(\mathcal{B})$ is bijective. Let $g \in \text{im}(\mathcal{B})$ such that $\mathcal{B}f = g$ for some $f \in D(\mathcal{T})$. By defining $\tilde{f} := (\text{id} - \Pi)f$, we obtain $\tilde{f} \in D(\mathcal{T}) \cap \ker(\mathcal{B})^\perp$ with

$\mathcal{B}\tilde{f} = \mathcal{B}f = g$, i.e., \mathcal{B} is surjective. The injectivity follows from the identity

$$\ker(\mathcal{B}|_{D(\mathcal{T}) \cap \ker(\mathcal{B})^\perp}) = \ker(\mathcal{B}) \cap \ker(\mathcal{B})^\perp = \{0\}.$$

According to Lemma 4.3.10 and due to $\mathcal{B}\Pi = 0$, we have

$$\mathcal{B}(\text{id} - \Pi)\tilde{\mathcal{B}}^{-1}f = \mathcal{B}\tilde{\mathcal{B}}^{-1}f = f, \quad f \in \ker(\mathcal{B})^\perp = \text{im}(\mathcal{B}).$$

Thus, $(\text{id} - \Pi)\tilde{\mathcal{B}}^{-1}$ is a right-inverse of $\mathcal{B}: D(\mathcal{T}) \cap \ker(\mathcal{B})^\perp \rightarrow \text{im}(\mathcal{B})$. Since above we have proven that the latter operator is bijective and because of (4.58), we conclude that $(\text{id} - \Pi)\tilde{\mathcal{B}}^{-1}$ is indeed the inverse of \mathcal{B} . Skew-symmetry of \mathcal{B}^{-1} can be seen from

$$\langle f, \mathcal{B}^{-1}g \rangle_H = \langle \mathcal{B}\mathcal{B}^{-1}f, \mathcal{B}^{-1}g \rangle_H = -\langle \mathcal{B}^{-1}f, \mathcal{B}\mathcal{B}^{-1}g \rangle_H = -\langle \mathcal{B}^{-1}f, g \rangle_H, \quad f, g \in \text{im}(\mathcal{B}), \quad (4.59)$$

because \mathcal{B} is skew-adjoint. The reversal of w -parity follows from the observation that $\tilde{\mathcal{B}}^{-1}$ reverses and $\text{id} - \Pi$ conserves w -parity since $\mathcal{H} \subset \ker(\mathcal{B})^\perp$ and functions in $\ker(\mathcal{B})$ are even in w .

It remains to show (g). For elements $f \in \text{im}(\mathcal{B}^2) = \text{im}(\mathcal{B})$, part (f) implies $\mathcal{B}^{-1}f \in \ker(\mathcal{B})^\perp \cap D(\mathcal{T})$ such that we can again apply \mathcal{B}^{-1} due to $\ker(\mathcal{B})^\perp = \text{im}(\mathcal{B})$ from part (e), which yields $\mathcal{B}^{-2}f \in \ker(\mathcal{B})^\perp \cap D(\mathcal{T})$. In order to provide $\mathcal{B}^{-2}f \in D(\mathcal{T}^2)$, we have to show $\mathcal{T}\mathcal{B}^{-2}f \in D(\mathcal{T})$. Since the proof of this is very similar to arguments employed in part (a) using Lemma 4.3.6(b), we leave out the details here. Together with $\ker(\mathcal{B})^\perp = \ker(\mathcal{B}^2)^\perp$ from part (e), we get that

$$\mathcal{B}^{-2}: \text{im}(\mathcal{B}^2) \rightarrow D(\mathcal{T}^2) \cap \ker(\mathcal{B}^2)^\perp$$

is well defined. The boundedness and conservation of w -parity are a consequence of (f). We show that \mathcal{B}^{-2} is the inverse of \mathcal{B}^2 in two steps: Firstly, for $f \in \text{im}(\mathcal{B}^2) = \text{im}(\mathcal{B})$ we obtain that

$$\mathcal{B}^2\mathcal{B}^{-2}f = \mathcal{B}(\mathcal{B}\mathcal{B}^{-1})\mathcal{B}^{-1}f = \mathcal{B}\mathcal{B}^{-1}f = f,$$

because of $\mathcal{B}^{-1}f \in \text{im}(\mathcal{B})$. Secondly, for $f \in D(\mathcal{T}^2) \cap \ker(\mathcal{B}^2)^\perp$ we deduce

$$\mathcal{B}^{-2}\mathcal{B}^2f = \mathcal{B}^{-1}(\mathcal{B}^{-1}\mathcal{B})\mathcal{B}f = \mathcal{B}^{-1}\mathcal{B}f = f,$$

due to $\mathcal{B}f \in D(\mathcal{T}) \cap \ker(\mathcal{B})^\perp$ and $f \in D(\mathcal{T}) \cap \ker(\mathcal{B})^\perp$ by part (e). Consequently, $\mathcal{B}^{-2} = (\mathcal{B}^2)^{-1}$. The symmetry of \mathcal{B}^{-2} can then be deduced from the self-adjointness of \mathcal{B}^2 similarly to (4.59).

At last, (h) follows immediately from the boundedness of \mathcal{B}^{-1} shown in (f). \square

Before we can tackle the spectral properties of the main operators, we need to show two so-called relative compactness results.

4.3.3 Two relative compactness results

In this section, we provide the necessary tools to characterize the essential spectrum of \mathcal{L} , \mathcal{B}^2 , and \mathcal{T}^2 in Section 4.3.4. First, we briefly cover the main properties of the response operator \mathcal{R} defined in Definition 4.2.2(c). Compared to \mathcal{T} and \mathcal{B} , the response operator behaves rather nicely, see also [47, Lem. 5.15]

Lemma 4.3.12. *The operator $\mathcal{R}: H \rightarrow H$ is bounded, symmetric, and non-negative in the sense of quadratic forms, i.e., $\langle \mathcal{R}f, f \rangle \geq 0$ for $f \in H$. The square root operator is applicable, and*

$$\sqrt{\mathcal{R}}: H \rightarrow H, \quad \sqrt{\mathcal{R}}f := 4\pi\sqrt{r}|\varphi'|e^{2\mu_0+\lambda_0}\sqrt{\frac{2r\mu'_0+1}{\mu'_0+\lambda'_0}}wjf$$

is bounded, symmetric, and non-negative as well. In particular, we have that $\sqrt{\mathcal{R}}\sqrt{\mathcal{R}} = \mathcal{R}$ on H . Moreover, $\sqrt{\mathcal{R}}f \in \mathcal{H}$ and $\mathcal{R}f \in \mathcal{H}$ for $f \in H$.

Proof. The well-definedness and boundedness is due to Lemma 4.3.6(a) and the compact support of the steady state. We immediately obtain

$$\langle \mathcal{R}f, g \rangle_H = 16\pi^2 \int_{R_{\min}}^{R_{\max}} e^{3\mu_0+\lambda_0}(2r\mu'_0+1)j_fj_g r^2 dr, \quad f, g \in H,$$

which yields the symmetry and non-negativity of \mathcal{R} due to $\mu'_0 \geq 0$, see (1.11). The claim for $\sqrt{\mathcal{R}}$ follows from similar considerations by employing (4.18), which eliminates the denominator $\mu'_0 + \lambda'_0$.¹⁵ The fact that $\mathcal{R}f$ and $\sqrt{\mathcal{R}}f$ are odd in w follows from $\varphi' = \varphi'(E(r, w, L), L)$, which is even in w . \square

Finally, we now show that the Antonov operator is well defined and self-adjoint.

Corollary 4.3.13. *The Antonov operator $\mathcal{L}: D(\mathcal{T}^2) \cap \mathcal{H} \rightarrow \mathcal{H}$ is self-adjoint as a densely defined operator on \mathcal{H} .*

Proof. We first note that \mathcal{L} is well defined by Proposition 4.3.5(b). In addition, since $\mathcal{B}^2|_{\mathcal{H}}$ is self-adjoint and the response operator \mathcal{R} is bounded and symmetric, the Kato-Rellich theorem [87, Thm. X.12] implies that \mathcal{L} is self-adjoint as well. \square

We recall the definition of relative compactness of two operators and a useful characterization in Definition B.8 and Lemma B.9 in the appendix. In general, relative compactness is a powerful method to control essential spectra [58, Ch. 14]. We apply the two upcoming results in the next section. For the Birman-Schwinger principle in Section 5.2, we have to prove that $\sqrt{\mathcal{R}}$ is relatively \mathcal{B}^2 -compact on \mathcal{H} as in [47, Lem. 5.16].

Lemma 4.3.14. *The operators $\sqrt{\mathcal{R}}|_{\mathcal{H}}$ and $\mathcal{R}|_{\mathcal{H}}$ are relatively $(\mathcal{B}^2|_{\mathcal{H}})$ -compact.*

¹⁵From the field equations, it follows that $\mu'_0 + \lambda'_0 = 4\pi r e^{2\lambda_0}(\rho_0 + p_0) > 0$ for $r \in]R_{\min}, R_{\max}[$.

Proof. We only prove the claim for $\sqrt{\mathcal{R}}|_{\mathcal{H}}$, since $\mathcal{R}|_{\mathcal{H}}$ is structurally the same with different radial weights. According to Proposition 4.3.5(b) and (g), the restricted operator $\mathcal{B}^2|_{\mathcal{H}}$ is self-adjoint and zero is an element of the resolvent set. By Lemma B.9, it is sufficient to show that

$$\sqrt{\mathcal{R}}: (\mathcal{D}(\mathcal{T}^2) \cap \mathcal{H}, \|\mathcal{B}^2 \cdot\|_H + \|\cdot\|_H) \rightarrow \mathcal{H}$$

is compact. Consider a bounded sequence $(f_n)_{n \in \mathbb{N}} \subset \mathcal{D}(\mathcal{T}^2) \cap \mathcal{H}$ such that $(\mathcal{B}^2 f_n)_{n \in \mathbb{N}}$ is bounded in \mathcal{H} as well. From the Poincaré-type estimate (4.34), we obtain that $(\mathcal{B} f_n)_{n \in \mathbb{N}}$ is also bounded in H , i.e., we can choose a subsequence, which we again denote by (f_n) , with $\mathcal{B} f_n \rightharpoonup h$ in H for $n \rightarrow \infty$ for some function $h \in H$. Since $\text{im}(\mathcal{B}) = \ker(\mathcal{B})^\perp$ from Proposition 4.3.5(e), we get

$$\langle h, g \rangle_H = \lim_{n \rightarrow \infty} \langle \mathcal{B} f_n, g \rangle_H = 0, \quad g \in \ker(\mathcal{B})$$

due to the weak convergence of $(\mathcal{B} f_n)$, and therefore $h \in \ker(\mathcal{B})^\perp = \text{im}(\mathcal{B})$, i.e., there exists $f \in \mathcal{D}(\mathcal{T})$ with $\mathcal{B} f = h$. The identity (4.41) yields

$$\sqrt{\mathcal{R}} f_n = -|\varphi'| e^{\mu_0} \sqrt{\frac{2r\mu'_0 + 1}{r(\mu'_0 + \lambda'_0)}} w \lambda_{\mathcal{B} f_n},$$

and (4.18) consequently implies

$$\begin{aligned} \|\sqrt{\mathcal{R}}(f_n - f)\|_H^2 &= 4\pi^2 \int_{R_{\min}}^{R_{\max}} e^{\lambda_0 + 2\mu_0} \frac{2r\mu'_0 + 1}{r(\mu'_0 + \lambda'_0)} |\lambda_{\mathcal{B} f_n} - \lambda_{\mathcal{B} f}|^2 \left(\int_0^\infty \int_{-\infty}^\infty w^2 |\varphi'| dw dL \right) dr \\ &= \int_{R_{\min}}^{R_{\max}} e^{\mu_0 - \lambda_0} (2r\mu'_0 + 1) |\lambda_{\mathcal{B} f_n} - \lambda_{\mathcal{B} f}|^2 dr \leq C \|\lambda_{\mathcal{B} f_n} - \lambda_{\mathcal{B} f}\|_{L^2([R_{\min}, R_{\max}])}^2, \end{aligned}$$

which goes to zero as $n \rightarrow \infty$ due to the compactness result from Lemma 4.3.6(a). \square

The second relative compactness is slightly more technical and lengthy. Recall that $\mathcal{B} = \mathcal{T} + \mathcal{S}$ from Definition 4.2.2.

Lemma 4.3.15. *The operator \mathcal{S} is relatively \mathcal{T} -compact.*

Proof. Due to Lemma B.9, we need to prove that

$$\mathcal{S}: (\mathcal{D}(\mathcal{T}), \|\mathcal{T} \cdot\|_H + \|\cdot\|_H) \rightarrow H$$

is compact. Let $(f_n)_{n \in \mathbb{N}} \subset \mathcal{D}(\mathcal{T})$ be bounded in H such that $(\mathcal{T} f_n)_{n \in \mathbb{N}}$ is bounded in $\mathcal{D}(\mathcal{T})$ as well. By choosing an appropriate subsequence, which we again name (f_n) , we get

$$f_n \rightharpoonup f, \quad \mathcal{T} f_n \rightharpoonup h, \quad \text{in } H \text{ for } n \rightarrow \infty$$

for some functions $f, h \in H$. Proposition 4.3.2(e) and $\mathcal{T} f_n \in \text{im}(\mathcal{T})$ yield that there exists $\tilde{f} \in \mathcal{D}(\mathcal{T})$ with $\mathcal{T} \tilde{f} = h$. The weak definition of the transport operator together

with the weak convergence above implies

$$-\langle f, \mathcal{T}\xi \rangle_H = -\lim_{n \rightarrow \infty} \langle f_n, \mathcal{T}\xi \rangle_H = \lim_{n \rightarrow \infty} \langle \mathcal{T}f_n, \xi \rangle_H = \langle \mathcal{T}\tilde{f}, \xi \rangle_H$$

for every $\xi \in C_c^1(\Omega_0)$, and therefore $\mathcal{T}f = \mathcal{T}\tilde{f}$ a.e. By linearity, we can assume that $f = 0$. We apply (4.42) in order to obtain

$$\mathcal{S}f_n = -4\pi r |\varphi'| e^{2\mu_0 + \lambda_0} w p_{f_n} - e^{-\lambda_0} |\varphi'| \frac{w^2}{\langle v \rangle} \lambda_{e^{\mu_0 + \lambda_0}} \mathcal{T}f_n.$$

Estimating this by using (4.18) yields

$$\|\mathcal{S}f_n\|_H \leq C \left(\|r^3 p_{f_n}\|_{L^2([R_{\min}, R_{\max}])} + \|r \lambda_{e^{\mu_0 + \lambda_0}} \mathcal{T}f_n\|_{L^2([R_{\min}, R_{\max}])} \right), \quad (4.60)$$

where $C > 0$ is a constant that only depends on steady state quantities and may change from line to line. The second term on the right-hand side goes to zero because of the compactness result from Lemma 4.3.6(a). This lemma also implies that $(r^3 p_{f_n})$ is bounded in $L^2([R_{\min}, R_{\max}])$. In addition, the weak derivative of $r p_{f_n}$ exists due to Lemma 4.3.6(b) and $f_n \in D(\mathcal{T})$. We further deduce that equation (4.35) holds in the weak sense which yields

$$\begin{aligned} & \|(r^3 p_{f_n})'\|_{L^2([R_{\min}, R_{\max}])} \\ & \leq C \left(\|r^3 \rho_{f_n}\|_{L^2([R_{\min}, R_{\max}])} + \|r^2 \rho_{f_n}\|_{L^2([R_{\min}, R_{\max}])} + \|r^3 j_{\mathcal{T}f_n}\|_{L^2([R_{\min}, R_{\max}])} \right) \\ & \leq C (\|f_n\|_H + \|\mathcal{T}f_n\|_H), \end{aligned}$$

where we again used that all the source terms can be bounded by $\rho_{|f_n|}$ and applied Lemma 4.3.6(a). From this, we obtain that $(r^3 p_{f_n})$ is bounded in $H^1([R_{\min}, R_{\max}])$.

Moreover, $r^3 p_{f_n}$ converges to zero weakly in $L^2([R_{\min}, R_{\max}])$, because for every $g \in L^2([R_{\min}, R_{\max}])$ it holds that

$$\begin{aligned} & \langle r^3 p_{f_n}, g \rangle_{L^2([R_{\min}, R_{\max}])} \\ & = \int_{R_{\min}}^{R_{\max}} r^3 p_{f_n}(r) g(r) dr = \frac{1}{4\pi} \left\langle |\varphi'| e^{-\lambda_0} r^3 g \frac{w^2}{\sqrt{1 + w^2 + \frac{L}{r^2}}}, f_n \right\rangle_H \rightarrow 0 \end{aligned}$$

for $n \rightarrow \infty$. Since $H^1([R_{\min}, R_{\max}])$ is compactly embedded in $L^2([R_{\min}, R_{\max}])$, we obtain that $(r^3 p_{f_n})$ converges (strongly) to zero in $L^2([R_{\min}, R_{\max}])$ after choosing an appropriate subsequence. To conclude, we have shown that the right-hand side of (4.60) goes to zero for this subsequence, which finishes the proof. \square

To complete the analysis of \mathcal{T} and \mathcal{B} , we will investigate the spectral properties of these operators next.

4.3.4 Spectral properties of \mathcal{T} and \mathcal{B}

The spectral analysis is heavily facilitated by the in-depth knowledge about the transport operator and the essential operator attained in the previous two sections. For a formal definition of the *spectrum*, *essential spectrum*, *discrete spectrum*, and further results that we use here, we refer to Appendix B.

We first determine the spectrum of \mathcal{T} and show that it is purely essential by making use of similar techniques as [55, Thm. 5.7] and [69, Lem. B.12], where the spectrum of the squared transport operator in the non-relativistic setting is considered. To this end, we initially investigate the spectrum of the derivative operator ∂_θ , because of the representation of \mathcal{T} given in Proposition 4.3.2(d), see [55, Lem. 5.6] for a related result.

Lemma 4.3.16. *The operator*

$$\partial_\theta: H_\theta^1 \rightarrow L^2(]0, 1[), \quad y \mapsto \dot{y}$$

is skew-adjoint as a densely defined operator on $L^2(]0, 1[)$, where H_θ^1 is defined in (4.19). The spectrum is given by

$$\sigma(\partial_\theta) = 2\pi i \mathbb{Z} := \{2\pi i k \mid k \in \mathbb{Z}\} = \sigma_d(\partial_\theta),$$

i.e., the spectrum is purely discrete. For $k \in \mathbb{Z}$, the eigenspace to the eigenvalue $2\pi i k$ is spanned by the function

$$]0, 1[\ni \theta \mapsto e^{2\pi i k \theta}. \quad (4.61)$$

Proof. The skew-adjointness follows immediately from integrating by parts in $H^1(]0, 1[)$. The boundary terms vanish due to the condition $y(0) = y(1)$ in the definition of H_θ^1 . We prove that $\sigma(\partial_\theta)$ only contains isolated eigenvalues of the form claimed above. For this, it is easy to check that the resolvent operator is given by¹⁶

$$[(\partial_\theta - \gamma \text{id})^{-1}y](\theta) = e^{\gamma\theta} \left(\frac{\int_0^1 e^{-\gamma\tau} y(\tau) d\tau}{e^{-\gamma} - 1} + \int_0^\theta e^{-\gamma\tau} y(\tau) d\tau \right), \quad y \in L^2(]0, 1[), \quad (4.62)$$

for $\gamma \notin 2\pi i \mathbb{Z}$, i.e., $\gamma \in \rho(\partial_\theta)$. For $\gamma \in \mathbb{C}$, the ODE

$$\partial_\theta y = \gamma y, \quad y(0) = y(1),$$

is solved if, and only if, $\gamma = 2\pi i k$ for some $k \in \mathbb{Z}$ and $y(\theta) = ce^{2\pi i k \theta}$ with $c \in \mathbb{C}$, which shows (4.61). \square

Knowledge about the operator ∂_θ can now be translated to the transport operator by using action-angle type variables.

¹⁶The formula for the resolvent can be derived by solving $\partial_\theta z - \gamma z = y$, $z(0) = z(1)$ via a variation of constants.

Proposition 4.3.17. *The spectrum of the operator $\mathcal{T}: D(\mathcal{T}) \rightarrow H$ is given by*

$$\sigma(\mathcal{T}) = \overline{\left(\frac{2\pi i \mathbb{Z}}{T(\tilde{\Omega}_0^{EL})} \right)} := \overline{\left\{ \frac{2\pi i k}{T(E, L)} \mid k \in \mathbb{Z}, (E, L) \in \tilde{\Omega}_0^{EL} \right\}},$$

and the spectrum is entirely essential, i.e., $\sigma_{\text{ess}}(\mathcal{T}) = \sigma(\mathcal{T})$.

Proof. The proof is similar to that of [55, Thm. 5.7]. We show that

$$\frac{2\pi i k}{T(\tilde{E}, \tilde{L})} \in \sigma_{\text{ess}}(\mathcal{T}), \quad (\tilde{E}, \tilde{L}) \in \tilde{\Omega}_0^{EL}, \quad k \in \mathbb{Z}, \quad (4.63)$$

by verifying Weyl's criterion Theorem B.7, i.e., we need to find a sequence $(f_n)_{n \in \mathbb{N}} \subset D(\mathcal{T})$ with the following properties:¹⁷

- (i) $\|f_n\|_H = 1$ for $n \in \mathbb{N}$,
- (ii) $\left\| \mathcal{T}f_n - \frac{2\pi i k}{T(\tilde{E}, \tilde{L})} f_n \right\|_H \rightarrow 0$ for $n \rightarrow \infty$,
- (iii) $f_n \rightarrow 0$ in H for $n \rightarrow \infty$.

Consider a smooth function $\zeta: \mathbb{R}^2 \rightarrow \mathbb{R}$ such that $\text{supp}(\zeta) \subset \tilde{\Omega}_0^{EL} \cap B_1(\tilde{E}, \tilde{L})$ and with

$$\iint_{\Omega_0^{EL}} \zeta^2(E, L) dEdL = \frac{1}{4\pi^2}.$$

We now define¹⁸

$$\zeta_n(E, L) := n\zeta(nE, nL), \quad (E, L) \in \mathbb{R}^2, \quad n \in \mathbb{N},$$

which fulfills

$$\text{supp}(\zeta_n) \subset \tilde{\Omega}_0^{EL} \cap B_{\frac{1}{n}}(\tilde{E}, \tilde{L}) \quad (4.64)$$

and

$$\iint_{\Omega_0^{EL}} \zeta_n^2(E, L) dEdL = \frac{1}{4\pi^2}. \quad (4.65)$$

With this at hand, we set

$$f_n(\theta, E, L) := \left(\frac{|\varphi'(E, L)|}{T(E, L)} \right)^{\frac{1}{2}} \zeta_n(E, L) e^{-2\pi i k \theta}, \quad (\theta, E, L) \in [0, 1] \times \Omega_0^{EL},$$

¹⁷To be precise, Theorem B.7 is formulated for self-adjoint operators. However, by using that $i\mathcal{T}$ is self-adjoint, we can still apply the result here.

¹⁸We can interpret this as an approximation of Dirac's delta distribution. In fact, the resulting "limit" of f_n , which we construct here, is in the sense of distributions sometimes referred to as an "eigendistribution".

via action-angle type variables and consequently show that this sequence satisfies (i)–(iii) above. Recall that the period function T is bounded away from zero on $\tilde{\Omega}_0^{EL}$ by assumption (S2). We compute

$$\|f_n\|_H^2 = 4\pi^2 \iint_{\Omega_0^{EL}} \frac{T(E, L)}{|\varphi'(E, L)|} \int_0^1 |f_n(\theta, E, L)|^2 d\theta dE dL = 4\pi^2 \iint_{\Omega_0^{EL}} \zeta_n^2(E, L) dE dL = 1,$$

because of (4.65), which shows (i). As to (ii), Proposition 4.3.2(d) yields

$$(\mathcal{T}f_n)(\theta, E, L) = \frac{2\pi ik}{T(E, L)} f_n(\theta, E, L)$$

almost everywhere, and therefore

$$\begin{aligned} \left\| \mathcal{T}f_n - \frac{2\pi ik}{T(\tilde{E}, \tilde{L})} f_n \right\|_H^2 &= \left\| 2\pi ik \left(\frac{1}{T} - \frac{1}{T(\tilde{E}, \tilde{L})} \right) f_n \right\|_H^2 \\ &= 4\pi^2 k^2 \iint_{\Omega_0^{EL}} \zeta_n(E, L)^2 \left(\frac{1}{T(E, L)} - \frac{1}{T(\tilde{E}, \tilde{L})} \right)^2 dE dL. \end{aligned}$$

The integrand goes to zero pointwise a.e. since T is continuous, as proven in Proposition 3.2.7. Equation (4.65) together with Lebesgue's theorem yields (ii). It remains to show that $f_n \rightharpoonup 0$ for $n \rightarrow \infty$. We let $h \in H$ and estimate

$$|\langle f_n, h \rangle_H| \leq \|f_n\|_H \|\mathbf{1}_{\text{supp}(\zeta_n)} h\|_H \rightarrow 0, \quad n \rightarrow \infty,$$

where we use the Cauchy-Schwarz inequality, $\|f_n\|_H = 1$, and (4.64) in order to apply Lebesgue's dominated convergence theorem once again. Riesz's representation theorem therefore shows (iii). As explained above, Weyl's criterion yields

$$\overline{\left(\frac{2\pi i \mathbb{Z}}{T(\tilde{\Omega}_0^{EL})} \right)} \subset \sigma_{\text{ess}}(\mathcal{T}) \subset \sigma(\mathcal{T}),$$

because the spectrum of an operator is always closed [58, Thm. 1.2], and since the boundary values are not isolated, i.e., they lie in the essential spectrum as well.¹⁹

In order to finish the proof, we show

$$\mathbb{C} \setminus \overline{\left(\frac{2\pi i \mathbb{Z}}{T(\tilde{\Omega}_0^{EL})} \right)} \subset \rho(\mathcal{T}),$$

¹⁹Note that the essential spectrum is always closed due to its definition and the definition of the discrete spectrum, see Definition B.4.

because this implies

$$\sigma(\mathcal{T}) \subset \overline{\left(\frac{2\pi i \mathbb{Z}}{T(\tilde{\Omega}_0^{EL})} \right)}.$$

For $\gamma \in \mathbb{C} \setminus \overline{\left(\frac{2\pi i \mathbb{Z}}{T(\tilde{\Omega}_0^{EL})} \right)}$, we first notice that there exists $c > 0$ that satisfies

$$\text{dist}(\gamma T(E, L), 2\pi i \mathbb{Z}) \geq c, \quad (E, L) \in \tilde{\Omega}_0^{EL}, \quad (4.66)$$

due to the lower boundedness of the period function prescribed in (S2). We use $\sigma(-\partial_\theta) = 2\pi i \mathbb{Z}$ from Lemma 4.3.16, i.e., $\gamma T(E, L) \in \rho(-\partial_\theta)$, and thus the operator $\mathcal{G}: H \rightarrow D(\mathcal{T})$ given by²⁰

$$(\mathcal{G}f)(\theta, E, L) := T(E, L)[(-\partial_\theta - \gamma T(E, L)\text{id})^{-1}f(\cdot, E, L)](\theta), \quad \theta \in [0, 1],$$

for a.e. $(E, L) \in \Omega_0^{EL}$, is well defined which follows from Proposition 4.3.2(d) and from $(-\partial_\theta - \gamma T(E, L)\text{id})^{-1}: L^2(]0, 1[) \rightarrow H_\theta^1$. From the definition of \mathcal{G} , we immediately deduce that \mathcal{G} is the inverse of

$$\mathcal{T} - \gamma \text{id} = \frac{1}{T(E, L)}(-\partial_\theta - \gamma T(E, L)\text{id}).$$

In addition, we estimate the resolvent operator

$$(-\partial_\theta - \gamma T(E, L))^{-1}: L^2(]0, 1[) \rightarrow H_\theta^1$$

by employing [58, Thm. 5.8] and (4.66) via

$$\|(-\partial_\theta - \gamma T(E, L))^{-1}y\|_{L^2(]0, 1[)} \leq \frac{1}{\text{dist}(\gamma T(E, L), 2\pi i \mathbb{Z})} \|y\|_{L^2(]0, 1[)} \leq \frac{1}{c} \|y\|_{L^2(]0, 1[)}$$

for every $y \in L^2(]0, 1[)$. Together with the upper boundedness of the period function prescribed in (S2), this yields that

$$\mathcal{G} = (\mathcal{T} - \gamma \text{id})^{-1}: H \rightarrow D(\mathcal{T})$$

is bounded, i.e., $\gamma \in \rho(\mathcal{T})$. □

It is now an easy task to determine the (essential) spectrum of $\mathcal{T}^2|_{\mathcal{H}}$, \mathcal{B} , $\mathcal{B}^2|_{\mathcal{H}}$, as well as \mathcal{L} from Lemma B.9 and the relative compactness results in Section 4.3.3. We summarize this in a spectral theorem since many of the properties derived in this chapter find their use here—directly or indirectly.

²⁰Note that, here “id” refers to the identity on $L^2(]0, 1[)$. We have determined the resolvent of $-\partial_\theta$ explicitly in (4.62).

Theorem 4.3.18 (The essential spectrum of \mathcal{L} , \mathcal{T}^2 , and \mathcal{B}^2). *The spectrum of the operator $-\mathcal{T}^2: \mathcal{D}(\mathcal{T}^2) \rightarrow H$ is given by*

$$\sigma(-\mathcal{T}^2) = \overline{\left(\frac{2\pi\mathbb{N}_0}{T(\tilde{\Omega}_0^{EL})}\right)^2} = \overline{\left\{\left(\frac{2\pi ik}{T(E, L)}\right)^2 \mid k \in \mathbb{N}_0, (E, L) \in \tilde{\Omega}_0^{EL}\right\}}. \quad (4.67)$$

The spectrum of $-\mathcal{T}^2$ is purely essential and

$$\sigma_{\text{ess}}(-\mathcal{B}^2) = \sigma_{\text{ess}}(-\mathcal{T}^2) = \sigma(-\mathcal{T}^2), \quad \sigma_{\text{ess}}(\mathcal{B}) = \sigma_{\text{ess}}(\mathcal{T}) \quad (4.68)$$

is valid. Moreover, for the spectrum of the restricted operator $-\mathcal{B}^2|_{\mathcal{H}}: \mathcal{D}(\mathcal{T}^2) \cap \mathcal{H} \rightarrow \mathcal{H}$ and the Antonov operator $\mathcal{L}: \mathcal{D}(\mathcal{T}^2) \cap \mathcal{H} \rightarrow \mathcal{H}$, it holds that

$$\sigma_{\text{ess}}(\mathcal{L}) = \sigma_{\text{ess}}(-\mathcal{B}^2|_{\mathcal{H}}) \subset \sigma_{\text{ess}}(-\mathcal{B}^2) \setminus \{0\} = \overline{\left(\frac{2\pi\mathbb{N}}{T(\tilde{\Omega}_0^{EL})}\right)^2}. \quad (4.69)$$

Proof. We observe that $-\mathcal{T}^2: \mathcal{D}(\mathcal{T}) \rightarrow H$ satisfies

$$\sigma(-\mathcal{T}^2) = -\sigma(\mathcal{T})^2 = -\sigma_{\text{ess}}(\mathcal{T})^2 = \overline{\left(\frac{2\pi\mathbb{N}_0}{T(\tilde{\Omega}_0^{EL})}\right)^2}, \quad (4.70)$$

which follows from Proposition 4.3.17 and Theorem B.11.²¹ According to Lemma 4.3.15, the operator \mathcal{S} , is relatively \mathcal{T} -compact. Weyl's theorem, see Theorem B.10, therefore implies $\sigma_{\text{ess}}(\mathcal{B}) = \sigma_{\text{ess}}(\mathcal{T})$. By applying Lemma B.12 twice, we consequently get

$$\sigma_{\text{ess}}(-\mathcal{B}^2) = -\sigma_{\text{ess}}(\mathcal{B})^2 = -\sigma_{\text{ess}}(\mathcal{T})^2 = \sigma_{\text{ess}}(-\mathcal{T}^2),$$

which together with (4.70) proves (4.68). It remains to show (4.69). Recall that \mathcal{L} is self-adjoint by Corollary 4.3.13. From Lemma 4.3.14, we know that $\mathcal{R}|_{\mathcal{H}}$ is relatively $(\mathcal{B}^2|_{\mathcal{H}})$ -compact. Therefore, Theorem B.10 yields $\sigma_{\text{ess}}(\mathcal{L}) = \sigma_{\text{ess}}(-\mathcal{B}^2|_{\mathcal{H}})$. In order to verify

$$\sigma_{\text{ess}}(-\mathcal{B}^2|_{\mathcal{H}}) \subset \sigma_{\text{ess}}(-\mathcal{B}^2) \setminus \{0\},$$

let $\gamma \in \sigma_{\text{ess}}(-\mathcal{B}^2|_{\mathcal{H}})$. Firstly, $\gamma \neq 0$ due to $\mathcal{H} \subset \ker(\mathcal{B})^\perp$ from Proposition 4.3.5(e). Secondly, let $(f_n)_{n \in \mathbb{N}} \subset \mathcal{H}$ be a Weyl sequence corresponding to γ , see Theorem B.7. We claim that (f_n) is also a Weyl sequence in H . For this, we only need to deal with the weak convergence as the other properties transfer immediately. By the Riesz representation theorem, $f_n \rightharpoonup 0$ in \mathcal{H} is equivalent to

$$\langle f_n, h \rangle_H \rightarrow 0, \quad n \rightarrow \infty, \quad \text{for every } h \in \mathcal{H}.$$

²¹As mentioned in footnote 17, these theorems are formulated for self-adjoint operators but can be applied for skew-adjoint ones as well.

Since every $g \in H$ can be decomposed into $g = g_+ + g_-$ and f_n is odd in w , we get that

$$\langle f_n, g \rangle_H = \langle f_n, g_- \rangle_H \rightarrow 0, \quad n \rightarrow \infty, \quad \text{for every } g \in H,$$

i.e., $f_n \rightarrow 0$ in H . Thus, we obtain $\gamma \in \sigma_{\text{ess}}(-\mathcal{B}^2)$. The last equality in (4.69) is valid due to (4.67) and (4.68). \square

As an aside, it is claimed in [47, Rem. 6.3] that $\sigma_{\text{ess}}(-\mathcal{B}^2|_{\mathcal{H}}) = \sigma_{\text{ess}}(-\mathcal{T}^2|_{\mathcal{H}})$ without a proof. Upon closer inspection, this is more difficult to show than previously assumed. In the theorem above, we are only able to confirm the inclusion $\sigma_{\text{ess}}(-\mathcal{B}^2|_{\mathcal{H}}) \subset \sigma_{\text{ess}}(-\mathcal{T}^2|_{\mathcal{H}})$.

In addition, we do not determine the discrete spectrum of $-\mathcal{B}^2|_{\mathcal{H}}$, and it might be the case that $\sigma_d(-\mathcal{B}^2|_{\mathcal{H}}) \neq \emptyset$. This remains an open problem. However, we can at least bound the spectrum away from zero as in [47, Cor. 5.13].

Corollary 4.3.19. *There exists $\varepsilon > 0$ such that*

$$\sigma(-\mathcal{B}^2|_{\mathcal{H}}) \subset [\varepsilon, \infty[.$$

Proof. From Proposition 4.3.5(e) and (h), we have $\mathcal{H} \subset \ker(\mathcal{B})^\perp$ as well as

$$\|\mathcal{B}f\|_H \geq C\|f\|_H, \quad f \in \text{D}(\mathcal{T}) \cap \ker(\mathcal{B})^\perp.$$

The skew-adjointness of \mathcal{B} yields

$$\langle -\mathcal{B}^2 f, f \rangle_H = \|\mathcal{B}f\|_H^2 \geq C^2\|f\|_H^2, \quad f \in \text{D}(\mathcal{T}^2) \cap \mathcal{H},$$

which implies the claim due to Lemma B.6. \square

Without an application of the properties derived in this chapter, all knowledge about the operators would be a sunk cost. We can now reward ourselves for the elaborate preparatory work by developing a criterion for linear stability of steady states to the Einstein-Vlasov system.

5 On linear stability of stationary solutions

But it remains the case that
you know what is wrong
with a lot more confidence
than you know what is right.

Nassim Nicholas Taleb

In this chapter, we finally come to a topic already suggested in the title of this work: stability of stationary solutions to the Einstein-Vlasov system. Since non-linear stability is still very much elusive for now, we only deal with linear stability issues by further analyzing the linearized system introduced in Chapter 4.

Throughout this chapter, we consider a steady state of the Einstein-Vlasov system, as described in Section 4.1 and employ the same notation as in that section. In particular, we prescribe the conditions (S1)–(S4) and make extensive use of the operators investigated in Section 4.3.

In Section 5.1, we define what we mean by linear stability of stationary solutions and describe the general idea behind the Birman-Schwinger principle. We also recap the (limited) knowledge about linear stability available in the literature. The Birman-Schwinger principle and its corresponding operator is rigorously established in Section 5.2 and subsequently reduced to an operator—the Mathur operator—acting on a one-dimensional L^2 -space in Section 5.3. From these properties, we characterize linear stability in Section 5.4, which is applied in order to show that small matter shells surrounding a Schwarzschild black hole are linearly stable.

5.1 Definition, previous results, and methodology

5.1.1 Definition of linear stability

For many readers, the term *linear stability* will be familiar from a variety of settings, e.g., from ordinary differential equations. Even though there might be an intuition of what linear stability means, we motivate and define how we use it in the following. The same notion of linear stability was introduced in [47, Def. 4.4], but we provide a more thorough description.

As mentioned in Lemma 4.2.4, the linearized Einstein-Vlasov system can be represented by the second-order evolution equation

$$\partial_t^2 f_- + \mathcal{L}f_- = 0 \tag{5.1}$$

for the odd-in- w part f_- of $f \in H$, where the Antonov operator \mathcal{L} is given in Definition 4.2.2(d) and H is a weighted L^2 -space, see (4.9). From [52, Lem. 4.20], we recall that there exists a conserved quantity which can be interpreted as the energy of the linearized Einstein-Vlasov system. This result can readily be extended to the second-order formulation, see [52, Lem. 4.21] and [62, Eqn. (24a;R)]

Lemma 5.1.1. *For solutions to the linearized Einstein-Vlasov system, the energy*

$$\mathcal{A}(f, f) := 4\pi^2 \iiint_{\Omega_0} \frac{e^{\lambda_0}}{|\varphi'|} f^2 dr dw dL - \int_{R_{\min}}^{R_{\max}} e^{\mu_0 - \lambda_0} (2r\mu'_0 + 1) \lambda_f^2 dr, \quad (5.2)$$

is formally conserved. Moreover, it holds that

$$\|\partial_t f_-\|_H^2 + \langle \mathcal{L}f_-, f_- \rangle_H = \mathcal{A}(\partial_t f, \partial_t f)$$

and this quantity is formally conserved along the flow of (5.1).

Proof. For sufficiently regular f , the first- and second-order formulations are equivalent, according to Lemma 4.2.4. By using the essential operator \mathcal{B} defined in Definition 4.2.2(b) and (4.4), the linearized Vlasov equation (4.2) can be written as

$$\partial_t f = \mathcal{B}f - e^{2\mu_0 - \lambda_0} \left(2\mu'_0 + \frac{1}{r} \right) |\varphi'| w \lambda_f.$$

We plug this into the time-derivative of the energy (5.2) and obtain¹

$$\begin{aligned} \frac{1}{2} \frac{d}{dt} \mathcal{A}(f, f) &= \left\langle \mathcal{B}f - e^{2\mu_0 - \lambda_0} \left(2\mu'_0 + \frac{1}{r} \right) |\varphi'| w \lambda_f, f \right\rangle_H - \int_{R_{\min}}^{R_{\max}} e^{\mu_0 - \lambda_0} (2r\mu'_0 + 1) \lambda_{\mathcal{B}f} \lambda_f dr \\ &= \left\langle \mathcal{B}f - e^{2\mu_0 - \lambda_0} \left(2\mu'_0 + \frac{1}{r} \right) |\varphi'| w \lambda_f, f \right\rangle_H + 4\pi \int_{R_{\min}}^{R_{\max}} r e^{2\mu_0} (2r\mu'_0 + 1) j_f \lambda_f dr \end{aligned}$$

after inserting (4.41). The second term in the scalar product cancels the last addend, and $\langle \mathcal{B}f, f \rangle_H = 0$ holds, since \mathcal{B} is skew-adjoint, see Proposition 4.3.5(a). This implies that $\partial_t \mathcal{A}(f, f) = 0$ and thus the energy is conserved.

As to the second part, we have $\partial_t f_+ = \mathcal{B}f_-$ and observe that

$$\begin{aligned} \langle \mathcal{L}f_-, f_- \rangle_H &= \langle \mathcal{B}f_-, \mathcal{B}f_- \rangle_H - \langle \mathcal{R}f_-, f_- \rangle_H \\ &= \|\partial_t f_+\|_H^2 - 16\pi^2 \int_{R_{\min}}^{R_{\max}} e^{3\mu_0 + \lambda_0} (2r\mu'_0 + 1) (j_{f_-})^2 r^2 dr \\ &= \|\partial_t f_+\|_H^2 - \int_{R_{\min}}^{R_{\max}} e^{\mu_0 - \lambda_0} (2r\mu'_0 + 1) (\lambda_{\mathcal{B}f_-})^2 r^2 dr, \end{aligned}$$

¹Note that $\lambda_{\partial_t f} = \lambda_{\mathcal{B}f}$ after parity considerations.

where we again used (4.41). This yields

$$\|\partial_t f_-\|_H^2 + \langle \mathcal{L} f_-, f_- \rangle_H = \|\partial_t f\|_H^2 - \int_{R_{\min}}^{R_{\max}} e^{\mu_0 - \lambda_0} (2r\mu'_0 + 1) (\lambda_{\partial_t f})^2 r^2 dr = \mathcal{A}(\partial_t f, \partial_t f),$$

since $\partial_t f_-$ is odd in w and $\partial_t f_+$ is orthogonal to $\partial_t f_-$ in H . In addition, we compute

$$\frac{1}{2} \partial_t (\|\partial_t f_-\|_H^2 + \langle \mathcal{L} f_-, f_- \rangle_H) = \langle \partial_t^2 f_-, \partial_t f_- \rangle + \langle \mathcal{L} f_-, \partial_t f_- \rangle_H = 0,$$

because \mathcal{L} is self-adjoint by Corollary 4.3.13. \square

This lemma is the foundation for the definition of linear stability as in [47, Def. 4.4] in the following sense:

Definition 5.1.2. *Consider a stationary solution to the Einstein-Vlasov system, as specified in Section 4.1.*

(a) *The steady state is called linearly stable if the spectrum of \mathcal{L} is positive, i.e.,*

$$\inf(\sigma(\mathcal{L})) > 0.$$

(b) *The steady state is called linearly unstable if there exists $\gamma \in \sigma(\mathcal{L})$ with $\gamma < 0$.*

(c) *The number of linearly independent eigenfunctions corresponding to negative eigenvalues is called the number of exponentially growing modes of the steady state. If zero is an eigenvalue of \mathcal{L} , we say that the steady state has a zero-frequency mode.*

A few remarks on the appropriateness of this definition are in order.

Remark 5.1.3. (a) *The Antonov operator is self-adjoint by Corollary 4.3.13, so the spectrum of \mathcal{L} is real [58, Thm. 5.5]. Moreover, Theorem 4.3.18 implies*

$$\sigma_{\text{ess}}(\mathcal{L}) \subset \overline{\left(\frac{2\pi\mathbb{N}}{T(\tilde{\Omega}_0^{EL})} \right)^2},$$

i.e., we get $\inf(\sigma_{\text{ess}}(\mathcal{L})) > 0$, since the period function is bounded from above by (S2). Therefore, every $\gamma \in \sigma(\mathcal{L})$ with

$$\gamma < \inf(\sigma_{\text{ess}}(\mathcal{L}))$$

is by definition in the discrete spectrum and thus an isolated eigenvalue with finite multiplicity. In particular, negative values in the spectrum are always isolated eigenvalues with finite multiplicity. Figure 5.1 illustrates how the spectrum of \mathcal{L} might qualitatively look like.

(b) *In the case where $\gamma = \inf(\sigma(\mathcal{L})) > 0$, we can deduce the Antonov-type inequality*

$$\langle \mathcal{L} f, f \rangle_H \geq \gamma \|f\|_H^2, \quad f \in \text{D}(\mathcal{L}), \quad (5.3)$$

as per Lemma B.6. Furthermore, Lemma 5.1.1 yields that

$$\|\partial_t f_-\|_H^2 + \langle f_-, \mathcal{L}f_- \rangle_H = \mathcal{A}(\partial_t f, \partial_t f)$$

is constant the flow of $\partial_t^2 f_- + \mathcal{L}f_- = 0$. From this, we can show that, for suitably chosen small initial data, the norms $\|f_-(t)\|_H$, $\|\partial_t f_-(t)\|_H$, $\|\partial_t f_+(t)\|_H$ stay small as well, i.e., we have linear stability in the sense of these norms. The claim for $\|\partial_t f_+(t)\|_H$ follows from $\partial_t f_+ = \mathcal{B}f_-$, by using the skew-adjointness of \mathcal{B} , and because \mathcal{R} is bounded.

- (c) On the other hand, consider an element $\gamma \in \sigma(\mathcal{L})$ with $\gamma < 0$ and thus, as discussed in (a), γ must be an isolated eigenvalue of \mathcal{L} . Let $f \in \mathcal{H}$ be an eigenfunction, i.e., $\mathcal{L}f = \gamma f$. Then $g(t) := e^{\sqrt{-\gamma}t} f$, $t \in \mathbb{R}$, solves (5.1), and we obtain a solution to the linearized Einstein-Vlasov system which grows exponentially in time. This is why we call g an exponentially growing mode and refer to the corresponding steady state as linearly unstable in this situation.
- (d) The terminology zero frequency mode, used if zero is an eigenvalue of \mathcal{L} , goes back to [62, Ch. IV(f)], where the authors argue that zero-frequency modes transfer the original equilibrium to another stationary solution nearby. If the eigenvalues are in some sense continuous along a family of steady states, this special case $0 \in \sigma(\mathcal{L})$ also corresponds to the point where linear stability can change. We will comment on this in more detail in Chapter 6.
- (e) From a non-linear perspective, the steady state f_0 is a critical point of the energy-Casimir functional²

$$\mathcal{H}_C(f) := 4\pi^2 \iiint_{\Omega_0} \left(\sqrt{1 + w^2 + \frac{L}{r^2}} f + e^\lambda \chi(f) \right) dr dw dL, \quad f \in H,$$

where $\chi \in C^1(\mathbb{R})$ with $\chi(0) = 0$ is chosen such that $\chi'(\varphi(E, L)) = -E$ for $(E, L) \in \Omega_0^{EL}$. For more details, we refer to [53, 54, 65]. The energy-Casimir functional has two important properties: \mathcal{H}_C is constant along solutions to the non-linear Einstein-Vlasov system and the second-order variation of \mathcal{H}_C at f_0 corresponds to the quadratic form \mathcal{A} induced by \mathcal{L} . Therefore, spectral knowledge of \mathcal{L} , and thus \mathcal{A} due to $\langle \mathcal{L}f, f \rangle_H = \mathcal{A}(\mathcal{B}f, \mathcal{B}f)$, should also be a natural step towards non-linear (in)stability. However, this is still an open problem.

5.1.2 Previous results on stability

We briefly recall what is known about (linear) stability for the Einstein-Vlasov system. For a more thorough review, we refer to the recent work in [92]. Linear stability in

²Here, the notation is a bit ambiguous. Only for this formula we write λ for the metric coefficient which is obtained by solving the non-linear field equation (1.10).

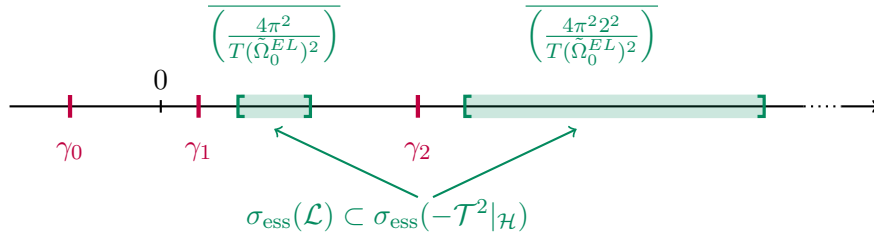


Figure 5.1: A possible qualitative configuration for the spectrum of the operator \mathcal{L} . The opaque parts represent the bounds for the essential spectrum of \mathcal{L} while $\gamma_0, \gamma_1, \gamma_2 \in \sigma_d(\mathcal{L})$ are isolated eigenvalues with finite multiplicity. In particular, γ_0 corresponds to an unstable mode, and γ_1, γ_2 induce an oscillating mode which we will deal with in Chapter 6. A-priori, we do not know whether $\sigma_d(\mathcal{L}) \neq \emptyset$.

the context of the singularity-free setting was first examined in [62]. The system is linearized around appropriate equilibria similar to Section 4.2, and the author shows that the spectral properties of the associated unbounded operator \mathcal{L} serve as the basis for studying linear stability. This is also the case for the non-relativistic counterpart to the Einstein-Vlasov system, i.e., the gravitational Vlasov-Poisson system, for which it is known that all physically relevant stationary solutions are both linearly and non-linearly stable [17, 33, 49, 66, 72].

As an aside, in [61] the analysis of linear stability leads to the claim that, along a family of suitably chosen equilibria, eigenvalues can only change sign at local extremal points of the binding energy $E_b = \frac{N-M}{N}$, as defined in (2.77); we discuss this in more depth in Chapter 7 and 8 where we consider numerical results on (non-)linear stability.

It was proven in [53, 54] that isotropic steady states of the Einstein-Vlasov, as constructed in our work, are stable for small values of the redshift κ , i.e., if the setting is not too relativistic. These stationary solutions become linearly unstable for large values of κ , as shown in [52]. The authors also establish a trichotomy in phase space divided into a stable, unstable, and center space. For future reference, we gather the main results from [52, 53, 54] in a theorem adapted to our setting. These conclusions will become very important in Chapter 6. As we deal with a κ -family in this theorem, we denote all relevant quantities with a subscript κ . In particular, the function space $\mathcal{H} = \mathcal{H}_\kappa$ and the operators depend on κ as well.

Theorem 5.1.4. *Consider a κ -family of isotropic steady states $(f_\kappa)_{\kappa>0}$, as in Definition 2.2.5, that satisfy the assumptions in Section 4.1.*

(a) *There exists $\kappa_{\text{st}} > 0$ such that for every $0 < \kappa < \kappa_{\text{st}}$ it holds that*

$$\langle \mathcal{L}_\kappa f, f \rangle_{\mathcal{H}_\kappa} \geq C_\kappa \|f\|_{\mathcal{H}_\kappa}^2, \quad f \in \mathcal{H}_\kappa, \quad (5.4)$$

for some $C_\kappa > 0$, where \mathcal{L}_κ is the Antonov operator corresponding to f_κ . The stationary solution f_κ is linearly stable for $0 < \kappa < \kappa_{\text{st}}$, according to Definition 5.1.2.

(b) There exists $\kappa_{\text{unst}} > 0$ such that for every $\kappa > \kappa_{\text{unst}}$ it holds that

$$\langle \mathcal{L}_\kappa f, f \rangle_{\mathcal{H}_\kappa} < 0,$$

for some $f \in \mathcal{H}_\kappa$. The stationary solution f_κ is linearly unstable for $\kappa > \kappa_{\text{unst}}$, according to Definition 5.1.2.

Proof. The main result in [54, Thm. 5.1]—translated to our notation and setting³—establishes a coercivity estimate in the following sense: There exists $C^* > 0$ and $\kappa_{\text{st}} > 0$ such that

$$\mathcal{A}_\kappa(\mathcal{B}_\kappa f, \mathcal{B}_\kappa f) \geq C^* \iiint \frac{1}{|\varphi'_\kappa|} \left(r^2 w^2 \left| \left\{ E, \frac{f}{r w} \right\} \right|^2 + \kappa^{1+2a} |f|^2 \right) dr dw dL \quad (5.5)$$

for every $0 < \kappa < \kappa_{\text{st}}$ and $f \in \mathcal{H}_\kappa$. Here, \mathcal{A}_κ is given by (5.2) and \mathcal{B}_κ is the essential operator corresponding to f_κ . In addition, we have $a = \frac{k}{2} + \frac{1}{4}$ with k given by $(\Phi 2)$. Due to the self-adjointness of \mathcal{B}_κ and from (4.41), we compute

$$\langle \mathcal{L}_\kappa f, f \rangle_{\mathcal{H}_\kappa} = \langle \mathcal{B}_\kappa f, \mathcal{B}_\kappa f \rangle_{H_\kappa} - \langle \mathcal{R}_\kappa f, f \rangle_{H_\kappa} = \mathcal{A}_\kappa(\mathcal{B}_\kappa f, \mathcal{B}_\kappa f). \quad (5.6)$$

We dispense with the first term in (5.5) and include a factor e^{λ_κ} in the integrand, in order to obtain (5.4). Using Lemma B.6 yields

$$\inf(\sigma(\mathcal{L}_\kappa)) \geq C_\kappa > 0, \quad 0 < \kappa < \kappa_{\text{st}},$$

and thus linear stability follows.

Similarly, we deduce from [52, Thm. 4.3] that there exists $\kappa_{\text{unst}} > 0$ such that for every $\kappa > \kappa_{\text{unst}}$, we have

$$\mathcal{A}_\kappa(\mathcal{B}_\kappa f, \mathcal{B}_\kappa f) < 0,$$

for some $f \in \mathcal{H}_\kappa$, which implies the first claim of (b) due to (5.6). In this case, we get

$$\inf(\sigma(\mathcal{L}_\kappa)) = \inf_{f \in \mathcal{H}_\kappa} \frac{\langle \mathcal{L}_\kappa f, f \rangle_{\mathcal{H}_\kappa}}{\|f\|_{\mathcal{H}_\kappa}^2} < 0$$

by applying the min-max principle for self-adjoint operators [88, Thm. XIII.1] and therefore obtain linear instability.⁴ \square

Note that in the original works [52, 54], the assumptions (S1) and (S2) are not imposed and thus the results in the theorem above hold in more generality. However, more work is required to obtain an exponentially growing mode from $\langle \mathcal{L}_\kappa f, f \rangle_{\mathcal{H}_\kappa} < 0$,

³Instead of using the essential operator \mathcal{B}_κ , the authors in [52, 54] formulate their results via the concept of *linearly dynamically accessible perturbations* which allows only for perturbations in $\text{im}(\mathcal{B}_\kappa)$ to begin with. All in all, the approach is equivalent to ours.

⁴To be precise, in order to apply [88, Thm. XIII.1], we have to show that $\mathcal{L} = -\mathcal{B}^2 - \mathcal{R}$ is bounded from below in the sense of quadratic forms. However, this follows from $-\mathcal{B}^2 \geq 0$ and the boundedness of \mathcal{R} .

see [52, Thm. 4.25], since the spectrum is not easily controlled if we do not prescribe (S1) and (S2).

To the authors knowledge, linear stability has been investigated numerically only in [61], where

$$\inf(\sigma(\mathcal{L}_\kappa)) = \inf_{f \in \mathcal{H}_\kappa} \frac{\langle \mathcal{L}_\kappa f, f \rangle_{\mathcal{H}_\kappa}}{\|f\|_{\mathcal{H}_\kappa}^2} \quad (5.7)$$

is approximated in order to estimate the bottom of the spectrum of \mathcal{L} . In [60], trial functions of the form $f(r, w, L) = |\varphi'|w C(r)$ are used—with an arguably limited number of radial test functions C . Modern computational power allows us to estimate (5.7) more accurately in Chapter 8.

We end this section with a comment on the issue of non-linear stability. It would be beneficial to obtain stationary solutions as minimizers of an appropriate energy-Casimir functional, as mentioned in Remark 5.1.3(e). This was tried in [113], but the work contains serious flaws, as pointed out in [9]. As a workaround, the Euler-Lagrange equation corresponding to critical points of the energy-Casimir functional is solved in [10]. However, actually finding steady states as minimizers of the energy-Casimir functional remains an open problem. This leaves us with numerically investigating non-linear stability which we discuss in Chapter 7.

5.1.3 Methodology of the Birman-Schwinger principle

As motivation and preparation for the following rigorous analysis, we outline the central idea behind the Birman-Schwinger principle. Originally, the Birman-Schwinger principle was designed in the context of quantum mechanics. For example, it is employed to investigate the eigenvalues of time-independent Schrödinger operators $-\Delta - V$, where $V \geq 0$ is an external potential. More precisely, it is used to determine or estimate the number of eigenvalues below a prescribed energy threshold. A small collection of where the Birman-Schwinger principle is applied in quantum mechanics is [73, Sc. 12.4], [74, Sc. 4.3], [88, Sc. XIII.3] as well as [110, Sc. III.3]; there is an abundance of other sources and applications which we do not list here. Recently, the Birman-Schwinger principle has attracted attention in the study of galactic dynamics for the Vlasov-Poisson system independently in [55] and [69], and subsequently in [56]. For the Einstein-Vlasov system, it has been applied in earlier work by the author and colleagues [47].

In our setting, the goal is to find a criterion to determine whether \mathcal{L} has or does not have an eigenvalue smaller than zero since this decides over linear stability, as defined in Definition 5.1.2. Now follows a formal derivation: We observe that zero is an eigenvalue of $\mathcal{L}_\beta = -\mathcal{B}^2 - \frac{1}{\beta}\mathcal{R}$ for $\beta > 0$ if, and only if, β is an eigenvalue of

$$Q := -\sqrt{\mathcal{R}}\mathcal{B}^{-2}\sqrt{\mathcal{R}},$$

which we call the *Birman-Schwinger operator*. This is the reason why we already determined $\sqrt{\mathcal{R}}$ and the invertibility of \mathcal{B}^2 in Section 4.3. With help of continuity in β and the auxiliary operators \mathcal{L}_β , we then prove that negative eigenvalues of \mathcal{L} can be charac-

terized by eigenvalues $\beta > 1$ of Q . In fact, even the multiplicities of the eigenvalues are conserved by this transformation. The procedure is discussed in detail in Section 5.2.

The spectral analysis of the Birman-Schwinger operator can be radically simplified by observing that $\text{im}(Q) \subset \text{im}(\sqrt{\mathcal{R}})$, which essentially reduces Q to an operator acting on a radial L^2 -space. More precisely, a function in $\text{im}(\sqrt{\mathcal{R}})$ can be written as $|\varphi'(E, L)|w \alpha_0(r) F(r)$ for some $F \in L^2([0, \infty[)$, where α_0 is a radial function depending only on steady state quantities. In fact, we can equivalently consider the operator $\mathcal{M}: L^2([0, \infty[) \rightarrow L^2([0, \infty[)$ given by

$$Q(|\varphi'(E, L)|w \alpha_0(r) F(r)) = |\varphi'(E, L)|w \alpha_0(r) (\mathcal{M}F)(r), \quad (5.8)$$

which we denote as the *Mathur operator*. This reduction process is due to Mathur [78], who considered a related problem for the non-relativistic setting with an external potential. Even though the Mathur operator acts on a radial L^2 -space instead of a three-dimensional phase space like Q and \mathcal{L} , we prove that Q and \mathcal{M} have the same eigenvalues, i.e., it is sufficient to investigate the spectrum of \mathcal{M} .

In Section 5.3, we show that the Mathur operator has advantageous properties by using the comprehensive knowledge on the essential operator from Section 4.3: It is compact, symmetric, bounded, non-negative, and a Hilbert-Schmidt operator with integral kernel K , cf. [89, Thm. VI.22 et seq]. This means that \mathcal{M} can be represented by

$$(\mathcal{M}F)(r) = \int_0^\infty K(r, s)F(s) dr, \quad F \in L^2([0, \infty[),$$

for an appropriate function $K \in L^2([0, \infty[^2)$. Unfortunately, we are only able to determine K semi-explicitly, as it involves the inverse of \mathcal{B}^2 , which is only known up to the projection onto $\ker(\mathcal{B})$, see Proposition 4.3.5(g).

As the main result of this chapter, we deduce a variational principle for \mathcal{M} , which is represented by integrating radially over the kernel K , in Section 5.4. Importantly, we prove that this fully characterizes linear stability of the steady state under investigation, i.e., whether negative eigenvalues of \mathcal{L} are present or not. As an application, we investigate linear stability of small matter shells with a Schwarzschild-singularity.

5.2 A Birman-Schwinger principle

After the brief introduction to the Birman-Schwinger principle in the previous section, we now implement it rigorously in order to obtain a criterion for linear stability which we can apply for a diverse collection of stationary solutions. As above, we consider a fixed steady state, as described in Section 4.1.

5.2.1 The operators \mathcal{L}_β

We consider the family of auxiliary operators

$$\mathcal{L}_\beta := -\mathcal{B}^2 - \frac{1}{\beta}\mathcal{R}: \mathcal{D}(\mathcal{T}^2) \cap \mathcal{H} \rightarrow \mathcal{H}, \quad \beta > 0, \quad (5.9)$$

which correspond to a shift of the Antonov operator $\mathcal{L} = -\mathcal{B}^2 - \mathcal{R}$. Analyzing the operators \mathcal{L}_β from a functional and spectral analytic point of view is again a tedious and abstract endeavor. However, it is essential to understand how the spectrum behaves in the parameter β . This will help later when analyzing $\mathcal{L} = \mathcal{L}_1$ in the following way: Formally speaking, if the spectrum of \mathcal{L}_β is “continuous” in $\beta > 0$, we would expect that it is in some sense increasing in β because $\mathcal{R} \geq 0$, as seen in Lemma 4.3.12. In addition, letting $\beta \rightarrow \infty$ should leave us solely with the spectrum of $-\mathcal{B}^2$, which is positive and strictly bounded away from zero by Corollary 4.3.19. If \mathcal{L} does indeed have a negative eigenvalue, the spectrum of \mathcal{L}_β therefore has to pass through zero for some value of β , and vice versa. It turns out easier to search for the eigenvalue zero of \mathcal{L}_β instead of negative eigenvalues of \mathcal{L} . We make these preliminary considerations much more precise. A very similar investigation can be found in [47, Sc. 6.1].

To begin, we prove that \mathcal{L}_β has essentially the same properties as the Antonov operator. In particular, we can control the essential spectrum in the same manner.

Lemma 5.2.1. *For $\beta > 0$, the operator $\mathcal{L}_\beta: \mathcal{D}(\mathcal{T}^2) \cap \mathcal{H} \rightarrow \mathcal{H}$ is self-adjoint as a densely defined operator on \mathcal{H} . The essential spectrum is given by*

$$\sigma_{\text{ess}}(\mathcal{L}_\beta) = \sigma_{\text{ess}}(-\mathcal{B}^2|_{\mathcal{H}}) = \sigma_{\text{ess}}(\mathcal{L}).$$

Proof. The self-adjointness follows analogously as for \mathcal{L} in Corollary 4.3.13. Moreover, Lemma 4.3.14 implies that $\frac{1}{\beta}\mathcal{R}|_{\mathcal{H}}$ is relatively $(\mathcal{B}^2|_{\mathcal{H}})$ -compact and thus $\sigma_{\text{ess}}(\mathcal{L}_\beta) = \sigma_{\text{ess}}(-\mathcal{B}^2|_{\mathcal{H}})$ by Weyl’s theorem, see Theorem B.10. \square

Having controlled the essential spectrum, we can thus resort to investigating the discrete spectrum of \mathcal{L}_β in dependence of β . What follows does not depend on the specific definition of \mathcal{B}^2 and \mathcal{R} but mainly comes down to the invertibility of \mathcal{B}^2 , the positivity of \mathcal{R} , and the relative compactness result from Lemma 4.3.14. As in [47, Prop. 6.4], we can characterize isolated eigenvalues by the well-known min-max-principle. We recall the notion of multiplicity of eigenvalues in Remark B.5.

Proposition 5.2.2. *For $\beta > 0$ and $n \in \mathbb{N}$, let*

$$\gamma_n(\beta) := \sup_{g_1, \dots, g_{n-1} \in \mathcal{H}} \left(\inf_{\substack{h \in \mathcal{D}(\mathcal{T}^2) \cap \mathcal{H}, \|h\|_H=1, \\ h \perp g_1, \dots, g_{n-1}}} \langle h, \mathcal{L}_\beta h \rangle_H \right). \quad (5.10)$$

Then $\gamma_n(\beta)$ is finite, and either

(i) $\gamma_n(\beta) < \inf(\sigma_{\text{ess}}(-\mathcal{B}^2|_{\mathcal{H}}))$. In this case, there exist at least n eigenvalues (counting multiplicities) of \mathcal{L}_β below $\inf(\sigma_{\text{ess}}(-\mathcal{B}^2|_{\mathcal{H}}))$, and $\gamma_n(\beta)$ is the n -th smallest eigenvalue (counting multiplicities) of \mathcal{L}_β ,

or

(ii) $\gamma_n(\beta) = \inf(\sigma_{\text{ess}}(-\mathcal{B}^2|_{\mathcal{H}}))$. In this case, there exist at most $n-1$ eigenvalues (counting multiplicities) of \mathcal{L}_β below $\inf(\sigma_{\text{ess}}(-\mathcal{B}^2|_{\mathcal{H}}))$, and $\gamma_{n+j}(\beta) = \inf(\sigma_{\text{ess}}(-\mathcal{B}^2|_{\mathcal{H}}))$ for $j \in \mathbb{N}$.

Proof. We can directly apply the min-max principle for self-adjoint operators that are bounded from below [88, Thm. XIII.1], [110, Prop. II.32]. Note that \mathcal{L}_γ is bounded from below due to

$$\langle f, \mathcal{L}_\beta f \rangle_H = \|\mathcal{B}f\|_H^2 - \frac{1}{\beta} \langle f, \mathcal{R}f \rangle_H \geq -\frac{\|\mathcal{R}\|_{H \rightarrow H}}{\beta}$$

for $f \in D(\mathcal{T}^2) \cap \mathcal{H}$ with $\|f\|_H = 1$, because \mathcal{R} is bounded. \square

We now investigate the mapping $]0, \infty[\ni \beta \mapsto \gamma_n(\beta)$ for $n \in \mathbb{N}$, as this tells us how the n -th eigenvalue of \mathcal{L}_β —if it exists—behaves in the parameter β . As motivated above, we can indeed show that γ_n is non-decreasing. A similar problem was, for example, considered in [88, XIII Problem 2] and [110, Thm. II.33].

Lemma 5.2.3. *For fixed $n \in \mathbb{N}$, the mapping $]0, \infty[\ni \beta \mapsto \gamma_n(\beta)$ is non-decreasing and*

$$|\gamma_n(\alpha) - \gamma_n(\beta)| \leq \left| \frac{1}{\alpha} - \frac{1}{\beta} \right| \|\mathcal{R}\|_{H \rightarrow H} \quad (5.11)$$

for $\alpha, \beta > 0$. In particular, $]0, \infty[\ni \beta \mapsto \gamma_n(\beta)$ is continuous.

Proof. We first show that the quadratic form is non-decreasing and continuous in β for a fixed test function, and afterwards we prove that this carries over to γ_n via the definition in (5.10). For $\beta > 0$ and $h \in D(\mathcal{T}^2) \cap \mathcal{H}$ with $\|h\|_H = 1$, we define

$$f_h(\beta) := \langle h, \mathcal{L}_\beta h \rangle_H.$$

Since \mathcal{R} is non-negative due to Lemma 4.3.12, we get

$$f_h(\beta) = \|\mathcal{B}h\|_H^2 - \frac{1}{\beta} \langle h, \mathcal{R}h \rangle_H \leq \|\mathcal{B}h\|_H^2 - \frac{1}{\alpha} \langle h, \mathcal{R}h \rangle_H = f_h(\alpha)$$

for $\beta \leq \alpha$. Moreover, the Cauchy-Schwarz inequality yields

$$|f_h(\beta) - f_h(\alpha)| = \left| \frac{1}{\beta} - \frac{1}{\alpha} \right| \langle h, \mathcal{R}h \rangle_H \leq \left| \frac{1}{\beta} - \frac{1}{\alpha} \right| \|\mathcal{R}\|_{H \rightarrow H}, \quad \alpha, \beta > 0. \quad (5.12)$$

In particular, the mapping $]0, \infty[\ni \beta \mapsto f_h(\beta)$ is non-decreasing and continuous. We illustrate the procedure for translating this to the estimate (5.11): For $\beta > 0$ and fixed

$g_1, \dots, g_{n-1} \in \mathcal{H}$, let

$$I_\beta(g_1, \dots, g_{n-1}) := \inf_{\substack{h \in \mathcal{D}(\mathcal{T}^2) \cap \mathcal{H}, \\ h \perp g_1, \dots, g_{n-1}, \\ \|h\|_H=1}} f_h(\beta).$$

For $\alpha, \beta > 0$ as well as $h \in \mathcal{D}(\mathcal{T}^2) \cap \mathcal{H}$ with $\|h\|_H = 1$ and $h \perp g_1, \dots, g_{n-1}$, we obtain

$$I_\beta(g_1, \dots, g_{n-1}) \leq f_h(\beta) \leq f_h(\alpha) + \left| \frac{1}{\beta} - \frac{1}{\alpha} \right| \|\mathcal{R}\|_{H \rightarrow H}$$

from (5.12). Taking the infimum over all such h 's and switching the role of β and α yields

$$|I_\beta(g_1, \dots, g_{n-1}) - I_\alpha(g_1, \dots, g_{n-1})| \leq \left| \frac{1}{\beta} - \frac{1}{\alpha} \right| \|\mathcal{R}\|_{H \rightarrow H}.$$

Since g_1, \dots, g_{n-1} are fixed, this implies that

$$\gamma_n(\beta) \geq I_\beta(g_1, \dots, g_{n-1}) \geq I_\alpha(g_1, \dots, g_{n-1}) - \left| \frac{1}{\beta} - \frac{1}{\alpha} \right| \|\mathcal{R}\|_{H \rightarrow H}, \quad \alpha, \beta > 0.$$

From this, we proceed in similar fashion by taking the supremum over all such g_j 's and switching the role of β and α , in order to obtain (5.11). \square

As hinted towards above, the monotonicity of γ_n can be attributed to the fact that increasing β in \mathcal{L}_β assigns more relative weight to the non-negative term $-\mathcal{B}^2$ instead of the non-positive term $-\frac{1}{\beta}\mathcal{R}$. Thus, the spectrum gets shifted towards more positive values. We can even show that this monotonicity is strict if γ_n is not part of the spectrum of $-\mathcal{B}^2|_{\mathcal{H}}$, see also [47, Lem. 6.7]. Remember that $\sigma(-\mathcal{B}^2|_{\mathcal{H}})$ is bounded away from zero by Corollary 4.3.19.

Lemma 5.2.4. *Fix $n \in \mathbb{N}$ and suppose that there exists $\beta_0 > 0$ such that*

$$\gamma_n(\beta_0) < \inf(\sigma(-\mathcal{B}^2|_{\mathcal{H}})).$$

Then $]0, \beta_0] \ni \beta \mapsto \gamma_n(\beta)$ is strictly increasing.

Proof. The proof is akin to [73, Proof of Thm. 12.1]. First observe that Proposition 5.2.2 and Lemma 5.2.3 yield $\gamma_j(\beta) < \inf(\sigma(-\mathcal{B}^2|_{\mathcal{H}}))$ and that $\gamma_j(\beta)$ is an eigenvalue of \mathcal{L}_β , for every $1 \leq j \leq n$ and $0 < \beta \leq \beta_0$. For every such j and β , we choose orthonormal eigenfunctions h_j^β , i.e.,

$$\mathcal{L}_\beta h_j^\beta = \gamma_j(\beta) h_j^\beta, \quad \|h_j^\beta\|_H = 1, \quad h_i^\beta \perp h_j^\beta \text{ for } i \neq j.$$

Fix $0 < \beta < \alpha \leq \beta_0$ and consider $\tilde{h} := \sum_{j=1}^n c_j h_j^\beta$ with $c_1, \dots, c_n \in \mathbb{R}$ selected such that

$$\|\tilde{h}\|_H^2 = \sum_{j=1}^n c_j^2 = 1, \quad \tilde{h} \perp h_1^\beta, \dots, h_{n-1}^\beta,$$

holds.⁵ We compute

$$\langle \tilde{h}, \mathcal{L}_\alpha \tilde{h} \rangle_H = \sum_{j=1}^n c_j^2 \gamma_j(\alpha) \leq \gamma_n(\alpha) \sum_{j=1}^n c_j^2 = \gamma_n(\alpha) < \inf(\sigma(-\mathcal{B}^2|_{\mathcal{H}})), \quad (5.13)$$

from which we deduce $\langle \tilde{h}, \mathcal{R} \tilde{h} \rangle_H > 0$ due to $\|\mathcal{B} \tilde{h}\|_H^2 \geq \inf(\sigma(-\mathcal{B}^2|_{\mathcal{H}}))$ from Lemma B.6. In conclusion, we estimate

$$\langle \tilde{h}, \mathcal{L}_\beta \tilde{h} \rangle_H = \|\mathcal{B} \tilde{h}\|_H^2 - \frac{1}{\beta} \langle \tilde{h}, \mathcal{R} \tilde{h} \rangle_H < \|\mathcal{B} \tilde{h}\|_H^2 - \frac{1}{\alpha} \langle \tilde{h}, \mathcal{R} \tilde{h} \rangle_H = \langle \tilde{h}, \mathcal{L}_\alpha \tilde{h} \rangle_H. \quad (5.14)$$

We claim that the supremum in $\gamma_n(\beta)$, see (5.10), is attained for $g_j = h_j^\beta$, $1 \leq j < n$. For this, we decompose $\mathcal{H} = \mathcal{H}_n \oplus \text{span}\{h_1^\beta, \dots, h_{n-1}^\beta\}$ —with \mathcal{H}_n chosen appropriately—and restrict \mathcal{L}_β to \mathcal{H}_n . Note that $\mathcal{L}_\beta|_{\mathcal{H}_n} : \mathcal{H}_n \rightarrow \mathcal{H}_n$ is well defined because h_j^β are eigenfunctions, it is self-adjoint, and as per Proposition 5.2.2, we get that $\gamma_n(\beta) < \inf(\sigma(-\mathcal{B}^2|_{\mathcal{H}}))$ is the smallest eigenvalue of $\mathcal{L}_\beta|_{\mathcal{H}_n}$. Therefore, the claim follows from case (i) in Proposition 5.2.2 and from [58, Prop. 12.1].

This observation together with (5.13) and (5.14) implies that

$$\gamma_n(\beta) = \inf_{\substack{h \in \mathcal{D}(\mathcal{T}^2) \cap \mathcal{H}, \|h\|_H=1, \\ h \perp h_1^\beta, \dots, h_{n-1}^\beta}} \langle h, \mathcal{L}_\beta h \rangle_H \leq \langle \tilde{h}, \mathcal{L}_\beta \tilde{h} \rangle_H < \langle \tilde{h}, \mathcal{L}_\alpha \tilde{h} \rangle_H \leq \gamma_n(\alpha),$$

and thus γ_n is strictly increasing on $]0, \beta_0]$. \square

In other words, we can only expect strict monotonicity of an eigenvalue in β if the eigenvalue “departs” from $\inf(\sigma(-\mathcal{B}^2|_{\mathcal{H}})) > 0$ as β decreases. We can verify that there exists a smallest eigenvalue which diverges for β tending to zero. Unfortunately, we do not know what happens for $n \geq 2$ as β gets small. In contrast, letting β go to infinity, we can prove that γ_n eventually reaches the infimum of the essential spectrum for every $n \in \mathbb{N}$; cf. [47, Lem. 6.8 & 6.9].

Lemma 5.2.5. *It holds that $\lim_{\beta \rightarrow 0} \gamma_1(\beta) = -\infty$. Moreover,*

$$\lim_{\beta \rightarrow \infty} \gamma_n(\beta) = \inf(\sigma(-\mathcal{B}^2|_{\mathcal{H}})) > 0$$

for every $n \in \mathbb{N}$.

⁵The existence of such coefficients c_1, \dots, c_n is a simple exercise from linear algebra.

Proof. The proof of the first assertion relies on the fact that the supremum in (5.10) is not present for $n = 1$. More precisely, we choose $g \in \mathcal{D}(\mathcal{T}^2) \cap \mathcal{H}$ with $\|g\|_H = 1$ and $\langle g, \mathcal{R}g \rangle_H > 0$, which implies that

$$\begin{aligned} \gamma_1(\beta) &= \inf_{\substack{h \in \mathcal{D}(\mathcal{T}^2) \cap \mathcal{H}, \\ \|h\|_H = 1}} \langle h, \mathcal{L}_\beta h \rangle_H = \inf_{\substack{h \in \mathcal{D}(\mathcal{T}^2) \cap \mathcal{H}, \\ \|h\|_H = 1}} \left(\|\mathcal{B}h\|_H^2 - \frac{1}{\beta} \langle h, \mathcal{R}h \rangle_H \right) \\ &\leq \|\mathcal{B}g\|_H^2 - \frac{1}{\beta} \langle g, \mathcal{R}g \rangle_H \rightarrow -\infty, \quad \beta \rightarrow 0. \end{aligned}$$

For the second part, we notice that the eigenvalue γ_n is non-decreasing and bounded due to Lemma 5.2.3, which implies that the limit for $\beta \rightarrow \infty$ exists. In addition, we estimate

$$\langle h, \mathcal{L}_\beta h \rangle_H = \|\mathcal{B}h\|_H^2 - \frac{1}{\beta} \langle h, \mathcal{R}h \rangle_H \geq \inf(\sigma(-\mathcal{B}^2|_{\mathcal{H}})) - \frac{\|\mathcal{R}\|_{H \rightarrow H}}{\beta},$$

for every $h \in \mathcal{D}(\mathcal{T}^2) \cap \mathcal{H}$ with $\|h\|_H = 1$ by Lemma B.6. \square

As we can see from these results, the zeros of the mappings $]0, \infty[\ni \beta \mapsto \gamma_n(\beta)$ are of particular interest since they are closely connected to negative eigenvalues of $\mathcal{L} = \mathcal{L}_1$.

Definition 5.2.6. For $n \in \mathbb{N}$, we define β_n^* as the unique zero of γ_n , if this zero exists. Otherwise, we set $\beta_n^* = 0$, if $\gamma_n > 0$ on $]0, \infty[$.

The quantity β_n^* is well defined because of the previous results: Lemma 5.2.3 asserts that γ_n is continuous while Lemma 5.2.4 yields that γ_n is strictly increasing if $\gamma_n < \inf(\sigma(-\mathcal{B}^2|_{\mathcal{H}}))$. Lemma 5.2.5 therefore implies that either $\gamma_n > 0$ or γ_n must have a unique zero on $]0, \infty[$. As an aside, we further note that $\beta_{n+1}^* \leq \beta_n^*$ for $n \in \mathbb{N}$ due to $\gamma_{n+1} \geq \gamma_n$.

Because γ_n is non-decreasing, we can identify the number of negative eigenvalues of $\mathcal{L} = \mathcal{L}_1$ with the zeros of γ_n , which are bigger than one, see [47, Prop. 6.11].

Proposition 5.2.7. It holds that

$$\#\{\text{negative eigenvalues of } \mathcal{L} \text{ (counting multiplicities)}\} = \#\{n \in \mathbb{N} \mid \beta_n^* > 1\}.$$

Note that each negative eigenvalue of \mathcal{L} has finite multiplicity since $\inf(\sigma_{\text{ess}}(\mathcal{L})) > 0$. Nonetheless, the number of negative eigenvalues could be infinite in principal.

Proof. As per Proposition 5.2.2,

$$\#\{\text{negative eigenvalues of } \mathcal{L} \text{ (counting multiplicities)}\} = \#\{n \in \mathbb{N} \mid \gamma_n(1) < 0\}.$$

The continuity and monotonicity deduced in Lemmas 5.2.3, 5.2.4, and 5.2.5 imply that $\gamma_n(1) < 0$ for some $n \in \mathbb{N}$ if, and only if, $\beta_n^* > 1$. \square

To conclude, we sketch the properties of γ_n in Figure 5.2 in order to clarify the results above.

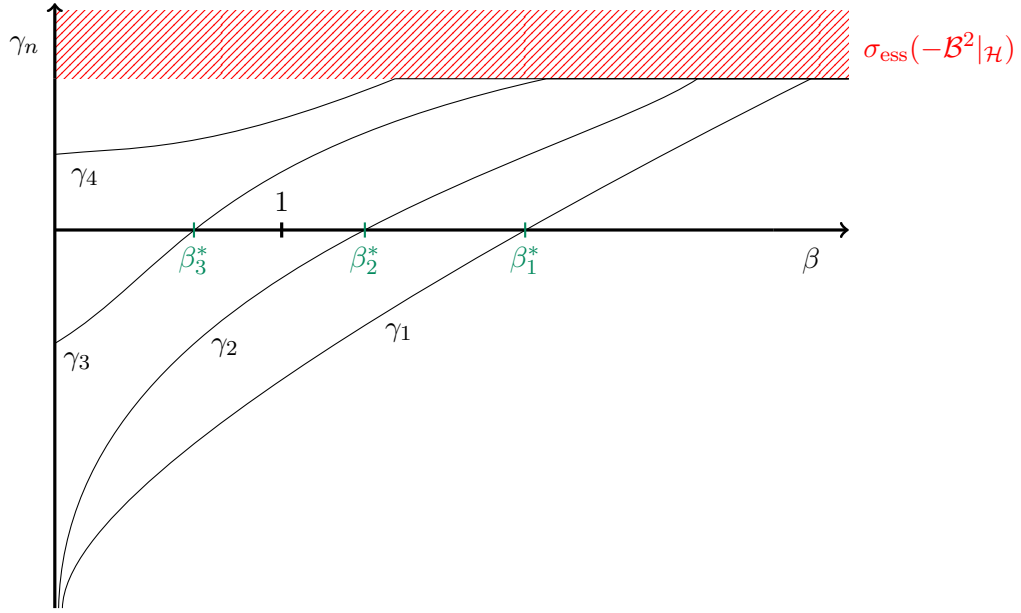


Figure 5.2: A conceivable qualitative behavior of the functions γ_n for $n \in \{1, 2, 3, 4\}$. The positions of the zeros of γ_n yield information about negative eigenvalues of \mathcal{L} . With Proposition 5.2.7, we get two negative eigenvalues of \mathcal{L} in this case since $\beta_3^* < 1 < \beta_2^* < \beta_1^*$. The functions γ_n are strictly increasing until they reach the bottom of the essential spectrum. After this they are constant.

5.2.2 The Birman-Schwinger operator

We have now provided enough groundwork to rigorously prove the steps outlined in Section 5.1.3. First, we introduce the Birman-Schwinger operator Q .⁶

Definition 5.2.8. *The operator*

$$Q := -\sqrt{\mathcal{R}}\mathcal{B}^{-2}\sqrt{\mathcal{R}} : \mathcal{H} \rightarrow \mathcal{H}$$

is called the Birman-Schwinger operator associated to \mathcal{L} .

The square root of the response operator \mathcal{R} was introduced in Lemma 4.3.12, whereas Proposition 4.3.5(g) establishes the existence of $\mathcal{B}^{-2} : \text{im}(\mathcal{B}^2) \rightarrow \text{D}(\mathcal{T}^2) \cap \ker(\mathcal{B}^2)^\perp$. Therefore, the Birman-Schwinger operator is well defined because $\mathcal{H} \subset \ker(\mathcal{B}^2)^\perp$ as well as $\text{im}(\sqrt{\mathcal{R}}) \subset \mathcal{H}$.

It is now possible to translate eigenvalues of the auxiliary operator \mathcal{L}_β from (5.9) to eigenvalues of Q as in [47, Prop. 6.13]. Results of this type are often referred to as a “Birman-Schwinger principle”.

⁶Our definition yields a symmetric Birman-Schwinger operator, which is the more common approach, see e.g., [69, Def. 4.1], [73, Thm. 12.4], or [88, Thm. XIII.10]. However, one could also consider $\mathcal{R}\mathcal{B}^{-2}$ as the Birman-Schwinger operator instead. This was, for example, done in [55, (8.1)] and the symmetry must be recovered a-posteriori by choosing the right function space for Q .

Proposition 5.2.9 (Birman-Schwinger principle). *Let $\beta > 0$. Then 0 is an eigenvalue of \mathcal{L}_β if, and only if, β is an eigenvalue of Q .*

In this case, the multiplicities of these eigenvalues are equal, and the associated eigenfunctions can be transformed explicitly into one another:

(a) *If $f \in \mathcal{D}(\mathcal{T}^2) \cap \mathcal{H}$ is an eigenfunction of \mathcal{L}_β to the eigenvalue 0, then*

$$g := \sqrt{\mathcal{R}} f \in \mathcal{H} \quad (5.15)$$

defines an eigenfunction of Q to the eigenvalue β .

(b) *If $g \in \mathcal{H}$ is an eigenfunction of Q to the eigenvalue β , then*

$$f := -\mathcal{B}^{-2} \sqrt{\mathcal{R}} g \in \mathcal{D}(\mathcal{T}^2) \cap \mathcal{H} \quad (5.16)$$

defines an eigenfunction of \mathcal{L}_β to the eigenvalue 0.

Proof. Let $f \in \mathcal{D}(\mathcal{T}^2) \cap \mathcal{H}$ be an eigenfunction of \mathcal{L}_β to the eigenvalue 0 with $\beta > 0$. Then $-\beta \mathcal{B}^2 f = \mathcal{R}f$ and applying $-\sqrt{\mathcal{R}} \mathcal{B}^{-2}$ to this equation yields

$$\beta g = \beta \sqrt{\mathcal{R}} f = -\sqrt{\mathcal{R}} \mathcal{B}^{-2} \mathcal{R}f = -\sqrt{\mathcal{R}} \mathcal{B}^{-2} \sqrt{\mathcal{R}} \sqrt{\mathcal{R}} f = Q(\sqrt{\mathcal{R}} f) = Qg,$$

where g is defined as in (5.15) and $g \in \mathcal{H}$. In addition, we deduce $g \neq 0$ from $f \neq 0$ and

$$f = -\frac{1}{\beta} \mathcal{B}^{-2} \mathcal{R}f = -\frac{1}{\beta} \mathcal{B}^{-2} \sqrt{\mathcal{R}} g,$$

which follows from $\mathcal{L}_\beta f = 0$; note that we are able to apply \mathcal{B}^{-2} to $\mathcal{R}f$, because $\mathcal{R}f \in \mathcal{H} \subset \text{im}(\mathcal{B}^2)$. This proves part (a).

For part (b), we consider an eigenfunction $g \in \mathcal{H}$ with $Qg = \beta g$ and define f as in (5.16). As argued above, we can apply \mathcal{B}^{-2} due to $\sqrt{\mathcal{R}} f \in \mathcal{H}$. Moreover, $f \in \mathcal{D}(\mathcal{T}^2) \cap \mathcal{H}$, because \mathcal{B}^{-2} conserves w -parity, see Proposition 4.3.5(g). We compute

$$\mathcal{L}_\beta f = -\mathcal{B}^2 f - \frac{1}{\beta} \mathcal{R}f = \sqrt{\mathcal{R}} g - \frac{1}{\beta} \sqrt{\mathcal{R}} Qg = 0$$

and $\sqrt{\mathcal{R}} f = Qg = \beta g \neq 0$, which implies that f is an eigenfunction of \mathcal{L}_β to the eigenvalue 0.

To finish the proof, we notice that in both cases the multiplicities of the eigenvalues are preserved since the transformations (5.15) and (5.16) conserve linear independence of eigenfunctions that are odd in w . \square

Together with Proposition 5.2.7 we now establish a connection between negative eigenvalues of the Antonov operator \mathcal{L} and eigenvalues > 1 of the Birman-Schwinger operator Q , see [47, Prop. 6.14].

Corollary 5.2.10. *It holds that*

$$\#\{\text{negative eigenvalues of } \mathcal{L}\} = \#\{\text{eigenvalues } > 1 \text{ of } Q\}.$$

In both sets the eigenvalues are counted including their multiplicities.

Proof. The claim is an immediate consequence of Propositions 5.2.7 and 5.2.9. \square

Let us summarize what we have shown: Instead of searching for negative eigenvalues for the (unbounded) Antonov operator \mathcal{L} , we can analyze the eigenvalues of the Birman-Schwinger operator Q . This is achieved by means of the auxiliary operator \mathcal{L}_β and the monotonicity properties of the corresponding eigenvalues. No “information” about the linear stability of the underlying steady state, as introduced in Definition 5.1.2, is lost during this process. At first glance, one could argue that this simply translates one difficult eigenvalue problem into another. However, the procedure is still beneficial since Q has much more favorable functional analytic properties compared to \mathcal{L} , as already observed in [47, Lem. 6.15].

Lemma 5.2.11. *The operator $Q = -\sqrt{\mathcal{R}} \mathcal{B}^{-2} \sqrt{\mathcal{R}} : \mathcal{H} \rightarrow \mathcal{H}$ is linear, bounded, symmetric, non-negative, and compact.*

Proof. We refer to Proposition 4.3.5(g) and Lemma 4.3.12 for properties of \mathcal{B}^{-2} and $\sqrt{\mathcal{R}}$. The Birman-Schwinger operator Q is linear, bounded, and symmetric because \mathcal{B}^{-2} and $\sqrt{\mathcal{R}}$ satisfy these properties. From Lemma 4.3.14, we know that $\sqrt{\mathcal{R}}|_{\mathcal{H}}$ is $\mathcal{B}^2|_{\mathcal{H}}$ -compact, i.e., according to Definition B.8, the operator $Q = \sqrt{\mathcal{R}} \mathcal{B}^{-2}$ is compact because $\sqrt{\mathcal{R}}$ is bounded and $\text{im}(\sqrt{\mathcal{R}}) \subset \mathcal{H}$. This implies that Q is compact. The non-negativity follows from the symmetry of $\sqrt{\mathcal{R}}$ and skew-symmetry of \mathcal{B}^{-1} , which yield

$$\langle Qf, f \rangle_H = \langle -\mathcal{B}^{-2} \sqrt{\mathcal{R}} f, \sqrt{\mathcal{R}} f \rangle_H = \|\mathcal{B}^{-1} \sqrt{\mathcal{R}} f\|_H^2 \geq 0, \quad f \in \mathcal{H}. \quad \square$$

Because of these properties, the spectrum of Q can be narrowed down significantly. We also obtain more information about the number of negative eigenvalues of \mathcal{L} .

Remark 5.2.12. (a) *The symmetry of Q implies $\sigma(Q) \subset [0, \infty[$. In addition, we have $\sigma(Q) \setminus \{0\} \subset \sigma_d(Q)$ and $\sigma_{\text{ess}}(Q) \subset \{0\}$ from the compactness of Q , according to the Riesz-Schauder theorem [58, Thm. 9.10]. The spectrum therefore only consist of positive, discrete eigenvalues with finite multiplicity and a possible accumulation point at 0, which can be an eigenvalue of infinite multiplicity.*

(b) *Since the spectrum of Q is bounded from above by the operator norm $\|Q\|_{\mathcal{H} \rightarrow \mathcal{H}} < \infty$, cf. [58, Thm. 1.7], and because the only possible accumulation point is at 0, there can only be a finite number of elements in $\sigma(Q)$, which are greater than 1. Together with Corollary 5.2.10, we therefore obtain that the Antonov operator \mathcal{L} can only have a finite number of negative eigenvalues (counting multiplicities).*

In the next section, we reduce the search for eigenvalues > 1 of the Birman-Schwinger operator to a setting in a radial L^2 -space due to the characteristic structure $Q = -\sqrt{\mathcal{R}} \mathcal{B}^{-2} \sqrt{\mathcal{R}}$.

5.3 The Mathur operator

5.3.1 Definition and functional analytic properties

The following reduction process start with a simple observation: If $f \in \mathcal{H}$ is an eigenfunction of the Birman-Schwinger operator $Q = -\sqrt{\mathcal{R}}\mathcal{B}^{-2}\sqrt{\mathcal{R}}$, necessarily $f \in \text{im}(\sqrt{\mathcal{R}})$ must hold. This is advantageous since elements in the range of $\sqrt{\mathcal{R}}$ can be characterized by radial L^2 -functions via

$$\text{im}(\sqrt{\mathcal{R}}) \subset \{f = f(r, w, L) = |\varphi'(E, L)|w\alpha_0(r)F(r) \text{ a.e.} \mid F \in L^2([R_{\min}, R_{\max}])\}, \quad (5.17)$$

where

$$\alpha_0(r) := \frac{e^{\frac{\lambda_0(r)}{2} + \frac{\mu_0(r)}{2}}}{\sqrt{r(\lambda'_0 + \mu'_0)(r)}}, \quad r \in]R_{\min}, \infty[,$$

is chosen such that F lies in an unweighted L^2 -space. Recall that R_{\min} and R_{\max} are the minimal and maximal radii appearing in the steady state support, as defined in (2.30). By the specific choice of α_0 and by (4.18), we get

$$\langle |\varphi'|w\alpha_0 F, |\varphi'|w\alpha_0 G \rangle_H = \langle F, G \rangle_{L^2([R_{\min}, R_{\max}])} \quad (5.18)$$

for every $F, G \in L^2([R_{\min}, R_{\max}])$, i.e., the mapping

$$\text{im}(\sqrt{\mathcal{R}}) \ni f \mapsto F \in L^2([R_{\min}, R_{\max}]),$$

given by the relation in (5.17), is an isomorphism. With these observations at hand, the following definition of the reduced operator is well defined.

Definition 5.3.1. *For every $F \in L^2([R_{\min}, R_{\max}])$, the function $Q(|\varphi'|w\alpha_0 F)$ lies in the range of $\sqrt{\mathcal{R}}$, i.e., there exists a unique $G \in L^2([R_{\min}, R_{\max}])$ such that*

$$Q(|\varphi'|w\alpha_0 F) = |\varphi'|w\alpha_0 G \quad \text{a.e. on } \Omega_0.$$

The resulting mapping

$$\mathcal{M}: L^2([R_{\min}, R_{\max}]) \rightarrow L^2([R_{\min}, R_{\max}]), \quad F \mapsto G$$

is called the reduced operator or Mathur operator.

By construction of this reduced operator, we do not lose information about eigenvalues when analyzing the Mathur operator instead of the Birman-Schwinger operator. In fact, the eigenvalues of these operators are equivalent, see [47, Lem. 6.18].

Lemma 5.3.2. *Let $\beta \in \mathbb{R} \setminus \{0\}$. Then β is an eigenvalue of Q if, and only if, β is an eigenvalue of \mathcal{M} . The multiplicities of these eigenvalues are equal.*

Proof. Consider that $Qg = \beta g$ if, and only if, $-\sqrt{\mathcal{R}}\mathcal{B}^{-2}\sqrt{\mathcal{R}}g = \beta g$ and $g \in \text{im}(\sqrt{\mathcal{R}})$, which means that there exists $G \in L^2([R_{\min}, R_{\max}])$ with $g = |\varphi'|w\alpha_0 G$. This relation

is therefore equivalent to

$$Q(|\varphi'|w\alpha_0 G) = \beta|\varphi'|w\alpha_0 G$$

and by definition of the Mathur operator we have $\mathcal{M}G = \beta G$. Note that obviously $g \neq 0$ if, and only if, $G \neq 0$.

The multiplicities of an eigenvalue for Q and \mathcal{M} are equal by (5.18), which implies that orthogonality of eigenfunctions is conserved. \square

Together with Proposition 5.2.10 it is therefore sufficient to analyze the spectrum of the Mathur operator since it encodes the full linear stability behavior of the steady state under consideration. It is also plausible that the spectral analysis of \mathcal{M} should be simpler than that of the Birman-Schwinger operator because Q acts on functions defined on the three-dimensional phase space, while \mathcal{M} is an operator on a radial L^2 -space only. This is also the reason why we refer to \mathcal{M} as a *reduced* operator. Fortunately, the nice properties of Q are directly inherited by \mathcal{M} .

Lemma 5.3.3. *The Mathur operator $\mathcal{M}: L^2([R_{\min}, R_{\max}]) \rightarrow L^2([R_{\min}, R_{\max}])$ is linear, bounded, symmetric, non-negative, and compact.*

Proof. This follows directly from the properties of Q proven in Lemma 5.2.11 and from the orthogonality relation (5.18). \square

5.3.2 Explicit representation

In the previous sections, we have introduced the Birman-Schwinger operator and the Mathur operator as mere abstract objects which might not be of much help when determining linear stability. At the heart of this chapter, we will now bring \mathcal{M} into a (semi-)explicit form that can be applied later. This is rather surprising at first glance because one would expect that \mathcal{B}^{-1} or the projection Π onto $\ker(\mathcal{B})$, see Proposition 4.3.5(f), are needed explicitly. However, additional knowledge is not necessary in order to infer further properties of \mathcal{M} . A similar calculation was done in [47, Sc. 6.3.2], but we provide a few more details here.

We start off with the Birman-Schwinger operator Q for which we only need to consider functions of the form $f = |\varphi'|w\alpha_0 F$ with $F \in L^2([R_{\min}, R_{\max}])$, as observed in the previous section. Plugging this ansatz into $\sqrt{\mathcal{R}}$ from Lemma 4.3.12 yields

$$\sqrt{\mathcal{R}} f = \sqrt{\mathcal{R}} (|\varphi'|w\alpha_0 F) = 4\pi\sqrt{r}|\varphi'|e^{2\mu_0+\lambda_0} \sqrt{\frac{2r\mu'_0+1}{\mu'_0+\lambda'_0}} w\alpha_0 F \frac{\pi}{r^2} \int_0^\infty \int_{\mathbb{R}} w^2 |\varphi'| dw dL,$$

and with (4.18) we get

$$\sqrt{\mathcal{R}} f = |\varphi'|w \frac{e^{\mu_0-\lambda_0}}{\sqrt{r}} \sqrt{(2r\mu'_0+1)(\lambda'_0+\mu'_0)} \alpha_0 F = |\varphi'|w \beta_0 F, \quad (5.19)$$

where we set⁷

$$\beta_0(r) := e^{\frac{3\mu_0(r) - \lambda_0(r)}{2}} \frac{\sqrt{2r\mu_0'(r) + 1}}{r}, \quad r \in]R_{\min}, \infty[. \quad (5.20)$$

Before we begin with the more elaborate computations, we refer the reader to Section 4.3 for the notational conventions that will also be used in the following.

We have to determine $\sqrt{\mathcal{R}}\mathcal{B}^{-2}\sqrt{\mathcal{R}}f = \sqrt{\mathcal{R}}\mathcal{B}^{-1}\tilde{\mathcal{B}}^{-1}\sqrt{\mathcal{R}}f$, so it makes sense to first bring $\mathcal{B}^{-1}\sqrt{\mathcal{R}}f$ into a suitable form. However, $\mathcal{B}^{-1} = (\text{id} - \Pi)\tilde{\mathcal{B}}^{-1}$ includes the unknown projection Π , as seen in Proposition 4.3.5(f); we postpone this problem for now. Since $\sqrt{\mathcal{R}}f$ is odd in w , the quantity $\lambda_{\sqrt{\mathcal{R}}f}$ vanishes, and the term stemming from the right-inverse is of the form

$$\tilde{\mathcal{B}}^{-1}\sqrt{\mathcal{R}} = \mathcal{T}^{-1}\sqrt{\mathcal{R}} + \mathcal{U}\mathcal{T}^{-1}\sqrt{\mathcal{R}}$$

for some suitable operator \mathcal{U} . Hence, it is reasonable to first calculate $\mathcal{T}^{-1}\sqrt{\mathcal{R}}f$. We make this more specific now:⁸

Step 1: Computing $\mathcal{T}^{-1}\sqrt{\mathcal{R}}f$

Since f as well as $\sqrt{\mathcal{R}}f$ are odd in w and \mathcal{T}^{-1} reverses w -parity—recall these properties from Lemma 4.3.12 and Proposition 4.3.2(f)—it is sufficient to consider $\theta \in [0, \frac{1}{2}]$, as remarked in (4.11) and (4.12). We plug (5.19) into the explicit formula for \mathcal{T}^{-1} in (4.23), apply Fubini's theorem, and obtain

$$\begin{aligned} & (\mathcal{T}^{-1}\sqrt{\mathcal{R}}f)(\theta, E, L) \\ &= -T(E, L)|\varphi'(E, L)| \left(\int_0^\theta W(\tau, E, L)\beta_0(R(\tau, E, L))F(R(\tau, E, L))d\tau \right. \\ & \quad \left. - \int_0^1 \int_\sigma^1 W(\sigma, E, L)\beta_0(R(\sigma, E, L))F(R(\sigma, E, L))d\tau d\sigma \right) \\ &= -T(E, L)|\varphi'(E, L)| \left(\int_0^\theta W(\tau, E, L)\beta_0(R(\tau, E, L))F(R(\tau, E, L))d\tau \right. \\ & \quad \left. + \int_0^1 \sigma W(\sigma, E, L)\beta_0(R(\sigma, E, L))F(R(\sigma, E, L))d\sigma \right) \end{aligned} \quad (5.21)$$

for $\theta \in [0, \frac{1}{2}]$ and a.e. $(E, L) \in \Omega_0^{EL}$ after observing that

$$\int_0^1 W(\sigma, E, L)\beta_0(R(\sigma, E, L))F(R(\sigma, E, L))d\sigma = 0,$$

⁷Note that β_0 here obviously has nothing to do with β_0 appearing in Lemma 5.2.4. Unfortunately, the Latin and Greek alphabets are finite.

⁸Though rather lengthy, we believe that this calculation is such a central and valuable part of our work that it would not do it justice if we outsourced it to the appendix.

because the integrand is an element in $L^{2,\text{odd}}(]0, 1[)$ for a.e. fixed (E, L) , see (4.11). This parity in the angle variable further implies

$$\begin{aligned}
 & \int_0^1 \sigma W(\sigma, E, L) \beta_0(R(\sigma, E, L)) F(R(\sigma, E, L)) d\sigma \\
 &= \int_0^{\frac{1}{2}} \sigma W(\sigma, E, L) \beta_0(R(\sigma, E, L)) F(R(\sigma, E, L)) d\sigma \\
 & \quad + \int_0^{\frac{1}{2}} (1 - \sigma) W(1 - \sigma, E, L) \beta_0(R(1 - \sigma, E, L)) F(R(1 - \sigma, E, L)) d\sigma \\
 &= \int_0^{\frac{1}{2}} (2\sigma - 1) W(\sigma, E, L) \beta_0(R(\sigma, E, L)) F(R(\sigma, E, L)) d\sigma. \tag{5.22}
 \end{aligned}$$

We put (5.22) into (5.21) and change variables via $s = R(\sigma, E, L)$, i.e., $\sigma = \theta(s, E, L)$, where θ is the angle function, as introduced in (2.69). This yields

$$\begin{aligned}
 (\mathcal{T}^{-1}\sqrt{\mathcal{R}}f)(\theta, E, L) &= -|\varphi'(E, L)| \left(\int_{r_-(E, L)}^{R(\theta, E, L)} E e^{(\lambda_0 - 2\mu_0)(s)} \beta_0(s) F(s) ds \right. \\
 & \quad \left. + \int_{r_-(E, L)}^{r_+(E, L)} (2\theta(s, E, L) - 1) E e^{(\lambda_0 - 2\mu_0)(s)} \beta_0(s) F(s) ds \right) \\
 &= |\varphi'(E, L)| E \left(\int_{R(\theta, E, L)}^{R_{\max}} e^{\lambda_0 - 2\mu_0} \beta_0 F ds \right. \\
 & \quad \left. - \int_{r_+(E, L)}^{R_{\max}} e^{\lambda_0 - 2\mu_0} \beta_0 F ds - 2 \int_{r_-(E, L)}^{r_+(E, L)} \theta(s, E, L) e^{\lambda_0 - 2\mu_0} \beta_0 F ds \right),
 \end{aligned}$$

where we rearranged the domains of integration in the last step. The last two terms only depend on (E, L) , and we introduce the shorthand

$$h_F(E, L) := -|\varphi'(E, L)| E \left(\int_{r_+(E, L)}^{R_{\max}} e^{\lambda_0 - 2\mu_0} \beta_0 F ds + 2 \int_{r_-(E, L)}^{r_+(E, L)} \theta(s, E, L) e^{\lambda_0 - 2\mu_0} \beta_0 F ds \right),$$

for a.e. $(E, L) \in \Omega_0^{EL}$. In order to see that $h_F \in H$, we observe that $\mathcal{T}^{-1}\sqrt{\mathcal{R}}f \in H$ as well as

$$|\varphi'(E, L)| E \int_{R(\theta, E, L)}^{R_{\max}} e^{\lambda_0 - 2\mu_0} \beta_0 F ds \in H$$

due to (S4) and $F \in L^2([R_{\min}, R_{\max}])$, i.e., h_F can be written as the sum of two elements in H . To summarize, we have shown for $\theta \in [0, \frac{1}{2}]$ and a.e. $(E, L) \in \Omega_0^{EL}$ that

$$(\mathcal{T}^{-1}\sqrt{\mathcal{R}}f)(\theta, E, L) = |\varphi'(E, L)| E \int_{R(\theta, E, L)}^{R_{\max}} e^{\lambda_0 - 2\mu_0} \beta_0 F ds + h_F(E, L). \tag{5.23}$$

Step 2: Computing $\mathcal{B}^{-1}\sqrt{\mathcal{R}}f$

Since $\sqrt{\mathcal{R}}f$ is odd in w according to Lemma 4.3.12, we get $\lambda_{\sqrt{\mathcal{R}}f} = 0$ from (4.8). By Definition 4.3.4, we thus obtain

$$\tilde{\mathcal{B}}^{-1}\sqrt{\mathcal{R}}f = \mathcal{T}^{-1}\sqrt{\mathcal{R}}f + 4\pi|\varphi'|Ee^{-\lambda_0-\mu_0} \int_r^{R_{\max}} e^{(3\lambda_0+\mu_0)(s)} p_{\mathcal{T}^{-1}\sqrt{\mathcal{R}}f}(s) s ds, \quad (5.24)$$

which itself is even in w due to Proposition 4.3.2(f). We use (5.23) and then (4.18) to compute

$$\begin{aligned} p_{\mathcal{T}^{-1}\sqrt{\mathcal{R}}f}(r) &= \frac{\pi e^{\mu_0(r)}}{r^2} \int_0^\infty \int_{\mathbb{R}} w^2 |\varphi'(E, L)| \left(\int_r^{R_{\max}} e^{\lambda_0-2\mu_0} \beta_0 F ds \right) dw dL + p_{h_F}(r) \\ &= \frac{e^{-2\lambda_0(r)} (\lambda'_0 + \mu'_0)(r)}{4\pi r} \int_r^{R_{\max}} e^{\lambda_0-2\mu_0} \beta_0 F ds + p_{h_F}(r) \end{aligned}$$

for $r \in]R_{\min}, \infty[$. Therefore, we get

$$\begin{aligned} \tilde{\mathcal{B}}^{-1}\sqrt{\mathcal{R}}f &= |\varphi'|E \int_r^{R_{\max}} e^{\lambda_0-2\mu_0} \beta_0 F ds + h_F \\ &\quad + |\varphi'|Ee^{-\lambda_0-\mu_0} \int_r^{R_{\max}} e^{(\lambda_0+\mu_0)(s)} (\lambda'_0 + \mu'_0)(s) \int_s^{R_{\max}} e^{\lambda_0-2\mu_0} \beta_0 F d\sigma ds \\ &\quad + 4\pi|\varphi'|Ee^{-\lambda_0-\mu_0} \int_r^{R_{\max}} e^{(3\lambda_0+\mu_0)(s)} p_{h_F}(s) s ds \\ &= |\varphi'|E \left(\int_r^{R_{\max}} e^{\lambda_0-2\mu_0} \beta_0 F ds + e^{-\lambda_0-\mu_0} \int_r^{R_{\max}} (e^{\lambda_0+\mu_0})' \int_s^{R_{\max}} e^{\lambda_0-2\mu_0} \beta_0 F d\sigma ds \right) \\ &\quad + h_F + 4\pi|\varphi'|Ee^{-\lambda_0-\mu_0} \int_r^{R_{\max}} e^{3\lambda_0+\mu_0} p_{h_F} s ds \\ &= |\varphi'|Ee^{-\lambda_0-\mu_0} \int_r^{R_{\max}} e^{2\lambda_0-\mu_0} \beta_0 F ds \\ &\quad + h_F + 4\pi|\varphi'|Ee^{-\lambda_0-\mu_0} \int_r^{R_{\max}} e^{3\lambda_0+\mu_0} p_{h_F} s ds. \end{aligned}$$

after an integration by parts in the last line. Remarkably, the last two terms together define an element in $\ker(\mathcal{B})$ with generator h_F , as described in Proposition 4.3.5(d) and Lemma 4.3.8. Notice that $h_F \in H$, as mentioned above, and h_F is a function in (E, L) only. Since $\mathcal{B}^{-1} = (\text{id} - \Pi)\tilde{\mathcal{B}}^{-1}$, as seen in Proposition 4.3.5(f), with Π being the orthogonal projection onto $\ker(\mathcal{B})$, we obtain

$$\mathcal{B}^{-1}\sqrt{\mathcal{R}}f = (\text{id} - \Pi)\tilde{\mathcal{B}}^{-1}\sqrt{\mathcal{R}}f = (\text{id} - \Pi) \left(|\varphi'|Ee^{-\lambda_0-\mu_0} \int_r^{R_{\max}} e^{2\lambda_0-\mu_0} \beta_0 F ds \right). \quad (5.25)$$

It is worth reflecting on what has happened in the two steps above: Naively, one would

assume that $\tilde{\mathcal{B}}^{-1}\sqrt{\mathcal{R}}f$ consists of four terms—two from $\mathcal{T}^{-1}\sqrt{\mathcal{R}}f$ and two from the second term in (5.24). Moreover, multiple separate integrations in r and (w, L) seem to appear. An integration by parts removes one of the terms while Fubini's theorem and the crucial identity (4.18) help to determine the integrals explicitly. The fact that we can write $\tilde{\mathcal{B}}^{-1}\sqrt{\mathcal{R}}f$ as one term plus an element in $\ker(\mathcal{B})$ then allows us to reduce $\mathcal{B}^{-1}\sqrt{\mathcal{R}}$ to just one term which behaves quite nicely.⁹

Step 3: Determining the Birman-Schwinger operator Q

Applying (4.41) yields

$$\begin{aligned} Qf &= -\sqrt{\mathcal{R}}\mathcal{B}^{-2}\sqrt{\mathcal{R}}f = -4\pi\sqrt{r}|\varphi'|e^{2\mu_0+\lambda_0}\sqrt{\frac{2r\mu'_0+1}{\lambda'_0+\mu'_0}}w j_{\mathcal{B}^{-2}\sqrt{\mathcal{R}}}f \\ &= |\varphi'|we^{\mu_0}\sqrt{\frac{2r\mu'_0+1}{r(\lambda'_0+\mu'_0)}}\lambda_{\mathcal{B}^{-1}\sqrt{\mathcal{R}}}f. \end{aligned} \quad (5.26)$$

This step is quickly implemented but has some powerful consequences, since it removes one \mathcal{B}^{-1} -term. Otherwise, it might not even be possible to determine $\mathcal{B}^{-2}\sqrt{\mathcal{R}}f$ in a suitable way because this would involve computing \mathcal{B}^{-1} of $\mathcal{B}^{-1}\sqrt{\mathcal{R}}f$, which itself is only known semi-explicitly through the projection Π . Moreover, we can now write $\lambda_{\mathcal{B}^{-1}\sqrt{\mathcal{R}}}f$ as a scalar-product in H , which allows us to use the symmetry in the projection to decouple the unknown function F and the projection Π in the following way: We insert (5.25) into (4.8) and get

$$\begin{aligned} \lambda_{\mathcal{B}^{-1}\sqrt{\mathcal{R}}}f(r) &= \frac{e^{2\lambda_0(r)}}{r} \left\langle |\varphi'|Ee^{-\lambda_0-\mu_0}\mathbb{1}_{[R_{\min},r]}, \mathcal{B}^{-1}\sqrt{\mathcal{R}}f \right\rangle_H \\ &= \frac{e^{2\lambda_0(r)}}{r} \left\langle (\text{id} - \Pi) \left(|\varphi'|Ee^{-\lambda_0-\mu_0}\mathbb{1}_{[R_{\min},r]} \right), |\varphi'|Ee^{-\lambda_0-\mu_0} \int_s^{R_{\max}} e^{2\lambda_0-\mu_0}\beta_0 F d\sigma \right\rangle_H, \end{aligned}$$

for $r \in]R_{\min}, \infty[$, where we have used the symmetry of Π . We write the scalar product as an integral again and subsequently integrate by parts which yields

$$\begin{aligned} \lambda_{\mathcal{B}^{-1}\sqrt{\mathcal{R}}}f(r) &= \frac{e^{2\lambda_0(r)}}{r} \int_{R_{\min}}^{R_{\max}} 4\pi s^2 \rho_{(\text{id}-\Pi)}(|\varphi'|Ee^{-\lambda_0-\mu_0}\mathbb{1}_{[R_{\min},r]})(s) \int_s^{R_{\max}} e^{2\lambda_0-\mu_0}\beta_0 F d\sigma ds \\ &= \frac{e^{2\lambda_0(r)}}{r} \int_{R_{\min}}^{R_{\max}} \partial_s \left(se^{-2\lambda_0} \lambda_{(\text{id}-\Pi)}(|\varphi'|Ee^{-\lambda_0-\mu_0}\mathbb{1}_{[R_{\min},r]})(s) \right) \int_s^{R_{\max}} e^{2\lambda_0-\mu_0}\beta_0 F d\sigma ds \\ &= \frac{e^{2\lambda_0(r)}}{r} \int_{R_{\min}}^{R_{\max}} se^{-\mu_0(s)} \lambda_{(\text{id}-\Pi)}(|\varphi'|Ee^{-\lambda_0-\mu_0}\mathbb{1}_{[R_{\min},r]})(s) \beta_0(s) F(s) ds \end{aligned}$$

after recalling (4.3) now applied to the projection term. Note that the boundary terms

⁹Overall, this whole process is rather surprising. We do not know if there is a deeper reason why the calculation works out as it does here but we disclose that several weeks—including different approaches—went into this single part of the work.

vanish at R_{\min} and R_{\max} due to $\lambda_{(\text{id}-\Pi)(\dots)}(R_{\min}) = 0$ and due to the domain of integration $[s, R_{\max}]$, respectively. We reveal a useful symmetry property in this integration term by considering the identity

$$\begin{aligned} & se^{-2\lambda_0(s)} \lambda_{(\text{id}-\Pi)(|\varphi'|Ee^{-\lambda_0-\mu_0}\mathbb{1}_{[R_{\min},r]})}(s) \\ &= \left\langle (\text{id} - \Pi) \left(|\varphi'|Ee^{-\lambda_0-\mu_0}\mathbb{1}_{[R_{\min},r]} \right), |\varphi'|Ee^{-\lambda_0-\mu_0}\mathbb{1}_{[R_{\min},s]} \right\rangle_H =: I(r, s), \end{aligned}$$

and since Π is symmetric, we obtain that $I(r, s) = I(s, r)$ for $r, s \in [R_{\min}, \infty[$. Putting these results into (5.26) and recalling the definition of β_0 in (5.20) implies that

$$Qf = |\varphi'|w \frac{e^{2\lambda_0+\mu_0}}{r} \sqrt{\frac{2r\mu'_0+1}{r(\lambda'_0+\mu'_0)}} \int_{R_{\min}}^{R_{\max}} e^{\frac{\mu_0(s)}{2}+\frac{3\lambda_0(s)}{2}} \frac{\sqrt{2s\mu'_0(s)+1}}{s} I(r, s) F(s) ds$$

for functions $f \in H$ of the form $f = |\varphi'|w\alpha_0 F$ with $F \in L^2([R_{\min}, R_{\max}])$.

Step 4: The Mathur operator \mathcal{M}

As the final step, we make the Mathur operator more explicit by using the representation of Q above. We prove a slightly stronger result compared to [47, Prop. 6.20], as we also show that the kernel K is continuous. We only have to adjust for the factor α_0 .

Proposition 5.3.4. *For $F \in L^2([R_{\min}, R_{\max}])$, we have*

$$(\mathcal{M}F)(r) = \int_{R_{\min}}^{R_{\max}} K(r, s) F(s) ds, \quad r \in [R_{\min}, R_{\max}],$$

where the kernel K is defined as

$$K(r, s) = e^{\frac{\mu_0(r)}{2}+\frac{3\lambda_0(r)}{2}} e^{\frac{\mu_0(s)}{2}+\frac{3\lambda_0(s)}{2}} \frac{\sqrt{2r\mu'_0(r)+1}\sqrt{2s\mu'_0(s)+1}}{rs} I(r, s), \quad (5.27)$$

with I given by

$$I(r, s) = \left\langle (\text{id} - \Pi) \left(|\varphi'|Ee^{-\lambda_0-\mu_0}\mathbb{1}_{[R_{\min},r]} \right), |\varphi'|Ee^{-\lambda_0-\mu_0}\mathbb{1}_{[R_{\min},s]} \right\rangle_H \quad (5.28)$$

for $r, s \in [R_{\min}, R_{\max}]$. The kernel K is symmetric, i.e., $K(r, s) = K(s, r)$, continuous on $[R_{\min}, R_{\max}]^2$ with $K = 0$ on $\partial([R_{\min}, R_{\max}]^2)$, and can be continuously extended by $K = 0$ onto $[0, \infty]^2$. Moreover, $K \in L^2([R_{\min}, R_{\max}]^2)$.

In particular, \mathcal{M} is a Hilbert-Schmidt operator, see [89, Thm. VI.22 et seq].

Proof. The representation of the Mathur operator and the formula for the kernel follow from Definition 5.3.1 and from the calculations made in Steps 1–3. We first show the continuity of the function I . For this, we let $(r, s), (\tilde{r}, \tilde{s}) \in [R_{\min}, R_{\max}]^2$ and estimate

via the Cauchy-Schwarz inequality that

$$\begin{aligned} & |I(r, s) - I(\tilde{r}, \tilde{s})| \\ & \leq \left\| (\text{id} - \Pi) \left(|\varphi'| E e^{-\lambda_0 - \mu_0} (\mathbf{1}_{[R_{\min}, r]} - \mathbf{1}_{[R_{\min}, \tilde{r}]}) \right) \right\|_H \left\| |\varphi'| E e^{-\lambda_0 - \mu_0} \mathbf{1}_{[R_{\min}, s]} \right\|_H \\ & \quad + \left\| (\text{id} - \Pi) \left(|\varphi'| E e^{-\lambda_0 - \mu_0} \mathbf{1}_{[R_{\min}, \tilde{r}]} \right) \right\|_H \left\| |\varphi'| E e^{-\lambda_0 - \mu_0} (\mathbf{1}_{[R_{\min}, s]} - \mathbf{1}_{[R_{\min}, \tilde{s}]}) \right\|_H. \end{aligned}$$

Due to $\|\text{id} - \Pi\| = 1$ and

$$\left\| |\varphi'| E e^{-\lambda_0 - \mu_0} \mathbf{1}_{[R_{\min}, r]} \right\|_H \leq \left\| |\varphi'| E e^{-\lambda_0 - \mu_0} \right\|_H \leq C, \quad r \geq R_{\min},$$

we get

$$\begin{aligned} |I(r, s) - I(\tilde{r}, \tilde{s})| & \leq C \left(\left\| |\varphi'| E e^{-\lambda_0 - \mu_0} (\mathbf{1}_{[R_{\min}, r]} - \mathbf{1}_{[R_{\min}, \tilde{r}]}) \right\|_H \right. \\ & \quad \left. + \left\| |\varphi'| E e^{-\lambda_0 - \mu_0} (\mathbf{1}_{[R_{\min}, s]} - \mathbf{1}_{[R_{\min}, \tilde{s}]}) \right\|_H \right), \end{aligned}$$

where $C > 0$ is a constant independent of (r, s) and (\tilde{r}, \tilde{s}) and may change from line to line. From the prescribed estimate (S4), we further obtain

$$\begin{aligned} \left\| |\varphi'| E e^{-\lambda_0 - \mu_0} (\mathbf{1}_{[R_{\min}, r]} - \mathbf{1}_{[R_{\min}, \tilde{r}]}) \right\|_H & \leq C \int_{\min(r, \tilde{r})}^{\max(r, \tilde{r})} \sigma^2 d\sigma \\ & \leq C |\max(r, \tilde{r})^3 - \min(r, \tilde{r})^3| = C |r^3 - \tilde{r}^3| \end{aligned}$$

for $r, \tilde{r} \geq R_{\min}$, and thus

$$|I(r, s) - I(\tilde{r}, \tilde{s})| \leq C (r^3 - \tilde{r}^3 + s^3 - \tilde{s}^3),$$

which yields continuity of I on $[R_{\min}, R_{\max}]^2$. In addition, this implies that $\frac{I(r, s)}{rs}$ can be extended continuously onto $[0, \infty]^2$ with

$$\lim_{r \rightarrow R_{\min}} \frac{I(r, s)}{rs} = \lim_{r \rightarrow R_{\min}} \frac{I(s, r)}{rs} = 0 = \lim_{r, s \rightarrow R_{\min}} \frac{I(r, s)}{rs}.$$

On the other hand, a straight-forward calculation shows that

$$|\varphi'| E e^{-\lambda_0 - \mu_0} = |\varphi'| E e^{-\lambda_0 - \mu_0} \mathbf{1}_{[R_{\min}, R_{\max}]} \in \ker(\mathcal{B}),$$

which implies $I(R_{\max}, s) = 0 = I(s, R_{\max})$ for $s > R_{\min}$ due to the symmetry of I . Overall, since λ_0 , μ_0 , and μ'_0 are continuous, we conclude that K is continuous and $K = 0$ on $\partial([R_{\min}, R_{\max}]^2)$. The claim that K is square-integrable follows immediately. \square

Having established this central representation of the Mathur operator, we can deduce even more properties of \mathcal{M} due to the fact that \mathcal{M} is Hilbert-Schmidt which is almost

as good as it gets from an operator theory point of view. For example, in the next section, we explicitly bound the number of negative eigenvalues of \mathcal{L} because \mathcal{M} is Hilbert-Schmidt.

Lemma 5.3.5. (a) *The Mathur operator \mathcal{M} can be extended to an operator*

$$\mathcal{M}: L^2([0, \infty[) \rightarrow L^2([0, \infty[).$$

All properties observed in Lemmas 5.3.2 and 5.3.3 remain valid for this extension.

(b) *The so-called Hilbert-Schmidt norm $\|\cdot\|_{HS}$ of \mathcal{M} is given by*

$$\|\mathcal{M}\|_{HS}^2 = \|K\|_{L^2([0, \infty[^2]}^2 = \int_0^\infty \int_0^\infty |K(r, s)|^2 dr ds, \quad (5.29)$$

see [89, Thm. VI.23]. If $\gamma_1 \geq \gamma_2 \geq \dots \geq 0$ are the eigenvalues of \mathcal{M} , where each eigenvalue is repeated according to its multiplicity, it holds that

$$\|\mathcal{M}\|_{HS}^2 = \sum_{j=1}^{\infty} \gamma_j^2, \quad (5.30)$$

where $\gamma_j := 0$ if necessary, i.e., if \mathcal{M} has finitely many eigenvalues.

(c) *The operator norm of $\mathcal{M}: L^2([0, \infty[^2] \rightarrow L^2([0, \infty[^2]$ is given by*

$$\|\mathcal{M}\| = \sup\{\langle F, \mathcal{M}F \rangle_{L^2([0, \infty[)} \mid F \in L^2([0, \infty[), \|F\|_{L^2([0, \infty[)} = 1\} = \max(\sigma(\mathcal{M})). \quad (5.31)$$

Proof. The proof relies on properties of Hilbert-Schmidt operators which are covered in [89, Sc. VI.6]. Part (a) follows by setting $K = 0$ on $[0, \infty[^2 \setminus [R_{\min}, R_{\max}]^2$, as done in Proposition 5.3.4. Because of the *Hilbert-Schmidt theorem* [89, Thm. VI.16], it is possible to choose an orthonormal basis of eigenfunctions of $L^2([0, \infty[)$ to the eigenvalues of \mathcal{M} . Using the symmetry of \mathcal{M} together with [89, Thm. VI.22(b)] then yields (5.30).

Since \mathcal{M} is symmetric, non-negative, and compact due to Lemma 5.3.3, the results in Lemma B.6 and [89, Thm. VI.6] yield that

$$\sup(\sigma(\mathcal{M})) = \max(\sigma(\mathcal{M})) = \|\mathcal{M}\|.$$

In addition, the operator norm is defined as and can be characterized by

$$\begin{aligned} \|\mathcal{M}\| &:= \sup\{\|\mathcal{M}F\|_{L^2([0, \infty[)} \mid F \in L^2([0, \infty[), \|F\|_{L^2([0, \infty[)} = 1\} \\ &= \sup\{\langle F, \mathcal{M}F \rangle_{L^2([0, \infty[)} \mid F \in L^2([0, \infty[), \|F\|_{L^2([0, \infty[)} = 1\}, \end{aligned}$$

where the latter equality holds because \mathcal{M} is symmetric and non-negative. \square

5.4 Results on linear stability

In this section, we apply the previous results in order to tackle linear stability issues for the steady state under consideration, as mentioned at the beginning of this chapter. It is useful to recall the definition of linear stability and the terminology introduced in Definition 5.1.2.

5.4.1 A reduced criterion for linear stability

First, we characterize linear stability via the Mathur operator and therefore establish some of this work's main theorems. For similar results, we refer to [47, Thm. 1.1 & Sc. 6.4].

Theorem 5.4.1 (A reduced variational principle). *A steady state, as described in Section 4.1, is linearly stable if, and only if,*

$$\|\mathcal{M}\| = \sup_{\substack{G \in L^2([0, \infty]) \\ \|G\|_2=1}} \int_0^\infty \int_0^\infty K(r, s)G(r)G(s) ds dr < 1.$$

If equality holds, there exists a zero-frequency mode but no exponentially growing mode.

Proof. Theorem 4.3.18 yields that $\inf(\sigma_{\text{ess}}(\mathcal{L})) > 0$, and thus $\sigma(\mathcal{L}) \setminus \sigma_{\text{ess}}(\mathcal{L})$ only consists of isolated eigenvalues of finite multiplicity. Linear stability of the underlying steady state is therefore equivalent to \mathcal{L} having no non-positive eigenvalues.

According to Corollary 5.2.10, the number of negative eigenvalues of \mathcal{L} and the number of eigenvalues of Q that are greater than one are the same (counting multiplicities). In addition, Lemma 5.3.2 shows that the same holds true for the Mathur operator \mathcal{M} instead of Q . This implies that \mathcal{L} has a negative eigenvalue if, and only if, the Mathur operator \mathcal{M} has an eigenvalue greater than one, i.e.,

$$\|\mathcal{M}\| = \sup_{\substack{G \in L^2([0, \infty]) \\ \|G\|_2=1}} \int_0^\infty \int_0^\infty K(r, s)G(r)G(s) ds dr > 1;$$

note that the representation of \mathcal{M} in Proposition 5.3.4 together with (5.31) yields the characterization of the operator norm $\|\mathcal{M}\|$.

Similarly, Proposition 5.2.9, Corollary 5.2.10, and Lemma 5.3.2 imply that zero is the smallest eigenvalue of \mathcal{L} if, and only if, $\|\mathcal{M}\| = 1$, i.e., one is an eigenvalue of \mathcal{M} .

Putting these observations together shows that linear stability is equivalent to $\|\mathcal{M}\| < 1$, and we deduce that $\|\mathcal{M}\| = 1$ implies that zero is an eigenvalue of \mathcal{L} but no negative eigenvalues exist. \square

From Theorem 5.4.1, we can derive a sufficient stability criterion which does not involve a variational principle.

Corollary 5.4.2 (A stability criterion). *A steady state, as described in Section 4.1, is linearly stable if $\|K\|_{L^2([0,\infty]^2)} < 1$.*

Proof. From (5.30) and (5.31) we get $\|\mathcal{M}\| \leq \|\mathcal{M}\|_{HS}$; note that this is true in general, as shown in [89, Thm. VI.22(d)]. The claim then follows by (5.29) together with Theorem 5.4.1. \square

The thorough analysis in Sections 5.2 and 5.3 furthermore yields an explicit bound on the number of exponentially growing modes by the L^2 -norm of K , as also observed in [47, Thm. 6.24]. Such bounds are often referred to as *Birman-Schwinger bounds* in the literature, cf. [74, Sc. 4.3] or [88, Thm. XIII.10].

Theorem 5.4.3 (A Birman-Schwinger bound on the number of growing modes). *It holds that*

$$\#\{\text{negative eigenvalues of } \mathcal{L} \text{ (counting multiplicities)}\} < \|K\|_{L^2([0,\infty]^2)}^2. \quad (5.32)$$

In particular, $K \neq 0$.

Proof. From Lemma 5.2.5, we know that $\beta_1^* > 0$, where β_1^* was introduced in Definition 5.2.6. Together with Proposition 5.2.9 and Lemma 5.3.2 this yields that the Mathur operator has at least one non-zero eigenvalue and hence $K \neq 0$. In order to prove (5.32), we note that Corollary 5.2.10 and Lemma 5.3.2 imply

$$\begin{aligned} \#\{\text{negative eigenvalues of } \mathcal{L} \text{ (counting multiplicities)}\} \\ = \#\{\text{eigenvalues greater one of } \mathcal{M} \text{ (counting multiplicities)}\}. \end{aligned}$$

In the case where \mathcal{M} has no eigenvalues greater one, \mathcal{L} has no negative eigenvalues and (5.32) is trivial. Otherwise, if we denote the eigenvalues of \mathcal{M} by $\gamma_1 \geq \gamma_2 \geq \dots \geq 0$ respecting multiplicities, we get by (5.29) and (5.30) that

$$\begin{aligned} \#\{\text{eigenvalues greater one of } \mathcal{M} \text{ (counting multiplicities)}\} \\ = \#\{j \in \mathbb{N} \mid \gamma_j > 1\} < \sum_{j \in \mathbb{N}, \gamma_j > 1} \gamma_j \leq \sum_{j \in \mathbb{N}} \gamma_j^2 = \|\mathcal{M}\|_{HS}^2 = \|K\|_{L^2([0,\infty]^2)}^2. \quad \square \end{aligned}$$

As a final remark, we mention that it might be the case that the stability criterion in Theorem 5.4.1 and the existence of a negative direction of the reduced differential operator S_κ in [52, Sc. 4.5] are equivalent. Interestingly, the authors encounter the same problem of not being able to explicitly determine the projection onto the kernel of \mathcal{B} . On the one hand, analyzing the bounded and compact Mathur operator is, of course, more pleasant compared to the unbounded operator S_κ from a function analysis point of view. On the other hand, for the results in [52], the use of action-angle type variables—and therefore a single-well structure—is not necessary, which makes these results applicable to more general settings. In the context of the Vlasov-Poisson system, a relation of the Mathur operator to a corresponding reduced differential operator has been observed in [69, Ch. 5].

5.4.2 Linear stability of matter shells with a Schwarzschild-singularity

As an application of the general results from the previous section, which hold for a large class of stationary solutions, we prove that small shells around a Schwarzschild black hole of mass M_0 are linearly stable. This was first proven in [47, Thm. 1.2]. We consider a δ -family $(f_\delta)_{\delta>0}$, as introduced in Definition 2.2.11, and employ the notation given in this definition, i.e., all quantities which depend on the steady state f_δ are denoted with a subscript δ . We emphasize that the following result does not require any additional assumptions on the steady states.

Theorem 5.4.4. *Let $(f_\delta)_{\delta>0}$ be a δ -family with $\Phi_0 \in C^1(\mathbb{R})$ and $\Phi'_0 > 0$. Then there exists $\delta_0 > 0$ such that for every $0 < \delta \leq \delta_0$, the steady state f_δ is linearly stable. As δ goes to zero, the metric coefficients converge uniformly on $]2M_0, \infty[$ to the vacuum Schwarzschild metric coefficients of mass M_0 , and the densities f_δ converge pointwise to zero on $\{x \in \mathbb{R}^3 \mid |x| > 2M_0\} \times \mathbb{R}^3$.*

Proof. We first need to verify that the stationary solutions f_δ satisfy the assumptions from Section 4.1 for small values of $\delta > 0$. The single-well structure, as prescribed in (S1), follows from Proposition 2.3.6 for $\delta \in]0, \delta_0]$, where $\delta_0 > 0$ is sufficiently small. In fact, the single-well structure is strict. The upper and lower bounds on the period function (S2) were shown in Propositions 2.3.9 and 2.3.16(a), respectively, because of $L_0 > 0$. Condition (S3) is fulfilled by the assumption that Φ_0 is continuously differentiable. Finally, (S4) is valid due to $L_0 > 0$, as argued in Remark 4.1.1(e).

As in Definition 2.2.11, we employ the notation

$$f_\delta(r, w, L) = \delta \varphi_0(E_\delta, L) = \delta \Phi_0 \left(1 - \frac{E_\delta}{E^\delta} \right) (L - L_0)_+^l.$$

The sufficient stability criterion in Corollary 5.4.2 yields that f_δ is linearly stable if $\|K_\delta\|_{L^2([0, \infty[^2]} < 1$, where as per Proposition 5.3.4

$$K_\delta(r, s) = e^{\frac{\mu_\delta(r)}{2} + \frac{3\lambda_\delta(r)}{2}} e^{\frac{\mu_\delta(s)}{2} + \frac{3\lambda_\delta(s)}{2}} \frac{\sqrt{2r(\mu_\delta)'(r) + 1} \sqrt{2s(\mu_\delta)'(s) + 1}}{rs} I_\delta(r, s) \quad (5.33)$$

and

$$I_\delta(r, s) = \left\langle (\text{id} - \Pi_\delta) \left(\delta |\varphi'_0| E_\delta e^{-\lambda_\delta - \mu_\delta} \mathbf{1}_{[R_{\delta, \min}, r]} \right), \delta |\varphi'_0| E_\delta e^{-\lambda_\delta - \mu_\delta} \mathbf{1}_{[R_{\delta, \min}, s]} \right\rangle_{H_\delta}$$

for $r, s > 2M_0$. Note that K_δ, I_δ are extended by zero onto $[0, \infty[^2$ and supported inside $[R_{\delta, \min}, R_{\delta, \max}]^2$, where $0 < R_{\delta, \min} < R_{\delta, \max}$ are the radial bounds of the steady state f_δ . Moreover, the orthogonal projection onto $\ker(\mathcal{B}_\delta)$ is denoted by Π_δ .

The Cauchy-Schwarz inequality yields

$$|I_\delta(r, s)| \leq \left\| \delta |\varphi'_0| E_\delta e^{-\lambda_\delta - \mu_\delta} \mathbf{1}_{[R_{\delta, \min}, r]} \right\|_{H_\delta} \left\| \delta |\varphi'_0| E_\delta e^{-\lambda_\delta - \mu_\delta} \mathbf{1}_{[R_{\delta, \min}, s]} \right\|_{H_\delta},$$

where we have used $\|\text{id} - \Pi_\delta\| = 1$, since Π_δ (and thus also $\text{id} - \Pi_\delta$) is an orthogonal projection. We bound

$$\frac{|I_\delta(r, s)|}{rs} \leq \frac{1}{(R_{\min}^0)^2} \left\| \delta |\varphi'_0| E_\delta e^{-\lambda_\delta - \mu_\delta} \right\|_{H_\delta}^2$$

due to $[R_{\delta, \min}, R_{\delta, \max}] \subset [R_{\min}^0, R_{\max}^0] \subset]3M_0, \infty[$ from Lemma 2.2.12(a). Recall that the correct integral weight in the Hilbert space H_δ is $\frac{e^{\lambda_\delta}}{\delta |\varphi'_0|}$. Therefore, we estimate

$$\frac{|I_\delta(r, s)|}{rs} \leq C_0 \delta \iint_{\Omega_\delta} |\varphi'_0| e^{-\lambda_\delta - 2\mu_\delta} E_\delta(\sigma, w, L)^2 d\sigma dw dL \quad (5.34)$$

for some δ -independent constant $C_0 > 0$, which may change from line to line. We now bound the remaining integral independently of δ as well. To this end, we use Lemma 2.2.12(b), which asserts that the metric coefficients μ_δ , μ'_δ , and λ_δ converge uniformly to the pure Schwarzschild quantities μ^0 , $(\mu^0)'$, and λ^0 on $]2M_0, \infty[$ as δ goes to zero; in particular they are bounded uniformly on $[R_{\min}^0, R_{\max}^0]$. We estimate $E_\delta \leq E^\delta < 1$ on the steady state support and show that the area of integration

$$\Omega_\delta = \{(r, w, L) \mid r > R_{\min}^0, E_\delta(r, w, L) < E^\delta\}$$

is uniformly bounded for small $\delta \in]0, \delta_0]$: For any $(r, w, L) \in \Omega_\delta$, we have established above that $r \in [R_{\min}^0, R_{\max}^0] \subset]3M_0, \infty[$, and thus

$$L_0 \leq L = r^2 \left(E_\delta^2 e^{-2\mu_\delta(r)} - 1 - w^2 \right) \leq r^2 e^{-2\mu_\delta(r)} \leq C_0,$$

which then yields a bound for w . After possibly shrinking δ_0 , we conclude that

$$\frac{|I_\delta(r, s)|}{rs} \leq C_0 \delta, \quad (r, s) \in]0, \infty[^2,$$

from the considerations above, (5.34), and since Φ'_0 is continuous. Inserting this estimate into (5.33) and again using the uniform bounds on the metric coefficients, implies that

$$\|K_\delta\|_{L^2([0, \infty[^2)} \leq C_0 \delta.$$

By choosing $\delta_0 < \frac{1}{C_0}$, we can apply Corollary 5.4.2 and obtain the linear stability of f_δ for $0 < \delta \leq \delta_0$. \square

In order to show linear stability in the setting above, a different approach consists of deriving a coercivity estimate for \mathcal{L}_δ for small values of δ . In fact, the methods used in [53, 54] simplify considerably in the case of a Schwarzschild-singularity, and one obtains a result similar to Theorem 5.4.1.

6 On oscillating solutions

The definition of a good
mathematical problem is the
mathematics it generates rather than
the problem itself.

Andrew Wiles

With the main results from Chapter 5 at hand, the goal of this chapter is to obtain oscillating solutions to the linearized Einstein-Vlasov system, as introduced in Chapter 4. This part and its results are entirely new and not yet part of previously published work.

We aim to show the *existence* of oscillating solutions and therefore restrict the investigation to singularity-free equilibria which are isotropic and sufficiently regular. However, we are certain that most of the upcoming arguments carry over to more general stationary solutions by more technical and elaborate reasoning.

For the Einstein-Vlasov system, the question whether galaxies can oscillate has not yet been considered in the literature. For the related Vlasov-Poisson system, the investigation of oscillating modes was initiated independently in [55] and [69] where an approach similar to that of Chapter 5 was used. The authors search for isolated eigenvalues in the *principal gap* $]0, \inf(\sigma_{\text{ess}}(\tilde{\mathcal{L}}))[,$ where $\tilde{\mathcal{L}}$ is the Antonov operator corresponding to the Vlasov-Poisson system, similar to \mathcal{L} for the Einstein-Vlasov system. In order to infer the existence of eigenvalues in the principal gap, the authors assume certain monotonicity properties for the period function. Without needing prescriptions on the period function, oscillating modes are rigorously established in the planar case studied in [55, Thm. 8.13] and for small shells with constant angular momentum surrounding a point mass [56, Thm. 1.2].

On a related note, we mention that there is research on the quantitative behavior of collisionless matter in an external potential where self-gravitation is neglected. For example, the Einstein-Vlasov system without self-gravitation and with a central black hole is studied in [101, 102]. In this situation, it is shown that *phase-mixing* occurs, which is strong evidence against the existence of oscillating modes. Whether this is also the case for stationary solutions with a Schwarzschild-singularity, as constructed in Section 2.2.2, is an open problem. It seems as though that the self-gravitation plays a major role for the existence or absence of oscillating modes.

This chapter is structured as follows: In Section 6.1, we specify the class of isotropic stationary solutions which we consider, and we describe the general idea behind our method. In Section 6.2, we prove some preliminary results: We approximate the quadratic form corresponding to the Antonov operator with smooth test functions and

show that the projection onto $\ker(\mathcal{B})$ can be characterized by a fixed-point equation. This yields the continuity of this projection in the redshift. In Section 6.3, we apply this to prove the existence of oscillating solutions by a continuity argument along the redshift.

6.1 The class of steady states and methodology

Instead of investigating one single steady state as in the previous two chapters, it is essential for our approach to consider a family of equilibria, since we want to make use of continuity arguments along this family.

More precisely, let $(f_\kappa)_{\kappa>0}$ be a κ -family of steady states, as given in Definition 2.2.5 and employ the notation mentioned there, i.e., every quantity corresponding to the steady state f_κ is labeled with a subscript κ unless stated otherwise. We do the same with every operator appearing in the previous two chapters because they obviously also depend on κ . We demand that f_κ fulfills similar assumptions as in Section 4.1:

(S1') For every $\kappa > 0$, the steady state f_κ has strict single-well structure, as introduced in Definition 2.3.1(a).

(S2') For every $0 < \kappa_1 < \kappa_2 < \infty$, there exists $C, c > 0$ such that

$$c \leq T_\kappa(E, L) \leq C, \quad (E, L) \in \tilde{\Omega}_\kappa^{EL}, \quad \kappa \in [\kappa_1, \kappa_2].$$

The period function T_κ is defined in (2.44), and $\tilde{\Omega}_\kappa^{EL}$ is the set of relevant (E, L) pairs, as defined in (2.43).

(S3') The ansatz function Φ is continuously differentiable on $]0, \infty[$ with $\Phi' > 0$. In particular, the microscopic equation of state φ_κ is continuously differentiable with respect to E on $\tilde{\Omega}_\kappa^{EL}$ with $\varphi'_\kappa := \partial_E \varphi_\kappa < 0$ on $\tilde{\Omega}_\kappa^{EL}$. On $\mathbb{R}^2 \setminus \tilde{\Omega}_\kappa^{EL}$, we set $\varphi'_\kappa := 0$.

(S4') The steady states are isotropic, i.e.,

$$f_\kappa(x, v) = \varphi_\kappa(E_\kappa(x, v)), \quad (x, v) \in \Omega_\kappa,$$

where Ω_κ is the interior of $\text{supp}(f_\kappa)$, defined in (2.41). In particular, $R_{\kappa, \min} = 0$.

(S5') There exists $C > 0$ such that $|\varphi'_\kappa(E)| \leq C$ for every $\kappa > 0$ and $E \in [0, 1]$.

Let us comment on these conditions which are very similar to the ones in Section 4.1. We refer to Remark 4.1.1 for a related discussion of (S1')–(S3').

Remark 6.1.1. *Conditions (S1') and (S3') are essentially the same assumptions as (S1) and (S3) extended to a family of steady states. In (S2'), we demand that the period function is uniformly bounded from below and above on compact κ -intervals. We have discussed the problem of bounding the period function in Section 3.2.2 and refer to Propositions 3.2.9 and 3.2.10 in particular. Conditions (S4') and (S5') are easily satisfied by*

choosing an appropriate ansatz function Φ and are imposed because of technical convenience.

We now describe the strategy for obtaining an oscillating mode for the linearized Einstein-Vlasov system by applying the techniques and results from Chapters 3 to 5. Consider an eigenvalue $\gamma > 0$ of the Antonov operator \mathcal{L}_κ with eigenfunction $g \in \mathcal{H}_\kappa$. Then

$$f(t) := e^{i\sqrt{\gamma}t}g, \quad t \in \mathbb{R}, \quad (6.1)$$

solves the second-order linearized system (4.16), and we get a solution which is periodic in time with period $\frac{2\pi}{\sqrt{\gamma}}$. In other words, the solution's amplitude *oscillates* in t . Real oscillating solutions are obtained by considering

$$\operatorname{Re}(f(t)) = \cos(\sqrt{\gamma}t)g, \quad \operatorname{Im}(f(t)) = \sin(\sqrt{\gamma}t)g, \quad t \in \mathbb{R}. \quad (6.2)$$

We refer to a solution of the type (6.1) or (6.2) as a (*linearly*) *oscillating mode* or *solution* corresponding to the underlying steady state. By means of the linearization, the oscillation is only visible in the magnitude of the solution f , whereas the support of f is fixed by the support of the underlying steady state. Numerically, it seems as though oscillating behavior also happens in quantities such as the maximal radial expansion for the non-linear case. This behavior can be reconciled by considering a different (but equivalent) linearization method, as discussed in [55, Sc. 3].

In order to determine the existence of an oscillating mode, three observations for steady states as above are key:

- (i) The steady state f_κ is linearly stable for small and linearly unstable for large values of κ by Theorem 5.1.4.
- (ii) The essential spectrum is (uniformly) bounded away from zero on compact κ -intervals by Theorem 4.3.18 and (S2').
- (iii) Every element outside of the essential spectrum $\sigma_{\text{ess}}(\mathcal{L}_\kappa)$ corresponds to an isolated eigenvalue by the standard min-max principle [88, Thm. XIII.1].

Now follows the general idea: If we assume that the infimum of the spectrum $\inf(\sigma(\mathcal{L}_\kappa))$ is continuous in κ , we know that an eigenvalue must depart from the essential spectrum at some value κ_{osc} and eventually turn negative at some larger value κ_0 , which induces the linear instability. Since $\inf(\sigma(\mathcal{L}_\kappa)) < \inf(\sigma_{\text{ess}}(\mathcal{L}_\kappa))$ is an isolated eigenvalue by (iii), this yields an oscillating mode for the linearized system, as described above, for some intermediate values that satisfy $\kappa_{\text{osc}} < \kappa < \kappa_0$. The continuity of the infimum of the spectrum of \mathcal{L}_κ should therefore be sufficient to infer the existence of oscillating solutions. This idea is illustrated in Figure 6.1 and sounds intriguing at first glance.

However, we are not able to show the continuity $\inf(\sigma(\mathcal{L}_\kappa))$ directly and do not know if this is possible with the current techniques. This difficulty can be attributed to the fact that the Antonov operator is an unbounded, densely defined operator and thus hard to control. At this point, the Mathur operator approach from Chapter 5 comes

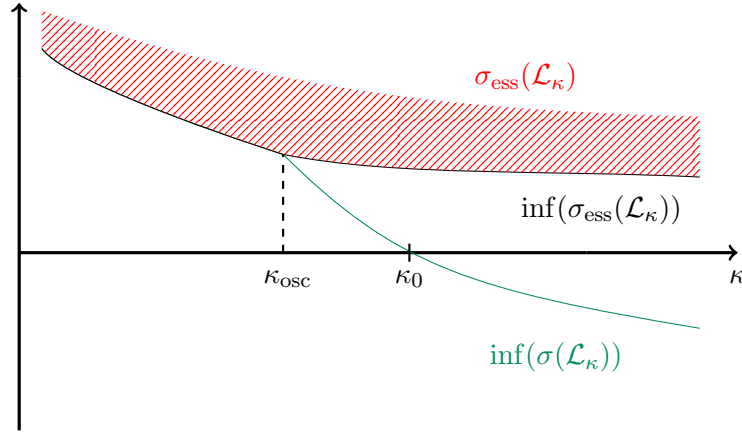


Figure 6.1: Depiction of the idea behind obtaining an eigenvalue that induces an oscillating mode. At κ_{osc} an eigenvalue departs from the essential spectrum and becomes negative for $\kappa > \kappa_0$, i.e., the steady state f_κ becomes unstable. An isolated eigenvalue exists in the principal gap $]0, \inf(\sigma_{\text{ess}}(\mathcal{L}_\kappa))$ for all intermediate values $\kappa_{\text{osc}} < \kappa < \kappa_0$.

in handy. As the Mathur operator \mathcal{M}_κ is much better behaved, see Lemma 5.3.3 and Proposition 5.3.4, we instead aim at showing that $\|\mathcal{M}_\kappa\|$ is continuous in κ . By the intermediate value theorem and Theorem 5.4.1, we obtain a (minimally chosen) value $\kappa_0 > 0$ such that $\|\mathcal{M}_{\kappa_0}\| = 1$, which is equivalent to $\inf(\sigma(\mathcal{L}_{\kappa_0})) = 0$. For small values of $\varepsilon > 0$, we then show the existence of a test function $f \in \mathcal{H}_{\kappa_0 - \varepsilon}$ such that

$$0 < \inf(\sigma(\mathcal{L}_{\kappa_0 - \varepsilon})) \leq \langle \mathcal{L}_{\kappa_0 - \varepsilon} f, f \rangle_{H_{\kappa_0 - \varepsilon}} < \inf(\sigma_{\text{ess}}(\mathcal{L}_{\kappa_0 - \varepsilon}))$$

via an approximation result for the quadratic form of the Antonov operator. In conclusion, we obtain the existence of an isolated eigenvalue and thus an oscillating mode.

The attentive reader will have noticed that—in the Mathur operator—the orthogonal projection onto $\ker(\mathcal{B})$ occurs. More precisely, we need to show that

$$\Pi_\kappa^s := \Pi_\kappa \left(|\varphi'_\kappa| E_\kappa e^{-\lambda_\kappa - \mu_\kappa} \mathbf{1}_{[0, s]} \right)$$

is continuous in κ in an appropriate sense for fixed $s \geq 0$. It is important to note that the function spaces depend on κ , which is why we have to reformulate the analysis to an unweighted L^2 -space over \mathbb{R}^3 and take care of the different function spaces by including indicator functions as well as the correct integration weights. By combining Lemmas 4.3.8 and 4.3.9, we are able to derive a fixed-point equation for the generator g_κ^s of Π_κ^s characterized by a compact fixed-point operator. This compactness then yields the continuity in κ in an unweighted L^2 -space. These technical and lengthy arguments will be thoroughly treated in the next section.

6.2 Preliminary results

Before we perform the search for an isolated eigenvalue in the spectrum, as described in the previous section, we need to provide some preliminary results that extend the knowledge from Chapter 3 and Section 4.3. As mentioned above, we want to infer the existence of an oscillating mode by a continuity argument in κ , for which we need to control the quadratic form corresponding to the Antonov operator and the orthogonal projection Π_κ onto $\ker(\mathcal{B}_\kappa)$. However, Π_κ is not known explicitly, which makes this endeavor much more challenging, as we have to show continuity through some involved arguments.

We first recall the necessary properties in κ from Chapter 3, apply them to our specific situation described in (S1')–(S5'), and gather them in the following lemma for future reference.

Lemma 6.2.1. *Consider a κ -family which satisfies (S1')–(S5'). For $\kappa_0 > 0$ and $\varepsilon > 0$, there exist $\delta > 0$ and compact sets K, U as well as a constant $C > 0$ such that the following holds for every $\kappa > 0$ with $|\kappa - \kappa_0| < \delta$:*

(a) $K \subset \Omega_\kappa \subset U$ with $\iint_{\Omega_\kappa \setminus K} dr dw dL < \varepsilon$ and $R_{\kappa, \max} \leq R_{\kappa_0, \max} + 1$, as well as

$$\iint_{\{(w, L) \mid (r, w, L) \in \Omega_\kappa \setminus K\}} dw dL < \varepsilon,$$

for every $r \in [R_{\kappa, \min}, R_{\kappa, \max}]$.

(b) The steady state quantities

$$[\kappa_0 - \delta, \kappa_0 + \delta] \times [0, R_{\kappa_0, \max} + 1] \ni (\kappa, r) \mapsto \mu_\kappa(r), \mu'_\kappa(r), \lambda_\kappa(r), \rho_\kappa(r), p_\kappa(r)$$

as well as

$$[\kappa_0 - \delta, \kappa_0 + \delta] \times K \ni (\kappa, r, w, L) \mapsto E_\kappa(r, w, L), |\varphi'_\kappa(E_\kappa(r, w, L))|^{\frac{1}{2}}$$

are bounded and uniformly continuous. The latter mapping is uniformly bounded away from zero.

(c) The period function

$$[\kappa_0 - \delta, \kappa_0 + \delta] \times K \ni (\kappa, r, w, L) \mapsto T_\kappa(E_\kappa(r, w, L), L),$$

is uniformly continuous as well as bounded from above and bounded away from zero. For fixed $(\kappa, E, L) \in \Gamma^{EL}$, the angle function $\theta_\kappa(\cdot, E, L)$ is continuous with $0 \leq \theta_\kappa(\cdot, E, L) \leq \frac{1}{2}$; recall (3.28) for the definition of Γ^{EL} .

(d) The solution to the characteristic system (4.17)

$$[0, 1] \times [\kappa_0 - \delta, \kappa_0 + \delta] \times K \ni (\theta, \kappa, r, w, L) \mapsto (R_\kappa, W_\kappa)(\theta, E_\kappa(r, w, L), L)$$

is bounded and uniformly continuous.

(e) For every $r \in]0, R_{\kappa_0, \max} + 1]$, it holds that

$$\frac{\pi}{r^2} \int_0^\infty \int_{\mathbb{R}} |\varphi'_\kappa(E_\kappa(r, w, L))| dw dL \leq C.$$

(f) For every $f \in H_\kappa$, it holds that

$$\int_0^{R_{\kappa_0, \max}+1} \rho_{|f|}(r) r dr \leq C \left(\int_0^{R_{\kappa_0, \max}+1} \rho_{|f|}(r)^2 r^2 dr \right)^{\frac{1}{2}} \leq C \|f\|_{H_\kappa}.$$

Proof. We first note that all the properties necessary to apply the results from Chapter 3 hold due to (S1')–(S5'). Part (a) follows directly from Lemmas 3.1.5 and 3.2.1. The uniform boundedness and continuity in (b) holds according to Proposition 3.1.4 and (S3'). Note that the compactness of K implies that the energy is bounded strictly away from the cut-off energy E^κ , and thus $|\varphi'| \geq c$ for some constant $c > 0$. The continuity of the period function and angle function is shown in Propositions 3.2.7 and 3.2.8, respectively. The lower and upper bounds of T are prescribed by (S2'). Lemma 3.2.5 and the continuity of the period function yield the claim in (d); recall the discussion at the beginning of Section 4.3 for the relation between (2.42) and (4.17). The claim in (e) is a consequence of (S5') and $\Omega_\kappa \subset U$, since the integral over the (w, L) -support yields a r^2 -term, see also (4.1) and the discussion thereafter.

The proof of (f) relies on similar techniques as that of Lemma 4.3.6(a). Due to the uniform bound of the radial support, we obtain

$$\int_0^{R_{\kappa_0, \max}+1} \rho_{|f|}(r) r dr \leq C \left(\int_0^{R_{\kappa_0, \max}+1} \rho_{|f|}(r)^2 r^2 dr \right)^{\frac{1}{2}}. \quad (6.3)$$

The density ρ_f can be estimated by the uniform bound $\Omega_\kappa \subset U$ and by the Cauchy-Schwarz inequality via

$$\begin{aligned} \rho_{|f|}(r) &\leq \frac{C}{r^2} \int_0^\infty \int_{\mathbb{R}} \frac{|\varphi'_\kappa|^{\frac{1}{2}}}{|\varphi'_\kappa|^{\frac{1}{2}}} |f| dw dL \leq \frac{C}{r^2} \left(\int_0^\infty \int_{\mathbb{R}} |\varphi'_\kappa| dw dL \right)^{\frac{1}{2}} \left(\int_0^\infty \int_{\mathbb{R}} \frac{|f|^2}{|\varphi'_\kappa|} dw dL \right)^{\frac{1}{2}} \\ &\leq \frac{C}{r} \left(\int_0^\infty \int_{\mathbb{R}} \frac{e^{\lambda_\kappa}}{|\varphi'_\kappa|} |f|^2 dw dL \right)^{\frac{1}{2}} \end{aligned}$$

for every $r > 0$, where we employed (b) and in the last step (e). Plugging this back into (6.3) yields

$$\left(\int_0^{R_{\kappa_0, \max}+1} \rho_{|f|}(r) r dr \right)^2 \leq C \int_0^{R_{\kappa_0, \max}+1} \frac{1}{r^2} \left(\int_0^\infty \int_{\mathbb{R}} \frac{e^{\lambda_\kappa}}{|\varphi'_\kappa|} |f|^2 dw dL \right) r^2 dr = C \|f\|_{H_\kappa}^2. \quad \square$$

6.2.1 Approximating the quadratic form

In the next lemma, we provide the necessary tools in order to control $\inf(\sigma(\mathcal{L}_\kappa))$, when κ is close to a fixed value $\kappa_0 > 0$. We do this by approximating the quadratic form with smooth functions.

Lemma 6.2.2. *Consider $\kappa_0 > 0$ and $g_0 \in \mathcal{H}_{\kappa_0} \cap \mathcal{D}(\mathcal{T}_{\kappa_0})$. For every $\varepsilon > 0$, there exists an odd-in- w function $g \in C_c^\infty(\Omega_{\kappa_0})$ and $\delta > 0$ such that for every $\kappa > 0$ with $|\kappa - \kappa_0| < \delta$ it holds that*

- (i) $g \in C_c^\infty(\Omega_{\kappa_0} \cap \Omega_\kappa)$,
- (ii) $|\langle \mathcal{B}_{\kappa_0} g_0, \mathcal{B}_{\kappa_0} g_0 \rangle_{H_{\kappa_0}} - \langle \mathcal{B}_\kappa g, \mathcal{B}_\kappa g \rangle_{H_\kappa}| < \varepsilon$,
- (iii) $|\langle \mathcal{R}_{\kappa_0} g_0, g_0 \rangle_{H_{\kappa_0}} - \langle \mathcal{R}_\kappa g, g \rangle_{H_\kappa}| < \varepsilon$.

Proof. In order to shorten notation, we write a subscript 0 instead of κ_0 for the necessary operators and quantities. Let $\varepsilon > 0$ and $\kappa_0 > 0$. By the approximation result in Proposition 4.3.5(c), there exists $g \in C_c^\infty(\Omega_0)$ with

$$\|g_0 - g\|_{H_0} + \|\mathcal{B}_0 g_0 - \mathcal{B}_0 g\|_{H_0} < \varepsilon \quad (6.4)$$

and

$$\|g\|_{H_0} + \|\mathcal{B}_0 g\|_{H_0} + \|\partial_r g\|_{H_0} + \|\partial_w g\|_{H_0} \leq C \quad (6.5)$$

for some constant $C > 0$, which is independent of ε . Since g_0 is odd in w , we can assume the same for g by restricting g to its odd-in- w part. For the fixed value of ε , we choose $\delta > 0$ and a compact set K according to Lemma 6.2.1(a) with the additional property that $\text{supp}(g) \subset K \subset \Omega_\kappa$ for every $\kappa > 0$ with $|\kappa - \kappa_0| < \delta$. In particular, we have $g \in C_c^\infty(\Omega_0 \cap \Omega_\kappa)$ for $|\kappa - \kappa_0| < \delta$. As to part (ii), we estimate

$$|\langle \mathcal{B}_0 g_0, \mathcal{B}_0 g_0 \rangle_{H_0} - \langle \mathcal{B}_\kappa g, \mathcal{B}_\kappa g \rangle_{H_\kappa}| \leq \left| \|\mathcal{B}_0 g_0\|_{H_0}^2 - \|\mathcal{B}_0 g\|_{H_0}^2 \right| + \left| \|\mathcal{B}_0 g\|_{H_0}^2 - \|\mathcal{B}_\kappa g\|_{H_\kappa}^2 \right|. \quad (6.6)$$

The first term can be controlled by

$$\begin{aligned} \left| \|\mathcal{B}_0 g_0\|_{H_0}^2 - \|\mathcal{B}_0 g\|_{H_0}^2 \right| &= \left(\|\mathcal{B}_0 g_0\|_{H_0} + \|\mathcal{B}_0 g\|_{H_0} \right) \left| \|\mathcal{B}_0 g_0\|_{H_0} - \|\mathcal{B}_0 g\|_{H_0} \right| \\ &\leq C \|\mathcal{B}_0 g_0 - \mathcal{B}_0 g\|_{H_0} < C\varepsilon, \end{aligned}$$

with $C > 0$ independent of ε due to (6.5). The last two steps follow from the reverse triangle inequality and from (6.4). We introduce the shorthand $\langle v \rangle = \sqrt{1 + w^2 + \frac{L}{r^2}}$ and note that the steady state supports and metric coefficients can be bounded uniformly in κ and ε by applying Lemma 6.2.1 (e.g. with $\varepsilon = 1$). Since g is odd in w and $\text{supp}(\mathcal{T}_\kappa g) \subset K$, we estimate the latter term in (6.6) by

$$\left| \|\mathcal{B}_0 g\|_{H_0}^2 - \|\mathcal{B}_\kappa g\|_{H_\kappa}^2 \right| = 4\pi^2 \left| \iiint_K \left(\frac{e^{\lambda_0}}{|\varphi'_0(E_0)|} (\mathcal{B}_0 g)^2 - \frac{e^{\lambda_\kappa}}{|\varphi'_\kappa(E_\kappa)|} (\mathcal{B}_\kappa g)^2 \right) dr dw dL \right|$$

$$\begin{aligned}
 &= 4\pi^2 \left| \iiint_K \left(\frac{e^{\lambda_0}}{|\varphi'_0(E_0)|} (\mathcal{T}_0 g + S_0 g)^2 - \frac{e^{\lambda_\kappa}}{|\varphi'_\kappa(E_\kappa)|} (\mathcal{T}_\kappa g + S_\kappa g)^2 \right) dr dw dL \right| \\
 &+ 4\pi \left| \iiint_{\Omega_0 \setminus K} \frac{e^{\lambda_0}}{|\varphi'_0|} (S_0 g)^2 dr dw dL \right| + 4\pi \left| \iiint_{\Omega_\kappa \setminus K} \frac{e^{\lambda_\kappa}}{|\varphi'_\kappa|} (S_\kappa g)^2 dr dw dL \right|, \quad (6.7)
 \end{aligned}$$

where we recall the operator \mathcal{S}_κ from Definition 4.2.2(b). The latter two terms can be estimated for every $\kappa > 0$ with $|\kappa - \kappa_0| < \delta$ via

$$\begin{aligned}
 &\left| \iiint_{\Omega_\kappa \setminus K} \frac{e^{\lambda_\kappa}}{|\varphi'_\kappa|} (\mathcal{S}_\kappa g)^2 dr dw dL \right| \leq C \iiint_{\Omega_\kappa \setminus K} |\varphi'_\kappa| |j_g(r)|^2 r^2 dr dw dL \\
 &\leq C \int_0^{R_{\kappa, \max}} \iint_{\{(w,L) \mid (r,w,L) \in \Omega_\kappa \setminus K\}} dw dL \rho_{|g|}(r)^2 r^2 dr < C\varepsilon \|g\|_{H_0}^2 \leq C\varepsilon
 \end{aligned}$$

by using (S5'), Lemma 6.2.1(a), (f), and (6.5). It remains to estimate the first term in (6.7), which we split further into

$$\begin{aligned}
 &4\pi^2 \left| \iiint_K \left(\frac{e^{\lambda_0}}{|\varphi'_0(E_0)|} (\mathcal{T}_0 g + S_0 g)^2 - \frac{e^{\lambda_\kappa}}{|\varphi'_\kappa(E_\kappa)|} (\mathcal{T}_\kappa g + S_\kappa g)^2 \right) dr dw dL \right| \\
 &\leq C \iiint_K \left| \frac{e^{\lambda_0}}{|\varphi'_0(E_0)|} (\mathcal{T}_0 g)^2 - \frac{e^{\lambda_\kappa}}{|\varphi'_\kappa(E_\kappa)|} (\mathcal{T}_\kappa g)^2 \right| dr dw dL \\
 &\quad + C \iiint_K \left| |\varphi'_0(E_0)| e^{4\mu_0 + 3\lambda_0} - |\varphi'_\kappa(E_\kappa)| e^{4\mu_\kappa + 3\lambda_\kappa} \right| j_g^2 r^2 dr dw dL \\
 &\quad + C \iiint_K \left| e^{2\mu_0 + 2\lambda_0} \mathcal{T}_0 g - e^{2\mu_\kappa + 2\lambda_\kappa} \mathcal{T}_\kappa g \right| |j_g| r dr dw dL \\
 &=: I_1 + I_2 + I_3.
 \end{aligned}$$

We treat the terms I_1, I_2, I_3 separately. To begin, we expand the square of the transport operator in I_1 and obtain

$$\begin{aligned}
 I_1 &\leq C \iiint_K \left| \frac{e^{2\mu_0 - \lambda_0}}{|\varphi'_0(E_0)|} - \frac{e^{2\mu_\kappa - \lambda_\kappa}}{|\varphi'_\kappa(E_\kappa)|} \right| \left(\partial_r g \frac{w}{\langle v \rangle} + \partial_w g \frac{L}{r^3 \langle v \rangle} \right)^2 dr dw dL \\
 &\quad + C \iiint_K \left| \frac{e^{2\mu_0 - \lambda_0}}{|\varphi'_0(E_0)|} (\mu'_0)^2 - \frac{e^{2\mu_\kappa - \lambda_\kappa}}{|\varphi'_\kappa(E_\kappa)|} (\mu'_\kappa)^2 \right| \langle v \rangle^2 (\partial_w g)^2 dr dw dL \\
 &\quad + C \iiint_K \left| \frac{e^{2\mu_0 - \lambda_0}}{|\varphi'_0(E_0)|} \mu'_0 - \frac{e^{2\mu_\kappa - \lambda_\kappa}}{|\varphi'_\kappa(E_\kappa)|} \mu'_\kappa \right| \left| \partial_w g \left(w \partial_r g + \frac{L}{r^3} \partial_w g \right) \right| dr dw dL.
 \end{aligned}$$

According to Lemma 6.2.1(b), the factors depending on κ in the integrands are uniformly continuous over $[\kappa_0 - \delta, \kappa_0 + \delta] \times K$. This implies that, for $\delta > 0$ small enough, we have

$$\begin{aligned} & \left| \frac{e^{2\mu_0 - \lambda_0}}{|\varphi'_0(E_0)|} - \frac{e^{2\mu_\kappa - \lambda_\kappa}}{|\varphi'_\kappa(E_\kappa)|} \right| + \left| \frac{e^{2\mu_0 - \lambda_0}}{|\varphi'_0(E_0)|} (\mu'_0)^2 - \frac{e^{2\mu_\kappa - \lambda_\kappa}}{|\varphi'_\kappa(E_\kappa)|} (\mu'_\kappa)^2 \right| \\ & + \left| \frac{e^{2\mu_0 - \lambda_0}}{|\varphi'_0(E_0)|} \mu'_0 - \frac{e^{2\mu_\kappa - \lambda_\kappa}}{|\varphi'_\kappa(E_\kappa)|} \mu'_\kappa \right| < \varepsilon \min(1, d^2) \end{aligned}$$

on K for $|\kappa - \kappa_0| < \delta$, where we defined

$$d := \min_{(r,w,L) \in K} r > 0;$$

note that this distance is positive since $K \subset \Omega_\kappa \subset]0, \infty[\times \mathbb{R} \times]0, \infty[$ is compact, and recall that K and ε are fixed throughout this whole process. In addition, we can bound the values of $\frac{L}{r^2}$ on K uniformly in κ as well due to $\frac{L}{r^2} \leq e^{-2\mu_\kappa(r)} E_\kappa^2$. Inserting this into the estimate for I_1 above yield that

$$\begin{aligned} I_1 & \leq C\varepsilon \min(1, d^2) \iiint_K \left| (\partial_r g)^2 + \frac{(\partial_w g)^2}{r^2} + (\partial_w g)^2 \right| dr dw dL \\ & \leq C\varepsilon \min(1, d^2) \iiint_K \frac{|\varphi'_0(E_0)|}{|\varphi'_0(E_0)|} \left| (\partial_r g)^2 + \frac{(\partial_w g)^2}{d^2} + (\partial_w g)^2 \right| dr dw dL \\ & \leq C\varepsilon \iiint_K \frac{1}{|\varphi'_0(E_0)|} |(\partial_r g)^2 + (\partial_w g)^2| dr dw dL \leq C\varepsilon (\|\partial_r g\|_{H_0}^2 + \|\partial_w g\|_{H_0}^2) \leq C\varepsilon \end{aligned}$$

due to (S5') and (6.5), with $C > 0$ still independent of ε . For the term I_2 , we make δ sufficiently small such that

$$\left| |\varphi'_0(E_0)| e^{4\mu_0 + 3\lambda_0} - |\varphi'_\kappa(E_\kappa)| e^{4\mu_\kappa + 3\lambda_\kappa} \right| < \varepsilon$$

on K for $|\kappa - \kappa_0| < \delta$, as above. This immediately implies

$$I_2 \leq C\varepsilon \int_0^{R_{0,\max}+1} |j_g(r)|^2 r^2 dr \leq C\varepsilon \|g\|_{H_0}^2 \leq C\varepsilon$$

because of $|j_f| \leq \rho_{|f|}$ and Lemma 6.2.1(f) as well as (6.5). The final term I_3 can be controlled analogously. Skipping over similar estimates, we obtain

$$I_3 \leq C \iiint_K \left| e^{3\mu_0 + \lambda_0} (1 + \mu'_0) - e^{3\mu_\kappa + \lambda_\kappa} (1 + \mu'_\kappa) \right| \left(|\partial_r g| + \frac{|\partial_w g|}{r} + |\partial_w g| \right) |j_g| r dr dw dL.$$

The Cauchy-Schwarz inequality, uniform continuity, and $r \geq d$ on K yields

$$I_3 \leq C\varepsilon (\|\partial_r g\|_{H_0} + \|\partial_w g\|_{H_0}) \int_0^{R_{0,\max}+1} |j_g(r)|^2 r^2 dr \leq C\varepsilon$$

as above with I_1 and I_2 . In conclusion, we deduce (ii) by putting the estimates above into (6.6), since $C > 0$ is independent of ε .

It remains to show that (iii) holds as well, for which we first estimate

$$\begin{aligned} |\langle \mathcal{R}_0 g_0, g_0 \rangle_{H_0} - \langle \mathcal{R}_\kappa g, g \rangle_{H_\kappa}| &\leq |\langle \mathcal{R}_0 g_0, g_0 \rangle_{H_0} - \langle \mathcal{R}_0 g, g \rangle_{H_0}| + |\langle \mathcal{R}_0 g, g \rangle_{H_0} - \langle \mathcal{R}_\kappa g, g \rangle_{H_\kappa}| \\ &\leq 16\pi^2 \int_0^{R_{0,\max}+1} e^{3\mu_0+\lambda_0} (2r\mu'_0 + 1) |j_{g_0}^2 - j_g^2| r^2 dr \\ &\quad + 16\pi^2 \int_0^{R_{0,\max}+1} \left| e^{3\mu_0+\lambda_0} (2r\mu'_0 + 1) - e^{3\mu_\kappa+\lambda_\kappa} (2r\mu'_\kappa + 1) \right| j_g^2 r^2 dr. \end{aligned}$$

Choosing δ small enough guarantees

$$\left| e^{3\mu_0+\lambda_0} (2r\mu'_0 + 1) - e^{3\mu_\kappa+\lambda_\kappa} (2r\mu'_\kappa + 1) \right| < \varepsilon$$

on $[0, R_{0,\max} + 1]$ for $|\kappa - \kappa_0| < \delta$. In addition, $|j_g^2 - j_{g_0}^2| = |j_g + j_{g_0}| |j_g - j_{g_0}|$, the Cauchy-Schwarz inequality, and Lemma 6.2.1(f) imply

$$|\langle \mathcal{R}_0 g_0, g_0 \rangle_{H_0} - \langle \mathcal{R}_\kappa g, g \rangle_{H_\kappa}| \leq C(\|g_0\|_{H_0} + \|g\|_{H_0}) \|g_0 - g\|_{H_0} + C\|g\|_{H_0}^2 \varepsilon \leq C\varepsilon$$

for $|\kappa - \kappa_0| < \delta$, where we used (6.4) as well as (6.5), and $C > 0$ is independent from ε . \square

It is now easy to infer the analogous result for the Antonov operator \mathcal{L}_κ by combining (ii) and (iii). This might also be useful for further applications beyond this work.

Corollary 6.2.3. *Consider $\kappa_0 > 0$ and $g_0 \in \mathcal{H}_{\kappa_0}$. For every $\varepsilon > 0$, there exists an odd-in- w function $g \in C_c^\infty(\Omega_{\kappa_0})$ and $\delta > 0$ such that $g \in C_c^\infty(\Omega_{\kappa_0} \cap \Omega_\kappa)$ and for every $\kappa > 0$ with $|\kappa - \kappa_0| < \delta$, it holds that*

$$|\langle \mathcal{L}_\kappa g, g \rangle_{H_\kappa} - \langle \mathcal{L}_{\kappa_0} g_0, g_0 \rangle_{H_{\kappa_0}}| < \varepsilon.$$

Proof. This follows directly from the skew-adjointness of \mathcal{B}_κ and the application of Lemma 6.2.2. \square

Remark 6.2.4. *At first glance, it is rather disturbing that Corollary 6.2.3 is not sufficient to show that $\kappa \mapsto \inf(\sigma(\mathcal{L}_\kappa))$ is continuous which would save a lot of work. Consider the same setup as in Corollary 6.2.3, where g and g_0 are normalized. Moreover, choose $g_0 \in \mathcal{H}_{\kappa_0}$ with $\langle \mathcal{L}_{\kappa_0} g_0, g_0 \rangle_{H_{\kappa_0}} < \inf(\sigma(\mathcal{L}_{\kappa_0})) + \varepsilon$. On the one hand, we immediately obtain*

$$\inf(\sigma(\mathcal{L}_\kappa)) \leq \langle \mathcal{L}_\kappa g, g \rangle_{H_\kappa} \leq \langle \mathcal{L}_{\kappa_0} g_0, g_0 \rangle_{H_{\kappa_0}} + \varepsilon \leq \inf(\sigma(\mathcal{L}_{\kappa_0})) + 2\varepsilon,$$

which implies upper semi-continuity of $\kappa \mapsto \inf(\sigma(\mathcal{L}_\kappa))$. On the other hand, we cannot, for example, rule out

$$\liminf_{\kappa \searrow \kappa_0} \inf(\sigma(\mathcal{L}_\kappa)) < \inf(\sigma(\mathcal{L}_{\kappa_0})),$$

as illustrated in Figure 6.2. It is easy to see that, in this case, Corollary 6.2.3 can still be valid, but $\kappa \mapsto \inf(\sigma(\mathcal{L}_\kappa))$ is not continuous in κ_0 . We do not know if and how this conundrum can be resolved directly. We work around the problem by employing the

Mathur operator approach developed in the previous chapter. Despite this observation, Corollary 6.2.3 will still be crucial in Section 6.3 for showing the existence of oscillating modes.

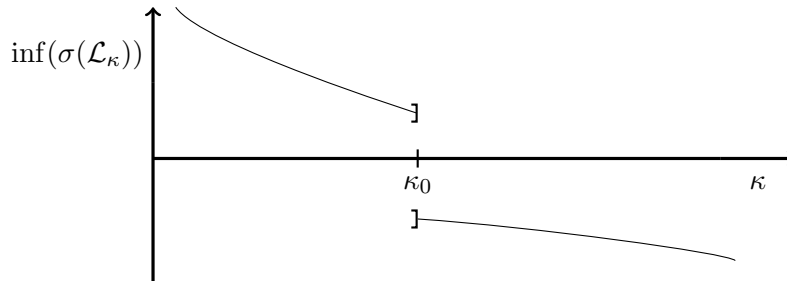


Figure 6.2: A conceivable behavior of $\inf(\sigma(\mathcal{L}_\kappa))$ along the redshift κ , which does not violate Corollary 6.2.3. The graph does not cross zero and the instability arises “suddenly” for values $\kappa > \kappa_0$. In particular, the strategy of obtaining an oscillating solution by a continuity argument, as described in Section 6.1 does not seem possible in this scenario.

6.2.2 A fixed-point method for the projection operator

We now establish a fixed-point equation that fully characterizes the orthogonal projection for some fixed value of the redshift κ , and we afterwards show that this leads to continuity of $\kappa \mapsto \Pi_\kappa$ in an appropriate sense. Only for the current section, we consider a fixed value $\kappa_0 > 0$, i.e., just the steady state f_{κ_0} . In order to lighten notation, we change from a subscript κ_0 to a subscript 0 or leave out the index completely such that the notation is the same as in Chapters 4 and 5.

The central difficulty when considering the kernel K from (5.27) is the term

$$\Pi^s := \Pi\left(|\varphi'|Ee^{-\lambda_0-\mu_0}\mathbb{1}_{[0,s]}\right). \quad (6.8)$$

Recall that $R_{\min} = 0$ holds due to isotropy. According to Lemma 4.3.8, there exists a unique function $g^s = g^s(E, L) \in \ker(\mathcal{T})$ such that

$$\Pi^s = g^s + 4\pi|\varphi'|Ee^{-\lambda_0-\mu_0} \int_r^{R_{\max}} e^{(3\lambda_0+\mu_0)(\sigma)} p_{g^s}(\sigma) \sigma d\sigma. \quad (6.9)$$

In this section, we show that g^s can be characterized by a fixed-point equation. As mentioned in Section 6.1, one of the main objectives is to eliminate the dependency on κ in the function spaces H_κ . Therefore, we formulate the following results in an unweighted L^2 -space which makes things more cumbersome to write down. The results from this section could have been shown much earlier in Section 4.3, but it did not feel appropriate to include them there.

Definition 6.2.5. For $s \geq 0$ and $j \in \{1, \dots, 5\}$, the auxiliary operators $G_j(s): H \rightarrow H$ are defined by

$$\begin{aligned}
 (G_1(s)g)(r, w, L) &:= 2|\varphi'|E \int_0^{\theta(s, E, L)} e^{-(\lambda_0 + \mu_0)(R(\theta))} d\theta \\
 (G_2(s)g)(r, w, L) &:= -4\pi|\varphi'|E \int_0^1 e^{-(\lambda_0 + \mu_0)(R(\theta))} \int_{R(\theta)}^{R_{\max}} e^{(3\lambda_0 + \mu_0)(\sigma)} p_g(\sigma) \sigma d\sigma d\theta, \\
 (G_3(s)g)(r, w, L) &:= 4\pi|\varphi'| \int_0^1 \frac{E^2 - \Psi_L^2(R(\theta))}{E} \frac{e^{2\lambda_0(R(\theta))}}{R(\theta)} \int_0^{\min(s, R(\theta))} \sigma^2 e^{-\lambda_0(\sigma)} M_{2, \varphi}(\sigma) d\sigma d\theta, \\
 (G_4(s)g)(r, w, L) &:= -4\pi|\varphi'| \int_0^1 \frac{E^2 - \Psi_L^2(R(\theta))}{E} \frac{e^{2\lambda_0(R(\theta))}}{R(\theta)} \int_0^{R(\theta)} \sigma^2 \rho_g(\sigma) d\sigma d\theta, \\
 (G_5(s)g)(r, w, L) &:= -16\pi^2|\varphi'| \int_0^1 \frac{E^2 - \Psi_L^2(R(\theta))}{E} \frac{e^{2\lambda_0(R(\theta))}}{R(\theta)} \int_0^{R(\theta)} \sigma^2 e^{-\lambda_0(\sigma)} M_{2, \varphi}(\sigma) \\
 &\quad \cdot \int_{\sigma}^{R_{\max}} e^{(3\lambda_0 + \mu_0)(\eta)} p_g(\eta) \eta d\eta d\sigma d\theta
 \end{aligned}$$

for $(r, w, L) \in \mathbb{R}^3$, where $E = E(r, w, L)$, $R(\theta) = R(\theta, E, L)$, and we have introduced the shorthand

$$M_{2, \varphi}(r) := \frac{\pi}{r^2} \int_0^\infty \int_{\mathbb{R}} \left(1 + w^2 + \frac{L}{r^2}\right) |\varphi'(E(r, w, L))| dw dL, \quad r > 0. \quad (6.10)$$

The fixed-point operator $G: L^2(\mathbb{R}^3) \rightarrow L^2(\mathbb{R}^3)$ corresponding to Π is given by

$$G(s)h := e^{\frac{\lambda_0}{2}} |\varphi'|^{-\frac{1}{2}} \sum_{j=1}^5 G_j(s) \left(e^{-\frac{\lambda_0}{2}} |\varphi'|^{\frac{1}{2}} h \right). \quad (6.11)$$

Recall the definition of the angle function $\theta = \theta(r, E, L)$ introduced in (2.69) and its continuous extension in the radial variable given in (3.30). We refrain from a derivation of $G(s)$, since Proposition 6.2.7 shows why we have defined this family of operators as we did. First, we prove that $G(s)$ is well defined.

Lemma 6.2.6. For every $s \geq 0$ and $j \in \{1, \dots, 5\}$, the operators $G_j(s): H \rightarrow H$ are well defined with $G_j(s) = G_j(R_{\max})$ for $s \geq R_{\max}$. In particular, the fixed-point operator $G: L^2(\mathbb{R}^3) \rightarrow L^2(\mathbb{R}^3)$ is well defined with $G(s) = G(R_{\max})$ for $s \geq R_{\max}$.

Proof. Throughout the proof, $C > 0$ denotes a constant depending only on steady state quantities. The operators G_1 and G_3 are constant. On the one hand, since the angle function is bounded by $\frac{1}{2}$, we can bound G_1 by

$$|G_1(s)g| \leq C|\varphi'|.$$

On the other hand, for G_3 we use Lemma 6.2.1(e) in order to obtain $M_{2,\varphi} \leq C$, and therefore

$$|G_3(s)g| \leq C|\varphi'|,$$

since the term R in the denominator gets canceled by the radial integral over σ . For the remaining terms, we apply Lemma 6.2.1(f), which yields

$$\frac{1}{r} \int_0^r (|\rho_g(\sigma)| + |p_g(\sigma)|)\sigma^2 d\sigma \leq \int_0^r (|\rho_g(\sigma)| + |p_g(\sigma)|)\sigma d\sigma \leq C\|g\|_H, \quad r > 0, \quad (6.12)$$

due to $|p_g| \leq \rho_{|g|}$. This estimate takes care of G_2 , G_4 , and G_5 simultaneously. For $j \in \{1, \dots, 5\}$ and $g \in H$, we therefore obtain

$$|G_j(s)g| \leq C(1 + \|g\|_H) |\varphi'|, \quad g \in H, \quad (6.13)$$

which implies $G_j(s)g \in H$ with

$$\|G_j(s)g\|_H \leq C(1 + \|g\|_H), \quad (6.14)$$

for every $s \geq 0$. When evaluating G_j at $s \geq R_{\max}$, we get $\theta(s, E, L) = \frac{1}{2}$, and $\min(s, R(\theta, E, L)) = R(\theta, E, L)$ for every $\theta \in [0, 1]$ and $(E, L) \in \tilde{\Omega}_0^{EL}$. Thus, G_j does not depend on s and $G_j(s) = G_j(R_{\max})$.

The well-definedness of $G(s): L^2(\mathbb{R}^3) \rightarrow L^2(\mathbb{R}^3)$ now follows from

$$\begin{aligned} \|G(s)h\|_{L^2(\mathbb{R}^3)} &\leq C \sum_{j=1}^5 \left\| G_j(s) \left(e^{-\frac{\lambda_0}{2}} |\varphi'|^{\frac{1}{2}} h \right) \right\|_H \\ &\leq C \left(1 + \left\| e^{-\frac{\lambda_0}{2}} |\varphi'|^{\frac{1}{2}} h \right\|_H \right) \leq C(1 + \|h\|_{L^2(\mathbb{R}^3)}) \end{aligned}$$

for every $h \in L^2(\mathbb{R}^3)$ after using (6.14) and that $e^{-\frac{\lambda_0}{2}} |\varphi'|^{\frac{1}{2}} h \in H$. \square

We now show the fixed-point equation that fully characterizes the generator of Π^s , as defined in (6.8). For the notion of the generator of a function in $\ker(\mathcal{B})$, recall Lemma 4.3.8.

Proposition 6.2.7. *For $s \geq 0$ the following holds:*

(a) *If $g^s \in \ker(\mathcal{T})$ is the generator of Π^s , the function*

$$h := \frac{e^{\frac{\lambda_0}{2}}}{|\varphi'|^{\frac{1}{2}}} g^s \in L^2(\mathbb{R}^3)$$

satisfies the equation $G(s)h = h$ a.e. on Ω_0 and $h = 0$ a.e. on $\mathbb{R}^3 \setminus \Omega_0$.

(b) If $h \in L^2(\mathbb{R}^3)$ solves $G(s)h = h$ a.e. on Ω_0 and $h = 0$ a.e. on $\mathbb{R}^3 \setminus \Omega_0$, the generator of Π^s is given by

$$g^s := e^{-\frac{\lambda_0}{2}} |\varphi'|^{\frac{1}{2}} h \in H.$$

Proof. From the definition of the orthogonal projection, (6.8), and the uniqueness of the generator, as shown in Lemma 4.3.8, we deduce that $g^s \in \ker(\mathcal{T})$ is the generator of Π^s if, and only if,

$$P^s(g^s) := |\varphi'| E e^{-\lambda_0 - \mu_0} \mathbf{1}_{[0,s]} - \left(g^s + 4\pi |\varphi'| E e^{-\lambda_0 - \mu_0} \int_r^{R_{\max}} e^{(3\lambda_0 + \mu_0)(\sigma)} p_{g^s}(\sigma) \sigma d\sigma \right)$$

is an element in $\ker(\mathcal{B})^\perp$. By Proposition 4.3.5(e), this is equivalent to

$$\int_0^1 \left(P^s(g^s) + |\varphi'| e^{2\mu_0(R(\theta))} \lambda_{P^s(g^s)}(R(\theta)) \frac{W^2}{E} \right) d\theta = 0 \text{ for a.e. } (E, L) \in \Omega_0^{EL},$$

where we employed the shorthand $R(\theta) = R(\theta, E, L)$ and $W(\theta) = W(\theta, E, L)$. For fixed $(E, L) \in \tilde{\Omega}_0^{EL}$, we insert the formula for $P^s(g^s)$ and arrive at

$$\begin{aligned} g^s(E, L) &= |\varphi'| E \int_0^1 e^{-(\lambda_0 + \mu_0)(R(\theta))} \mathbf{1}_{[0,s]}(R(\theta)) d\theta \\ &\quad - 4\pi |\varphi'| E \int_0^1 e^{-(\lambda_0 + \mu_0)(R(\theta))} \int_{R(\theta)}^{R_{\max}} e^{(3\lambda_0 + \mu_0)(\sigma)} p_{g^s}(\sigma) \sigma d\sigma d\theta \\ &\quad + |\varphi'| \int_0^1 \frac{E^2 - \Psi_L^2(R(\theta))}{E} \left(\lambda_{|\varphi'| E e^{-\lambda_0 - \mu_0} \mathbf{1}_{[0,s]}}(R(\theta)) - \lambda_{g^s}(R(\theta)) \right. \\ &\quad \left. - 4\pi \lambda_{|\varphi'| E e^{-\lambda_0 - \mu_0} \int_\sigma^{R_{\max}} e^{(3\lambda_0 + \mu_0)(\eta)} p_{g^s}(\eta) \eta d\eta}(R(\theta)) \right) d\theta. \end{aligned} \tag{6.15}$$

Here we have used that $g^s = g^s(E, L)$, according to Proposition 4.3.2(e), and the identity $e^{2\mu_0(R(\theta))} W^2 = E^2 - \Psi_L^2(R(\theta))$. For the first term, we note that the integrand is even in w such that

$$\int_0^1 e^{-(\lambda_0 + \mu_0)(R(\theta))} \mathbf{1}_{[0,s]}(R(\theta)) d\theta = 2 \int_0^{\frac{1}{2}} e^{-(\lambda_0 + \mu_0)(R(\theta))} \mathbf{1}_{[0,s]}(R(\theta)) d\theta;$$

recall (4.12). The following cases can appear due to $r_-(E, L) \leq R(\theta, E, L) \leq r_+(E, L)$: If $s < r_-(E, L)$, the indicator function vanishes on $[0, \frac{1}{2}]$, and if $s > r_+(E, L)$, the indicator function is always 1. In the remaining case, where $r_-(E, L) \leq s \leq r_+(E, L)$, the indicator function vanishes for $\theta > \theta(s, E, L)$. In all three cases, we conclude

$$\int_0^1 e^{-(\lambda_0 + \mu_0)(R(\theta))} \mathbf{1}_{[0,s]}(R(\theta)) d\theta = 2 \int_0^{\theta(s, E, L)} e^{-(\lambda_0 + \mu_0)(R(\theta))} d\theta, \tag{6.16}$$

because of the continuous extension of the angle function in (3.30). Moreover, from the explicit formula in (4.8), we get

$$\begin{aligned}\lambda_{|\varphi'|E} e^{-\lambda_0 - \mu_0} \mathbf{1}_{[0,s]}(r) &= \frac{4\pi e^{2\lambda_0(r)}}{r} \int_0^{\min(r,s)} e^{-(\lambda_0 + \mu_0)(\sigma)} \rho_{|\varphi'|E}(\sigma) \sigma^2 d\sigma \\ &= \frac{4\pi e^{2\lambda_0(r)}}{r} \int_0^{\min(r,s)} e^{-\lambda_0(\sigma)} M_{2,\varphi}(\sigma) \sigma^2 d\sigma\end{aligned}\quad (6.17)$$

as well as

$$\begin{aligned}\lambda_{|\varphi'|E} e^{-\lambda_0 - \mu_0} \int_{\sigma}^{R_{\max}} e^{(3\lambda_0 + \mu_0)(\eta)} p_{g^s}(\eta) \eta d\eta(r) \\ &= \frac{4\pi e^{2\lambda_0(r)}}{r} \int_0^r \left(\int_{\sigma}^{R_{\max}} e^{(3\lambda_0 + \mu_0)(\eta)} p_{g^s}(\eta) \eta d\eta \right) e^{-(\lambda_0 + \mu_0)(\sigma)} \rho_{|\varphi'|E}(\sigma) \sigma^2 d\sigma \\ &= \frac{4\pi e^{2\lambda_0(r)}}{r} \int_0^r \sigma^2 e^{-\lambda_0(\sigma)} M_{2,\varphi}(\sigma) \int_{\sigma}^{R_{\max}} e^{(3\lambda_0 + \mu_0)(\eta)} p_{g^s}(\eta) \eta d\eta d\sigma,\end{aligned}\quad (6.18)$$

for every $r > 0$, where $M_{2,\varphi}$ is defined in (6.10). Putting the three identities (6.16)–(6.18) back into (6.15) yields that g^s is the generator of Π^s if, and only if,

$$g^s = \sum_{j=1}^5 G_j(s) g^s$$

for the auxiliary operators G_j introduced in Definition 6.2.5. From this, the claims in (a) and (b) follow immediately when we consider the different weights that appear in the operator $G(s)$. \square

We need to analyze the fixed-point operator $G(s)$ further in order to find out more about the generator of Π^s . In fact, we establish a compactness result for $G(s)$, which will play a crucial role later when proving a continuity result for Π^s in the redshift κ .

Lemma 6.2.8. *For every $s \geq 0$, the operator $G(s): L^2(\mathbb{R}^3) \rightarrow L^2(\mathbb{R}^3)$ is compact in the sense that*

$$G(s)h_n \rightarrow G(s)h \text{ in } L^2(\mathbb{R}^3) \text{ for } n \rightarrow \infty,$$

if $h_n \rightarrow h$ in $L^2(\mathbb{R}^3)$ for $n \rightarrow \infty$.¹

Proof. Let $h_n \rightarrow h$ in $L^2(\mathbb{R}^3)$ for $n \rightarrow \infty$. From the definition $G(s)$ in (6.11), we have

$$\|G(s)h_n - G(s)h\|_{L^2(\mathbb{R}^3)} \leq \left\| \frac{e^{\frac{\lambda_0}{2}}}{|\varphi'|^{\frac{1}{2}}} \sum_{j \in \{2,4,5\}} G_j(s) \left(e^{-\frac{\lambda_0}{2}} |\varphi'|^{\frac{1}{2}} (h_n - h) \right) \right\|_{L^2(\mathbb{R}^3)},$$

¹Note that $G(s)$ is not linear but includes affine terms that do not depend on the argument. Compactness for $G(s)$ thus refers to compactness in the sense of affine transformations which is defined analogously as for linear operators.

since the terms involving $G_1(s)$ and $G_3(s)$ vanish in the difference. We consider the three addends separately. Throughout the proof, $C > 0$ denotes a constant which may change from line to line and is independent of n . The weak convergence implies

$$\begin{aligned} & \left| \int_{R(\theta, E, L)}^{R_{\max}} e^{(3\lambda_0 + \mu_0)(r)} p_{|\varphi'|^{\frac{1}{2}}(h_n - h)}(r) r \, dr \right| \\ & \leq C \left| \iiint_{\Omega_0} e^{(3\lambda_0 + \mu_0)(r)} \frac{\mathbf{1}_{[R(\theta, E, L), R_{\max}]}(r)}{r} \frac{w^2}{\langle v \rangle} |\varphi'|^{\frac{1}{2}}(h_n - h)(r, w, L) \, dr \, dw \, dL \right| \\ & \leq C \left| \left\langle \mathbf{1}_{\Omega_0} e^{(3\lambda_0 + \mu_0)(r)} \frac{\mathbf{1}_{[R(\theta, E, L), R_{\max}]}(r)}{r} \frac{w^2}{\langle v \rangle} |\varphi'|^{\frac{1}{2}}, h_n - h \right\rangle_{L^2(\mathbb{R}^3)} \right| \rightarrow 0, \quad n \rightarrow \infty, \end{aligned}$$

for a.e. $(\theta, E, L) \in [0, 1] \times \tilde{\Omega}_0^{EL}$. In addition, Lemma 6.2.1(f) yields the bound

$$\left| \int_{R(\theta, E, L)}^{R_{\max}} e^{(3\lambda_0 + \mu_0)(r)} p_{|\varphi'|^{\frac{1}{2}}(h_n - h)}(r) r \, dr \right| \leq C \|(h_n - h) |\varphi'|^{\frac{1}{2}}\|_H \leq C \|h_n - h\|_{L^2(\mathbb{R}^3)} \leq C$$

for a.e. $(\theta, E, L) \in [0, 1] \times \tilde{\Omega}_0^{EL}$, since weakly convergent sequences are bounded. Lebesgue's theorem thus proves that

$$\lim_{n \rightarrow \infty} \int_0^1 \int_{R(\theta, E, L)}^{R_{\max}} e^{(3\lambda_0 + \mu_0)(r)} p_{|\varphi'|^{\frac{1}{2}}(h_n - h)}(r) r \, dr \, d\theta = 0$$

for a.e. $(E, L) \in \tilde{\Omega}_0^{EL}$, and this sequence is again bounded in n and a.e. in (E, L) . By again applying Lebesgue's theorem and using (S5'), we obtain

$$\lim_{n \rightarrow \infty} \left\| |\varphi'|^{\frac{1}{2}} \int_0^1 \int_{R(\theta)}^{R_{\max}} e^{(3\lambda_0 + \mu_0)(r)} p_{|\varphi'|^{\frac{1}{2}}(h_n - h)}(r) r \, dr \, d\theta \right\|_{L^2(\mathbb{R}^3)} = 0. \quad (6.19)$$

The term involving G_2 can now be estimated by

$$\left| \frac{e^{\frac{\lambda_0}{2}}}{|\varphi'|^{\frac{1}{2}}} G_2(s) \left(e^{-\frac{\lambda_0}{2}} |\varphi'|^{\frac{1}{2}}(h_n - h) \right) \right| \leq C |\varphi'|^{\frac{1}{2}} \int_0^1 \left| \int_{R(\theta)}^{R_{\max}} e^{(3\lambda_0 + \mu_0)(r)} p_{|\varphi'|^{\frac{1}{2}}(h_n - h)}(\sigma) \sigma \, d\sigma \right| d\theta,$$

which converges to zero for $n \rightarrow \infty$ in $L^2(\mathbb{R}^3)$ due to (6.19). Similarly, we estimate

$$\left| \frac{e^{\frac{\lambda_0}{2}}}{|\varphi'|^{\frac{1}{2}}} G_4(s) \left(e^{-\frac{\lambda_0}{2}} |\varphi'|^{\frac{1}{2}}(h_n - h) \right) \right| \leq C |\varphi'|^{\frac{1}{2}} \int_0^1 \frac{1}{R(\theta)} \left| \int_{R(\theta)}^{R_{\max}} \rho_{|\varphi'|^{\frac{1}{2}}(h_n - h)}(\sigma) \sigma^2 \, d\sigma \right| d\theta. \quad (6.20)$$

Analogous to the case above, we get

$$\lim_{n \rightarrow \infty} \frac{1}{R(\theta, E, L)} \int_0^{R(\theta, E, L)} \rho_{|\varphi'|^{\frac{1}{2}}(h_n - h)}(\sigma) \sigma^2 \, d\sigma = 0$$

for a.e. $(\theta, E, L) \in [0, 1] \times \tilde{\Omega}_0^{EL}$, where the integrable majorant is obtained by

$$\left| \frac{1}{R(\theta, E, L)} \int_0^{R(\theta, E, L)} \rho_{|\varphi'|^{\frac{1}{2}}(h_n - h)}(\sigma) \sigma^2 d\sigma \right| \leq \int_0^{R_{\max}} \rho_{|\varphi'|^{\frac{1}{2}}|h_n - h|}(\sigma) \sigma d\sigma \leq C$$

after again using Lemma 6.2.1(f). From this point, we continue as with G_2 to obtain convergence of (6.20) in $L^2(\mathbb{R}^3)$.

For the last term G_5 , we proceed in exactly the same manner, but we have to eliminate one more radial integral; recall that $M_{2, \varphi}$ is uniformly bounded, as shown in Lemma 6.2.1(e). \square

We emphasize that we change back to the notation mentioned at the beginning of Section 6.1 since we now consider a family of steady states (f_κ) .

6.2.3 Continuity of the projection operator

The goal of this subsection is to show that the projection term

$$\Pi_\kappa^s := \Pi_\kappa \left(|\varphi'_\kappa| E_\kappa e^{-\lambda_\kappa - \mu_\kappa} \mathbb{1}_{[0, s]} \right) \quad (6.21)$$

is continuous in κ for every $s \geq 0$. From Lemma 4.3.8, we know that Π_κ^s is characterized by its generator $g_\kappa^s = g_\kappa^s(E, L) \in \ker(\mathcal{T})$ via

$$\Pi_\kappa^s = g_\kappa^s + 4\pi |\varphi'_\kappa| E_\kappa e^{-\lambda_\kappa - \mu_\kappa} \int_r^{R_{\kappa, \max}} e^{(3\lambda_\kappa + \mu_\kappa)(\sigma)} p_{g_\kappa^s}(\sigma) \sigma d\sigma. \quad (6.22)$$

The procedure is as follows: We consider a sequence $(\kappa_n) \subset]0, \infty[$ such that $\kappa_n \rightarrow \kappa_0 > 0$ and show that the corresponding generators $(g_{\kappa_n}^s)$ are bounded uniformly in n . We then extract a weakly convergent subsequence from $(g_{\kappa_n}^s)$ and use that $G(s)$ is compact in the sense of Lemma 6.2.8. From the fixed-point equation and a “sub-subsequence” argument, we obtain the continuity of the generators in κ , which consequently yields the continuity of Π_κ^s . We start by bounding the generators uniformly in κ . The proof involves many properties of the operators derived in Section 4.3 and relies on a Sobolev-embedding in the angle-variable.

Lemma 6.2.9. *Let $\kappa_0 > 0$ and $s \geq 0$. There exist $\delta > 0$ and $C > 0$ such that for every $|\kappa - \kappa_0| < \delta$ the generators g_κ^s corresponding to Π_κ^s satisfy*

$$\|g_\kappa^s\|_{H_\kappa} \leq C.$$

In particular, the functions

$$h_\kappa^s := e^{\frac{\lambda_\kappa}{2}} |\varphi'_\kappa|^{-\frac{1}{2}} g_\kappa^s$$

are uniformly bounded in $L^2(\mathbb{R}^3)$ for $|\kappa - \kappa_0| < \delta$.

Proof. Throughout the proof, $C > 0$ denotes a constant which does not depend on $\kappa > 0$ with $|\kappa - \kappa_0| < \delta$ and may change from line to line. Lemma 4.3.8 yields that the generator

of Π_κ^s is given by the equation

$$g_\kappa^s(E, L) = \Pi_\kappa^s\left(\frac{1}{2}, E, L\right) - 4\pi|\varphi'_\kappa(E, L)|E \int_{r_{\kappa,+}(E,L)}^{R_{\kappa,\max}} e^{2\lambda_\kappa(\sigma)} p_{\Pi_\kappa^s}(\sigma) \sigma d\sigma \quad (6.23)$$

for a.e. $(E, L) \in \Omega_\kappa^{EL}$. In the first step, we control $\Pi_\kappa^s(\frac{1}{2}, E, L)$. Due to the fact that $\Pi_\kappa^s \in \ker(\mathcal{B}) \subset \mathcal{D}(\mathcal{T})$ and because of Proposition 4.3.2(d), we obtain

$$\Pi_\kappa^s(\cdot, E, L) \in H_\theta^1$$

for a.e. $(E, L) \in \Omega_\kappa^{EL}$, where H_θ^1 is defined in (4.19). The Sobolev embedding $H^1(]0, 1[) \hookrightarrow C([0, 1])$ implies the existence of $C > 0$ independent from (E, L) with

$$|\Pi_\kappa^s(\theta, E, L)| \leq C \|\Pi_\kappa^s(\cdot, E, L)\|_{H_\theta^1}, \quad \theta \in [0, 1],$$

for the continuous representative of $\Pi_\kappa^s(\cdot, E, L)$ and a.e. $(E, L) \in \Omega_\kappa^{EL}$. We express the norm of Π_κ^s in action-angle type variables, see Lemma 2.3.17(c), and consequently estimate

$$\begin{aligned} \left\| \Pi_\kappa^s\left(\frac{1}{2}, \cdot, \cdot\right) \right\|_{H_\kappa}^2 &= 4\pi^2 \iint_{\Omega_\kappa^{EL}} \frac{T_\kappa(E, L)}{|\varphi'_\kappa(E, L)|} \int_0^1 \left| \Pi_\kappa^s\left(\frac{1}{2}, E, L\right) \right|^2 d\theta dEdL \\ &\leq C \iint_{\Omega_\kappa^{EL}} \frac{T_\kappa(E, L)}{|\varphi'_\kappa(E, L)|} \|\Pi_\kappa^s(\cdot, E, L)\|_{H_\theta^1}^2 dEdL \\ &= C \iint_{\Omega_\kappa^{EL}} \frac{T_\kappa(E, L)}{|\varphi'_\kappa(E, L)|} \int_0^1 (|\Pi_\kappa^s(\theta, E, L)|^2 + |\partial_\theta \Pi_\kappa^s(\theta, E, L)|^2) d\theta dEdL \\ &= C (\|\Pi_\kappa^s\|_{H_\kappa}^2 + \|\partial_\theta \Pi_\kappa^s\|_{H_\kappa}^2). \end{aligned} \quad (6.24)$$

The more difficult part is to control the derivative $\partial_\theta \Pi_\kappa^s$. We apply the representation of elements in $\ker(\mathcal{B})$ given in Lemma 4.3.8(a) to Π_κ^s and differentiate this relation in θ , which yields

$$\begin{aligned} \partial_\theta \Pi_\kappa^s(\theta, E, L) &= 4\pi|\varphi'_\kappa(E, L)|E \partial_\theta \left(\int_{R_\kappa(\theta, E, L)}^{R_{\kappa,\max}} e^{2\lambda_\kappa(\sigma)} p_{\Pi_\kappa^s}(\sigma) \sigma d\sigma \right) \\ &= -4\pi|\varphi'_\kappa(E, L)|E (\partial_\theta R_\kappa)(\theta, E, L) e^{2\lambda_\kappa(R_\kappa(\theta, E, L))} p_{\Pi_\kappa^s}(R_\kappa(\theta, E, L)) R_\kappa(\theta, E, L) \\ &= -4\pi|\varphi'_\kappa(E, L)| \left(e^{(2\mu_\kappa + \lambda_\kappa)(R_\kappa)} T_\kappa W_\kappa p_{\Pi_\kappa^s}(R_\kappa) R_\kappa \right) (\theta, E, L), \end{aligned}$$

where we used the characteristic equation (4.17a). Because of Lemma 6.2.1, we bound

$$e^{(2\mu_\kappa + \lambda_\kappa)(R_\kappa)} W_\kappa \leq C$$

independently from κ and (θ, E, L) . By assumption (S2'), the period function is bounded

uniformly as well. In conclusion, we have

$$|\partial_\theta \Pi_\kappa^s| \leq C |\varphi'_\kappa| r |p_{\Pi_\kappa^s}|$$

a.e. on Ω_κ . Therefore, Lemma 6.2.1 implies that

$$\|\partial_\theta \Pi_\kappa^s\|_{H_\kappa} \leq C \|\varphi'_\kappa\|_{H_\kappa} \|r p_{\Pi_\kappa^s}\|_{H_\kappa} \leq C \|r p_{\Pi_\kappa^s}\|_{L^2([0, R_{\kappa, \max}])} \leq C \|\Pi_\kappa^s\|_{H_\kappa}$$

after possibly shrinking δ . Together with (6.24), we get

$$\left\| \Pi_\kappa^s \left(\frac{1}{2}, \cdot, \cdot \right) \right\|_{H_\kappa} \leq C \|\Pi_\kappa^s\|_{H_\kappa} \quad (6.25)$$

and have thus eliminated the derivative along θ . Equation (6.23) and estimate (6.25) yield

$$\begin{aligned} \|g_\kappa^s\|_{H_\kappa} &= \left\| \Pi_\kappa^s \left(\frac{1}{2}, \cdot, \cdot \right) - 4\pi |\varphi'_\kappa| E_\kappa \int_{r_{\kappa,+}}^{R_{\kappa, \max}} e^{2\lambda_\kappa(\sigma)} p_{\Pi_\kappa^s}(\sigma) \sigma \, d\sigma \right\|_{H_\kappa} \\ &\leq \left\| \Pi_\kappa^s \left(\frac{1}{2}, E, L \right) \right\|_{H_\kappa} + C \left\| |\varphi'_\kappa| \int_0^{R_{\kappa_0, \max}+1} p_{\Pi_\kappa^s}(\sigma) \sigma \, d\sigma \right\|_{H_\kappa} \leq C \|\Pi_\kappa^s\|_{H_\kappa} \end{aligned}$$

for every $\kappa > 0$ with $|\kappa - \kappa_0| < \delta$ which again is due to the bounds and estimates established in Lemma 6.2.1. In the final step, we use that the operator norm of an orthogonal projection satisfies $\|\Pi_\kappa\| \leq 1$, which implies that

$$\begin{aligned} \|g_\kappa^s\|_{H_\kappa} &\leq C \|\Pi_\kappa^s\|_{H_\kappa} = C \left\| \Pi_\kappa \left(|\varphi'_\kappa| E_\kappa e^{-\lambda_\kappa - \mu_\kappa} \mathbf{1}_{[0, s]} \right) \right\|_{H_\kappa} \\ &\leq C \left\| |\varphi'_\kappa| E_\kappa e^{-\lambda_\kappa - \mu_\kappa} \mathbf{1}_{[0, s]} \right\|_{H_\kappa} \leq C \end{aligned}$$

due to Lemma 6.2.1(b) and (e). The last claim in the lemma follows immediately since $\|g_\kappa^s\|_{H_\kappa} = \|h_\kappa^s\|_{L^2(\mathbb{R}^3)}$ by definition. \square

Before we can finally come to the continuity of the generator g_κ^s in κ , we have to further investigate the fixed-point operator. We first show a boundedness result for $G(s)$ in an appropriate sense.

Lemma 6.2.10. *For $\kappa_0 > 0$ and $s \geq 0$, there exist $\delta > 0$ and $C > 0$ such that for every $\kappa > 0$ with $|\kappa - \kappa_0| < \delta$ it holds that*

$$|G_\kappa(s)h| \leq C |\varphi'_\kappa|^{\frac{1}{2}} (1 + \|h\|_{L^2(\mathbb{R}^3)}), \quad h \in L^2(\mathbb{R}^3),$$

almost everywhere.

Proof. The proof comes down to similar arguments that were already established in the proof of Lemma 6.2.6, now being applied locally uniformly in κ . We thus keep

the reasoning rather short. By making δ small enough, we can uniformly bound the metric coefficients in κ and in r due to Lemma 6.2.1. Recall the auxiliary operators $G_{\kappa,j}$ defined in Definition 6.2.5, which now depend on κ as well. For fixed $h \in L^2(\mathbb{R}^3)$ and $g_\kappa := e^{-\frac{\lambda_\kappa}{2}} |\varphi'_\kappa|^{\frac{1}{2}} h$, we get

$$|G_{\kappa,1}(s)g_\kappa|, |G_{\kappa,3}(s)g_\kappa| \leq C|\varphi'_\kappa|,$$

almost everywhere. Here, $C > 0$ is a constant which does not depend on κ or h and may change from line to line. From Lemma 6.2.1(f), we get

$$\frac{1}{r} \int_0^r (|\rho_{g_\kappa}(\sigma)| + |p_{g_\kappa}(\sigma)|)\sigma^2 d\sigma \leq \int_0^{R_{\kappa_0} + \max + 1} (|\rho_{g_\kappa}(\sigma)| + |p_{g_\kappa}(\sigma)|)\sigma d\sigma \leq C\|g_\kappa\|_{H_\kappa} \quad (6.26)$$

for $r > 0$. As in (6.13), we thus obtain

$$|G_{\kappa,j}(s)g_\kappa| \leq C|\varphi'_\kappa|(1 + \|g_\kappa\|_{H_\kappa}) \leq C|\varphi'_\kappa|(1 + \|h\|_{L^2(\mathbb{R}^3)}),$$

a.e. for $j \in \{1, \dots, 5\}$. In particular,

$$|G_\kappa(s)h| \leq C|\varphi'_\kappa|^{-\frac{1}{2}} \sum_{j=1}^5 |G_{\kappa,j}(s)g_\kappa| \leq C|\varphi'_\kappa|^{\frac{1}{2}}(1 + \|h\|_{L^2(\mathbb{R}^3)}). \quad \square$$

Next, we show that $G_\kappa(s)h$ is continuous in κ for a fixed choice of h . From this point on, the continuity and differentiability results from Chapter 3 are indispensable.

Lemma 6.2.11. *For $s \geq 0$ and $\kappa_0 > 0$, it holds that²*

$$\lim_{\kappa \rightarrow \kappa_0} \|G_\kappa(s) - G_{\kappa_0}(s)\| := \lim_{\kappa \rightarrow \kappa_0} \sup_{\substack{h \in L^2(\mathbb{R}^3) \\ \|h\|_{L^2(\mathbb{R}^3)} = 1}} \|G_\kappa(s)h - G_{\kappa_0}(s)h\|_{L^2(\mathbb{R}^3)} = 0.$$

Proof. Fix $\kappa_0 > 0$ and $\varepsilon > 0$. Let $h \in L^2(\mathbb{R}^3)$ with $\|h\|_{L^2(\mathbb{R}^3)} = 1$ be arbitrary. According to Lemma 6.2.1(a), there exists a compact set K and $\delta > 0$ such that for every $\kappa > 0$ with $|\kappa - \kappa_0| < \delta$ it holds that $K \subset \Omega_\kappa$ and

$$\iiint_{\Omega_\kappa \setminus K} drdwdL < \varepsilon.$$

From the definition of $G_\kappa(s)$, we get

$$\begin{aligned} & \|G_\kappa(s)h - G_{\kappa_0}(s)h\|_{L^2(\mathbb{R}^3)} \\ & \leq \|G_\kappa(s)h - G_{\kappa_0}(s)h\|_{L^2(K)} + \|G_\kappa(s)h\|_{L^2(\Omega_\kappa \setminus K)} + \|G_{\kappa_0}(s)h\|_{L^2(\Omega_{\kappa_0} \setminus K)} \end{aligned}$$

²For linear operators, this corresponds to continuity in the operator norm. Since G_κ is affine linear, this can be interpreted as an analogous result.

and estimate the latter two terms via the bound from Lemma 6.2.10, which implies the existence of $C > 0$ such that

$$\|G_\kappa(s)h\|_{L^2(\Omega_\kappa \setminus K)} \leq C \|\varphi'_\kappa\|_{L^2(\Omega_\kappa \setminus K)} \leq C\varepsilon$$

for every $|\kappa - \kappa_0| < \delta$ small enough due to (S5'). Note that C does not depend on h because of $\|h\|_{L^2(\mathbb{R}^3)} = 1$. Since $\varepsilon > 0$ is arbitrary, it is sufficient to show that

$$\sup_{\substack{h \in L^2(\mathbb{R}^3) \\ \|h\|_{L^2(\mathbb{R}^3)} = 1}} \|G_\kappa(s)h - G_{\kappa_0}(s)h\|_{L^2(K)} \rightarrow 0, \quad \kappa \rightarrow \kappa_0, \quad (6.27)$$

where K is now a fixed compact set. From now on, we do not write the index κ_0 anymore but instead the index 0 for better readability. The constant $C > 0$ does not depend on κ or h and may change from line to line.

We analyze the five terms appearing in definition (6.11) separately, now restricted to the compact set K and $h \in L^2(\mathbb{R}^3)$ with $\|h\|_{L^2(\mathbb{R}^3)} = 1$.

Term no. 1: As to the first term, the estimate

$$\begin{aligned} & \left\| e^{\frac{\lambda_\kappa}{2}} |\varphi'_\kappa|^{-\frac{1}{2}} G_{\kappa,1}(s) \left(e^{-\frac{\lambda_\kappa}{2}} |\varphi'_\kappa|^{\frac{1}{2}} h \right) - e^{\frac{\lambda_0}{2}} |\varphi'_0|^{-\frac{1}{2}} G_{0,1}(s) \left(e^{-\frac{\lambda_0}{2}} |\varphi'_0|^{\frac{1}{2}} h \right) \right\|_{L^2(K)} \\ &= \left\| 2e^{\frac{\lambda_\kappa}{2}} |\varphi'_\kappa|^{\frac{1}{2}} E_\kappa \int_0^{\theta_\kappa(s, E_\kappa, L)} e^{-(\lambda_\kappa + \mu_\kappa)(R_\kappa(\theta, E_\kappa, L))} d\theta \right. \\ & \quad \left. - 2e^{\frac{\lambda_0}{2}} |\varphi'_0|^{\frac{1}{2}} E_0 \int_0^{\theta_0(s, E_0, L)} e^{-(\lambda_0 + \mu_0)(R_0(\theta, E_0, L))} d\theta \right\|_{L^2(K)} \\ &\leq C \left\| e^{\frac{\lambda_\kappa}{2}} |\varphi'_\kappa|^{\frac{1}{2}} E_\kappa - e^{\frac{\lambda_0}{2}} |\varphi'_0|^{\frac{1}{2}} E_0 \right\|_{L^2(K)} \\ & \quad + C \left\| |\varphi'_0|^{\frac{1}{2}} \int_{\theta_0(s, E_0, L)}^{\theta_\kappa(s, E_\kappa, L)} e^{-(\lambda_\kappa + \mu_\kappa)(R_\kappa(\theta, E_\kappa, L))} d\theta \right\|_{L^2(K)} \\ & \quad + C \left\| |\varphi'_0|^{\frac{1}{2}} \int_0^{\theta_0(s, E_0, L)} \left(e^{-(\lambda_\kappa + \mu_\kappa)(R_\kappa(\theta, E_\kappa, L))} - e^{-(\lambda_0 + \mu_0)(R_0(\theta, E_0, L))} \right) d\theta \right\|_{L^2(K)} \\ &=: I_{11} + I_{12} + I_{13} \end{aligned}$$

follows from the (uniform) boundedness of the metric coefficients, $\theta_\kappa \leq \frac{1}{2}$, and the triangle inequality applied twice. The term I_{11} converges to zero due to the uniform continuity of the integrand in κ over K , as discussed in Lemma 6.2.1, which also yields bounds on μ_κ and λ_κ . These bounds imply

$$\left| \int_{\theta_0(s, E_0, L)}^{\theta_\kappa(s, E_\kappa, L)} e^{-(\lambda_\kappa + \mu_\kappa)(R_\kappa(\theta, E_\kappa, L))} d\theta \right| \leq C |\theta_\kappa(s, E_\kappa, L) - \theta_0(s, E_0, L)|.$$

We claim that the right-hand side converges pointwise to zero for $\kappa \rightarrow \kappa_0$ a.e. on K . In the case where $s \in]r_{0,-}(E_0, L), r_{0,+}(E_0, L)[$, this follows from the continuity of the energy, $r_{\kappa,\pm}$, and the angle-function, as shown in Corollary 3.2.4 and Proposition 3.2.8. If $s < r_{0,-}(E_0, L)$, we have $\lim_{\kappa \rightarrow \kappa_0} \theta_\kappa(s, E_\kappa, L) = 0 = \theta_0(s, E_0, L)$ by (3.30), since $r_{\kappa,-}$ is continuous. Similar reasoning yields $\lim_{\kappa \rightarrow \kappa_0} \theta_\kappa(s, E_\kappa, L) = 1 = \theta_0(s, E_0, L)$, if $r_{0,+}(E_0, L) < s$. The remaining edge cases form a set of measure zero in K . By using the L^1 -majorant $C|\varphi'_0|$, Lebesgue's theorem implies $I_{12} \rightarrow 0$ for $\kappa \rightarrow \kappa_0$. The uniform continuity mentioned above further yields

$$\int_0^{\theta_0(s, E_0, L)} \left(e^{-(\lambda_\kappa + \mu_\kappa)(R_\kappa(\theta, E_\kappa, L))} - e^{-(\lambda_0 + \mu_0)(R_0(\theta, E_0, L))} \right) d\theta \rightarrow 0, \quad \kappa \rightarrow \kappa_0,$$

a.e. on K , and via the same argument as for I_{12} , we deduce convergence of I_{13} to zero.

Term no. 2: We proceed in similar manner as for the first term and estimate

$$\begin{aligned} & \left\| e^{\frac{\lambda_\kappa}{2} |\varphi'_\kappa|^{-\frac{1}{2}}} G_{\kappa,2}(s) \left(e^{-\frac{\lambda_\kappa}{2} |\varphi'_\kappa|^{\frac{1}{2}} h} \right) - e^{\frac{\lambda_0}{2} |\varphi'_0|^{-\frac{1}{2}}} G_{0,2}(s) \left(e^{-\frac{\lambda_0}{2} |\varphi'_0|^{\frac{1}{2}} h} \right) \right\|_{L^2(K)} \\ & \leq C \left\| \left(e^{\frac{\lambda_\kappa}{2} |\varphi'_\kappa|^{\frac{1}{2}} E_\kappa} - e^{\frac{\lambda_0}{2} |\varphi'_0|^{\frac{1}{2}} E_0} \right) \right. \\ & \quad \cdot \int_0^1 e^{-(\mu_\kappa + \lambda_\kappa)(R_\kappa(\theta, E_\kappa, L))} \int_{R_\kappa(\theta, E_\kappa, L)}^{R_{\kappa, \max}} e^{(\frac{5}{2} \lambda_\kappa + \mu_\kappa)(\sigma)} p_{|\varphi'_\kappa|^{\frac{1}{2}} h}(\sigma) \sigma d\sigma d\theta \left. \right\|_{L^2(K)} \\ & + C \left\| |\varphi'_0|^{\frac{1}{2}} \int_0^1 \left(e^{-(\mu_\kappa + \lambda_\kappa)(R_\kappa(\theta, E_\kappa, L))} - e^{-(\mu_0 + \lambda_0)(R_0(\theta, E_0, L))} \right) \right. \\ & \quad \cdot \int_{R_\kappa(\theta, E_\kappa, L)}^{R_{\kappa, \max}} e^{(\frac{5}{2} \lambda_\kappa + \mu_\kappa)(\sigma)} p_{|\varphi'_\kappa|^{\frac{1}{2}} h}(\sigma) \sigma d\sigma d\theta \left. \right\|_{L^2(K)} \\ & + C \left\| |\varphi'_0|^{\frac{1}{2}} \int_0^1 e^{-(\mu_0 + \lambda_0)(R_0(\theta, E_0, L))} \left(\int_{R_\kappa(\theta, E_\kappa, L)}^{R_{\kappa, \max}} e^{(\frac{5}{2} \lambda_\kappa + \mu_\kappa)(\sigma)} p_{|\varphi'_\kappa|^{\frac{1}{2}} h}(\sigma) \sigma d\sigma \right. \right. \\ & \quad \left. \left. - \int_{R_0(\theta, E_0, L)}^{R_{0, \max}} e^{(\frac{5}{2} \lambda_0 + \mu_0)(\sigma)} p_{|\varphi'_0|^{\frac{1}{2}} h}(\sigma) \sigma d\sigma \right) d\theta \right\|_{L^2(K)} \\ & =: I_{21} + I_{22} + I_{23}. \end{aligned}$$

We observe that

$$\left| \int_{R_\kappa(\theta, E_\kappa, L)}^{R_{\kappa, \max}} e^{(\frac{5}{2} \lambda_\kappa + \mu_\kappa)(\sigma)} p_{|\varphi'_\kappa|^{\frac{1}{2}} h}(\sigma) \sigma d\sigma \right| \leq \int_0^{R_{0, \max} + 1} |p_{|\varphi'_\kappa|^{\frac{1}{2}} h}(\sigma)| \sigma d\sigma \leq C \|h\|_{L^2(\mathbb{R}^3)} \leq C$$

for $|\kappa - \kappa_0| < \delta$ as per Lemma 6.2.1(f). This together with the uniform bounds on the metric coefficients implies that

$$I_{21} \leq C \left\| e^{\frac{\lambda_\kappa}{2} |\varphi'_\kappa|^{\frac{1}{2}} E_\kappa} - e^{\frac{\lambda_0}{2} |\varphi'_0|^{\frac{1}{2}} E_0} \right\|_{L^2(K)} = C I_{11},$$

which converges to zero for $\kappa \rightarrow \kappa_0$, as shown above. Similarly, we get that

$$I_{22} \leq C \left\| |\varphi'_0|^{\frac{1}{2}} \int_0^1 \left(e^{-(\mu_\kappa + \lambda_\kappa)(R_\kappa(\theta, E_\kappa, L))} - e^{-(\mu_0 + \lambda_0)(R_0(\theta, E_0, L))} \right) d\theta \right\|_{L^2(K)}$$

approaches zero for $\kappa \rightarrow \kappa_0$ due to the uniform convergence in the θ -integral and Lebesgue's theorem applied with majorant $C|\varphi'_0|$ in analogy to I_{13} . The third term I_{23} requires a more elaborate argument. We fix $\theta \in [0, 1]$, $(r, w, L) \in K$, and define

$$d := \min_{(\sigma, \tilde{w}, \tilde{L}) \in K} \sigma > 0.$$

For the fixed values $E_\kappa = E_\kappa(r, w, L)$ and $E_0 = E_0(r, w, L)$, we can estimate

$$\begin{aligned} & \left| \int_{R_\kappa(\theta, E_\kappa, L)}^{R_{\kappa, \max}} e^{(\frac{5}{2}\lambda_\kappa + \mu_\kappa)(\sigma)} p_{|\varphi'_\kappa|^{\frac{1}{2}}h}(\sigma) \sigma d\sigma - \int_{R_0(\theta, E_0, L)}^{R_{0, \max}} e^{(\frac{5}{2}\lambda_0 + \mu_0)(\sigma)} p_{|\varphi'_0|^{\frac{1}{2}}h}(\sigma) \sigma d\sigma \right| \\ & \leq C \int_0^\infty \int_{\mathbb{R}} \int_0^\infty \left| \left(e^{(\frac{5}{2}\lambda_\kappa + \mu_\kappa)(\sigma)} |\varphi'_\kappa(E_\kappa(\sigma, \tilde{w}, \tilde{L}))|^{\frac{1}{2}} \mathbf{1}_{[R_\kappa(\theta, E_\kappa, L), R_{\kappa, \max}]}(\sigma) \right. \right. \\ & \quad \left. \left. - e^{(\frac{5}{2}\lambda_0 + \mu_0)(\sigma)} |\varphi'_0(E_0(\sigma, \tilde{w}, \tilde{L}))|^{\frac{1}{2}} \mathbf{1}_{[R_0(\theta, E_0, L), R_{0, \max}]}(\sigma) \right) \frac{|h(\sigma, \tilde{w}, \tilde{L})|}{\sigma} \right| d\tilde{L} d\tilde{w} d\sigma \\ & \leq \frac{C}{d} \|h\|_{L^2(\mathbb{R}^3)} \left(\int_0^\infty \int_{\mathbb{R}} \int_0^\infty \left| e^{(\frac{5}{2}\lambda_\kappa + \mu_\kappa)(\sigma)} |\varphi'_\kappa(E_\kappa(\sigma, \tilde{w}, \tilde{L}))|^{\frac{1}{2}} \mathbf{1}_{[R_\kappa(\theta, E_\kappa, L), R_{\kappa, \max}]}(\sigma) \right. \right. \\ & \quad \left. \left. - e^{(\frac{5}{2}\lambda_0 + \mu_0)(\sigma)} |\varphi'_0(E_0(\sigma, \tilde{w}, \tilde{L}))|^{\frac{1}{2}} \mathbf{1}_{[R_0(\theta, E_0, L), R_{0, \max}]}(\sigma) \right|^2 d\tilde{L} d\tilde{w} d\sigma \right)^{\frac{1}{2}}, \quad (6.28) \end{aligned}$$

where we used the Cauchy-Schwarz inequality in the last step. The remaining integrand converges pointwise to zero a.e. as $\kappa \rightarrow \kappa_0$ because of Lemmas 3.2.1 and 6.2.1. Condition (S5') and the various bounds mentioned above yield

$$\begin{aligned} & \left| e^{(\frac{5}{2}\lambda_\kappa + \mu_\kappa)(\sigma)} |\varphi'_\kappa(E_\kappa(\sigma, \tilde{w}, \tilde{L}))|^{\frac{1}{2}} \mathbf{1}_{[R_\kappa(\theta, E_\kappa, L), R_{\kappa, \max}]}(\sigma) \right. \\ & \quad \left. - e^{(\frac{5}{2}\lambda_0 + \mu_0)(\sigma)} |\varphi'_0(E_0(\sigma, \tilde{w}, \tilde{L}))|^{\frac{1}{2}} \mathbf{1}_{[R_0(\theta, E_0, L), R_{0, \max}]}(\sigma) \right| \leq C \mathbf{1}_U(\sigma, \tilde{w}, \tilde{L}) \quad (6.29) \end{aligned}$$

uniformly in $\theta \in [0, 1]$, $(r, w, L) \in K$, and κ , where U is a compact set with $\Omega_\kappa \subset U$, according to Lemma 6.2.1(a). Lebesgue's theorem therefore yields pointwise convergence of (6.28) to zero for $\kappa \rightarrow \kappa_0$ for a.e. $\theta \in [0, 1]$, $(r, w, L) \in K$. In particular, we obtain

$$\left| \int_0^1 e^{-(\mu_0 + \lambda_0)(R_0(\theta, E_0, L))} \left(\int_{R_\kappa(\theta, E_\kappa, L)}^{R_{\kappa, \max}} e^{(\frac{5}{2}\lambda_\kappa + \mu_\kappa)(\sigma)} p_{|\varphi'_\kappa|^{\frac{1}{2}}h}(\sigma) \sigma d\sigma \right. \right.$$

$$- \int_{R_0(\theta, E_0, L)}^{R_{0, \max}} e^{(\frac{5}{2}\lambda_0 + \mu_0)(\sigma)} p_{|\varphi'_0|^{\frac{1}{2}}h}(\sigma) \sigma d\sigma \Big| \rightarrow 0, \quad \kappa \rightarrow \kappa_0$$

for a.e. $(r, w, L) \in K$ after again applying Lebesgue's theorem using the bound (6.29). In addition, this difference is bounded by a constant as well. We repeat the same argument on the outer integral over K with majorant $C|\varphi'_0|$ and thus get $I_{23} \rightarrow 0$ for $\kappa \rightarrow \kappa_0$.

Term no. 3: Fortunately, the arguments for the remaining three terms are very similar, so we can cover them more quickly. We introduce the shorthand

$$P_\kappa(\theta, E, L) := \frac{E^2 - \Psi_{\kappa, L}^2(R_\kappa(\theta, E, L))}{E} e^{2\lambda_\kappa(R_\kappa(\theta, E, L))}$$

for $\theta \in [0, 1]$ and $(E, L) \in \tilde{\Omega}_\kappa^{EL}$. This quantity is uniformly bounded in κ . We split the third term into

$$\begin{aligned} & \left\| e^{\frac{\lambda_\kappa}{2}} |\varphi'_\kappa|^{-\frac{1}{2}} G_{\kappa, 3}(s) \left(e^{-\frac{\lambda_\kappa}{2}} |\varphi'_\kappa|^{\frac{1}{2}} h \right) - e^{\frac{\lambda_0}{2}} |\varphi'_0|^{-\frac{1}{2}} G_{0, 3}(s) \left(e^{-\frac{\lambda_0}{2}} |\varphi'_0|^{\frac{1}{2}} h \right) \right\|_{L^2(K)} \\ & \leq C \left\| \left(e^{\frac{\lambda_\kappa}{2}} |\varphi'_\kappa|^{\frac{1}{2}} E_\kappa - e^{\frac{\lambda_0}{2}} |\varphi'_0|^{\frac{1}{2}} E_0 \right) \right. \\ & \quad \cdot \left. \int_0^1 \frac{P_\kappa(\theta, E_\kappa, L)}{R_\kappa(\theta, E_\kappa, L)} \int_0^{\min(s, R_\kappa(\theta, E_\kappa, L))} \sigma^2 e^{-\lambda_\kappa(\sigma)} M_{\kappa, 2, \varphi_\kappa}(\sigma) d\sigma d\theta \right\|_{L^2(K)} \\ & + C \left\| |\varphi'_0|^{\frac{1}{2}} \int_0^1 \frac{|P_\kappa - P_0|(\theta, E_\kappa, L)}{R_\kappa(\theta, E_\kappa, L)} \int_0^{\min(s, R_\kappa(\theta, E_\kappa, L))} \sigma^2 e^{-\lambda_\kappa(\sigma)} M_{\kappa, 2, \varphi_\kappa}(\sigma) d\sigma d\theta \right\|_{L^2(K)} \\ & + C \left\| |\varphi'_0|^{\frac{1}{2}} \int_0^1 P_0(\theta, E_0, L) \left(\frac{1}{R_\kappa(\theta, E_\kappa, L)} \int_0^{\min(s, R_\kappa(\theta, E_\kappa, L))} \sigma^2 e^{-\lambda_\kappa(\sigma)} M_{\kappa, 2, \varphi_\kappa}(\sigma) d\sigma d\theta \right. \right. \\ & \quad \left. \left. - \frac{1}{R_0(\theta, E_0, L)} \int_0^{\min(s, R_0(\theta, E_0, L))} \sigma^2 e^{-\lambda_0(\sigma)} M_{0, 2, \varphi_0}(\sigma) d\sigma d\theta \right) \right\|_{L^2(K)} \\ & =: I_{31} + I_{32} + I_{33}. \end{aligned}$$

In addition, we bound

$$\frac{1}{R_\kappa(\theta, E_\kappa, L)} \int_0^{\min(s, R_\kappa(\theta, E_\kappa, L))} \sigma^2 e^{-\lambda_\kappa(\sigma)} M_{\kappa, 2, \varphi_\kappa}(\sigma) d\sigma d\theta \leq C \quad (6.30)$$

for $\theta \in [0, 1]$ and $(r, w, L) \in K$ after noting that the term R_κ appearing in the denominator can be eliminated by the integral over σ ; by Lemma 6.2.1(e), we uniformly bound $M_{\kappa, 2, \varphi_\kappa}$. We thus obtain $I_{31} \rightarrow 0$ for $\kappa \rightarrow \kappa_0$ in a manner similar to I_{11} and I_{21} . Using (6.30) and the uniform continuity results from Lemma 6.2.1 yields that I_{32} also converges to zero after applying Lebesgue's theorem twice. The third term I_{33} can be

treated similarly to I_{23} , because

$$\begin{aligned} & \frac{1}{R_\kappa(\theta, E_\kappa, L)} \int_0^{\min(s, R_\kappa(\theta, E_\kappa, L))} \sigma^2 e^{-\lambda_\kappa(\sigma)} M_{\kappa, 2, \varphi_\kappa}(\sigma) d\sigma \\ &= \frac{\pi}{R_\kappa(\theta, E_\kappa, L)} \int_0^\infty \int_{\mathbb{R}} \int_0^\infty e^{-\lambda_\kappa(\sigma)} \left(1 + \tilde{w}^2 + \frac{\tilde{L}}{\sigma^2}\right) |\varphi'_\kappa(E_\kappa(\sigma, \tilde{w}, \tilde{L}))| \\ & \quad \cdot \mathbb{1}_{[0, \min(s, R_\kappa(\theta, E_\kappa, L))]}(\sigma) d\tilde{L} d\tilde{w} d\sigma \end{aligned}$$

converges as $\kappa \rightarrow \kappa_0$ for fixed values of $\theta \in [0, 1]$ and $(r, w, L) \in K$ by Lebesgue's theorem using the majorant $C \mathbb{1}_U$, as with term I_{23} . Applying Lebesgue's theorem twice more—once in $\theta \in [0, 1]$ with a constant majorant and then over K with the majorant $C|\varphi'_0|$ —as with I_{23} yields that $I_{33} \rightarrow 0$ as $\kappa \rightarrow \kappa_0$.

Terms no. 4 and 5: For the terms involving $G_{\kappa, 4}$ and $G_{\kappa, 5}$, we combine the techniques from the previous three steps. Differences only arise in the details. We first split the terms with the triangle inequality. We have to consider ρ instead of p in the fourth term and eliminate the function h with the Cauchy-Schwarz inequality as in (6.28) and bound the integrand similar to (6.29); note that this is simpler for the fourth term, since σ does not arise in the denominator. Lebesgue's theorem applied with majorant $C \mathbb{1}_U$ yields the pointwise convergence of the inner integral a.e. in θ and on K . In order to obtain a majorant for the integral over θ , we notice that $R_\kappa(\theta, E_\kappa, L)$ in the denominator can be eliminated by one power of σ in the innermost integral. The outer integral over K can again be dealt with as above. For the fifth term, the innermost integral is the same as the integral appearing in term no. 2. The convergence of one more layer of radial integration has to be shown, which is again achieved by Lebesgue's theorem, since all terms there are bounded. As the fourth and fifth terms are structurally very similar to the first three, we judge it unnecessary to repeat the slightly different reasoning in detail.

Bringing these five steps together proves (6.27). It is important to note that all the convergences above were uniform in h due to $\|h\|_{L^2(K)} = 1$, which implies convergence in the supremum. \square

The compactness and continuity result for the fixed-point operator as well as the uniform boundedness of the generators come together nicely so that we can prove the continuity of g_κ^s in the following sense:

Proposition 6.2.12. *Let g_κ^s be the generator of Π_κ^s defined in (6.8) for $s \geq 0$ and $\kappa > 0$. The mapping*

$$]0, \infty[\ni \kappa \mapsto h_\kappa^s := e^{\frac{\lambda_\kappa}{2}} |\varphi'_\kappa|^{-\frac{1}{2}} g_\kappa^s \in L^2(\mathbb{R}^3)$$

is continuous for every $s \geq 0$.

Proof. Fix $\kappa_0 > 0$ and consider a sequence $(\kappa_n)_{n \in \mathbb{N}} \subset]0, \infty[$ with $\kappa_n \rightarrow \kappa_0$. Then there exists $C > 0$ with

$$\|h_{\kappa_n}^s\|_{L^2(\mathbb{R}^3)} = \|g_{\kappa_n}^s\|_{H_{\kappa_n}} \leq C, \quad n \in \mathbb{N},$$

due to Lemma 6.2.9, and thus, we have weak convergence

$$h_{\kappa_{n_j}}^s \rightharpoonup \tilde{h}, \quad j \rightarrow \infty,$$

in $L^2(\mathbb{R}^3)$ for a subsequence $(\kappa_{n_j})_{j \in \mathbb{N}}$ to some limiting function $\tilde{h} \in L^2(\mathbb{R}^3)$. We estimate

$$\begin{aligned} & \|G_{\kappa_{n_j}}(s)h_{\kappa_{n_j}}^s - G_{\kappa_0}(s)\tilde{h}\|_{L^2(\mathbb{R}^3)} \\ & \leq \|G_{\kappa_{n_j}}(s)h_{\kappa_{n_j}}^s - G_{\kappa_0}(s)h_{\kappa_{n_j}}^s\|_{L^2(\mathbb{R}^3)} + \|G_{\kappa_0}(s)(h_{\kappa_{n_j}}^s - \tilde{h})\|_{L^2(\mathbb{R}^3)}. \end{aligned}$$

For the former term, the uniform boundedness of the (sub)sequence implies

$$\|G_{\kappa_{n_j}}(s)h_{\kappa_{n_j}}^s - G_{\kappa_0}(s)h_{\kappa_{n_j}}^s\|_{L^2(\mathbb{R}^3)} \leq C\|G_{\kappa_{n_j}}(s) - G_{\kappa_0}(s)\| \rightarrow 0, \quad j \rightarrow \infty,$$

due to Lemma 6.2.11. The compactness result from Lemma 6.2.8 yields

$$\|G_{\kappa_0}(s)(h_{\kappa_{n_j}}^s - \tilde{h})\|_{L^2(\mathbb{R}^3)} \rightarrow 0, \quad j \rightarrow \infty.$$

Therefore,

$$\lim_{j \rightarrow \infty} G_{\kappa_{n_j}}(s)h_{\kappa_{n_j}}^s = G_{\kappa_0}(s)\tilde{h}$$

in $L^2(\mathbb{R}^3)$. However, $h_{\kappa_{n_j}}^s$ is the unique solution of the fixed-point problem $G_{\kappa_{n_j}}(s)h = h$, according to Proposition 6.2.7. This implies that

$$G_{\kappa_0}(s)\tilde{h} = \lim_{j \rightarrow \infty} G_{\kappa_{n_j}}(s)h_{\kappa_{n_j}}^s = \lim_{j \rightarrow \infty} h_{\kappa_{n_j}}^s$$

holds. Thus, $h_{\kappa_{n_j}}^s$ converges both weakly and strongly in $L^2(\mathbb{R}^3)$, from which we conclude that

$$G_{\kappa_0}(s)\tilde{h} = \tilde{h} \text{ a.e. on } \Omega_{\kappa_0}, \quad \tilde{h} = 0 \text{ a.e. on } \mathbb{R}^3 \setminus \Omega_{\kappa_0}. \quad (6.31)$$

The fact that \tilde{h} a.e. on $\mathbb{R}^3 \setminus \Omega_{\kappa_0}$ follows from the weak convergence and Lemma 6.2.1(a). More precisely, we have

$$\|\tilde{h}\|_{L^2(\mathbb{R}^3 \setminus \Omega_{\kappa_0})}^2 = \lim_{j \rightarrow \infty} \left| \iiint_{(\mathbb{R}^3 \setminus \Omega_{\kappa_0}) \cap (\Omega_{\kappa_{n_j}} \setminus K)} h_{\kappa_{n_j}}^s \tilde{h} dr dw dL \right| \leq C\varepsilon \|\tilde{h}\|_{L^2(\mathbb{R}^3 \setminus \Omega_{\kappa_0})}$$

where $\varepsilon > 0$ is independent of C and K is as in Lemma 6.2.1(a). In conclusion, (6.31) yields $\tilde{h} = h_{\kappa_0}^s$ by Proposition 6.2.7 and we have

$$h_{\kappa_0}^s = \lim_{j \rightarrow \infty} h_{\kappa_{n_j}}^s \text{ in } L^2(\mathbb{R}^3).$$

These arguments work for any sequence of generators which converges weakly in $L^2(\mathbb{R}^3)$.

In particular, any subsequence $(h_{\kappa_{n_j}}^s) \subset (h_{\kappa_n}^s)$ has a subsequence $(h_{\kappa_{n_{j_k}}}^s) \subset (h_{\kappa_{n_j}}^s)$ with

$$h_{\kappa_0}^s = \lim_{k \rightarrow \infty} h_{\kappa_{n_{j_k}}}^s \text{ in } L^2(\mathbb{R}^3).$$

From the standard “sub-subsequence-argument”, we obtain

$$h_{\kappa_0}^s = \lim_{n \rightarrow \infty} h_{\kappa_n}^s \text{ in } L^2(\mathbb{R}^3),$$

and the proof is finished. \square

From the continuity of the generators, we now infer continuity of the projection $\kappa \mapsto \Pi_\kappa^s$, which was the main objective of this technical section.

Theorem 6.2.13. *For every $s \geq 0$, the mapping*

$$]0, \infty[\ni \kappa \mapsto e^{\frac{\lambda_\kappa}{2}} |\varphi'_\kappa|^{-\frac{1}{2}} \Pi_\kappa^s \in L^2(\mathbb{R}^3)$$

is continuous, where Π_κ^s is given by (6.8).

Proof. Fix $\kappa_0 > 0$. By similar arguments as in the proof of Lemma 6.2.11, it is sufficient to show

$$\left\| e^{\frac{\lambda_\kappa}{2}} |\varphi'_\kappa|^{-\frac{1}{2}} \Pi_\kappa^s - e^{\frac{\lambda_{\kappa_0}}{2}} |\varphi'_{\kappa_0}|^{-\frac{1}{2}} \Pi_{\kappa_0}^s \right\|_{L^2(K)} \rightarrow 0, \quad \kappa \rightarrow \kappa_0, \quad (6.32)$$

where K is a fixed compact set independent of κ , as in Lemma 6.2.1(a). In addition, we only have to consider $\kappa > 0$ with $|\kappa - \kappa_0| < \delta$, where $\delta > 0$ is small and fixed. We again write a subscript 0 instead of κ_0 for better readability. We define

$$h_\kappa^s := e^{\frac{\lambda_\kappa}{2}} |\varphi'_\kappa|^{-\frac{1}{2}} g_\kappa^s \in L^2(\mathbb{R}^3),$$

where g_κ^s is the generator of Π_κ^s , as defined in Lemma 4.3.8. From the representation of Π_κ^s in (6.9), we get

$$\begin{aligned} & \left\| e^{\frac{\lambda_\kappa}{2}} |\varphi'_\kappa|^{-\frac{1}{2}} \Pi_\kappa^s - e^{\frac{\lambda_0}{2}} |\varphi'_0|^{-\frac{1}{2}} \Pi_0^s \right\|_{L^2(K)} \\ & \leq \|h_\kappa^s - h_0^s\|_{L^2(\mathbb{R}^3)} \\ & \quad + \left\| 4\pi E_\kappa |\varphi'_\kappa|^{\frac{1}{2}} e^{-\lambda_\kappa - \mu_\kappa} \int_r^{R_{\kappa, \max}} e^{(\frac{5}{2}\lambda_\kappa + \mu_\kappa)(\sigma)} p_{|\varphi'_\kappa|^{\frac{1}{2}} h_\kappa^s}(\sigma) \sigma d\sigma \right. \\ & \quad \left. - 4\pi E_0 |\varphi'_0|^{\frac{1}{2}} e^{-\lambda_0 - \mu_0} \int_r^{R_{0, \max}} e^{(\frac{5}{2}\lambda_0 + \mu_0)(\sigma)} p_{|\varphi'_0|^{\frac{1}{2}} h_0^s}(\sigma) \sigma d\sigma \right\|_{L^2(K)} \\ & =: I_1 + I_2. \end{aligned}$$

By Proposition 6.2.12, we know that $h_\kappa^s \rightarrow h_0^s$ for $\kappa \rightarrow \kappa_0$ in $L^2(\mathbb{R}^3)$. The term I_1 therefore goes to zero for $\kappa \rightarrow \kappa_0$, whereas I_2 here is structurally comparable to $I_{21} + I_{22} + I_{23}$

in the proof of Lemma 6.2.11, and we use very similar arguments to control it. We estimate I_2 via

$$\begin{aligned} I_2 &\leq C \left\| \left(E_\kappa |\varphi'_\kappa|^{\frac{1}{2}} e^{-\lambda_\kappa - \mu_\kappa} - E_0 |\varphi'_0|^{\frac{1}{2}} e^{-\lambda_0 - \mu_0} \right) \int_r^{R_{\kappa, \max}} p_{|\varphi'_\kappa|^{\frac{1}{2}} h_\kappa^s}(\sigma) \sigma \, d\sigma \right\|_{L^2(K)} \\ &\quad + C \left\| |\varphi'_0|^{\frac{1}{2}} \left(\int_r^{R_{\kappa, \max}} e^{\left(\frac{5}{2}\lambda_\kappa + \mu_\kappa\right)(\sigma)} p_{|\varphi'_\kappa|^{\frac{1}{2}} h_\kappa^s}(\sigma) \sigma \, d\sigma \right. \right. \\ &\quad \quad \quad \left. \left. - \int_r^{R_{0, \max}} e^{\left(\frac{5}{2}\lambda_0 + \mu_0\right)(\sigma)} p_{|\varphi'_0|^{\frac{1}{2}} h_0^s}(\sigma) \sigma \, d\sigma \right) \right\|_{L^2(K)} \\ &\quad + C \left\| |\varphi'_0|^{\frac{1}{2}} \int_r^{R_{0, \max}} p_{|\varphi'_0|^{\frac{1}{2}} (h_\kappa^s - h_0^s)}(\sigma) \sigma \, d\sigma \right\|_{L^2(K)} =: I_{21} + I_{22} + I_{23}, \end{aligned}$$

where $C > 0$ does not depend on κ . Recall that the metric coefficients, the steady state supports, and h_κ^s are uniformly bounded for $|\kappa - \kappa_0| < \delta$ as per Lemmas 6.2.1 and 6.2.9. In particular, Lemma 6.2.1(f) yields that

$$\left| \int_r^{R_{\kappa, \max}} p_{|\varphi'_0|^{\frac{1}{2}} h_\kappa^s}(\sigma) \sigma \, d\sigma \right| \leq C \|h_\kappa^s\|_{L^2(\mathbb{R}^3)} \leq C$$

for $|\kappa - \kappa_0| < \delta$ and $r > 0$. Due to the uniform convergences from Lemma 6.2.1(b), we deduce that $I_{21} \rightarrow 0$ for $\kappa \rightarrow \kappa_0$. The term I_{22} is the same as the term I_{23} in the proof of Lemma 6.2.11 with h_κ^s instead of h and without an additional integral over the angle variable θ . However, this does not change the arguments—we again need that h_κ^s are uniformly bounded—and we get the convergence of I_{22} to zero for $\kappa \rightarrow \kappa_0$. As to the final term, we again employ Lemma 6.2.1(f) and obtain

$$\left| \int_r^{R_{0, \max}} p_{|\varphi'_0|^{\frac{1}{2}} (h_\kappa^s - h_0^s)}(\sigma) \sigma \, d\sigma \right| \leq C \|h_\kappa^s - h_0^s\|_{L^2(\mathbb{R}^3)} \rightarrow 0, \quad \kappa \rightarrow \kappa_0.$$

In conclusion, we get $I_2 \rightarrow 0$ for $\kappa \rightarrow \kappa_0$ and thus (6.32) holds. \square

6.3 Existence of oscillating solutions

6.3.1 Continuity of the Mathur operator

All the effort in the previous section was put in solely to be able to show that the Mathur operator is continuous in κ with respect to the operator norm. Because the Mathur operator is of Hilbert-Schmidt type and can be written via an integral kernel, as seen in Proposition 5.3.4, it is sufficient to show that this integral kernel

$$]0, \infty[\ni \kappa \mapsto K_\kappa \in L^2([0, \infty[^2)$$

is continuous. The integral kernel and the Mathur operator depend κ and are extended to $[0, \infty[^2$ and $L^2([0, \infty[)$, respectively, as in Proposition 5.3.4 and Lemma 5.3.5(a).

Lemma 6.3.1. *The integral kernel*

$$]0, \infty[\ni \kappa \mapsto K_\kappa \in L^2([0, \infty[^2)$$

is continuous, i.e., for every $\kappa_0 > 0$, it holds that

$$\lim_{\kappa \rightarrow \kappa_0} \|K_\kappa - K_{\kappa_0}\|_{L^2([0, \infty[^2)} = 0. \quad (6.33)$$

Proof. Let $\kappa_0 > 0$ and choose $\delta > 0$ as in Lemma 6.2.1(a) such that

$$R_{\kappa, \max} \leq R_{\kappa_0, \max} + 1 =: R$$

for $\kappa > 0$ with $|\kappa - \kappa_0| < \delta$. Recalling equation (5.27), we write $K_\kappa(r, s) = A_\kappa(r, s) \frac{I_\kappa(r, s)}{rs}$, where

$$\begin{aligned} A_\kappa(r, s) &:= e^{\frac{\mu_\kappa(r)}{2} + \frac{3\lambda_\kappa(r)}{2}} e^{\frac{\mu_\kappa(s)}{2} + \frac{3\lambda_\kappa(s)}{2}} \sqrt{2r\mu'_\kappa(r) + 1} \sqrt{2s\mu'_\kappa(s) + 1}, \\ I_\kappa(r, s) &:= \left\langle (\text{id} - \Pi_\kappa) \left(|\varphi'_\kappa| E_\kappa e^{-\lambda_\kappa - \mu_\kappa} \mathbf{1}_{[0, r]} \right), |\varphi'_\kappa| E_\kappa e^{-\lambda_\kappa - \mu_\kappa} \mathbf{1}_{[0, s]} \right\rangle_{H_\kappa}, \end{aligned}$$

for $(r, s) \in [0, \infty[^2$. We aim to show (6.33) by applying Lebesgue's theorem. The quantity A_κ is uniformly bounded and uniformly continuous over $[0, R]^2$ because of Lemma 6.2.1(b). For fixed $(r, s) \in [0, \infty[^2$, we write the scalar product as

$$\begin{aligned} I_\kappa(r, s) &= \left\langle (\text{id} - \Pi_\kappa) \left(|\varphi'_\kappa| E_\kappa e^{-\lambda_\kappa - \mu_\kappa} \mathbf{1}_{[0, r]} \right), |\varphi'_\kappa| E_\kappa e^{-\lambda_\kappa - \mu_\kappa} \mathbf{1}_{[0, s]} \right\rangle_{H_\kappa} \\ &= \left\langle |\varphi'_\kappa|^{\frac{1}{2}} E_\kappa e^{-\frac{\lambda_\kappa}{2} - \mu_\kappa} \mathbf{1}_{[0, r]}, |\varphi'_\kappa|^{\frac{1}{2}} E_\kappa e^{-\frac{\lambda_\kappa}{2} - \mu_\kappa} \mathbf{1}_{[0, s]} \right\rangle_{L^2(\mathbb{R}^3)} \\ &\quad - \left\langle e^{\frac{\lambda_\kappa}{2}} |\varphi'_\kappa|^{-\frac{1}{2}} \Pi_\kappa^r, |\varphi'_\kappa|^{\frac{1}{2}} E_\kappa e^{-\frac{\lambda_\kappa}{2} - \mu_\kappa} \mathbf{1}_{[0, s]} \right\rangle_{L^2(\mathbb{R}^3)}, \end{aligned} \quad (6.34)$$

where we employ the notation introduced in (6.21). Theorem 6.2.13 proves that $e^{\frac{\lambda_\kappa}{2}} |\varphi'_\kappa|^{-\frac{1}{2}} \Pi_\kappa^r \in L^2(\mathbb{R}^3)$ is continuous in κ . In order to pass to the limit in (6.34) as $\kappa \rightarrow \kappa_0$, it is therefore sufficient to show that the mapping

$$]0, \infty[\ni \kappa \mapsto |\varphi'_\kappa|^{\frac{1}{2}} E_\kappa e^{-\frac{\lambda_\kappa}{2} - \mu_\kappa} \mathbf{1}_{[0, r]} \in L^2(\mathbb{R}^3) \quad (6.35)$$

is continuous for fixed $r > 0$. As in the proofs of Lemma 6.2.11 and Theorem 6.2.13, we can restrict the analysis to a compact set K independent of κ , as described in Lemma 6.2.1(a), by making $\delta > 0$ small enough. We obtain that

$$|\varphi'_\kappa|^{\frac{1}{2}} E_\kappa e^{-\frac{\lambda_\kappa}{2} - \mu_\kappa} \mathbf{1}_{[0, r]}$$

converges pointwise a.e. on K . In addition, this function can be bounded by a constant independent of κ by (S5') as well as the boundedness of the metric coefficients.

Lebesgue's theorem implies

$$\left\| |\varphi'_\kappa|^{\frac{1}{2}} E_\kappa e^{-\frac{\lambda_\kappa}{2} - \mu_\kappa} \mathbb{1}_{[0,r]} - |\varphi'_{\kappa_0}|^{\frac{1}{2}} E_{\kappa_0} e^{-\frac{\lambda_{\kappa_0}}{2} - \mu_{\kappa_0}} \mathbb{1}_{[0,r]} \right\|_{L^2(K)} \rightarrow 0, \quad \kappa \rightarrow \kappa_0,$$

and thus the continuity of the mapping (6.35). In particular, we obtain $I_\kappa \rightarrow I_{\kappa_0}$ for $\kappa \rightarrow \kappa_0$ pointwise on $]0, \infty[^2$. Moreover,

$$\begin{aligned} \left| \frac{I_\kappa(r, s)}{rs} \right| &\leq \frac{1}{rs} \left| \left\langle (\text{id} - \Pi_\kappa) \left(|\varphi'_\kappa| E_\kappa e^{-\lambda_\kappa - \mu_\kappa} \mathbb{1}_{[0,r]} \right), |\varphi'_\kappa| E_\kappa e^{-\lambda_\kappa - \mu_\kappa} \mathbb{1}_{[0,s]} \right\rangle_{H_\kappa} \right| \\ &\leq \frac{1}{rs} \left\| |\varphi'_\kappa| E_\kappa e^{-\lambda_\kappa - \mu_\kappa} \mathbb{1}_{[0,r]} \right\|_{H_\kappa} \left\| |\varphi'_\kappa| E_\kappa e^{-\lambda_\kappa - \mu_\kappa} \mathbb{1}_{[0,s]} \right\|_{H_\kappa} \end{aligned}$$

holds for $(r, s) \in]0, \infty[^2$ because of $\|\text{id} - \Pi\| \leq 1$ and the Cauchy-Schwarz inequality. We compute

$$\left\| |\varphi'_\kappa| E_\kappa e^{-\lambda_\kappa - \mu_\kappa} \mathbb{1}_{[0,r]} \right\|_{H_\kappa} \leq \iiint_{\Omega_\kappa} |\varphi'_\kappa(E_\kappa)| \mathbb{1}_{[0,r]}(\sigma) dLdwd\sigma \leq Cr$$

with $C > 0$ independent of $\kappa > 0$ and $r > 0$ by using (S5') and bounding the steady state supports uniformly, as in Lemma 6.2.1(a). Putting these estimates together yields

$$\left| \frac{I_\kappa(r, s)}{rs} \right| \leq C, \quad (r, s) \in]0, \infty[^2.$$

In conclusion, we get $K_\kappa \rightarrow K_{\kappa_0}$ for $\kappa \rightarrow \kappa_0$ pointwise on $]0, \infty[^2$. Recall that K_κ vanishes outside of $[0, R]^2$ due to $R_{\kappa, \max} \leq R$ and Proposition 5.3.4. In addition, we have shown a uniform bound on K_κ . This allows us to apply Lebesgue's theorem and (6.33) is proven. \square

The continuity of the integral kernel can now be translated to the continuity of the Mathur operator directly from the representation of the Mathur operator in Proposition 5.3.4.

Proposition 6.3.2. *The Mathur operator $]0, \infty[\ni \kappa \mapsto \mathcal{M}_\kappa \in \mathcal{L}(L^2([0, \infty[); L^2([0, \infty[)))$ is continuous in the operator norm, i.e.,*

$$\lim_{\kappa \rightarrow \kappa_0} \|\mathcal{M}_\kappa - \mathcal{M}_{\kappa_0}\| = \lim_{\kappa \rightarrow \kappa_0} \sup_{\substack{F \in L^2([0, \infty[) \\ \|F\|_{L^2([0, \infty[)} = 1}} \|\mathcal{M}_\kappa F - \mathcal{M}_{\kappa_0} F\|_{L^2([0, \infty[)} = 0 \quad (6.36)$$

for every $\kappa_0 > 0$. In particular, the operator norm of the Mathur operator $\|\mathcal{M}_\kappa\|$ is continuous in $\kappa \in]0, \infty[$.

Proof. For every $F \in L^2([0, \infty[)$ with $\|F\|_{L^2([0, \infty[)} = 1$, Proposition 5.3.4 and the Cauchy-Schwarz inequality yield

$$\begin{aligned} \|\mathcal{M}_\kappa F - \mathcal{M}_{\kappa_0} F\|_{L^2([0, \infty[)}^2 &= \int_0^\infty \left| \int_0^\infty (K_\kappa(r, s) - K_{\kappa_0}(r, s)) F(s) ds \right|^2 dr \\ &\leq \left(\int_0^\infty \int_0^\infty |K_\kappa(r, s) - K_{\kappa_0}(r, s)|^2 ds dr \right) \|F\|_{L^2([0, \infty[)}^2 = \|K_\kappa - K_{\kappa_0}\|_{L^2([0, \infty]^2)}^2. \end{aligned}$$

Therefore,

$$\|\mathcal{M}_\kappa - \mathcal{M}_{\kappa_0}\| = \sup_{\substack{F \in L^2([0, \infty[) \\ \|F\|_{L^2([0, \infty[)} = 1}} \|\mathcal{M}_\kappa F - \mathcal{M}_{\kappa_0} F\|_{L^2([0, \infty[)} \leq \|K_\kappa - K_{\kappa_0}\|_{L^2([0, \infty]^2)},$$

which converges to zero as $\kappa \rightarrow \kappa_0$ due to Lemma 6.3.1. \square

This is a very helpful result for our upcoming application and, hopefully, for more applications to come. For steady states, as described in Section 6.1, the continuity of $\|\mathcal{M}_\kappa\|$ shows that linear stability along a κ -family is well-behaved in κ since it is fully characterized by the value of $\|\mathcal{M}_\kappa\|$, as shown in Theorem 5.4.1.

Despite the technical nature of the continuity results in κ —especially the continuity of the projection term which was crucial in the proof of Lemma 6.3.1—it is not too surprising that all the necessary quantities depend continuously on κ , since we can (to some extent) wish for the regularity of the steady states by choosing appropriate ansatz functions φ . However, the in-depth knowledge attained in these preliminary results, enables us to now prove the existence of oscillating solutions.

6.3.2 On eigenvalues in the principal gap

We begin by combining the previously known linear stability results, which we have recalled in Theorem 5.1.4, with the characterization of linear stability in Theorem 5.4.1. Note that we still consider a family of steady state, as introduced in Section 6.1.

Proposition 6.3.3. *There exists $\kappa_0 > 0$ such that $\|\mathcal{M}_{\kappa_0}\| = 1$. In particular, the steady state f_{κ_0} has a zero-frequency mode, as defined in Definition 5.1.2(c).*

Proof. Since the steady states $(f_\kappa)_{\kappa > 0}$ are isotropic by (S4'), Theorem 5.1.4 implies the existence of $0 < \kappa_{\text{st}} < \kappa_{\text{unst}}$ such that f_κ is linearly stable for $0 < \kappa < \kappa_{\text{st}}$ and linearly unstable for $\kappa > \kappa_{\text{unst}}$. According to Theorem 5.4.1, this is equivalent to $\|\mathcal{M}_\kappa\| < 1$ for $0 < \kappa < \kappa_{\text{st}}$ and $\|\mathcal{M}_\kappa\| > 1$ for $\kappa > \kappa_{\text{unst}}$. Note that all the assumptions from Section 4.1 are also satisfied by the conditions prescribed in Section 6.1. Since $\|\mathcal{M}_\kappa\|$ is continuous in κ , as proven in Proposition 6.3.2, we obtain the existence of $\kappa_0 > 0$ with $\|\mathcal{M}_{\kappa_0}\| = 1$ from the intermediate value theorem. Furthermore, Theorem 5.4.1 implies that f_{κ_0} has a zero-frequency mode. \square

With this setup and the previous results at hand, we now establish the existence of positive eigenvalues in the principal gap for two related situations. In consequence, we obtain the existence of oscillating solutions.

Theorem 6.3.4 (Existence of oscillating solutions). *Consider a κ -family $(f_\kappa)_{\kappa>0}$ of steady states as in Definition 2.2.5, which satisfies (S3')–(S5'). Moreover, assume that*

(i) *the conditions (S1') and (S2') hold,*

or

(ii) *the inequality*

$$\frac{2m_\kappa(r)}{r} < \frac{1}{3}, \quad r > 0,$$

is satisfied for $\kappa \in]0, \kappa_{\text{unst}}[$, where κ_{unst} is given by Theorem 5.1.4(b).

Then there exists $\kappa > 0$ and an eigenvalue γ of \mathcal{L}_κ such that $0 < \gamma < \inf(\sigma_{\text{ess}}(\mathcal{L}_\kappa))$. The eigenvalue γ induces an oscillating mode of f_κ , as described in Section 6.1.

Proof. We first consider case (i). By Proposition 6.3.3, there exists $\kappa_0 > 0$ such that $\|\mathcal{M}_{\kappa_0}\| = 1$, i.e., zero is the smallest eigenvalue of \mathcal{L}_{κ_0} by Theorem 5.4.1 and the definition of linear stability in Definition 5.1.2. In addition, we choose κ_0 as small as possible. This choice is well defined because the value κ_0 is bounded away from zero due to Theorem 5.1.4 and since $\|\mathcal{M}_\kappa\|$ is continuous as per Proposition 6.3.2. In particular, we have

$$\|\mathcal{M}_\kappa\| < 1, \quad \kappa < \kappa_0. \tag{6.37}$$

We denote an eigenfunction corresponding to \mathcal{L}_{κ_0} by $g_0 \in \mathcal{H}_{\kappa_0} \cap D(\mathcal{T}_{\kappa_0})$, i.e., $\mathcal{L}_{\kappa_0}g_0 = 0$. By Theorem 4.3.18, we have

$$\sigma_{\text{ess}}(\mathcal{L}_\kappa) \subset \overline{\left(\frac{2\pi\mathbb{N}}{T(\tilde{\Omega}_\kappa^{EL})}\right)^2}.$$

Because the period function is uniformly bounded from above by (S2'), there exists $C_{\text{ess}} > 0$ such that

$$\inf(\sigma_{\text{ess}}(\mathcal{L}_\kappa)) \geq C_{\text{ess}}$$

for every $\kappa > 0$ with $|\kappa - \kappa_0| < \delta$ and $0 < \delta < \kappa_0$. The approximation result in Corollary 6.2.3 yields the existence of $g \in C_c^\infty(\Omega_0)$ and $\delta > 0$ with

$$|\langle \mathcal{L}_{\kappa_0}g_0, g_0 \rangle_{H_{\kappa_0}} - \langle \mathcal{L}_\kappa g, g \rangle_{H_\kappa}| = |\langle \mathcal{L}_\kappa g, g \rangle_{H_\kappa}| < C_{\text{ess}} \tag{6.38}$$

for every $\kappa > 0$ with $|\kappa - \kappa_0| < \delta$ due to $\mathcal{L}_{\kappa_0}g_0 = 0$. Equation (6.37) and Theorem 5.4.1 imply that f_κ is linearly stable for $\kappa < \kappa_0$ which, by Definition 5.1.2, means that $\inf(\sigma(\mathcal{L}_\kappa)) > 0$. In particular, we deduce $\langle \mathcal{L}_\kappa g, g \rangle_{H_\kappa} > 0$ for $\kappa < \kappa_0$ from Lemma B.6. The estimate (6.38) consequently yields

$$0 < \inf(\sigma(\mathcal{L}_\kappa)) < C_{\text{ess}} \leq \inf(\sigma_{\text{ess}}(\mathcal{L}_\kappa))$$

for every $\kappa < \kappa_0$ with $|\kappa - \kappa_0| < \delta$. For any such value of κ , we choose $\gamma := \inf(\sigma(\mathcal{L}_\kappa))$, which is an eigenvalue of \mathcal{L}_κ , by applying the min-max principle for self-adjoint operators [88, Thm. XIII.1], since γ cannot be an element in the essential spectrum. This proves the claim in scenario (i).

In case (ii), we apply Proposition 2.3.5, which shows that f_κ has strict single-well structure for $\kappa \in]0, \kappa_{\text{unst}}[$, since the steady state is isotropic by (S4'). In addition, Propositions 3.2.9 and 3.2.10 yield that the period function is uniformly bounded and bounded away from zero on compact sub-intervals of $]0, \kappa_{\text{unst}}[$. Thus, (S1') and (S2') hold, not for $\kappa > 0$ but for $\kappa \in]0, \kappa_{\text{unst}}[$. Note that all the results from this chapter can be derived for $\kappa \in]0, \kappa_{\text{unst}}[$ instead of $\kappa \in]0, \infty[$, since they are “local” in κ . This is sufficient to be able to repeat the same arguments as above for case (i) since necessarily $\kappa_0 < \kappa_{\text{unst}}$ by the continuity of $\|\mathcal{M}_\kappa\|$ in κ . \square

To finish this section, we add a few comments to this new result. We argue that the situations (i) or (ii) are quite general and put the existence of oscillating solutions into context with related work on the Vlasov-Poisson system.

Remark 6.3.5. (a) *Condition (i) in Theorem 6.3.4 is, of course, very demanding and not easy to verify. However, it is unavoidable to know about the single-well structure and the boundedness of the period function since our whole approach is based on these assumptions. Condition (ii) is in some sense less stringent since we do not need to prescribe knowledge about the period function but only about the macroscopic mass function m_κ . The mass function can be analyzed much more easily and condition (ii) can be accurately verified from a numerical point of view. The boundedness of the period function is then simply a consequence of Propositions 3.2.9 and 3.2.10.*

- (b) *For a detailed discussion on the validity of conditions (i) and (ii), we refer to Remarks 2.3.2 and 2.4.2. In short, it seems as though (i) holds for any isotropic steady state, while (ii) holds for large classes of stationary solutions. It is, however, still an open problem to rigorously show this.*
- (c) *Our idea of inferring the existence of an isolated eigenvalue, as it departs from the essential spectrum and crosses zero, is not possible for the Vlasov-Poisson system since all relevant steady states are linearly stable there. This means that no eigenvalue will cross zero and this approach breaks down. Paradoxically, the search for oscillating solutions is thus simplified because we know that unstable equilibria exist for the Einstein-Vlasov system.*

7 Numerical investigation of non-linear stability

The first principle is that you must not fool yourself—and you are the easiest person to fool.

Richard Feynman

As described in the previous chapters several times, non-linear stability of steady states for the spherically symmetric Einstein-Vlasov system, as constructed in Chapter 2, remains difficult to tackle analytically. A large corpus of the literature which we recall in Section 7.1 has therefore dealt with numerical modeling of this system. The most common approach is the so-called particle-in-cell (PIC) method which is based on a decomposition of phase space into disjoint cells. We describe the PIC method in more detail in Section 7.2. This algorithm is then used to examine singularity-free steady states in Section 7.3. We address different manifestations of stability as well as instability and present convincing evidence that the so-called *binding energy hypothesis* is not true. Furthermore, we show the existence of *heteroclinic* orbits, which were first observed by the author and colleagues in [45]. We conclude the chapter with a new study of the stability of shells surrounding a black hole in Section 7.4 and present the different types of stability behaviors there as well.

7.1 Setup and previous results

We choose to simulate the Einstein-Vlasov system in maximal areal coordinates, as introduced in Section 1.1.2. This was also done in [15, 45, 48, 79] and allows us to detect the emergence of *trapped surfaces* which signal the inevitable development of a black hole [80]. This is not possible in Schwarzschild coordinates. In addition, we can better simulate collapsing matter in maximal areal coordinates since this allows us to “freeze” the particles once they are inside a trapped surface. Fortunately, it is easy to see that stationary solutions in Schwarzschild coordinates are equivalent to stationary solutions in maximal areal coordinates through the relation

$$\alpha = e^\mu, \quad a = e^\lambda,$$

as discussed in [15, 45, 48]. This is due to the fact that $\beta = 0 = j$ must necessarily hold for time-independent solutions in maximal areal coordinates. It should be noted that

the stability behavior of steady states seems to be independent of the actual coordinates used [45, 48]. This is a-priori not obvious, as there is no canonical way of comparing metric coefficients across different coordinate systems, cf. [48, 62] for a more detailed discussion.

Before we begin with the numerical analysis, we briefly comment on the previous findings in the literature where the stability of stationary solutions to the Einstein-Vlasov system is numerically investigated. We refer to [48, Sc. 1.2] for a comprehensive and in-depth review. The work towards numerical stability analysis was initiated by [60] and subsequently [42] who consider linear stability by approximating the bottom of the spectrum of the Antonov operator (4.14). The first simulation of the dynamics for the non-linear system using a PIC method was presented in [107, 108]. More classes of steady states are investigated in [21, 85], where the authors claim to find stable equilibria with an arbitrarily large central redshift. The authors of [85, 86] approximate the particle density directly in phase space instead of using a PIC method. Initial research on the axisymmetric Einstein-Vlasov system is carried out in [2, 109] and was recently reconsidered in [3].

A study of the stability of anisotropic steady states of the polytropic type (2.5) is conducted in [15] using maximal areal coordinates. This research is extended to multiple coordinate systems by the author and colleagues in [45, 48]. In [45], heteroclinic orbits are first described, while [48] provides evidence for steady state families with multiple stability changes, see Section 7.3 for more details.

Remark 7.1.1. *(a) In the literature, it was long believed that the binding energy hypothesis holds. This hypothesis states that stability along a family of stationary solutions—parametrized by an appropriate redshift-factor—changes only at extremal points of the binding energy. Earlier numerical evidence supported this [2, 15, 45, 60, 85, 86, 107, 108, 109]. In fact, in these references, stability seems to change exactly at the first local maximum of the binding energy. In addition, arguments from a physics point of view made the hypothesis plausible as well [61, 114, 115]. Overall, the stability behavior along families of steady states seemed to be solved in the sense that stability can be determined by examining the binding energy curve.*

However, the author and colleagues recently provided compelling evidence in [48] that the binding energy hypothesis is generally not true for isotropic steady states by considering the piecewise linear model (2.76). We elaborate on this in Section 7.3.3.

(b) A weaker form of the binding energy hypothesis states that, along a family of steady states parametrized by an appropriate redshift-factor, the equilibria are stable at least up to the first local maximum of the binding energy curve. This assertion still holds true for all the evidence obtained in the references above. Our work continues to support it as well, but we do not go further into detail here. An analytical proof of this hypothesis remains an open problem.

As an aside, the Einstein-Vlasov system was of interest in the question whether highly relativistic matter distributions can be stable in order to explain the discovery of quasars [22, 23, 62, 114]. One could say that this initiated the activity in the field and the subsequent numerical investigations mentioned above. Unstable steady states also play a role in the study of critical collapse and might become useful for explaining the type I behavior observed for the Einstein-Vlasov system [15, 79, 98]. This is tightly related to the cosmic censorship hypothesis which is a central open problem in general relativity [81].

7.2 The numerical method

In this section, we describe the numerical scheme employed to simulate the Einstein-Vlasov system in maximal areal coordinates. We use a particle-in-cell (PIC) method which is a common choice in plasma physics and for Vlasov equations in general [20]. The use of a PIC method allows for both the efficient tracking of the evolution of the distribution over time and the simulation of the collective behavior of large numbers of particles. This makes the PIC method particularly well-suited for problems that involve the interaction of particles with each other and with external fields. It has been used in [3, 15, 45, 48, 98, 107] for the Einstein-Vlasov system and in [84] for the Vlasov-Poisson system. This method has been shown to converge for the Einstein-Vlasov system in Schwarzschild coordinates in [99] and for the spherically symmetric Vlasov-Poisson system in [103]. We expect that the PIC method also converges in the case of maximal areal coordinates, but leave this open for future research.

In essence, the PIC method involves a discretization of the simulation domain, i.e., phase space, into a grid of disjunct cells. Each cell is represented by a particle which is assigned a weight that corresponds to the distribution function f to be approximated. The densities and metric coefficients are then calculated from this distribution using the formulas (1.26)–(1.29) of the Einstein-Vlasov system in maximal areal coordinates. These formulas are subsequently employed to update the positions and velocities of the particles using the characteristic system that corresponds to the Vlasov equation (1.25).

The method involves a time-stepping process where each step entails a computation of the source terms on the grid based on the particle positions, an approximation of the metric coefficients on the grid via the field equations, and an update of the positions and velocities of the particles according to the characteristic system. The process is repeated for multiple time steps to simulate the evolution of the distribution function f over time. We now make this process more precise but only describe the algorithm for the singularity-free case. Translating the PIC method to the Einstein-Vlasov system with a black hole at the center requires handling the boundary conditions appropriately.

Initialization: For technical reasons, we do not use (r, w, L) variables¹ in order to initialize the numerical particles from a given spherically symmetric distribution f° , but

¹It turns out that the initialization process does not work well in (r, w, L) variables. It is not fully clear to the author why this is the case. However, one reason seems to be that particles with small angular momentum L are not represented appropriately when using an equidistant grid in (r, w, L) .

choose to write

$$\mathring{f} = \mathring{f}(x, v) = \mathring{f}(r, w, L) = \mathring{f}(r, u, \psi),$$

where $u \geq 0$ and $\psi \in [0, \pi]$ are given by

$$u^2 = w^2 + \frac{L}{r^2}, \quad w = u \cos(\psi).$$

It is easy to see that every spherically symmetric distribution can be written in the variables (r, u, ψ) . Illustratively, u corresponds to the absolute value $|v|$ of the momentum $v \in \mathbb{R}^3$ of a particle, whereas ψ determines the angle between the position $x \in \mathbb{R}^3$ and the momentum $v \in \mathbb{R}^3$. We define

$$N_r := \frac{R_{\max} - R_{\min}}{\Delta r}, \quad \Delta u := \frac{U_{\max}}{N_u}, \quad \Delta \psi := \frac{\pi}{N_\psi},$$

where $N_u, N_\psi \in \mathbb{N}$ and $\Delta r > 0$ are prescribed, and U_{\max} is the maximal value of u appearing in the support of \mathring{f} . The grid is then set up on the points (r_i, u_j, ψ_k) given by

$$r_i = R_{\min} + \left(i - \frac{1}{2}\right) \Delta r, \quad u_j = \left(j - \frac{1}{2}\right) \Delta u, \quad \psi_k = \left(k - \frac{1}{2}\right) \Delta \psi,$$

where $i, j, k \in \mathbb{N}$. The weight corresponding to the point (r_i, u_j, ψ_k) is defined as

$$\mathring{f}_{ijk} := \mathring{f}(r_i, u_j, \psi_k) 8\pi^2 r_i^2 u_j^2 \sin(\psi_k) \Delta r \Delta u \Delta \psi. \quad (7.1)$$

These weights include the phase space volume element, i.e., the volume of the corresponding cell which the particles were placed into, and the weights have to be propagated accordingly in the time-step. Including the volume element is advantageous when computing the approximate densities $\bar{\rho}$, \bar{S} , and \bar{j} , which we describe below. Note that points only contribute to the initialization if $\mathring{f}_{ijk} > 0$ and get discarded otherwise.

In reality, the initialization scheme is somewhat more sophisticated. For example, when r_i is fixed, we choose the step sizes Δu and $\Delta \psi$ adaptively to guarantee a certain amount of minimal steps into each variable direction. Moreover, the distribution \mathring{f} is not evaluated sharply at one point, but we sample over multiple points inside the cell and take the average. These and other refinements make the initialization more efficient and accurate.

Once the particles are initialized, the grid in (r, u, ψ) is no longer needed. By changing back to (r, w, L) -variables, we obtain a set of points

$$(\bar{r}, \bar{w}, \bar{L}, \bar{f}) \in ([0, \infty[\times \mathbb{R} \times [0, \infty[\times [0, \infty[)^N, \quad (7.2)$$

which approximates the initial distribution \mathring{f} , where $N \in \mathbb{N}$ is the number of particles/cells used. In the following, approximated quantities are always denoted with a bar to distinguish them from the analytical quantities.

Time propagation: From the setup after the initialization, we now describe the time-step. Assume that we have a set of points as in (7.2) at time $t = 0$. We fix a radial grid with step size Δr . The first step consists of computing the densities ρ , p , and S . In order to smoothen the approximation, we smear out the particles radially via the hat-function

$$\chi(s) := \begin{cases} 1 - \frac{|s|}{\Delta r}, & |s| \leq \Delta r, \\ 0, & |s| > \Delta r. \end{cases}$$

Since the weights \bar{f} contain the volume elements, we obtain an approximation to the source terms by summing

$$\bar{\rho}(r) = \frac{1}{4\pi r^2} \sum_{n=1}^N \sqrt{1 + \bar{w}_n^2 + \frac{\bar{L}_n}{\bar{r}_n^2}} \chi(r - \bar{r}_n) \bar{f}_n, \quad (7.3)$$

$$\bar{S}(r) = \frac{1}{4\pi r^2} \sum_{n=1}^N \frac{\bar{w}_n^2 + \frac{\bar{L}_n}{\bar{r}_n^2}}{\sqrt{1 + \bar{w}_n^2 + \frac{\bar{L}_n}{\bar{r}_n^2}}} \chi(r - \bar{r}_n) \bar{f}_n, \quad (7.4)$$

$$\bar{j}(r) = \frac{1}{4\pi r^2} \sum_{n=1}^N \bar{w}_n \chi(r - \bar{r}_n) \bar{f}_n, \quad (7.5)$$

where r is chosen from the fixed radial grid. We plug $\bar{\rho}$ and \bar{j} into the field equations (1.27) and (1.28), which decouple from (1.29). In contrast to Schwarzschild coordinates, we cannot solve for the metric coefficients explicitly. We thus use a standard fourth-order Runge-Kutta (RK4) method to solve for \bar{a} and \bar{K}_θ^θ . We put these two quantities into the elliptic-type field equation (1.29), which leaves the linear second-order differential equation

$$\alpha'' = \alpha' \left(\frac{\bar{a}'}{\bar{a}} - \frac{2}{r} \right) + 6\alpha \bar{a}^2 (\bar{K}_\theta^\theta)^2 + 4\pi \alpha \bar{a}^2 (\bar{S} + \bar{\rho}), \quad (7.6)$$

where the boundary condition $\alpha(\infty) = 1$ makes solving this more delicate. Instead of using a sufficiently large radial grid and approximating the boundary condition at infinity as in [15, 45], we employ a different strategy which is inspired by the analytical procedure of solving for α developed in [46]. We first solve (7.6) with boundary condition $\alpha(R_{\min}) = 1$ via the RK4 method and obtain an approximate solution. We then rescale because of linearity in order to obtain $\bar{\alpha}$, which is an approximate solution of (7.6) with $\bar{\alpha}(\infty) = 1$.

Hence, we have computed the source terms and the metric coefficients of the current distribution represented by $(\bar{r}, \bar{w}, \bar{L}, \bar{f})$. The actual time step is implemented by propagating the particles according to the characteristic system corresponding to the Vlasov equation (1.25). For this, we use a prescribed time step of size $\Delta t > 0$. The necessary quantities are interpolated from the radial grid. By nature of (r, w, L) -coordinates being adapted to spherical symmetry, the propagation leads to difficulties and possibly large numerical errors if the radius \bar{r}_n gets small. To work around this problem, we propagate

the particles in Cartesian coordinates (x, v) , which removes the artificial singularity at the origin. This is a bit more computationally expensive but much more accurate. At this point, the new coordinates $(\bar{r}_{\Delta t}, \bar{w}_{\Delta t}, \bar{L}_{\Delta t})$ of the particles are known at time $t = \Delta t$. In addition, we update the weights \bar{f} during each time step and take care of the volume element contained in \bar{f} . More precisely, we have

$$\bar{f}_{\Delta t} = \bar{f} - \Delta t \left(\frac{\alpha(\bar{r}_n)}{\bar{a}^2(\bar{r}_n)} \bar{a}'(\bar{r}_n) \frac{\bar{w}_n}{\sqrt{1 + \bar{w}_n^2 + \frac{\bar{L}_n^2}{\bar{r}_n^2}}} - \bar{\beta}'(\bar{r}_n) - 2\bar{\alpha}(\bar{r}_n) \bar{K}_\theta^\theta(\bar{r}_n) \right) \bar{f}$$

as the new weights at time $t = \Delta t$, see also [15]. We now iterate this time step until we reach a final time T or until a certain condition is met to stop the simulation. A pseudo-code of the entire procedure can be found in Appendix D.2.

As to the numerical parameters, we typically use in the order of 10^7 particles for isotropic steady states and 10^6 particles for shells surrounding a black hole; in the latter case, fewer particles are sufficient since the particles are bounded away from the spatial origin, and the external potential from the black hole contributes to better numerical stability. During the time evolution we employ up to 10^6 time steps. Good choices for the step sizes Δr and Δt depend on the initial distribution under consideration.

Numerical refinements and validity checks: We actually use a RK4 method for the time propagation as well instead of the basic Euler stepping method suggested above. More precisely, a copy of the particles is propagated with a Euler method for a half time step $\frac{1}{2}\Delta t$ —we save the source terms and metric coefficients at the half step—, then a midpoint method is used to propagate the copy of the particles to $t = \Delta t$, and we again save the resulting source terms and metric coefficients. The actual particles are then propagated by employing RK4 and using the quantities calculated at $t = \frac{1}{2}\Delta t$ and $t = \Delta t$. This is numerically quite costly but worthwhile to prevent the particle trajectories from drifting from their actual path. Since the propagation of one particle is independent from the others, the PIC method can be parallelized efficiently, as discussed in detail in [68].

In the case of collapsing matter, the densities and metric coefficients become quite peaked and the simulation eventually gets inaccurate or breaks down. In order to prevent this from happening, we are able to freeze the particles which are inside a trapped surface, as defined in (1.34). This does not change the behavior of the solution outside of the trapped surface since information starting from the inside cannot reach the outside of a trapped surface. It does, however, prevent the quantities from exploding at the center, and the simulation of the dynamics outside of the trapped surface can continue. Note that this would not work in Schwarzschild coordinates which cannot cover trapped surfaces.

In order to keep track of the dynamical evolution, we output macroscopic quantities such as the radii \bar{R}_{\max} , \bar{R}_{\min} , the ADM-mass \bar{M} , the number of particles \bar{N} , and the central value $\bar{\alpha}(0)$, etc., at every time step. If necessary, we also output the metric coefficients and source terms as functions in r . Since the ADM-mass and the number

of particles are conserved quantities along solutions to the Einstein-Vlasov system, we track the relative errors

$$\frac{|\bar{M} - M|}{M}, \quad \frac{|\bar{N} - N|}{N}$$

during the time propagation. The errors stay remarkably small in the order of 10^{-6} (or even much lower) as long as the solution does not develop a trapped surface which may lead to errors up to 10^{-3} . We also verify that the initialization algorithm, which translates a given distribution \mathring{f} to the PIC method, is sufficiently accurate. For example, we compute the approximate L^1 -difference

$$\left[\frac{R_{\max} - R_{\min}}{\Delta r} \right] \sum_{k=0} \left| \bar{\rho}(R_{\min} + k\Delta r) - \rho_{\mathring{f}}(R_{\min} + k\Delta r) \right| (R_{\min} + k\Delta r)^2$$

and check that this difference is sufficiently small; otherwise we have to use more particles or a finer initialization grid.

Perturbing a steady state: The process described above does not draw on the investigation of stationary solutions but holds for general distributions \mathring{f} . However, in this work we are mainly interested in studying the stability behavior of steady states of the Einstein-Vlasov system. In order to investigate stability, we have to employ a scheme of slightly perturbing stationary solutions.² We use the same dynamically accessible perturbation method as in [45, 48]: We add the divergence-free term $(0, \gamma \frac{x}{r}) \in \mathbb{R}^3 \times \mathbb{R}^3$ to the right-hand side of the characteristic system during the particle propagation for an initial time interval $[0, T_{\text{pert}}]$. Here $\gamma \in \mathbb{R}$ is a small factor that determines the strength of the perturbation. This type of perturbation is physically reasonable since it conserves all Casimir functionals (1.35) and can be interpreted as an external force exerted on the individual particles. We typically use $T_{\text{pert}} = 10M$, whereas the value of γ might depend on the specific steady state: for isotropic equilibria $|\gamma| \approx 10^{-3}$ is reasonable while for shells with a black hole we need larger values of $|\gamma|$. In order to determine the strength of the applied perturbation method, we consider the difference $\Delta\alpha(t) := |e^{\mu_0}(t, 0) - \alpha(t, 0)|$ for $t \in [0, T_{\text{pert}}]$, which should stay quite small. Note that errors in the initialization and during the time evolution tend to lead to increased values of $\Delta\alpha(t)$. This necessitates a delicate balance, where γ must be sufficiently large to counterbalance initialization errors, yet not so large that it disproportionately perturbs the steady state.

Generally, the sign of γ determines whether the solution tends towards dispersion ($\gamma > 0$) or towards collapse ($\gamma < 0$). This is attributable to the fact that particles get slightly accelerated outwards for $\gamma > 0$ and inwards for $\gamma < 0$, which promotes dispersion in the former and collapse in the latter case. This was also observed in [45, 48].

It should be mentioned, however, that other types of perturbations basically lead to the same results as the dynamically accessible perturbation introduced above. In

²Numerical errors also naturally lead to a perturbation away from the steady state. However, as we observe different behaviors for different perturbation “directions”, we cannot rely on numerical errors as the driving factor.

particular, simply rescaling the static distribution f° by a factor close to one or slightly shifting all particles radially in- or outwards leads to similar results [15]. We have no reason to believe that the specific type of perturbation is decisive for the phenomena observed in the following.

Limitations: One of the main limitations of the PIC method is numerical noise introduced by random motion of the particles which can lead to fluctuations in the source terms and—to less extent—in the metric coefficients. Furthermore, the accuracy of the particle method is inherently limited by the cell size chosen during the initialization. In addition, we need to choose multiple numerical parameters which can affect the accuracy of the results. Lastly, the particle-in-cell method requires a large number of particles to accurately simulate the system, resulting in high computational costs.

7.3 Singularity-free steady states

For this part of the numerical investigation, we only consider singularity-free steady states which are isotropic. We present the distinction between stable and unstable steady states and how it manifests in the metric coefficients and macroscopic quantities in Sections 7.3.1 and 7.3.2. Furthermore, we recall the main result from [48], where the authors provide numerical evidence that contradicts the binding energy hypothesis. For the case of anisotropic equilibria, analogous results hold, and we refer the interested reader to [15, 45] for related studies.

For two main reasons, we use $\alpha(t, 0)$ as the main quantity to illustrate the time-development of a perturbed steady state: Firstly, it is the general relativistic counterpart of the Newtonian gravitational potential at the spatial origin. Thus, the development of $\alpha(t, 0)$ provides insights into whether the configuration is becoming more relativistic (indicated by decreasing values of $\alpha(t, 0)$) or less relativistic (indicated by increasing values of $\alpha(t, 0)$). As we will see in Section 7.3.2, the quantity $\alpha(t, 0)$ goes to zero if matter collapses to a black hole, whereas it converges to one as the matter disperses (fully). Secondly, from a mathematical point of view, $\alpha(t, 0)$ is obtained by integrating over $[0, \infty[$, which means that it takes the whole structure of the setting into account, rendering it more numerically stable. For an illustration of the density $\rho(t, \cdot)$ during the time evolution, we refer to [15, 45].

Another way to visualize the current configuration is to plot the (r, E) -space for a representative subset of the particles, as first introduced in [45]. This approach provides a detailed insight into the radial positioning of particles as well as their corresponding energies, thereby providing an indication of the system's behavior at the particle level in phase space.

7.3.1 Stable steady states

We find that stationary solutions that are not too relativistic are stable when perturbed slightly for $\gamma > 0$ and $\gamma < 0$, where γ is the parameter of the dynamically accessible perturbation introduced in Section 7.2. This is consistent with the results of Theo-

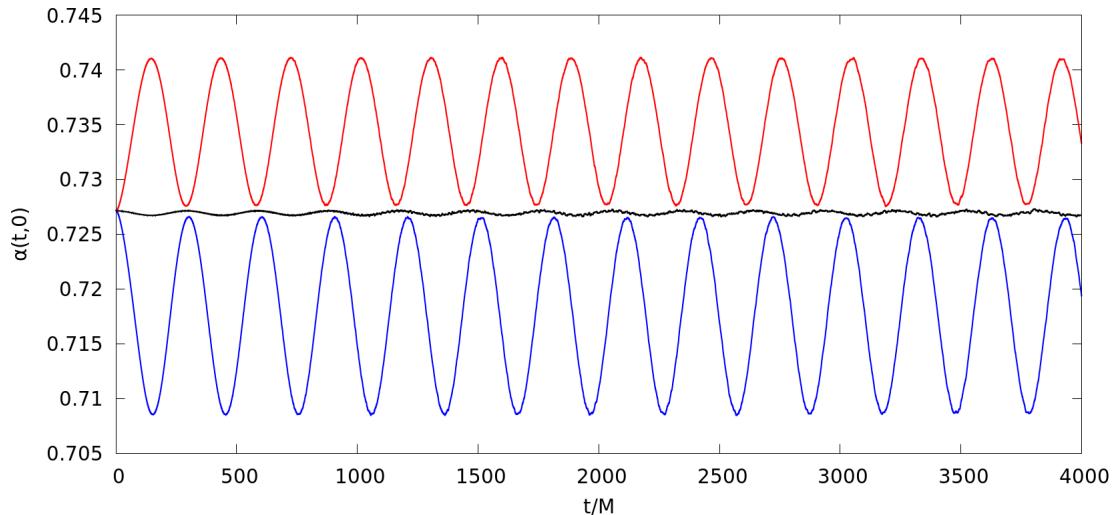


Figure 7.1: Time evolution of the quantity $\alpha(t,0)$ for the King model with $\kappa = 0.25$ perturbed with $\gamma < 0$ (blue line), $\gamma > 0$ (red line), and unperturbed $\gamma = 0$ (black line).

rem 5.1.4(a). Stability here does not mean that the configuration remains unchanged but manifests itself in two different types of behavior which we describe in the following.

Oscillation: A small perturbation of the static configuration often leads to oscillations of various quantities, for example in the density terms ρ and p , as well as in the metric coefficients α and a . This pulsating behavior has already been observed in [15, 45, 48] and is also known for the Vlasov-Poisson system [84]. We illustrate it for the King model in Figure 7.1, which also shows the effect of the sign of γ when perturbing a steady state. For $\gamma > 0$, the value of $\alpha(t,0)$ initially increases, whereas for $\gamma < 0$ it initially decreases. This is a general feature which we observe for all equilibria considered. In all three simulations, an oscillation sets in at roughly the same period. Even the unperturbed steady state ($\gamma = 0$) pulsates slightly due to inherent numerical errors from the initialization and time evolution. The period depends on the specific model under consideration as well as the strength of the perturbation. However, if the perturbation is small enough, the period appears to “converge” to a fixed value.

It is worth noting that such oscillations are particularly pronounced and easily recognizable when one is close to the stability change along a κ -family of steady states $(f_\kappa)_{\kappa>0}$, see Section 7.3.3. This should not come as a surprise, as we have proven the existence of linearly oscillating modes under suitable assumptions in Theorem 6.3.4 by considering values of κ close to the point where stability changes.

Damping: We observe damping effects for stationary solutions if the ansatz function Φ is sufficiently smooth and the redshift κ is small enough. For example, perturbed isotropic polytropes (2.5) with different values of k and $\kappa = 0.05$ are shown in Figure 7.2. On the one hand, if the polytropic index k is small, i.e., the ansatz function Φ is not dif-

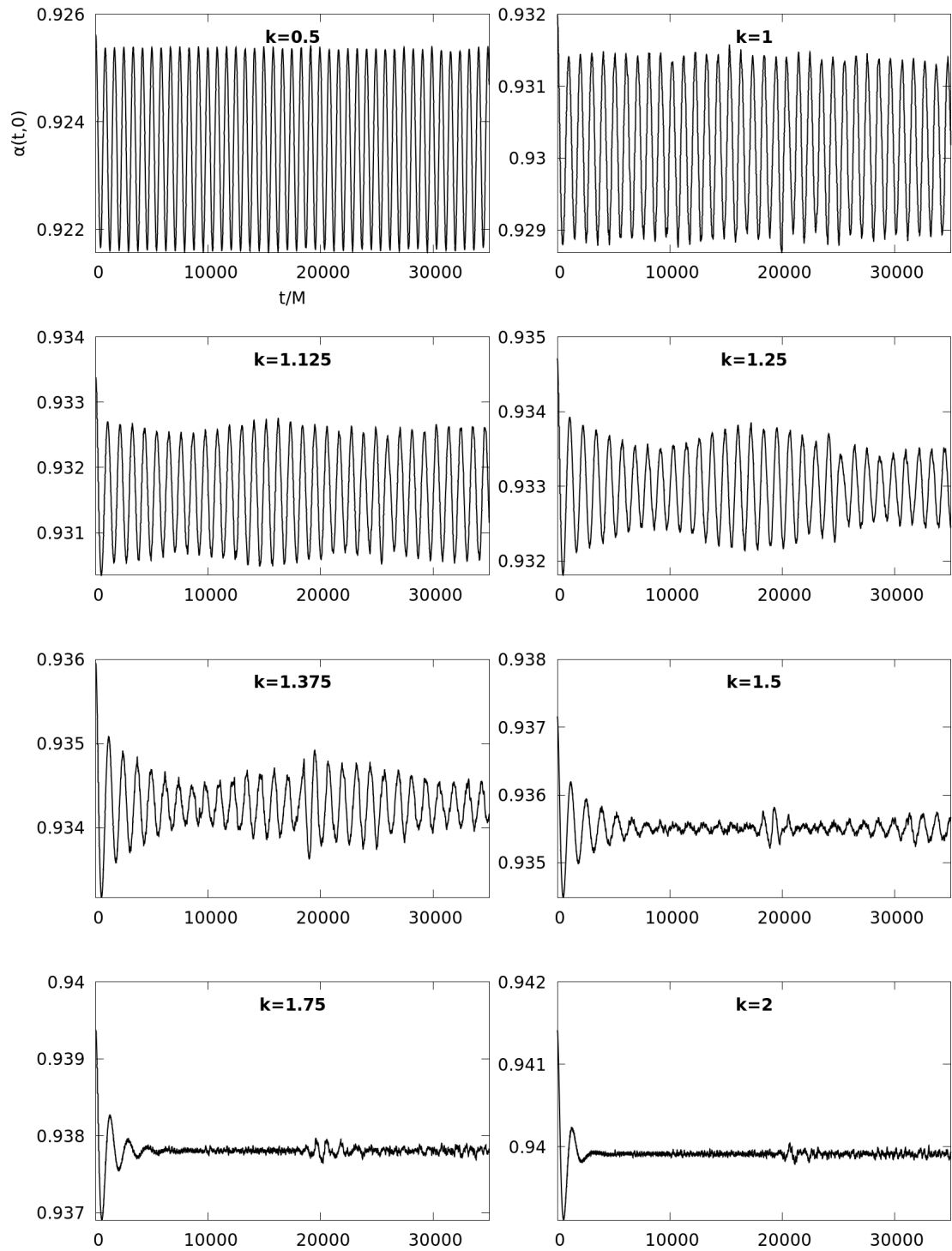


Figure 7.2: Time evolution of the quantity $\alpha(t, 0)$ for isotropic polytropes with different values of the polytropic exponent k and $\kappa = 0.05$ perturbed with $\gamma < 0$.

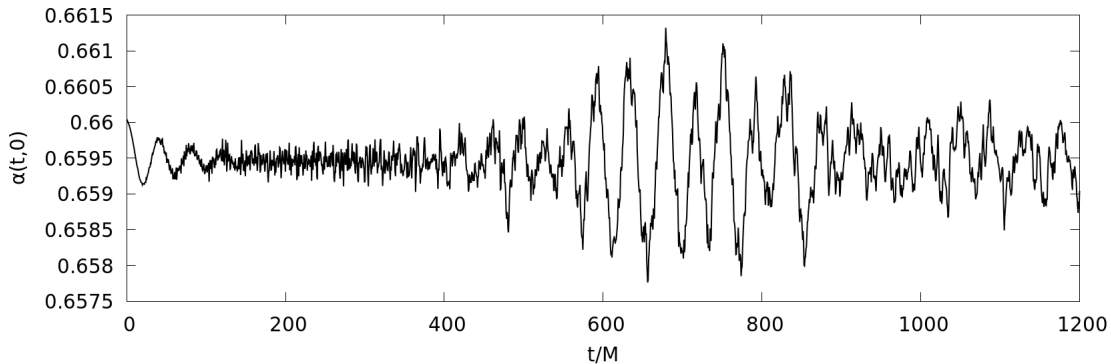


Figure 7.3: Time evolution of the quantity $\alpha(t, 0)$ for the piecewise model with $n = 130$ and $\kappa = 0.4$ perturbed with $\gamma < 0$. See Figure 2.8 for the corresponding weighted mass density $4\pi r^2 \rho$.

ferentiable at zero, undamped oscillations are present. On the other hand, for $k \geq 1.5$ we obtain damping that becomes more intense as k increases. The damping is represented by the progressive decrease of the deflection of the quantity $\alpha(t, 0)$, until an unchanged state is reached where $\alpha(t, 0)$ remains almost constant for large values of t . Note that $k > 1$ corresponds to an ansatz function Φ that is continuously differentiable at zero. However, it is not feasible to numerically determine the threshold value of k , which leads to damping rather than oscillation. In particular, it is unclear whether $k = 1.25$ and $k = 1.375$ can be considered damped or if we obtain a superposition of two oscillations. As in [84, Fig. 7], we observe models where oscillations get damped for small t and after some large time seemingly get re-initiated, e.g., for the case $k = 1.5$.

To the authors' knowledge, damping effects for perturbed steady states of the Einstein-Vlasov system have not yet been described in the literature. Our results are consistent with the observation of [84], where the authors numerically discover damping for Newtonian isotropic polytropes with $k \geq 1.2$. Since we observe damping for small values of κ , the steady states can be considered close to Newtonian, and similar behavior as in the Vlasov-Poisson system should be expected. We speculate that damping will not be present near the point where stability changes, even for larger values of k , in accordance with Theorem 6.3.4. This may also be the reason why damping has not yet been observed in the literature.

For the linearized Vlasov-Poisson system with a point-mass, damping has been proven in the recent work [56] for small, smooth shells. Remarkably, in this case the polytropic index k fully determines whether oscillation or damping is present. As we do not go into more detail here, we refer to [56] and the references there for further information.

We emphasize that it is often not possible to differentiate between damping and oscillation. For example, depending on the model and the strength of the perturbation, the relevant quantities might stay static or flicker diffusely. Such behavior might arise because numerical errors dominate compared to the small perturbation. Recall the steady state induced by the piecewise model with $n = 130$ and $\kappa = 0.4$ shown in Figure 2.8. It

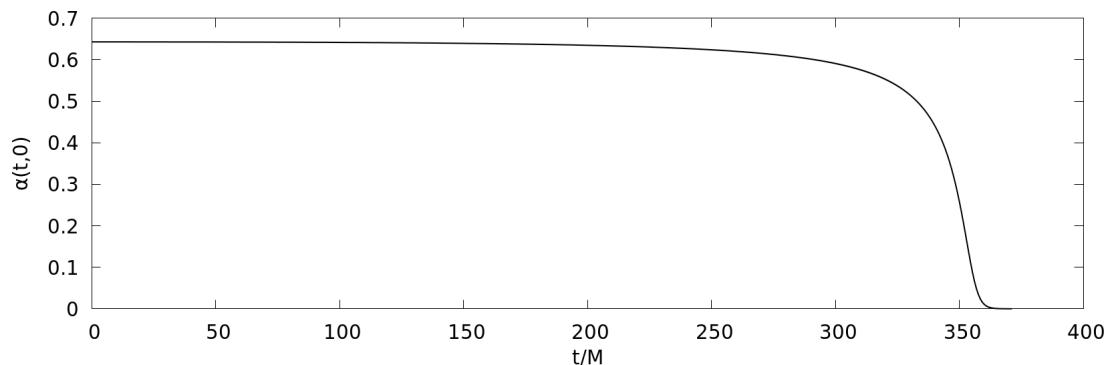


Figure 7.4: Time evolution of the quantity $\alpha(t,0)$ for the King model with $\kappa = 0.36$ perturbed with $\gamma < 0$.

has a very dense core and a long tail which is much less relativistic. It turns out that such a setting can be stable, as illustrated in Figure 7.3. The quantity $\alpha(t,0)$ behaves quite randomly after an initial oscillation for roughly two periods. This oscillation apparently comes back stronger later in time, but numerical effects make it hard to say anything more specific. The evolution of $\alpha(t,0)$ is reminiscent of the case $k = 1.5$ in Figure 7.2. This perturbed steady state is also considered but not presented explicitly in [48].

Overall, the results above provide new insights on the behavior of steady states of the Einstein-Vlasov systems and may have important implications for the formation and evolution of astrophysical structures. Further research is needed to fully understand the damping mechanisms and to develop new methods for studying their long-term behavior.

7.3.2 Unstable steady states

One of the most interesting facets of the Einstein-Vlasov system is the existence of unstable steady states that arise when choosing a sufficiently large value of the redshift κ , cf. Theorem 5.1.4(b). If the system is initially perturbed slightly away from the steady state, the perturbation can grow exponentially over time, leading to a rapid change of the configuration. This evolution can take various forms depending on the specific properties of the underlying steady state, such as the ansatz function Φ , the value of κ , as well as the direction of the perturbation, i.e., the sign of γ .

We observe a dichotomy in the sense that we generally obtain two types of behavior for unstable steady states: The perturbation can cause the system to collapse to a black hole, which means that a trapped surface develops, or it can cause the system to disperse and become more homogeneous. We describe this in more detail below.

Total collapse: For a large class of the unstable steady states, a small perturbation towards collapse ($\gamma < 0$) leads to the total collapse of the matter. Every numerical particle irreversibly leaves its orbit and rushes towards the center until, eventually, a trapped surface forms. We confirm the findings of previous studies that the radius at which the first trapped surface forms is much larger than the radial step size Δr .

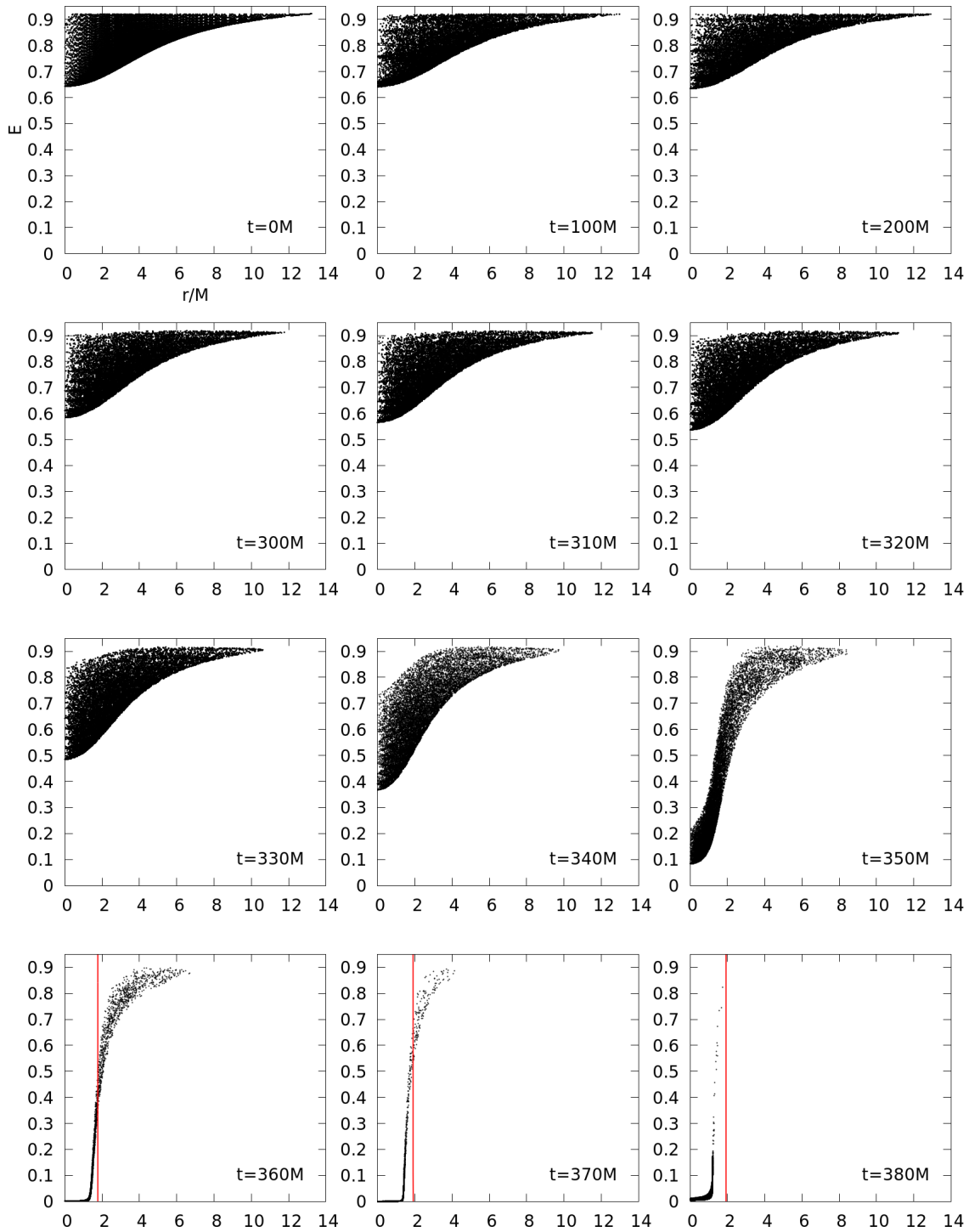


Figure 7.5: Time evolution of the radius-energy space for the King model with $\kappa = 0.36$ perturbed with $\gamma < 0$. The red line correspond to the radius r_{TS} , i.e., the outermost trapped surface which first appears at $t \approx 357M$.

This supports that the weak cosmic censorship hypothesis holds for the Einstein-Vlasov system. Moreover, the mass density ρ gets more peaked as the matter focuses towards the center, whereas the value of $\alpha(t, 0)$ converges to zero. The latter is often referred to as the “collapse of the lapse” in the literature since $\alpha(t, \cdot)$ determines the rate of proper time elapsing on the hypersurface of constant t . The exponential decay of the lapse function α is studied more closely in [45, Sc. 4.3]. We either stop the simulation, if a trapped surface is present, or freeze the particles inside of it, as described in Section 7.2. In order to detect a trapped surface, we check if

$$\frac{1}{a(t, r)} < r K_{\theta}^{\theta}(t, r) \quad (7.7)$$

is valid at some radius $r > 0$. For fixed $t > 0$, we call the largest value of r , where (7.7) holds, the (*outermost*) *trapped radius* and denote it as $r_{\text{TS}}(t)$. The smallest point in time t , where (7.7) is satisfied, is referred to as the *collapse time* and denoted by t_{TS} . Accordingly, the *trapped mass* $M_{\text{TS}}(t)$ corresponds to the mass inside the trapped radius $r_{\text{TS}}(t)$.

The typical process of a total collapse for an unstable steady state induced by the King model is presented in Figures 7.4 and 7.5, for the quantity $\alpha(t, 0)$ and in the radius-energy space, respectively. Initially, the configuration appears almost unchanged for $t \leq 300M$ until the instability sets in rapidly. The value $\alpha(t, 0)$ converges to 0 and we stop the simulation as the numerical errors get too large. Figure 7.5 clearly illustrates that all particles get sucked towards the center. At roughly $t_{\text{TS}} \approx 357M$, the first trapped surface forms, and shortly afterwards, all particles cross the radius $r_{\text{TS}}(t)$. Note that the collapse time t_{TS} depends on the strength of the perturbation as well as the numerical accuracy employed. It is worth mentioning that in the final configuration at $t = 380M$ we have $r_{\text{TS}}(t) \approx 2M$.

Partial collapse: It is not always the case that all the matter eventually collapses into the black hole. For example, unstable core-halo configurations exist, as shown in Figure 7.6. In this setting, the dense core typically collapses rapidly when the steady state is perturbed with $\gamma < 0$, while the large Newtonian halo remains mostly unchanged. In contrast to the aforementioned scenario, we do not observe that all matter moves into the trapped surface but continues to orbit the newly formed black hole in a stable manner. Although individual particles may occasionally move beyond the trapped radius, this phenomenon diminishes over time and could be primarily attributed to numerical errors. We are confident that the bulk of the matter stays confined away from the trapped surface. In particular, if we run the simulation long enough, an apparently stable shell surrounding the newly formed black hole remains. In this sense, we observe a heteroclinic orbit from an unstable, singularity-free isotropic equilibrium to a stable shell with a Schwarzschild singularity at the center. We note that the inner radius of the remaining shell is very close to the photon sphere $r = 3M_{\text{TS}}$. However, it is unclear what the final setting actually is and by what model it can be described. Further research is needed to fully understand the final configuration. It is worth noting that the trapped radius r_{TS} is small compared to the remaining matter, but it still contains a significant

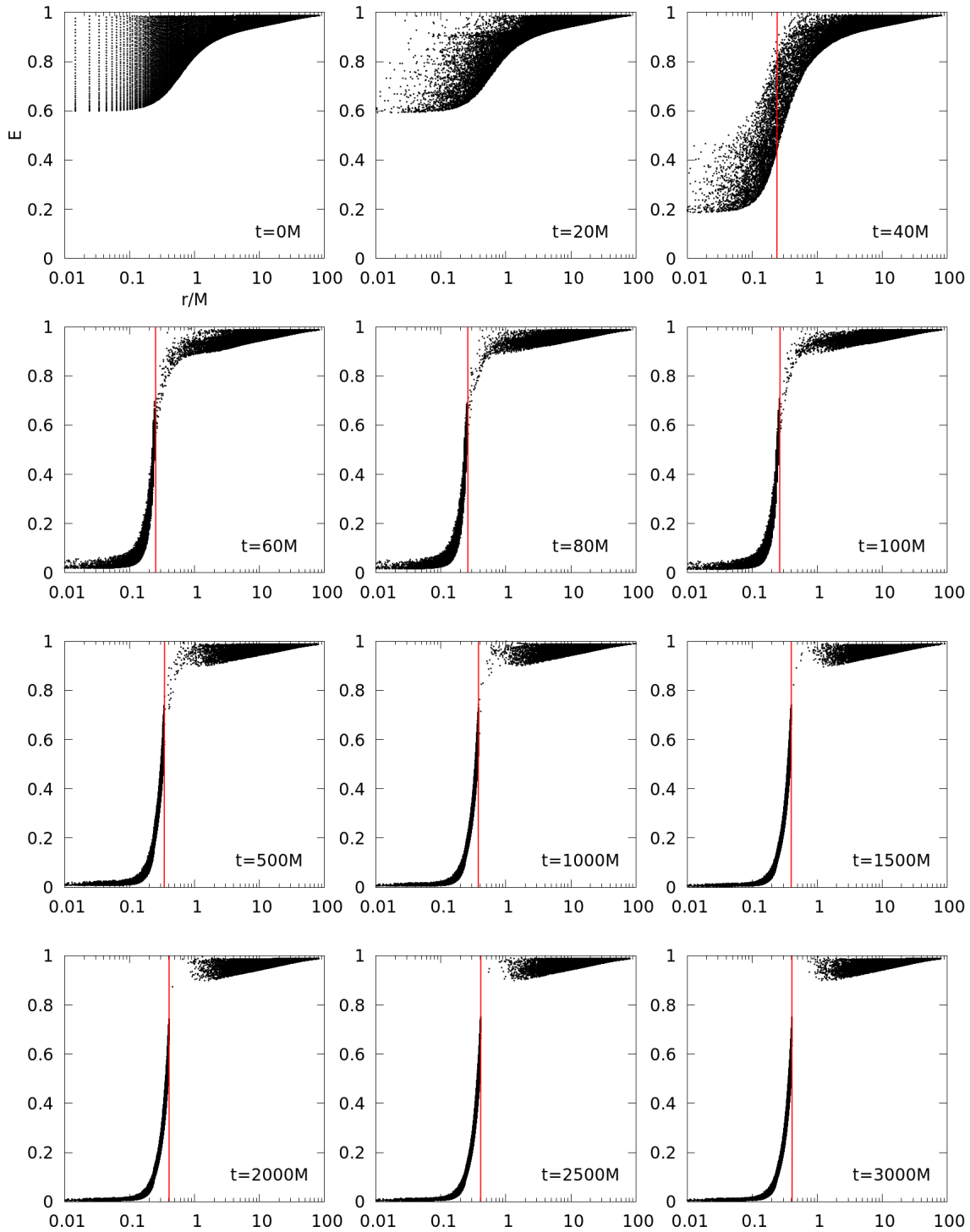


Figure 7.6: Time evolution of the radius-energy space for the piecewise model with $n = 130$ and $\kappa = 0.5$ perturbed with $\gamma < 0$. Particles inside of a trapped surface are frozen in order to continue the simulation outside. The red line corresponds to the trapped radius r_{TS} . Note the logarithmic scale.

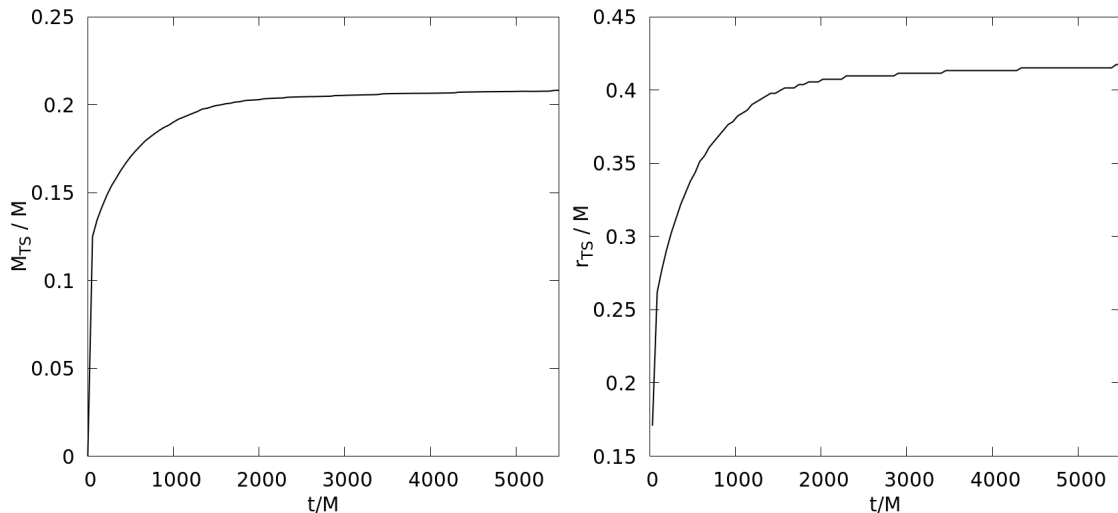


Figure 7.7: Time evolution of the trapped mass M_{TS} and the trapped radius r_{TS} in multiples of the ADM mass M , corresponding to the model used in Figure 7.6

fraction of the total mass of the initial steady state. The time evolution of the trapped mass and the trapped radius is shown in Figure 7.7. This presents further evidence that the configuration eventually settles near a new equilibrium. In conclusion, the partial collapse highlights another complex behavior that can occur for unstable steady states. It is important to study such scenarios in more detail to better understand the behavior of Vlasov matter under highly relativistic conditions.

So far, we have considered collapse promoting perturbations. Next, we study the scenario of $\gamma > 0$, i.e., perturbations that promote dispersion which leads to significantly different behavior for unstable steady states.

Partial dispersion (heteroclinic orbits): Perturbing an unstable equilibrium with a dispersion promoting perturbation can lead to *heteroclinic orbits* in the sense that the unstable isotropic steady state is transformed to a less relativistic, stable static solution which still seems to be isotropic. Such behavior was first observed in [45].

The perturbation leads to an initial dispersion and relaxation of the solution. More precisely, the matter is distributed more homogeneously in phase space, and the corresponding spacetime becomes flatter. If the initial steady state is not too relativistic, the solution reimplodes at some point, and a new structure appears to form around the center which begins to oscillate. In terms of $\alpha(t, 0)$, this means that the quantity initially increases due to the relaxation but starts to decrease after the solution reimplodes. After this, it oscillates around an approximately fixed value which is larger than $\alpha(0, 0)$, indicating a less relativistic configuration. This behavior is depicted in Figure 7.8 for the King model and occurs across all unstable isotropic models that we have considered, when they are perturbed towards dispersion and the redshift is not too large.

In terms of the individual particles, we observe that the initial dispersion leads to

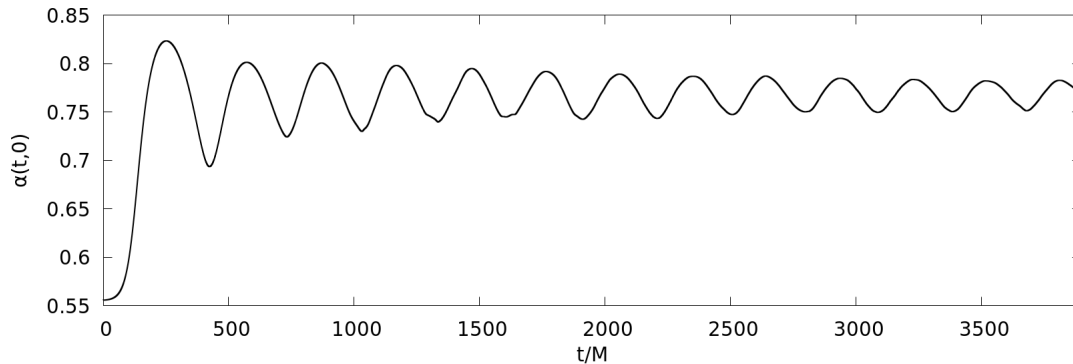


Figure 7.8: Heteroclinic orbit for the King model and $\kappa = 0.5$ illustrated by the time evolution of the quantity $\alpha(t, 0)$. The steady state is perturbed with $\gamma > 0$.

clusters of particles being ejected completely from the setting—they keep moving away from the spatial origin during the whole simulation—while other particles return after some time. The process of particles getting expelled and returning repeats a handful of times until the solution settles (and pulsates) around a new, apparently stationary configuration. For the same simulation as in Figure 7.8, the evolution of the radius-energy space is shown in Figure 7.9. The ejection of particles is clearly visible for $t = 400M$ and $t = 500M$. For $t > 2000M$, the solution has settled down and does not change much anymore apart from the pulsating behavior.

The final configuration, which remains after the dispersion and reimplosion, is less relativistic and only depends on the initial steady state. In particular, it is independent of the (small) perturbation. For dynamical systems, such a new state is generally a stable static solution to the system, and the behavior described above is suggestive of a heteroclinic orbit since the initial equilibrium migrates to a new one following the perturbation.

As noted in [45], it is a delicate task to identify the new state since it is not possible to decide which particles constitute the new state and which particles are simply trapped inside of the gravitational potential of the new state without actually “belonging” to it. The abundance of stationary solutions to the Einstein-Vlasov system further complicates this process, leaving the problem unsolved and thus requiring additional research.

There are two additional important observations concerning heteroclinic orbits: Firstly, it is not always the case that particles get expelled. In some cases, the steady state simply moves to a slightly less relativistic state which is stable. This usually happens if the steady state is located close to the point where stability changes along a κ -family. In fact, it appears to be a smooth process in κ from stable steady states to heteroclinic orbits without ejection of particles to heteroclinic orbits with ejection of particles. This progression is demonstrated in Figure 7.10 for the King model. Secondly, it has been speculated [108] that negative binding energy together with a dispersion promoting perturbation leads to the full dispersion of the steady state. This is expanded to and confirmed for anisotropic polytropes in [15]. However, the author and colleagues

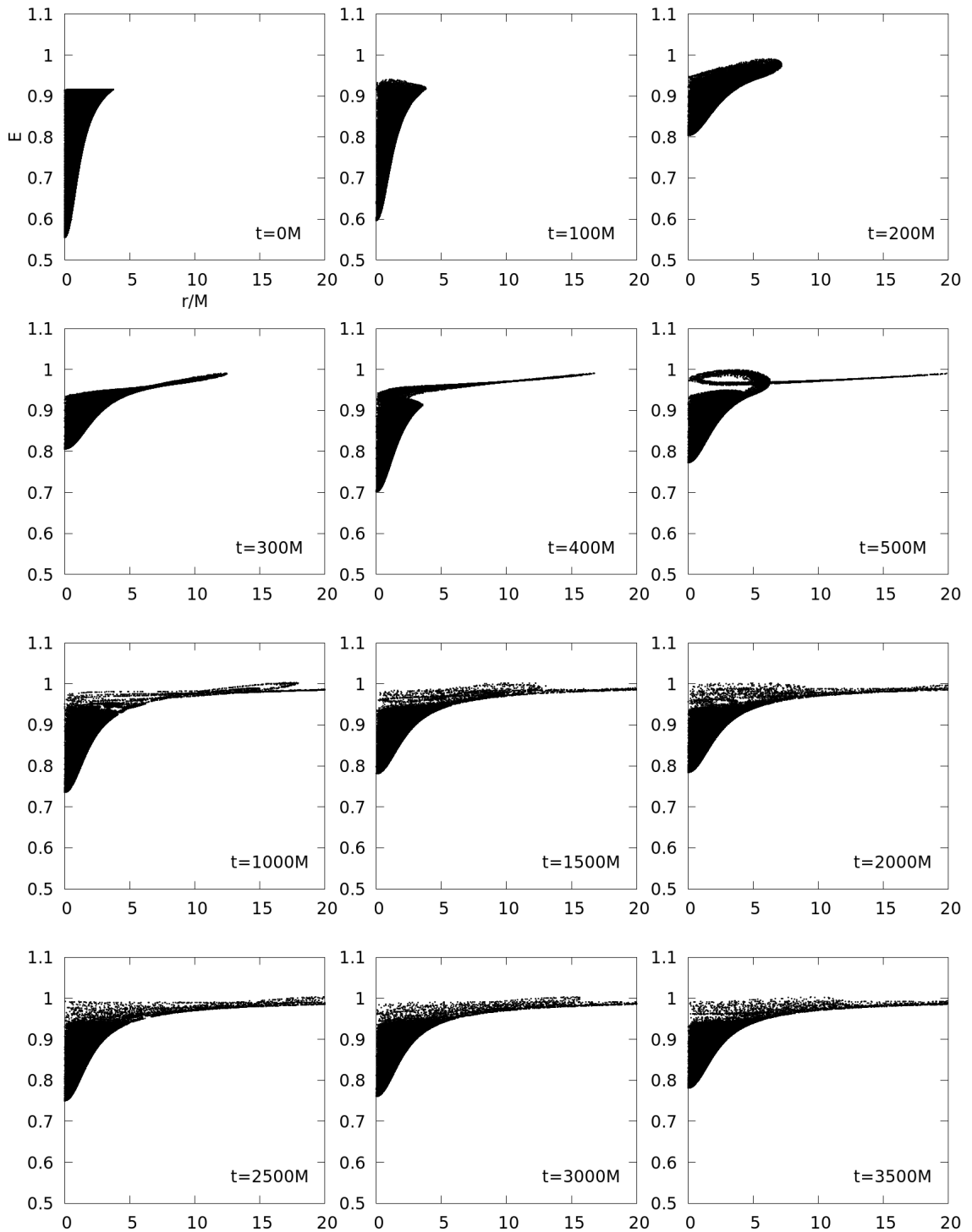


Figure 7.9: Time evolution of the radius-energy space for the King model with $\kappa = 0.5$ perturbed with $\gamma > 0$.

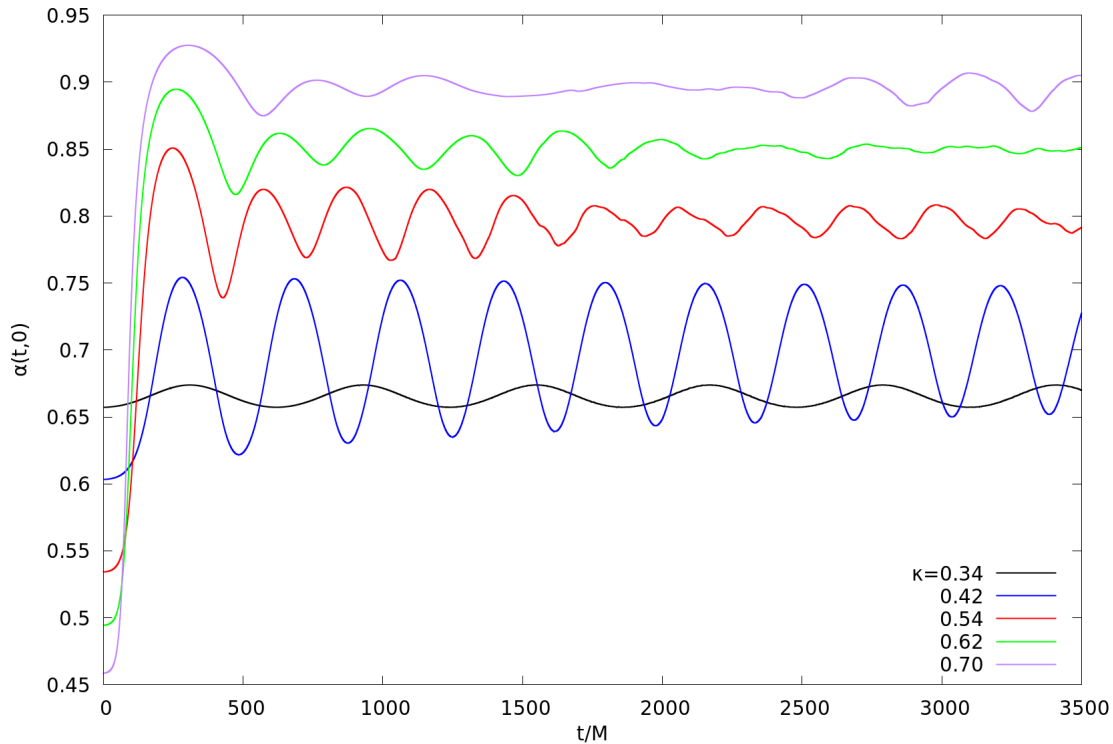


Figure 7.10: Heteroclinic orbits along the King model for different values of κ illustrated by the time evolution of the quantity $\alpha(t,0)$. The steady states are perturbed with $\gamma > 0$.

present evidence against this hypothesis in [45], where heteroclinic orbits are observed even if the initial equilibrium has negative binding energy. In addition, we observe and hypothesize that heteroclinic orbits always exist for unstable steady states with positive binding energy. This means that even highly relativistic stationary solutions perturbed towards dispersion perform a heteroclinic orbit to a less relativistic configuration and do not fully disperse or show other unstable behavior. For example, we have checked the piecewise model with $n = 130$ and $\kappa = 1.5$, which corresponds to a central redshift factor of $z_c \approx 3.624$ and a binding energy of $E_b \approx 0.01793$. Despite the very relativistic initial equilibrium, we indubitably obtain a heteroclinic orbit.

We come back to the question whether the sign of the binding energy determines the dispersion behavior later in Section 7.4 when we investigate shells surrounding a black hole. Nevertheless, fully dispersing solutions are still present for the isotropic steady states for the Einstein-Vlasov system in some cases.

Full dispersion: For some κ -families of singularity-free steady states, it happens that the heteroclinic orbit ceases to exist if the value of κ is large enough. In this case, a dispersion promoting perturbation leads to a full dispersion in the sense that the metric coefficients approach that of Minkowski space, i.e., $\alpha = 1 = a$ and $K_\theta^\theta = 0$. The evolution

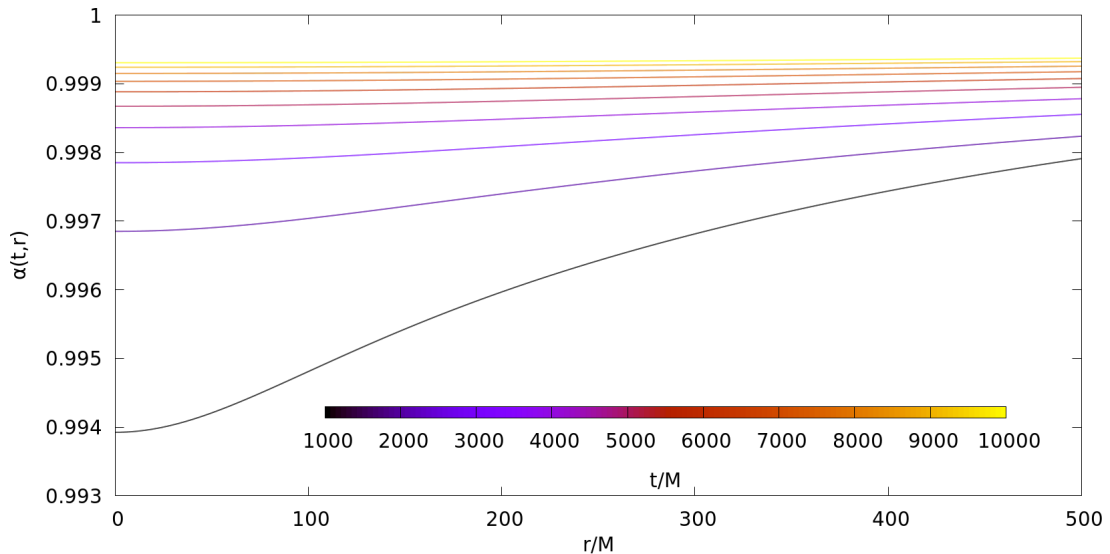


Figure 7.11: The metric coefficient $\alpha(t, \cdot)$ for different values of $t \geq 1000M$ for the isotropic polytrope with $k = \frac{1}{2}$ and $\kappa = 1$ perturbed with $\gamma > 0$.

of the metric coefficient $\alpha(t, \cdot)$ is presented in Figure 7.11 for the isotropic polytropes with $k = \frac{1}{2}$ and $\kappa = 1$.

For every fixed radius $r > 0$, the value of $\alpha(t, r)$ is monotonically increasing in time t and thus the overall setting gets less relativistic. In particular, $\alpha(t, 0)$ keeps increasing until it approaches one, unlike for heteroclinic orbits where this value eventually decreases again. The individual particles spread out more and more homogeneously over the radial space. Some particles escape towards spatial infinity and appear not to return, while others stay close to the origin. The particles close to the center do not move on periodic orbits anymore but have very small momentum. We emphasize that we only find evidence for full dispersion if the binding energy E_b is sufficiently negative. In Section 7.4.2, we will see that the dispersing behavior of shells surrounding a black hole is qualitatively different.

7.3.3 Stability behavior along κ -families

Throughout the analysis of the stability of steady states of the Einstein-Vlasov system in Chapters 5 and 6, considering families of stationary solutions parametrized by the redshift κ was of particular interest and useful from a mathematical point of view. This is also the case for the numerical stability analysis. As mentioned in Section 7.1, the point where stability changes along a one-parameter family of steady states has already been studied quite extensively in the literature. Most of the earlier numerical work found that κ -families $(f_\kappa)_{\kappa > 0}$ behave in a manner that f_κ is stable for $\kappa < \kappa_0$ and becomes unstable for $\kappa \geq \kappa_0$, where κ_0 is a threshold value signaling the onset of instability. For example, this is the case for isotropic and anisotropic polytropes [15, 45] as well as for

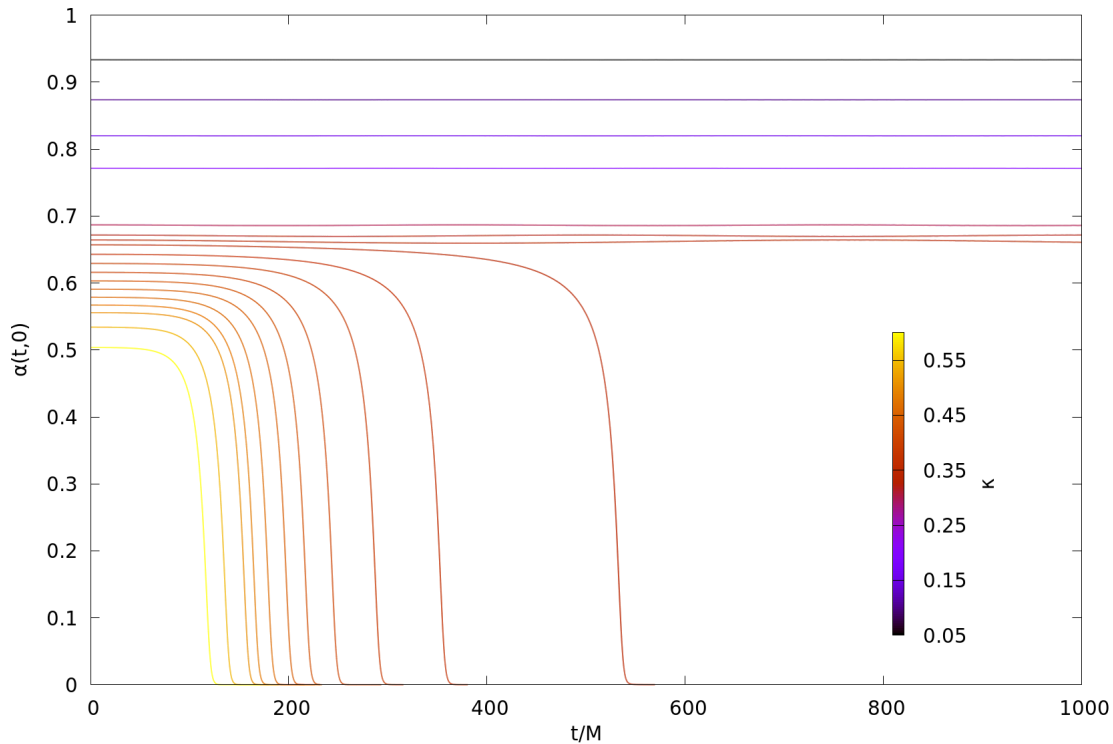


Figure 7.12: Stability behavior of the King model for different values of κ illustrated by the time evolution of the quantity $\alpha(t, 0)$. The steady states are perturbed with $\gamma < 0$.

Maxwell-Boltzmann distributions [60, 108]. In Figure 7.12, we recall the behavior for the King model and provide the typical stability behavior along a family of isotropic equilibria perturbed with $\gamma < 0$; this is also included in [45], . We find that the steady states are stable for $\kappa \leq 0.3325$ and unstable for $\kappa \geq 0.335$. There is only one change in stability behavior, and the value $\kappa = 0.3325$ is very close to the maximizer of the binding energy curve. In the case of a stable configuration, the perturbed steady state stays mostly unchanged. Despite the plot being limited to $t \leq 1000M$, we have simulated the system much longer in the stable case. The perturbation might lead to an oscillation which is more visible when κ is close to the point where stability changes. In the case of collapse, a trapped surface eventually forms and all particles cross this barrier after some time. In addition, Figure 7.12 shows that—for unstable steady states—the collapse time, i.e., the time after which a trapped surface is first formed, is increasing in κ .³

As mentioned in Remark 7.1.1, the author and colleagues provide strong evidence in [48] that stability changes do not necessarily occur at a critical point of the binding

³For this observation, we have to employ the same “strength” of the perturbation and numerical accuracy across all models. Otherwise, the collapse time can vary much more and may not decrease if κ increases.

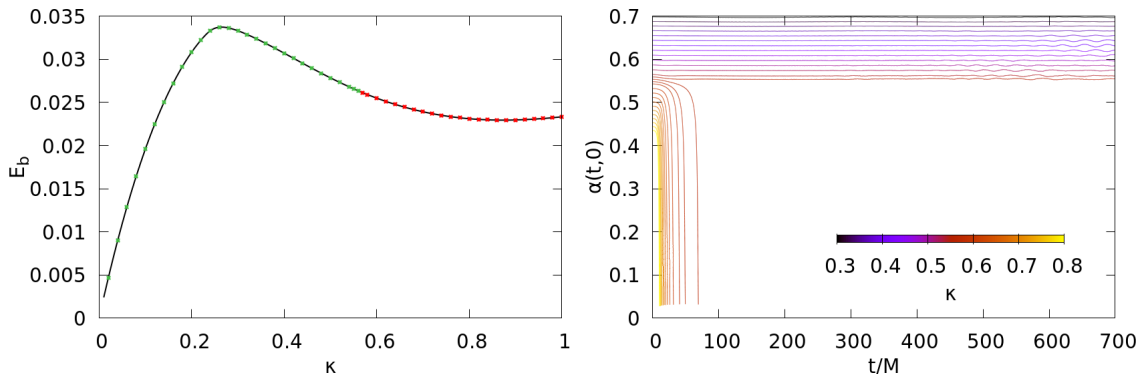


Figure 7.13: Stability behavior of the piecewise model with $n = 200$ for different values of κ . The left hand side shows the binding energy along κ ; green dots mark stable steady states and red dots unstable ones. On the right hand side, the time evolution of the quantity $\alpha(t,0)$ is plotted. The steady states are perturbed with $\gamma < 0$. See also [48, Fig. 5].

energy, which was long believed to be the crucial quantity for the onset of instability. For the sake of completeness, we briefly recall the main findings of [48, Sc. 5.1] which contains much more information on the topic and a comprehensive numerical analysis of the piecewise model (2.76).

In Figure 7.13, we present the binding energy curve as a function in κ and the corresponding time evolution of $\alpha(t,0)$ along certain values of κ for the piecewise model with $n = 200$, see also [48, Fig. 5]. The steady states are stable for $\kappa \leq 0.56$ and unstable for $\kappa \geq 0.57$, whereas the first local maximum of the binding energy is attained at $\kappa \approx 0.265$. Moreover, the change in stability cannot be attributed to other critical points of the binding energy curve. Other criteria that might be connected to the onset of instability are discussed further in [48, Ch. 6], e.g., a *local* binding energy, a modification of the binding energy by using a different Casimir functional, a threshold value of $\sup_{r>0} \frac{2m}{r}$, etc. However, these ideas were to no avail and no universal criterion is known. It remains a conundrum why the binding energy serves as a reliable indicator of stability in models such as the King model or the polytropes but fails to do so in the case of the piecewise model.

For the King model and polytropes, previous studies always found just one point along κ , where stability changes from stability to instability. In this regard, the piecewise model displays another interesting feature: For $255 \leq n \leq 290$ stability changes multiple times along the family of steady states parametrized by the redshift. This was first detected and described in [48, Sc. 5.2].

In the case $n = 270$, the stability behavior and the multiple stability changes on the level of the evolution of $\alpha(t,0)$ are depicted in Figure 7.14. The steady states are stable for $\kappa \leq 0.32$ and become unstable for $0.33 \leq \kappa \leq 0.47$. After the initial unstable region, a second stability domain sets in for $0.48 \leq \kappa \leq 0.63$, which consists of much more relativistic stationary solutions compared to the first stable domain. By increasing the

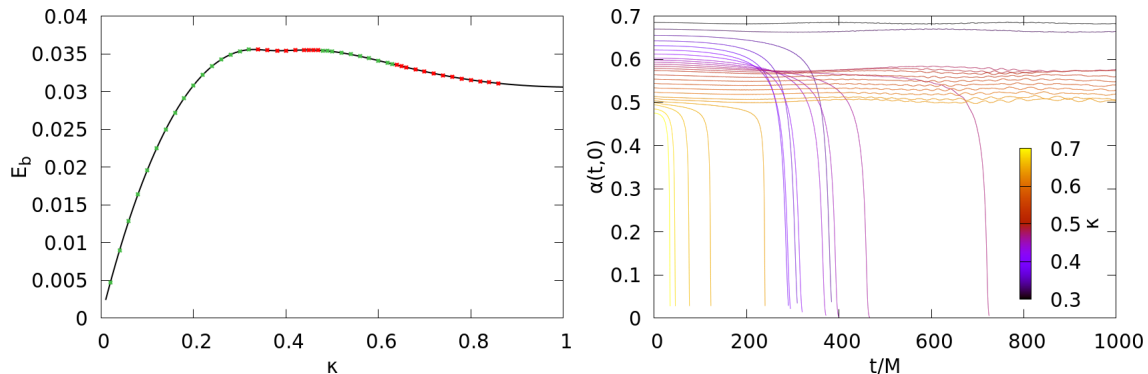


Figure 7.14: Stability behavior of the piecewise model with $n = 270$ for different values of κ . The left hand side shows the binding energy along κ ; green dots mark stable steady state and red dots unstable ones. On the right hand side, the time evolution of the quantity $\alpha(t,0)$ is plotted. The steady states are perturbed with $\gamma < 0$. See also [48, Fig. 6].

redshift further, we eventually reach another point where instability sets in, and the steady states are unstable for $\kappa \geq 0.64$. The points where stability changes are close to critical points of the binding energy curve which is quite flat for the relevant values of κ . It is unclear if this has anything to do with the peculiar behavior observed here. We do not observe a third stability domain for the piecewise model, but it is conceivable that stability may change even more often when considering other ansatz functions.

7.4 Steady states surrounding a Schwarzschild black hole

Besides isotropic steady states, static shells surrounding a Schwarzschild black hole of mass M_0 form the other central class of equilibria considered throughout this work. We describe the different types of stability behavior for shells, as constructed in Section 2.2.2. To avoid exceeding the scope of this study, we refrain from analyzing the stability behavior along families of steady states. To the author's knowledge, this is the first time that non-linear stability of stationary solutions to the Einstein-Vlasov system with a singularity is explored.

As maximal areal coordinates only cover the region where $r > 2M_0$, we cannot use the evolution of $\alpha(t,0)$ for illustrating the stability behavior of the steady state in time. Instead, we use $\alpha(t,3M_0)$, which can be viewed as an analogous quantity to $\alpha(t,0)$ in the setting with a singularity. Note that $3M_0 < R_{\min}$ necessarily holds due to condition (P2), i.e., $\alpha(t,3M_0)$ is guaranteed to take into account the whole structure of the steady state—at least in its initial, unperturbed state—since it is obtained by integrating from infinity inwards. Furthermore, we usually consider the time and radial variables in multiples of

$$M_{\text{tot}} = M_0 + M,$$

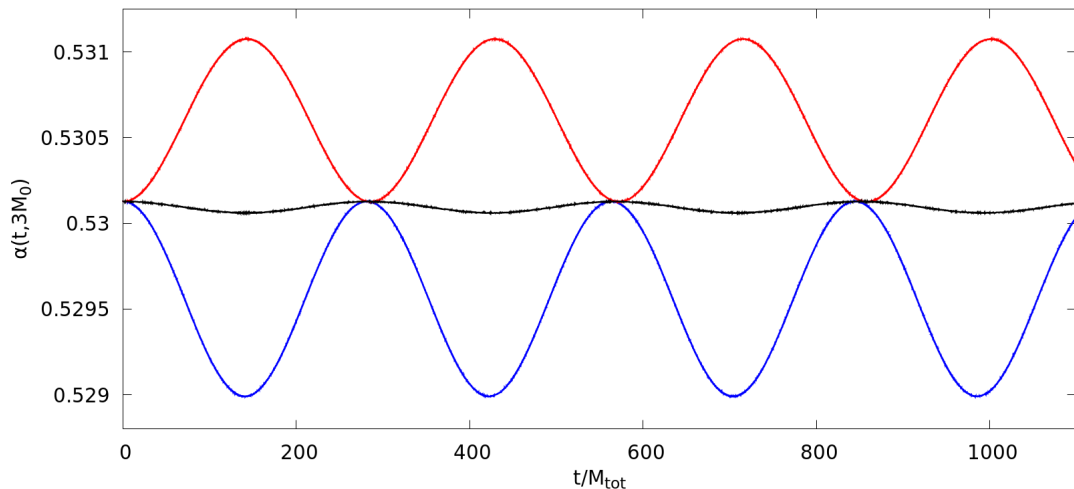


Figure 7.15: Time evolution of the quantity $\alpha(t, 3M_0)$ for a stable shell surrounding a black hole of mass $M_0 = 1$ perturbed with $\gamma < 0$, $\gamma > 0$, and unperturbed ($\gamma = 0$). The model is given by the polytropic ansatz with $k = 1$, $l = 1$, $L_0 = 50$, and $\kappa = 0.01$.

where M is the Vlasov mass of the steady state, see (2.27). This makes the time and radial variables more comparable across different models. Finally, as in Section 2.4, we consider only single shell solutions and leave the study of equilibria with multiple shells open for future work.

7.4.1 Stable shells

Given Theorem 5.4.4, the existence of non-linearly stable shells surrounding a black hole should come as no surprise. Stability manifests itself in several ways, analogous to the singularity-free case studied earlier:

Oscillation: A small perturbation can induce an oscillation of the source and metric terms which is very similar to the behavior described in Section 7.3.1. We illustrate this for a polytropic model in Figure 7.15 where we consider the time development of $\alpha(t, 3M_0)$ in the three cases of a perturbation towards collapse, towards dispersion, and the unperturbed solution. This should be compared to Figure 7.1 which shows the same qualitative behavior. It is noteworthy that the period of the oscillation is only marginally dependent on the strength and type of the perturbation. In addition, the unperturbed solution exhibits a slight pulsation caused by numerical artifacts.⁴

⁴Without going into more detail, we note that—as in the singularity-free case—oscillations are better visible and obtainable when the model is “close” to unstable steady states. Even if the theory from Chapter 6 does not apply here, the same mechanism for the linearized system should be valid, i.e., there will most likely be an eigenvalue that transitions into the negative and thus stimulates an oscillating mode.

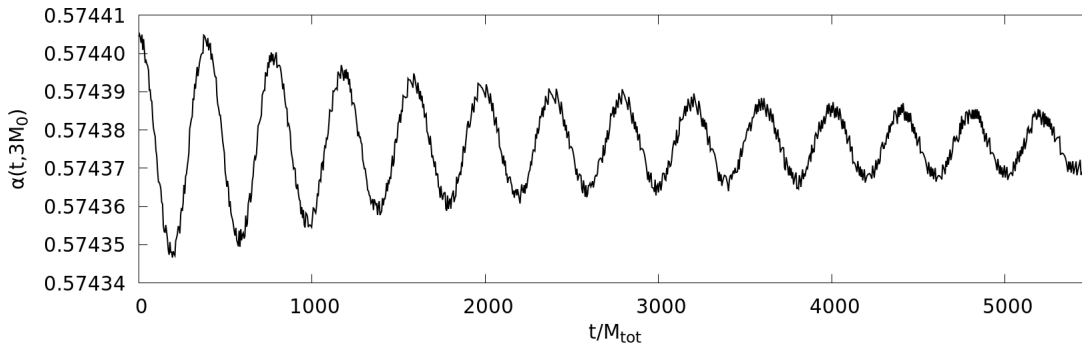


Figure 7.16: Time evolution of the quantity $\alpha(t, 3M_0)$ for a stable shell surrounding a black hole of mass $M_0 = 1$ perturbed with $\gamma < 0$. The model is obtained by considering a δ -family for the polytropic ansatz with $k = 2$, $l = 1$, $L_0 = 15$, $E^{0,\text{vac}} = 0.97$, and $\delta = 10$.

Damping: We also find static shells that show damping when perturbed. The effects are very similar to those described in Section 7.3.1. In order to obtain better observable and stronger damping effects, the steady state should not be too close to unstable shells and the ansatz functions should be smooth, e.g., have high values of k for the polytropes. In Figure 7.16, we depict this for the polytropic model with $k = 2$, $M_0 = 1$, $l = 1$, $L_0 = 15$, and $E^{0,\text{vac}} = 0.97$, parametrized via a δ -family with $\delta = 10$ by considering the evolution of $\alpha(t, 3M_0)$. This shell is rather small in the sense that its Vlasov mass is approximately $M \approx 0.052M_0$. The non-smooth variation of $\alpha(t, 3M_0)$ can be attributed to numerical round-off errors since the vertical scale is very small in relative terms. Searching for damping in the case of shells surrounding a black hole turns out more delicate than in the singularity-free case since the central black hole often dominates the motion of the particles. We comment further on this in the following third behavior which can be observed.

No effects or indeterminable behavior: When considering small shells compared to the black hole, i.e., $M \ll M_0$, we could expect a similar behavior as in the Vlasov-Poisson system with a point mass, as studied in [56], since this is the Newtonian counterpart of our setting; recall also the discussion of [56] in the previous section. However, we often do not see any effect after the perturbation of a sufficiently small shell. More precisely, the gravitational field generated by the black hole at the center dominates the self-gravitating part of the Vlasov matter by orders of magnitude. The particles seem to move on orbits which are almost identical to the orbits in the vacuum Schwarzschild solution. In particular, we cannot observe oscillations or other behavior, but the steady state just stays where it is, despite using rather strong perturbations.⁵ Such small shells can, for example, be obtained by fixing a δ -family and making δ sufficiently small,

⁵Of course, if the perturbation is strong enough, we would see effects. However, we doubt the sense of this approach.

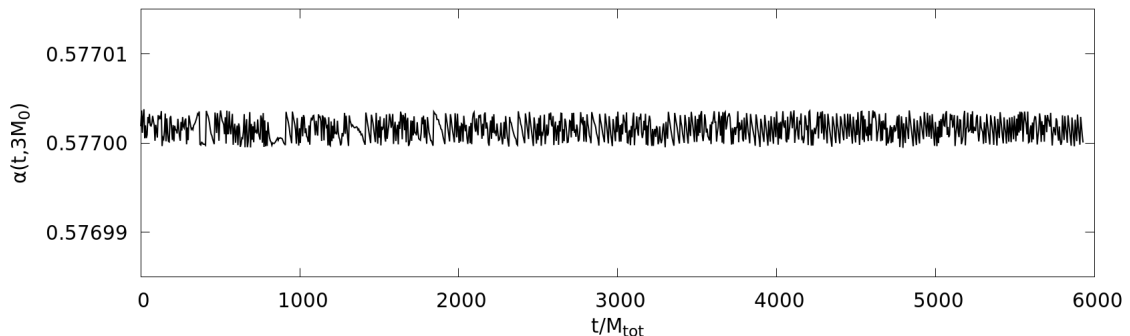


Figure 7.17: Time evolution of the quantity $\alpha(t, 3M_0)$ for a stable shell surrounding a black hole of mass $M_0 = 1$ perturbed with $\gamma < 0$. The model is obtained by considering a δ -family for the polytropic ansatz with $k = 2$, $l = 1$, $L_0 = 15$, $E^{0,\text{vac}} = 0.97$, and $\delta = 1$.

cf. Definition 2.2.11. From Lemma 2.2.12, we know that this yields solutions close to the vacuum Schwarzschild solution. The evolution of $\alpha(t, 3M_0)$ is shown in Figure 7.17 for the same model as used in Figure 7.16 but with the smaller value $\delta = 1$, which yields $M \approx 0.0065M_0$. Even an increase of the strength of the perturbation does not lead to better observable effects. Instead, the question whether oscillation or damping happens seems to get obscured by the central black hole.

In conclusion, the non-linear numerical stability analysis of stable shells confirms that the findings of [56] concerning linear stability can, to some extent, be transferred to the Einstein-Vlasov system. More precisely, we observe that damping seems to occur for smoother ansatz functions, i.e., larger values of k , if the shell is “small”. However, these results have to be taken with a pinch of salt, as we cannot make the shells arbitrarily small compared to the central black hole since in this case the strong external gravitational field dominates the dynamical behavior of the Vlasov matter.

7.4.2 Unstable shells

Besides stable shells, as described above, we also observe instability for steady states surrounding a black hole. As in the isotropic case, unstable steady states behave differently if perturbed with $\gamma < 0$ or $\gamma > 0$, i.e., towards collapse or dispersion, respectively. The former case always leads to the collapse into the black hole at the center. The latter case $\gamma > 0$ is a bit more interesting, as we could expect heteroclinic orbits, as described in Section 7.3.2, especially because such heteroclinic orbits are also obtained in [45] for singularity-free shells. However, it seems that this is not the case for shells surrounding a black hole. Instead, we observe a “homoclinic orbit” if we perturb an unstable shell towards dispersion. We describe the behavior in more detail in the following.

Collapse: If we increase the redshift κ for the same models as used in Figure 7.15, we eventually reach unstable equilibria. One possible scenario is the collapse of the matter

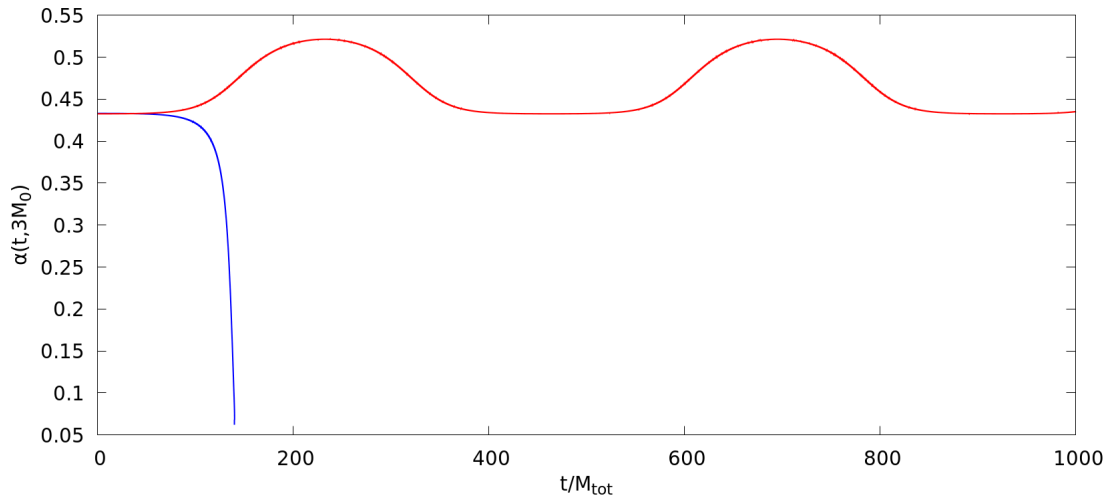


Figure 7.18: Time evolution of the quantity $\alpha(t, 3M_0)$ for an unstable shell surrounding a black hole of mass $M_0 = 1$ perturbed with $\gamma < 0$ (blue line) and $\gamma > 0$ (red line). The former corresponds to a collapsing solution while the latter represents a homoclinic orbit. The model is given by the polytropic ansatz with $k = 1$, $l = 1$, $L_0 = 50$, and $\kappa = 0.1$.

after it gets perturbed slightly towards collapse, i.e., with $\gamma < 0$. The mechanism is quite similar to that described in Section 7.3.2 with the main difference being that the matter now approaches the black hole at the center and eventually gets absorbed by it. The entire shell moves towards the central singularity, and a new outermost trapped surface forms abruptly at a radius $r_{\text{TS}} > 2M_0$, which signals the development of a new, larger black hole at the center. Such a scenario is depicted in Figure 7.18 for the quantity $\alpha(t, 3M_0)$, which decreases rapidly due to the instability. On a particle level, the solution behaves qualitatively the same as the King model illustrated in Figure 7.5: All particles rush towards the center and ultimately cross the outermost trapped surface after which we terminate the simulation. Note that we did not search for the phenomenon of *partial* collapse which should be easily obtainable by constructing two separate shells where the outer shell is stable and the inner shell is unstable. Research towards such results is currently underway. In addition, it would be interesting whether partial collapse can happen for single-shell solutions, similar to the model used in Figure 7.6.

Homoclinic orbit: When perturbing unstable shells surrounding a black hole towards dispersion, i.e., with $\gamma > 0$, the solution performs a *homoclinic orbit* for a large class of models. These orbits often arise in dynamical systems such as ordinary differential equations and connect a saddle equilibrium to itself. In our setting, the perturbed stationary solution relaxes to a less relativistic configuration, the radii of the particles increase significantly, but no particles reach escape velocity. Eventually, the whole configuration appears to return to its original state. This can be observed across all quantities

that we have considered. However, as the original state is unstable, the configuration again begins to expand and starts a new cycle of the same behavior. This leads to a type of oscillatory behavior which should not be confused with the oscillations of stable steady states.⁶ We illustrate a homoclinic orbit in Figure 7.18, which shows the process of repeated expansion followed by an implosion represented by the quantity $\alpha(t, 3M_0)$. We continued with the simulation much longer than depicted in Figure 7.18 and it appears that the cycle of expansion and reimplosion continues indefinitely. In addition, Figure 7.19 shows one full cycle in radius-energy space, which better clarifies the evolution of the whole configuration as well as of the individual particles. From Figure 7.19, it is evident that this behavior should be regarded as unstable. It is rather remarkable that the system returns exactly to its original state after approximately $t = 440M$ and that no particles are expelled which is most likely due to the external potential generated by the central black hole.

Full dispersion: By increasing the value of κ even further, we usually encounter fully dispersing solutions when the static shell is perturbed towards dispersion. We depict this in Figure 7.20 for the evolution of $\alpha(t, 3M_0)$. For large time t , the value of $\alpha(t, 3M_0)$ approaches $\frac{1}{\sqrt{3}}$, which is the value corresponding to the vacuum Schwarzschild solution. Furthermore, the maximal radius of the particles increases linearly in time. The particles get expelled violently from their initial configuration and do not return but escape towards infinity, as shown in the bottom plot in Figure 7.20.

One crucial difference compared to full dispersion for perturbed isotropic steady states, as discussed in Section 7.3.2, is that the particles do not disperse over a large radial region, but remain in a rather compact bundle and move away "uniformly" towards spatial infinity. To our numerical accuracy, the configuration does not return which is indicated by the energy of the particles being larger than one in Figure 7.20.

It is of interest if there exists a simple criterion that determines whether the perturbed equilibrium performs a homoclinic orbit or fully disperses. Before we address this issue in more detail, let us briefly comment on our observation regarding the stability of families of stationary solutions.

Remark 7.4.1. (a) *There is a multitude of possibilities to parametrize static shells surrounding a black hole, even if the ansatz function is fixed. For example, we could vary the parameters M_0 , L_0 , κ , or even consider δ -families, as defined in Definition 2.2.11. For more details, we refer to Section 2.2.2. We have limited the analysis to mainly studying families along either κ or δ , where $M_0 = 1$ and L_0 are fixed. Recall that κ has a lower and upper bound determined by (P3).*

(b) *Usually, equilibria are stable for κ close to its lower bound. This case corresponds to small shells compared to the central black hole and is consistent with the result in Theorem 5.4.4. The same behavior can be observed if δ is small along a δ -family.*

⁶For isotropic, singularity-free steady states, we did not explicitly observe homoclinic orbits. However, it is reasonable to assume that homoclinic orbits also exist if the model is close to the point where stability changes. In this case, it is delicate to differentiate between heteroclinic and homoclinic behavior since the system does not undertake a large structural change.

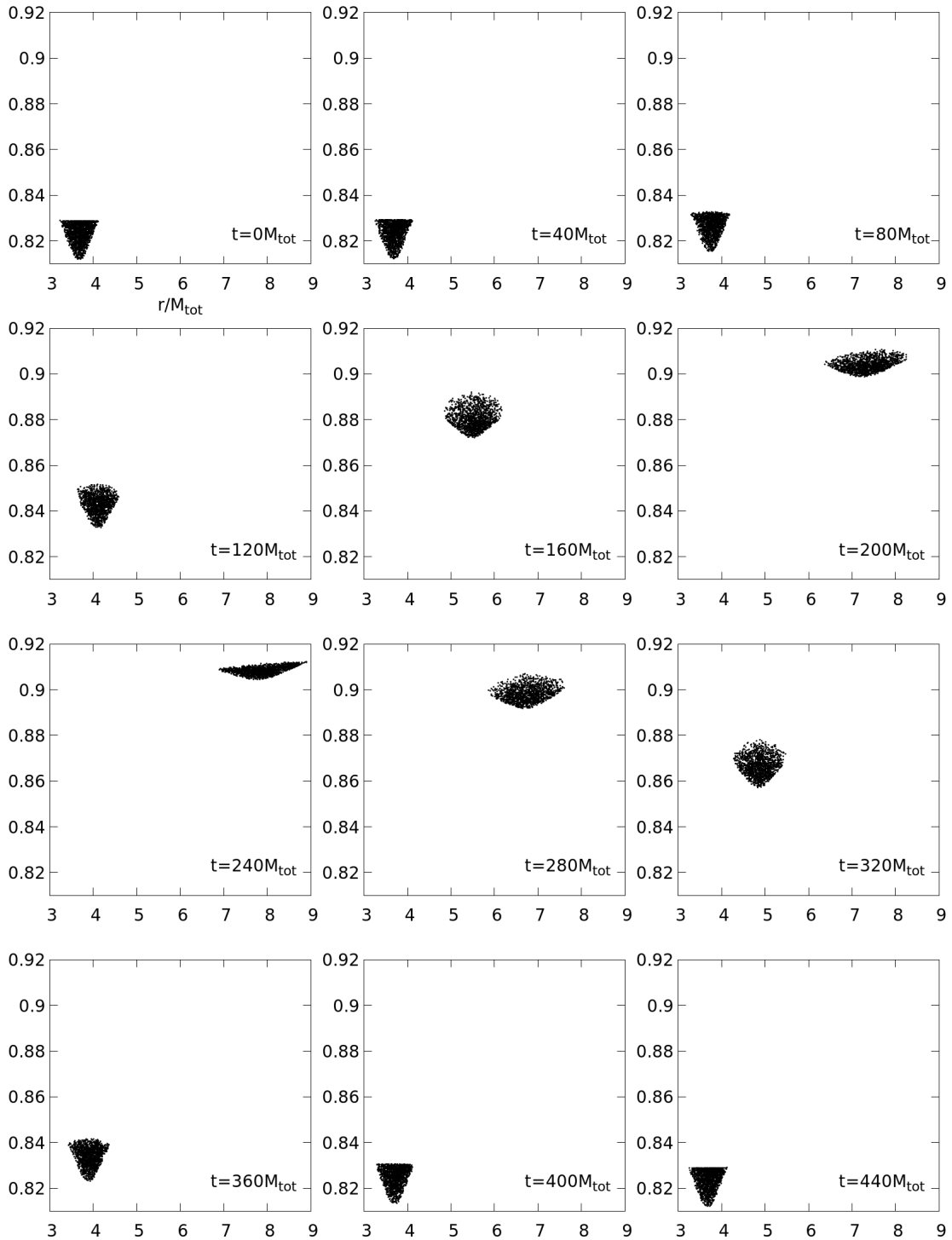


Figure 7.19: Time evolution of the radius-energy space for an unstable shell surrounding a black hole of mass $M_0 = 1$ perturbed with $\gamma > 0$. The model is given by the polytropic ansatz with $k = 1$, $l = 1$, $L_0 = 50$, and $\kappa = 0.1$.

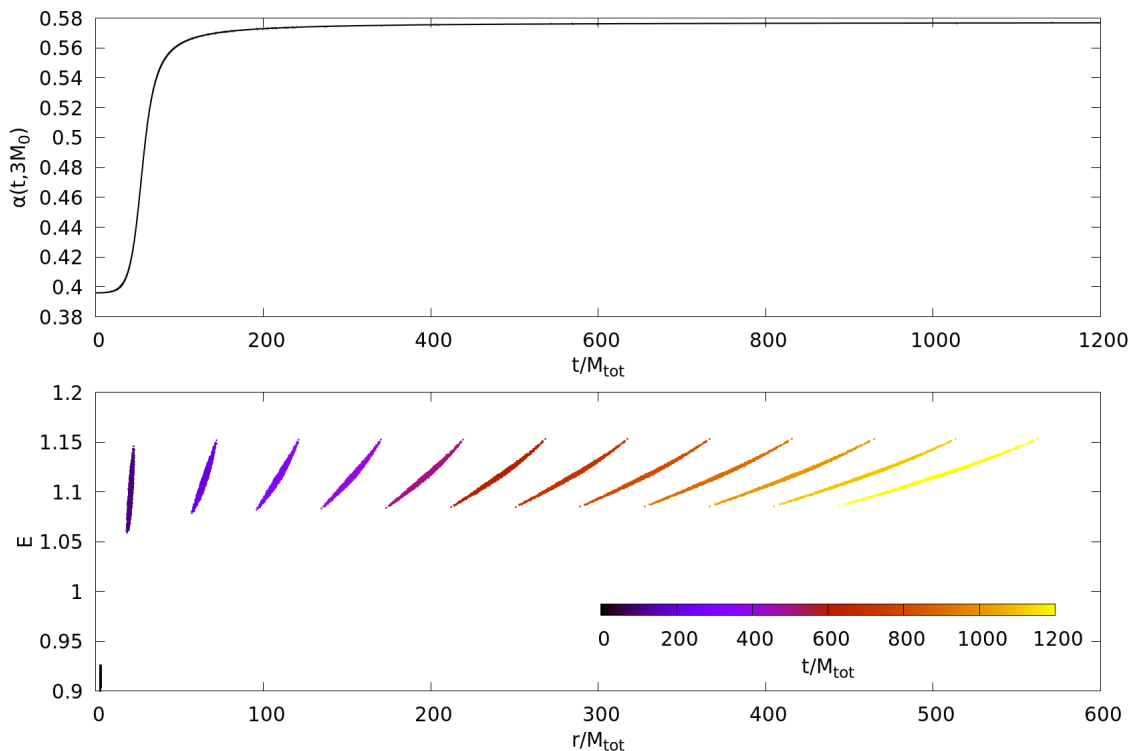


Figure 7.20: Time evolution of $\alpha(t, 3M_0)$ and the radius-energy space for an unstable shell surrounding a black hole of mass $M_0 = 1$ perturbed with $\gamma > 0$. The model is given by the polytropic ansatz with $k = 1$, $l = 1$, $L_0 = 50$, and $\kappa = 0.3$.

- (c) *When increasing κ or δ , we often obtain unstable shells of the types described above. In some sense, this can be interpreted similarly to the singularity-free case since increasing κ or δ usually yields more relativistic settings. It is, however, not clear whether this is necessarily the case along families in κ , since κ is bounded from above.*

A binding energy criterion: It appears that the change of behavior from homoclinic orbits to full dispersion happens suddenly when parametrizing families of shells along κ or considering δ -families. In particular, we do not observe any heteroclinic orbits. We hypothesize that it is a general feature of shells surrounding a black hole that heteroclinic orbits do not exist due to the central black hole. Instead, the sign of the binding energy seems to be tightly connected to the question whether the solution full disperses. For shells surrounding a black hole, the binding energy is defined as $E_b = \frac{N-M}{N}$, where M is the Vlasov mass of the shell, which does not include the mass M_0 of the central singularity. When increasing κ , the time to complete the homoclinic orbit generally increases. For a family along κ , our results are presented in Figure 7.21 by visualizing the evolution of $\alpha(t, 3M_0)$. In Table 7.1, we provide the corresponding binding energy

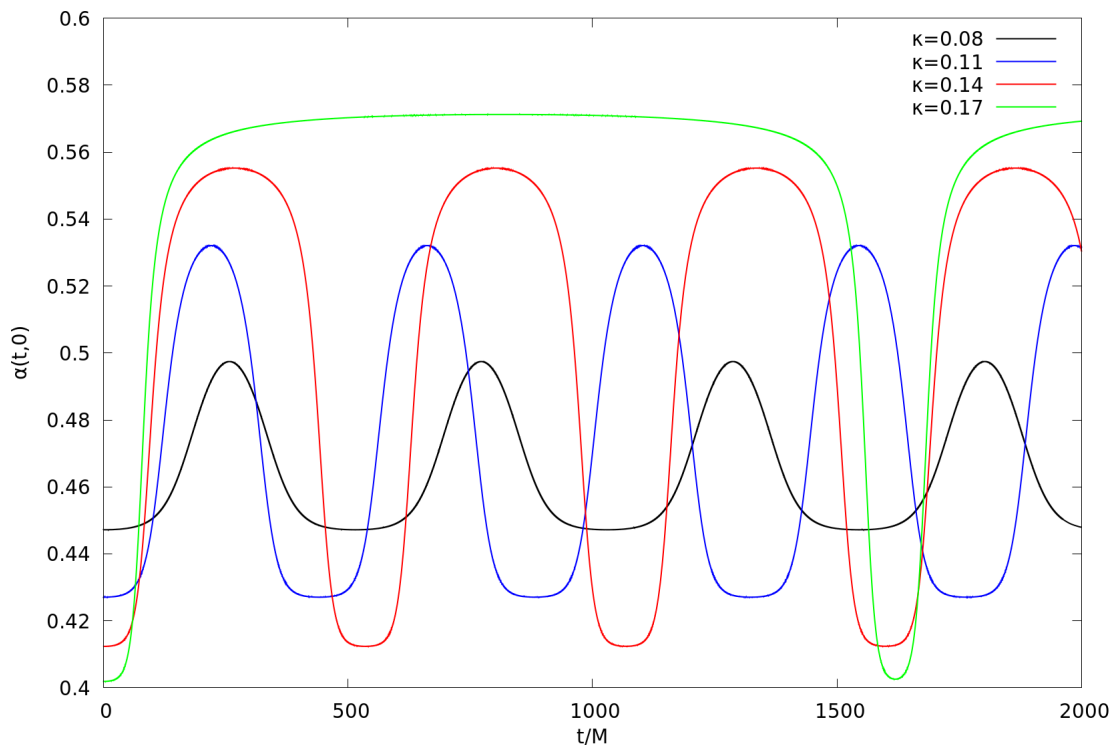


Figure 7.21: Homoclinic orbits for different values of κ illustrated by the time evolution of the quantity $\alpha(t,0)$. The shells are given by $M_0 = 1$, $k = 1$, $l = 1$, $L_0 = 50$, and are perturbed with $\gamma > 0$.

κ	0.14	0.15	0.16	0.17	0.18	0.19	0.20
E_b	0.0284	0.0230	0.0170	0.0105	0.0036	-0.0038	-0.012
Full dispersion?	No	No	No	No	Yes	Yes	Yes
$\frac{T_{\text{HCO}}}{M_{\text{tot}}}$	535	655	891	1618	–	–	–

Table 7.1: The binding energy, the dispersing behavior, and the approximate time taken to complete one homoclinic orbit T_{HCO} for multiple values of κ . The model is given by the polytropes with $M_0 = 1$, $k = 1$, $l = 1$, and $L_0 = 50$.

of the models as well as the approximate time T_{HCO} it takes for one homoclinic orbit to complete—if it exists. For $\kappa = 0.18$, we observe a full dispersion, according to our numerical accuracy, despite of positive binding energy which seemingly contradicts our claims above. However, firstly, the binding energy is very close to zero for this model and it is difficult to determine whether the solution fully disperses or returns after some (possibly very long) time. Secondly, numerical errors could also be the reason why we obtain that $\kappa = 0.18$ disperses fully. For a second κ -family, the results are quite similar,

κ	0.07	0.08	0.09	0.10	0.11	0.12	0.13
E_b	0.0340	0.0252	0.0148	0.0035	-0.013	-0.0319	-0.0584
Full dispersion?	No	No	No	Yes	Yes	Yes	Yes
$\frac{T_{\text{HCO}}}{M_{\text{tot}}}$	458	613	1145	-	-	-	-

Table 7.2: The binding energy, the dispersing behavior, and the approximate time taken to complete one homoclinic orbit T_{HCO} for multiple values of κ . The model is given by the polytropes with $M_0 = 1$, $k = \frac{1}{2}$, $l = 0$, and $L_0 = 25$.

as shown in Table 7.2.⁷ In conclusion, a more elaborate and structured analysis of families of shells with a singularity is needed in order to get a better understanding of their stability behavior and features.

⁷We do not consider δ -families here, as they appear to never fully disperse and, in particular, always have positive binding energy. This might be explainable by the fact that the gravitational potential induced by the central black hole is more dominant for δ -families, because of the different way these shells are constructed, see Section 2.2.2. For example, we have that the minimal and maximal radii are a-priori and uniformly bounded in δ , as proven in Lemma 2.2.12.

8 Numerical investigation of linear stability

An algorithm must be seen
to be believed.

Donald Knuth

As we have outlined in the previous chapter, most of the literature concerning numerical stability of steady states of the Einstein-Vlasov system deals with non-linear stability issues. In this chapter, we aim to analyze linear stability from the perspective of spectral analysis by numerically approximating the bottom of the spectrum of the Antonov operator \mathcal{L} introduced in Definition 4.2.2(d).

We begin by outlining the general idea behind our method in Section 8.1 and assess how this analysis complements the work in Chapter 7. We also present the relevant calculations and considerations necessary for minimizing the quadratic form corresponding to the Antonov operator. In Section 8.2, the concrete numerical method is introduced along with its limitations. In Section 8.4, we then apply this numerical method in order to test for the agreement of linear and non-linear stability of stationary solutions to the Einstein-Vlasov system. In Section 8.5, we search for oscillating solutions, which expands the knowledge gained from the rigorous investigation in Chapter 6. In addition, we probe for evidence of damping which should be tightly connected to that observed in Section 7.3.1 for the non-linear system.

Since this chapter should mainly be viewed as a “proof of concept” and, as we need a steady state f_0 with strict single-well structure—at least when using arguments that involve the period function—, we restrict the analysis to isotropic equilibria which fulfill the conditions (S1)–(S4) introduced in Chapter 4. Recall that we put forth the conjecture in Remark 2.4.1 that the (strict) single-well structure holds for all isotropic stationary solutions. However, it is in principle possible to expand the investigation to anisotropic steady states, which may or may not surround a black hole, if the formulas are adjusted accordingly. We use the same notation as introduced in Chapter 4.

8.1 Preliminaries and setup of the variational principle

In Section 4.2, we have seen that the spectral properties of the Antonov operator \mathcal{L} fully describe the linear stability behavior of a steady state of the Einstein-Vlasov system. Since the Antonov operator acts as an unbounded operator on an infinite-dimensional Hilbert space, the best that we can reasonably hope to achieve, is to approximate the

bottom of the spectrum of \mathcal{L} . Therefore, our goal is to numerically find

$$\inf(\sigma(\mathcal{L})) = \inf_{f \in \mathcal{H}} \frac{\langle \mathcal{L}f, f \rangle_H}{\|f\|_H^2} = \inf_{f \in \mathcal{H}, \|f\|_H=1} \langle \mathcal{L}f, f \rangle_H, \quad (8.1)$$

where the first equality follows from applying the min-max principle for self-adjoint operators [88, Thm. XIII.1], and \mathcal{H} is the appropriate Hilbert space defined in (4.10) consisting of odd-in- w functions. Approximating the bottom of the spectrum of \mathcal{L} still entails a lot of information about the stability behavior of the underlying steady state. We refer to Remark 5.1.3 for a more detailed discussion of the following.

In the case $\inf(\sigma(\mathcal{L})) > 0$, we have that the equilibrium is linearly stable, as per Definition 5.1.2. If in addition $\inf(\sigma(\mathcal{L})) < \inf(\sigma(-\mathcal{T}^2))$ holds, this implies the existence of an oscillating mode, since

$$\inf(\sigma(-\mathcal{T}^2)) \leq \inf(\sigma_{\text{ess}}(\mathcal{L})), \quad (8.2)$$

according to Theorem 4.3.18, and thus $\inf(\sigma(\mathcal{L}))$ must be an isolated, positive eigenvalue. Recall that the question whether equality holds in (8.2) is an open problem, as discussed in Section 4.3.4. In case $\inf(\sigma(\mathcal{L})) \geq \inf(\sigma(-\mathcal{T}^2))$ holds, it is difficult to assess the qualitative behavior of the linearized system without further knowledge, but it is plausible that damping may take place. For the Vlasov-Poisson system, the existence of damping is rigorously proven in [56]. There, the authors observe that no eigenvalue exists when $\inf(\sigma(\mathcal{L})) \geq \inf(\sigma(-\mathcal{T}^2))$. In the case $\inf(\sigma(\mathcal{L})) < 0$, we deduce the existence of an exponentially growing mode, as argued in Remark 5.1.3, and thus the stationary solution is linearly unstable.

In conclusion, we can thus check if linear and non-linear stability coincide for the Einstein-Vlasov system—especially in the case of multiple stability changes observed in Section 7.3.2—, expand the search for linearly oscillating modes, and find equilibria for which damping on a linear level is possible.

Linear stability is studied via a similar approach in [60]. The author plugs different heuristic test functions of the form $f = \varphi' w F(r)$ into the variational principle (8.1) in order to get an approximation of the sign of $\inf(\sigma(\mathcal{L}))$. The radial function $F = F(r)$ is the only part that is subject to variation in the attempt to find (8.1). The distribution functions under consideration are given by families of isotropic, isothermal clusters as well as isotropic, polytropic equilibria; note that these are different polytropes compared to ours introduced in (2.5). The results of [60] are expanded upon in [42], where the author optimizes the radial trial function F for similar distribution functions. Our goal is to build upon the previous work from [60] and use a much larger class of test functions as well as more advanced techniques in order to better approximate the bottom of the spectrum of \mathcal{L} .

It is important to note that, while having attempted to numerically minimize the functional (8.1) over the infinite-dimensional function space \mathcal{H} , the author of this work is by no means an expert in this field. The work here is simply an ad-hoc solution that has been developed as a proof of concept. A more rigorous and methodologically

sound approach would require refined expertise in areas such as numerical optimization. Nonetheless, our efforts provide a foundation for further exploration and development.

The reduced variational principle: Before we approximate the infimum in (8.1), we have to bring the scalar product $\langle \mathcal{L}f, f \rangle_H$ into a form suitable to be implemented on the computer. Recall from Definition 4.2.2 that the Antonov operator can be written as

$$\mathcal{L} = -\mathcal{B}^2 - \mathcal{R} = -(\mathcal{T} + \mathcal{S})^2 - \mathcal{R}, \quad (8.3)$$

where \mathcal{S} and \mathcal{R} are bounded operators which introduce non-local terms, and \mathcal{T} is the transport operator which acts as a differential operator along characteristics of the steady state. This interplay between the differential terms arising from the transport operator \mathcal{T} as well as the non-local terms generated by \mathcal{S} and \mathcal{R} , causes the main difficulty in reducing the scalar product $\langle \mathcal{L}f, f \rangle_H$ to a nice and compact form. In addition, we have to construct and choose test functions in the three independent variables (r, w, L) .

We employ separated test functions of the form

$$f_{ikm}(r, w, L) = |\varphi'(E)| \psi_i(r) a_k(w) b_m(E(r, w, L)), \quad (r, w, L) \in \Omega_0, \quad (8.4)$$

for $i, k, m \in \mathbb{N}_0$; we specify ψ_i, a_k, b_m later. For the sake of the following formal derivation, it is sufficient to prescribe that $\psi_i, a_k, b_m \in C^1(\mathbb{R})$ are bounded and a_k is odd in w . It will become clear later why it is advantageous to choose a separated ansatz not in (r, w, L) but in (r, w, E) . From a mathematical point of view, this should not make the test functions less general.

We start by applying the relevant operators to a test function f_{ikm} as in (8.4). For the transport operator, we get

$$\begin{aligned} (\mathcal{T}f_{ikm})(r, w, L) &= |\varphi'(E)| e^{(2\mu_0 - \lambda_0)(r)} b_m(E) \cdot \\ &\cdot \left(-\frac{w}{E} \psi_i'(r) a_k(w) + \left(e^{-2\mu_0(r)} \mu_0'(r) E - \frac{L}{r^3 E} \right) \psi_i(r) a_k'(w) \right) \end{aligned} \quad (8.5)$$

by using definition (4.13). Applying the bounded operators \mathcal{S} and \mathcal{R} yields

$$(\mathcal{S}f_{ikm})(r, w, L) = 4\pi |\varphi'(E)| \frac{w^2}{E} r e^{(3\mu_0 + \lambda_0)(r)} j_{f_{ikm}}(r), \quad (8.6)$$

$$(\mathcal{R}f_{ikm})(r, w, L) = 4\pi |\varphi'(E)| w e^{3\mu_0(r)} (2r \mu_0'(r) + 1) j_{f_{ikm}}(r), \quad (8.7)$$

since f_{ikm} is odd in w . In order to appropriately minimize (8.1), we need to plug two test functions f_{ikm} and f_{jln} , where $i, j, k, l, m, n \in \mathbb{N}_0$, of the form (8.4) into the scalar product

$$\begin{aligned} \langle \mathcal{L}f_{ikm}, f_{jln} \rangle_H &= \langle \mathcal{B}f_{ikm}, \mathcal{B}f_{jln} \rangle_H - \langle \mathcal{R}f_{ikm}, f_{jln} \rangle_H \\ &= \langle \mathcal{T}f_{ikm}, \mathcal{T}f_{jln} \rangle_H + \langle \mathcal{S}f_{ikm}, \mathcal{T}f_{jln} \rangle_H + \langle \mathcal{T}f_{ikm}, \mathcal{S}f_{jln} \rangle_H \\ &\quad + \langle \mathcal{S}f_{ikm}, \mathcal{S}f_{jln} \rangle_H - \langle \mathcal{R}f_{ikm}, f_{jln} \rangle_H, \end{aligned} \quad (8.8)$$

where we have used (8.3) and the fact that \mathcal{B} is skew-adjoint on H , as shown in Proposition 4.3.5(a). In addition, we need to calculate $\langle f_{ikm}, f_{jln} \rangle_H$ as well as $j_{f_{ikm}}(r)$ for $r > 0$, which arise from the variational principle. For the derivation, it is useful to introduce the shorthand

$$g(r, E) := e^{-2\mu_0(r)} E^2 - 1 \quad (8.9)$$

and the auxiliary function

$$A_h^{(s)}(x) := \int_0^x h(\sqrt{y}) y^{\frac{s-1}{2}}, \quad x \geq 0, \quad (8.10)$$

where $h \in C([0, \infty[)$ and $s \geq 0$.

We present all relevant equations needed for the reduced variational principle on page 229. In a nutshell, these formulas are derived using (8.5)–(8.10) and multiple changes of variables. We provide more details of these laborious calculations in Appendix C. In this generality, the reduced equations are not of much use, which is why we have to specify the test functions ψ_i, a_k, b_m next.

The class of test functions: One of the numerically most expensive tasks is the computation of the integrals appearing in (8.11) and (8.12). In fact, currently three integrals appear which we would have to approximate numerically. The idea now is to first define suitable functions a_k that span a satisfactory subspace in w and at the same time allow us to explicitly compute the necessary integrals $A_h^{(s)}$. Our choice for the test functions along w consists of

$$a_k(w) = \begin{cases} w, & k = 0, \\ \sin\left(\frac{k\pi w}{w_{\max}}\right), & k \geq 1, \end{cases} \quad (8.14)$$

for $w \in [-w_{\max}, w_{\max}]$ and $k \in \mathbb{N}_0$, where $w_{\max} := \sup\{w \mid (r, w, L) \in \text{supp}(f_0)\}$. Recall that the functions f_{ikm} need to be odd in w . We include the linear term $a_0(w) = w$, since the family $(a_k)_{k \geq 1}$ cannot cover general test functions due to the boundary conditions $a_k(0) = 0 = a_k(1)$ and $a'_k(0) = 1 = a'_k(1)$ for $k \geq 1$.¹ All integrals $A_h^{(s)}$ appearing in (8.11) and (8.12) can now be calculated by hand for the different cases, e.g., recursively in s . As an aside, we mention that this maneuver is only possible since we have chosen a separated ansatz in (r, w, E) instead of (r, w, L) . In conclusion, only two-dimensional integrals remain to be computed in the equations for the reduced variational principle, which reduces the numerical workload considerably.

Since the equation of state φ depends on the specific steady state under consideration, we cannot generally eliminate the integral over E as well. In our case, after probing

¹Loosely speaking, we need to ensure that the functions $(a_k)_{k \geq 0}$ span a basis over $H^1([0, 1])$ in an appropriate sense. Without the linear term, $(a_k)_{k \geq 1}$ defines a basis over $H_0^1([0, 1])$, which is not optimal to approximate the most general functions possible in \mathcal{H} .

The equations for the reduced variational principle:

$$\begin{aligned}
 & \langle \mathcal{L} f_{ikm}, f_{jln} \rangle_H \\
 &= 8\pi^2 \int_0^{R_{\max}} \int_{e^{\mu_0(r)}}^{E^0} r^2 e^{2\mu_0 - \lambda_0} |\varphi'(E)| b_m(E) b_n(E) \cdot \\
 & \cdot \left\{ (\psi_i \psi_j)(r) \left[A_{a'_k a'_l}^{(0)}(g(r, E)) \left(e^{-4\mu_0} (\mu'_0)^2 E^3 - 2e^{-2\mu_0} \mu'_0 \frac{g(r, E)E}{r} + \frac{g(r, E)^2}{r^2 E} \right) \right. \right. \\
 & \quad \left. \left. + A_{a'_k a'_l}^{(2)}(g(r, E)) \left(\frac{2e^{-2\mu_0} E \mu'_0}{r} - \frac{2g(r, E)}{r^2 E} \right) + \frac{A_{a'_k a'_l}^{(4)}(g(r, E))}{r^2 E} \right] \right. \\
 & \quad - (\psi'_i \psi_j)(r) \left[A_{a_k a'_l}^{(1)}(g(r, E)) \left(e^{-2\mu_0} \mu'_0 E - \frac{g(r, E)}{rE} \right) + \frac{A_{a_k a'_l}^{(3)}(g(r, E))}{rE} \right] \\
 & \quad - (\psi_i \psi'_j)(r) \left[A_{a'_k a_l}^{(1)}(g(r, E)) \left(e^{-2\mu_0} \mu'_0 E - \frac{g(r, E)}{rE} \right) + \frac{A_{a'_k a_l}^{(3)}(g(r, E))}{rE} \right] \\
 & \quad \left. \left. + (\psi'_i \psi'_j)(r) \frac{A_{a_k a_l}^{(2)}(g(r, E))}{E} \right\} dE dr \\
 &+ 32\pi^3 \int_0^{R_{\max}} \int_{e^{\mu_0(r)}}^{E^0} r^3 e^{3\mu_0 + \lambda_0} j_{f_{jln}}(r) |\varphi'(E)| b_m(E) \cdot \\
 & \cdot \left\{ \psi_i(r) \left[A_{a'_k}^{(2)}(g(r, E)) \left(e^{-2\mu_0} \mu'_0 E - \frac{g(r, E)}{rE} \right) + \frac{A_{a'_k}^{(4)}(g(r, E))}{rE} \right] - \psi'_i(r) \frac{A_{a_k}^{(3)}(g(r, E))}{E} \right\} dE dr \\
 &+ 32\pi^3 \int_0^{R_{\max}} \int_{e^{\mu_0(r)}}^{E^0} r^3 e^{3\mu_0 + \lambda_0} j_{f_{ikm}}(r) |\varphi'(E)| b_n(E) \cdot \\
 & \cdot \left\{ \psi_j(r) \left[A_{a'_l}^{(2)}(g(r, E)) \left(e^{-2\mu_0} \mu'_0 E - \frac{g(r, E)}{rE} \right) + \frac{A_{a'_l}^{(4)}(g(r, E))}{rE} \right] - \psi'_j(r) \frac{A_{a_l}^{(3)}(g(r, E))}{E} \right\} dE dr \\
 &+ \frac{256}{5} \pi^4 \int_0^{R_{\max}} \int_{e^{\mu_0(r)}}^{E^0} r^4 e^{4\mu_0 + 3\lambda_0} j_{f_{ikm}}(r) j_{f_{jln}}(r) g(r, E)^{\frac{5}{2}} \frac{|\varphi'(E)|}{E} dE dr \\
 &- 16\pi^2 \int_0^{R_{\max}} \int_{e^{\mu_0(r)}}^{E^0} r^4 e^{\mu_0 + \lambda_0} (2r\mu'_0 + 1) j_{f_{ikm}}(r) \psi_j(r) A_{a'_l}^{(1)}(g(r, E)) |\varphi'(E)| b_n(E) E dE dr,
 \end{aligned} \tag{8.11}$$

$$\langle f_{ikm}, f_{jln} \rangle_H = 8\pi^2 \int_0^{R_{\max}} \int_{e^{\mu_0(r)}}^{E^0} r^2 e^{\lambda_0 - 2\mu_0} (\psi_i \psi_j)(r) A_{a_k a_l}^{(0)}(g(r, E)) |\varphi'(E)| (b_m b_n)(E) E dE dr, \tag{8.12}$$

$$j_{f_{ikm}}(r) = 2\pi e^{-2\mu_0(r)} \psi_i(r) \int_{e^{\mu_0(r)}}^{E^0} A_{a_k}^{(1)}(g(r, E)) |\varphi'(E)| b_m(E) E dE, \quad r > 0. \tag{8.13}$$

several test functions in E , the best numerical performance has been achieved with

$$b_m(E) = \begin{cases} 1, & m = 0, \\ E, & m = 1, \\ \cos\left(\frac{2\pi m(E - e^{\mu_0(0)})}{(E^0 - e^{\mu_0(0)})}\right), & m \geq 2, \end{cases} \quad (8.15)$$

for $E > 0$ and $m \in \mathbb{N}_0$. We leave out the sine from this family of functions since it only provides marginal gains in numerical testing. By similar considerations as for a_k and b_m above, we employ the radial test functions

$$\psi_i(r) = \begin{cases} r, & i = 0, \\ \cos\left(\frac{\pi(i-1)r}{R_{\max}}\right), & i \geq 1 \text{ odd}, \\ \sin\left(\frac{\pi i r}{R_{\max}}\right), & i \geq 2 \text{ even}, \end{cases} \quad (8.16)$$

for $r \in [0, R_{\max}]$ and $i \in \mathbb{N}_0$.

We emphasize that, in principle, there are many other ways to choose the test functions and ours is most likely not the best choice overall. However, we employ the functions above because they provide a satisfactory mix of simplicity, usefulness, and numerical performance.

8.2 The numerical method

We now come to the actual method for approximating

$$\inf(\sigma(\mathcal{L})) = \inf_{f \in \mathcal{H}, \|f\|_H=1} \langle \mathcal{L}f, f \rangle_H. \quad (8.17)$$

First, we present the mathematical formulation which reduces the problem to a finite-dimensional one. In the second step, we provide the algorithms and solvers employed for our problem. Finally, we lay out the main difficulties and limitations of the method.

Mathematical formulation: We fix $i_{\max}, k_{\max}, m_{\max} \in \mathbb{N}_0$ and consider the family of test functions

$$(f_{ikm})_{0 \leq i \leq i_{\max}, 0 \leq k \leq k_{\max}, 0 \leq m \leq m_{\max}}$$

as defined in (8.4). We assume that these test functions are linearly independent which is plausible by their definition; from a numerical point of view, this should always be the case. For a more concise formulation, we re-index the family of test functions through $(f_n)_{1 \leq n \leq n_{\max}}$, where $n_{\max} = (i_{\max} + 1)(k_{\max} + 1)(m_{\max} + 1)$. The infimum in (8.17) is

approximated by solving the optimization problem

$$\begin{aligned} & \text{minimize} && \left\langle \mathcal{L} \left(\sum_{n=1}^{n_{\max}} c_n f_n \right), \sum_{n=1}^{n_{\max}} c_n f_n \right\rangle_H, \\ & \text{subject to} && \left\| \sum_{n=1}^{n_{\max}} c_n f_n \right\|_H = 1, \end{aligned} \tag{8.18}$$

where $c = (c_1, \dots, c_{n_{\max}}) \in \mathbb{R}^{n_{\max}}$ acts as the unknown. We define the shorthand

$$L_{nm} := \langle \mathcal{L} f_n, f_m \rangle_H, \quad F_{nm} := \langle f_n, f_m \rangle_H, \tag{8.19}$$

which define real, symmetric matrices $L = (L_{nm}), F = (F_{nm}) \in \mathbb{R}^{n_{\max} \times n_{\max}}$. Note that F is invertible and positive definite since we assume that (f_n) is linearly independent. With this, (8.18) is equivalent to determining

$$\min \{ c^T L c \mid c^T F c = 1, c \in \mathbb{R}^{n_{\max}} \}, \tag{8.20}$$

which can be solved with the method of Lagrange multipliers. We define

$$\gamma_{\min} := \min \{ c^T L c \mid c^T F c = 1, c \in \mathbb{R}^{n_{\max}} \}, \tag{8.21}$$

which obviously depends on the particular family of test functions employed.

The algorithm and solvers: Since the non-local terms $j_{f_{ikm}}$ appear in the formula (8.11), we have to compute these terms for the relevant values of i, k, m in advance. Due to (8.13), we only have to compute

$$\int_{e^{\mu_0(r)}}^{E^0} A_{a_k}^{(1)}(g(r, E)) |\varphi'(E)| b_m(E) E dE, \quad 0 \leq k \leq k_{\max}, 0 \leq m \leq m_{\max},$$

for $r > 0$ on a radial grid; we use the same grid as for the computation of the underlying steady state. Recall that for our choice of a_k , cf. (8.14), we can explicitly calculate $A_{a_k}^{(1)}$. Thus, for every $r > 0$ a one-dimensional integral over $]e^{\mu_0(r)}, E^0[$ remains that we approximate with the CUBA library in C++, which is a collection of numerical integration and Monte Carlo methods for multi-dimensional problems [57]. With the same library, we evaluate the scalar products (8.11) and (8.12) needed for the matrices L and F , as defined in (8.19). For each element L_{nm} and F_{nm} , this amounts to a two-dimensional integral in (r, E) -space.²

Once L and F are determined, we can solve for γ_{\min} . Instead of inverting F , which can be numerically delicate, we search for the minimal value of λ , which solves $Lc = \lambda Fc$ for some $c \in \mathbb{R}^{n_{\max}} \setminus \{0\}$ with $c^T F c = 1$. This is equivalent to determining (8.21). In the literature, γ_{\min} is referred to as the smallest generalized eigenvalue of the pair (L, F) ,

²The necessary integrals need to be normalized to integrals ranging over the domain $[0, 1]$ in order to use the methods provided in the CUBA library. This is a mere technicality which we do not explicate further.

cf. [24, Example 3.37]. We use the *GeneralizedEigenSolver* from the Eigen library in C++ to find γ_{\min} . For an overview of the code, we refer to Appendix D.3.

We use about 10^4 and 10^7 evaluations of the integrands for the approximation of one-dimensional and two-dimensional integrals, respectively. The radial grid consists of at least 10^3 steps, but we tend to employ much more accuracy when considering more relativistic steady states, as measured in the value of the redshift κ . Before we run the algorithm, we normalize the test functions which seems to improve accuracy.

Refinements: The main bottleneck of the algorithm consists of the two-dimensional integrals that need to be calculated for the entries of the matrices L and F . As n_{\max} increases, the amount of necessary two-dimensional integrals grows as n_{\max}^2 . When considering a family of the form (f_{ikm}) , this translates to a growth of the order $(i_{\max} k_{\max} m_{\max})^2$, which limits our ability to choose a large number of test functions in order to keep the computation time reasonable. In addition, due to numerical errors adding up from the computation of $j_{f_{ikm}}$ and from the lengthy formulas for the integrands in (8.11) and (8.12), the search for γ_{\min} can lead to errors once we employ too many test functions. These errors manifest themselves in the fact that γ_{\min} suddenly changes its value drastically when another test function is added to the family (f_{ikm}) . These errors can be eliminated at the cost of increasing the computational resources sufficiently.

Due to the numerical errors and the fast growing number of necessary integrals, we sometimes employ a different strategy for finding γ_{\min} . In short, it consists of splitting the optimization process in (r, w, E) into two separate optimization problems in r and (w, E) : Consider a family of test functions (f_{ikm}) as above. For every fixed pair (k_0, m_0) with $0 \leq k_0 \leq k_{\max}, 0 \leq m_0 \leq m_{\max}$, we first find the best approximation according to the algorithm described above for the family $(f_{ik_0 m_0})_{0 \leq i \leq i_{\max}}$. We denote this value as $\gamma_{\min}^{(k_0, m_0)}$. Concretely, we obtain a vector $c = (c_0, \dots, c_{i_{\max}}) \in \mathbb{R}^{i_{\max}+1}$ such that

$$g_{k_0 m_0} := \psi(r) |\varphi'(E)| a_{k_0}(w) b_{m_0}(E) := \left(\sum_{i=0}^{i_{\max}} c_i \psi_i(r) \right) |\varphi'(E)| a_{k_0}(w) b_{m_0}(E)$$

defines the solution of (8.18) for the family $(f_{ik_0 m_0})_{0 \leq i \leq i_{\max}}$. For the fixed pair (k_0, m_0) , the radial function ψ is now determined. We then repeat the same optimization process for the family $(g_{km})_{0 \leq k \leq k_{\max}, 0 \leq m \leq m_{\max}}$, which yields a final best approximation γ_{\min} to $\inf(\sigma(\mathcal{L}))$. Necessarily, it holds that $\gamma_{\min} \leq \gamma_{\min}^{(k, m)}$. Due to the separation of the radial optimization process from the optimization in (w, E) , we refer to this method as *radial separation* in the following. Although this procedure may appear unconventional, it boasts its own unique benefits and is justified by its performance which we investigate in the next section. On the one hand, we lose numerical accuracy by splitting up the optimization process since we do not approximate the infimum exactly. On the other hand, this loss in accuracy can be overcompensated by the fact that it allows us to employ many more test functions since the number of relevant two-dimensional integrals is of the order $k_{\max} m_{\max} (i_{\max}^2 + k_{\max} m_{\max})$. In fact, for this method the calculation of the necessary functions $j_{f_{ikm}}$ takes up the majority of the computation time.

Limitations: The reduced variational principle, which we solve numerically, constitutes an optimization problem over a finite-dimensional subspace of the Hilbert space \mathcal{H} . This naturally leads to suboptimal results and an overestimation of $\inf(\sigma(\mathcal{L})) \leq \gamma_{\min}$. In addition, there is no known error estimate. This makes it difficult to assess the accuracy of the results obtained, which is why we test the method thoroughly in the next section. In addition, higher values of the redshift κ seem to make the numerical method more prone to errors, so a significant increase in computational resources is required to obtain reliable results. There are of course multiple numerical parameters, e.g., $(i_{\max}, k_{\max}, m_{\max})$, the radial step size Δr , etc., which need to be prescribed and affect the algorithm's accuracy as well as its performance.

Next, we specify how we verify the accuracy of the algorithm, and we test various combinations of $(i_{\max}, k_{\max}, m_{\max})$ with and without the radial separation method.

8.3 Testing and verification

For reliable results, we need to verify our implementation described in the previous section. In addition, we have to find suitable values for $i_{\max}, k_{\max}, m_{\max}$, which determine the family of test functions (f_{ikm}) and lead to a good numerical approximation. As a benchmark, we consider the (isotropic) King model (2.4), which we have already investigated on a non-linear level in Section 7.3.

There are two possible ways by which we can verify that our code works correctly and that γ_{\min} is, in fact, close to the actual value $\inf(\sigma(\mathcal{L}))$. Firstly, we check whether the value of γ_{\min} converges as we iterate through $1 \leq n \leq n_{\max}$. Additionally, we need to use different values of $(i_{\max}, k_{\max}, m_{\max})$ to compare which combination of these numbers provides the most reliable results. In this context, more reliable results by definition means that we are looking for $(i_{\max}, k_{\max}, m_{\max})$ that lead to the smallest values for γ_{\min} . Secondly, we compare the linear stability results with the non-linear stability investigation from Section 7.3, where we have considered the King model along the redshift κ in Figure 7.12. Recall that, according to Definition 5.1.2, an equilibrium is linearly unstable if $\inf(\sigma(\mathcal{L})) < 0$. Thus, we can check if the sign of γ_{\min} becomes negative at roughly the same value of κ that corresponds to the onset of instability in the non-linear case. Of course, this assumes that linear and non-linear stability coincide which is by no means an obvious fact for the Einstein-Vlasov system.

As to the convergence of γ_{\min} , we have tested various combinations of $(i_{\max}, k_{\max}, m_{\max}) \in \mathbb{N}_0^3$ for the King model with $\kappa = 0.2$ and kept track of γ_{\min} as we increase n to n_{\max} . We present our results in Figure 8.1. The value of γ_{\min} seems to slowly converge in all the cases that we have studied. However, the final value at n_{\max} depends quite strongly on the class of test functions used which is determined by the indices $(i_{\max}, k_{\max}, m_{\max})$. Since the approximation performs worst for $(i_{\max}, k_{\max}, m_{\max}) = (0, 7, 7)$, choosing an appropriate number for i_{\max} , i.e., sufficiently many radial test functions, appears to be essential for a good approximation to $\inf(\sigma(\mathcal{L}))$. Nevertheless, the extreme setting of employing only radial test functions, as in the case $(i_{\max}, k_{\max}, m_{\max}) = (50, 0, 0)$, does not lead to the best result either.

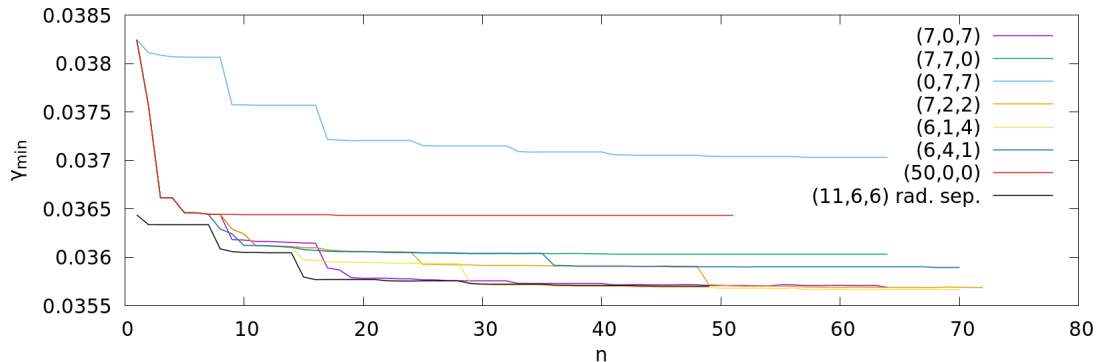


Figure 8.1: The approximation γ_{\min} to $\inf(\sigma(\mathcal{L}))$ for the King model with $\kappa = 0.2$ along increasing values of $1 \leq n \leq n_{\max} = (i_{\max} + 1)(k_{\max} + 1)(m_{\max} + 1)$ for different values of $(i_{\max}, k_{\max}, m_{\max})$.

Recall that the previous work in [60] exclusively considered the case where variation is only applied in r . It seems as if a good mixture of different ansatz functions in (r, w, E) performs the best, as is the case, e.g., for $(i_{\max}, k_{\max}, m_{\max}) = (7, 2, 2)$. It is rather remarkable, however, that the final values of γ_{\min} are fairly close to each other for many of the different combinations of $(i_{\max}, k_{\max}, m_{\max})$, and notably also for the case where $(i_{\max}, k_{\max}, m_{\max}) = (11, 6, 6)$ with the method of radial separation employed, as explained in Section 8.2. We interpret this as another indication that the results are reliable.

In addition to the performance for one fixed steady state, we have tested different combinations for $(i_{\max}, k_{\max}, m_{\max})$ along the King model. In conclusion, it does not appear that one set of $(i_{\max}, k_{\max}, m_{\max})$ always performs best, but that a mix of multiple test functions in each variable r, w , and E are necessary for the best possible approximation. In addition, the method of radial separation works quite well overall because it saves valuable computation time, leads to better numerical stability due to smaller matrices that need to be considered, and yields a satisfactory value of γ_{\min} when compared to the other cases.

As our last test, we check if the numerical results for linear stability are consistent with the results from non-linear stability from Section 7.3.1. The value of γ_{\min} along the redshift κ for the King model for different values of $(i_{\max}, k_{\max}, m_{\max})$ is provided in Figure 8.2. The roots along the plots indicate the point where linear stability changes, according to our approximate value. Non-linear stability changes between $0.3325 < \kappa < 0.335$, which is illustrated by the vertical, dashed grey lines in Figure 8.2. Again, the results are quite consistent across the different combinations of $(i_{\max}, k_{\max}, m_{\max})$. On the one hand, perturbed stationary solutions in the non-linear system are more prone to develop instabilities due to numerical errors stemming from the dynamics. On the other hand, by nature of the numerical method, we always overes-

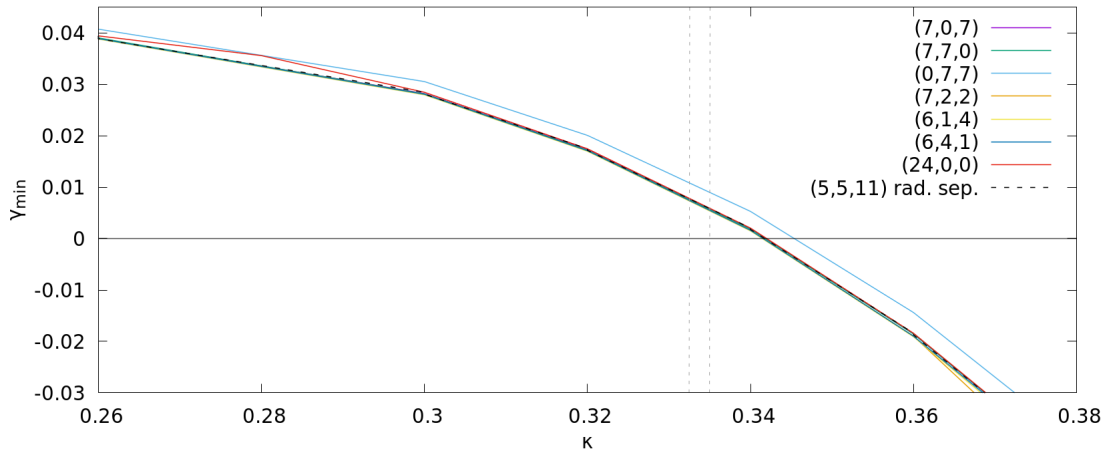


Figure 8.2: The value of γ_{\min} along the redshift κ for the King model for different values of $(i_{\max}, k_{\max}, m_{\max})$. The vertical, dashed gray lines at $\kappa = 0.3325$ and $\kappa = 0.335$ indicate the corridor where stability changes non-linearly according to the PIC method, see Figure 7.12 and its description in Section 7.3.1.

timate linear stability since $\inf(\sigma(\mathcal{L})) < \gamma_{\min}$ must necessarily hold. These observations should be able to explain the (small) discrepancy between our results on linear and non-linear stability. Overall, we believe that this confirms that our method is working well, but improvements to the algorithm’s accuracy and efficiency would be welcome.

At least for the King model, linear and non-linear stability seem to coincide up to numerical accuracy. This is the first time that results concerning linear and non-linear stability are compared for steady states of the Einstein-Vlasov system. We expand on this in the upcoming section.

8.4 Results on linear stability

As we have already indicated above, we can approximate the linear stability behavior of equilibria by determining the sign of γ_{\min} . The results for the King model, as presented in Figure 8.2, indicate that the onset of linear and non-linear stability happens at roughly the same value of κ . This raises the question if linear stability always coincides with non-linear stability. We will not analyze this question in depth, but investigate the two models for which new non-linear stability behavior has been observed in Section 7.4.2, namely the piecewise model (2.76) for $n = 200$ and for $n = 270$. In particular, we analyze if the *binding energy hypothesis* explained in Section 7.3.3 holds for linear stability.³ In addition, it is of interest whether multiple stability changes for $n = 270$ are also observable in the linear case.

³This might seem odd at first glance. However, the only “formal” derivation of the binding energy hypothesis is performed in [61] by investigating linear stability. Therefore, it could in principle be a phenomenon that is only present on the linearized level.

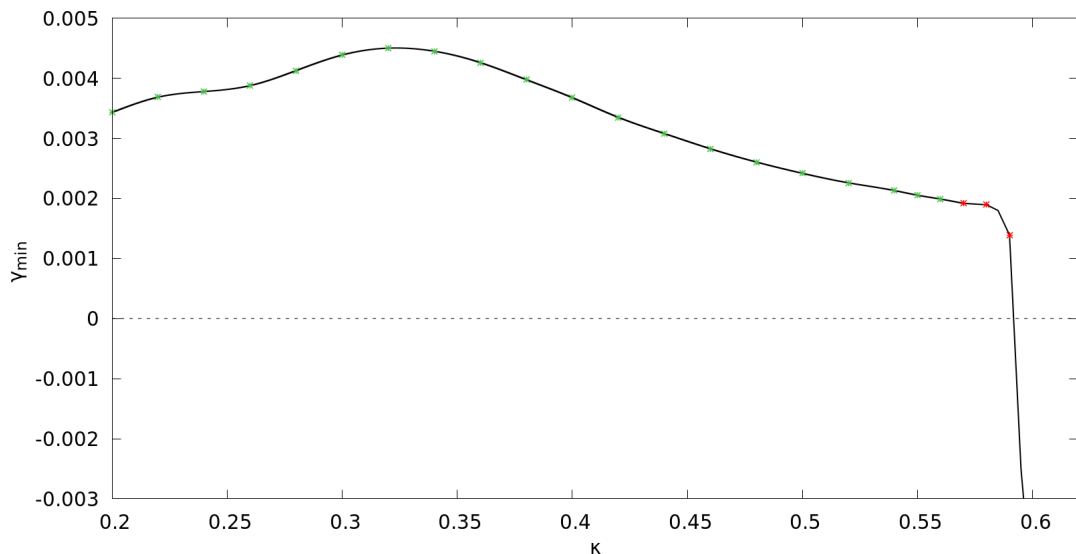


Figure 8.3: The value of γ_{\min} along the redshift κ for the piecewise model with $n = 200$. The set of test functions is given by $(i_{\max}, k_{\max}, m_{\max}) = (9, 2, 6)$ and the method of radial separation is used. The green and red dots indicate non-linearly stable and unstable equilibria, respectively, as obtained in Section 7.3.3.

We begin by presenting the piecewise model for $n = 200$ along the redshift κ . Especially if κ is large, i.e., roughly $\kappa \geq 0.5$, we need to massively ramp up the numerical accuracy. In particular, the step size dr and the number of integrand evaluations need to be increased sufficiently, which means that we cannot use too many test functions. Due to its good performance and smaller computation time, we employ the radial separation method and choose $(i_{\max}, k_{\max}, m_{\max}) = (9, 2, 6)$, thereby putting more emphasis on the test functions along r and E instead of w . This performs better and is numerically more stable. The results on linear stability are depicted in Figure 8.3 where we also compare them to the results from the non-linear stability investigation from Section 7.3.3. Our numerical results yield that the model is linearly stable for $\kappa \leq 0.59$ and unstable for $\kappa \geq 0.595$. The linear instability sets in rapidly for $\kappa \geq 0.595$, for which we provide the values of γ_{\min} in Table 8.1. It is quite delicate to determine the exact value where γ_{\min} becomes negative, but we can still confidently rule out the binding energy hypothesis for the linearized system since the first maximizer of the binding energy curve is located at $\kappa \approx 0.265$, see Figure 7.13, and no other extremal point is close to $\kappa = 0.59$.

Comparing this to the result from the non-linear stability analysis from Section 7.3.3, where the threshold value for the onset of instability is $\kappa = 0.57$, yields that the two results are quite similar. In addition, the observation that γ_{\min} decreases rapidly in the unstable domain may be correlated with the low collapse time which can be seen in Figure 7.13.

κ	0.595	0.60	0.61	0.62	0.63	0.64	0.65
γ_{\min}	-0.00250	-0.00471	-0.0628	-0.161	-0.176	-0.270	-0.344

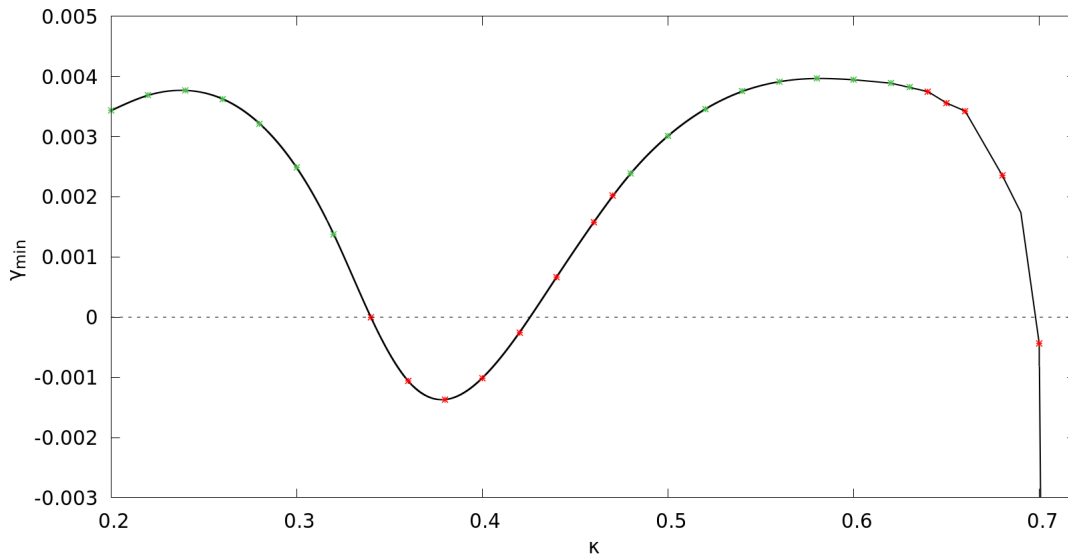
Table 8.1: The value of γ_{\min} in the unstable domain for the model used in Figure 8.3.

Figure 8.4: The value of γ_{\min} along the redshift κ for the piecewise model with $n = 270$. The set of test functions is given by $(i_{\max}, k_{\max}, m_{\max}) = (9, 2, 6)$ and the method of radial separation is used. The green and red dots indicate non-linearly stable and unstable equilibria, respectively, as obtained in Section 7.3.3.

As a second example, we consider the piecewise model with $n = 270$, for which we have investigated non-linear stability in Section 7.3.3. The distinct feature of this family of steady states is the existence of multiple non-linear stability changes. Indeed, linear stability also changes multiple times for $n = 270$, as we illustrate in Figure 8.4 by plotting the values of γ_{\min} . For $\kappa \leq 0.33$, the value of γ_{\min} is positive. This initial linear stability domain is followed by the range $0.34 \leq \kappa \leq 0.42$, which yields $\gamma_{\min} < 0$, i.e., the existence of an exponentially growing mode. For $0.43 \leq \kappa \leq 0.68$, we obtain a second linear stability domain after which the steady states become linearly unstable again for $\kappa \geq 0.70$. Similar to the case $n = 200$ above, it is difficult to determine the boundary values for κ with much precision, so these results should be considered more as a rough overview of linear stability for this model. The important finding is that multiple stability changes occur linearly as well as non-linearly.

This should be compared with the results obtained in Section 7.3.3. As for the case $n = 200$, the threshold values for κ differ with the algorithm for linear stability, where

the steady states are always judged to be stable more often—as measured in κ —than with the non-linear PIC method. However, the results are still reasonably consistent considering the highly relativistic setting for the large values of κ and the inherent fact that we only approximate $\inf(\sigma(\mathcal{L}))$ on a finite-dimensional subspace.

In conclusion, we provide evidence that the binding energy hypothesis does not hold for linearized stability and that multiple stability changes can occur also for the linearized system. More generally, we confirm that linear and non-linear stability coincide up to numerical accuracy for the two examples of the piecewise model with $n = 200$ and $n = 270$, which are distinguished by their unusual stability behavior. The fact that there is a discrepancy between the results for linear and non-linear stability may be explicable by the limitations of the numerical method, as mentioned in Section 8.2. The consistency of the linear and non-linear results, which are obtained by entirely different methods—through a variational principle induced by a unbounded differential operator in the former and through a particle method in the latter case—, serve as an indication that our numerical results are reliable and accurately represent the features of the analytical system.

8.5 Results on oscillating modes and damping

The second application of the numerical analysis of the linearized Einstein-Vlasov system deals with the search for linearly oscillating solutions whose existence we showed rigorously in Theorem 6.3.4 for isotropic steady states under certain conditions. The goal of this section is to numerically explore whether

$$0 < \inf(\sigma(\mathcal{L})) < \inf(\sigma_{\text{ess}}(\mathcal{L})) \tag{8.22}$$

holds which yields an oscillating mode, as described in Section 6.1. From the analysis of the essential spectra in Theorem 4.3.18, we obtain

$$\sigma_{\text{ess}}(\mathcal{L}) = \sigma_{\text{ess}}(-\mathcal{B}^2|_{\mathcal{H}}) \subset \overline{\left(\frac{2\pi\mathbb{N}}{T(\tilde{\Omega}_0^{EL})} \right)^2} = \sigma_{\text{ess}}(-\mathcal{T}^2|_{\mathcal{H}}).$$

Together with (8.22), this shows that the estimate

$$0 < \inf(\sigma(\mathcal{L})) < \inf_{(E,L) \in \tilde{\Omega}^{EL}} \frac{4\pi^2}{T(E,L)^2}$$

necessarily implies the presence of an oscillating mode. We also search for damping for the linearized system, as we have observed non-linear damping for stable steady states in Section 7.3. It is unclear how to determine the existence of damping from the analysis of the bottom of the spectrum of \mathcal{L} . However, it is plausible that damping takes place in the case

$$\inf(\sigma(\mathcal{L})) = \inf(\sigma_{\text{ess}}(\mathcal{L})),$$

since this is the case in [56] for the Vlasov-Poisson system. Unfortunately, we do not have an exact formula for $\inf(\sigma_{\text{ess}}(\mathcal{L}))$, but it is reasonable to assume

$$\inf(\sigma_{\text{ess}}(\mathcal{L})) = \inf_{(E,L) \in \hat{\Omega}^{EL}} \frac{4\pi^2}{T(E,L)^2} = \inf(\sigma_{\text{ess}}(-\mathcal{T}^2|_{\mathcal{H}})), \quad (8.23)$$

which is indirectly claimed in [47, Rem. 6.3].

We therefore approximate $\inf(\sigma(\mathcal{L}))$ with γ_{\min} , as outlined in Section 8.2, and compare this with the value of $\inf_{(E,L) \in \hat{\Omega}^{EL}} \frac{4\pi^2}{T(E,L)^2}$, which we compute numerically as in Section 2.4. If we find

$$0 < \gamma_{\min} < \inf_{(E,L) \in \hat{\Omega}^{EL}} \frac{4\pi^2}{T(E,L)^2} = \inf(\sigma_{\text{ess}}(-\mathcal{T}^2|_{\mathcal{H}})) \quad (8.24)$$

and assume that the steady state is, in fact, linearly stable, we can conclude with good confidence that an oscillating mode does indeed exist since the algorithm always yields $\inf(\sigma(\mathcal{L})) \leq \gamma_{\min}$. On the other hand, if

$$\gamma_{\min} > \inf_{(E,L) \in \hat{\Omega}^{EL}} \frac{4\pi^2}{T(E,L)^2} = \inf(\sigma_{\text{ess}}(-\mathcal{T}^2|_{\mathcal{H}})) \quad (8.25)$$

holds, it is possible that damping takes place for the steady state under consideration; however, this has to be taken with a pinch of salt. In particular, if (8.23) is indeed true, the estimate (8.25) is always due to numerical inaccuracy. As we minimize the quadratic form over only a finite-dimensional subspace, such errors are expected, especially since elements in the essential spectrum can only be approximated in a distributional sense which is hard to obtain from our numerical method.

We focus on the isotropic polytropes (2.5) which are parametrized by the polytropic index k determining the smoothness of the ansatz function. As we have observed in Figure 7.2, for the fixed value of the redshift $\kappa = 0.05$, damping appears to set in when k is increased sufficiently. For the same setting, we present our findings regarding the linearized system in Figure 8.5 and additionally consider $\kappa \in \{0.01, 0.005, 0.001\}$. Note that the vertical scale, i.e., the value of γ_{\min} , is logarithmic. Three observations stand out: Firstly, we obtain an oscillating mode for approximately $k \leq 1.31$ for the case $\kappa = 0.05$, after which (8.25) is fulfilled, indicating that damping might be present. This is consistent with the non-linear results depicted in Figure 7.2. However, as in the non-linear case, it is difficult to determine the exact threshold value for k , where oscillation changes to damping. Secondly, in the limit $\kappa \rightarrow 0$, it appears that $k = 1.2$ is close to the value which decides over oscillating or damping behavior. We do not know whether $k = 1.2$ is of any deeper analytical meaning or if it is an artifact of numerical inaccuracy. However, it is worth mentioning that $k = 1.2$ also arises as a critical value in the results of [84] for the Vlasov-Poisson system. Finally, there seems to be a negative exponential relation between γ_{\min} and k as well as between $\sigma_{\text{ess}}(-\mathcal{T}^2|_{\mathcal{H}})$ and k , as we get an almost perfectly straight line in the logarithmic plot. We speculate that this is

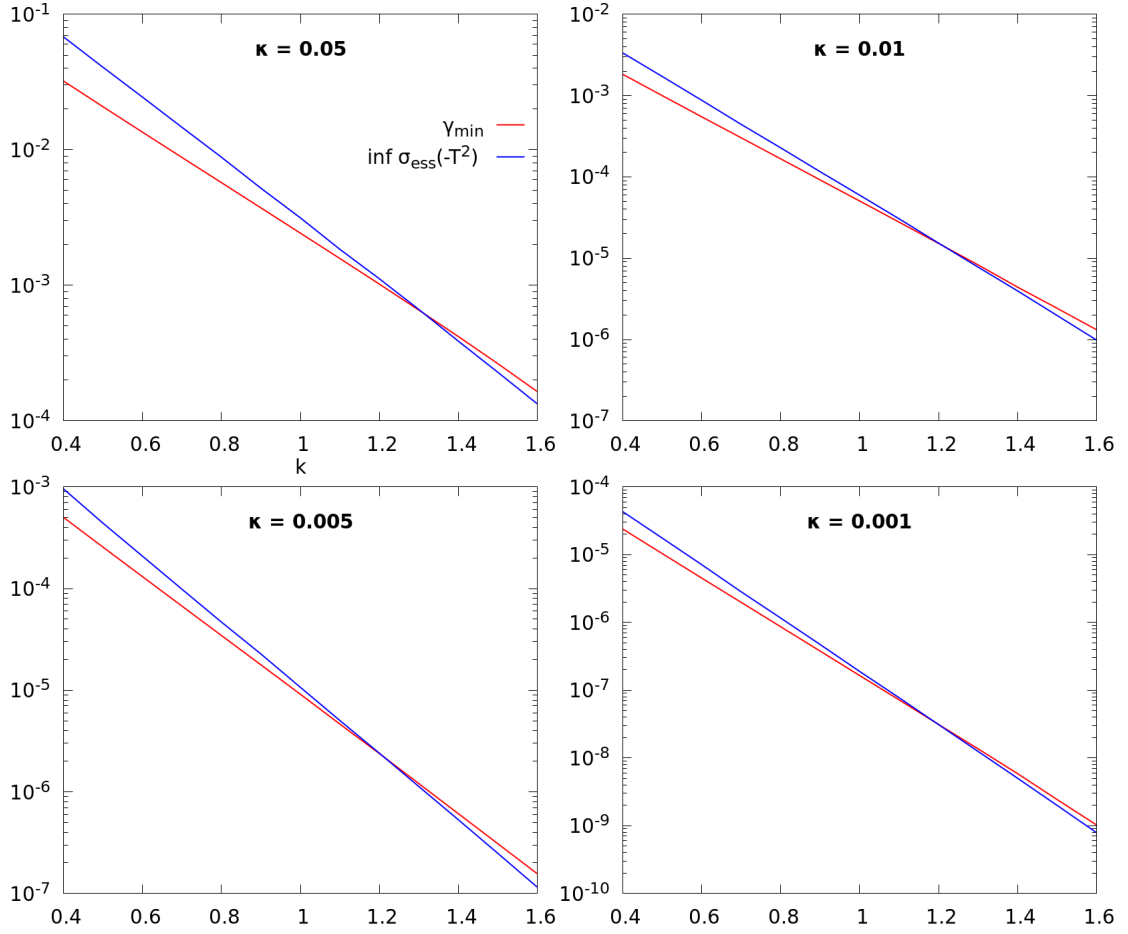


Figure 8.5: The values of γ_{\min} and $\sigma_{\text{ess}}(-\mathcal{T}^2)$ for the isotropic polytropes along the polytropic index k for multiple values of κ . The set of test functions is given by $(i_{\max}, k_{\max}, m_{\max}) = (6, 1, 4)$.

due to the polytropic nature of the ansatz function. The quantity $\sigma_{\text{ess}}(-\mathcal{T}^2|_{\mathcal{H}})$ falls off less quickly than γ_{\min} in k , which is why the two functions eventually cross. It remains unclear whether there is a deeper analytical reason behind this behavior for polytropes, so more research in this direction is needed.

Instead of scanning along k for a fixed value of κ , we next investigate a fixed polytrope along κ . We provide the ratio γ_{\min} over $\inf(\sigma_{\text{ess}}(-\mathcal{T}^2))$ in Figure 8.6 for $k \in \{\frac{1}{2}, 1, \frac{3}{2}, 2\}$. In the case where the ratio is between zero and one, the estimate (8.24) is valid which corresponds to the existence of an oscillating mode. If the ratio is greater than one, (8.25) holds, indicating the possibility of damped solutions. For $k \leq 1$, we always obtain oscillating solutions for all values of κ for which the steady state is linearly stable. For $k \geq 1.5$, we observe the validity of (8.25) for an interval in κ which appears to start at 0. For example, in the case $k = 1.5$, the estimate (8.25) seems to hold for

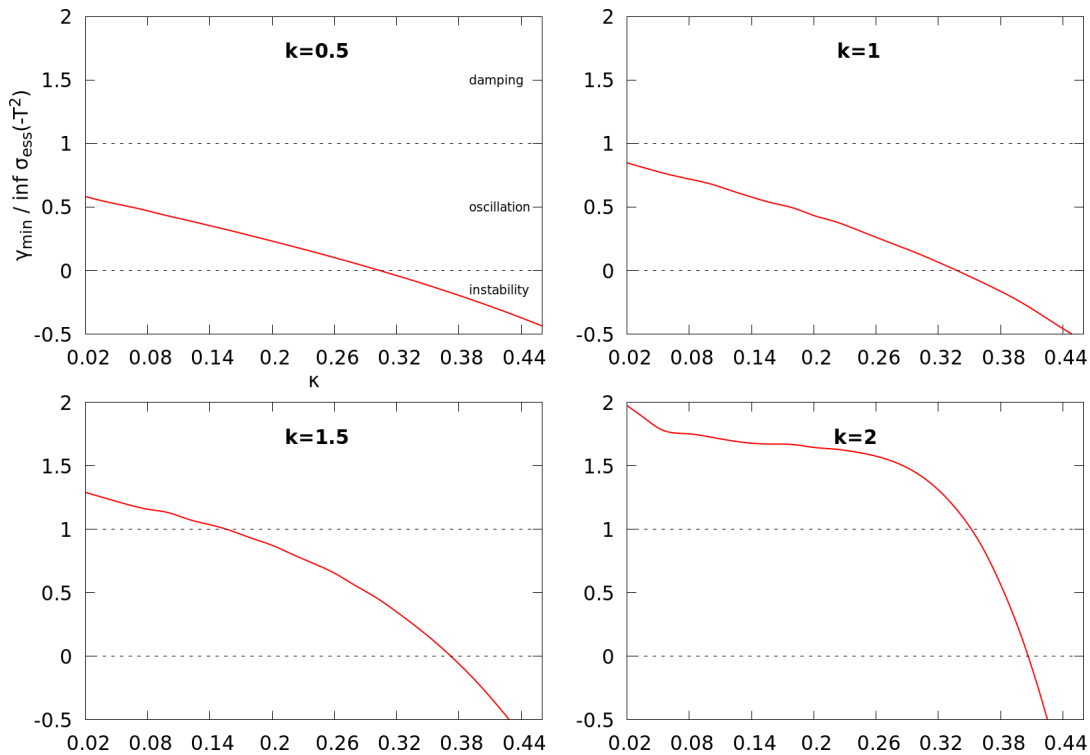


Figure 8.6: The ratio of γ_{\min} over $\inf(\sigma_{\text{ess}}(-\mathcal{T}^2))$ for the isotropic polytropes along the redshift κ for multiple values of k . The set of test functions is given by $(i_{\max}, k_{\max}, m_{\max}) = (9, 4, 4)$ and the method of radial separation is employed.

$0 < \kappa \leq 0.15$. Moreover, this interval gets larger as k increases, e.g., for $k = 2$ it ranges from $0 < \kappa \leq 0.35$, supporting the hypothesis that the smoothness of the ansatz function is tightly connected to the question whether an oscillating mode exists or damping occurs.

However, if we consider κ close to the value of the redshift where stability changes, we always obtain oscillating modes, as an eigenvalue departs from the essential spectrum and eventually crosses zero, leading to an exponentially growing mode. This fits very well to the general idea stated and used in Chapter 6 in order to obtain oscillating modes analytically.

9 Conclusion, open problems, and possible areas of further research

We live on an island surrounded by a
sea of ignorance. As our island of
knowledge grows, so does the shore of
our ignorance.

John Archibald Wheeler

In this final chapter, we provide a brief summary of our main results and address open problems. We also list areas for possible further research which are beyond the scope of this work.

The main focus of this dissertation was to investigate stability issues of steady states and the existence of oscillating solutions to the spherically symmetric, asymptotically flat Einstein-Vlasov system. As the foundation, we have constructed stationary solutions, analyzed their properties, and derived the linearized Einstein-Vlasov system in Chapters 2 to 4. In Theorem 4.3.18, we have gathered spectral properties of the Antonov operator \mathcal{L} which governs over the dynamics of the linearized system. Through a Birman-Schwinger principle, we have characterized and reduced the issue of linear stability to a one-dimensional variational problem for the Mathur operator \mathcal{M} in Theorem 5.4.1. This has lead directly to a Birman-Schwinger bound on the number of exponentially growing modes in Theorem 5.4.3 and, as an application, to the linear stability of small stationary shells surrounding a black hole in Theorem 5.4.4. We have established the existence of linearly oscillating modes for isotropic equilibria under suitable conditions in Theorem 6.3.4. For the proof, we have shown in Theorem 6.2.13 that the projection onto the kernel of the essential operator \mathcal{B} is continuous along the redshift. In the numerical study in Chapter 7, we have considered and described non-linear qualitative and quantitative stability behavior in the isotropic case as well as in the setting with a Schwarzschild singularity. We have provided evidence against the binding energy hypothesis and for the existence of multiple stability changes along certain families of isotropic equilibria. In Chapter 8, we have closed with a brief numerical investigation of linear stability by means of approximating the bottom of the spectrum of \mathcal{L} . We have found that linear and non-linear stability coincides up to numerical accuracy and analyzed the existence of oscillating modes versus damping behavior for polytropes.

Nevertheless, numerous problems remain open and unsolved. It would be of interest to show the linear stability result from Theorem 5.1.4(a) with the Mathur operator approach. This should be possible by considering the limit $\kappa \rightarrow 0$, which yields solutions close to Newtonian, see [54, Sc. 3], together with the continuity result for the Mathur

operator from Theorem 6.3.2 as well as the Birman-Schwinger principle for the Vlasov-Poisson system derived in [55]. Understanding the projection Π onto the kernel of \mathcal{B} better and finding an explicit representation would open up possibilities to specify the variational principle for determining linear stability further, possibly leading to an explicit stability characterization. Furthermore, a better understanding of the spectral properties of \mathcal{L} is necessary to determine whether linearly oscillating modes exist or if damping happens. In this context, it is unclear what precisely is the connection between our work in Chapter 5 and the linear stability analysis of [52]. The main assumption which we make throughout our study is the existence of the single-well structure, which we have shown, e.g., for isotropic steady states which are not too relativistic. Numerical evidence indicates that the single-well structure holds for general isotropic equilibria, but proving this is an open problem. A concept for a generalized single-well structure for (multi-)shell solutions could be a next natural step in order to expand our findings to anisotropic steady states.

For projects involving numerical analysis, a more structured investigation of families of shells surrounding black holes is needed. For example, it is unknown whether κ - or δ -families always lead to unstable steady states when increasing κ or δ , respectively. In addition, one should study the effects of multi-shell solutions to answer the question whether different qualitative behavior occurs in comparison to single shells.¹ As to the method for approximating the infimum of $\sigma(\mathcal{L})$ via a variational principle, it is clear that our algorithm would benefit from a more sophisticated approach and a numerically more stable implementation.

One major long-term open problem for the Einstein-Vlasov system consists of (dis-)proving the cosmic censorship hypothesis [81] and showing global in-time existence of classical solutions in Schwarzschild coordinates launched by compactly supported initial data. These two issues are most likely tightly intertwined. The non-linear stability of steady states is another important topic which is out of reach using the current techniques. The search for non-linearly stable equilibria should most likely begin by obtaining stationary solutions close to Newtonian as minimizers of an appropriate functional. The non-linear behavior of unstable steady states, i.e., the existence of collapsing solutions, heteroclinic and homoclinic orbits, requires further deep understanding of the dynamical system. A first step into this direction would be to translate the existence of an exponentially growing mode for the linearized system to instability in the non-linear case in a suitable sense.

Throughout this thesis, we have recalled and applied previous results, proven open research questions, and stated new problems that require further investigation. It remains crucial to consider the spherically symmetric Einstein-Vlasov system in order to gain a more comprehensive conceptual understanding of collisionless matter within the framework of general relativity.

¹A research group associated with the author is currently working on this topic.

A Derivation of the linearized system

We provide a formal derivation of the linearized system which is missing in the literature. We only consider the singularity-free case, as the same techniques can be applied almost one-to-one to the setting with a Schwarzschild black hole at the center. To simplify the computations, we assume that f_0 is a classical solution of the Vlasov equation (1.24), and we employ the same notation and assumptions, as introduced in Section 4.1. For $0 < \varepsilon \ll 1$ and a suitably smooth, spherically symmetric function $f: \mathbb{R} \times \mathbb{R}^6 \rightarrow \mathbb{R}$ supported on the steady state support, we insert¹

$$\tilde{f} = f_0 + \varepsilon f + \mathcal{O}(\varepsilon^2)$$

into the Einstein-Vlasov system and ignore terms of order $\mathcal{O}(\varepsilon^2)$. Consequently, we get

$$\rho_{\tilde{f}} = \rho_0 + \varepsilon \rho_f + \mathcal{O}(\varepsilon^2), \quad p_{\tilde{f}} = p_0 + \varepsilon p_f + \mathcal{O}(\varepsilon^2),$$

and the quasi-local mass (of \tilde{f}) is given by

$$m = m_0 + \varepsilon m_f + \mathcal{O}(\varepsilon^2),$$

where m_f is the quasi-local mass (1.23) corresponding to f . Moreover, we deduce equations for the linearized metric coefficients λ_f, μ_f by expressing the metric coefficients μ, λ induced by \tilde{f} as

$$\lambda = \lambda_0 + \varepsilon \lambda_f + \mathcal{O}(\varepsilon^2), \quad \mu = \mu_0 + \varepsilon \mu_f + \mathcal{O}(\varepsilon^2). \quad (\text{A.1})$$

By explicitly solving (1.10) for λ , we obtain by a first-order Taylor expansion that

$$\lambda = -\frac{1}{2} \ln \left(1 - \frac{2(m_0 + \varepsilon m_f + \mathcal{O}(\varepsilon^2))}{r} \right) = -\frac{1}{2} \ln \left(1 - \frac{2m_0}{r} \right) + \varepsilon \frac{\frac{m_f}{r}}{1 - \frac{2m_0}{r}} + \mathcal{O}(\varepsilon^2)$$

and thus

$$\lambda_f(r) = \frac{\frac{m_f(r)}{r}}{1 - \frac{2m_0(r)}{r}} = \frac{4\pi e^{2\lambda_0}}{r} \int_{R_{\min}}^r \rho_f(s) s^2 ds. \quad (\text{A.2})$$

¹Here $\mathcal{O}(\varepsilon^2)$ stands for a function $g_\varepsilon: \mathbb{R} \times \mathbb{R}^6 \rightarrow \mathbb{R}$ such that $|g_\varepsilon| \leq \varepsilon^2 |g|$ for a fixed function $g: \mathbb{R} \times \mathbb{R}^6 \rightarrow \mathbb{R}$ and small values of $\varepsilon > 0$. We use this symbol quite loosely in our derivation but note that it could be made more rigorous.

Moreover (1.11), yields

$$(\mu_0 + \varepsilon\mu_f)' + \mathcal{O}(\varepsilon^2) = e^{2(\lambda_0 + \varepsilon\lambda_f)} \left(\frac{m_0 + \varepsilon m_f}{r^2} + 4\pi r(p_0 + \varepsilon p_f) \right) + \mathcal{O}(\varepsilon^2).$$

We use the Taylor expansion

$$e^{2(\lambda_0 + \varepsilon\lambda_f)} = e^{2\lambda_0}(1 + 2\varepsilon\lambda_f) + \mathcal{O}(\varepsilon^2)$$

as well as

$$\mu'_0 = e^{2\lambda_0} \left(\frac{m}{r^2} + 4\pi r p_0 \right)$$

and (A.2), in order to obtain (4.4). Expressing (A.2) as a differential equation yields (4.3). Inserting \tilde{f} and relation (A.1) into the Vlasov equation (1.24) gives

$$\begin{aligned} 0 = & \partial_t f_0 + \varepsilon \partial_t f + e^{\mu_0 - \lambda_0} (1 + \varepsilon(\mu_f - \lambda_f)) \frac{v}{\sqrt{1 + |v|^2}} \cdot (\partial_x f_0 + \varepsilon \partial_x f) \\ & + \left(4\pi r e^{\lambda_0 + \mu_0} (1 + \varepsilon(\lambda_f + \mu_f)) (j_0 + \varepsilon j_f) \frac{x \cdot v}{r} \right. \\ & \left. - e^{\mu_0 - \lambda_0} (1 + \varepsilon(\mu_f - \lambda_f)) (\mu'_0 + \varepsilon \mu'_f) \sqrt{1 + v^2} \right) \frac{x}{r} \cdot (\partial_v f_0 + \varepsilon \partial_v f) + \mathcal{O}(\varepsilon^2), \end{aligned}$$

where we have employed multiple first-order Taylor expansions in ε . This equation can be simplified considerably by eliminating terms of order ε^2 and using that f_0 is a stationary solution to the Einstein-Vlasov system. In particular, we have $\partial_t f_0 = 0$, $j_0 = 0$, and

$$\frac{v}{\sqrt{1 + |v|^2}} \cdot \partial_x f_0 = \mu'_0 \sqrt{1 + |v|^2} \frac{x}{r} \cdot \partial_v f_0. \quad (\text{A.3})$$

Therefore, we obtain

$$\begin{aligned} 0 = & \partial_t f + e^{\mu_0 - \lambda_0} (\mu_f - \lambda_f) \frac{v}{\sqrt{1 + |v|^2}} \cdot \partial_x f_0 \\ & + \left(4\pi r e^{\lambda_0 + \mu_0} j_f \frac{x \cdot v}{r} - e^{\mu_0 - \lambda_0} (\mu'_f + (\mu_f - \lambda_f) \mu'_0) \sqrt{1 + v^2} \right) \frac{x}{r} \cdot \partial_v f_0 \\ & + e^{\mu_0 - \lambda_0} \left(\frac{v}{\sqrt{1 + |v|^2}} \partial_x f - \mu'_0 \sqrt{1 + |v|^2} \frac{x}{r} \cdot \partial_v f \right), \end{aligned}$$

which can be rewritten by again using (A.3) such that

$$\begin{aligned} 0 = & \partial_t f + e^{\mu_0 - \lambda_0} \left(\frac{v}{\sqrt{1 + |v|^2}} \partial_x f - \mu'_0 \sqrt{1 + |v|^2} \frac{x}{r} \cdot \partial_v f \right) \\ & + \left(4\pi r e^{\lambda_0 + \mu_0} j_f \frac{x \cdot v}{r} - e^{\mu_0 - \lambda_0} \mu'_f \sqrt{1 + v^2} \right) \frac{x}{r} \cdot \partial_v f_0. \end{aligned}$$

We use the Poisson bracket of two differentiable functions g, h

$$\{g, h\} = \partial_x g \cdot \partial_v h - \partial_v g \cdot \partial_x h = \partial_r g \partial_w h - \partial_w g \partial_r h,$$

and, since $f_0(x, v) = \varphi(E(x, v), L(x, v))$ and $\frac{x \cdot v}{r} = w$, we get

$$0 = \partial_t f + e^{-\lambda_0} \{f, E\} + \left(4\pi r e^{3\mu_0 + \lambda_0} \frac{w^2}{E} j_f - e^{2\mu_0 - \lambda_0} w \mu'_f \right) \varphi',$$

which is equivalent to (4.2) because of $\varphi' < 0$ by (S3).

B Results from operator and spectral theory

We recall the definition of closed, self-adjoint, and skew-adjoint operators from the seminal work [89, Ch. VIII].

Definition B.1. Consider a densely defined operator T on a Hilbert space $(H, \langle \cdot, \cdot \rangle)$ with domain $D(T)$.

- (a) The operator is called closed if its graph $\{(Tf, f) \mid f \in D(T)\}$ is a closed subset of $H \times H$.
- (b) Let $D(T^*)$ be the set of $f \in H$ such that there exists $g \in H$ with

$$\langle Th, f \rangle = \langle h, g \rangle, \quad h \in D(T).$$

The operator $T^* : D(T^*) \rightarrow H$, given by the relation $T^*f = g$, is referred to as the adjoint of T .

- (c) The operator T is called self-adjoint if $D(T) = D(T^*)$ and $T = T^*$.
- (d) The operator T is called skew-adjoint if $D(T) = D(T^*)$ and $T = -T^*$.

The orthogonal projection onto a (closed) subspace plays an important role in determining the inverse of the essential operator \mathcal{B} . For the existence theory of such projections, see, e.g., [25, Section 5.1] or [58, Section 5.4].

Definition B.2 ([58], Def. 5.15). A bounded operator P acting on a Hilbert space H is called a projection if $P^2 = P$. If P is self-adjoint, it is called an orthogonal projection.

Lemma B.3 ([58], Prop. 5.16). If M is a closed subspace of a Hilbert space H , there exists a unique orthogonal projection P such that $\text{im}(P) = M$. In addition, H can be decomposed into

$$H = \ker(P) \oplus \text{im}(P).$$

There is a plethora of literature that provides an introduction to spectral theory. For our purpose, we refer to [58] and [89] as the main works on which we orient ourselves. We only formulate the following for self-adjoint operators but note that many results and properties can be generalized to much less restrictive settings. As in [58], we define the spectrum of an operator acting on a Hilbert space $(H, \langle \cdot, \cdot \rangle)$ as follows:

Definition B.4 ([89], Ch. VI & Ch. VIII). Let T be a self-adjoint operator on a Hilbert space H with domain $D(T)$.

(a) The resolvent set of T is defined as

$$\rho(T) := \{\lambda \in \mathbb{C} \mid T - \lambda \text{id} \text{ is invertible with bounded inverse}\}.$$

The spectrum of T is given by $\sigma(T) := \mathbb{C} \setminus \rho(T)$.

(b) The discrete spectrum of T is defined as

$$\sigma_d(T) := \{\lambda \in \sigma(T) \mid \lambda \text{ is isolated and an eigenvalue of } T \text{ with finite multiplicity}\}.$$

The essential spectrum of T is given by $\sigma_{\text{ess}}(T) := \sigma(T) \setminus \sigma_d(T)$.

We need to specify what is meant by “multiplicity” of an eigenvalue in the case of a self-adjoint operator. For a more detailed discussion, we refer to [58, Sc. 7.1].

Remark B.5. Let T be a self-adjoint operator on a Hilbert space H with domain $D(T)$. Then $\gamma \in \mathbb{R}$ is an eigenvalue of T if there exists $f \in D(T) \setminus \{0\}$ such that $Tf = \gamma f$. The multiplicity of γ is defined as $\dim(\ker(T - \gamma \text{id})) \in \mathbb{N} \cup \{\infty\}$. By the definition above, the multiplicity of γ is finite if $\gamma \notin \sigma_{\text{ess}}(T)$.

Fortunately, for self- and skew-adjoint operators the spectrum has some nice a-priori properties. For example, it is easy to see that the spectrum of self-adjoint operators is real, see [58, Thm. 5.5]. The following characterization of coercivity is used at various points of our investigation:

Lemma B.6. Let T be a self-adjoint operator on a Hilbert space H and $\gamma \geq 0$. The coercivity estimate $\langle Tf, f \rangle \geq \gamma \|f\|^2$ holds for $f \in H$ if, and only if, $\sigma(T) \subset [\gamma, \infty[$.

Proof. We observe that $\langle Tf, f \rangle \geq \gamma \|f\|^2$ for $f \in H$ if, and only if, the operator $T_\gamma := T - \gamma \text{id}$ fulfills

$$\langle T_\gamma f, f \rangle = \langle Tf, f \rangle - \gamma \|f\|^2 \geq 0.$$

Since T_γ is self-adjoint as well, this is equivalent to $\sigma(T_\gamma) \subset [0, \infty[$ according to [58, Prop. 5.12]. This means that for every $\eta < 0$, the operator

$$T_\gamma - \eta \text{id} = T - (\gamma + \eta) \text{id}$$

is invertible with bounded inverse, i.e., $\gamma + \eta \in \rho(T)$ and thus $\sigma(T) \subset [\gamma, \infty[$ □

A famous theorem is *Weyl's criterion*, which characterizes elements in the essential spectrum by an approximation result. We formulate the following properties for self-adjoint operators but emphasize that they can be defined and applied for skew-adjoint operators T analogously since in this case iT is self-adjoint.

Theorem B.7 ([58], Thm. 7.2). Let T be a self-adjoint operator. It holds that $\lambda \in \sigma_{\text{ess}}(T)$ if, and only if

$$\exists (f_n)_{n \in \mathbb{N}} \subset D(T) \text{ with } \|f_n\| = 1 : \quad f_n \rightharpoonup 0, \quad (T - \lambda \text{id})f_n \rightarrow 0 \text{ for } n \rightarrow \infty.$$

In this case, $(f_n)_{n \in \mathbb{N}}$ is called a Weyl sequence.

Let us recall the definition of relative compactness of two operators which we only define for self-adjoint operators.

Definition B.8 ([58], Def. 14.1). *Let T be a self-adjoint operator. An operator S is called relatively T -compact if $D(S) \supset D(T)$ and $S(T - \lambda \text{id})^{-1}$ is compact for some (and thus every) $\lambda \in \rho(T)$.*

Note that in [58, Def. 14.1], this is formulated for *closed* operators. However, self-adjoint operators are always closed with a non-empty resolvent set. By using the definition and result from [40, III. Def 2.15 & Exercise 2.18.(1)], we can characterize relative compactness as follows:

Lemma B.9. *Let T be a self-adjoint operator on a Hilbert space H . An operator S is relatively T -compact if, and only if, $D(T) \subset D(S)$ and*

$$S: (D(T), \|T \cdot\|_H + \|\cdot\|_H) \rightarrow H$$

is compact.

Using the notion of relative compactness, *Weyl's theorem* proves that the essential spectrum of an operator remains unchanged under relatively compact *perturbations*.

Theorem B.10 ([58], Thm. 14.6). *Let T and S be self-adjoint operators and let $T - S$ be relatively T -compact. Then,*

$$\sigma_{\text{ess}}(T) = \sigma_{\text{ess}}(S).$$

The next technical result—referred to as a *spectral mapping theorem*—relates the spectrum of a polynomial of an operator with the polynomial of the spectrum.

Theorem B.11 ([111], Cor. 5.5). *Let T be a self-adjoint operator. For a locally analytic function $F: \mathbb{C} \rightarrow \mathbb{C}$, it holds that*

$$F(\sigma(T)) = \sigma(F(T)).$$

As with many assertions above, this holds for a much broader range of operators, e.g., closed operators. With this result, we are able to show that the essential spectra are mapped accordingly as well. We only prove this in our adapted situation.

Lemma B.12. *For a self-adjoint operator T , it holds that*

$$\sigma_{\text{ess}}(T^2) = \sigma_{\text{ess}}(T)^2.$$

Proof. We note that $\sigma_{\text{ess}}(T^2)$ as well as $\sigma_{\text{ess}}(T)^2$ contain only real, non-negative elements since T is self-adjoint. For the first inclusion, consider $\lambda \in \sigma_{\text{ess}}(T^2)$, i.e., $\lambda \in \sigma(T^2)$, but λ is not an isolated $\sigma(T^2)$ or its multiplicity is infinite. In the case where λ is not isolated,

$\pm\sqrt{\lambda}$ is also not isolated in $\sigma(T)$ due to $\sigma(T)^2 = \sigma(T^2)$ from Theorem B.11. On the other hand, if λ is an eigenvalue with infinite multiplicity, i.e.,

$$\dim(\ker(T^2 - \lambda \text{id})) = \infty,$$

we can estimate

$$\begin{aligned} \dim(\ker(T^2 - \lambda \text{id})) &= \dim(\ker((T - \sqrt{\lambda} \text{id})(T + \sqrt{\lambda} \text{id}))) \\ &= \dim(\ker(T + \sqrt{\lambda} \text{id}) \oplus (\ker(T - \sqrt{\lambda} \text{id}) \cap \text{im}(T + \sqrt{\lambda} \text{id}))) \\ &\leq \dim(\ker(T + \sqrt{\lambda} \text{id})) + \dim(\ker(T - \sqrt{\lambda} \text{id})). \end{aligned}$$

Hence, one of $\pm\sqrt{\lambda}$ must have infinite multiplicity as well. Overall, this yields that one of $\pm\sqrt{\lambda}$ is in $\sigma_{\text{ess}}(T)$ and thus $\lambda \in \sigma_{\text{ess}}(T)^2$.

The reverse inclusion follows in a similar manner: For $\lambda \in \sigma_{\text{ess}}(T)^2$, we assume $\sqrt{\lambda} \in \sigma_{\text{ess}}(T)$ without restriction of generality. In case $\sqrt{\lambda}$ is not isolated in $\sigma(T)$, then $\lambda \in \sigma(T)^2 = \sigma(T^2)$ is not isolated in $\sigma(T^2)$ either. If $\sqrt{\lambda}$ has infinite multiplicity, we immediately get

$$\infty = \dim(\ker(T - \sqrt{\lambda} \text{id})) \leq \dim(\ker(T^2 - \lambda \text{id}))$$

These two cases prove $\lambda \in \sigma_{\text{ess}}(T^2)$. □

C Derivation of the equations for the reduced variational principle

The basis of the numerical investigation in Chapter 8 is given by the equations for the reduced variational principle (8.11)–(8.13). We provide the details on how to obtain these formulas here. Recall the setting in Section 8.1 and consider $f_{ikm}, f_{jln} \in \mathcal{H}$ as in (8.4). In the following, we repeatedly use equations (8.5)–(8.8).

We begin with the term

$$\begin{aligned} & \langle \mathcal{T} f_{ikm}, \mathcal{T} f_{jln} \rangle_H \\ &= 4\pi^2 \iiint_{\Omega_0} e^{4\mu_0 - \lambda_0} |\varphi'(E)|(b_m b_n)(E) \left[(\psi_i \psi_j)(r)(a'_k a'_l)(w) \left(e^{-2\mu_0} \mu'_0 E - \frac{L}{r^3 E} \right)^2 \right. \\ & \quad - \left((\psi'_i \psi_j)(r)(a_k a'_l)(w) + (\psi_i \psi'_j)(r)(a'_k a_l)(w) \right) \frac{w}{E} \left(e^{-2\mu_0} \mu'_0 E - \frac{L}{r^3 E} \right) \\ & \quad \left. + (\psi'_i \psi'_j)(r) \frac{w^2}{E^2} (a_k a_l)(w) \right] dw dL dr, \end{aligned}$$

where we recall that E has to be considered as a function $E = E(r, w, L)$. Changing variables from $w \geq 0$ to E via $w = \sqrt{e^{-2\mu_0} E^2 - \frac{L}{r^2} - 1}$ and applying Fubini's theorem yields

$$\begin{aligned} & \langle \mathcal{T} f_{ikm}, \mathcal{T} f_{jln} \rangle_H \\ &= 8\pi^2 \int_0^{R_{\max}} \int_{e^{\mu_0}(r)}^{E^0} \int_0^{r^2(e^{-2\mu_0} E^2 - 1)} e^{2\mu_0 - \lambda_0} |\varphi'(E)|(b_m b_n)(E) \cdot \\ & \quad \cdot \left[(\psi_i \psi_j)(r) \frac{(a'_k a'_l) \left(\sqrt{e^{-2\mu_0} E^2 - \frac{L}{r^2} - 1} \right)}{\sqrt{e^{-2\mu_0} E^2 - \frac{L}{r^2} - 1}} E \left(e^{-2\mu_0} \mu'_0 E - \frac{L}{r^3 E} \right)^2 \right. \\ & \quad - \left((\psi'_i \psi_j)(r)(a_k a'_l) \left(\sqrt{e^{-2\mu_0} E^2 - \frac{L}{r^2} - 1} \right) + (\psi_i \psi'_j)(r)(a'_k a_l) \left(\sqrt{e^{-2\mu_0} E^2 - \frac{L}{r^2} - 1} \right) \right) \\ & \quad \left. \cdot \left(e^{-2\mu_0} \mu'_0 E - \frac{L}{r^3 E} \right) \right] \end{aligned}$$

$$+ (\psi'_i \psi'_j)(r)(a_k a_l) \left(\sqrt{e^{-2\mu_0} E^2 - \frac{L}{r^2} - 1} \right) \frac{\sqrt{e^{-2\mu_0} E^2 - \frac{L}{r^2} - 1}}{E} \Big] dL dE dr.$$

The boundaries of the integrals are due to $\Omega_0 = \{(r, w, L) \mid E(r, w, L) < E^0\}$. Another change of variables defined through $y = e^{-2\mu_0} E^2 - \frac{L}{r^2} - 1$, where $r \in]0, R_{\max}[$ and $E \in]e^{\mu_0}(r), E^0[$ are fixed, implies

$$\begin{aligned} & \langle \mathcal{T} f_{ikm}, \mathcal{T} f_{jln} \rangle_H \\ &= 8\pi^2 \int_0^{R_{\max}} \int_{e^{\mu_0}(r)}^{E^0} \int_0^{e^{-2\mu_0} E^2 - 1} r^2 e^{2\mu_0 - \lambda_0} |\varphi'(E)| (b_m b_n)(E) \cdot \\ & \quad \cdot \left[(\psi_i \psi_j)(r) \frac{(a'_k a'_l)(\sqrt{y})}{\sqrt{y}} E \left(e^{-2\mu_0} \mu'_0 E + \frac{1 + y - e^{-2\mu_0} E^2}{rE} \right)^2 \right. \\ & \quad - \left. \left((\psi'_i \psi_j)(r)(a_k a'_l)(\sqrt{y}) + (\psi_i \psi'_j)(r)(a'_k a_l)(\sqrt{y}) \right) \left(e^{-2\mu_0} \mu'_0 E + \frac{1 + y - e^{-2\mu_0} E^2}{rE} \right) \right. \\ & \quad \left. + (\psi'_i \psi'_j)(r)(a_k a_l)(\sqrt{y}) \frac{\sqrt{y}}{E} \right] dy dE dr. \end{aligned}$$

We expand the square and sort in the different powers of y in order to obtain

$$\begin{aligned} & \langle \mathcal{T} f_{ikm}, \mathcal{T} f_{jln} \rangle_H \\ &= 4\pi^2 \int_0^{R_{\max}} \int_{e^{\mu_0}(r)}^{E^0} r^2 e^{2\mu_0 - \lambda_0} |\varphi'(E)| (b_m b_n)(E) \cdot \\ & \quad \cdot \left\{ (\psi_i \psi_j)(r) \left[\left(e^{-4\mu_0} (\mu'_0)^2 E^3 - 2e^{-2\mu_0} \mu'_0 \frac{g(r, E)E}{r} + \frac{g(r, E)^2}{r^2 E} \right) \int_0^{g(r, E)} \frac{(a'_k a'_l)(y)}{\sqrt{y}} dy \right. \right. \\ & \quad \left. \left. + \left(\frac{2e^{-2\mu_0} E \mu'_0}{r} - \frac{2g(r, E)}{r^2 E} \right) \int_0^{g(r, E)} (a'_k a'_l)(y) \sqrt{y} dy + \frac{1}{r^2 E} \int_0^{g(r, E)} (a'_k a'_l)(y) y^{\frac{3}{2}} dy \right] \right. \\ & \quad - (\psi'_i \psi_j)(r) \left[\left(e^{-2\mu_0} \mu'_0 E - \frac{g(r, E)}{rE} \right) \int_0^{g(r, E)} (a_k a'_l)(y) dy + \frac{1}{rE} \int_0^{g(r, E)} (a_k a'_l)(y) y dy \right] \\ & \quad - (\psi_i \psi'_j)(r) \left[\left(e^{-2\mu_0} \mu'_0 E - \frac{g(r, E)}{rE} \right) \int_0^{g(r, E)} (a'_k a_l)(y) dy + \frac{1}{rE} \int_0^{g(r, E)} (a'_k a_l)(y) y dy \right] \\ & \quad \left. + \frac{(\psi'_i \psi'_j)(r)}{E} \int_0^{g(r, E)} (a_k a_l)(y) \sqrt{y} dy \right\} dE dr, \end{aligned}$$

where we recall the shorthand $g(r, E) = e^{-2\mu_0(r)} E^2 - 1$. By using the auxiliary quantity (8.10), we arrive at the first integral addend in (8.11). The exact same steps are now repeated for the remaining terms for which we keep the derivation shorter. For the

mixed terms involving \mathcal{T} and \mathcal{S} , we get

$$\begin{aligned}
& \langle \mathcal{T} f_{ikm}, \mathcal{S} f_{jln} \rangle_H \\
&= 16\pi^3 \iiint_{\Omega_0} r e^{5\mu_0 + \lambda_0} j_{f_{jln}}(r) |\varphi'(E)| b_m(E) \cdot \\
&\quad \cdot \left[\psi_i(r) a'_k(w) \frac{w^2}{E} \left(e^{-2\mu_0} \mu'_0 E - \frac{L}{r^3 E} \right) - \psi'_i(r) a_k(w) \frac{w^3}{E^2} \right] dw dL dr \\
&= 32\pi^3 \int_0^{R_{\max}} \int_{e^{\mu_0(r)}}^{E^0} \int_0^{e^{-2\mu_0} E^2 - 1} r^3 e^{3\mu_0 + \lambda_0} j_{f_{jln}}(r) |\varphi'(E)| b_m(E) \cdot \\
&\quad \cdot \left[\psi_i(r) a'_k(\sqrt{y}) \sqrt{y} \left(e^{-2\mu_0} \mu'_0 E + \frac{1+y - e^{-2\mu_0} E^2}{rE} \right) - \psi'_i(r) a_k(\sqrt{y}) \frac{y}{E} \right] dy dE dr \\
&= 32\pi^3 \int_0^{R_{\max}} \int_{e^{\mu_0(r)}}^{E^0} r^3 e^{3\mu_0 + \lambda_0} j_{f_{jln}}(r) |\varphi'(E)| b_m(E) \cdot \\
&\quad \cdot \left\{ \psi_i(r) \left[\left(e^{-2\mu_0} \mu'_0 E - \frac{g(r, E)}{rE} \right) \int_0^{g(r, E)} a'_k(\sqrt{y}) \sqrt{y} dy + \frac{1}{rE} \int_0^{g(r, E)} a'_k(\sqrt{y}) y^{\frac{3}{2}} dy \right] \right. \\
&\quad \left. - \frac{\psi'_i(r)}{E} \int_0^{g(r, E)} a_k(\sqrt{y}) y dy \right\} dE dr,
\end{aligned}$$

which yields the second and, by symmetry, the third term in (8.11). Next, we compute

$$\begin{aligned}
\langle \mathcal{S} f_{ikm}, \mathcal{S} f_{jln} \rangle_H &= 64\pi^4 \iiint_{\Omega_0} r^2 e^{6\mu_0 + 3\lambda_0} (j_{f_{ikm}} j_{f_{jln}})(r) |\varphi'(E)| \frac{w^4}{E^2} dw dL dr \\
&= 128\pi^4 \int_0^{R_{\max}} \int_{e^{\mu_0(r)}}^{E^0} r^4 e^{4\mu_0 + 3\lambda_0} (j_{f_{ikm}} j_{f_{jln}})(r) \frac{|\varphi'(E)|}{E} \int_0^{e^{-2\mu_0} E^2 - 1} y^{\frac{3}{2}} dE dr \\
&= \frac{256}{5} \pi^4 \int_0^{R_{\max}} \int_{e^{\mu_0(r)}}^{E^0} r^4 e^{4\mu_0 + 3\lambda_0} (j_{f_{ikm}} j_{f_{jln}})(r) \frac{|\varphi'(E)|}{E} g(r, E)^{\frac{5}{2}} dE dr
\end{aligned}$$

leading to the fourth addend in (8.11). Before we deduce the last term in (8.11), we calculate

$$\begin{aligned}
j_{f_{ikm}}(r) &= \frac{2\pi}{r^2} \psi_i(r) \int_0^\infty \int_0^\infty |\varphi'(E)| w a_k(w) b_m(E) dw dL \\
&= 2\pi e^{-2\mu_0} \psi_i(r) \int_{e^{\mu_0(r)}}^{E^0} |\varphi'(E)| b_m(E) E \int_0^{g(r, E)} a_k(\sqrt{y}) dy dE
\end{aligned}$$

for $r > 0$ in similar fashion to the terms above, which implies (8.13). By plugging this

into the term involving the residual operator \mathcal{R} , we obtain

$$\begin{aligned} \langle \mathcal{R}f_{ikm}, f_{jln} \rangle_H &= 8\pi^2 \iiint_{\Omega_0} r^2 e^{3\mu_0 + \lambda_0} (2r\mu'_0 + 1) (j_{f_{ikm}} j_{f_{jln}})(r) dr \\ &= 16\pi^2 \int_0^{R_{\max}} \int_{e^{\mu_0(r)}}^{E^0} r^4 e^{\mu_0 + \lambda_0} (2r\mu'_0 + 1) j_{f_{ikm}}(r) \psi_j(r) |\varphi'(E)| b_n(E) E \int_0^{g(r,E)} a_l(\sqrt{y}) dy dE dr, \end{aligned}$$

and thus, we have completed the derivation of (8.11). To conclude, the scalar product

$$\begin{aligned} \langle f_{ikm}, f_{jln} \rangle_H &= 4\pi^2 \iiint_{\Omega_0} e^{\lambda_0} |\varphi'(E)| (\psi_i \psi_j)(r) (a_k a_l)(w) (b_m b_n)(E) dr dw dL \\ &= 8\pi^2 \int_0^{R_{\max}} \int_{e^{\mu_0(r)}}^{E^0} r^2 e^{\lambda_0 - 2\mu_0} (\psi_i \psi_j)(r) |\varphi'(E)| (b_m b_n)(E) E \int_0^{g(r,E)} \frac{(a_k a_l)(\sqrt{y})}{\sqrt{y}} dy dE dr \end{aligned}$$

yields (8.12), and all necessary equations from page 229 are shown.

D Pseudo-codes

In this chapter, we provide the pseudo-codes of the algorithms used throughout the work. As we aim for a comprehensive presentation, it is not possible to lay out all the details of the codes. We denote the radial grid points as $r_k = k\Delta r$. The metric coefficients, the auxiliary function y , and the source terms at the radial step r_k are denoted with a subscript $k \in \mathbb{N}$.

D.1 The steady state computation

For the setting covered in Section 2.2, we numerically approximate steady state solutions as follows.

```

Input :  $\Phi, \kappa, M_0, L_0, l$ 
Output: Metric coefficients, source terms, and macroscopic quantities, e.g.,  $M, N, E^0, R_{\max}$ 
if  $M_0 > 0$  then
  | Check whether (P1) and (P3) are satisfied;
end
Compute  $R_{\min}$ , metric coefficients, and  $y_k$  for  $r_k \leq R_{\min}$ ;
 $r_k \leftarrow R_{\min}, m_k \leftarrow 0$ ;
while  $e^{-y_k} \sqrt{1 + \frac{L_0}{r_k^2}} < 1$  do
  | Calculate  $g(r_k, y_k)$  and  $h(r_k, y_k)$  via Simpson rule, see (2.9) and (2.10);
  |  $m_k \leftarrow m_k + 4\pi r^2 g_k \Delta r$ ;
  | Use midpoint method to compute  $y_{k+1}$  according to (2.6).
end
if maximum number of wanted shells is reached or no more shell exists then
  | return metric coefficients, source terms, and macroscopic quantities;
else
  | Repeat while-loop above for next shell;
end

```

Algorithm 1: Approximating steady states

D.2 The particle-in-cell method

Compared to the pseudo-code below, the actual PIC code includes additional features such as the ability to freeze particles inside a trapped surface and a more elaborate sampling in the initialization process.

Input : Steady state \mathring{f} from Algorithm 1, perturbation scheme, and T_{final}

Output: Time evolution of metric coefficients, radius-energy space, and macroscopic quantities

Initialization of particles;

for $i = 1, \dots, N_r, j = 1, \dots, N_u, k = 1, \dots, N_\psi$ **do**

if $\mathring{f}\left(\left(i - \frac{1}{2}\right)\Delta r, j\Delta u, k\Delta\psi\right) > 0$ **then**

 Generate particle at $\left(i - \frac{1}{2}\right)\Delta r, j\Delta u,$ and $k\Delta\psi$ with weight f given

 by (7.1);

 Transform back to (r, w, L) coordinates and write (r_i, w_i, L_i, f_i) for i -th particle's representation;

end

end

if *there are not enough particles* **then**

 Increase N_r, N_u, N_ψ ;

end

Check accuracy of initialization by comparing the result to the steady state;

Partition the particles for parallelization onto the individual threads;

The time loop;

$t \leftarrow 0$;

while $t < T_{\text{final}}$ **do**

 Calculate source terms $\rho_k, j_k,$ and S_k on radial grid via formulas (7.3)–(7.5);

 Solve for a_k and $(K_\theta^\theta)_k$ on radial grid with RK4 method;

 Solve for α_k with RK4 method while $a_k, (K_\theta^\theta)_k$ are fixed and use linearity to handle boundary condition at $r = \infty$;

if $\frac{1}{a_k} < r_k(K_\theta^\theta)_k$ **then**

 trapped surface has developed;

end

foreach *thread in parallel* **do**

 Transform particle positions (r_i, w_i, L_i) to Cartesian coordinates (x_i, v_i) ;

 Propagate particle positions and weights f_i according to Vlasov equation (1.24) using RK4 method;

if $t < T_{\text{pert}}$ **then**

 Include dynamically accessible perturbation if wanted;

end

 Transform particle positions back to (r_i, w_i, L_i) coordinates;

end

 Output errors, metric coefficients, and radius-energy distribution if wanted;

$t \leftarrow t + \Delta t$;

end

Algorithm 2: Particle-in-cell method

D.3 The variational principle

Last but not least, here is a sketch of the algorithm used in Chapter 8 to approximate the bottom of the spectrum of the Antonov operator \mathcal{L} .

Input : Steady state \mathring{f} from Algorithm 1, $(i_{\max}, k_{\max}, m_{\max}) \in \mathbb{N}_0^3$

Output: Approximation to $\inf(\sigma(\mathcal{L}))$

Setup;

Create class of normalized test functions $f = |\varphi'|\psi_i a_k b_m$ and use CUBA library to compute $\|f\|_H$;

Calculate j_f according to (8.13);

Approximation of $\inf(\sigma(\mathcal{L}))$;

if *radial separation method is employed* **then**

for $0 \leq j \leq j_{\max}, 0 \leq k \leq k_{\max}$ **do**

 Compute matrices $L = (\langle \mathcal{L}(|\varphi'|\psi_i a_k b_m), |\varphi'|\psi_j a_l b_n \rangle_H)_{0 \leq i, j \leq i_{\max}}$ and $F = (\langle |\varphi'|\psi_i a_k b_m, |\varphi'|\psi_j a_l b_n \rangle_H)_{0 \leq i, j \leq i_{\max}}$ according to (8.11) and (8.12) using CUBA library;

 Find smallest generalized eigenvalue of the pair (L, F) and a corresponding eigenvector c using Eigen library;

$\psi_{km} \leftarrow \sum_{i=0}^{i_{\max}} c_i \psi_i$;

end

 Compute matrices $L = (\langle \mathcal{L}(|\varphi'|\psi_{km} a_k b_m), |\varphi'|\psi_{ln} a_l b_n \rangle_H)_{k, l, m, n}$ and

$F = (\langle |\varphi'|\psi_{km} a_k b_m, |\varphi'|\psi_{ln} a_l b_n \rangle_H)_{k, l, m, n}$;

 Find smallest generalized eigenvalue γ_{\min} of the pair (L, F) ;

return γ_{\min} ;

else

 Compute matrices $L = (\langle \mathcal{L}(|\varphi'|\psi_i a_k b_m), |\varphi'|\psi_j a_l b_n \rangle_H)_{i, j, k, l, m, n}$ and

$F = (\langle |\varphi'|\psi_i a_k b_m, |\varphi'|\psi_j a_l b_n \rangle_H)_{i, j, k, l, m, n}$;

 Find smallest generalized eigenvalue γ_{\min} of the pair (L, F) ;

return γ_{\min} ;

end

Algorithm 3: Approximating $\inf(\sigma(\mathcal{L}))$ via a variational principle

Bibliography

- [1] ABBOTT, B. P. ET AL., Observation of Gravitational Waves from a Binary Black Hole Merger. *Phys. Rev. Lett.* **116**, 061102 (2019).
- [2] ABRAHAMS, A. M., COOK, G. B., SHAPIRO, S. L., TEUKOLSKY, S. A., Solving Einstein's equations for rotating spacetimes: Evolution of relativistic star clusters. *Phys. Rev. D* **49**, 5153–5164 (1994).
- [3] AMES, E., ANDRÉASSON, H., RINNE, O., Dynamics of gravitational collapse in the axisymmetric Einstein-Vlasov system. *Class. Quantum Gravity* **38**, 105003 (2021).
- [4] ANDRÉASSON, H., On Static Shells and the Buchdahl Inequality for the Spherically Symmetric Einstein-Vlasov System. *Commun. Math. Phys.* **274**, 409–425 (2007).
- [5] ANDRÉASSON, H., Sharp bounds on $2m/r$ of general spherically symmetric static objects. *J. Differ. Equ.* **245** (8), 2243–2266 (2008).
- [6] ANDRÉASSON, H., The Einstein-Vlasov System/Kinetic Theory. *Living Rev. Relativ.* **14**, 4 (2011).
- [7] ANDRÉASSON, H., Black Hole Formation from a Complete Regular Past for Collisionless matter. *Ann. Henri Poincaré* **13**, 1511–1536 (2012).
- [8] ANDRÉASSON, H., Existence of Steady States of the Massless Einstein–Vlasov System Surrounding a Schwarzschild Black Hole. *Ann. Henri Poincaré* **22**, 4271–4297 (2021).
- [9] ANDRÉASSON, H., KUNZE, M., Comments on the paper ‘Static solutions of the Vlasov–Einstein system by G. Wolansky. *Arch. Ration. Mech. Anal.* **235**, 783–791 (2020).
- [10] ANDRÉASSON, H., KUNZE, M., Static solutions to the spherically symmetric Einstein-Vlasov system: a particle-number-Casimir approach. *Preprint arXiv:2202.01835v1*, 41pp. (2022).
- [11] ANDRÉASSON, H., KUNZE, M., REIN G., Global Existence for the Spherically Symmetric Einstein-Vlasov System with Outgoing Matter. *Commun. Partial Differ. Equ.* **33** (4), 656–668 (2008).
- [12] ANDRÉASSON, H., KUNZE, M., REIN G., Gravitational collapse and the formation of black holes for the spherically symmetric Einstein-Vlasov system. *Q. Appl. Math.* **68**, 17–42 (2010).

- [13] ANDRÉASSON, H., KUNZE, M., REIN G., The formation of black holes in spherically symmetric gravitational collapse. *Math. Ann.* **350**, 683–705 (2011).
- [14] ANDRÉASSON, H., KUNZE, M., REIN G., Existence of Axially Symmetric Static Solutions of the Einstein-Vlasov System. *Commun. Math. Phys.* **308**, 23–47 (2011).
- [15] ANDRÉASSON, H., REIN, G., A numerical investigation of the stability of steady states and critical phenomena for the spherically symmetric Einstein-Vlasov system. *Class. Quantum Gravity* **23** (11), 3659–3677 (2006).
- [16] ANDRÉASSON, H., REIN, G., On the steady states of the spherically symmetric Einstein-Vlasov system. *Class. Quantum Gravity* **24** (7), 1809–1832 (2007).
- [17] ANTONOV, V. A., Remarks on the problems of stability in stellar dynamics. *Soviet Astronomy* **4**, 859–867 (1960).
- [18] ARNOL'D, V. I., *Mathematical Methods of Classical Mechanics* (second edition), Graduate Texts in Mathematics **60**, Springer-Verlag, New York 1989.
- [19] BATT, J., FALTENBACHER, W., HORST, E., Stationary spherically symmetric models in stellar dynamics. *Arch. Ration. Mech. Anal.* **93**, 159–183 (1986).
- [20] BIRDSALL, C. K., LANGDON, A. B., *Plasma Physics via Computer Simulation*, Series in Plasma Physics, Taylor & Francis Group, New York 1991.
- [21] BISNOVATYI-KOGAN, G. S., MERAFINA, M., RUFFINI, R., VESPERINI, E., Stability of Dense Stellar Clusters against Relativistic Collapse. II. Maxwellian Distribution Functions with Different Cutoff Parameters. *Astrophys. J.* **500**, 217–232 (1998).
- [22] BISNOVATYI-KOGAN, G. S., THORNE, K. S., Relativistic gas spheres and clusters of point masses with arbitrarily large central redshifts: can they be stable? *Astrophys. J.* **160**, 875–885 (1970).
- [23] BISNOVATYI-KOGAN, G. S., ZEL'DOVICH, YA. B., Models of clusters of point masses with great central red shift. *Astrofizika*, **5**, 223–234 (1969).
- [24] BOYD, S., VANDENBERGHE, L., *Convex Optimization*, Cambridge University Press, Cambridge 2004.
- [25] BREZIS, H., *Functional Analysis, Sobolev Spaces and Partial Differential Equations*, Universitext, Springer, New York 2011.
- [26] BUCHDAHL, H. A., General Relativistic Fluid Spheres. *Phys. Rev.* **116** (4), 1027–1034 (1959).
- [27] CHANDRASEKHAR, S., *The Mathematical Theory of Black Holes*, International Series of Monographs on Physics **69**, Oxford University Press, New York 1983.

-
- [28] CHRISTODOULOU, D., On the global initial value problem and the issue of singularities *Class. Quantum Gravity* **16**, A23–A35 (1999).
- [29] CHOQUET-BRUHAT, Y., Problème de Cauchy pour le système intégro-différentiel d'Einstein-Liouville. *Ann. de l'Institut Fourier* **21**, 181–201 (1971).
- [30] DAFERMOS, M., HOLZEGEL, G., RODNIANSKI, I., TAYLOR, M., The non-linear stability of the Schwarzschild family of black holes. *Preprint arXiv:2104.08222v1*, 513pp. (2021).
- [31] DAFERMOS, M., Spherically symmetric spacetimes with a trapped surface. *Class. Quantum Gravity* **22**, 2221–2232 (2005).
- [32] DAFERMOS, M., RENDALL, A. D., An extension principle for the Einstein-Vlasov system in spherical symmetry. *Ann. Henri Poincaré* **6**, 1137–1155 (2005).
- [33] DOREMUS, J.-P., FEIX, M. R., BAUMANN, G., Stability of Encounterless Spherical Stellar Systems. *Phys. Rev. Lett.* **26**, 725–728 (1971).
- [34] DYSON, F. W., EDDINGTON, A. S., DAVIDSON, C., A determination of the deflection of light by the sun's gravitational field, from observations made at the total eclipse of May 29, 1919. *Philos. Trans. Royal Soc. A* **220**, 291–333 (1920).
- [35] EHLERS, J., *Survey of general relativity theory*, in: *Relativity, Astrophysics and Cosmology* D. Reidel Publishing Company, Dordrecht 1973.
- [36] EINSTEIN, A., Über den Einfluß der Schwerkraft auf die Ausbreitung des Lichtes. *Ann. Phys.* **340** (10), 898–908 (1911).
- [37] EINSTEIN, A., Zur allgemeinen Relativitätstheorie. *Sitzungsber. der Königl. Preuß. Akad. der Wissenschaften* **1915**, 778–786 (1915).
- [38] EINSTEIN, A., Die Feldgleichungen der Gravitation. *Sitzungsber. der Königl. Preuß. Akad. der Wissenschaften* **1915**, 844–847 (1915).
- [39] EINSTEIN, A., Erklärung der Perihelbewegung des Merkur aus der allgemeinen Relativitätstheorie. *Sitzungsber. der Königl. Preuß. Akad. der Wissenschaften* **1915**, 831–839 (1915).
- [40] ENGEL, K.-J., NAGEL, R., *One-Parameter Semigroups for Linear Evolution Equations*, Graduate Texts in Mathematics **194**, Springer, New York 1999.
- [41] EVENT HORIZON TELESCOPE COLLABORATION ET AL., First Sagittarius A* Event Horizon Telescope Results. I. The Shadow of the Supermassive Black Hole in the Center of the Milky Way. *Astrophys. J. Lett.* **930** (2), L12 (2022).
- [42] FACKERELL, E. D., Relativistic, Spherically Symmetric Star Clusters. IV. A Sufficient Condition for Instability of Isotropic Clusters against Radial Perturbations. *Astrophys. J.* **160**, 859–874 (1970).

- [43] FAJMAN, D., JOUDIQUX, J., SMULEVICI, J., The stability of the Minkowski space for the Einstein-Vlasov system. *Anal. PDE* **14**, 425-531 (2021).
- [44] GÜNTHER, S., The Einstein-Vlasov system in maximal areal coordinates—Local existence and continuation. *Master thesis*, University of Bayreuth, 78p. (2019).
- [45] GÜNTHER, S., KÖRNER, J., LEBEDA, T., PÖTZL, B., REIN, G., STRAUB, C., WEBER, J., A numerical stability analysis for the Einstein-Vlasov system. *Class. Quantum Gravity* **38**, 035003 (2021).
- [46] GÜNTHER, S., REIN, G., The Einstein-Vlasov system in maximal areal coordinates—Local existence and continuation. *Kinet. Relat. Models*, **15(4)**, 681–719 (2021).
- [47] GÜNTHER, S., REIN, G., STRAUB, C., A Birman-Schwinger Principle in General Relativity: Linearly Stable Shells of Collisionless Matter Surrounding a Black Hole. *Preprint: arXiv:2204.10620*, 58pp, (2022).
- [48] GÜNTHER, S., STRAUB, C., REIN, G., Collisionless Equilibria in General Relativity: Stable Configurations beyond the First Binding Energy Maximum. *Astrophys. J.* **918**, 48 (2021).
- [49] GUO, Y., REIN, G., Stable Steady States in Stellar Dynamics. *Arch. Ration. Mech. Anal.* **147**, 225–243 (1999).
- [50] GUO, Y., REIN, G., A Non-Variational Approach to Nonlinear Stability in Stellar Dynamics Applied to the King Model. *Commun. Math. Phys.* **271**, 489–509 (2007).
- [51] HADŽIĆ, M., LIN, Z., Turning Point Principle for Relativistic Stars. *Commun. Math. Phys.* **387**, 729–759 (2021).
- [52] HADŽIĆ, M., LIN, Z., REIN, G., Stability and Instability of Self-Gravitating Relativistic Matter Distributions. *Arch. Ration. Mech. Anal.* **241**, 1–89 (2021).
- [53] HADŽIĆ, M., REIN, G., Stability for the spherically symmetric Einstein-Vlasov system—a coercivity estimate. *Math. Proc. Cambridge Philos. Soc.* **155** (3), 529–556 (2013).
- [54] HADŽIĆ, M., REIN, G., On the small redshift limit of steady states of the spherically symmetric Einstein-Vlasov system and their stability. *Math. Proc. Cambridge Philos. Soc.* **159** (3), 529–546 (2015).
- [55] HADŽIĆ, M., REIN, G., STRAUB, C., On the Existence of Linearly Oscillating Galaxies. *Arch. Ration. Mech. Anal.* **243**, 611–696 (2022).
- [56] HADŽIĆ, M., REIN, G., STRAUB, C., SCHRECKER, M., Damping versus oscillations for a gravitational Vlasov-Poisson system. *Preprint: arXiv:2301.07662v1*, 49pp, (2023).

-
- [57] HAHN, T., Cuba—a library for multidimensional numerical integration. *Comput. Phys. Commun.* **168** (2), 78–95 (2005).
- [58] HISLOP, P. D., SIGAL, I. M., *Introduction to Spectral Theory*, Applied Mathematical Sciences **113**, Springer, New York 1996.
- [59] IPSER, J. R., Relativistic, Spherically Symmetric Star Clusters. II. Sufficient Conditions for Stability against Radial Perturbations. *Astrophys. J.* **156**, 509–527 (1969).
- [60] IPSER, J. R., Relativistic, Spherically Symmetric Star Clusters. III. Stability of Compact Isotropic Models. *Astrophys. J.* **158**, 17–43 (1969).
- [61] IPSER, J. R., A binding-energy criterion for the dynamical stability of spherical stellar systems in general relativity. *Astrophys. J.* **238**, 1101–1110 (1980).
- [62] IPSER, J. R., THORNE, K. S., Relativistic, Spherically Symmetric Star Clusters. I. Stability Theory for Radial Perturbations. *Astrophys. J.* **154**, 251–270 (1968).
- [63] JABIRI, F. E., Static Spherically Symmetric Einstein-Vlasov Bifurcations of the Schwarzschild Spacetime. *Ann. Henri Poincaré* **22**, 2355–2406 (2021).
- [64] JABIRI, F. E., Stationary axisymmetric Einstein-Vlasov bifurcations of the Kerr spacetime. *Preprint: arXiv:2202.10245*, 239pp. (2022).
- [65] KANDRUP, H., MORRISON, P., Hamiltonian structure of the Vlasov-Einstein system and the problem of stability for spherical relativistic star clusters. *Ann. Phys.* **225** (1), 114–166 (1993).
- [66] KANDRUP, H. E., SYGNET, J. F., A simple proof of dynamical stability for a class of spherical clusters. *Astrophys. J.* **298**, 27–33 (1985).
- [67] KING, I., The Structure of Star Clusters. III. Some Simple Dynamical Models. *Astron. J.* **71**, 64–75 (1966).
- [68] KORCH, M., RAMMING, R., REIN, G., Parallelization of Particle-in-Cell Codes for Nonlinear Kinetic Models from Mathematical Physics, *2013 42nd International Conference on Parallel Processing (ICPP)*, IEEE Computer Society, 523–529 (2013).
- [69] KUNZE, M., *A Birman-Schwinger Principle in Galactic Dynamics*, Progress in Mathematical Physics **77**, Birkhäuser, Cham 2021.
- [70] LANDAU, L. D., LIFSHITZ, E. M., *Mechanics* (third edition), Course of Theoretical Physics **1**, Butterworth-Heinemann 1976.
- [71] LEMOU, M., MÉHATS, F., RAPHAËL, P., A New Variational Approach to the Stability of Gravitational Systems. *Commun. Math. Phys.* **302**, 161–224 (2011).
- [72] LEMOU, M., MÉHATS, F., RAPHAËL, P., Orbital stability of spherical galactic models. *Invent. Math.* **187**, 145–194 (2012).

- [73] LIEB, E. H., LOSS, M., *Analysis* (second edition), Graduate Studies in Mathematics **14**, American Mathematical Society, Providence 2001.
- [74] LIEB, E. H., SEIRINGER, R., *The Stability of Matter in Quantum Mechanics*, Cambridge University Press, Cambridge 2010.
- [75] LINDBLAD, H., TAYLOR, M., Global Stability of Minkowski Space for the Einstein-Vlasov System in the Harmonic Gauge. *Arch. Ration. Mech. Anal.* **235**, 517–633 (2020).
- [76] LIONS, P. L., PERTHAME, B., Propagation of moments and regularity for the 3-dimensional Vlasov-Poisson system. *Invent. Math.* **105** 415–430 (1991).
- [77] LYNDEN-BELL, D., Lectures on stellar dynamics. *Lecture Notes in Phys.* **433**, 3–31 (1994).
- [78] MATHUR, S. D., Existence of oscillation modes in collisionless gravitating systems. *Mon. Notices Roy. Astron. Soc.* **243**, 529–536 (1990).
- [79] OLABARRIETA, I., CHOPTUIK, M. W., Critical phenomena at the threshold of black hole formation for collisionless matter in spherical symmetry, *Phys. Rev. D.* **65**, 024007 (2002).
- [80] PENROSE, R., Gravitational Collapse and Space-Time Singularities. *Phys. Rev. Lett.* **14**, 57–59 (1965).
- [81] PENROSE, R. Gravitational Collapse: The Role of General Relativity. *Gen. Relativ. Gravit.* **34**, 1141–1165 (2002).
- [82] PFAFFELMOSER, K. Global Classical Solutions of the Vlasov-Poisson System in Three Dimensions for General Initial Data. *J. Differ. Equ.* **95**, 281–303 (1992).
- [83] RAMMING, R., REIN, G., Spherically Symmetric Equilibria for Self-Gravitating Kinetic or Fluid Models in the Nonrelativistic and Relativistic Case—A Simple Proof for Finite Extension. *SIAM J. Math. Anal.* **45** (2), 900–914 (2013).
- [84] RAMMING, R., REIN, G., Oscillating solutions of the Vlasov-Poisson system—A numerical investigation. *Physica D* **365**, 72–79 (2018).
- [85] RASIO, F. A., SHAPIRO, S. L., TEUKOLSKY, S. A., On the Existence of Stable Relativistic Star Clusters With Arbitrarily Large Central Redshifts. *Astrophys. J.* **336**, L63–L66 (1989).
- [86] RASIO, F. A., SHAPIRO, S. L., TEUKOLSKY, S. A., Solving the Vlasov Equation in General Relativity. *Astrophys. J.* **344**, 146–157 (1989).
- [87] REED, M., SIMON, B., *II. Fourier Analysis, Self-Adjointness*, Methods of Modern Mathematical Physics, Academic Press, New York – London 1975.

-
- [88] REED, M., SIMON, B., *IV. Analysis of Operators*, Methods of Modern Mathematical Physics, Academic Press, New York – London 1978.
- [89] REED, M., SIMON, B., *I. Functional analysis* (second edition), Methods of Modern Mathematical Physics, Academic Press, Inc., New York 1980.
- [90] REIN, G., Static solutions of the spherically symmetric Vlasov-Einstein system. *Math. Proc. Cambridge Philos. Soc.* **115**(3), 559–570 (1994).
- [91] REIN, G., *The Vlasov-Einstein System with Surface Symmetry*, Habilitationsschrift, München 1995.
- [92] REIN, G., Stability and instability results for equilibria of a (relativistic) self-gravitating collisionless gas—A review *Preprint: arXiv:2305.02098*, 71pp, (2023).
- [93] REIN, G., RENDALL, A. D., Global existence of solutions of the spherically symmetric Vlasov-Einstein system with small initial data. *Commun. Math. Phys.* **150**, 561–583 (1992). Erratum: *Commun. Math. Phys.* **176**, 475–478 (1996).
- [94] REIN, G., RENDALL, A. D., The Newtonian limit of the spherically symmetric Vlasov-Einstein system. *Commun. Math. Phys.* **150**, 585–591 (1992).
- [95] RENDALL, A. D., An introduction to the Vlasov-Einstein system. *Banach Center Publ.* **41**, 35–68 (1997).
- [96] REIN, G., RENDALL, A. D., Compact support of spherically symmetric equilibria in non-relativistic and relativistic galactic dynamics. *Math. Proc. Cambridge Philos. Soc.* **128** (2), 363–380 (2000).
- [97] REIN, G., RENDALL, A. D., SCHAEFFER, J., A Regularity Theorem for Solutions of the Spherically Symmetric Vlasov-Einstein System. *Commun. Math. Phys.* **168**, 467–478 (1995).
- [98] REIN, G., RENDALL, A. D., SCHAEFFER, J., Critical collapse of collisionless matter: A numerical investigation. *Phys. Rev. D* **58**, 044007 (1998).
- [99] REIN, G., RODEWIS, T., Convergence of a Particle-in-cell Scheme for the Spherically Symmetric Vlasov-Einstein System. *Indiana Univ. Math. J.* **52**, 821–861 (2003).
- [100] REIN, G., STRAUB, C., On the transport operators arising from linearizing the Vlasov-Poisson or Einstein-Vlasov system about isotropic steady states. *Kinet. Relat. Models* **13**, 933–949 (2020).
- [101] RIOSECO, P., SARBACH, O., Accretion of a relativistic, collisionless kinetic gas into a Schwarzschild black hole. *Class. Quantum Gravity* **34**, 095007 (2017).
- [102] RIOSECO, P., SARBACH, O., Phase space mixing in an external gravitational central potential. *Class. Quantum Gravity* **37**, 195027 (2020).

- [103] SCHAEFFER, J. Discrete approximation of the Poisson-Vlasov system. *Q. Appl. Math.* **45**, 59–73 (1987).
- [104] SCHAEFFER, J., A Class of Counterexamples to Jeans' Theorem for the Vlasov-Einstein System. *Commun. Math. Phys.* **204**, 313–327 (1999).
- [105] SCHULZE, A., Existence and stability of static shells for the Vlasov-Poisson system with a fixed central point mass. *Math. Proc. Cambridge Philos. Soc.* **146** (2), 489–511 (2009).
- [106] SCHWARZSCHILD, K., Über das Gravitationsfeld eines Massenpunktes nach der Einstein'schen Theorie. *Sitzungsber. der Königl. Preuß. Akad. der Wissenschaften* **1916**, 189–196 (1916).
- [107] SHAPIRO, S. L., TEUKOLSKY, S. A., Relativistic Stellar Dynamics on the Computer. I. Motivation and Numerical Method. *Astrophys. J.* **298**, 34–57 (1985).
- [108] SHAPIRO, S. L., TEUKOLSKY, S. A., Relativistic Stellar Dynamics on the Computer. II. Physical Applications. *Astrophys. J.* **298**, 58–79 (1985).
- [109] SHAPIRO, S. L., TEUKOLSKY, S. A., Relativistic Stellar Systems with Rotation. *Astrophys. J.* **419**, 636–647 (1993).
- [110] SIMON, B., *Quantum Mechanics for Hamiltonians Defined as Quadratic Forms*, Princeton Series in Physics **1**, Princeton University Press 1971.
- [111] TAYLOR, A. E., LAY, D. C., *Introduction to Functional Analysis* (second edition), John Wiley & Sons, New York 1980.
- [112] WALD, R. M., *General Relativity*, University of Chicago Press, Chicago – London 1984.
- [113] WOLANSKY, G., Static Solutions of the Vlasov-Einstein System. *Arch. Ration. Mech. Anal.* **156**, 205–230 (2001).
- [114] ZEL'DOVICH, Y. B., NOVIKOV, I. D., *Relativistic Astrophysics. Vol. 1: Stars and Relativity*, University of Chicago Press, Chicago 1971.
- [115] ZEL'DOVICH, Y. B., PODURETS, M. A., The Evolution of a System of Gravitationally Interacting Point Masses. *Soviet Astronomy* **9**, 742–749 (1966).